FULL-SCALE EXPERIMENTAL AND ANALYTICAL STUDIES

ON HIGH-STRENGTH CONCRETE COLUMNS

by

Henry Wook Yun

VOLUME I

A Dissertation Presented to the
FACULTY OF THE GRADUATE SCHOOL
UNIVERSITY OF SOUTHERN CALIFORNIA
In Partial Fulfillment of the
Requirements for the Degree
DOCTOR OF PHILOSOPHY
(CIVIL ENGINEERING)

July 2003

Copyright 2003   Henry Wook Yun

UMI Number: 3116810

INFORMATION TO USERS

The quality of this reproduction is dependent upon the quality of the copy
submitted. Broken or indistinct print, colored or poor quality illustrations and
photographs, print bleed-through, substandard margins, and improper
alignment can adversely affect reproduction.

   In the unlikely event that the author did not send a complete manuscript
and there are missing pages, these will be noted. Also, if unauthorized
copyright material had to be removed, a note will indicate the deletion.
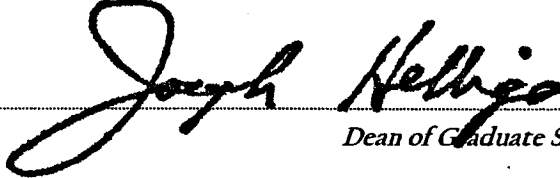
UMI®

UMI Microform 3116810

UNIVERSITY OF SOUTHERN CALIFORNIA
The Graduate School
University Park
LOS ANGELES, CALIFORNIA 90089-1695

This dissertation, written by

<u>Henry Wook Yun</u>

Under the direction of h.i.s.... Dissertation
Committee, and approved by all its members,
has been presented to and accepted by The
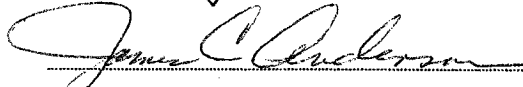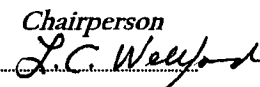*Graduate School, in partial fulfillment of*
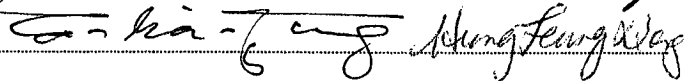*requirements for the degree of*

DOCTOR OF PHILOSOPHY

Dean of Graduate Studies

Date   August 12, 2003

DISSERTATION COMMITTEE

Chairperson

DEDICATION

To my wife, Sue

ACKNOWLEDGMENTS

An experimental research in structural engineering involves tremendous time, perseverance, financial support, and most of all, dedication. The process of reaching an ultimate goal to discover and to pursue for knowledge in depth serves the humankind in much greater dimensions. I would like to acknowledge the support of my parents and my wife for their encouragements throughout my studies. This dissertation would not have been possible without the guidance of my dissertation advisor, Dr. Yan Xiao, for his expertise, encouragements, and financial support. His inputs over the course of past six years have greatly helped me to reach my academic and career goals. I greatly appreciate the members of the dissertation committee, Dr. James C. Anderson, Dr. Landon Carter Wellford, Dr. Hung Leung Wong, and Dr. Ta-Liang Teng for their comments and encouragements that have greatly helped me to push forward toward reaching my lifetime goals. Cooperation from laboratory manager, Mr. R. Bueche is appreciated. Special thanks are due to Mr. Hui Wu, Mr. Tolga Yaprak, Ph.D. candidates, and Dr. Asadollah Esmaeily of the Department of Civil and Environmental Engineering, University of Southern California, for their helps in testing and for collaborative engagements in other structural laboratory activities of various structural research topics over the course of past several years.

iii

Technical findings and conclusions described in this disseration are solely those of the author, and do not necessarily reflect the views of the sponsors and collaborators. The report does not constitute a standard, specification or regulation. Anyone making use of the information stated in this report assumes all liability arising from such use.

TABLE OF CONTENTS

LIST OF TABLES

LIST OF FIGURES

xiii

LIST OF VARIABLES

$a = \dfrac{M}{V}$, ratio of moment to shear at critical section or inclination of diagonal compression strut (due to axial load P)

a = Upper bound of integration defined

a_1 a_2, a_3, a_4, a_5= Constants evaluated performing a regression analysis

b = width of the cross section

b_c and d_c or (b_{cx} and b_{cy}) = Core dimensions to centerlines of perimeter hoop in x and y directions, respectively

b_c = the width of the confined concrete core

b_w = Web width taken as D and b for circular and rectangular columns, respectively

c = Concrete cover thickness or depth of the compression zone

c_x and c_y = widths of the concrete core parallel to the x and the y axis, repectively

d = Effective depth, normally taken as $0.8h$ or $0.8D$ for rectangular or circular columns, respectively

d = Nominal diameter of longitudinal steel bars in inches

d_b, d = Diameter of column bars

d_{lb} = Longitudinal bar diameter

d'' = Nominal diameter of lateral ties in inches

$\widetilde{e}_c$ = uniaxial strain corresponding to $\widetilde{\sigma}_c$ $(\widetilde{e}_c \prec 0)$

$^t\widetilde{e}$ = uniaxial strain

$\widetilde{e}_c^{\,\prime}$ = Uniaxial strain corresponding to $\widetilde{\sigma}_c^{\,\prime}$ for multiaxial stress conditions

$^t e_{pi}$ = Strain corresponding to principal stress

e_{p3} = Strain increment

$^t e_{p3}$ = Strain component at time t measured in direction of the principal stress $^t\sigma_{p3}$

$\widetilde{e}_u$ = ultimate uniaxial compressive strain $(\widetilde{e}_u \prec 0)$

$\widetilde{e}_u^{\,\prime}$ = Ultimate uniaxial compressive strain corresponding to $\widetilde{\sigma}_u^{\,\prime}$ for multiaxial stress conditions

f_c, f = Compressive confined concrete stress

$f_c^{\prime}$, f_{co} = Compressive strength of concrete

f'_{cc}, f_{cc} = Peak compressive stress of confined concrete

f'_{co} = Peak stress of unconfined concrete

f_{hcc} = Stress in the transverse reinforcement at the maximum strengths of confined concrete

f_{hcc} = Stress in the lateral reinforcement at peak strength of confined strength

f_i = Confined concrete stress at ε_i

f_o = Peak confined concrete stress

f_l = Lateral pressure from the transverse reinforcement or uniform passive confinement pressure for spirally reinforced circular column

f_l' = Effective lateral confining pressure

f_{le} = Effective confinement pressure applied to the nominal concrete core

f_{lex} and f_{ley} = Equivalent lateral pressures acting perpendicular to core dimensions in x and y directions, respectively

f_{lx} = Lateral confining stress on the concrete in the x direction

f_{lx}' = Effective lateral confining stress in x direction

f_{ly} = Lateral confining stress on the concrete in the y direction

f_{ly}' = Effective lateral confining stress in y direction

$\bar{f}_r$ = Average transverse confining pressure

f_s = Tensile stress in tranverse reinforcement at peak concrete stress

f_s = Steel stress

f_s = Steel stress of the outmost longitudinal reinforcement

f_s = Stress in extreme tensile bars

f_{su} = Ultimate tensile strength of steel

f_U = Ultimate tensile strength of reinforcement

f_{uh} = Peak stress when strain-energy capacity of the transverse reinforcement is reached

f_y = Yield strength of steel

f_y = Yield strength of longitudinal reinforcement

$$f_y' = \begin{cases} f_y \\ E_s \varepsilon_y' \end{cases} \text{ for } \begin{array}{l} \varepsilon_s \leq \varepsilon_{sh} \\ \varepsilon_s \succ \varepsilon_{sh} \end{array}$$

f_y'' = Yielding stress of the lateral steel in psi

f_{ye} = Effective stress of transverse reinforcement at the point of maximum strength

f_{yeff} = Effective stress in confining steel for the condition when the specimen has reached to its maximum strength

f_{yh}, f_y = Transverse reinforcement yield stress

f_{yh} = Tie yield strength

f_{yh} = Specified yield strength of transverse reinforcement

f_{yt} = Yield strength of the transverse steel

f_{2i} = Confined concrete stress at ε_{2i}

g' = the distance between the centers of the longitudinal bars in the extreme faces divided by the core dimension

h = Column height for single curvature bending

h = Full column height during double curvature bending

h = Rectangular column depth

h = Depth of the cross section

h_c = The depth of the confined concrete core or cross sectional dimension of column core measured center-to-center of out-most peripheral hoops

h_e = Effective column length considering the plastic hinge length

h_x = Maximum horizontal spacing of hoop or crosstie legs of column face

$h'' $ = Dimension of core of rectangular or square column at right angels to direction of transverse bars under consideration measured to the outside of the perimeter hoop

$h'' $ = Length of one side of the rectangular ties in inches

k = Concrete shear component factor dependent on the member displacement ductility level and on whether loading is uniaxial or biaxial

k, k_1, k_2, k_3, k_4 = Empirical coefficients

k_e = Confinement effectiveness coefficient

l = total column length

l_{cons} = Segment of constant length close to the column base

l_e, h_e = Effective plastic hinge length

l_p = Plastic hinge length or length of the transition region between the point of the first longitudinal reinforcement yielding and the column base

l_s = Shear span length (one half of column height for double curvature bending)

l_{trans} = Transition length

$$m = \frac{f_y}{0.85 f_c'}$$

xxxiv

n = Number of the legs of the transverse reinforcement in the vertical cross section within the spacing, s

n = Number of longitudinal steel bars

$$p = \frac{\tilde{e}_u}{\tilde{e}_c}$$

$$p_t = \frac{A_{st}}{A_g} = \text{Gross longitudinal reinforcement ratio}$$

q = Number of tie legs that cross the side of core concrete for which the average lateral pressure f_l is being computed

$$r = \frac{E_{50}}{E_{50} - E_{sec}} \text{ or } \frac{E_c}{E_c - E_{sec}}$$

s, s_x, s_h = Spacing of transverse reinforcements

s_l = Spacing of longitudinal reinforcement

s' = Clear vertical spacing between spiral or hoop bars

w_i' = Clear spacing between longitudinal reinforcements

$$x = \frac{\varepsilon_c}{\varepsilon_{cc}}$$

$$A = \frac{E_c \varepsilon_o}{f_o}$$

A_b = Area of the longitudinal bars reliant on tie

A_c = Area of core of section enclosed by the center lines of the perimeter spiral or hoop

A_{cc} = Area of confined concrete defined as the area of the concrete within the center lines of the perimeter spiral or hoop (Nominal concrete core area)

A_{ch}, A_c = Cross sectional area of a column measured out-to-out of transverse reinforcement

A_e = Area of the effectively confined concrete core

$A_e = 0.8A_{gross}$ for both circular and rectangular columns

A_e = Area of effectively confined concrete core at midway between the levels of transverse hoop reinforcement

$A_e = 0.8bh = 0.8A_g$ for rectangular columns

$A_e = 0.8D^2 = 1.02A_g$ for circular columns

A_g = Gross concrete section area

A_g = Gross sectional area of the column

A_i = Total plane area of ineffectually confined core concrete at the hoop level

A_{sh} = Area of transverse reinforcement

$A_{sh(ACI)}$ = Total cross-sectional area of rectilinear ties required equired by ACI 318-95 code

A_{shx} and A_{shy} or (A_{sx} and A_{sy}) = total cross sections of the lateral steel bars perpendicular to the x and the y axis, respectively

A_{st} = Total area of longitudinal column reinforcement

A_{sx} and A_{sy} = The total area of transverse bars in x and y directions, respectively

A_t = Cross sectional area of one leg of transverse reinforcement

A_{te} = Area of one leg of a stirrup-tie in the direction of potential buckling of the longitudinal bars

A_v = Total transverse reinforcement area per layer

$$B = \left[\frac{(A-1)^2}{0.55} \right] - 1$$

$$C = \left[\frac{(\varepsilon_{2i} - \varepsilon_i)}{\varepsilon_o} \right] \left\{ \left[\frac{\varepsilon_{2i} E_i}{(f_o - f_i)} \right] - \left[\frac{4\varepsilon_i E_{2i}}{(f_o - f_{2i})} \right] \right\}$$

$\hat{C}$ = Stress-strain matrix corresponding to isotropic conditions

C_1 = Experimental constant for shear effect

C_1 = Transformation constant

C_2, $\mathcal{E}$ = Experimental constant for yield penetration

C_2 = Transformation constant

D = Column section depth

$$D = (\varepsilon_i - \varepsilon_{2i}) \left\{ \left[\frac{E_i}{(f_o - f_i)} \right] - \left[\frac{4E_{2i}}{(f_o - f_{2i})} \right] \right\}$$

D = Circular column diameter

D' = the distance between centers of the peripheral hoop or spiral

E = Young's Modulus of Reinforcement

E_c = Tangent modulus of elasticity of the concrete = $5,000\sqrt{f'_{co}}$ MPa, $27.55w^{1.5}\sqrt{f'_c}$, $3200\sqrt{f'_{co}} + 6900$ MPa, $4700\sqrt{f'_{co}}$ MPa, $3,320\sqrt{f'_c}(MPa)6,900$, $57,000\sqrt{f'_c}(lb/in^2)$, $4,730\sqrt{f'_c}(MPa)$, or $18,000\sqrt{f'_c} + 2.1 \times 10^6$ (psi)

$$E_i = f_i \Big/ \varepsilon_i$$

$'E$ = Young's modulus

$$'E_{ij} = \frac{\left|{}^t\sigma_{pi}\right|{}^t\widetilde{E}_{pi} + \left|{}^t\sigma_{pj}\right|{}^t\widetilde{E}_{pj}}{\left|{}^t\sigma_{pi}\right| + \left|{}^t\sigma_{pj}\right|} \ , \text{ where } i \neq j$$

$\widetilde{E}_0$ = uniaxial initial tangent modulus (all uniaxial variables are designated with ~ symbol over them)

$'\widetilde{E}_{pi}$ = Tangent Young's modulus corresponding to each principal stress

E_s = Modulus of elasticity of steel

$\widetilde{E}_s$ = uniaxial secant modulus corresponding to uniaxial maximum stress,

$$\widetilde{E}_s = \frac{\widetilde{\sigma}_c}{\widetilde{e}_c}$$

E_{sec} = Secant modulus of elasticity of the concrete = $\dfrac{f'_{cc}}{\varepsilon_{cc}}$ or $\dfrac{f'_{cc}}{\varepsilon_1}$

E_{SEC} = Secant modulus at the peak strength of confined concrete

$E_{sec u} = \dfrac{f'_{co}}{\varepsilon_{co}}$ = Secant modulus of elasticity of unconfined concrete

E_{sh} = Strain-hardening modulus of steel

$$\widetilde{E}_u = \frac{\widetilde{\sigma}_u}{\widetilde{e}_u} \ \text{ or } \ \frac{\widetilde{\sigma}_u - \widetilde{\sigma}_c}{\widetilde{e}_u - \widetilde{e}_c}$$

$$E_{2i} = f_{2i} \Big/ \varepsilon_{2i}$$

xxxviii

$E_{50} = 46,000 \times k_2 \times \sqrt{f'_{co}}$ (psi) (Empirical confined concrete modulus of elasticity)

$E_{50u} = 46,000 \times \sqrt{f'_{co}}$ (psi) (Empirical unconfined concrete modulus of elasticity)

H_e = Effective height of the column taking into consideration the plastic hinge formation

I_g = Moment of inertia of the column gross section

K, K_e = Effective confinement

L = Distance from the point of contraflexure to the point of maximum moment

L_h = Length of plastic hinge

M_{ACI} = Moment capacity of the columns based on the ACI 318-95 Code

M_i = Ideal flexural capacity

M_{max} = Maximum moment value

$_{EXP}M_{MAX}$, M_{MAX}, $_{EXP}M_{MAX(Avg.)}$ = Maximum experimental moment capacity

M_U = Ultimate flexural capacity

M_U = moment at the critical section of column base

M_y = Moment at the first yield of longitudinal steel

M_y = yield moment for the existing axial load

$_{MAN}M_{1Y}$ = Analytical yield moment based on Mander model

$_{MAR}M_{1Y}$ = Analytical yield moment based on Martirossyan model

$M_{1y(Avg.)}$ = Experimental yield moment

P = control parameter for increase in the steel stress relevant to strain in the strain-hardening region

P , N^* , N_U = Axial load

P_e = Maximum design axial load in compression at a given eccentricity

P_o = Axial load

P_o , N_o = Axial load capacity

V = Shear force

V_c = Sum of strength of the concrete shear resisting mechanism

V_c = Concrete shear component dependent on ductility level

V_f = Shear force

V_{fACI} , V_{ACI} = Flexural capacity per ACI requirement

$_{TRUE}V_{MAX}$ = Maximum true shear force

$_{EXP}V_{MAX}$, V_{MAX} = Maximum experimental shear capacity

V_n = Nominal shear force

V_p = Axial level shear component dependent on column aspect ratio

V_s = Truss shear component dependent on content of transverse reinforcement

V_s = Truss-mechanism strength of transverse reinforcement

V_U = Factored shear force or lateral shear force at development of ultimate flexural capacity

V_y = Shear force corresponding to the first yield of longitudinal steel

$$X = \varepsilon_c \Big/ \varepsilon_o$$

$$Y = f_c \Big/ f_o$$

Y_P = Parameter to take into account the axial load effect

Y_ϕ = Parameter to take into account sectional ductility demand

$$\alpha = \frac{0.25 \dfrac{f_c' - 0.6}{f_o}}{3.13K\left[1.4\left(\dfrac{\varepsilon_o}{K}\right) + 0.0003\right]} = \text{Empirical coefficient}$$

or configuration efficiency factor total cross-sectional area of rectilinear ties

$\alpha = s' \Big/ h$ for square or rectangular sections

α_s = Modification factor

β = Coefficient for the slope control of descending branch

$$\beta = b_c \Big/ h_c$$

$$\beta = \left(0.048 f_{co}' - 2.14\right) - \left(0.098 f_{co}' - 4.57\right)\sqrt{\frac{f_l'}{f_{co}'}}$$

ε = Concrete strain

ε, ε_y = Yield strain

xli

ε_c = Longitudinal compressive confined concrete strain

ε_{cc} = Peak longitudinal compressive confined concrete strain

$\varepsilon_{co}, \varepsilon_1$ = Unconfined concrete strain at corresponding f'_{co} (Assumed as 0.002)

$$\varepsilon_{co} = \frac{0.7\left(f'_{co}\right)^{0.3}}{1000} = \text{Strain at peak stress of the unconfined concrete}$$

ε_{cu} = Ultimate confined concrete strain (with an assumption that a conservative limitation of ultimate confined concrete compressive strain is when fracture of a hoop first occurs due to substantial buckling of longitudinal bars)

ε_{hcc} = Tie steel strain

ε_i = Arbitrarily selected empirical strain on the descending branch of confined concrete stress-strain relationship

ε_o = Peak confined concrete strain corresponding to f_o

$$\varepsilon_o = \begin{cases} 0 \\ \left(\varepsilon_{sh} - \dfrac{f_y}{E_s}\right) \end{cases} \text{for} \quad \begin{matrix} \varepsilon_s \leq \varepsilon_{sh} \\ \varepsilon_s \succ \varepsilon_{sh} \end{matrix}$$

ε_s = Steel strain

ε_{sh} = Steel strain at commencement of strain hardening

ε_{sp} = Concrete strain at spalling

ε_{su} = Steel strain at f_{su}

ε_y = Steel strain

$$\varepsilon_y' = \frac{1}{E_s(1-\rho')}\left[(f_{su} - f_y) - (\varepsilon_{su} - \varepsilon_{sh})E_s\rho'\right]$$

ε_{C50C} = Strain at which the stress drops to 50% of the peak strength of confined concrete

ε_{C50U} = Strain at which the stress drops to 50% of the peak strength of unconfined concrete (May be assumed as 0.004)

ε_{01} = Strain at peak unconfined concrete stress

ε_{085} = Unconfined concrete strain corresponding to 85% of peak stress

ε_1 = Strain at peak confined concrete stress

$\varepsilon_{2i} = 2\varepsilon_i - \varepsilon_o$ = Arbitrarily selected empirical strain on the descending branch of confined concrete stress-strain relationship

ε_{85} = Confined concrete strain corresponding to 85% of peak stress

ϕ = Reduction factor for concrete members in compression

ϕ = Curvature or strength reduction factor

ϕ_{lp} = Curvature at the top of the plastic hinge

ϕ_t = Curvature at the top of transition length

ϕ_u = Curvature at the critical region of the column base or ultimate curvature at column failure

ϕ_y = Curvature corresponding to the first yield of longitudinal steel

$$\delta' = \begin{cases} \delta_o & \\ \left(\dfrac{\varepsilon_{sh}}{\varepsilon_y} - 1\right)^2 \delta_o & \end{cases} \text{for} \quad \begin{array}{l} \varepsilon_s \leq \varepsilon_{sh} \\ \varepsilon_s \succ \varepsilon_{sh} \end{array}$$

$\mu_{\phi 80}$ = Curvature ductility factor from the moment-curvature relationship of the column section in the plastic hinge region when the strength loss of the column is smaller than or equal to 20% of the maximum bending moment

ν = Poisson's ratio at the maximum strength of confined concrete, where 0.5 is used at the peak strength of confined concrete

ν_b = Basic shear stress

ρ = Volumetric ratio of longitudinal reinforcement

ρ_c = Longitudinal reinforcement ratio in the core section

ρ_{cc} = Ratio of area of longitudinal reinforcement to area of core of section

ρ_{cc} = Longitudinal reinforcement ratio

ρ_h = Volumetric ratio of the transverse reinforcement

ρ_s = Volumetric ratio of the transverse reinforcement

ρ_s = Volumetric ratio of reinforcements to concrete or ratio of volume of transverse circular hoop or spiral steel to volume of concrete core of column

ρ_t = Transverse reinforcement ratio

ρ_w = Ratio of longitudinal tension reinforcement, taken as $0.5\rho_t$ for columns

ρ_x = Transverse confinement ratio in x direction

ρ_y = Transverse confinement ratio in y direction

xliv

$$\rho' = \begin{cases} 0 \\ \dfrac{E_h}{E_s} \end{cases} \text{for} \quad \begin{matrix} \varepsilon_s \leq \varepsilon_{sh} \\ \varepsilon_s \succ \varepsilon_{sh} \end{matrix}$$

$\rho'' =$ Volumetric ratio of lateral reinforcement

$'\widetilde{\sigma} =$ uniaxial stress

$\widetilde{\sigma}_c =$ maximum uniaxial compressive stress ($\widetilde{\sigma}_c \prec 0$)

$\widetilde{\sigma}_c' =$ Maximum uniaxial compressive stress for multiaxial stress conditions

$'\sigma_{pi}$, $'\sigma_{p3} =$ Principal stresses

$\widetilde{\sigma}_u =$ ultimate uniaxial compressive stress ($'\widetilde{\sigma} \prec 0$)

$\widetilde{\sigma}_u' =$ Ultimate uniaxial compressive stress for multiaxial stress condition

τ_{ss}, τ_{tt}, $\tau_{rr} =$ Normal stresses

τ_{rs}, τ_{rt}, $\gamma_{st} =$ Shear stresses

$\Delta =$ Total flexural deflection or total lateral displacement

$\Delta_e =$ Elastic flexural deflection

$\Delta_f =$ Total deformation due to flexural bending

$\Delta_{f1} =$ Deformation due to plastic hinge rotation

$\Delta_{f2} =$ Actual flexural deformation of the column

$\Delta_i =$ Total displacement

$\Delta_p =$ Deflection due to the rotation of the plastic hinge area

Δ_s = Shear deformation

Δ_{sy}, Δ_Y = Shear deformation corresponding to first yield of longitudinal steel

Δ_U = Lateral displacement at development of ultimate flexural capacity

ABSTRACT

Six full-scale high-strength concrete columns were tested under cyclic lateral force and a constant axial load equal to 20% to 34% of the column axial load capacity. The 510 mm (20 in.) square columns were reinforced with 4 No. 29 (ASTM No.9) and 4 No. 36 (ASTM No.11) bars constituting a longitudinal steel ratio of 2.6% of the column gross sectional area. The main experimental parameter was transverse reinforcement detail. It was found that the hysteretic behavior and ultimate deformability of high-strength concrete columns are significantly influenced by the amount and details of transverse reinforcement in the potential plastic hinge regions as well as the axial load levels. Excellent hysteretic behavior achieving a drift ratio of 6% without degradation of load carrying capacity was developed by columns with 82% or more of confinement specified in the seismic design provision of the ACI 318-95 code, when the axial load ratio was 20%. However, similar columns only achieved an ultimate drift ratio of 3% when the axial load was above 30% of the column axial load capacity. Reasonably good hysteretic behavior up to an ultimate drift ratio of 4% was possible for columns reinforced with transverse reinforcement providing as low as 57% of confinement required by the ACI code, when the axial load ratio was 20%. For the same transverse reinforcement configuration and testing condition, improved behavior was observed for the model column where the transverse

reinforcement was of a higher strength. New performance-based design for required transverse reinforcements for high-strength concrete columns subjected to seismic loading is investigated. Macro-analysis was performed to predict the column behavior at various stages of seismic loading. The analytical results show that currently available confined high-strength concrete stress-strain theories implemented in a new curvature-based moment-curvature program analysis is able to predict the lateral shear versus displacement relationship of the specimens. A micro-analysis was performed with ADINA (Automatic Dynamic Non-linear Analysis), a finite element analysis software, by constructing three-dimensional finite element models. The results, with all parameters properly prescribed, provide good correlation with the experimental values. The finite element method can provide detailed analytical results of stress and crack distributions and provide insights in stress and crack variations during the stages of loading as well as verification of the experimental results.

xlviii

PREFACE

My aspiration is to present a dissertation that does not only make a small but significant contribution to scientific progress, but that also provides significant help to the civil engineering practice.

This dissertation addresses crucial experimental and analytical work in contribution to performance-based design and analysis of reinforced concrete structural members whose importance has been increasing steadily over the decade. The development of analytical tools to predict the seismic-performance of high performance structural members is gaining momentum because of emerging need for increased productivity. The trend toward the efficient use of high-strength materials in the next century is evident.

Former researchers in the field of testing seismic components of structures have set up an aggressive basis to learn the mechanics in seismic performance of reinforced concrete members. All researchers face problems in enhancement of currently available tools, and all of them will face problems of learning and resolving pertinent problems that are addressed in this dissertation. I hope that the concepts from my dissertation will ease the lives of my future colleagues.

xlix

Originally, I had thought of my intended dissertation work as a kind of adventure because it was uncertain what would be the next problem I face. Judging from what successful colleagues had told me, finding a worthwhile Ph.D. thesis, writing a dissertation, and persisting in all trials is like descending to hell, being eaten alive, and returning to the surface while trying to maintain a normal life. This did not seem to occur to me since I managed to obtain the approval of thesis proposal in 1999, continued with my research and its consolidation in 2002, and finished writing up the dissertation in 2003. One reason for this is that I could build on my earlier research work dating back to 1997.

The dissertation went through a number of revisions throughout all stages of research. My faculty advisors commented on all of the releases, and I am indebted to all of them for their insightful comments that helped me improve this dissertation, and I am grateful to all of my colleagues who have collaborated with me in the fabrication and testing of the specimens and also shared with me their research works.

1

CHAPTER 1

INTRODUCTION

1.1   GENERAL

History of Concrete Usage

Going back to the early civilization, the lime mortar was used in a hardened form for building materials. Clay and timber were one of the earliest forms of building materials to build habitats (Smith et. al., 1989). Then through evolution came more advanced form of material concrete. It consists of several different components that were mixed together for better strength and stiffness. There are much aspects to consider when it comes the formulation of concrete with desired properties for a specific purpose. One of the first attempts to use reinforced concrete began in 1800's for building structures. Since then, various research have been undertaken over past century to understand and improve the properties and the behavior of concrete materials and their usage in reinforced concrete members of structures.

1

The high strength concrete (HSC) was first introduced since 1950's, with its strength gradually increasing. The design strength of commercially available HSC has almost tripled in certain areas of the United States (US). Its usage has gradually increased. In 1972, the first 62 MPa (9000 psi) concrete was produced and was used in the 50-story Mid-Continental Plaza building which is located in Chicago. Other cities such as Chicago, Houston, New York, and Seattle followed the usage of HSC for the construction of high-rise building structures. Throughout the United States, HSC of strengths between 52 and 69 MPa (7500 and 10,000 psi) are being used. In Chicago, concrete strengths of up to 96 MPa (14,000 psi) have been used in buildings. It is expected that in the near future, use of 69 to 83 MPa (10,000 to 12,000 psi) concrete may become fairly common. The ingredients of high-strength concrete is undergoing continual development. It is predicted that 138 MPa (20,000 psi) HSC may be in use by the beginning of the 21st century.

High-strength concrete is defined in terms of strength and durability. Many different definitions have been used depending on the curing period, geographical locations, and different mix designs. In all aspects, it is found to be extremely important to pay special attention to the material selection, mix design, and to overall quality control in every phase of the concrete-making process.

2

1.2 PURPOSE

Various research have been undertaken on the usage of high strength concrete for axially loaded reinforced concrete columns that are subjected to seismic loading. However, it is apparent that further investigation is necessary due limited research data on full-scale specimens. The purpose is to investigate the seismic behavior of high strength concrete columns and to make comparisons between existing concrete stress-strain models and analytical behaviors based on the new data on high strength concrete columns. By analyzing the behavior of these full-scale columns, the criteria will be established to understand the effect of different crucial column parameters on the overall performance, capacities, and behavior of the HSC columns. Further, existing design criteria will be investigated to determine adequate design method in consideration for HSC application on columns subjected to seismic loads.

The behavior of reinforced high strength concrete under simulated seismic load was investigated to study the effect of different reinforcement configurations, deformability, flexural capacity, shear capacity, failure characteristics, yield points, ultimate failure, and ductility. Quasi-static loading was applied to the specimens to best simulate the seismic behavior with displacement control. From this investigation it is hoped that better understanding and methods to improve the

3

high strength concrete column members is deduced based on the analysis of the test data. Material tests for the material that were used to construct the specimens have been performed. After analysis of the test data, the results and the behavior of the specimens were analyzed and discussed in detail to better understand the nature of the failures at various stages of the experiments.

Prediction of Column Behavior

An appropriate column model will be devised in order to establish a realistic model that can predict the performance and behavior of high strength reinforced concrete columns which consist of high-strength materials in order to achieve desired level of seismic performance level as well as ideal ductile behavior when subjected to various axial load levels. The variation of behavior due to steel configurations as well as analytical models to predict such behavior will be considered. The behavior of columns may be understood and predicted upon successful completion of experimental phase and once proper analytical techniques have been devised. It is hoped that detailed analysis and observance of the specimens may provide accurate prediction of the high-strength concrete column behaviors.

4

1.3 LAYOUT OF DISSERTATION

First, the material properties of High Strength Concrete will be investigated in order to understand the nature of the material. In order to understand the behavior of columns, it is important to consider the material properties and behavior of HSC for use in high strength concrete columns. Material composition, various ingredients, deformability and other characteristics that affect the behavior of high strength reinforced concrete columns will be discussed. Current application of HSC in the construction industry and its advantages will be discussed.

Second, in consideration for the application of HSC in reinforced columns, the stress-strain characteristics of unconfined and confined high strength concrete under axial loading will be discussed. Previous researches that have been undertaken in consideration for typical effects of seismic loading will be considered. The material properties of the steel reinforcements also will be considered.

By modeling the stress-strain characteristics of unconfined and confined high strength concrete under seismic loading, a reliable moment to curvature relationship is then generated in order to assess the flexural strength and deformation capacity from reinforced high strength concrete sections confined by different yield grades of reinforcement and axial load levels. The experimental

5

program, which will be discussed, consists of concentric compressive axial loads applied on six full-scale high strength concrete reinforced columns. Simultaneously, quasi-static cyclic lateral load was applied in order to simulate a typical earthquake loading. The concrete compressive strength were either 62.1 or 64.1 MPa (9.0 or 9.3 ksi). The column sections were 508 x 508 mm (20 x 20 inch) square sections, and a combination of Grade 420 No. 29 and No. 36 (ASTM Grade 60 #9 and #11) longitudinal bars and either Grade 420 or 520 No. 16 (ASTM Grade 60 or 75 #5) transverse reinforcements were used. The arrangement of transverse hoops was such that two cross ties were used, and their details are shown in Chapter 3. The axial load ranged between 3331.7 and 5450.8 kN (749 and 1225.4 kips).

The flexural strength in relation to different parameters such as yield grade of the reinforcements and transverse reinforcement details will be assessed. Through analysis, the strain behavior of the steel reinforcements in the plastic hinge region and other critical regions are observed to understand the cause and nature of failure patterns on the column and to properly model column behavior throughout the loading stages and therefore, accurately predict the column capacities. Theoretical considerations will be made to generalize the theoretical prediction of the flexural capacity of reinforced high strength concrete columns subjected to high or low axial loads. The appropriateness of the ACI 318-95 and 318-99 seismic design provisions, existing seismic provision of New Zealand, and

6

recommended transverse reinforcement by Shiekh, et. al. for high strength concrete columns will be considered. The Macro-analysis will be performed which consists of moment-curvature analysis as well as cyclical analysis. The comparisons will be made among the existing seismic provisions of transverse reinforcement based on the experimental data. The Micro-analysis will utilize the Finite Element Method to model and confirm the results obtained from the experiment.

7

CHAPTER 2

RESEARCH BACKGROUND

2.1 CONVENTIONAL USE OF STRUCTURAL MATERIALS

For the axially loaded column design, the individual strength contributions of the concrete and steel are added. The lateral steel (transverse reinforcements) are used to laterally confine the core concrete to prevent lateral expansion. The lateral steel also increases the axial capacity and ductility of the column. The use of high-strength concrete typically increases the range of the linear elastic response to compression because the internal microcracking is delayed until higher ultimate load is reached. However, its material ductility is less than that of lower strength concretes, and therefore has lower creep coefficient. Despite such different qualities of the high strength concrete, much of the design practices are based on normal strength concrete. Therefore, investigation is necessary to examine the currently available design equations.

8

2.1.1 Material Properties and Characteristics of High Strength Concrete

Characteristics

In order to attain the desired high strength, additional admixtures such as fly ash or superplasticizer are added to the concrete mix, to increase the strength to as high as 100 MPa (14,000 psi). It is crucial to use the proper type of aggregates, cement, supplementary cementing materials, and superplasticizers among many types that are available to obtain the desired strength.

The water to cementitious ratio for high strength concrete is low, and the strength of the cement-aggregate bond is mostly the strength controlling factor. Thus, there is no clear correlation between the water to cementitious ratio in relation to the compressive strength. As compared to the normal strength concrete, the content of the cementitious materials (cement, fly ash, slag, silica fume) for the high strength concrete are much higher, and the amount of supplementary cementing materials such as superplasticizers and silica fume are adjusted as necessary to further increase the workability and the strengths.

Different mix designs of high strength concrete can give the same concrete strength because of variance in the specific material properties from different geographical locations and due to different types of cementitious and

9

supplementary cementing materials that are available.   Therefore, the high strength concrete should be proportioned based on trial mixes.

The strength of the high strength concrete is sensitive to its curing conditions, the type of mold used, capping techniques, the specimen size, and to the load capacity and rigidity of the testing machine.   Therefore, the quality control should be maintained throughout the entire production process.

The selection of materials and their proper usage require a fundamental understanding of mechanics and trial and error experiences.   Further, a well-rounded knowledge in the properties of different material components of concrete and their behavior in combination with steel reinforcements as well as thorough analysis of research and analysis are necessary to understand the behavior of reinforced concrete members.

In order to understand the behavior of concrete, the compressive tests are performed to measure the displacement and ultimate strength at failure.   Also, tensile tests are performed to understand the stress-strain behavior and the ultimate strength of the steel reinforcements.   Actual reinforced concrete specimens are then tested often subjected to static or dynamic loads to understand their behavior and capacity.   Although there are sufficient amount of available knowledge about normal strength concrete, the investigation of high strength

10

concrete is quite limited. With several disastrous earthquakes in the recent years and increasing need for more efficient usage of materials that can provide safe and economic means of construction have led to increase in the high strength concrete usage in recent years. Many different countries have undertaken research in high strength concrete with 28-day strengths typically greater than 41.4 MPa (6 ksi). Mechanical properties, tensile strength, creep, shrinkage, temperature effects, fatigue, bond properties, permeability, corrosion resistance, frost resistance, fire resistance, abrasion-erosion resistance, fracture mechanics, the effect of load rate, stress gradient and ductility are some of the considerations which were made to understand the nature of the high strength concrete material.

Material Properties

The high strength concrete, with developments in the recent decade, can have strength as high as 96.5 to 110.3 MPa (14 to 16 ksi). Many countries are actively using high strength concrete technology for construction. The various aspects of the high strength concrete materials will be discussed based on the recent research results of the past decade.

With lower water to cement ratio as compared to normal strength concrete, the strength of high-strength concrete is based on the participation of all of its ingredients including aggregates, cement, chemical admixtures, and water. For normal strength concrete, the strength of the cement-aggregate bond or the hardened cement paste is the controlling factor that determines its strength. In other words, for high strength concrete, the strength of all of its components are optimized with each of them considered in the design.

The superplasticizers are used to increase the workability and other cementitious materials are also needed to attain its high strengths. For very high strengths, the use of silica fume or fly ash or ground granulated blast furnace slag is needed as additional materials.

The fineness and chemical composition of the cement and other supplementary materials are needed to properly produce trial mixes of proper strength level. There are various types of cements meeting the ASTM Standard Specification C150 for Types I, II, and III Portland cements. When mixed with other admixtures, the same cements of the same type may have different strength characteristics. Thus, it is necessary to consider the fineness and chemistry when choosing Portland cements. The chemical compositions of other supplementary

12

cementing materials also affect the overall strength behavior of the high strength concrete.

With regards to the aggregates, the coarse aggregate should be crushed aggregates free of any other types of particles. It has been found that equi-dimensional crushed coarse aggregates from various rock types are proper to provide sufficient cement-aggregate bond. The fine aggregates with fineness modulus of 3.0 or greater is recommended. The ratio of coarse to fine aggregate is typically 2.0 for high strength concrete.

The proper casting and curing methods are essential for high strength concrete mixes to obtain proper strengths. Different types of casting cylindrical mold, capping materials, and the stiffness of the testing machine all can affect the final strength of high strength concrete. There are various factors which affect the strength of high strength concrete such as dimensions, aggregate porosity, matrix porosity, moisture state, rate of stress application, water to cement ratio, degree of hydration, air content, aggregate grading, curing time, curing temperature, humidity, and chemical interaction between aggregate and cement paste. The surface texture of the coarse, for example, affects the bond strength between the aggregates and the cement paste, and therefore, affect the stress level at which the microcracking begins. The larger aggregate size generally results in lower

13

strength since the larger aggregates have less specific surface area, and therefore, the bond between aggregates and paste is lower. The proper hydration while curing is necessary to properly reduce the porosity to attain the desired strength. It has been found that moist-cured specimens had higher strength as compared to air-cured specimens. The amount of condensed silica fume or cement type has been found to not to substantially affect the strength of the high strength concrete. However, higher the curing temperature, the strengths were generally found to be higher as compared to low temperature curing. After above considerations, the maintenance of adequate temperature and moisture level which provide sufficient hydration during curing process are found to be very important. The higher rates of loading has been found to increase the measured compressive strength. Based on the test data, Ahmad and Shah proposed a relationship to estimate the strength under very fast loading.

The tensile strengths of high strength concrete have been performed and based on the test data the relationships have been obtained for tensile strengths. In general, it has been found that higher the compressive strength, the tensile strengths are greater.

Several different empirical formulas are available for the static and dynamic elastic modulus. The modulus of static elasticity is profoundly more common

14

since it's easier to perform static tests. Higher the elasticity of the coarse aggregate, the elasticity of the concrete is higher. The mineralogical characteristics of the aggregates also affect the properties of resulting concrete. Dynamic modulus is general is higher than static modulus.

After various compression tests, it has been found that the shape of the descending part of the stress-strain relationship of high strength concrete is in general more linear and steeper, and the strain at maximum stress is also slightly higher. Also, for high strength concrete, it goes through less volume dilation during compression tests as compared to normal strength concrete which means that high strength concrete undergo less internal micro-cracking.

Shrinkage of high strength concrete is generally affected by the change in the moisture content of the concrete and physio-chemical changes of the cement paste. However, it is significantly affected by the stiffness of the coarse aggregate. Whenever an admixture changes the pore structure of the paste, it will affect the shrinkage. For example, pozzolan generally increase pore refinement increasing the shrinkage. As moisture evaporate from concrete after few days of casting, plastic shrinkage will occur. Drying shrinkage also may occur after the concrete has set after chemical hydration process of the cement has been completed. Since setting of cement is a highly exothermic chemical process, the

15

temperature rises and differential contractions in various parts may lead to cracking. As the concrete sets, the formation of hydrates around the grains leads to the crystal coalesce which changes the concrete from a suspension to a continuous solid. As self-desiccation ends, the liquid phase changes to gaseous phase which then immobilizes the liquid after which the chemical reaction reaches its equilibrium state.

Basic creep is affected by various factors such as the mix-design parameters, volume of hydrates, and mainly by free water in the micro-structure. Various analytical models have been proposed to estimate the creep behavior. Drying creep is affected by differential drying which relaxes part of the self-stresses. Therefore, it decreases the deformation caused by self-desiccation.

The creep of the high strength concrete affected by the amount of free water in the microstructure and the total volume of the hydrates. It has been recognized that shrinkage resistant concrete also has low creep potential. However, the information of creep of high strength concrete is limited. Lower the volume of hydrates and the water content, creep decreases. A number of analytical models are available for estimating creep. The compressive strength is often used as a parameter to evaluate the basic creep. Also, the creep significantly decreases after 28 days for the high strength concretes. The second type of creep is drying creep

which is caused by differential drying. An increase in the water content and the amount of cement increases drying creep because this results in greater water movement and expansion of hydrates. Large aggregate size reduces drying creep because it induces restraining effect. Creep in general is smaller than that of normal strength concrete.

Drying shrinkage occurs as the concrete dries. Although a very limited information is available for drying shrinkage of high strength concrete, it has been found that long-term drying shrinkage of high strength concrete is smaller as compared to that of normal strength concrete. The shrinkage is inversely proportional to time.

The thermal properties of high strength concrete shows a decrease in its strength at temperature range of 100 to 300 Celsius (212 to 572 Fahrenheit) and increases up to about 400 Celsius (752 Fahrenheit). For higher temperatures, its strength decreases up to 800 Celsius (1472 Fahrenheit). It has been found that for some test specimen, explosive failures were observed at temperature range of 320 to 360 Celsius (608 to 680 Fahrenheit). The strength of high strength concrete is strongly dependent on the strength of its cement paste matrix as compared to that of normal strength concrete. Therefore, in case of fire, high strength concrete

17

may lose its strength along with explosive spalling once the cement paste matrix loses its strength.

Understanding of the aforementioned behavior enhances the prediction of the long-term time dependent performance and the design of high strength concrete structures.

The fatigue of concrete is not very well understood. The available data on the fatigue behavior of high strength concrete is very limited. Fatigue on concrete is typically encountered in structures subjected to earthquake, mass rapid transit structures, pavements, and bridges. After subjected to various kinds of load fluctuation, the accumulated damage on concrete results in crack propagation. The mechanism of fatigue is not clearly understood. However, it is known to be associated with the initiation and propagation of internal microcracks at the cement past-aggregate interface and/or within the cement paste itself. It is so far known that fatigue on high strength concrete is not different from that of normal strength concrete. Also, concrete with smaller aggregate size were found to have shorter fatigue life due to brittle nature of concrete with smaller aggregate. When concrete is subjected to reversed loading, the fatigue strength of concrete is reduced. Higher the fatigue loading rate, it has been found that the fatigue strength increased when triangular wave form with contant loading and unloading rate was applied. For lower strength concrete, however, the fatigue loading rate did not affect the overall fatigue strength. The moisture condition significantly

18

affect the fatigue strength. Lower the moisture content, the fatigue strength decreased, and greater the age of concrete, the fatigue life increased. The air content and the coarse aggregate type had the largest influence on fatigue strength. Also, smaller the specimen, the fatigue life increased. Concrete subjected to biaxial states of stress had higher fatigue strength as compared to those in uniaxial states. Bond failures in concrete occur in four type of interfaces which are interfaces within hydrated cement paste, interfaces between hydrated cement paste and cement particles, and interfaces between hydrated cement paste and aggregates, and interfaces between the concrete matrix and the steel reinforcement.

The studies have shown that the thickness of the transition zone at the cement paste and aggregate interfaces is reduced as pozzolanic materials are added for high strength concrete. This results in an improved bond at the hydrated cement paste and aggregate interfaces. Such a strong bond allows the strength of the coarse aggregate to be the limiting factor of the high strength concrete strength. The bearing stresses that develop between the steel reinforcement ribs and the surrounding concrete is another major factor that prevents bond failure. Lower the bond diameter, the average bond strength increased due to large specific bond surface area. If lateral confinement was provided or if the silica fume was used,

19

the showed an improving effect on the bond strength. The aforementioned aspects of fatigue were the same for normal strength concrete.

Fracture Mechanics

The topic of fracture mechanics is has been investigated by researchers such as Griffith, Irwin, Knott and Broek, Glucklich, Mindess, Hillerborg, and Ohgishi [Ref.]. The fracture models were considered to represent the brittle behavior of high strength concrete. Considering the brittle nature of high strength concrete, the mechanical behavior was studied using linear elastic and nonlinear fracture mechanics. The crack propagation is characterized in several different ways such as: (1) microcracking which occurs due to the stress concentration ahead of a crack near flaws, (2) crack bridging which occurs when the propagating crack is forced to go around a strong particle such as unhydrated cement grain, gravel, or sand grain, and (3) crack-bowing which is caused by unevenness of the crack front and the crack follows the paths of least resistance. The fracture mechanics also considers notch sensitivity and size effects on the failure modes based on experimental results and by using energy-based fracture mechanics and various crack models. The concrete composition, loading rate, temperature, humidity, and loading history influence the fracture parameters that are used for the various

20

crack models. The fracture models may be applied to study the collapse mechanisms of structures. However, such application is beyond the scope of this research.

Compressive Stress Distribution

The differences in the types of flexural compressive stress distributions for reinforced concrete beams was found to provide similar capacity values. However, for reinforced concrete columns, the differences in concrete stress distributions resulted in quite a large differences in the results. The strength predicted by the ACI equivalent rectangular stress block was unconservative by as much as 12% as compared to strength based on continuous stress block. Such a difference is more pronounced for high strength concrete materials and for high axial load application. The reinforced concrete column capacity is governed by material properties and the geometry of the cross section. Therefore, improved methods for dimensioning and utilization of high strength concrete and reinforcing steels. According to Park et al., it is recommended to use triangular compressive stress block for high-strength concrete reinforced concrete columns. Further, the current design procedures of ACI code for concrete columns may need some adjustments in material parameters such as elastic modulus and the

factor beta used in the slender column analysis for high strength concrete columns.

High Strength Concrete Column Deformability

The high-strength concrete has high stress capacity, but cannot maintain its load-carrying capacity for a large range of strains. Its load-carrying capacity drops quickly after reaching its peak stress level. However, with sufficient confinement of the core concrete, the inelastic deformability of high-strength concrete columns can be substantially increased. The column deformability is determined based on its displacement ductility ratio that is defined as the ratio of maximum displacement prior to exceeding 20% strength decay under cyclic loading to the yield displacement. The parameters which affect column deformability are: (1) Axial load level, (2) shear stress (minor effect), (3) loading history, (4) loading rate (minor effect), (5) volumetric ratio of confinement reinforcement, (6) confinement reinforcement strength, (7) transverse reinforcement spacing, (8) transverse reinforcement configuration, (9) column section geometry and size, (10) concrete strength and properties, and (11) unit weight of aggregate.

22

2.1.2 Advantage of High Strength Concrete

High Strength Concrete usage has increased in the recent years for their applications in high rise building structures since high-strength concrete has smaller cross-sectional area for a given load, providing more floor space. As compared to normal strength concrete, the high strength concrete behaves quite differently due to its special composition. There are many advantages for using high strength concrete.

Several advantages of using high-strength concrete exist in building construction (Smith et. al., 1989). The principal advantage is the economic benefits from its use in primary structural members such as columns. With an increase in concrete strength, the engineer can design a smaller member size to carry the same loads that a larger member of ordinary strength concrete would carry. The reduced member size increases the amount of rentable space and is especially beneficial when there are architectural restrictions on column sizes. Further, in several individual studies, it has been demonstrated that the increased cost of using high-strength concrete was offset by a significant decrease in the quantity of material used with reduced member sizes designed with high-strength concrete. Also, the percentage of reinforcing steel was reduced while concrete strength was increased. The study concluded that the most economical design was a column with a

23

minimum percent of reinforcing steel. A study was conducted in 1984 to investigate the cost savings in the design of over 1700 columns in a 45-story high-rise building that was already under construction in Chicago. Utilizing a computer program, the outcome of the study was that the most economical column uses about 1% vertical reinforcing steel in conjunction with high-strengh concrete. Moreno and Zils et. al. examined the optimum design of high-rise buildings in 1985. Three column sizes were selected and construction costs were computed per kip of axial load due to gravity loads. The reinforcement ratio 1 to 8 percent, the cost items included concrete material and placement, reinforcement, and column formwork. Cost to load evaluation showed that cost per kip of axial load decreased as the concrete strength increased, although this study did not include construction cost of columns in unbraced frames subjected to lateral loads. The high early strength of high-strength concrete also allows the early stripping of the shoring or formworks which reduces the total amount of rental time on the forms and shoring equipment over the period of the construction project. Data received from various contractors indicated that the estimated time saved ranges from 10 to 25 percent of the normal construction period. From the comparative cost analysis of the reinforced concrete columns, it is evident that more economy can be obtained with the use of high-strength than with normal-strength concrete. The relative reduction in the column-construction cost is on the order of 26

percent for 55-MPa (8000-psi) concrete and 42 percent for 83-MPa (12,000 psi) concrete.

There are great advantages of high-strength concrete for the construction of high-rise buildings which are:

Strength/unit cost

Strength/unit weight

Stiffness/unit cost

The high strength per unit weight is a great advantage for high seismic regions. Since the modulus of elasticity of concrete is proportional to the square root of the compressive strength of concrete, higher stiffness per unit weight and unit cost is obtained. Such a large stiffness of high strength concrete offers low value of creep, therefore, small amount of differential settlement in the vertical members of high-rise buildings. Further, the usable square footage of the building space can be substantially increased since high strength concrete columns dimensions are in general more slender as compared to normal strength concrete columns. The high strength concrete in column construction will increase around the world. With careful construction techniques for the high strength concrete columns such as efficient integration with normal strength slabs, reduction of heat of hydration,

preventing plastic shrinkage cracks, and plastic settlement cracks, the construction procedures using high-strength concrete is similar to those for conventional concrete. Proper testing procedures should be followed including the correction type of capping materials. More recent applications prove that the high strength concrete can have same benefits for shorter building.

Moment-Interaction Diagram

The Figure 2.1 shows the advantage of using high-strength concrete as compared to normal strength concrete. PCA Column program was used to show the increased capacity for using high strength concrete as compared to the normal strength concrete. The dotted line is a moment-axial capacity relationship for an arbitrary 508 x 508 mm (20 x 20 in.) high strength concrete column section with $f_c' = 68.95$ MPa (10 ksi), where the solid line is that of normal strength concrete with the same column section with $f_c' = 34.48$ MPa (5 ksi). It can be seen that both the moment capacity and axial load capacity of the column cross section can be substantially increased with increased concrete strength. The figure also demonstrates that capacity of the column section is increased by using high strength concrete, since the location of the balanced point shifts upward which

26

increases area of the tensile failure region below the balanced point as well as the compressive failure region above the balanced point.

The Figure 2.2 demonstrates the possibility of smaller column section by using high strength concrete for the same load demand. The dotted line is a moment-axial capacity relationship for an aribitrary 508 x 508 mm (20 x 20 in) high strength concrete column section with $f_c' = 68.95$ MPa (10 ksi), where the solid line is that of normal strength column section with $f_c' = 34.48$ MPa (5 ksi) and with increased dimension of 584.2 x 584.2 mm (23 x 23 in). The original 508 x 508 mm (20 x 20 in) column section was increased by 32.25% in order to achieve the same moment capacity. From this it is apparent that substantial decrease in the column sectional area can be achieved by the use of high strength concrete. For both figures 2.1 and 2.2, the strength reduction factors were left as 1.0 for illustrative purposes.
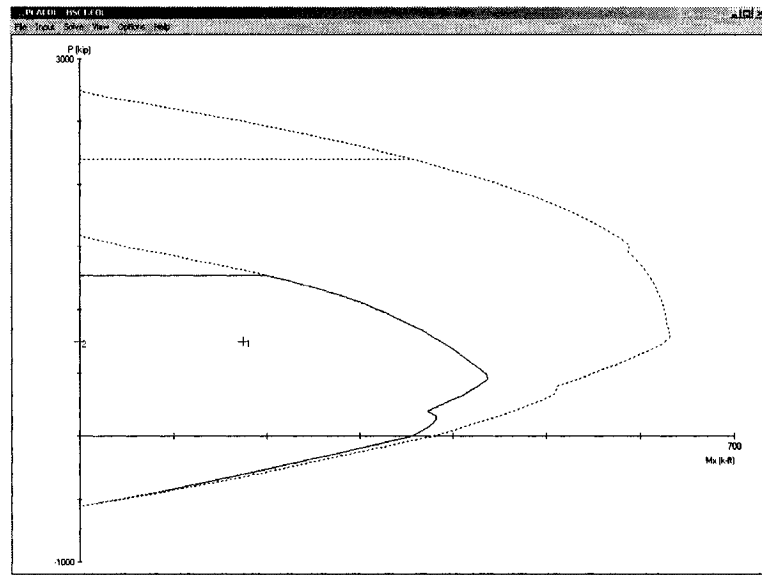
Fig. 2.1-Comparison of moment capacities with use of high-strength
$f_c' = 68.95$ **MPa (10 ksi) and normal-strength** $f_c' = 34.48$ **MPa (5 ksi)**
concrete for a 508 x 508mm (20 x 20 in) column section.
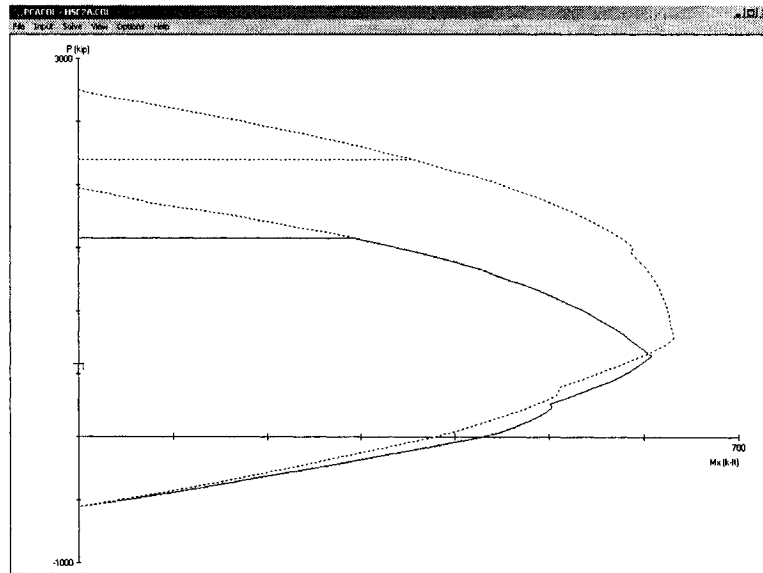
Fig. 2.2-Comparison of 584.2x 584.2mm(23 x 23 in) to 508 x 508mm(20 x 20
in) column sections to achieve similar moment capacity.

28

The merit of high strength concrete usage is clear. Some of the disadvantages would be its limited workability unless proper amount of superplasticizer is used and limited research data. The conventional normal strength concrete can tolerate minor changes in its properties due to slight differences in the mixing proportions. However, for high strength concrete, its properties are very sensitive to small changes in the mixing proportions. Therefore, there is a need for reliable quality control for all aspects of the high strength concrete production from the proper admixture mixing procedures and checking the uniformity of the raw materials to proper transportation method, vibration, curing, and testing. A main problem with high strength concrete design is that there is a lack of test data for full-scale experiments. With increased usage of high strength concrete for high rise buildings as well as for short buildings, it is important to understand the behavior of high strength concrete columns.

2.2 HIGH STRENGTH CONCRETE CONSTRUCTION

Background Information on HSC

According to the guide for selecting proportions of high strength concrete with Portland cement and fly ash, it considers the methods for selecting proportions over normal strength concrete in the range of 13.8 to 41.4 MPa (2000 to 6000 psi).

29

For high strength concrete the mix proportion is more critical. Specially selected pozzolanic and the chemical admixtures are employed and attainment of a low water to cement dismaterial ratio is considered essential.

High-range water-reducing admixtures (HRWR), also known as superplasticizers, are most effective in concrete mixtures that are rich in cement and other cementitious materials. HRWR works by helping the dispersion of cement particles, and it can reduce mixing water requirements by up to 30 percent, increasing concrete compressive strength.

The performance of the admixtures is influenced by the particular cementitious materials used (ACI 211.4R-93). The optimum dosage of an admixture or combination of admixtures should be determined by trial mixtures using varying amounts of admixtures.

Micro-analysis of the HSC column provides a basis for making long-range predictions of performance that incorporates a mechanistic understanding of behavior. This is especially important for successful use of high strength concrete materials with entirely new properties. Present empirical relationships are inadequate when applied to materials with properties outside the normal range of traditional materials.

Accelerated construction requiring high early-age strength and increased use of high-strength concrete require accelerating admixtures or additional cement and high cement content.

The development of high-rise building was and remains a strong impetus for high-strength concrete research. High-strength concrete is considered in design of buildings to achieve greater heights, to reduce column sections, and to provide greater stiffness.

A new liquid admixture to improve the strength of concrete is a dispersion of silica fume in water with additives to provide stability and proper viscosity (Rosenburg and Gaidis, 1989).

It has been found that the when silica fume is used in concrete, porosity does not necessarily decrease. Porosity is primarily controlled by water-cement ratio, which can be lowered with the use of a superplasticizer, high range water reducing agent (HRWRA). However, the permeability is dramatically reduced. The shrinkage is also decreased due to slower water loss from concrete made with silica fume. At the cement paste-aggregate interface, large crystals of $Ca(OH)_2$ precipitate and ettringite are formed. The bond strength to steel for concrete with silica fume increased almost proportionally to the strength of the concrete. The ettringite, which is an equilibrium compound formed from sulfate, calcium, and

31

aluminate ions in solution, the reduction in lime would be expected to reduce ettringite formation. The silica fume also accelerates the hydration of C3S due to reaction of silica fume with the Ca(OH)2, which is a product of the hydration of C3S, which encourages further hydration. On the other hand, it is also possible that silica fume could provide seed crystals to facilitate precipitation of C-S-H. Such acceleration of hydration would also help account for the reduced amount of ettringite found. Although interface areas are known to have relatively high porosity and consist of large crystals of calcium hydroxide and ettringite that precipitates in a water layer around the aggregates, the evidence was found in concrete with the new admixture of water and silica fume that a water layer does not form, reducing the amounts of calcium hydroxide and ettringite and leading to a stronger interfacial paste.

High Strength Concrete Construction

In the last five years, several building projects in downtown Seattle have specified high-strength concrete (Giraldi, 1989). The 76-story Columbia Center has reinforced structural columns of 65.5 MPa (9500 psi.) concrete. The 30-story Century Square used 69 MPa (10,000 psi.) concrete and the 12-story First & Stewart Building has 76 MPa (11,000 psi.) concrete in its columns. Specifying a

32

14 MPa (2000 psi.) greater concrete strength eliminated 20 No. 36 (ASTM #11) reinforcing bars for a net saving of $400 per column. Also, increasing the concrete compressive strength from 34.5 MPa (5000 psi.) to 69 MPa (10,000 psi.) when designing for gravity loads, the cross sectional area of the column is cut by nearly half. Further, since the tenants provide lease income, high-strength concrete provides smaller columns and more leasable space. More space and more tenants mean more income. Turner Construction's Frank Anderson stated that the 58-story Two Union Square Building in Seattle, which used 96.5 MPa (14,000 psi.) concrete in its columns, has only 5.5 kg (12 lbs.) of steel per 0.09 m^2 (square feet) in comparison to a typical steel-framed 58-story building which would have 10 to 12 kg (23 to 27 lbs.) of steel per 0.09 m^2 (ft^2). Further the building has more leasable space than any building in Seattle, in addition to the cost savings feature of concrete over steel.

With building and construction interests in earthquake-prone areas consider use of high strength concretes, the development of high-strength concrete began in Chicago in 1962 with 41 MPa (6000 psi.) concrete (Moreno, 1990). In 1989, the silica fume mixture of 96 MPa (14,000 psi.) for six stories of columns and one 117 MPa (17,000 psi.) experimental column was used for 225 W. Wacker project. High strength concrete from 31 to 96 MPa (4500 to 14,000 psi.) was used in the columns as an economical means to satisfy the structural requirements for this job,

33

with first five stories and the basement columns of the building containing 96 MPa (14,000 psi.) concrete. The majority of the columns consisted of approximately 1 percent reinforcement, which produced the most economical columns. Also, optimum use of cement, fly ash, additives, and granulometry in the mixture resulted in concrete strength of over 96 MPa (14,000 psi.) without the use of silica fume.

The availability of new construction methods and innovative technology in the construction industry along with improved equipments, structural systems, and computer peripherals dramatically increased the height of the concrete buildings along with the increased availability of the high strength concrete (Jensen, J.J., 1990). Since 1950's to recent years, many high rise buildings have been built with high strength concrete strength as high as 130 Mpa (19,000 psi.).

2.3 PREVIOUS RESEARCH ON HIGH STRENGTH CONCRETE COLUMNS

2.3.1 General Structures

The design of structures for earthquake resistance is complicated in nature due to uncertainty in the design load and the configuration of structural elements.

34

Through decades of research and analysis, a rational understanding has been obtained through refinements of knowledge based on accumulation of research results. In order to meet the demand of earthquake forces, it has been attempted to increase the capacity of reinforced concrete structures through experiments. The inelastic behavior of reinforced columns is necessary for economic design, and their ductile behavior is crucial to improve the safety of structures. A good understanding of critical regions of the structural elements as well as the nature of the behavior of the columns is necessary to further improve current available knowledge.

Transverse reinforcement in reinforced concrete columns provides confinement to compressed concrete, prevents premature buckling of compressed longitudinal bars, and and acts as shear reinforcement. The current approach to the design of moment-frame can use a strong column-weak beam approach to reduce the plastic hinging in the column during an earthquake. However, according to Park and Paulay et al. (1975), it is impossible to completely eliminate the plastic hinging in columns. Especially in high rise buildings, the bending moment distribution among frame members are not always uniform. The significant flexural mode or higher-mode response under dynamic loading can often cause plastic hinge region to spread over a longer length than would normally occur. In this case, it is recommended that the confinement reinforcement is provided over the full height

of the column. The detailing of the transverse reinforcement in column for seismic resistance should allow proper amount of ductility during earthquake loading.

The New Zealand Code requirement of reinforced concrete columns that are subjected to axial and cyclical lateral force loading is that under high axial load, the confinement region in the plastic hinge area of the column need to be extended by 1.5 times the usual assumed length for high axial load levels exceeding 0.36 $\phi f'_c A_g$, where $\phi = 0.75$. Despite this fact, ACI 318-95 and 318-99 codes do not specify a special requirement for different axial load levels. Further, there is no specific guideline that considers the effect of the axial load levels on the transverse reinforcements in the plastic hinge region.

The research in the fundamental behavior of reinforced concrete has progressed greatly since the 1960's. Various models and theories were created based on experimental studies. However, the studies on the behavior of high strength concrete columns are still quite limited. Further, the ACI 318-95 and 318-99 codes do not specify a confinement requirement for plastic region of the reinforced high strength concrete columns.

Over the past decades, numerous researches have been undertaken in the topic of the adequacy of the confinement for reinforced concrete columns subjected to seismic demand.

Azizinamini et. al. (1994) conducted a study investigating flexural capacity and ductility of square high strength concrete columns that were subjected to constant axial load and cyclic lateral loads. The concrete compressive strength used was as high as 103.8 MPa (15,050 psi.). It was concluded that the high strength concrete columns subjected to axial load levels below 20 percent of their axial load capacity and designed based on the seismic provisions of ACI 318-89 have sufficient ductility. However, it was found that the code overestimates the flexural capacity of high strength concrete columns subjected to both axial and bending moment. A modification of ACI 318 was suggested to conservatively calculate the flexural capacity of high strength concrete columns. The authors claim that current ACI 318-89 overestimates flexural capacity of high-strength concrete columns subjected to both axial and bending moment. Their proposal indicates that modification to be incorporated into ACI 318 to calculate the flexural capacity of high-strength concrete columns conservatively. Nine $\frac{2}{3}$ scale columns with square cross sections subjected to constant axial load and cyclic lateral loads were tested. It was concluded that high-strength concrete columns subjected to less than 20 percent of axial load capacity fulfilled the

37

seismic provision of ACI318-89 and provided sufficient ductility, but the ACI 318-89 was found to over-estimate the flexural capacity of high-strength columns when subjected to both axial and bending moment.

Watson et. al. (1994) designed equations to determine the quantities of transverse reinforcement required for specific ductility levels, and they were derived on the basis of the design charts. A refined analysis has been attempted considering parameters such as the axial load level, the longitudinal reinforcement ratio, and stress strain relationship of the concrete. It was found that the code equations for transverse reinforcement for concrete confinement resulted in more than sufficient confining reinforcement for columns with low to medium axial-load ratios. However, for large axial load ratios, it was found that the code based confining reinforcement was insufficient.

2.3.2 Previous Seismic Research on High Strength Concrete Columns

2.3.2.1 Mander, Priestley, and Park

In 1984, Mander et. al. proposed a model to predict the cyclic stress-strain behavior for various grades of reinforcing steel at any strain level. Also, in 1984

38

and 1988, Mander et. al. developed the stress-strain relationship for confined and unconfined concrete to determine the compressive stress distribution in the core concrete and the cover concrete, respectively, for a given extreme fiber compression strain.

In 1975, Park and Paulay proposed a theoretical moment-curvature relationships for reinforced concrete-column sections. To compute the moment-curvature relationship for a given column section and axial load level, the column section was divided into a number of discrete subsections. The longitudinal steel reinforcements were idealized as equivalent thin tube with equivalent wall thickness to give the same total area of longitudinal reinforcement or considered as a discrete number of bars of reinforcing steel. Then, the moment due to the compressive force on the concrete subsections and the forces due to the longitudinal steel reinforcements were calculated for each increment of curvature.

2.3.2.2 Sheik, Shah, and Khoury

A high strength concrete with compressive strength ranging between 31 and 59 MPa (4500 and 8500 psi) was used for the testing of HSC reinforced columns which were subjected to constant axial load and cyclic lateral loads simulating

39

earthquake (Sheikh et. al., 1994). It was found that the required amount of confining steel is proportional to the strength of concrete for a certain column performance if the axial load is measured in terms of P_o instead of as a fraction of $f'_c A_g$. According to this research, the plastic hinge length is independent of variables such as steel configuration, axial load level, amount of confining steel, and concrete strength. All specimens that were tested contained eight No. 20 (ASTM #6) longitudinal bars uniformly distributed around the core perimeter. Four corner bars were supported by bends in perimeter ties and internal diamond ties provided support to the middle bars. The ends of all the ties were hooked inside the core. One specimen was a square prismatic column with dimensions of 305 x 305 x 2438 mm (12 x 12 x 96 in.) and three non-prismatic specimens consisted of a 305 x 305 x 1473 mm (12 x 12 x 58 in.) and a 508 x 762 x 813 mm (20 x 30 x 32 in.) stub at one end. For this test, the cyclic load was applied either on the center of the prismatic column or on the edge of the column stub for the non-prismatic column. The test results showed a significant increase in the capacity of high strength concrete reinforced columns as compared to the normal strength reinforced columns, and the confining steel designed according to North American building code was found to provide satisfactory column behavior for a certain situation. However, it was found that for other situations, such as varied steel detailing, axial load level, and different performance requirements, etc., the design may be either overly conservative or unsafe.

40

According to a research undertaken by Sheikh and Toklucu in 1993, similar tests for normal strength reinforced concrete columns confined by circular spirals and hoops have shown the effects of different variables on confined concrete behavior such as effect of volumetric ratio of lateral steel, effect of lateral steel spacing, and the effect of specimen size. In all cases, the increased volumetric ratio and decreased lateral spiral hoop spacing improved the behavior of the confined concrete with respect to strength and ductility. However, regarding the effect of specimen size, it was found that in several cases, higher loads were resisted by larger columns at small strains. It was observed that the participation of cover concrete in larger specimens may have been better than that of smaller specimens. This difference was more pronounced among larger specimens as compared to among smaller specimens. From this, it can be concluded that the full-scale high strength concrete reinforced column testing as discussed in this report is one of the most ideal means of understanding the column behavior.

In 1982, Ahmad and Shah determined the stress strain curves of normal strength concrete of a compressive strength of up to 68.9 MPa (10,000 psi) and two types of lightweight concrete confined with spiral reinforcement. The influence of compressive strength, aggregate type, and the spacing and yield strength of hoop reinforcement was investigated. A theoretical model was developed to predict the stress strain curves of confined concrete based on the properties of the hoop

41

reinforcement and constitutive relationship of plain concrete. It was found that the theoretical model predicts experimental data well for different concrete strengths, for steel grades, and for spiral spacing. However, this experiment did not provide longitudinal reinforcements, and square hoops were not tested.

2.3.2.3 Park

One of the earlier attempts to understand the behavior of reinforced concrete members with cyclic loading is that of Park et. al. in 1972. A theoretical moment-curvature relationship was developed based on assumptions that the longitudinal strain in the steel and concrete at the various levels is directly proportional to distance from the neutral axis. Also, it was assumed that the stress-strain curve for steel under cyclic loading in the yield region has the unloading path for both positive and negative stresses which follow the initial elastic slope as the reloading path. However, after the first yield, the loading curve was assumed to become nonlinear at low stresses due to the Bauschinger effect. The loading part of the stress-strain curve was developed by Kent et. al. According to Park et. al., 1982, the envelope curve for compressive stress was represented by the relationship developed by Kent and Park for concrete confined by rectangular hoops under monotonic loading. Park, et. al. developed a computer program to

42

compute the bending moment and curvature for cyclically loaded reinforced concrete for rectangular sections with or without constant axial compression. The program can be operated within assumed curvature cycles. An iterative technique was used to calculate points on the moment-curvature curves.

From the observation of previous research on reinforced concrete columns, it is apparently necessary to investigate the behavior of high strength reinforced concrete columns since the experimental tests are very limited. A full-scale testing can provide a realistic behavior of high strength concrete columns subjected to earthquake forces.

2.4 CONFINED HIGH STRENGTH CONCRETE STRESS-STRAIN MODELS

2.4.1 General Concrete Stress-Strain Models

In practice, the core concrete is commonly confined by transverse reinforcement either in the form of spiral or rectangular hoops. In this case, the rectangular hoops were considered which represent much of the column types used in high-rise or short building structures in order to understand their behaviors under

43

seismic conditions. The behavior of confined concrete depends very much on the nature of the confinement, axial load levels, and stages of application. The order in which concrete reaches its maximum stress first or the confining steel reaches its yield strength may have drastic effect on the column capacity. Further, high strength concrete delays the confinement due to its low poisson's ratio. Thus, it has been found that use of high yield grade steel helps increase the ultimate deformability of high strength concrete columns. Several concrete stress-strain models which represent a result of many cumulative studies on confined and unconfined concrete stress-strain models are presented in the following section.

Confined HSC Stress-Strain Models

Effect of different parameters on the behavior of the HSC reinforced concrete columns have been considered in order to enhance the understanding of the column behavior when they are subjected to forces.

When reinforced concrete columns are subjected to axial loads, the nominal strength of a column is calculated by adding the strength contributions of the concrete and steel. It has been found that for high-strength concrete, the steel will yield at constant stress until the concrete reaches its maximum stress, where for

44

normal strength concrete, the concrete reaches non-linear deformation while the steel is still in its elastic range. The transverse reinforcements increase the strength of the core concrete through confinement against lateral expansion. It also increases ductility of the column by increasing the axial strain capacity.

Various research have been undertaken to study the behavior of confined and reinforced normal strength concrete columns leading to research studies specifically for high-strength reinforced concrete columns over recent years. The use of spiral reinforcement is found to increase strength and ductility of the confined concrete, and it has been found that rectangular hoops and tie confinement in square sections is not as effective as the spiral confinement. However, the square sections provide higher moment capacity as compared to circular sections, especially at large deformations.

Existing HSC Stress-Strain Theories

2.4.2 Mander, Priestley, and Park

In 1984, Mander et al. proposed a unified stress-strain theory for confined concrete for both circular and rectangular shaped transverse reinforcement. The stress-strain model is based on an equation suggested by Popovics (1973) for slow

45

(quasi-static) strain rate and monotonic loading (Popovics, 1973). Based on the experiments on full-scale confined reinforced normal strength concrete columns with concrete strength of 30 MPa (4.35 ksi.) and steel yield strength of about 300 MPa (43.5 ksi), the longitudinal compressive concrete stress f_c is given by

$$f_c = \frac{f'_{cc} \, xr}{r - 1 + x^r} \tag{2.2}$$

where f'_{cc} = compressive strength of confined concrete.

$$x = \frac{\varepsilon_c}{\varepsilon_{cc}} \tag{2.3}$$

where ε_c = longitudinal compressive concrete strain.

$$\varepsilon_{cc} = \varepsilon_{co} \left[1 + 5 \left(\frac{f'_{cc}}{f'_{co}} - 1 \right) \right] \tag{2.4}$$

According to Richart et. al. (1928), f'_{co} and ε_{co} are the unconfined concrete strength and the corresponding strain, respectively, where 0.002 can be assumed for ε_{co}.

$$r = \frac{E_c}{E_c - E_{sec}} \tag{2.5}$$

where $E_c = 5{,}000\sqrt{f'_{co}}$ Mpa is the tangent modulus of elasticity of the concrete (1 MPa = 145 psi), and

$$E_{sec} = \frac{f'_{cc}}{\varepsilon_{cc}} \tag{2.6}$$

46

The stress-strain behavior of the cover concrete outside the confined core concrete is defined as the part of the falling branch in the strain range of $\varepsilon_c > 2\varepsilon_{co}$ which is assumed to be a straight line which reaches zero stress at the spalling strain, ε_{sp}.

The effective lateral confining pressure and the confinement effectiveness coefficient are defined taking into consideration the area of ineffectively confined concrete. The area of confined concrete is defined as the area of the concrete within the center lines of the perimeter spiral or hoop, A_{cc}. The area of the effectively confined concrete core is defined as A_e which will be defined later.

The effective lateral confining pressure is defined as:

$$f'_l = f_l k_e \qquad (2.7)$$

where f_l = lateral pressure from the transverse reinforcement, which is assumed to be uniformly distributed over the surface of the concrete core.

$$k_e = \frac{A_e}{A_{cc}} = \text{confinement effectiveness coefficient} \qquad (2.8)$$

A_e = area of effectively confined concrete core

$$A_{cc} = A_c(1 - \rho_{cc}) \qquad (2.9)$$

ρ_{cc} = ratio of area of longitudinal reinforcement to area of core of section.

A_c = area of core of section enclosed by the center lines of the perimeter spiral or hoop.

47

For the confinement effectiveness for rectangular concrete sections confined by rectangular hoops with or without cross ties, the area of an effectively confined concrete at hoop level is determined by subtracting the areas containing the ineffectively confined concrete. The total plan area of ineffectually confined core concrete at the hoop level for n longitudinal bar is defined as:

$$A_i = \sum_{i=1}^{n} \frac{(w'_i)^2}{6} \tag{2.10}$$

The area of effectively confined concrete core at midway between the levels of transverse hoop reinforcement is

$$A_e = \left(b_c d_c - \sum_{i=1}^{n} \frac{(w'_i)^2}{6} \right)\left(1 - \frac{s'}{2b_c}\right)\left(1 - \frac{s'}{2d_c}\right) \tag{2.11}$$

where b_c and d_c = core dimensions to centerlines of perimeter hoop in x and y directions, respectively, where $b_c \geq d_c$. Where A_{cc} was defined earlier, the confinement effectiveness coefficient for rectangular hoops is defined by

$$k_e = \frac{\left(1 - \sum_{i=1}^{n} \frac{(w'_i)^2}{6b_c d_c}\right)\left(1 - \frac{s'}{2b_c}\right)\left(1 - \frac{s'}{2d_c}\right)}{(1 - \rho_{cc})} \tag{2.12}$$

where s' = clear vertical spacing between spiral or hoop bars.

The quantities of transverse confining steel in the x and y directions are defined by

48

$$\rho_x = \frac{A_{sx}}{sd_c} \text{ and } \rho_y = \frac{A_{sy}}{sb_c} \qquad (2.13)$$

where A_{sx} and A_{sy} = the total area of transverse bars running in the x and y directions, respectively.

The lateral confining stress on the concrete (total transverse bar force divided by vertical area of confined concrete) is given in the x direction as

$$f_{lx} = \frac{A_{sx}}{sd_c} f_{yh} = \rho_x f_{yh} \qquad (2.14a)$$

and in the y direction as

$$f_{ly} = \frac{A_{sy}}{sb_c} f_{yh} = \rho_y f_{yh} \qquad (2.14b)$$

From the previously defined expression for the effective lateral confining stress,

$$f'_{lx} = k_e \rho_x f_{yh} \qquad (2.15a)$$

and $\qquad f'_{ly} = k_e \rho_y f_{yh} \qquad (2.15b)$

where k_e is defined previously.

The confined concrete compressive strength f'_{cc} is given by

$$f'_{cc} = f'_{co} \left(-1.254 + 2.254 \sqrt{1 + \frac{7.94 f'_l}{f'_{co}}} - 2 \frac{f'_l}{f'_{co}} \right) \qquad (2.16)$$

where f'_{co} = unconfined concrete compressive strength, and f'_l is defined above.

The confinement effective coefficient k_e considers the efficiency of the

49

transverse reinforcement for both circular and rectangular confinement. The range of steel and concrete materials that this model is based on, are limited.

2.4.3 Young, Nour, and Nawy Model

In 1988, Young et. al. introduced empirical model for the stress-strain curve of rectilinearly confined high strength concrete based on linear regression of the results obtained from the small-scale experiment of twenty four 457 mm (18 in.) long square columns which were subjected to short-term monotonic concentric loading until failure. High strength concrete with compressive strength ranging from 83.6-93.5 MPa (12,130-13,560 psi.) and rectilinear confinement which consisted of rectangular lateral ties and longitudinal rebars were used. The cross sectional dimensions of specimens are 152 x 152 mm (6 x 6 in.), and No. 10 (ASTM Grade 60 #3) longitudinal bars and No. 3 (ASTM Grade 60 #1) lateral ties were used. The maximum axial load applied to this small-scale test was 2185.4 kN (491.3 kips) (Yong et. al., 1988).

The coordinates of the stress-strain curve are based on empirical parameters which are: (1) peak stress corresponding strain, f_o and ε_o; (2) the stress and

50

strain, f_{2i} and ε_{2i} , an arbitrarily selected point on the descending branch, where

ε_{2i} is equal to $(2\varepsilon_i - \varepsilon_o)$. The peak stress f_o is equal to $K f_c'$, where K and f_c'

are the effective confinement and the concrete cylinder strength, respectively.

The following are the defined expressions for K.

$$K = 1 + 0.0091\left(1 - \frac{0.245s}{h''}\right)\left(\rho'' + \frac{nd''}{8sd}\rho\right)\frac{f_y''}{\sqrt{f_c'}} \qquad (2.17)$$

s = the center-to-center spacing of the lateral ties in inches

h'' = length of one side of the rectangular ties in inches

n = number of longitudinal steel bars

d'' = nominal diameter of lateral ties in inches

d = nominal diameter of longitudinal steel bars in inches

ρ = volumetric ratio of longitudinal reinforcement

ρ'' = volumetric ratio of lateral reinforcement

f_y'' = yielding stress of the lateral steel in psi

An expression to predict the peak strain ε_o is expressed as:

51

$$\varepsilon_o = 0.00265 + \frac{0.0035\left(1 - \frac{0.734s}{h''}\right)\left(\rho'' f_y''\right)^{2/3}}{\sqrt{f_c'}} \qquad (2.18)$$

The values f_i, ε_i, and f_{2i} are calculated using equations obtained by following equations:

$$f_i = f_o\left[0.25\left(\frac{f_c'}{f_o}\right) + 0.4\right] \qquad (2.19)$$

$$\varepsilon_i = K\left[1.4\left(\frac{\varepsilon_o}{K}\right) + 0.0003\right] \qquad (2.20)$$

$$f_{2i} = f_o\left[0.025\left(\frac{f_o}{1000}\right) - 0.065\right] \geq 0.3 f_o \qquad (2.21)$$

The following proposed equations models stress-strain behavior of rectilinearly confined high-strength axially loaded concrete for the ascending and descending branches of the stress-strain curve.

$$Y = \frac{AX + BX^2}{1 + (A-2)X + (B+1)X^2} \qquad \text{for } \varepsilon_c \leq \varepsilon_o \qquad (2.22)$$

52

where $Y = \dfrac{f_c}{f_o}$; $X = \dfrac{\varepsilon_c}{\varepsilon_o}$; $A = \dfrac{E_c \varepsilon_o}{f_o}$; $B = \left[\dfrac{(A-1)^2}{0.55} \right] - 1$;

$E_c = 27.55 w^{1.5} \sqrt{f_c'}$;

and f_c and ε_c are the concrete stress and strain, respectively. The descending branch starts from the peak stress and strain and is expressed by:

$$Y = \frac{CX + DX^2}{1 + (C-2)X + (D+1)X^2} \qquad \text{for } \varepsilon_c \ge \varepsilon_o \qquad (2.23)$$

where $C = \left[\dfrac{(\varepsilon_{2i} - \varepsilon_i)}{\varepsilon_o} \right] \left\{ \left[\dfrac{\varepsilon_{2i} E_i}{(f_o - f_i)} \right] - \left[\dfrac{4\varepsilon_i E_{2i}}{(f_o - f_{2i})} \right] \right\}$ (2.24)

$D = (\varepsilon_i - \varepsilon_{2i}) \left\{ \left[\dfrac{E_i}{(f_o - f_i)} \right] - \left[\dfrac{4E_{2i}}{(f_o - f_{2i})} \right] \right\}$ (2.25)

$E_i = \dfrac{f_i}{\varepsilon_i}$ and $E_{2i} = \dfrac{f_{2i}}{\varepsilon_{2i}}$

It has been found through this experiment that the stress-strain curves were similar for all types of specimens tested with linear stress-strain relations which author found to be typical of high-strength concretes. Due to brittle nature of the

53

high-strength concrete, the confined specimens axial strength after reaching its first peak and after spalling of the cover concrete, the axial load dropped to a stable value then gradually increased to its second peak due to its lateral confinement at approximately 85-90% of the first peak. At the final stage, there was a sudden drop in the axial load as transverse reinforcement failed at one or more ties. Further, it has been found that the effective confinement K was observed to increase with the increase of volumetric ratio of the lateral steel disproportionately. Providing greater number of longitudinal and lateral ties resulted in greater ductility. In comparison to normal strength concrete, the reinforcing steel confinement is found to be not as effective. It also has been observed that the reinforcement did not begin to act until the concrete stress almost reached its unconfined ultimate stress. At this time, none of the models were able to accurately predict the descending portion of the stress-strain curve.

2.4.4 Azizinamini, Kuska, Brungardt, and Hatfield Model

In 1994, Azizinamini et. al. tested nine 2/3 scale test columns subjected to constant axial load and cyclic lateral loads. Each column had a cross section of 305 x 305 mm (12 x 12 in.) and a height of 2.44 m (8 ft.) which represents a 2/3 scale model of an 457 x 457 mm (18 x 18 in.) prototype column. The test

54

specimen represented the column extending upward from a beam-column connection to approximately the point of inflection. The provided beam stub at a point of application of lateral load strengthened the joint region so that plastic hinging occurred in the column rather than at the joint. The height of the upper column was greater than the height of the lower column to force hinging into the upper column. For all specimens, 8-No. 20 (ASTM #6) longitudinal rebars and No. 9 or 10 (ASTM #3 or #4) transverse reinforcements of 413.8 ksi yield strength (ASTM Grade 60) were used for the majority of the cases, except for two of the nine specimens, a transverse reinforcement with yield strength of 827.4 MPa (120 ksi.) was used. The compressive strength of the high-strength concrete used ranged from 54 to 101 Mpa (7790 to 14,620 psi.). The applied axial loads ranged from 0.2 P_o to 0.4 P_o with 2.44 percent vertical reinforcement provided for all specimens (Azizinamini et. al., 1994). Mutiples of two cycles at each displacement increment were applied to the specimens to induce displacement ductilities.

Azizinamini et. al. used the information presented by Yong et. al. to propose a new model for prediction of the stress-strain curve for confined high-strength concrete. This model assumes that the confined model consists of linear segments for both ascending and descending portions of the curve. The high-strength

concrete columns with compressive strength greater than $f_c^{'} = 69$ MPa (10,000 psi.) were tested, and the results using this model compared in good agreement with analytically obtained moment-curvature relationships. In order to model the behavior of confined high-strength concrete, the peak stress and strain f_o and ε_o given by Young et al. were used to model the ascending portion which is defined by:

$$f = \left(\frac{f_o}{\varepsilon_o} \right) \varepsilon \qquad \text{for } 0 \leq \varepsilon \leq \varepsilon_o \qquad (2.26)$$

The descending portion of the curve was defined based on the experimental data and is expressed by:

$$f = f_o [1 - \alpha(\varepsilon - \varepsilon_o)] \geq 0.3 f_o \qquad (2.27)$$

where

$$\alpha = \frac{0.25 \dfrac{f_c^{'} - 0.6}{f_o}}{3.13 K \left[1.4 \left(\dfrac{\varepsilon_o}{K} \right) + 0.0003 \right]} \qquad (2.28)$$

56

The curvature in the plot of the experimental result was obtained using gages located within approximately 102 mm (4 in.) above the column stub. A typical yield strain of transverse reinforcement was approximately 2100 microstrains at about 178 mm (7 in.) from the column stub. It has been observed that the peak confined stress of high-strength was reached at an axial concrete strain between approximately 0.0024 and 0.003. In consideration of its linear behavior, the author proposed to use triangular compressive stress blocks assuming maximum compressive stress is 0.85 f_c' at compressive strain of 0.003. From the triangular stress block, equivalent rectangular compression block was devised with its stress intensity proportionately reduced for unconfined concrete strength exceeding 69 MPa (10,000 psi.). The use of this modified concrete stress block for concrete strength exceeding 69 MPa (10,000 psi.) resulted in more conservative prediction of high-strength column flexural capacity.

The experiment gave conclusion that high-strength concrete columns subjected to less than 20% of their axial load capacity designed in compliance to ACI318-89 has sufficient ductility. However, it has been found that ACI318-89 overestimated the flexural capacity of high-strength columns subjected to both axial and bending moment. Also, it has been found that use of high-strength steel for high-strength columns resulted in larger spacing and in compliance to ACI 318-89 seismic provisions, although this leads to early buckling of longitudinal bars. It is recommended that for axial load level below 20 percent of column's

57

axial capacity, transverse reinforcement yield strength of 414 MPa (60 ksi.) is used.

2.4.5 Bing Model (1994)

Based on series of tests on circular and square high-strength reinforced concrete columns, Li and Park proposed a modified version of confined concrete stress-strain model of Mander et. al. from 1988 (Li and Park, 1994). Various types of reinforcement configurations were tested, and the model has different estimation of the peak stress for the confined concrete as compared to Mander model. For columns with square cross sections, the following parameters were proposed.

$$f_{cc}^{'} = f_{co}^{'} \left(1.413 \sqrt{1 + \frac{11.4 f_{l}^{'}}{f_{co}^{'}}} - \frac{2 f_{l}^{'}}{f_{co}^{'}} - 0.413 \right) \qquad (2.29)$$

where,

$f_{cc}^{'}$ = the peak longitudinal compressive stress for confined concrete

$f_{co}^{'}$ = peak stress of the unconfined concrete

ε_{o} = corresponding strain at peak stress of the unconfined concrete

58

$f_l' =$ the effective lateral confining stress

$$f_l' = \frac{1}{2} K_e \rho_s f_{yh} \tag{2.30}$$

$$K_e = \frac{(1-0.5\alpha)^2 (\beta - 0.5\alpha)}{\beta(1-1.6g'\rho_{cc})} \left[1 - \frac{8(0.58+0.11g')}{\beta}\left(\frac{w_i'}{h_c}\right)^2 + \frac{0.93}{\beta}\left(\frac{w_i'}{h_c}\right)^3 \right] \tag{2.31}$$

for square column sections.

$K_e =$ confinement effectiveness coefficient

$\rho_s =$ volumetric ratio of the transverse reinforcement

$f_{yh} =$ transverse reinforcement yield stress

$\alpha = s'/h$ for square or rectangular sections

$s' =$ clear spacing of transverse reinforcement

$h =$ depth of the cross section

$b =$ width of the cross section

$g' =$ the distance between the centers of the longitudinal bars in the extreme faces divided by the core dimension

$\beta = b_c/h_c$

b_c = the width of the confined concrete core

h_c = the depth of the confined concrete core

w'_i = the dimension between longitudinal bars taken from inside to inside

ρ_{cc} = longitudinal reinforcement ratio

Li and Park proposed the following confined concrete strains:

$$\varepsilon_{cc} = \varepsilon_{co}\left[1.0 + 11.3\left(\frac{f'_l}{f'_{co}}\right)^{0.7}\right] \qquad \text{for } 60\text{ MPa} \leq f'_{co} \leq 80\text{ MPa} \qquad (2.32)$$

$$\varepsilon_{cc} = \varepsilon_{co}\left[-8.1 + 9.1\exp\left(\frac{f'_l}{f'_{co}}\right)\right] \qquad \text{for} \qquad f'_{co} \geq 80\text{ MPa} \qquad (2.33)$$

The stress-strain curve by Li and Park is expressed by:

$$f_c = E_c \varepsilon_c + \frac{f'_{co} - E_c \varepsilon_{co}}{\varepsilon_{co}^2}\varepsilon_c^2 \qquad \text{for } 0 \leq \varepsilon_c \leq \varepsilon_{co} \qquad (2.34a)$$

$$f_c = f'_{cc} - \frac{f'_{cc} - f'_{co}}{(\varepsilon_{cc} - \varepsilon_{co})^2}(\varepsilon_c - \varepsilon_{co})^2 \qquad \text{for } \varepsilon_{co} \leq \varepsilon_c \leq \varepsilon_{cc} \qquad (2.34b)$$

60

$$f_c = f'_{cc} - \beta \frac{f'_{cc}}{\varepsilon_{cc}} (\varepsilon_c - \varepsilon_{cc}) \geq 0.4 f'_{cc} \quad \text{for } \varepsilon_{cc} \leq \varepsilon_c \tag{2.34c}$$

where,

$$\beta = (0.048 f'_{co} - 2.14) - (0.098 f'_{co} - 4.57) \sqrt{\frac{f'_l}{f'_{co}}} \tag{2.35}$$

Following equations according to ACI Committee 363 (1980) Recommendations,

$$E_c = 3200 \sqrt{f'_{co}} + 6900 \qquad \text{MPa} \tag{2.36}$$

and according to Code of Practice of the Design of Concrete Structures of the New Zealand (NZS 3101, Part 1, 1982),

$$E_c = 4700 \sqrt{f'_{co}} \qquad \text{MPa} \tag{2.37}$$

were used to determine the modulus of elasticity of concrete.

The strain at peak stress of the unconfined concrete ε_{co} was determined by:

61

$$\varepsilon_{co} = \frac{0.7\left(f_{co}'\right)^{0.3}}{1000} \qquad\qquad (2.38)$$

An ultimate strain ε_{cu} was proposed as:

$$\varepsilon_{cu} = \varepsilon_{co}\left[2 + \left(122.5 - 0.92 f_{co}'\right)\sqrt{\frac{f_l'}{f_{co}'}}\right] \qquad \text{for} \qquad f_{co}' \leq 80\ \text{MPa} \qquad (2.39a)$$

$$\varepsilon_{cu} = \varepsilon_{co}\left[2 + \left(82.75 - 0.37 f_{co}'\right)\sqrt{\frac{f_l'}{f_{co}'}}\right] \qquad \text{for} \qquad f_{co}' \geq 80\ \text{MPa} \qquad (2.39b)$$

2.4.6 Cusson and Paultre Model

In 1994, Cusson and Paultre performed an experimental study on large-scale high-strength concrete columns under concentric loading. The parameters defining the requirements for lateral confining reinforcement in current codes are the results of tests done on reinforced concrete members with concrete compressive strengths lower than 40 MPa (5.8 ksi) (ACI Committee 318, 1989), and existing confined concrete stress-strain models are based on test results from normal-strength

62

concrete columns, which may not be adequate for high strength concrete. This experimental study observed the behavior of thirty concentrically loaded large-scale columns confined by rectangular ties. The column cross sectional dimension is 235 x 235 x 1400 mm (9.25 x 9.25 x 55 in.). The concrete compressive strengths ranged from 60 to 120 Mpa (8.7 to 17.4 ksi.), the longitudinal reinforcement provided ranged from 2.2 to 3.6 percent, and yield stress of the reinforcements ranged from 392 to 482 MPa (57 to 70 ksi.) for the longitudinal reinforcement and from 392 to 770 MPa (57 to 112 ksi.) for the transverse reinforcements. From the experimental results, an analytical stress-strain model for confined HSC has been developed. It has been found that axial load-strain curve showed an initial strength gain and later reached a second peak when the confined concrete core reached its maximum stress. It was observed that the yield stress of the reinforcement was reached only for well-confined specimens. For poorly confined specimens, the stresses of the transverse reinforcements were much lower than that of the tie yield stresses. The ultimate failure of the specimens was caused by tie rupture, buckling of longitudinal bars, and inclined shear surfaces in the confined concrete core with a sudden drop in the axial capacity. The inclination of the shear sliding plane with respect to the vertical axis varied from 25 degrees for low-confined specimens to 45 degrees for highly confined specimens. The compressive strain of the confined concrete ranged between 0.0022 to 0.0034 during its first peak and between 0.0033 to

0.0321 during its second peak. At 50% of the maximum confined strength on the descending portion of the stress-strain curve, the confined concrete strain ranged from 0.0052 for low-confinement to 0.0459 for well-confined specimens. It was observed that the tie yield strength is fully developed at the peak strength of confined concrete, when the confinement efficiency is high. On the other hand, when the tie yield strength is not fully developed, the confinement efficiency is observed to be relatively low. Larger amount of longitudinal bars with greater diameter was found to prevent buckling of longitudinal bars.

The authors felt that the present code provisions, which are based on the parameters defining the lateral confinement requirements for low compressive strength concretes, are used without any special considerations for the safety of high-strength concrete constructions. They considered various refined stress-strain models based on normal-strength concrete columns may be inappropriate for high-strength concrete columns. The results from axial compression tests on fifty large-scale columns with concrete compressive strengths of 60, 80, 100, and 120 MPa (8.7, 11.6, 14.5, and 17.4 ksi.) with lateral reinforcement with yield strengths ranging from 400 to 800 MPa (58 to 116 ksi.) were used to propose following confined stress-strain model (Cusson and Paultre, 1994).

The nominal lateral pressure based on the equilibrium of lateral pressure exerted onto the concrete core of rectangular tied columns and the confining reinforcement forces in both orthogonal directions is expressed as:

$$f_l = \frac{f_{hcc}}{s} \left(\frac{A_{shx} + A_{shy}}{c_x + c_y} \right)$$

(2.40)

where,

f_{hcc} = stress in the transverse reinforcement at the maximum strengths of confined concrete

s = center-to-center tie spacing

A_{shx} and A_{shy} = total cross sections of the lateral steel bars perpendicular to the x and the y axis, respectively

c_x and c_y = widths of the concrete core parallel to the x and the y axis, repectively

The concept of effectively confined concrete area is used to calculate the confinement effective coefficient, K_e which is a ratio of the effectively confined concrete area in the midpoint between two layers of ties to the nominal concrete core area, A_{cc}. K_e is defined as:

65

$$K_e = \frac{\left(1 - \frac{\sum w_i^2}{6c_x c_y}\right)\left(1 - \frac{s'}{2c_x}\right)\left(1 - \frac{s'}{2c_y}\right)}{(1 - \rho_c)}$$

(2.41)

where,

$\sum w_i^2$ = sum of the squares of all the clear spacings between adjacent longitudinal steel bars in a rectangular section

s' = clear spacing of ties

ρ_c = longitudinal reinforcement ratio in the core section

The effective confinement pressure applied to the nominal concrete core, f_{le}, is expressed by:

$$f_{le} = K_e f_l = \frac{K_e f_{hcc}}{s}\left(\frac{A_{shx} + A_{shy}}{c_x + c_y}\right)$$

(2.42)

where for a square section, equation (2.42) is reduced to

66

$$f_{le} = \frac{K_e f_{hcc} A_{sh}}{sc} \qquad (2.43)$$

The confinement index $\dfrac{\rho_h f_{yh}}{f_c'}$ is used as an indicator of the efficiency of the confinement for reinforced concrete columns according to Park et al. (1982), Muguruma et al.(1983), and Saatcioglu et al. (1993), where ρ_h is the volumetric ratio of the transverse reinforcement, f_{yh} is the tie yield strength, and f_c' is the cylinder strength of plain concrete. According to Cusson and Paultre, different tie configurations or tie spacings with same confinement index value may result in different responses. When the yield stress is not reached in the transverse reinforcement when the confined concrete reaches its maximum strength, the confinement index values will over-estimate the confinement of the column.

Thus, a more accurate indicator of confinement efficient which considers the arching action in the concrete core and the actual peak strength stress in the transverse reinforcement was proposed as:

$$\text{Effective confinement index} = \frac{f_{le}}{f_{co}} \qquad (2.44)$$

The effective confinement index is used in the development of the empirical equations of the proposed confinement model. Using regression analysis, the

67

relationship was established between the strength gain of the confined concrete, f_{cc}/f_{co} and the effective confinement index, f_{le}/f_{co} expressed as:

$$f_{cc}/f_{co} = 1.0 + 2.1\left(f_{le}/f_{co}\right)^{0.7} \tag{2.45}$$

where,

f_{cc} = maximum strength of confined concrete in a member

f_{co} = maximum strength of unconfined concrete in a member

The strain gain is defined as the difference between the peak strain of the confined concrete, ε_{cc}, and that of unconfined concrete, ε_{co}. The ductility gain is defined as the difference between the strains at which the stress drops to 50% of the peak strength of confined concrete, ε_{C50C}, and that of the unconfined concrete, ε_{C50U}. The least absolute deviations were used to propose the equations for the concrete strains ε_{cc} and ε_{C50C} expressed as:

68

$$\varepsilon_{cc} = \varepsilon_{co} + 0.21\left(\frac{f_{le}}{f_{co}}\right)^{1.7} \qquad (2.46)$$

$$\varepsilon_{C50C} = \varepsilon_{C50U} + 0.15\left(\frac{f_{le}}{f_{co}}\right)^{1.1} \quad \text{with} \quad f_{hcc} = f_{yh} \qquad (2.47)$$

If no experimental data is available for ε_{C50U}, the value of 0.004 may be used. Since it is anticipated that transverse bars are yielding at large deformations, the effective confinement pressure, f_{le} from equation (2.43), is calculated by setting f_{hcc} equal to the yield strength of the transverse reinforcement for the determination of ε_{C50C}.

It has been observed that for HSC columns confined with high-strength steel ties, the yield strength of the transverse reinforcement was developed only at the peak strength of the well-confined concrete specimens. The tie yield strength which was used for the lateral pressure computation of normal-strength concrete columns may not apply to HSC columns. Depending on the degree of confinement as defined by effective confinement index, the tie yield stress may or may not be reached at the peak strength of the confined HSC columns. Thus, an expression for tie steel strain, ε_{hcc}, to compute the stress in the lateral reinforcement, f_{hcc}, at peak strength of confined strength, was proposed assuming

69

equal lateral concrete strains and confining stresses in both transverse directions and is expressed as:

$$\varepsilon_{hcc} = \nu\varepsilon_{cc} - \frac{(1-\nu)f_{le}}{E_{SEC}}$$

(2.48)

where,

E_{SEC} = secant modulus at the peak strength of confined concrete

ν = Poisson's ratio at the maximum strength of confined concrete, where 0.5 is used at the peak strength of confined concrete.

Since it is anticipated that tie strain ε_{hcc} may be in error for highly confined concrete columns with its peak strength strain larger than the tie yield strain, equation (2.48) was reduced to:

$$\varepsilon_{hcc} = 0.5\varepsilon_{cc}\left[1-\left(\frac{f_{le}}{f_{cc}}\right)\right]$$

(2.49)

70

The adjustment of the three unknowns f_{le}, peak strength of confined concrete f_{cc}, and ε_{cc} in equation (2.49) depends on the tie stress f_{hcc}, the strain ε_{hcc} and the stress f_{hcc} in the transverse reinforcement at the peak strength of confined concrete are computed in following manner.

1. Compute the effective confinement pressure, f_{le}, letting $f_{hcc} = f_{yh}$.

2. Estimate f_{cc} and corresponding ε_{cc}.

3. Estimate ε_{hcc} using equation (2.49)

4. Calculate the resulting stress f_{hcc} in the transverse reinforcement using the stress-strain relationship of the tie reinforcement bars

5. Recalculate the effective confinement pressure, f_{le}, using the new value of the stress f_{hcc} in the transverse reinforcement, only if $f_{hcc} < f_{yh}$.

6. Repeat steps 2 to 6 until convergence.

The proposed ascending portion of the stress-strain curve of confined HSC is written as:

71

$$f_c = f_{cc} \left[\frac{k \left(\dfrac{\varepsilon_c}{\varepsilon_{cc}} \right)}{k - 1 + \left(\dfrac{\varepsilon_c}{\varepsilon_{cc}} \right)^k} \right] \qquad \text{for } \varepsilon_c \leq \varepsilon_{cc} \qquad (2.50)$$

where,

$$k = \frac{E_c}{E_c - \left(\dfrac{f_{cc}}{\varepsilon_{cc}} \right)} \qquad (2.51)$$

E_c = tangent modulus of concrete

The descending part of the stress-strain curve is written as:

$$f_c = f_{cc} \exp \left[k_1 \left(\varepsilon_c - \varepsilon_{cc} \right)^{k_2} \right] \qquad \text{for } \varepsilon_c \geq \varepsilon_{cc} \qquad (2.52)$$

where,

$$k_1 = \frac{\ln 0.5}{\left(\varepsilon_{C50C} - \varepsilon_{cc} \right)^{k_2}} \qquad (2.53)$$

$$k_2 = 0.58 + 16 \left(f_{le} / f_{co} \right)^{1.4} \qquad (2.54)$$

72

The proposed model may be used for the behavior prediction of unconfined concrete by using $k_2 = 1.5$.

The prediction responses showed good agreement with different test results. Since this model is based on concentric loading on specimens, it provides effective high-strength confinement model without consideration of seismic loading.

2.4.7 Martirossyan Model

2.4.7.1 Confined

In 1998, Martirossyan proposed the following revised version of Popovics (1973) equation applicable to high-strength confined concrete (Xiao and Martirossyan, 1997).

$$f_c = \frac{f'_{cc} \, xr}{r - 1 + x^{k_3 r}}$$

(2.55)

where $x = \dfrac{\varepsilon_c}{\varepsilon_{cc}}$

(2.56)

73

$$r = \frac{E_{50}}{E_{50} - E_{sec}}$$ (2.57)

$$E_{sec} = \frac{f'_{cc}}{\varepsilon_{cc}}$$ (2.58)

$$f'_{cc} = f'_{co} + 3.96 \bar{f}_r$$ (2.59)

$$\varepsilon_{cc} = \varepsilon_{co}\left[1 + k_1\left(\frac{f'_{cc}}{f'_{co}} - 1\right)\right]$$ (2.60)

The expression k_1 was used in the above equation for the peak strain of confined concrete instead of the number "5" which was suggested by Richard et al. (1928). In 1988, Mander et al. has shown that "5" in this equation is not constant and varies with the concrete strength. Martirossyan used regression technique and performed the necessary simplifications to determine the expression for k_1.

$$k_1 = 5 + 1.3 \times \rho_t \frac{f_y}{f'_{co}}$$ (2.61)

where, ρ_t is the transverse reinforcement ratio defined as $\frac{nA_t}{b's}$; f_y is the yield strength of transverse reinforcement, and f'_{co} is the plain concrete strength; b' is the width measured from the center lines of the out-most perimeter hoops; and s is the spacing of one pair of transverse steel. n is the number of the legs of the transverse reinforcement in the vertical cross section within the spacing, s. The coefficient n considers the effect of the confinement configuration. A_t is the cross

74

sectional area of one leg of transverse reinforcement; $\bar{f}_r$ is defined as the average transverse confining pressure, a passive confining pressure.

$$\bar{f}_r = \rho_t f_{yeff} \qquad (2.62)$$

where f_{yeff} is the effective stress in confining steel for the condition when the specimen has reached to its maximum strength.

$$f_{yeff} = \min\left(f_y, f_{ye}\right) \qquad (2.63)$$

where f_{ye} is the effective stress of transverse reinforcement at the point of maximum strength of HSC confined column defined as

$$f_{ye} = 11.6 \times \left(\frac{1}{\rho_t} \times \frac{f_y}{f'_c}\right)^{0.26} \quad \text{(ksi)} \qquad (2.64)$$

f_y and f'_c are strengths of transverse steel and the concrete, respectively.

In order to control the stiffness of ascending part of the stress-strain curve and for better accuracy, E_{50} was introduced instead of regular E_c (Xiao and Martirossyan, 1998).

$$E_{50} = 46{,}000 \times k_2 \times \sqrt{f'_{co}} \quad \text{(psi)} \qquad (2.65)$$

where $\qquad k_2 = \left(\frac{f_{yeff}}{f_y}\right)^{0.2} \qquad (2.66)$

The coefficient k_3 in the Xiao and Martirossyan's revised Popovics (1973) equation was designed to control the descending part of the stress-strain curve and

75

to allow the curve to pass through initially defined point $(\varepsilon_{cu}, 0.8f'_{cc})$. Using the best fitted empirical line and based on proposed energy balance method of Mander et. al. (1988), Xiao and Martirossyan (1998), proposed the ultimate strain of confined HSC columns to be expressed as

$$\varepsilon_{cu} = 0.005 + 0.19 \times \left(\rho_t \frac{f_y}{f_c} \right)^{1.5} \tag{2.67}$$

where this ultimate strain is defined as the strain corresponding to 80% of post-peak stress.

$$k_3 = \left\{ \begin{array}{c} 1 \\ \dfrac{Ln\left[1 - r + \dfrac{1.25\varepsilon_{cu}r}{\varepsilon_{cc}}\right]}{rLn\left[\dfrac{\varepsilon_{cu}}{\varepsilon_{cc}}\right]} \end{array} \right\} \tag{2.68}$$

In the above expression, upper expression value "1" is used for $0 \le \varepsilon_c \le \varepsilon_{cc}$, and the lower expression is used for $\varepsilon_{cc} < \varepsilon_c < \varepsilon_{cu}$.

2.4.7.2   Unconfined

The above stress-strain model for confined concrete may be simplified for unconfined concrete by using the appropriate parameter values for unconfined

concrete where necessary. Assuming that the ultimate strain of unconfined concrete is 0.005, the expressions for unconfined concrete stress-strain model are:

$$\varepsilon_{co} = \frac{1.4(f'_{co})^{0.27}}{1000} \qquad \text{(ksi)} \qquad (2.69)$$

$$f_c = \frac{f'_{co}\, xr}{r - 1 + x^{k_3 r}} \qquad \text{(ksi)} \qquad (2.70)$$

$$x = \frac{\varepsilon_c}{\varepsilon_{co}} \qquad (2.71)$$

$$r = \frac{E_{50u}}{E_{50u} - E_{secu}} \qquad (2.72)$$

$$E_{50u} = 46{,}000 \times \sqrt{f'_{co}} \qquad \text{(psi)} \qquad (2.73)$$

$$E_{secu} = \frac{f'_{co}}{\varepsilon_{co}} \qquad (2.74)$$

77

$$k_3 = \left\{ \begin{array}{c} 1 \\ \dfrac{Ln\left[1 - r + \dfrac{0.00625r}{\varepsilon_{co}}\right]}{rLn\left[\dfrac{0.005}{\varepsilon_{co}}\right]} \end{array} \right\}$$

(2.75)

In the above expression, upper expression value "1" is used for $0 \le \varepsilon_c \le \varepsilon_{co}$, and

the lower expression is used for $\varepsilon_{co} < \varepsilon_c < 0.005$.

2.4.8 Razvi and Saatcioglu Model

In 1999, Razvi and Saatcioglu proposed a mathematical model to express the

stress-strain relationship of high-strength concrete confined by transverse

reinforcement. The model, which is applicable to both normal-strength and high-

strength concretes is based on testing of concrete with unconfined strength

between 30 and 130 MPa (4.35 to 18.9 ksi). The model is developed on the basis

of "equivalent uniform confinement pressure" concept also proposed by

Saatcioglu and Razvi (1992) for testing of 96 columns, using normal strength

concrete. The new proposed model was based on 46 near full-size columns of

concrete strength ranging from 60 to 124 MPa (8.7 to 18 ksi) (Razvi and

Saatcioglu 1996a; Saatcioglue and Razvi 1998). Additional data obtained from

78

124 tests of high-strength concrete conducted by others were utilized. For the ascending branch of the stress-strain relationship is expressed as:

$$f_c = \frac{f_{cc}'\left(\dfrac{\varepsilon_c}{\varepsilon_1}\right)r}{r - 1 + \left(\dfrac{\varepsilon_c}{\varepsilon_1}\right)^r} \tag{2.76}$$

$$r = \frac{E_c}{E_c - E_{sec}} \tag{2.77}$$

where E_{sec} = secant modulus of elasticity of confined concrete and is expressed as:

$$E_{sec} = \frac{f_{cc}'}{\varepsilon_1} \tag{2.78}$$

where E_c = modulus of elasticity of unconfined concrete. An expression originally proposed by Carrasquillo et al. (1981) was found to agree well with the experimental results.

$$E_c = 3{,}320\sqrt{f_c'}\,6{,}900 \tag{2.79}$$

where f_c' is in megapascals. E_c should be greater than E_{sec}.

$$f_{cc}' = f_{co}' + k_1 f_{le} \tag{2.80}$$

$$k_1 = 6.7(f_{le})^{-0.17} \tag{2.81}$$

$$f_{le} = k_2 f_l \qquad \text{(MPa)} \tag{2.82}$$

$$f_l = \frac{\sum_{i=1}^{q}(A_s f_s \sin\alpha)_i}{sb_c} \tag{2.83}$$

where q = number of tie legs that cross the side of core concrete for which the

average lateral pressure f_l is being computed.

The stress f_s used in equation for f_l is the tensile stress in tranverse

reinforcement at peak concrete stress, although f_s is often assumed to equal to

yield strength f_{yt} of the transverse steel.

The value of $f_s = E_s\left(0.0025 + 0.04 * \sqrt[3]{\dfrac{k_2\rho_c}{f'_{co}}}\right) \le f_{yt}$ \hfill (2.84)

where f'_{co} is in megapascals. The upper limit of yield strength f_{yt} may be taken as

1,400 MPa (203 ksi) as used in the experiments. The reduction of lateral

pressure is expressed using coefficient k_2 expressed as:

$$k_2 = 0.15\sqrt{\left(\frac{b_c}{s}\right)\left(\frac{b_c}{s_l}\right)} \le 1.0 \tag{2.85}$$

where s = spacing of transverse reinforcement and s_l = spacing of longitudinal

reinforcement. The equivalent uniform lateral pressure that produces same effect

as nonuniform pressure f_{le} defined above is applicable to square and circular

80

sections have the same confinement pressure in two orthogonal directions. For rectangular and square columns with different pressures in orthogonal directions due to different tie arrangements in two directions, f_{le} is expressed as:

$$f_{le} = \frac{f_{lex}b_{cx} + f_{ley}b_{cy}}{b_{cx} + b_{cy}}$$

(2.86)

where the equivalent lateral pressures f_{lex} and f_{ley} acting perpendicular to core dimensions b_{cx} and b_{cy} can be computed separately. The originally proposed expression for parabolic ascending portion, which is for normal-strength concrete was found to overestimate the initial modulus of elasticity when applied to high strength concrete. Therefore, the relationship proposed by Nagashima et al. (1992) and Cusson and Paultre (1995) for high-strength concrete as adopted for the ascending branch of the proposed model.

For the descending branch of the stress-strain relationship, the expressions proposed earlier for normal-strength concrete (Saatcioglue and Razvi 1992) were modified to reflect the use of increased concrete and steel strength by the use of new coefficients k_3 and k_4 as given below, where the strain at peak concrete stress ε_1 is expressed as:

$$\varepsilon_1 = \varepsilon_{01}(1 + 5k_3 K)$$

(2.87)

81

It consists of a linear segment starting from the peak with descending slope defined by the strain corresponding to 85% of peak stress ε_{85}. The strain corresponding to 85% of peak stress ε_{85} is expressed as

$$\varepsilon_{85} = 260 k_3 \rho_c \varepsilon_1 \left[1 + 0.5 k_2 (k_4 - 1) \right] + \varepsilon_{085} \qquad (2.88)$$

$$\text{where } \rho_c = \frac{\displaystyle\sum_{i=1}^{n} (A_{sx})_i + \sum_{j=1}^{m} (A_{sy})_j}{\left[s(b_{cx} + b_{cy}) \right]} \qquad (2.89)$$

=volumetric ratio, $k_3 = \dfrac{40}{f_{co}'} \le 1.0$, $k_4 = \dfrac{f_{yt}}{500} \ge 1.0$, and f_{yt} = yield strength of transverse reinforcement.

The strength enhance coefficient is expressed as: $K = \dfrac{k_1 f_{le}}{f_{co}'}$. $\qquad (2.90)$

The unconfined properties, ε_{01} and ε_{085} are expressed as:

$$\varepsilon_{01} = 0.0028 - 0.0008 k_3 \qquad (2.91)$$

$$\varepsilon_{085} = \varepsilon_{01} + 0.0018 k_3^2 \qquad (2.92).$$

It is recommended that the unconfined strains ε_{01} and ε_{085} should not exceed the above equations if the experimental values are available.

82

The proposed model is applicable up to transverse reinforcements of 1,400 MPa

(203 ksi) yield strength. The model considers all relevant parameters of

confinement from 30 MPa (4.35 ksi) normal-strength concrete to 130 MPa (18.9

ksi) high-strength concrete for confinements provided by spirals, hoops, crossties,

welded wire fabric, and combinations of these reinforcements.

2.4.9 Bing et. al. Model (2001)

A total of 40 small-scale high-strength reinforced concrete columns with concrete

strength ranging from 35.2 to 82.5 MPa (5.1 and 12 ksi) and transverse yield

strength of Grade 430 $f_{yh} = 445$ MPa (64.5 ksi) and Grade 1300 $f_{yh} = 1318$ MPa

(191 ksi: ultra-high-strength) and subjected to quasi-static axial loading tests were

tested by Bing et. al. in 2001. The model consists of three branches followed by a

tail with a constant stress of $0.4 f_{cc}'$ as following:

When $0 \leq \varepsilon_c \leq \varepsilon_{co}$

$$f_c = E_c \varepsilon_c + \frac{\left(f_{co}' - E_c \varepsilon_{co} \right)}{\varepsilon_{co}^2} \varepsilon_c^2 \qquad (2.93a)$$

when $\varepsilon_{co} \leq \varepsilon_c \leq \varepsilon_{cc}$

83

$$f_c = f'_{cc} - \frac{\left(f'_{cc} - f'_{co}\right)}{\left(\varepsilon_{cc} - \varepsilon_{co}\right)^2} \times \left(\varepsilon_c - \varepsilon_{cc}\right)^2 \qquad (2.93b)$$

when $\varepsilon > \varepsilon_{cc}$

$$f_c = f_{cc} - \beta \frac{f'_{cc}}{\varepsilon_{cc}} \times \left(\varepsilon_c - \varepsilon_{cc}\right) \geq 0.4 f'_{cc} \qquad (2.93c)$$

where,

f'_{cc} = maximum strength of confined concrete

ε_{cc} = axial strain at maximum strength

β = coefficient for the slope control of descending branch

The authors found that the previous model proposed by Mander et. al. over-estimated the f'_{cc} for the concrete confined by high yield strength steel due to the fact that the ultra high yield strength of steel is not developed until high transverse strains are reached as the confinement of the high-strength concrete is substantially delayed in comparison to normal-strengthh concrete. Thus, a modification was made with an introduction of a modification factor α_s. The proposed expressions are as follows:

84

$$f'_{cc} = f'_{co}\left[-1.254 + 2.254\sqrt{1 + 7.94\alpha_s \frac{f'_l}{f'_{co}}} \right] - 2\alpha_s \frac{f'_l}{f'_{co}}$$ (2.94)

When $f'_{co} \leq 52MPa$, $\alpha_s = (21.2 - 0.35f'_{co})\frac{f'_l}{f'_{co}}$ (2.95a)

When $f'_{co} > 52MPa$, $\alpha_s = 3.1\frac{f'_l}{f'_{co}}$, (2.95b)

where f'_l is the effective lateral confining pressure expressed as:

$$f'_l = 0.5K_e(\rho_x + \rho_y)f_{yh}$$ (2.96)

where ρ_x = lateral confining steel parallel to x-axis and ρ_y = lateral confining

steel parallel to y-axis.

Confinement effective coefficient based on area ratio,

$$K_e = \frac{\left[1 - \sum_{i=1}^{n}\frac{C_i^2}{6b_c d_c}\right] \times \left[1 - 0.5\frac{s'}{b_c}\right] \times \left[1 - 0.5\frac{s'}{d_c}\right]}{1 - \rho_{cc}}$$ (2.97)

ρ_{cc} = volumetric ratio of confining reinforcement to core concrete.

For rectilinear confinement with ordinary-strength steel,

$$\frac{\varepsilon_{cc}}{\varepsilon_{co}} = 1.0 + 11.3\left[\frac{f'_l}{f'_{co}}\right]^{0.7}$$ (2.98)

85

For rectilinear confinement with ultra-high-strength steel,

$$\frac{\varepsilon_{cc}}{\varepsilon_{co}} = 2.0 + \left(87 - 1.06 f_{co}'\right)\sqrt{\frac{f_l'}{f_{co}'}} \text{ when } f_{co}' \leq 50MPa \qquad (2.99a)$$

$$\frac{\varepsilon_{cc}}{\varepsilon_{co}} = 2.0 + \left(53.4 - 0.42 f_{co}'\right)\sqrt{\frac{f_l'}{f_{co}'}} \text{ when } f_{co}' > 50MPa \qquad (2.99b)$$

For concrete confined by rectilinear confinement,

$$\beta = \left(0.048 f_{co}' - 2.14\right) - \left(0.098 f_{co}' - 4.57\right)\left(\frac{f_l'}{f_{co}'}\right)^{\frac{1}{3}} \qquad (2.100a)$$

when $f_{yh} \leq 550MPa$ and $f_{co}' > 75MPa$

$$\beta = 0.07 \qquad (2.100b)$$

when $f_{yh} > 1200MPa$ and $f_{co}' \leq 80MPa$

$$\beta = 0.1 \qquad (2.100c)$$

when $f_{yh} > 1200MPa$ and $f_{co}' > 80MPa$

where β does not apply all ranges of material strength with continuity for

rectilinear confinement with ordinary yield strength ($f_{yh} \leq 550MPa$).

The maximum concrete strain ε_{cu} was also defined with an assumption that a

conservative limitation of ultimate concrete compressive strain is when fracture of

a hoop first occurs due to substantial buckling of longitudinal bars.

86

For rectilinear confinement with normal-strength steel,

$$\frac{\varepsilon_{cu}}{\varepsilon_{co}} = 2.0 + \left(122.5 - 0.92 f_{co}'\right)\sqrt{\frac{f_l'}{f_{co}'}} \quad \text{when} \quad f_{co}' < 80 MPa \qquad (2.101a)$$

$$\frac{\varepsilon_{cu}}{\varepsilon_{co}} = 2.0 + \left(82.75 - 0.37 f_{co}'\right)\sqrt{\frac{f_l'}{f_{co}'}} \quad \text{when} \quad f_{co}' \geq 80 MPa \qquad (2.101b)$$

For rectilinear confinement with ultra-high-strength steel,

$$\frac{\varepsilon_{cu}}{\varepsilon_{co}} = 2.0 + \left(70.0 - 0.6 f_{co}'\right)\sqrt{\frac{f_l'}{f_{co}'}} \quad \text{when} \quad f_{co}' \leq 50 MPa \qquad (2.102a)$$

$$\frac{\varepsilon_{cu}}{\varepsilon_{co}} = 2.0 + \left(49.0 - 0.2 f_{co}'\right)\sqrt{\frac{f_l'}{f_{co}'}} \quad \text{when} \quad f_{co}' > 50 MPa \qquad (2.102b)$$

It was found from this experiment that none of the available high-strength concrete models are able to predict the experimentally measured stress-strain behavior of both circular and rectangular transverse reinforcements of different yield strength. The ascending portions the stress-strain relationships were predicted well. However, the descending portions were consistent in comparison to experimental results. It was found that all models under-predicted the concrete strength giving a very conservative prediction for concrete confined by ultra high yield strength steel. It was found that the influence of concrete compressive

87

strength on performance is important, especially for concrete compressive strengths exceeding 60 MPa (8.7 ksi). The increase in transverse reinforcement spacing reduces the efficiency of the confinement. Otherwise, the model was found to provide reasonable predictions of the experimental results for both circular and square high-strength concrete specimens for both normal or high yield strength transverse reinforcement.

2.5 COMPARISON OF EXISTING STRESS-STRAIN MODELS

The latest confined concrete stress-models which most realistically predict seismic behaviors of high-strength columns have been used to observe the fundamental stress-stress behaviors of both confined and unconfined concrete. Using the parameters and material properties of the full-scale columns mentioned above, sample calculations have been performed for the comparison of confined and unconfined behavior of the concrete based on Mander and Martirossyan confined concrete stress-stress theories.

Figure 2.3 shows concrete stress-strain relationship for the Mander model for Grade 420 (ASTM Grade 60) transverse reinforcement spaced at 100, 125, and 150 mm (4, 5, and 6 inches). It can be noticed that in general 100 mm (4 inch)

88

spacing resulted in greater concrete stress values as compared to 150mm (6 inch) spacing as a consequence of greater confinement values provided for the core concrete by smaller spacing. The unconfined concrete stress-strain curve is also shown for comparison to confined cases.

In the Figure 2.4, Grade 520 (ASTM Grade 75) transverse reinforcement gave overall greater values of confined stresses as compared to the Grade 420 (ASTM Grade 60) curves from Figure 2.3.
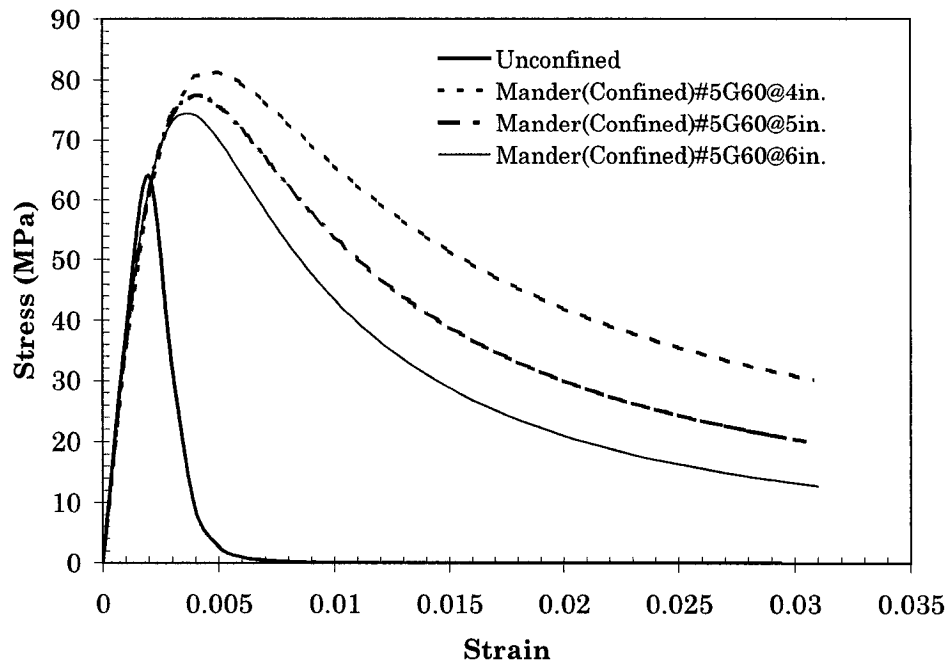
Fig. 2.3-Comparison of confined and unconfined high-strength concrete behavior at transverse reinforcement spacing of 100, 125, and 150 mm (4, 5, and 6 in.) using Mander model and Grade 420 (ASTM Grade 60) steel.

90
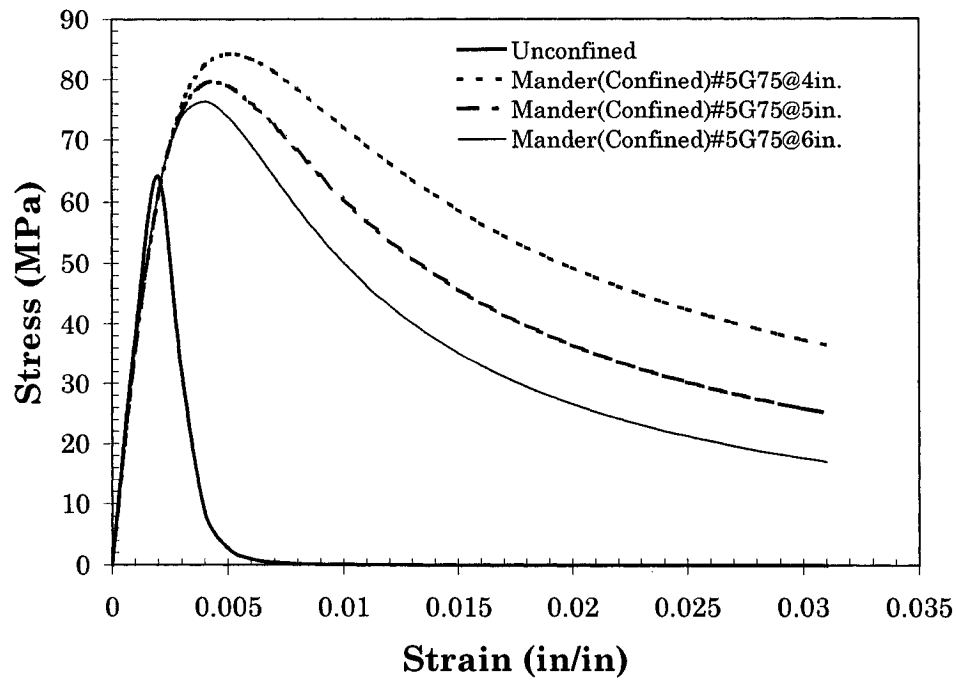
Fig. 2.4- Comparison of confined and unconfined high-strength concrete behavior at transverse reinforcement spacing of 100, 125, and 150 mm (4, 5, and 6 in.) using Mander model and Grade 520 (ASTM Grade 75) steel.

91

Similarly, Figures 2.5 and 2.6 based on Martirossyan concrete stress-strain theory are depicted for different transverse reinforcement spacing and grades. It is apparent that smaller spacing of the transverse reinforcement as well as higher grade type used resulted in larger concrete strain values.

When the results based on the Mander concrete stress-strain theory is compared to that of Martirossyan theory, the first depicts greater value of concrete modulus of elasticity, therefore, a steeper ascending portion of the curve as shown in the figures above. This is because new value of E_{50} was introduced into Martirossyan model instead of the conventional E_c in order to control the stiffness of the ascending part of the curve for better accuracy. On the other hand,

Martirossyan model has a steeper descending curve since the model includes the coefficient k_3 which was designed to control the descending part of the model to allow the curve to pass through the initially defined point ($\varepsilon_{cu}, 0.8f'_{cc}$). A glitch in the unconfined stress-strain models for both Mander and Martirossyan models can be noticed from above figures due to a noticeable differences in the initial stiffnesses of the ascending curves between the unconfined and confined curves. Further investigation by aforementioned authors may be necessary in order to correct such a discrepancies between the ascending portions of the confined and unconfined curves.

92
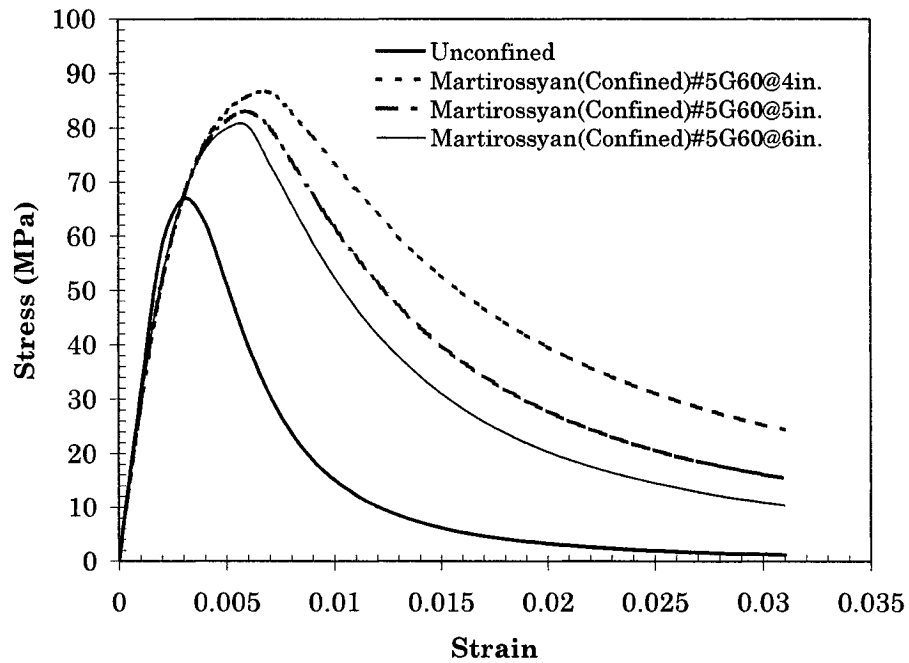
Fig. 2.5-Comparison of confined and unconfined high-strength concrete behavior at transverse reinforcement spacing of 100, 125, and 150 mm (4, 5, and 6 in.) using Martirossyan model and Grade 420 (ASTM Grade 60) steel.

93
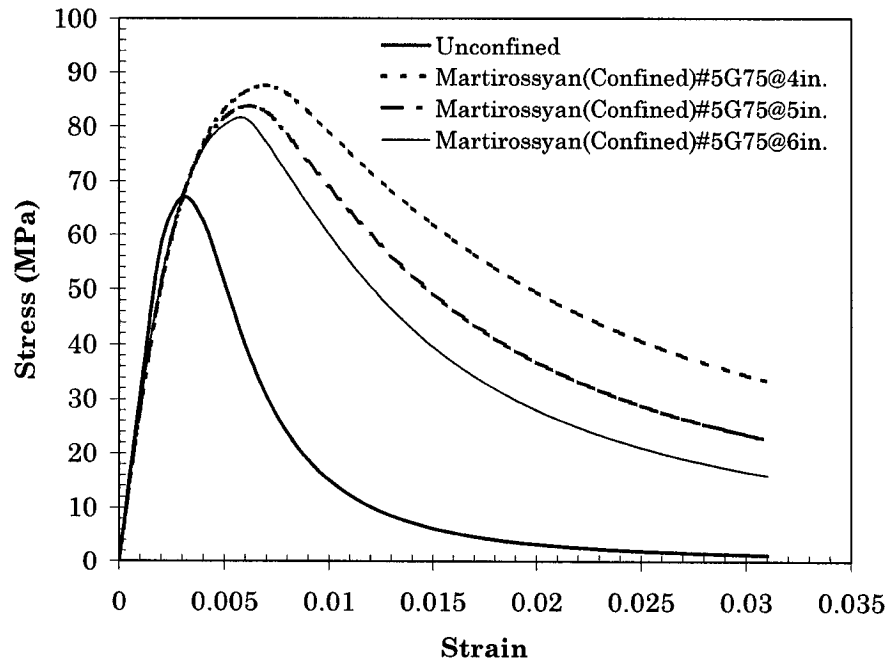
Fig. 2.6- Comparison of confined and unconfined high-strength concrete behavior at transverse reinforcement spacing of 100, 125, and 150 mm (4, 5, and 6 in.) using Martirossyan model and Grade 520 (ASTM Grade 75) steel.

94

2.6 STEEL STRESS-STRAIN MODELS

An assumption of bi-linear stress-strain relationship is used for ACI rectangular stress block where,

$$f_S = E_S \varepsilon_S \quad \text{for} \quad \varepsilon_S \leq \varepsilon_Y \tag{2.103a}$$

and

$$f_S = f_Y \quad \text{for} \quad \varepsilon_S > \varepsilon_Y \tag{2.103b}$$

The yield strain $\varepsilon_Y = \dfrac{f_Y}{E_S}$, where f_Y = yield stress

The typical stress-strain behavior of steel reinforcement during monotonic loading tests can be idealized into its linear elastic and non-linear strain-hardening behavior. In 1984, Mander et al. predicted the non-linear strain-hardening region of the stress-strain curve, where the elastic region remains the same as mentioned above for the steel tensile stress-strain relationship for the ACI rectangular stress block. In the strain-hardening region defined as $\left(\varepsilon_{sh} \leq \varepsilon_s \leq \varepsilon_{su} \right)$, the following equation is proposed (King et. al., 1986).

95

$$f_s = f_{su} - \left(f_{su} - f_y\right)\left(\frac{\varepsilon_{su} - \varepsilon_s}{\varepsilon_{su} - \varepsilon_{sh}}\right)^P \qquad (2.104)$$

where,

ε_s = steel strain

ε_{sh} = steel strain at commencement of strain hardening

ε_{su} = steel strain at f_{su}

f_s = steel stress

f_{su} = ultimate tensile strength of steel

f_y = yield strength of steel

E_{sh} = strain-hardening modulus of steel

The increase in the stress relevant to strain in the strain-hardening region was determined by taking into account the strain rate determined by using the relevant control parameter values as:

$$P = E_{sh}\left(\frac{\varepsilon_{su} - \varepsilon_{sh}}{f_{su} - f_y}\right) \qquad (2.105)$$

96

The ultimate tensile strength of steel is approximated as $1.5 f_y$ for both mild and high strength steel. The following are assumptions are made for ε_{sh} and ε_{su} as shown in Table 2.1.

TABLE 2.1-Assumed steel strain values

	MILD STEEL	HIGH STRENGTH STEEL
ε_{sh}	$14\varepsilon_y$	$3.24\varepsilon_y$
ε_{su}	$0.14 + \varepsilon_{sh}$	0.12

The normal design values of yield stress f_y for mild steel is considered to be 275 MPa (40 ksi) and 380 MPa (55 ksi) for high strength steel. There is no guideline for steel grades higher than those mentioned above. However, the behavior in the strain-hardening region are assumed to be similar for higher grade steels. Mander et. al. (1984) also predicted the cyclic stress-strain behavior of steels with different grades. The envelopes of the cyclic stress-strain behavior are found to be identical to that of the monotonic stress-strain relationship. Therefore, for the purpose of this research the monotonic stress-strain relationship will be used to model the behavior of the test specimens.

Figure 2.7 shows typical stress-strain relationships for mild and high strength steels with strain-hardening behavior which were mentioned above considered.

97
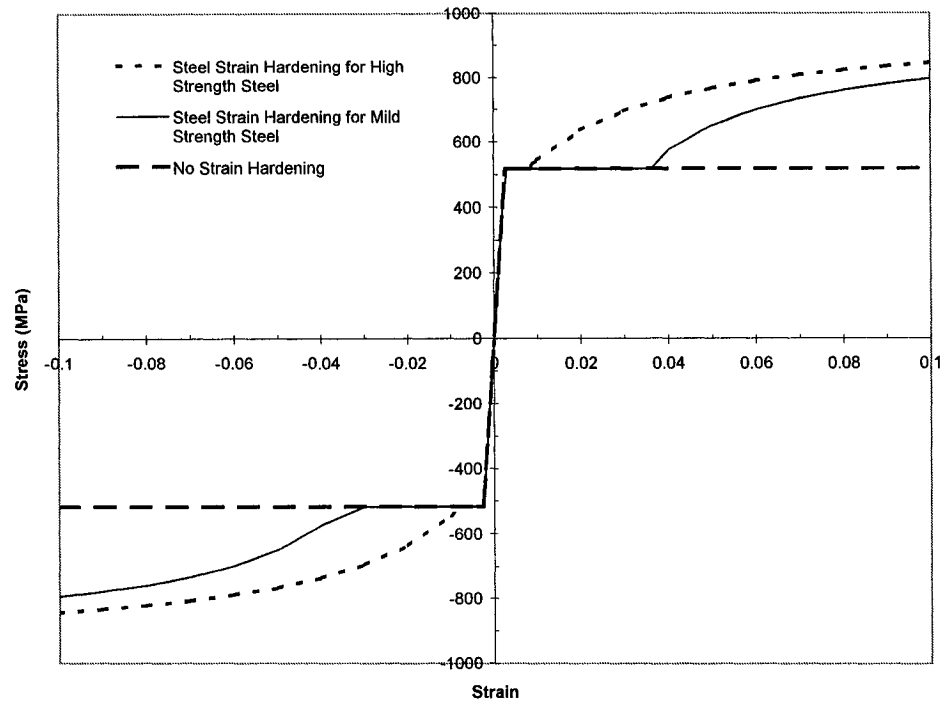
Fig. 2.7-Mander Steel Stress-Strain Relationships

98

2.6.1 Strain Hardening for Mild and High Strength Steels

The stress strain relationship of steel depends on the types of steel used whether they are cold-rolled or cast iron. Due to brittle nature of the material, stress-stress relationship of the cold-rolled and cast iron steels are difficult to model. For mild-steel, on the other hand, have been modeled based on experimental stress-strain relationships. The bi-linear model has been widely used in the past. However, in consideration of strain-hardening in post-elastic region, the stress-strain proposed by Mander et al. which has been discussed previously has been used within the scope of this research.

2.6.2 New Macroscopic Steel Stress-Strain Model for Ordinary and High-Strength Reinforcing Steel

In an attempt to simulate the hysteretic behavior of all types of steel, Balan et. al., 1998, introduced a new steel stress-strain relationship based on the evaluation of the nonlinear hysteretic response of reinforced concrete structures. The model is expressed in natural stress and strain so that a single curve can express both tension and compression behaviors. The material parameters are based on calibration of monotonic tests, and strength degradation relations are derived from cyclic test data. The use of natural stress allows the same curves for both tension

99

and compression stress and strain relationship. The proposed monotonic stress-strain relation is simplified from curve to simplified idealized bilinear curve. A single equation defines both linear elastic region and the strain-hardening regions as follows:

$$f_s = f_y' \frac{\left(1-\rho'\right)}{2}\left[1+\frac{\left(1+\rho'\right)}{\left(1-\rho'\right)}\frac{\varepsilon_s - \varepsilon_o}{\varepsilon_y'} - \sqrt{\left(\frac{\varepsilon_s - \varepsilon_o}{\varepsilon_y'}-1\right)^2 + \delta'}\right] \tag{2.106}$$

where,

$$f_y' = \begin{cases} f_y & \\ E_s \varepsilon_y' & \end{cases} \text{for} \quad \begin{matrix} \varepsilon_s \leq \varepsilon_{sh} \\ \varepsilon_s \succ \varepsilon_{sh} \end{matrix} \tag{2.107}$$

$$\rho' = \begin{cases} 0 & \\ \dfrac{E_h}{E_s} & \end{cases} \text{for} \quad \begin{matrix} \varepsilon_s \leq \varepsilon_{sh} \\ \varepsilon_s \succ \varepsilon_{sh} \end{matrix} \tag{2.108}$$

$$\delta' = \begin{cases} \delta_o & \\ \left(\dfrac{\varepsilon_{sh}}{\varepsilon_y}-1\right)^2 \delta_o & \end{cases} \text{for} \quad \begin{matrix} \varepsilon_s \leq \varepsilon_{sh} \\ \varepsilon_s \succ \varepsilon_{sh} \end{matrix} \tag{2.109}$$

$$\varepsilon_o = \begin{cases} 0 & \\ \left(\varepsilon_{sh} - \dfrac{f_y}{E_s}\right) & \end{cases} \text{for} \quad \begin{matrix} \varepsilon_s \leq \varepsilon_{sh} \\ \varepsilon_s \succ \varepsilon_{sh} \end{matrix} \tag{2.110}$$

$$\varepsilon_y' = \frac{1}{E_s\left(1-\rho'\right)}\left[\left(f_{su} - f_y\right) - \left(\varepsilon_{su} - \varepsilon_{sh}\right)E_s\rho'\right] \tag{2.111}$$

100

2.7 PLASTIC HINGE MODEL

The concept of plastic hinge was used to determine the force-displacement relationship using the moment-curvature relationship that was obtained using various confined HSC stress-strain models.

A plastic hinge method proposed by Priestley and Park estimates the flexural deflection divided into two parts:

$$\Delta = \Delta_e + \Delta_P \tag{2.112}$$

where Δ_e is the elastic flexural deflection contributed by assuming that the curvature distribution outside the plastic hinge region prior to reaching the yield curvature is linear expressed by:

$$\Delta_e = \frac{1}{3}\phi_Y (l_e - l_P)^2 \tag{2.113}$$

where $l_e = l + \varepsilon f_s d_b$ \hfill (2.114)

f_s is the steel stress of the outmost longitudinal reinforcement and d_b is the diameter of the main longitudinal reinforcement.

and where Δ_p is a deflection due to the rotation of the plastic hinge area expressed as:

$$\Delta_P = \phi_P l_P \left(l_e - \frac{l_P}{2} \right) \tag{2.115}$$

101

The definition of plastic hinge length was devised by Priestly and Park in 1987 as follows (Priestley et. al., 1987):

$$l_p = 0.08L + 0.15d_b f_y \qquad\qquad (2.116)$$

$$l_p = 0.08L + 0.022d_b f_y \qquad\qquad \text{(in metric system)}$$

where,

L = distance from the point of contraflexure to the point of maximum moment,

d_b = diameter of column bars, and

f_y = yield stress of the reinforcement (in ksi)

The term $0.08L$ is an empirically determined expression for a length measured from the column stub through which the steel behaves inelastically and $0.15d_b f_y$ is an estimated length of the yield penetration into the column stub.

To perform the plastic-hinge analysis, it was assumed that hinges formed near the ends of the columns.

102

FURTHER DISCUSSION

The practical modeling for the prediction of flexural displacement of a reinforced column involves consideration of moment-curvature relationship by assuming uniform properties in all sections and theoretical curvature distributions. The elastic deformation, cracked stages, and actual plastic hinge region rotation can be taken into account to model the flexural displacement of columns. Figure 2.8 shows a basic lateral force versus flexural displacement relationship.
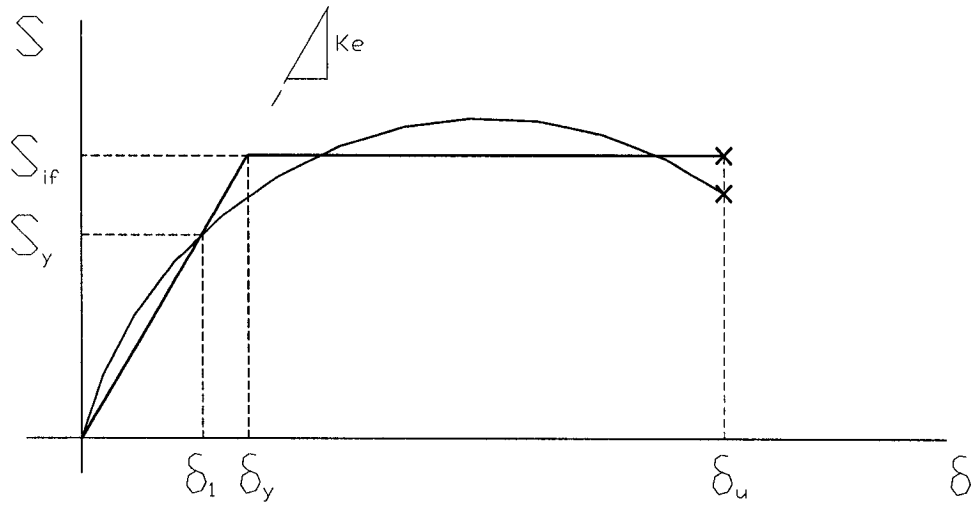
Fig. 2.8-Basic lateral force versus flexural displacement relationship

103

However, such a basic curve distribution does not include two important effects which are the influence of inclined shear cracking and fixed end rotation due to imperfect longitudinal reinforcement anchorage.

Tjd Effect

In the fixed end region of the column, the column section is subjected to Tjd effect as the column undergoes a flexural deformation. The Tjd effect is the result of a constant value of tensile force 'T' which exists in column axial direction over a certain length from the fixed end that balances the compressive force 'C' a distance 'jd' from 'T' in the compressive zone. The tensile steel Force 'T' of the longitudinal reinforcement remains constant over a certain axial length from the fixed end of the column. Therefore, the steel stress remain constant. This means that "plane" hypothesis is no longer applicable and that there is a spread of plasticity.

Furthermore, the yield penetrations and bond degradation of the longitudinal reinforcement in the fixed end region can cause an additional plastic rotation.

104
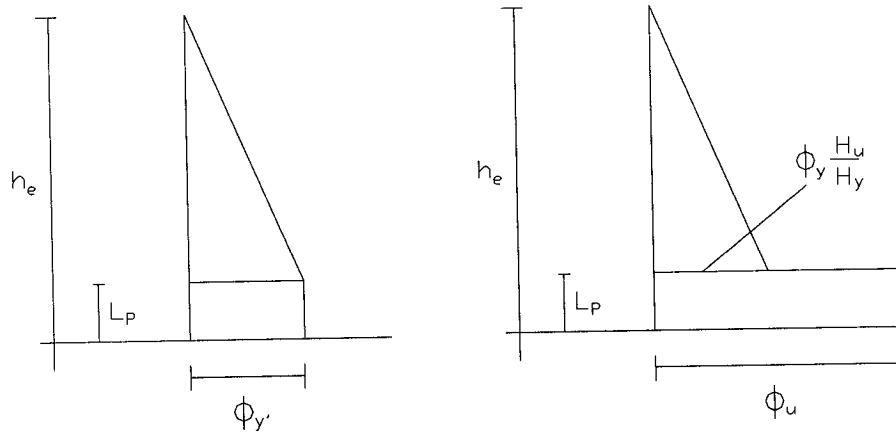
Fig. 2.9-Concept of plastic hinge

Here, $L_p = C_1 h + C_2$ (2.117)

where C_1 = Experimental constant for shear effect

C_2 = Experimental constant for yield penetration

The pure theory can not give prediction of plastic hinge length. Therefore, the definition of plastic hinge region was determined based on experimental results by Priestley et al.

If we assume that elasto-plastic model applies,

105

$$\Delta_P = (\phi - \phi_Y)L_P(L - \frac{L_P}{2}) \qquad (2.118)$$

$$\Delta_P = \Delta - \Delta_Y \qquad (2.119)$$

Since Δ_Y and ϕ_Y can be experimentally determined or reasonably predicted, the values of Δ and ϕ can be obtained by solving the following equation.

$$\Delta - \Delta_Y = (\phi - \phi_Y)L_P\left(L - \frac{L_P}{2}\right). \qquad (2.120)$$

In 1984, Paulay and Priestley proposed the following equation.

$$L_P = 0.08h + \xi d_b \quad \text{where } \xi = 0.15f_y. \qquad (2.121)$$

$$\xi = 0.022f_y \text{ (in metric system)}$$

The effective length considering the plastic hinge length is defined as:

$$h_e = h + \xi d_b \qquad (2.122)$$

where h = Column height for single curvature bending

106

However, the above equations were not calibrated against high axial load. Therefore, the following equations were proposed.

The definition of "plastic hinge length" was defined for bridge columns (Priestley et. al., 1994) and was modified by Xiao and Ma in 1994. It is defined as:

$$L_h = 0.08 l_s \frac{f_s}{f_y} + 0.02 d_{lb} f_s \qquad \text{(MPa)} \qquad (2.123a)$$

$$L_h = 0.08 l_s \frac{f_s}{f_y} + 0.15 d_{lb} f_s \qquad \text{(ksi)} \qquad (2.123b)$$

where,

L_h = Length of plastic hinge

l_s = Shear span length (one half of column height for double curvature bending)

f_s = Stress in extreme tensile bars

f_y = Yield strength of longitudinal reinforcement

d_{lb} = Longitudinal bar diameter

107

The effective height of the column taking into consideration the plastic hinge formation is defined as:

$$H_e = h + \left(2 \times 0.02 d_{lb} f_s\right) \qquad \text{(MPa)} \qquad (2.124a)$$

$$H_e = h + \left(2 \times 0.15 d_{lb} f_s\right) \qquad \text{(ksi)} \qquad (2.124b)$$

where,

h = Full column height during double curvature bending.

In order to calculate the force-displacement relationship, the concept of shear and flexural deformations need to be defined.

Since the majority of the columns failures are the result of flexural deformation, the shear deformation are also considered as a secondary effect.

The total displacement is defined below as the sum of flexural and shear deformation for single curvature bending for the specimens that were tested, where it is multiplied by two for the cases of double curvature bending.

108

$$\Delta_i = \Delta_f + \Delta_s \qquad (2.125)$$

where,

Δ_f = Total deformation due to flexural bending

Δ_s = Shear deformation

Δ_i = Total displacement

Δ_f is the sum of deformation due to plastic hinge rotation Δ_{f1} and the actual flexural deformation of the column Δ_{f2}.

$$\Delta_f = \Delta_{f1} + \Delta_{f2} \qquad (2.126)$$

where,

$$\Delta_{f1} = \left(\frac{H_e}{2} - \frac{L_h}{2} \right) \times L_h \times \phi_i \qquad (2.127)$$

$$\Delta_{f2} = \int_0^a \phi(x) x\, dx \qquad (2.128)$$

109

Variable x in equation 2.91 is a variable which increases along the length of the column, and a is the upper bound of integration defined as:

$$a = \frac{h}{2} - 0.08 \frac{h}{2} \frac{f_s}{f_y} \qquad (2.129)$$

Assuming a linear distribution of the moment along the column height, equation 2.91 is simplified as:

$$\Delta_{f2} = \frac{1}{3} \phi_i \times \left(\frac{h}{2} - 0.08 \frac{h}{2} \frac{f_s}{f_y} \right)^2 \qquad (2.130)$$

The shear deformation Δ_s is expressed by a linear relationship based on the linear deformation of the longitudinal bar up to its yield point as:

$$\Delta_s = \frac{V}{V_y} \Delta_{sy} \qquad (2.131)$$

where,

Δ_s = Relative displacement caused by shear deformation between column ends

V = The shear force

110

V_y = Shear force corresponding to the first yield of longitudinal steel

Δ_{sy} = Shear deformation corresponding to first yield of longitudinal steel defined

by Priestley et al., 1994, as:

$$\Delta_{sy} = \frac{V_y l_s}{0.9 A_g \times (0.4 E_c)} \frac{E_c I_g}{(M_y / \phi_y)} \tag{2.132}$$

where,

l_s = Shear span length (one half of column height for double curvature bending)

E_c = Modulus of elasticity of the concrete

I_g = Moment of inertia of the column gross section

A_g = Gross sectional area of the column

M_y = Moment at the first yield of longitudinal steel

ϕ_y = The curvature corresponding to the first yield of longitudinal steel

In 2001, Esmaeily revised the latest plastic hinge model mentioned above in consideration of the actual location of plastic hinge a distance away from the

111

column stub as observed in his experimental tests of columns that were subjected to cyclical loading. Two approaches in the estimation of variations in plastic hinge length during monotonic or cyclical loading are introduced. The first approach assumes that the curvature between the point of the first longitudinal reinforcement yielding and the base of columns varies linearly and is only applicable to monotonic loading cases. The length of the transition region between the point of the first longitudinal reinforcement yielding and the column base is expressed as:

$$l_p = l\left(1 - \frac{M_y}{M_u}\right) \qquad (2.133)$$

where,

l = total column length

M_y = yield moment for the existing axial load

M_U = moment at the critical section of column base

$$M_y = \frac{(l - l_p)}{l} M_U \qquad (2.134)$$

The curvature at the top of the plastic hinge is expressed as:

$$\phi_{l_p} = \phi_y\left(\frac{M_U}{M_y}\right)\frac{(l - l_p)}{l} \qquad (2.135)$$

The total displacement is expressed as:

$$\Delta = \Delta_e + \Delta_p \qquad (2.136)$$

112

where,

$$\Delta_e = \frac{1}{3}\phi_{l_p}\left(l - l_p\right)^2 \text{ and } \Delta_p = \phi_{l_p}l_p\left(l - \frac{l_p}{2}\right) + \frac{1}{2}\left(\phi_u - \phi_{l_p}\right)l_p\left(l - \frac{l_p}{3}\right)$$ (2.137)

ϕ_u = curvature at the critical region of the column base

In order to approximate the total lateral displacement in consideration of variation of plastic hinge length, the following steps are used:

1.   With value of initial plastic hinge length l_p equal zero, the initial yield lateral displacement is obtained by $\Delta_y = \frac{1}{3}\phi_y l^2$.

2.   If $|\Delta| \leq \Delta_y$, $\phi_u = \frac{3\Delta}{l^2} \rightarrow M_U \rightarrow$ Lateral Force $F = \frac{M_U}{l}$, where similar process applies to during the reversal loading while $|\Delta| \leq \Delta_y$

3.   Once the lateral displacement $|\Delta|$ exceeds Δ_y, a new curvature $\phi_u > \phi_y$ is found by trial and error so that $l_p = l\left(1 - \frac{M_y}{M_U}\right)$, and the curvature at the top of transition zone l_p is ϕ_y as shown in equation (2.135). The maximum achieved value of l_p so far is retained.

4.   The curvature at the top of the plastic hinge is used to obtain the total lateral displacements as shown in equations (2.136) and (2.137).

113

The trial and error approach allows the determination of a location and the value of the curvature at the top of the transition zone in relation to the column length, column base moment, yield curvature, and yield moment, thus providing proper total lateral displacement in consideration of the variations in the plastic hinge length.

The second approach, proposed by Park and Priestley, is applicable to both monotonic or hysteretic cases. In this case it has been applied for variable axial load. The plastic hinge model assumes that the total column length is divided into three parts, the part with a constant curvature with a length of $0.08l + 0.15f_yd$ or the section depth, a transition length $0.15f_yd_b$ along which the curvature varies linearly from the curvature of the previous segment to a curvature that is dependent on the first yield curvature due to the existing axial load and lateral force, and the remaining length which always remain elastic. For a given lateral displacement and axial load, a proper displacement are obtained in consideration of the variation in the plastic hinge length. This is achieved by obtaining new curvatures at the column base by trial and error, where the new curvatures are dependent on the base curvature at the critical section of the column. The procedure is as follows:

114

1. The segment of constant length, l_{cons}, is assumed equal to D, where D is the section depth, where $l_{cons} = 0.08l$ for columns with height to depth ratio of more than 12.5.

2. ϕ_y and M_y are evaluated from a moment-curvature analysis.

3. A new column base curvature is assumed and the corresponding moment is calculated using a moment-curvature analysis for the new target displacement.

4. The curvature at the top of transition length ϕ_t is obtained as by:

$$\phi_t = \phi_y \left(\frac{M_U}{M_y} \right) \frac{(l - l_{cons} - l_{trans})}{l} \qquad (2.138)$$

where,

ϕ_y = yield curvature

M_y = yield moment for the current axial load level

M_U = column base moment

l = column height

l_{cons} = length of the segment close to the base

l_{trans} = transition length

5. The lateral displacement is evalued as $\Delta = \Delta_e + \Delta_p$

where,

$$\Delta_p = \phi_t l_{trans}\left(l - l_{cons} - \frac{l_{trans}}{2}\right) + \frac{1}{2}(\phi_u - \phi_t)l_{trans}\left(l - l_{cons} - \frac{l_{trans}}{3}\right) + \phi_u l_{cons}\left(l - \frac{l_{cons}}{2}\right)$$

$$(2.139)$$

$$\Delta_e = \frac{1}{3}\phi_t\left(l - l_{cons} - l_{trans}\right)^2 \qquad (2.140)$$

6. The obtained total lateral displacement Δ is then compared to the target displacement previously set and the process is iterated from step 2. above until the desired tolerance is achieved.

This approach is similar to that of the first approach, except a region of constant plastic curvature has been added to the region varying plastic hinge length.

2.8 REINFORCED HIGH-STRENGTH CONCRETE COLUMNS

The use of high-strength concrete (HSC) in earthquake resistant tall buildings can offer many advantages compared with normal strength concrete, such as reduced column sectional dimensions. However, due to the lack of sufficient research data for the development of seismic design guidelines, the use of HSC in lateral load resisting systems has been non-existing in Southern California, one of the major regions in the US with high seismicity.

116

This study is part of a comprehensive experimental program aimed at developing design provisions for the use of HSC in the regions of high seismicity. The objective of this particular study is to investigate confinement requirements to ensure proper ductility in HSC columns utilized in lateral load resisting frames. Further, currently available code equations will be examined for its application for HSC columns. Efforts will be made to explore existing material models in order to introduce an appropriate analytical methods for HSC columns.

Although an increasing amount of experimental database on seismic behavior of HSC columns are becoming available including those from the studies by the author, test data on full-scale HSC columns are extremely rare. The main reason is due to the difficulties of testing. A new equipment recently developed at the University of Southern California enables full-scale experimental study on structural columns. This report presents the experimental results on six full-scale HSC columns subjected to simulated seismic loading.

Note: SI units are used as the main units throughout the paper, with the corresponding English units provided in the parenthesis. The sizes and grades of reinforcing bars are described based on so-called soft conversions (CRSI, 1997).

117

CHAPTER 3

EXPERIMENTAL PROGRAM

3.1 GENERAL

In an attempt to investigate the behavior of the full-scale high strength reinforced concrete columns subjected to high axial loads and lateral seismic loads, an experimental program was designed to provide extensive data and analysis. From the fabrication of the specimens and the test system to acquiring and analyzing the experimental data required tremendous effort in pre-planning and time scheduling. The material preparations, strain gage installations, construction of the steel cage as well as the formwork, and data analysis were accomplished with careful attention to the details. The data acquisition was performed by a 40 channel logger which monitored and measured all the strains, displacements, and forces within the test system. Extensive material testing on the high strength concrete cylinders and steel reinforcements were performed. Proper capping procedures were followed for the compression tests, and the true stress-strain values were measured using strain gages and force cells for the tensile tests. The details of the steel test system components were sketched with AUTOCAD Release 13 and were fabricated through a local steel fabricator. The welding and

118

connections of the steel component were typically plug welds, fillet welds, 483 MPa (70 ksi), or full penetration welds for crucial connections to ensure rigidity of the test system. All components were assembled in the structural laboratory prior to testing.

Extensive data analysis as well as experimental documentation were needed in order to understand and determine the yielding points, maximum capacities, and overall behavior of the specimens. These are also to be discussed in Chapters 4 to 6.

3.2 SPECIMEN DESIGN

3.2.1 Introduction

Six full-scale model columns were designed to simulate columns in a cast in-situ multi-story building in Los Angeles. The testing matrix is shown in Table-3.1 and the model details are illustrated in Fig. 3.1 and Fig. 3.2. The columns were 510 mm (20 in.) square section with a height of 1,778 mm (70 in.) from the point of lateral loading to the top of the load stub. The columns were reinforced with four No.36 (ASTM No.11, nominal diameter =35.8 mm =1.41 in.) bars plus four No.29 (ASTM No.9, nominal diameter =28.7 mm =1.128 in.) bars, constituting a

119

longitudinal reinforcement ratio of 2.6%. (ACI Committee 318, 1995) The main

testing parameter was the transverse reinforcement detail. In the seismic design

provisions of ACI 318 code (1995), the total cross-sectional area of transverse

reinforcement of columns is specified by the following two equations,
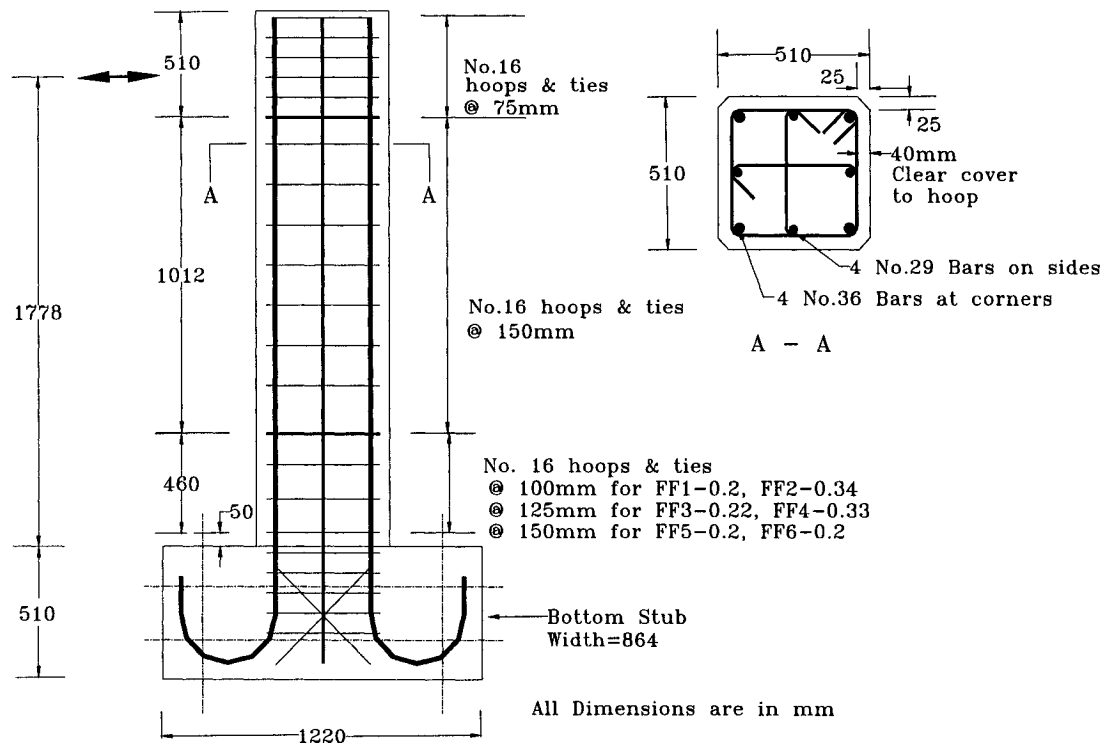
Fig. 3.1-Specimen details.

120
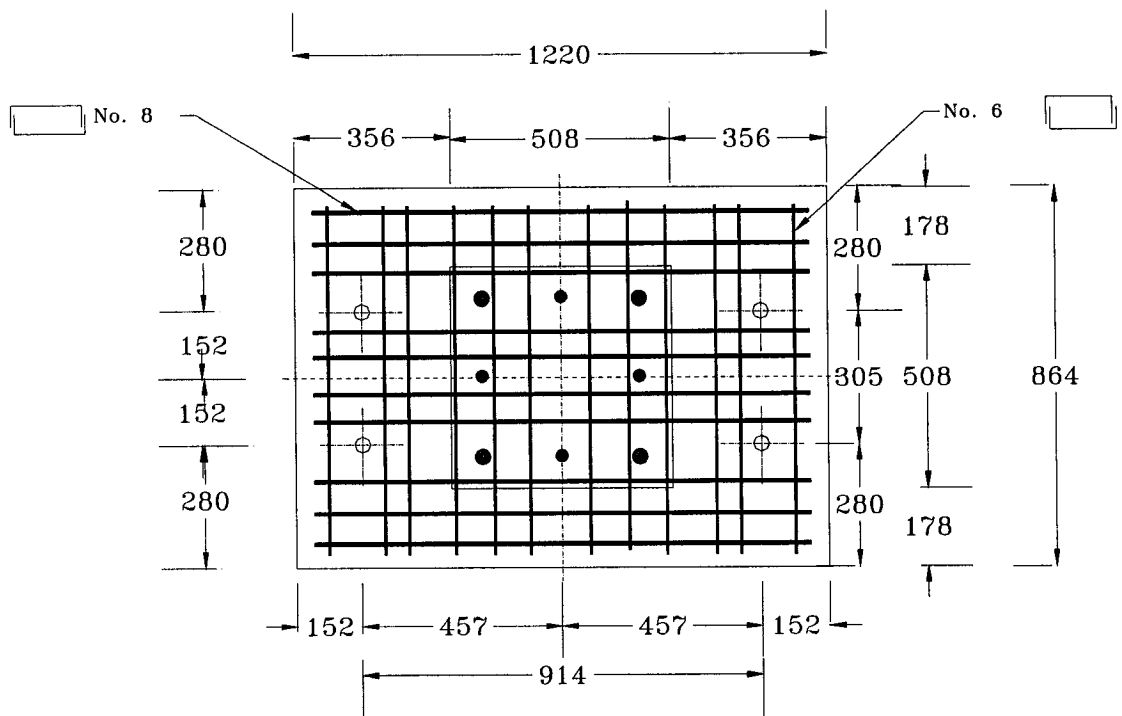
All Dimensions are in mm

Foundation Plan View

Fig. 3.2-Foundation details.

121

TABLE 3.1-Testing matrix.

Specimen	Longitudinal Steel	Transverse Steel for Column Potential Plastic Hinge Region	Concrete Strength f'_c (MPa)	Axial Load Ratio $P/A_g f'_c$ (Axial Load)
FHC1-0.2		No.16 hoops &ties @100mm (f_y=445MPa)	64.1	0.2 (3334 kN)
FHC2-0.34	4 No.29 &	No.16 hoops &ties @100mm (f_y=445MPa)	62.1	0.34 (5373 kN)
FHC3-0.22	4 No.36	No.16 hoops &ties @125mm (f_y=524MPa)	62.1	0.22 (3630 kN)
FHC4-0.33	(f_y=473MPa)	No.16 hoops &ties @125mm (f_y=525MPa)	62.1	0.33 (5240 kN)
FHC5-0.2		No.16 hoops &ties @150mm (f_y=445MPa)	64.1	0.2 (3334 kN)
FHC6-0.2		No.16 hoops &ties @150mm (f_y=524MPa)	64.1	0.2 (3334 kN)

Note: i. Specimen name designation example: HSC-FF1-0.2 represents High-Strength Concrete Full-scale Flexural testing model column No.1 with an axial load ratio of 0.2;

ii. Concrete strength is based on average strength of three 152mm × 305mm (6in × 12in) cylinders cured in the air-dry condition;

iii. Axial load ratio = $P/(A_g f'_c)$;

iv. The nominal diameter is 28.7mm (1.128in) for No.29 (No.9) bars; 35.8mm (1.41in) for No.36 (No.11) bars; and 15.9mm (0.625in) for No.16 (No.5) bars.

$$A_{sh} \geq 0.3 \frac{s h_c f'_c}{f_{yh}} \left(\frac{A_g}{A_{ch}} - 1 \right)$$

(3.1a)

or,

$$A_{sh} \geq 0.09 s h_c \frac{f'_c}{f_{yh}}$$

(3.1b)

where, A_{sh} is the total transverse steel cross sectional area within spacing s; h_c is the cross sectional dimension of column core measured center-to-center of out-most peripheral hoops; f'_c is specified compressive strength of concrete; f_{yh} is specified yield strength of transverse reinforcement; A_g is gross area of column section; and A_{ch} is cross sectional area of a column measured out-to-out of transverse reinforcement. The spacing of the hoops is limited to less than one-

122

quarter of the minimum dimension of the member or 100 mm (4 in.), whichever smaller.

Fig.3.3 compares equation (3.1a) and (3.1b) for square columns with a constant cover thickness of 38mm (1.5in). In Fig.3.3, the vertical axis shows total cross-sectional area, A_{sh}, divided by $(sh_c f'_c/f_{yh})$, while the horizontal axis shows width of the square columns considered. As evidenced from Fig.3.3, equation (3.1a) governs the design of square columns with side length less than approximately 610mm (about 24in), while equation (3.1b) controls the design for larger sections. The relative values of the transverse reinforcement for the hinge regions of the six full-scale model columns based on actual material strengths are also plotted in Fig.3.3. For the selected dimension of the specimens tested in this research, equation (3.1a) governs the design of A_s.

Model columns FHC1-0.2 and FHC2-0.34 were transversely reinforced with No.16 (ASTM #5, nominal diameter =15.9 mm =5/8 in.) hoops and cross ties spaced at 100 mm (4 in.) for their potential plastic hinge regions with a length measured 510 mm (20 in.) from the top of the stub, whereas spaced at 150 mm (6 in.) there upper. The hoop spacing of these two specimens also satisfied the ACI 318-95 requirements. The transverse reinforcement in the hinge regions of these
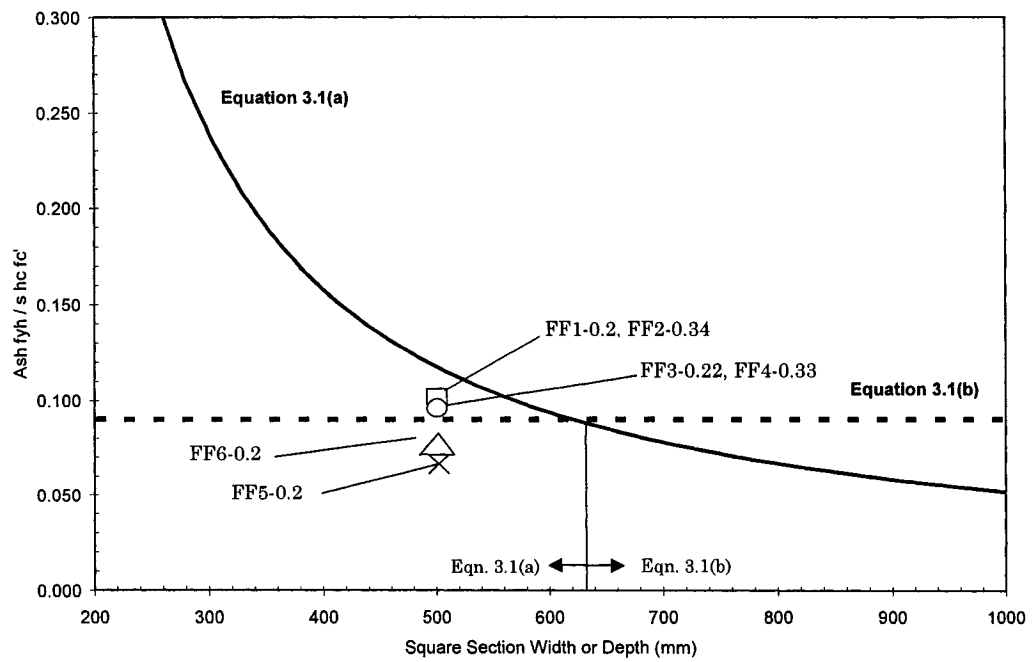
Fig. 3.3-ACI Code 318-95 requirement for transverse reinforcement.

124

two specimens provided approximately 86% of the required confinement steel based on the ACI 318-95 equation (3.1a).

In model columns FHC3-0.22 and FHC4-0.33, the spacing of the No.16 (ASTM #5) transverse reinforcement in the potential plastic hinge regions was increased to 125 mm (5 in.), which was 1.25 times wider than the maximum spacing requirement for transverse reinforcement based on ACI 318-95 code. However, due to the use of higher strength transverse reinforcement in these two columns, the confinement was about 82% of the ACI 318-95 code requirement, comparatively close to that for the specimens FHC1-0.2 and FHC2-0.34.

Model column FHC5-0.2 was reinforced with No.16 (ASTM #5) hoops and ties spaced at 150 mm (6 in.), which was 1.5 times wider than the maximum spacing requirement for transverse reinforcement based on ACI 318-95 code. Consequently, FHC5-0.2 had approximately 57% of the confinement required by ACI code in the column hinge region. Higher strength steel was used in the transverse reinforcement for model column FHC6-0.2, where the hoops and ties were spaced at 150 mm (6 in.). The total cross-sectional area of transverse reinforcement approximately equaled to 68% given by equation (3.1).

125

All the hoops and ties satisfied the detailing requirements of current ACI code. Each set of the transverse reinforcement was made of a peripheral hoop with 135° hooks and a pair of cross ties with 135° hook at one end and 90° hook at the other end.

The columns were constructed into 1,219 × 864 × 508 mm (48 × 34 × 20 in.) load stubs, which were post-tensioned to the loading frame during the testing. The column stubs were proportioned and reinforced to assure a rigid behavior during testing.

3.2.2 Existing U.S. High Strength Concrete Provisions

ACI 318-95 Building Code provide special provisions for earthquake resistance for reinforced concrete column subjected to earthquake-induced forces. The limitations on material properties are discussed for a minimum specified concrete strength f'_c of 20.7 MPa (3,000 psi.) and a maximum specified reinforcement yield strength f_y of 413.7 MPa (60,000 psi.). The code did not have specific provisions for high strength concrete design since test data on high strength concrete usage is limited. For high strength lightweight concrete members under reversed cyclic loading, a limitation of 27.6 MPa (4,000 psi.) is advised.

126

ACI 318-99 Building Code provisions for seismic load application for columns are also derived for normal-strength concrete columns and are not applicable to high-strength concrete columns (Murat and Salim, 2002).

3.2.3 ACI Code Provision

The special seismic provisions in Chapter 21 of ACI318-95 and ACI318-99 require transverse reinforcements for the confinement of columns in potential plastic-hinge region and is based on the ultimate axial capacity of columns that are concentrically loaded. However, the required ultimate curvature deformation of columns that are also subjected to end moments or eccentrical loading are crucial for seismic performance. Therefore, New Zealand Concrete Design Code (NZS 3101) also provide equations for the transverse reinforcement design in the plastic-hinge region which have modification factor to consider the axial compressive load level and its related ultimate curvature deformation. This modification factor is found from the theoretical monotonic moment-curvature analysis using conservative stress-strain curves for normal strength confined concrete. Mander et al. (1984) and other researchers analyzed the concentric confined concrete loading test results and developed confined concrete stress-

127

strain models, considering the effect of the passive effective lateral confining pressure exerted by the transverse reinforcement on the core concrete.

A general review of different seismic design codes shows considerable differences in the reinforcement requirements for rectangular reinforced concrete columns, and specifically for high strength reinforced concrete columns, there is no specific design provisions in ACI318-95 or ACI318-99 Codes. However, in New Zealand Concrete Design Code, there is a design provision for high strength reinforced concrete columns. A recent journal publication by Park et. al. explains the differences in the shape of the stress block for high strength concrete in comparison to the that of normal strength concrete. Such difference stems from the fundamental differences in the material properties of high strength concrete as compared to normal strength concrete, where high strength concrete undergoes a brittle nature. With proper confinement, however, it has been found that the high strength concrete can provide sufficient ductility.

The confinement requirements of the ACI 318-99 Building Code for reinforced concrete columns were derived for normal-strength concrete columns and are not applicable to high-strength concrete columns. The design criterion of the ACI 318-99 assumes that confined columns maintain their concentric capacities after spalling of cover concrete by providing sufficient core concrete confinements.

128

The confinement is assumed to provide strength and ductility enhancements when subjected to seismic loads, maintaining overall strength and stability of a structure. The basis of the derivation of ACI 318-99 equations is as follows:

The strength gain in the core concrete provided by confinement is expressed as:

$\left(f_{cc}' - f_{co}'\right) = 4.1 f_l$ where f_l represents uniform passive confinement pressure for spirally reinforced circular column. The strength gain in the core equated to the concentric capacity of cover concrete. After a substitutions and simplifications, a required the volumetric ratio of ACI 318-99 code, $\rho_s = 0.45\left(\dfrac{A_g}{A_c} - 1\right)\dfrac{f_c'}{f_{yh}}$, is obtained. The lower bound of the expression, providing a limitation on A_g / A_c ratio, is expressed as $\rho_s = 0.12\dfrac{f_c'}{f_{yh}}$. For square and rectangular columns, the two equations are revised with an assumption of a one third increase in required steel to achieve the same deformabilities as that of circular columns. As a result the requirements of transverse steel for square or rectangular columns are expressed as follows:

$$A_{sh} \geq 0.3 s h_c \frac{f_c'}{f_{yh}}\left(\frac{A_g}{A_c} - 1\right) \qquad (3.2a)$$

129

or

$$A_{sh} \geq 0.09 s h_c \frac{f_c'}{f_{yh}}$$ (3.2b)

where A_{sh} is the total transverse steel cross-sectional area within the spacing s;

h_c is the cross-sectional dimension of the column core measured center-to-center

of the outermost peripheral hoops; f_c' is the specified compressive strength of

concrete; f_{yh} is the specified yield strength of the transverse reinforcement; A_g is

the gross area of the column section; and A_c is the cross-sectional area of a

column measured out-to-out of transverse reinforcement. In earlier versions of

the ACI 318 code, the hoop spacing is limited to ¼ of the minimum dimension of

the column or 100 mm (4 in.), whichever is smaller. The hoop spacing in the ACI

318-99 code, however, is changed to not exceeding: ¼ of the minimum dimension

of the member; six times the diameter of the longitudinal reinforcement; and s_x,

given as

$$s_x = 4 + \left(\frac{14 - h_x}{3} \right)$$ (3.3)

where h_x is the maximum horizontal spacing of hoop or crosstie legs on the faces

of the column, and both s_x and h_x are measured in inches. This change relaxed

the requirements of the transverse requirement spacing in the potential plastic

130

hinge region up to 150 mm (6 in.). As it can be observed in Figure 3.3, the ACI 318-99 requirements for transverse reinforcement remains almost the same except for a minor changes in the spacing requirements in the plastic hinge region.

Further, the ACI 318-99 equations does provide representation of experimental observations and performance criterias. It has been found that poorly confined columns designed based on ACI 318 requirements can be unsafe for axial load greater than 40% of the column concentric capacity P_o defined as:

$$0.85 f_c' \left(A_g - A_{sh} \right) + f_y A_{st} .$$

The equations 3.2a and 3.2b are based on an assumption that the efficiency of rectangular transverse reinforcements are approximately 75% of that of spiral transverse reinforcements.

The square columns represent a case of worst behavior among columns of various transverse reinforcement and longitudinal reinforcement arrangements for the same amount and spacing of confinement reinforcements. It is intended in this research to observe the behavior of square columns, to study available analytical models, and to consider design approaches based on the experimental results.

131

The above ACI provision is intended to maintain the ultimate strength of columns subjected to axial loading at concrete cover spalling. However, it does not take into consideration of the ductility or axial load level and the confinement requirements in the plastic hinge region.

3.2.4 New Zealand Code Provision

The New Zealand code considers the effect of different axial load level, while it aims to obtain a curvature ductility factor of at least 10 for highly ductile columns (NZS 3101, 1982).

According to New Zealand Seismic Code (NZS 3101:1982), the following are the requirements for transverse reinforcement in columns and piers in potential plastic hinge regions for rectangular hoops with or without supplementary cross-ties.

The area of hoops bars and supplementary cross-ties in each of the principal directions of the cross-section within spacing s_h shall not be less than the greater of

$$A_{sh} = 0.3 s_h h'' \left(\frac{A_g}{A_c} - 1 \right) \frac{f'_c}{f_{yh}} \left(0.5 + 1.25 \frac{P_e}{\phi f'_c A_g} \right) \qquad \text{(3.3a) (Code Equation 8.24a)}$$

or

$$A_{sh} = 0.12 s_h h'' \frac{f'_c}{f_{yh}} \left(0.5 + 1.25 \frac{P_e}{\phi f'_c A_g} \right)$$
(3.3b) (Code Equation 8.24b)

except that where permitted by section 6.5.4.3 (c) of aforementioned NZS code, A_{sh} may be reduced by one-half, allowing a 50% reduction for columns for frames protected against plastic hinging by capacity design procedures. Further, for columns and piers, section 6.5.1 states that the maximum design axial load in compression at a given eccentricity P_e shall not exceed $0.7\phi f'_c A_g$, unless it can be shown that P_e is less than $0.7\phi P_o$

where,

$$P_o = 0.85 f'_c \left(A_g - A_{st} \right) + f_y A_{st}$$
(3.4)

This limitation was found to ensure that the specified curvature ductility factor ϕ_u / ϕ_y in columns are available for axial compressive levels up to $0.7\phi f'_c A_g$.

133

The limitation of longitudinal reinforcement in columns and piers shall be as follows per section 6.5.4.2:

(a)   Area of longitudinal reinforcement shall be not less than 0.008 A_g.

(b)   Area of longitudinal reinforcement shall be not greater than 0.06 A_g for Grade 275 (ASTM Grade 40) steel nor greater than 0.045 for Grade 380 (ASTM Grade 55) steel, except that in the region of lap splices the total area shall not exceed 0.08 A_g for Grade 275 steel nor 0.06 A_g for Grade 380 steel.

NZS 3101:1995, New Zealand Concrete Structures Standard, Part 1- The Design of Concrete Structures further provides revised requirements for earthquake effects and are made more dependent on the level of axial loads. (NZS 3101, Part 1, 1995) The new requirement states that the transverse reinforcement in columns and piers shall conform to sections 7.5.4 and 7.5.5 which state that the area and limits on spacing and arrangement of rectangular hoops with or without supplementary cross ties in members shall conform to section 8.5.4.3 and to section 11.4.4 which state the horizontal joint shear reinforcement requirements for beam-column joints.

Per Section 8.5.4.3, the tranverse reinforcement shall be placed as follows:

134

(b)   In potential plastic hinge regions, as defined in 8.5.4.1, when rectangular hoops with or without supplementary cross-ties are used:

(i)   The total effective area of hoop bars and supplementary cross-ties in each of the principal directions of the cross section within spacing s_h shall not be less than that given by the greater of code equations 8-23 or 8-26.

$$A_{sh} = \frac{(1.3 - p_t m)s_h h^{"}}{3.3} \frac{A_g}{A_c} \frac{f_c^{'}}{f_{yt}} \frac{N^*}{\phi f_c^{'} A_g} - 0.006 s_h h^{"} \qquad (3.5)(Code\ Eq.\ 8-26)$$

where A_g / A_c shall not be permitted to be greater than 1.5 unless it can be shown that the design strength of the column core can resist the design actions and $p_t m$ shall not be taken greater than 0.4 and f_{yt} shall not be taken larger than 800 Mpa.

(ii)   The center-to-center spacing of hoop sets along the member shall no exceed the smaller of ¼ of the least lateral dimension of the cross section or 6 times the diameter of the longitudinal bar to be restrained.

135

(iii)   Each longitudinal bar or bundle of bars shall be laterally supported by the corner of a hoop having an included angle of not more than 135° or by a supplementary cross-tie, except that the following 2 cases of bars are exempt from this requirement:

(a)   Bars or bundles of bars which lie between 2 laterally supported bars or bundle of bars supported by the same hoop where the distance between the laterally supported bars or bundles of bars does not exceed the larger of ¼ of the adjacent lateral dimension of the cross section or 200 mm between centers.

(b)   Inner layers of reinforcing bars within the concrete core centered more than 75 mm from the inside of hoop bars.

(c)   In frames where columns are designed with sufficient strength to provide a high degree of protection against plastic hinging, the required quantity of transverse reinforcement placed in the regions of columns defined as potential plastic hinge regions in 8.5.4.1 shall be 70% of that required by equation 8-26 but not less than that required by equation 8-23, but all other provisions of 8.5.4 shall be conformed to.   This reduction in the quantity of transverse reinforcement in potential plastic hinge region shall not be permitted at the top and bottom of the

136

columns of the first story nor in any story in which a column sideway mechanism could occur with plastic hinges forming in the columns.

(d)   Outside potential plastic hinge regions of a column or pier the transverse reinforcement over the length of column or pier between the potential plastic hinge regions shall be as follows:

(i)   The center-to-center spacing of transverse reinforcement along the member shall not exceed the smaller of one-third of the diameter in the case of a circular cross section or one-third of the least lateral dimension in the case of a rectangular cross section, or 10 times the diameter of the longitudinal bar to be restrained.

(ii)   The quantity of transverse reinforcement shall not be less than 70% of that required in the potential plastic hinge region.

(e)   Spirals, hoops, and ties placed according to section 8.5.4.3 extending around longitudinal bars in the compression and tension faces of the member cross section shall be assumed to contribute to the shear strength of the member.

(f)   For column bars that are not restrained against buckling by beams, the distance between the first spiral, hoop or tie in the column and that within the

beam-column joint shall not exceed 6 times the diameter of the column bar to be restrained.

Per section 8.5.3.4, the transverse reinforcement in the form of stirrup-ties shall be placed in potential plastic hinge regions of beams, as defined in section 8.5.3.1, as follows:

(b)   The diameter of the stirrup-ties shall not be less than 5 mm(0.197 in.), and the area of one leg of a stirrup-tie in the direction of potential buckling of the longitudinal bars shall not be less than:

$$A_{te} = \frac{\sum A_b f_y}{96 f_{yt}} \frac{s}{d_b}$$
                                                                                    (3.6)(Code Eq. 8-23)

where $\sum A_b$ is the sum of the areas of the longitudinal bars reliant on the tie, including the tributary area of any bars exempted from being tied in accordance with section 8.5.3.4(a) and f_{yt} shall not be taken larger than 800 MPa (116 ksi). *Longitudinal bars centered more than 75 mm* (2.953 in.) *from the inner face of stirrup-ties need not be considered in determining the value of $\sum A_b$.*

138

In addition to the consideration of axial load level, the code recommend different transverse reinforcement for plastic hinge region and outside plastic hinge areas. A reduction of 70% in required transverse reinforcement placed in the plastic hinge regions is recommended when columns are designed such that it has sufficient strength to provide a high degree of protection against plastic hinging . Further, there is a separate requirements to provide sufficient amount to longitudinal bars in the plastic hinge region to prevent pre-mature longitudinal bar buckling.

According to New Zealand Concrete Structures Standard 1995 (NZS 3101), Part 2- Commentary on The Design of Concrete Structures, an interpretation of the newly revised requirements has been provided for the transverse reinforcements in consideration for levels of axial load and performance (NZS 3101, Part 2, 1995).

Per commentary section C8.5.4.3 (a) and (b), it is stated that Watson and Park have used the design charts for ductility derived by Zahn et. al. to obtain refined design equations for the quantities of transverse confining reinforcement required in the potential plastic hinge regions of reinforced concrete columns.

The following shows the basis of NZS transverse reinforcement requirements.

139

Typical ranges of the axial load ratio $N^*/f_c'A_g$, the concrete compressive strength f_c', the mechanical reinforcing ratio $p_t m$, and the cover ratios c/h for square and rectangular columns or c/D for circular columns, were considered, where c = concrete cover thickness and h and D = overall depth and diameter of rectangular or square and circular cross sections, respectively. The 95% upper-tail values of the area of transverse reinforcement obtained from the design charts and a regression analysis were used to obtain the best-fit equations by the least squares method.

The derived equation for rectangular column cross sections is as follows:

$$\frac{A_{sh}}{s_h h''} = \left\{ \frac{A_g}{A_c} \frac{\left\{ \left(\phi_U/\phi_Y \right) - 33 p_t m + 22 \right\}}{111} \frac{f_c'}{f_{yt}} \frac{N^*}{\phi f_c' A_g} \right\} - 0.006 \qquad \text{(3.7)(Code Eq. C8-4)}$$

where,

A_{sh} = total effective area of transverse bars in direction under consideration within center to center spacing of hoop sets s_h

$h^{"}$ = dimension of core of rectangular or square column at right angels to direction of transverse bars under consideration measured to the outside of the perimeter hoop (Note- The definition of $h^{"}$ permits $h^{"}$ to be measured to the outside of the perimeter hoop)

A_g = gross area of column

A_c = core are of column

ϕ_U / ϕ_Y = curvature ductility factor

$p_t = A_{st} / A_g$, A_{st} = total area of longitudinal column reinforcement,

$m = f_y / 0.85 f_c'$

f_y = lower characteristic strength yield strength of longitudinal steel

f_{yt} = lower characteristic strength yield strength of transverse steel

f_c' = concrete compressive cylinder strength

N^* = axial compressive load on column

ϕ = strength reduction factor

ρ_s = ratio of volume of transverse circular hoop or spiral steel to volume of concrete core of column

141

Code Excerpt:

A value of curvature ductility factor $\phi_U/\phi_Y = 20$ *could be used in the above*

equations when plastic hinging of ductile columns or piers is expected in a severe

earthquake. For example, at the bottom story of ductile building frames, or in the

columns of one or two story ductile frames where strong beam-weak column

design is permitted, or in ductile bridge piers where plastic hinging is expected in

a severe earthquake. Code Equations 8-24 and 8-26 were obtained from the

above equations by substituting $\phi_U/\phi_Y = 20$. *Unless special studies are*

undertaken the maximum curvature ductility factor ϕ_U/ϕ_Y *should not exceed or*

assumed to be greater than 20.

At low axial load levels the need of transverse reinforcement for concrete

confinement becomes less and the provision of sufficient transverse reinforcement

to prevent buckling of the longitudinal reinforcement becomes more critical. The

quantity of transverse reinforcement required to prevent buckling of longitudinal

reinforcement is given by equation 8-25 for spiral or circular hoop reinforcement

and by equation 8-23 for rectangular hoops or supplementary cross-ties. Code

equation 8.25 is not shown here since it is the outside the scope of this research.

142

The transverse reinforcement should not be less than the greater of that required for concrete confinement and restraint against bar buckling.

Equations 8-24 and 8-26 were derived for concrete with compressive strength f_c' up to 40 MPa (5.8 ksi.). Recently they have been shown to apply approximately to concrete with compressive strength f_c' up to 100 MPa (14.5 ksi.). Note that test on columns with f_c' of 100 MPa (14.5 ksi.) have shown that very high strength concrete is extremely brittle when not confined adequately and that the required confinement will be considerably greater than for normal strength concrete columns.

Section C8.5.4.3 (c): In order to take into account possible beam overstrength, higher mode effects and concurrent earthquake forces when determining the design actions for columns, it is considered that the amount of confining reinforcement can be reduced to 70% of that required by equations 8-24 and 8-26. This should allow the column to achieve a curvature ductility factor ϕ_U/ϕ_Y of at least 10 if necessary. However, protection against bar buckling is still required, and some concrete confinement is necessary, and hence all the other requirements of detailing of section 8.5.4 are still necessary.

143

The derivation of the NZS transversement reinforcement apparently assumes a maximum ductility level of about 20 for high levels of axial loads and provides sufficient transverse reinforcements for low levels of axial loads to prevent longitudinal bar buckling. The NZS equation is based on concrete strengths up to about 40 MPa (5,801 psi). However, it recently has been shown to apply approximately to high strength concrete columns. For high strength concrete columns, the required confinement will be considerably greater than for normal strength concrete columns. Thus, refined equations for high strength concrete were proposed based on cyclic moment-curvature analysis using the constitutive model of confined high strength concrete as follows:

Rectilinear Columns Confined by High Yield Strength Steel

$$\frac{A_{sh}}{s_h h_c} = \left(\frac{A_g}{A_c} \frac{\left(\phi_u / \phi_y \right) - 30\rho_t m + 22}{83.7} \frac{f_c'}{f_{yh}} \frac{P_e}{\phi f_c' A_g} \right) \tag{3.8}$$

144

Circular Column Confined by High Yield Strength Steel

$$\rho_s = \left(\frac{A_g}{A_c} \frac{\left(\frac{\phi_u}{\phi_y} \right) - 54.5 \rho_t m + 22}{78.7} \frac{f_c'}{f_{yh}} \frac{P_e}{\phi f_c' A_g} \right)$$

(3.9)

It has been found that the above proposed equations can allow the use of high yield joint confinement reinforcement up to 1300 MPa (188.5 ksi.) and the use of concrete compressive strength of up to 100 MPa (14.5 ksi.). It is recommended that when using high strength concrete, special attention should be paid to strength and stiffness degradation at the joint due to shear and bond stresses.

3.2.5 Sheikh, Shah, and Khoury Proposal

Bayrak and Sheikh Confinement Reinforcement Design Criteria

With very limited amount of experimental data available in the literature, following are reviews of currently available guidelines of confinement reinforcement design of ductile HSC columns.

With greater usage of HSC by design engineers, there has been a greater need to determine the ways to design for HSC columns. Further, both ACI 318-95 and ACI 318-99 do not consider the effect of different levels of axial load. Current New Zealand design code (NZS3101:1995), although it considers the effect of different levels of axial load, was derived based on experimental results using normal strength concrete (NSC).

In 1997, experiments were performed by Bayrak and Sheikh using large-scale reinforced concrete columns made from 72 Mpa (10.44 ksi) concrete which were tested under constant axial load and large cyclic inelastic lateral displacements. When the results were compared to previous experiments using similar specimens of concrete strengths between 31 and 55 Mpa (4.49 and 7.98 ksi), it has been found that the required amount of lateral steel was proportional to the strength of concrete for a certain column performance, measuring axial load levels as a fraction of P_O. Also, as for NSC columns, it has been found that the behavior of HSC column is substantially influenced by the provided rectangular tie confinement. These columns were tested under moderate to high axial load levels, from $\dfrac{P}{P_O}$ = 0.36 to 0.50. The reinforcing steel used to construct the specimens had yield stress in the range from 463 to 542 Mpa (67 to 78.6 ksi).

146

It was observed that the amount of provided lateral steel is proportional to the improvements in ductility, energy absorption, and dissipation capacity. On the other hand, the moment capacity was less proportional to the amount of the provided lateral steel.

In 1998, Bayrak and Sheikh performed further experiments using large-scale column specimens using ultra high strength concrete (UHSC) of strengths ranging from 101.8 to 102.2 MPa (14.76 to 14.8 ksi) with the same types of reinforcing steels that were used for their previous experiments in 1997 which was mentioned above. These columns were tested under relatively high levels of axial load levels, from $\dfrac{P}{P_O}$ = 0.48 to 0.50, since most of the concrete design codes allow high axial loads.

In 1997, Sheikh and Khoury performed experiments using NSC columns and proposed a procedure for the design of confinement reinforcements for a given ductile performance and axial load level. When this procedure was used to predict the amount of the required confinement for UHSC and HSC specimens tested by Bayrak and Sheikh in 1997 and 1998, it was found that its prediction was as much as 37% greater than the average experimental values. The original model by Sheikh and Khoury (1997) for NSC is as follows:

$$A_{sh} = \left[A_{sh(ACI)} \right] \bullet \alpha \bullet Y_P \bullet Y_\phi \qquad\qquad (3.10)$$

where,

$A_{sh(ACI)}$ = total cross-sectional area of rectilinear ties required by ACI 318-

95 code.

α = configuration efficiency factor

    (=1 when all longitudinal bars are laterally supported by tie bends)

    (>1 when some of the longitudinal bars are not supported by tie bends)

Y_P = parameter to take into account the axial load effect

$$= a_1 + a_2 \bullet \left(\frac{P}{P_O} \right) \bullet a_3 \qquad\qquad (3.5)$$

Y_ϕ = parameter to take into account sectional ductility demand

$$= a_4 \bullet \left(\mu_{\phi 80} \right) \bullet a_5 \qquad\qquad (3.6)$$

where,

a_1 to a_5 = constants that were evaluated performing a regression analysis

using results from test series in which f_c' ranged from 30 to 55 MPa (4.35 to 7.98

ksi.).

148

The curvature ductility factor, $\mu_{\phi 80}$, is obtained from the moment-curvature relationship of the column section in the plastic hinge region when the strength loss of the column is smaller than or equal to 20% of the maximum bending moment.

In order to apply the above procedure to specimens having concrete strengths ranging from 72 to 102 MPa (10.44 to 14.8 ksi.), Bayrak and Sheikh performed regression analysis using the results from their UHSC and HSC column experimental results. From the application of above equations to the specimens with concrete strengths between 72 and 102 MPa (10.44 to 14.8 ksi.), it was found that the constants a_1, a_2, and a_3, which considers the axial load effects, remained constant and constants a_4 and a_5, which considers the ductility effect, changed.

From regression analysis and least-squares analysis, a_4 and a_5 were determined to be 1/8.12 and 0.82, respectively, for concrete strengths ranging from 72 to 102 MPa (10.4 to 14.8 ksi). The average of the predicted curvature ductility ratios were roughly equal to the average experimental values using these values. Regression analysis for a_1, a_2, and a_3 were based on concrete strengths ranging from 30 to 102 MPa (4.35 to 14.8 ksi.).

149

The experimental result of Bayrak and Sheikh showed that the concrete strength did not significantly affect different axial load levels and lateral reinforcement. Also, the curvature ductility demand, which solely considers the strength loss of smaller or equal to 20% of the maximum bending moment, did not affect the overall behavior of columns.

In 1998, Bayrak and Sheikh proposed a design equation of confinement reinforcement which considers ductility requirement as well as the axial load level for High Strength concrete columns. The requirement amount of lateral reinforcement in tied columns are assumed to be:

$$A_{sh} = \left[A_{sh(ACI)}\right] \bullet \alpha \bullet \left[1 + 13\left(\frac{P}{P_O}\right)^5\right] \bullet \left[\frac{\left(\mu_{\phi 80}\right)^{0.82}}{8.12}\right] \qquad (3.11)$$

for $f_c' = 55$ MPa (7.98 ksi.) to over 100 MPa (14.5 ksi.)

For the proposed equation (3.7), the factor α can be assumed to be unity for columns in which a minimum of three longitudinal bars are effectively supported by tie corners on each face of the column and hooks are anchored into the core concrete. For HSC columns with high ductility, configuration which produces $\alpha = 1$ should be used.

150

When comparison of the area of the confinement reinforcement using ACI 318-95 is made to that using the proposed equation, it can be observed that ACI 318-95 does not consider the effect of different levels of axial load and the expected sectional performance or curvature ductility. At low levels of axial load, ACI provision does not provide sufficient levels of ductility. At axial load level of $0.5 P_O$, ACI 318-95 provides a curvature ductility factor that is not sufficiently high for highly ductile columns. For highly ductile HSC columns, the proposed equation requires larger amount of lateral reinforcements as compared to ACI code, even for low levels of axial load such as $0.2 P/P_O$.

It is recommended that for HSC with highly ductile performance, configuration which allows a value of $\alpha = 1$ should be used.

151

3.2.6 Comparison of Design Codes

Table 3.2 Transverse Reinforcement Provided in Comparison to ACI and New Zealand Code Requirements

Specimen	Ash(ACI) (in^2)	Ash(NZS) (in^2)	Ash,provided/Ash(ACI)	Ash, provided/Ash(NZS)
FHC1-0.2	1.09	0.97	0.86	0.96
FHC2-0.34	1.05	1.21	0.88	0.77
FHC3-0.22	1.12	1.04	0.83	0.90
FHC4-0.33	1.12	1.27	0.83	0.74
FHC5-0.2	1.63	1.46	0.57	0.64
FHC6-0.2	1.39	1.24	0.67	0.75

Note: A_{sh} Provided = 600 mm^2 (0.93 in^2)

Table 3.2 shows a comparison of amount of transverse reinforcements provided to those required by both ACI 318-95/99 and NZS 1995. All specimens were provided with less than

the transverse reinforcement requirement of both codes. It is apparent that ACI code does not require greater transverse reinforcements even for those specimens FF2 and FF4 which were subjected to higher levels of axial loads. NZS code, on the other hand, requires greater amount of steel for the specimens subjected to higher axial loads.

152

Fig. 3.4-Comparison of transverse reinforcement indexes for specimens, ACI318-95/99 Codes, and New Zealand (NZS 3101, 1995) Code Requirements.

Above comparison shows that NZS 3101 code requirements considers greater confinement for high axial load levels, where as ACI 318-95 and ACI 318-99 do not consider axial load levels into consideration. Further, ACI 318-95 and ACI 318-99 state that rectilinear transverse reinforcements improves ductility consistently. However, it has been considered difficult to express reliably the effect of rectilinear transverse reinforcement in terms of critical material properties. The code states that in general, more confinement should be provided per unit length of member for rectilinear confinement to provide confinement

153

comparable to that of spiral reinforcement. Neither NZS 3101 nor ACI 318-95/99 codes directly takes into account the seismic performance level of the specimens.

COMPARISON OF TRANSVERSE REINFORCEMENT INDEXES FOR BAYRAK AND SHEIKH REQUIREMENTS

The following confinement index versus column size charts show that the Bayrak and Sheikh criteria for providing confinement considers all column parameters and axial load levels as well as the performance level. They also provide a comparison between experimental and the required transverse confinement index based on seismic performance demand. The determination of performance-based confinement requires a section analysis of the specimens in the plastic hinge region to acquire their respective ductility performance levels when the strength loss of the column is smaller than or equal to 20% of the maximum bending moment. This has been accomplished, and it can be deduced from the charts that better performances can be achieved for lower axial load levels. In other words, the confinement index obtained based on the Bayrak and Sheikh performance-based criteria was higher for those specimens subjected to lower axial loads such as specimens FHC1-0.2, FHC3-0.22, FHC5-0.2, and FHC6-0.2. For specimens subjected to higher axial loads such as specimens FHC2-0.34 and FHC4-0.33, the confinement index decreased due to their lower ductility performance levels. In

154

comparison of specimens FHC5-0.2 and FHC6-0.2 with all parameters equal except for the yield stress of the transverse reinforcements [445 MPa (64.5 ksi.) and 524 MPa (76 ksi.), respectively], specimen FHC6-0.2 with greater transverse reinforcement yield stress and analytical ductility level had greater confinement index as shown on Figures 3.9 and 3.10. From these results it can be deduced that performance-based design of the specimens is important. Comparing Figures 3.5 and 3.6, it can be observed that for specimen FHC1-0.2, the required confinement is actually greater than that required for specimen FHC2-0.34 which is subjected to a higher axial load, because specimen FHC1-0.2 is analytically predicted to achieve greater ductility performance-level. In either case, it can be noticed that the transverse reinforcements provided for the specimens per ACI 318-95/99 requirement are greater than those required by Bayrak and Shiekh criteria. The similar pattern can be noticed for comparison between Figures 3.7 and 3.8 for specimens FHC3-0.22 and FHC4-0.33, respectively. In this case, specimen FHC3-0.22 requires greater confinement due to its higher ductility level although it is subjected to lower axial load level.

Figures 3.9 and 3.10 show a difference in the required confinement, even though both specimens FHC5-0.2 and FHC6-0.2 are subjected to the same axial loads and transverse reinforcement spacing. This is because according to Bayrak and Sheikh criteria, the specimen FHC6-0.2, which was provided with higher grade

155

transverse reinforcements, required greater confinement, as it is predicted to achieve greater ductility performance-level.
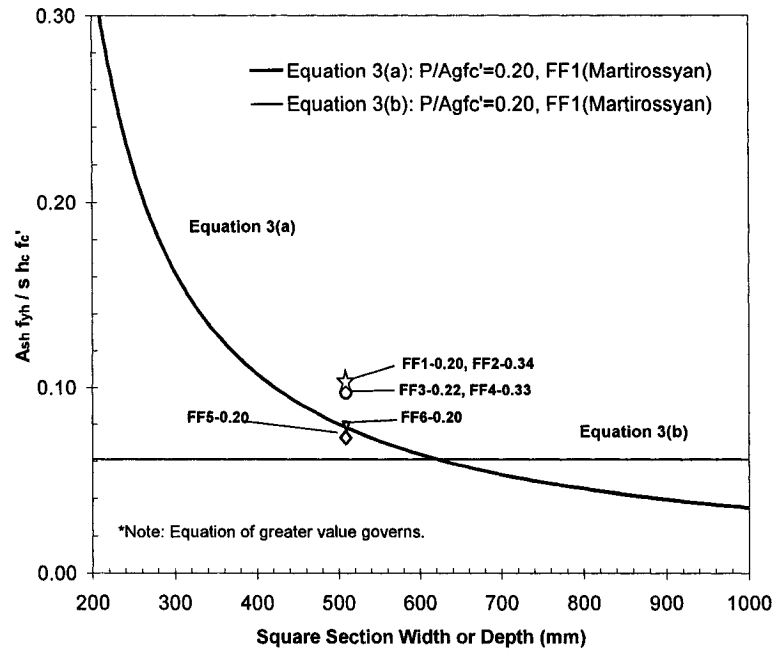
Fig. 3.5-Confinement index versus column section size per Bayrak and Sheikh criteria for specimen FHC1-0.2.
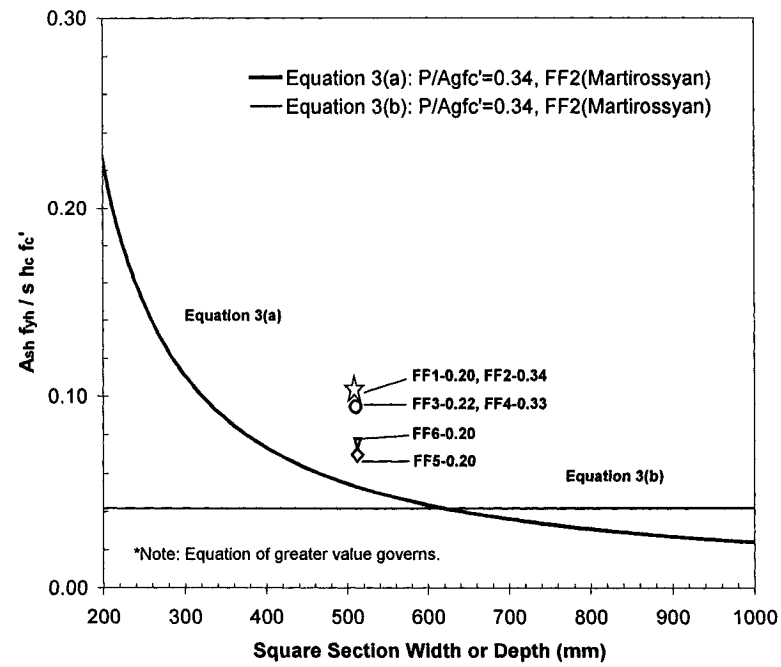
Fig. 3.6-Confinement index versus column section size per Bayrak and Sheikh criteria for specimen FHC2-0.34.

157
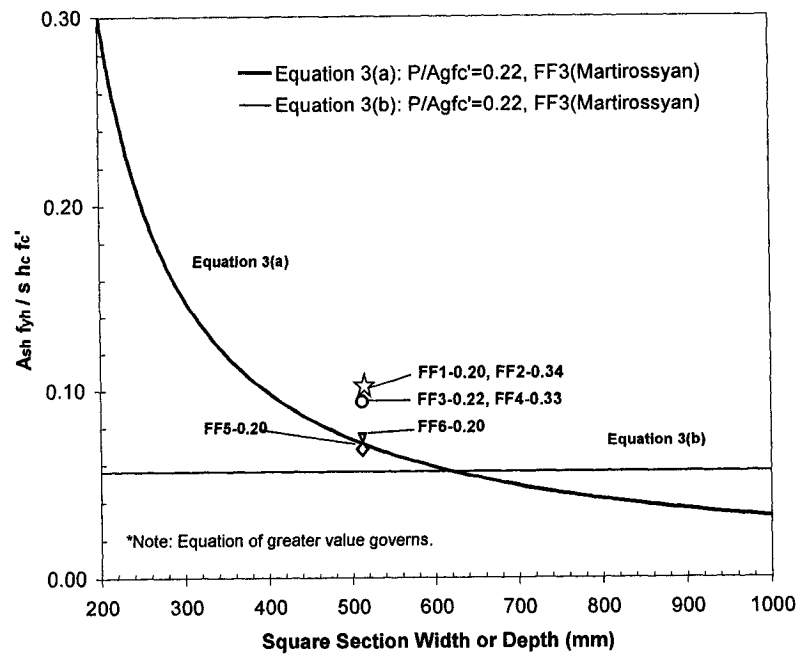
Fig. 3.7-Confinement index versus column section size per Bayrak and Sheikh criteria for specimen FHC3-0.22.

158
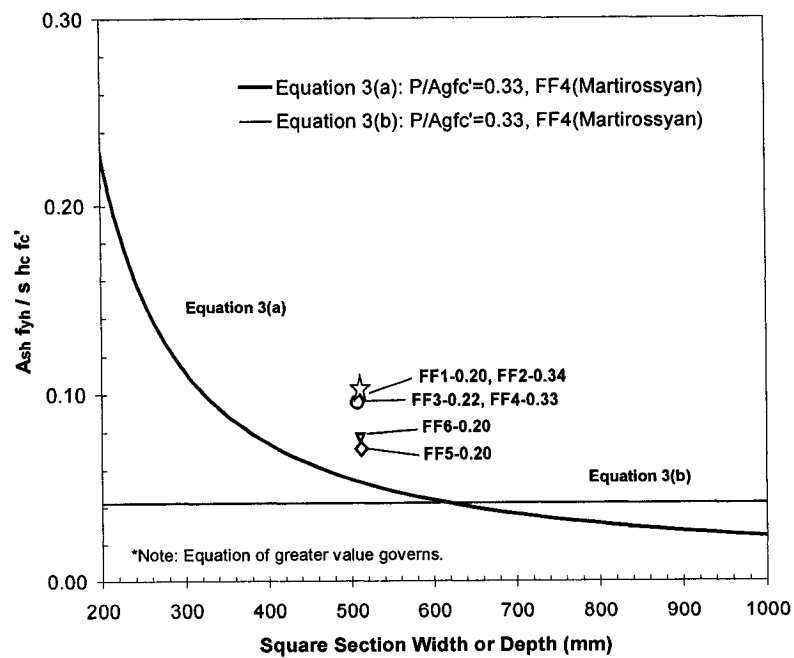
Fig. 3.8-Confinement index versus column section size per Bayrak and Sheikh criteria for specimen FHC4-0.33.

159
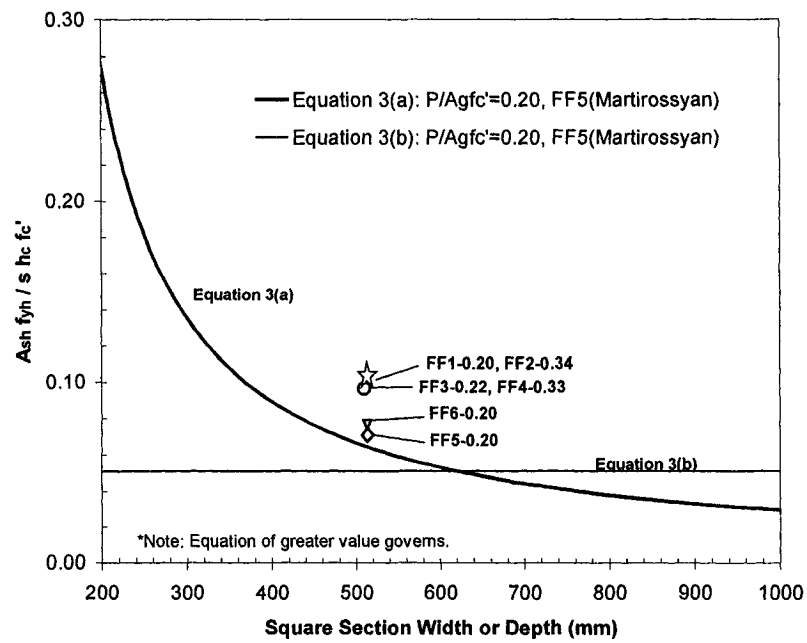
Fig. 3.9-Confinement index versus column section size per Bayrak and Sheikh criteria for specimen FHC5-0.2.

160
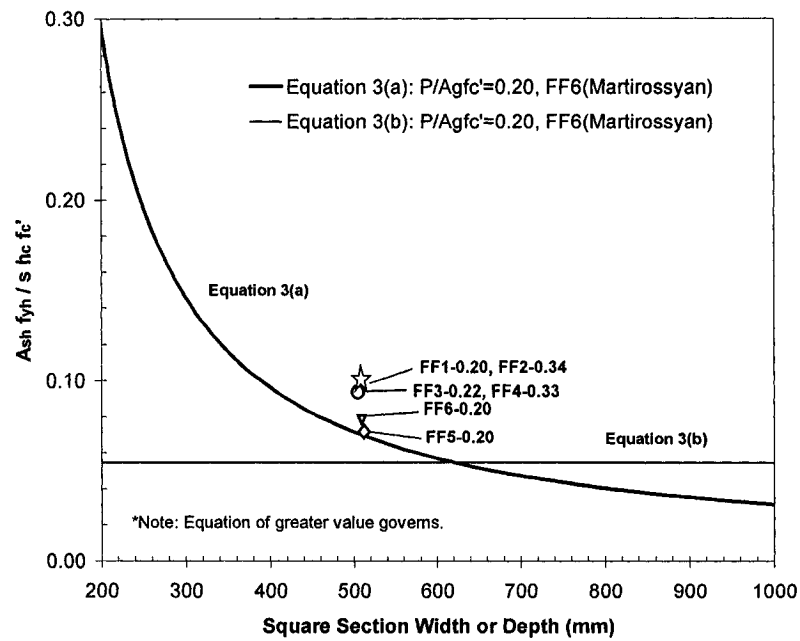
Fig. 3.10-Confinement index versus column section size per Bayrak and Sheikh criteria for specimen FHC6-0.2.

161

The NZS transverse reinforcement requirement for the seismic design of reinforced concrete columns considers axial load levels into consideration. The similar requirement based on Bayrak and Sheikh's criteria considers seismic performance levels as well as the axial load levels into consideration to determine the amount of transverse reinforcement of HSC columns. Using the moment-curvature relationships that are based on various confined HSC stress-strain relationships, the transverse reinforcement requirements are summarized in the Table 3.3.

Among the various stress-strain theories that are used in the moment-curvature program, one of the most recent models for HSC are those by Martirrosyan and Azizinamini. However, the classic Mander model still remains as the most fundamental theory although it is based on NSC tests.

From the observation of the various moment-curvature relationships integrating currently available HSC stress-strain models, it is apparent that some models show greater peak than others, and some of them have more abrupt drops after the peak values reached in comparison to others. However, the most recent models demonstrate more gradual drops in the capacity as column goes through various stages of behavior and with increase in curvature and displacement.

162

The crucial point is that different HSC models are based on various steel reinforcement configurations and properties, model sizes, axial load levels, and concrete strength. Therefore, it is necessary to compare various factors to determine which model is most appropriate to compare to the current full-scale experiment result.

The linear regression performed by Bayrak and Sheikh's proposal considers above mentioned factors into consideration. Therefore, it is most reasonable to compare Bayrak and Sheikh's model to the full-scale experimental results. The following Table 3.3 shows that transverse reinforcement required by Bayrak and Sheikh's critera is more conservative in comparison to NZS and ACI requirements for the specimens which were tested, especially for those specimens exerted by high axial load. Further, it considers the curvatures and displacement ductility as well as the steel configuration, shape of the column section, material properties of HSC concrete, and quantity of the lateral reinforcement and its configuration.

The combination of the most recent HSC confined stress-strain models, a moment-curvature relationship based on these models, the consideration of axial load levels and performance levels in terms of the ductility requirements, and the results of full-scale HSC column tests and its detailed analysis can provide a basis

163

for better future prediction of performance-based HSC behavior for seismic loading.

The Bayrak and Sheikh's transverse reinforcement requirement shown in Table 3.3 considers all of these factors into consideration and therefore its basis for design consideration is different from those of NZS and ACI requirements. The values shown on Table 3.2 for ACI and NZS requirements are shown in Table 3.3 for comparison.

Table 3.3-Transverse Reinforcement Comparison.

Specimen	FF1	FF2 (H)	FF3	FF4 (H)	FF5	FF6
Ash(ACI)	1.09	1.05	1.12	1.12	1.63	1.39
Ash(NZS)	0.97	1.21	1.04	1.27	1.46	1.24
Ash(Bayrak and Sheikh)						
Mander et. al.	2.07	1.13	2.0	1.13	1.86	1.92
Martirossyan	2.18	1.2	2.11	1.19	1.96	2.02
Li and Park(Bing et. al. 1994)	1.44	1.14	2.0	1.13	1.86	1.92
Cusson and Paultre	0.61	1.19	2.09	1.18	1.95	2.01
Young et. al.	0.24	1.13	2.0	1.13	1.86	1.92
Azizinamini et. al.	0.82	1.13	2.0	1.13	1.86	1.92
Ash, provided/Ash(ACI)	0.86	0.88	0.83	0.83	0.57	0.67
Ash, provided/Ash(NZS)	0.96	0.77	0.9	0.74	0.64	0.75
Ash, provided/Ash(Bayrak and Sheikh)						
Mander	0.45	0.82	0.47	0.82	0.5	0.49
Martirossyan	0.43	0.78	0.44	0.78	0.47	0.46
Li and Park(Bing et. al. 1994)	0.64	0.82	0.46	0.82	0.5	0.48
Cusson and Paultre	1.52	0.78	0.44	0.79	0.48	0.46
Young et. al.	3.92	0.82	0.47	0.82	0.5	0.49
Azizinamini et. al.	1.14	0.82	0.47	0.82	0.5	0.49

Note: All values are in units of in^2 unless otherwise noted.
A_{sh} Provided = 600 mm^2 (0.93 in^2)   (H) Denotes High Axial Loads

164

Evaluation based on Bing et. al. 2001 and Razvi and Saatcioglu (1999) models will be added.

The performance-based transverse reinforcement by Bayrak and Sheikh varies depending the ultimate ductility of each specimen and based on which mechanism is predicted to fail first using the column section analysis which will be introduced later. In general, after performing the column section analysis for each specimen, the performance-based transverse reinforcement required for each specimen is shown in Table 3.3. Greater the axial load level, less transverse reinforcement, A_{sh}, was needed due to lower analytical ductility level achieved; those specimens subjected to high levels of axial loads achieved lower ultimate curvature ductility. Also, it can be observed that when greater transverse reinforcement spacing is proposed, less A_{sh} is needed since greater spacing resulted in lower performance level. For those specimens with greater transverse reinforcement yield stress, more A_{sh} seems to be needed to accommodate greater curvature ductility. Those specimens with greater unconfined concrete strength seems to require less A_{sh} due to greater effective confinement provided by increased concrete strength. Thus, all parameters including the anticipated ductility level have impact on the amount of confinement required in design.

165

Table 3.4 Summary of transverse reinforcement requirements.

Requirement / Variables	ACI 318	NZS 3101	Bayrak and Sheikh
Transverse Reinforcement	A_{sh}	A_{sh}	A_{sh}
Yield Stress, Axial Load Level	f_y, Not Applicable	$f_y, \dfrac{P}{P_o}$	$f_y, \dfrac{P}{P_o}$
Seismic Performance Level	Not Applicable	Ductility of up to 20 assumed	Ductility Level obtained from $M - \phi$ relationship

Table 3.4 shows the fundamental differences between currently available seismic requirements for transverse reinforcements of reinforced concrete columns. Where ACI and NZS codes are based on normal strength concrete testing, Bayrak and Sheikh requirements are based on high-strength concrete testing. Further, Bayrak and Sheikh approach considers analytical performance-levels into consideration.

166

3.3 SPECIMEN CONSTRUCTION AND DETAILS

Construction of the specimens was carried out at the Structural Laboratory of the University of Southern California. The six columns were divided into two groups with three specimens in each group for construction. The reinforcing bars were manufactured

by a local reinforcing steel manufacturer, and the steel caging was carried out by professional iron workers. Fig.3.11 shows the preparations of the steel cages. Forms were prepared by the research team. Column stubs were formed and cast first, as shown in Fig.3.12 (a). After curing the column stubs for more than one week, the columns were formed as shown in Fig.3.12 (b). Casting of concrete also took place in the laboratory using ready-mix HSC from a local ready-mix concrete plant. After casting, the top concrete surfaces of the specimens were kept moist using wet burlaps for one week to avoid cracking due to shrinkage. As shown in Fig. 3.12 (c), the forms were removed two weeks after casting. Then, the specimens were cured in an air-dry condition until testing.

167

3.4 MATERIAL PROPERTIES

3.4.1 Concrete Strength

Material strengths for various specimens are also summarized in Table 3.6. The HSC was supplied by a local ready-mix concrete plant. Proportions for 1 m^3 HSC were 187 kg water; 415 kg cement; 148 kg Class-F fly ash; 45 kg silica fume; 868 kg coarse aggregates; and 710 kg fine aggregates. The water-to-cementitious materials ratio was 30%. Superplasticizer was also used to improve workability and setting time. The average slump at casting was 150 mm (6 in.). The average concrete strength at the test age was 64.1 MPa (9.3 ksi.). It should be pointed out that the mix proportion was developed based on extensive trial mixes conducted at the University of Southern California using materials available to Southern California which is one of the regions with highest seismicity in the US. The strength level yielded by this mix typically doubles the upper strength limit of 34.5 MPa (5 ksi.) permitted for general use of concrete in seismic resisting elements by the City of Los Angeles (according to an internal memo of Los Angeles city).

Note that the concrete strength values shown in Table 3.6 were based on compression tests on concrete cylinders with 150 mm (6 in.) diameter and 300 mm (12 in.) height. They were prepared and cured at the site of construction. Fig.

168

3.13(a) shows the strength development of concrete for the first three-specimen group. For the construction of the second group, the cylinders were cured both in the air-dry condition at the construction site and in standard curing condition using curing tank that contains water at a constant temperature.

Quite significant difference can be seen in Fig. 3.13(b) for concrete strength obtained from cylinders with different curing conditions. Such drastic discrepancy hints the urgent need to investigate the actual strength development in HSC structural elements in the near future. For current study, it is assumed that the concrete strength of air-cured cylinders approximately represents the actual strength.

Grade 420 (ASTM A615 Grade 60) steel was used for longitudinal reinforcing bars throughout all six columns and for transverse reinforcements in three of the six specimens. The other three specimens (FHC3-0.22, FHC4-0.33, and FHC6-0.2) had Grade 520 (ASTM Grade 75) bars for transverse reinforcement.

169
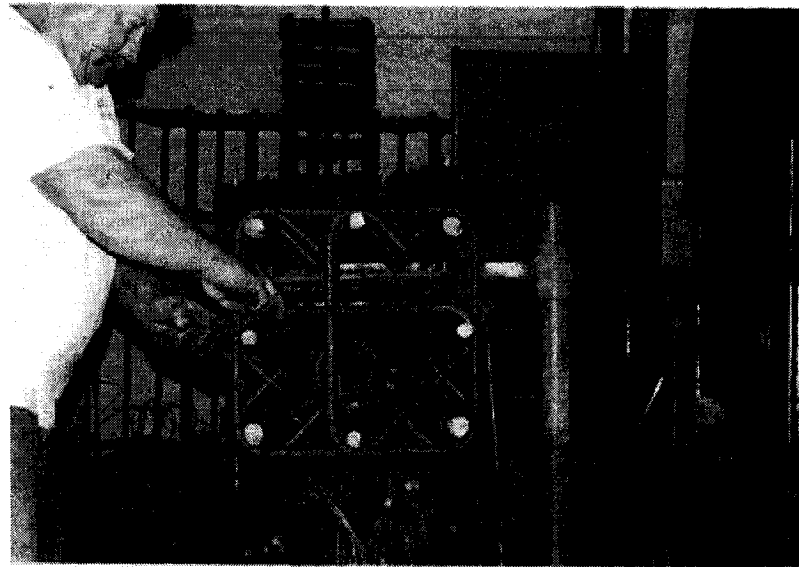
Fig. 3.11-Preparation of steel cages.

170
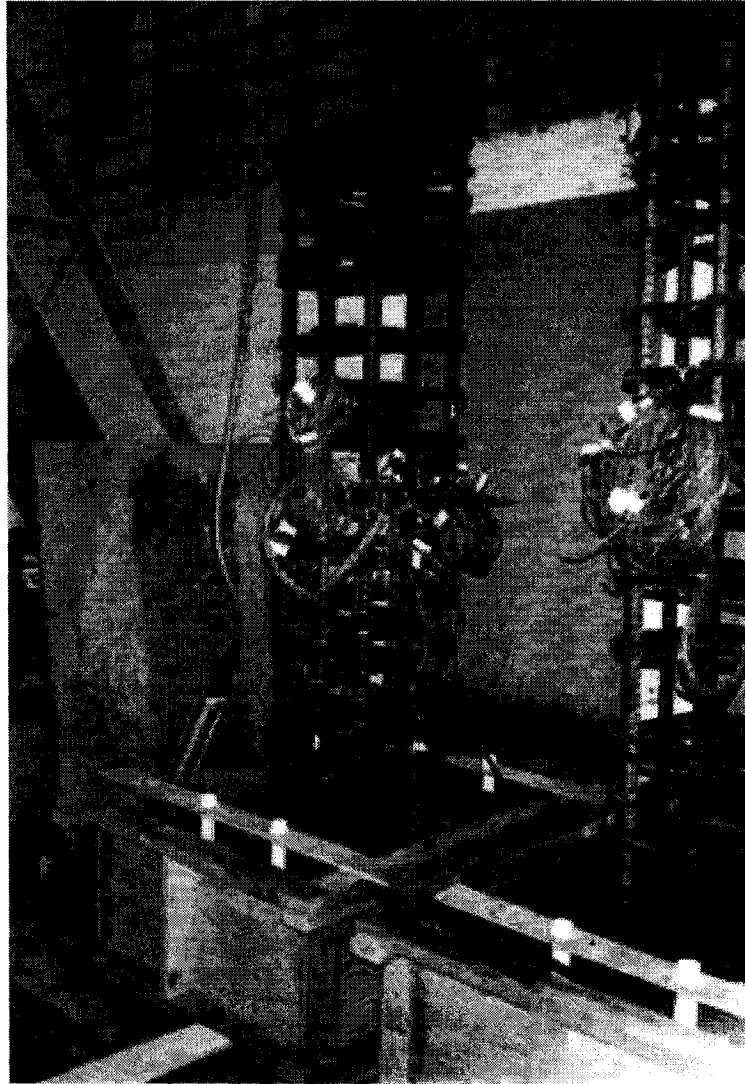
Fig. 3.12(a)-Formwork for column stub.

171

Fig. 3.12(b)-Formwork for columns (continued).

FIG. 3.12(c)-Columns after construction.

172

Compressive Strength
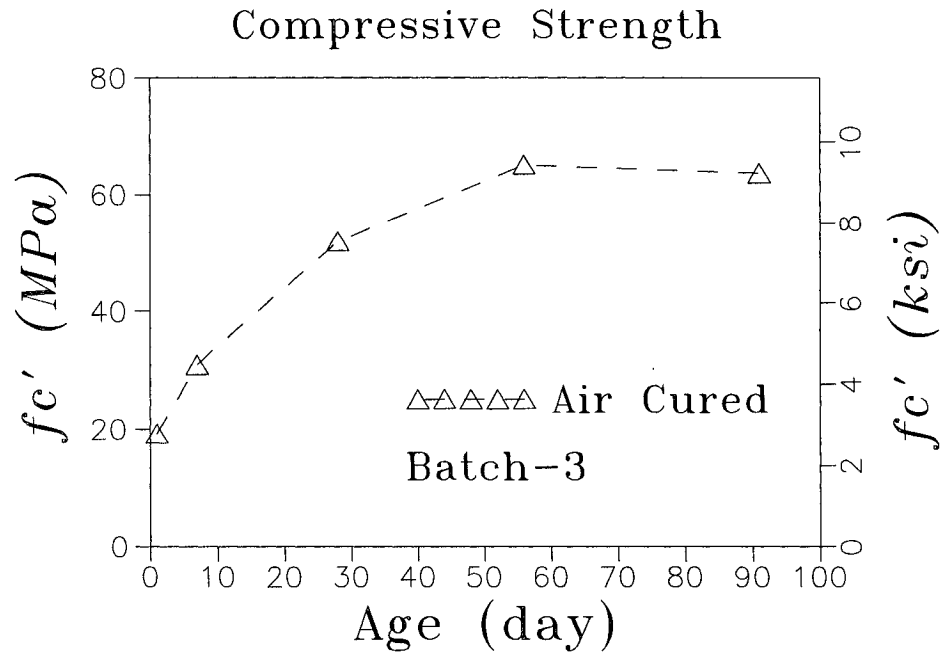
(a) For FHC1-0.2, FHC5-0.2, and FHC6-0.2 (Air-Cured Only)

Compressive Strength
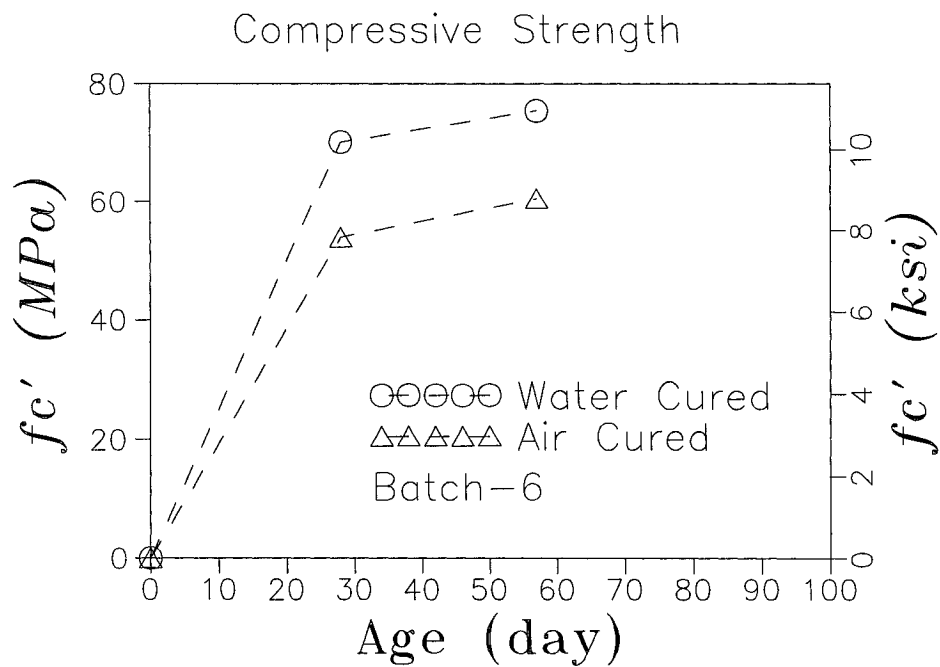
(b) For FHC2-0.34, FHC3-0.22, and FHC4-0.33 (Water and Air Cured)

Fig. 3.13-Compressive strength development of high-strength concrete

173

3.4.2 Stress versus Strain Behavior

In order to determine the true stress-strain behaviors of the steel reinforcements, a series of tensile tests were conducted in order to measure strain directly from the strain gauge which was installed on individual bar, where strain was also measured by the 600 kip SATEC machine simultaneously. From the test result, the Young's Modulus and the Yield Strains were accurately obtained using a force cell of 2669 kN (600 kip) SATEC machine and strain gages. No. 16 (#5) bars ultimately deformed over 25 mm (1 in.), and No. 29 (#9) or No. 36 (No. 11) bars deformed as much as over 75 mm (3 in.) until they ruptured. This far exceeded the specified strain limitation of the strain gauges. Therefore, the strain measurement was interrupted from a specific strain values typically at strains greater than approximately 0.06. However, the complete test data for the full range of tensile load and strains until the bars reached the ultimate failure were simultaneously obtained using the 2669 kN (600 kip) SATEC machine mentioned above. The ultimate tensile strength, f_U was obtained from the SATEC machine data. The values of the Young's Modulus were obtained from the slope of the true stress-strain curves which are shown in the following section. The following is the summary of the test results.

174

TABLE 3.5-Steel reinforcement yield properties.

Grade 75, #5					
Bar Specimen Code	Yield Stress f_y, MPa (ksi)	Ultimate Tensile Strength, f_U MPa (ksi)	Young's Modulus E, MPa (ksi)	Yield Strain ε (in/in)	
75HC5-1	544 (78.9)	754 (109.3)	173740 (25198)	0.003131	
75HC5-2	534 (77.4)	789 (114.4)	170596 (24742)	0.003128	
75HC5-3	478 (69.3)	758 (109.9)	164425 (23847)	0.002906	ε (in/in)
75HC5-4	480 (69.6)	754 (109.3)	166094 (24089)	0.002889	From Avg.
Average:	509 (73.8)	763 (110.7)	168714 (24469)	0.003013699	**0.003016**
Grade 60, #5					
Bar Specimen Code	Yield Stress f_y (ksi)	Ultimate Tensile Strength, f_U (ksi)	Young's Modulus E (ksi)	Yield Strain ε (in/in)	
60HC5-1	452 (65.6)	801 (116.2)	187041 (27127)	0.002418	
60HC5-2	400 (58)	803 (116.4)	142602 (20682)	0.002804	ε (in/in)
60HC5-3	407 (59)	772 (111.9)	159440 (23124)	0.002551	From Avg..
Average:	420 (60.9)	792 (114.8)	163025 (23644)	0.002591363	**0.002574**
Grade 60, #9					
Bar Specimen Code	Yield Stress f_y (ksi)	Ultimate Tensile Strength, f_U (ksi)	Young's Modulus E (ksi)	Yield Strain ε (in/in)	
60HC9-1	456 (66.13)	754 (109.4)	177498 (25743)	0.002569	
60HSC9-1	459 (66.6)	752 (109.1)	191260 (27739)	0.002401	ε (in/in)
60HSC9-2	483 (70.1)	751 (108.9)	221281 (32093)	0.002184	From Avg.
Average:	466 (67.6)	752 (109.1)	196680 (28525)	0.002384694	**0.00237**
Grade 60, #11					
Bar Specimen Code	Yield Stress f_y (ksi)	Ultimate Tensile Strength, f_U (ksi)	Young's Modulus E (ksi)	Yield Strain ε (in/in)	
60HC11-1	475 (68.89)	780 (113.1)	178360 (25868)	0.002663	
60HC11-1A	464 (67.28)	812 (117.7)	177491 (25742)	0.002614	ε (in/in)
60HC11-3	471 (68.35)	777 (112.7)	210146 (30478)	0.002243	From Avg.
Average:	470 (68.2)	789 (114.5)	188668 (27363)	0.002506455	**0.002491**

Note: The strain values in bold are calculated from the average values of the Yield Stress and Young's Modulus. These values were used to locate the yielding points of the specimens.

175

3.4.3 No. 16 (#5), No. 29 (#9), and No. 36 (#11) Grade 420(60) or 520(75) Steel Reinforcements

Figure 3.14 shows typical true stress-strain behavior of No. 16(#5), No. 29(#9), and No. 36(#11) steel reinforcements which were obtained by performing the tensile tests. Both grades 420 and 520 (ASTM grade 60 and 75) were tested. The first number in the specimens designations show the grade type in English unit.

Legend:
— 60HC5-1
— — 75HC5-2
- - - 60HSC9-2
— 60HC11-3
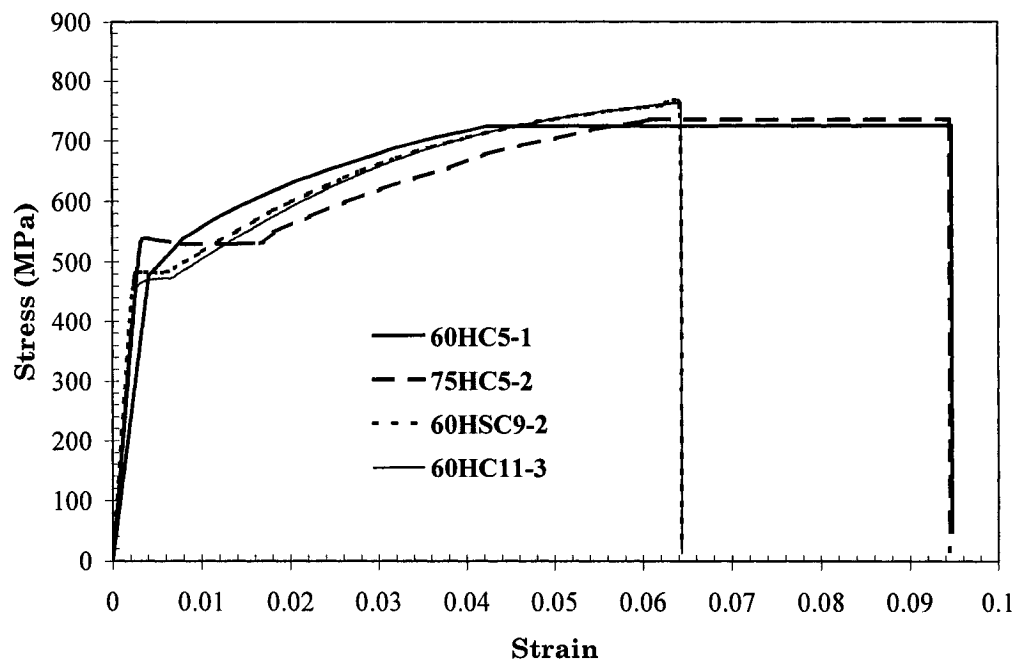
Fig. 3.14-Experimental steel tensile stress versus strain relationship.

176

For Grade 420 No. 16 (ASTM Grade 60 #5) steel bars, 0.001 strain offset method was used to determine the Young's Modulus and the Yield Stress. For all other steel bars, the Yield Stress values were also obtained directly from the Fig 3.14.

177

Table 3.6-Specimen parameters.

Specimen	Logitudinal Reinforcement	Transverse Reinforcement	Concrete Compressive Strength, f'_c	Applied Axial Load Ratio
FHC1-0.2	4 No. 29 (#9) 4 No. 36 (#11) f_y = 473 Mpa (68.6 ksi)	No. 16 (#5) @ 100mm=4 inches f_y =445 Mpa (64.54 ksi)	64.1 Mpa (9.3 ksi)	$\dfrac{P}{A_g f'_c} = 0.2$ P=3331.7 kN (749 kips)
FHC2-0.34	4 No. 29 (#9) 4 No. 36 (#11) f_y = 473 Mpa (68.6 ksi)	No. 16 (#5) @ 100mm=4 inches f_y =445 Mpa (64.54 ksi)	62.1 Mpa (9.0 ksi)	$\dfrac{P}{A_g f'_c} = 0.34$ P=5450.85 kN (1225.4 kips)
FHC3-0.22	4 No. 29 (#9) 4 No. 36 (#11) f_y = 473 Mpa (68.6 ksi)	No. 16 (#5) @ 125mm=5 inches f_y =524 Mpa (76 ksi)	62.1 Mpa (9.0 ksi)	$\dfrac{P}{A_g f'_c} = 0.22$ P=3526.9 kN (792.9 kips)
FHC4-0.33	4 No. 29 (#9) 4 No. 36 (#11) f_y = 473 Mpa (68.6 ksi)	No. 16 (#5) @ 125mm=5 inches f_y =525 Mpa (76.14 ksi)	62.1 Mpa (9.0 ksi)	$\dfrac{P}{A_g f'_c} = 0.33$ P=5290.27 kN (1189.3 kips)
FHC5-0.20	4 No. 29 (#9) 4 No. 36 (#11) f_y = 473 Mpa (68.6 ksi)	No. 16 (#5) @ 150mm=6 inches f_y =445 Mpa (64.54 ksi)	64.1 Mpa (9.3 ksi)	$\dfrac{P}{A_g f'_c} = 0.20$ P=3331.7 kN (749 kips)
FHC6-0.20	4 No. 29 (#9) 4 No. 36 (#11) f_y = 473 Mpa (68.6 ksi)	No. 16 (#5) @ 150mm=6 inches f_y =524 Mpa (76 ksi)	64.1 Mpa (9.3 ksi)	$\dfrac{P}{A_g f'_c} = 0.20$ P=3331.7 kN (749 kips)

178

3.5 EXPERIMENTAL SETUP

A testing system that enables the testing of high-strength concrete columns in full-scale model has been recently developed at the University of Southern California. As shown in Fig.3.15(a), the testing system utilizes two actuators with 1,334 kN (300 kip) capacity for cyclic loading in both lateral and axial directions of the column specimen. An axial force

as large as 6,000 kN (about 1,300 kip) can be loaded to the specimen through a specially

designed lever arm that amplifies the force output of the vertical actuator by six times. Fig.3.15(b) schematically illustrates the concepts of the lever arm system for axial loading. As shown in Fig.3.15(b), by setting the distance between the axis of vertical connectors and the column axis to be 1/5 of the distance between the vertical actuator and the column axis, a force of 5 times the actuator force can be generated in the vertical connectors. By considering the vertical equilibrium condition of the lever arm, one can easily understand that the applied axial load to the column specimen is 6 times of the vertical actuator force.

As also shown in Fig.3.15(b), if a lateral displacement Δ is induced, the applied axial load becomes inclined, and thus the true vertical load subjected by the column is the vertical component of the applied axial load. It can be shown that

179

for small deformation, the true vertical load and the applied axial load can be considered approximately the same. On the other hand, the inclination of the applied axial load corresponding to Δ also has a horizontal component. Because this horizontal component is not negligible comparing with the lateral load capacity of the column, it must be subtracted from the applied lateral load to obtain the true lateral force carried by the column specimen.

Fig. 3.15(c) illustrates the concept of the horizontal and vertical components of the applied loads which are calculated based on angle α', where L' is considered as the corresponding length of the column. The test setup and a completed formwork are shown in Figures 3.16 (a) and (b).

3.6 INSTRUMENTATION

Calibrated load cells were used to monitor the applied forces. The lateral displacement at the application point of the lateral load was measured by a 500mm stroke linear potentiometer. Six pairs of liner potentiometers, as shown in Fig.3.17 and 3.19(b), were mounted near the lower end of the column on the two faces in the loading direction to measure the average curvatures. Electrical-resistance strain gauges were mounted on the surfaces of the longitudinal

180

reinforcing and transverse bars at selected positions in the column specimen, as shown in Fig.3.18 and 3.19(a).

3.7 LOADING PROCEDURE

During the testing, the axial load was maintained approximately constant, whereas the lateral force was cycled based on lateral displacement control. One loading cycle was applied corresponding to an increment of 0.25% drift ratio, Δ/H, until $\Delta/H=1\%$ was reached. Three loading cycles were attempted for each of the drift ratios, $\Delta/H=1\%$, 1.5%, 2%, 3%, 4%, and 6% as shown in Fig.3.20. For specimen HSC-FF1-0.2, an additional cycle at 8% drift was also attempted.

181
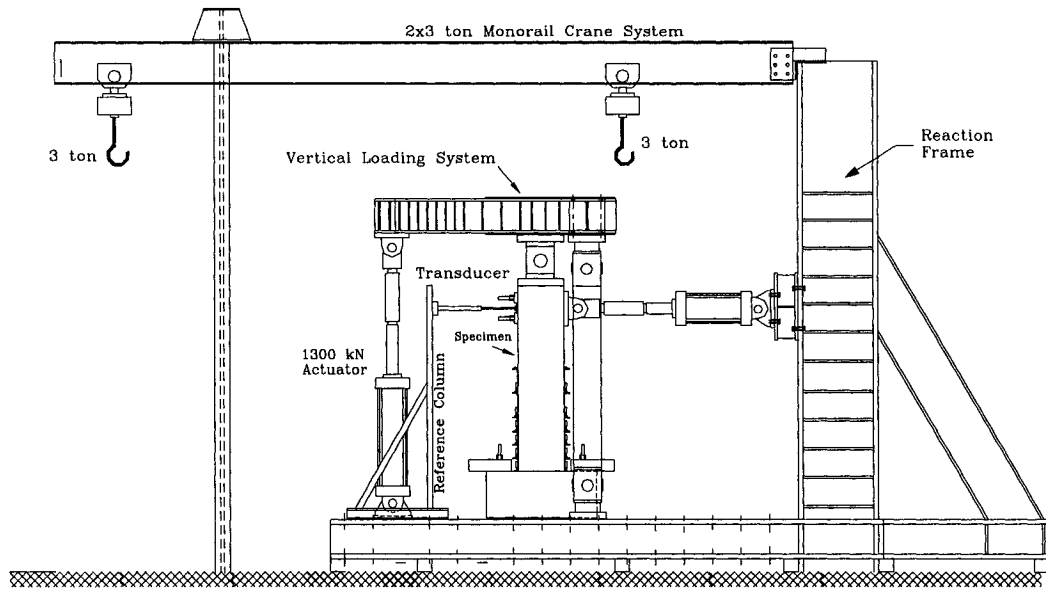
Fig. 3.15(a)-Test frame setup.
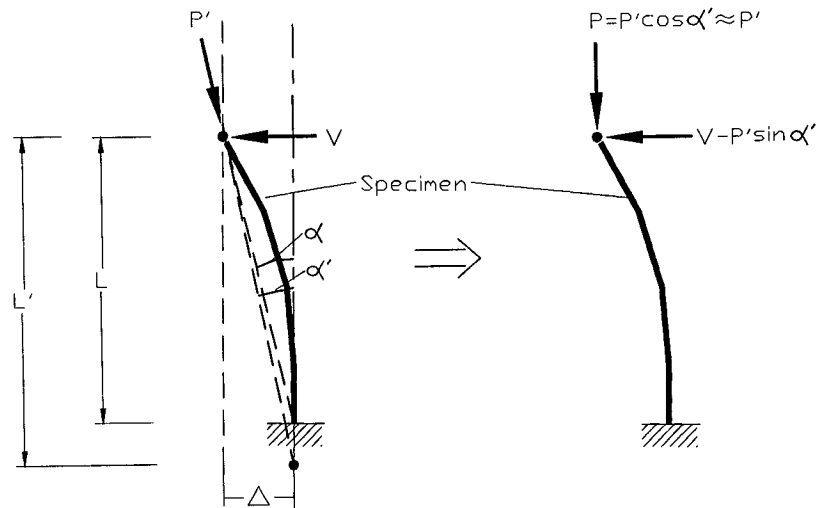
Fig. 3.15(b)-Horizontal and vertical components of the applied axial load.

182
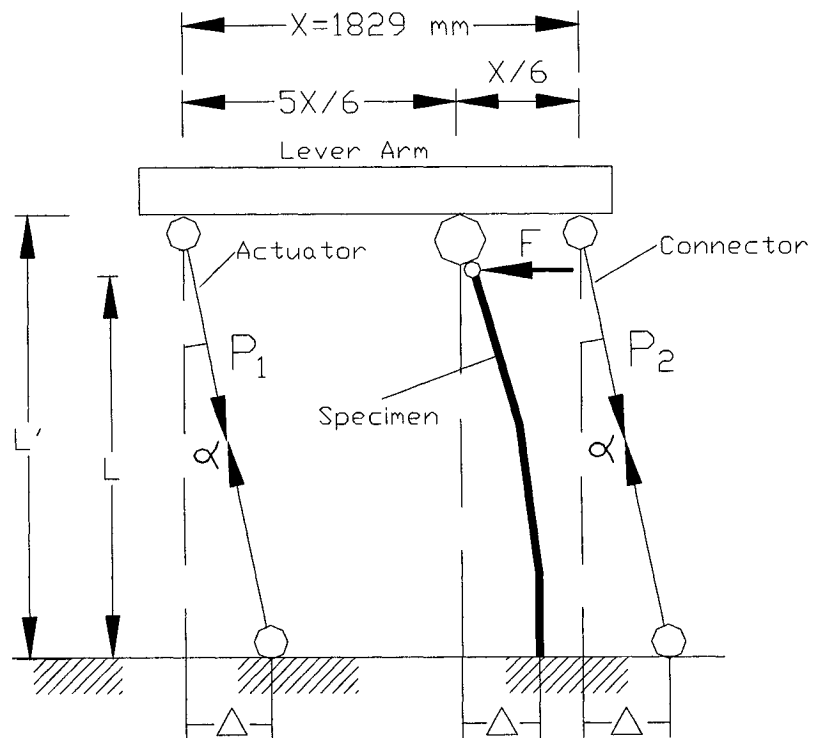
Fig. 3.15(c)-Lever arm system for axial loading.

Fig. 3.16- Test setup.

183

Loading Direction

Loading Direction

203

A–A

A   A

Linear Potentiometer

254

254

127

127

127

127
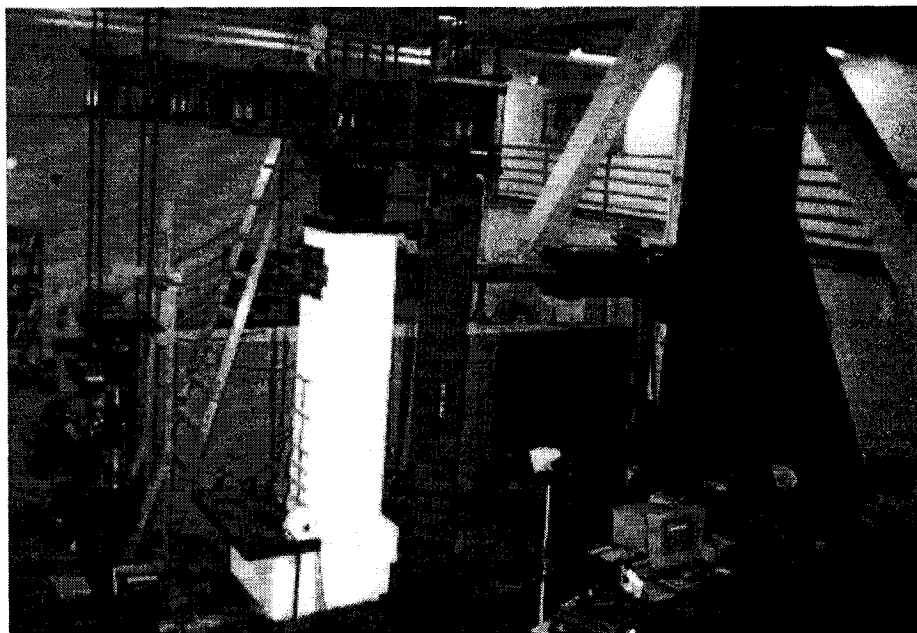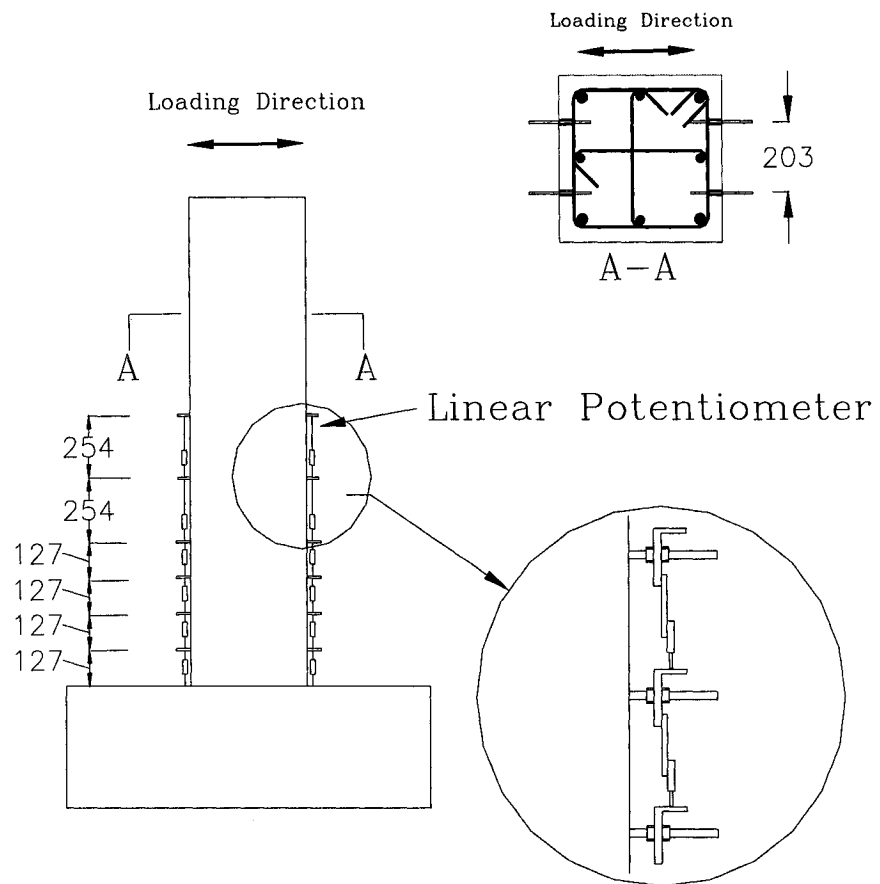
All Dimensions are in mm

Fig. 3.17-Vertical Linear Potentiometers.

184
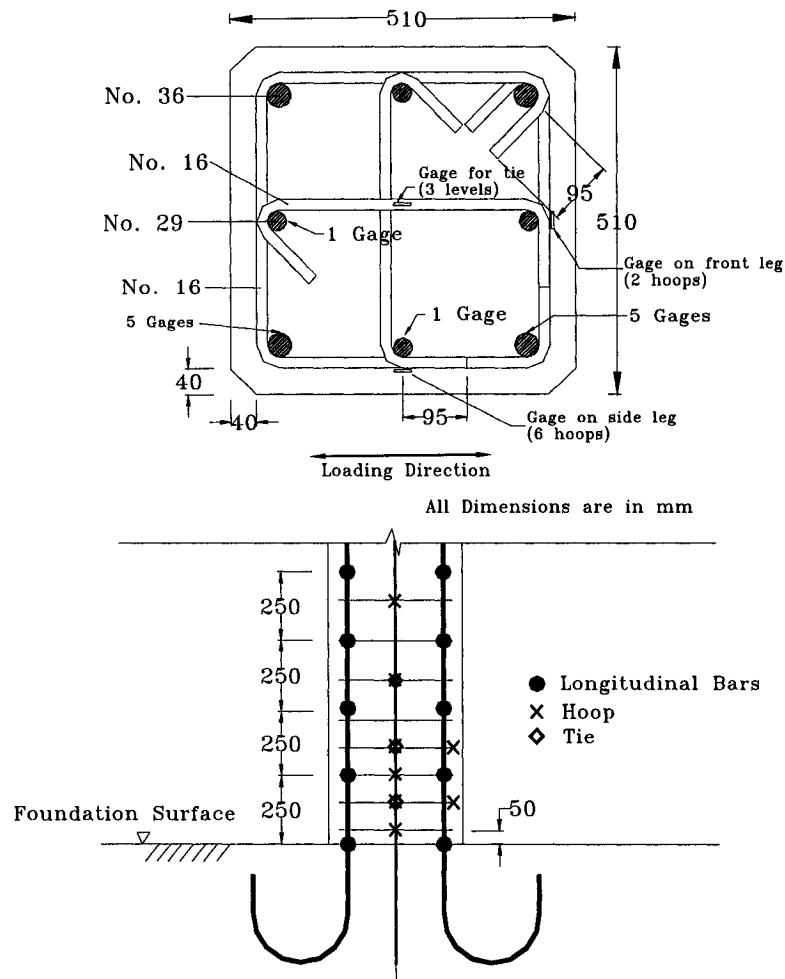
Fig. 3.18-Strain gage locations.

185
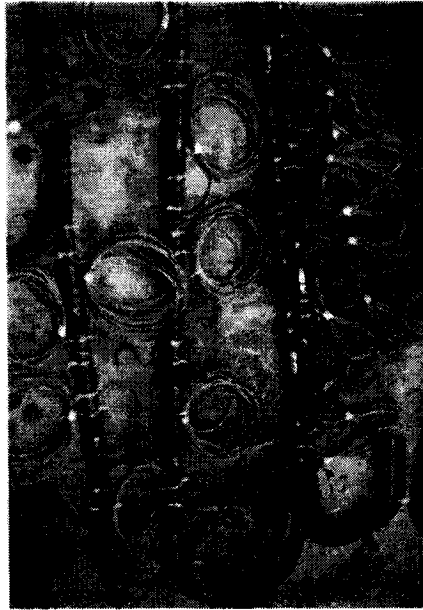
(a)
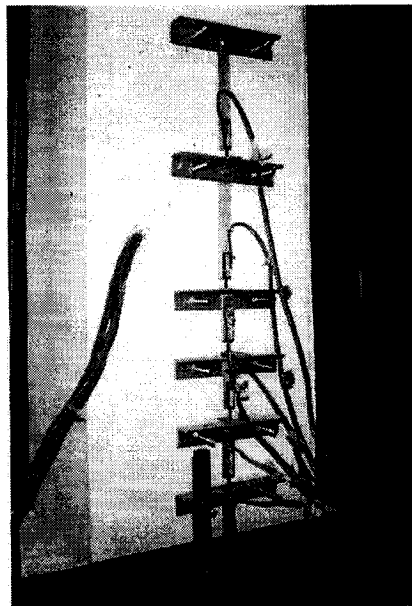
(b)

Fig. 3.19-Instrumentations: (a) Strain Gages Installed on Longitudinal Bars; (b) Installed Vertical Linear Potentiometers.

186

Drift Ratio versus Number of Cycles
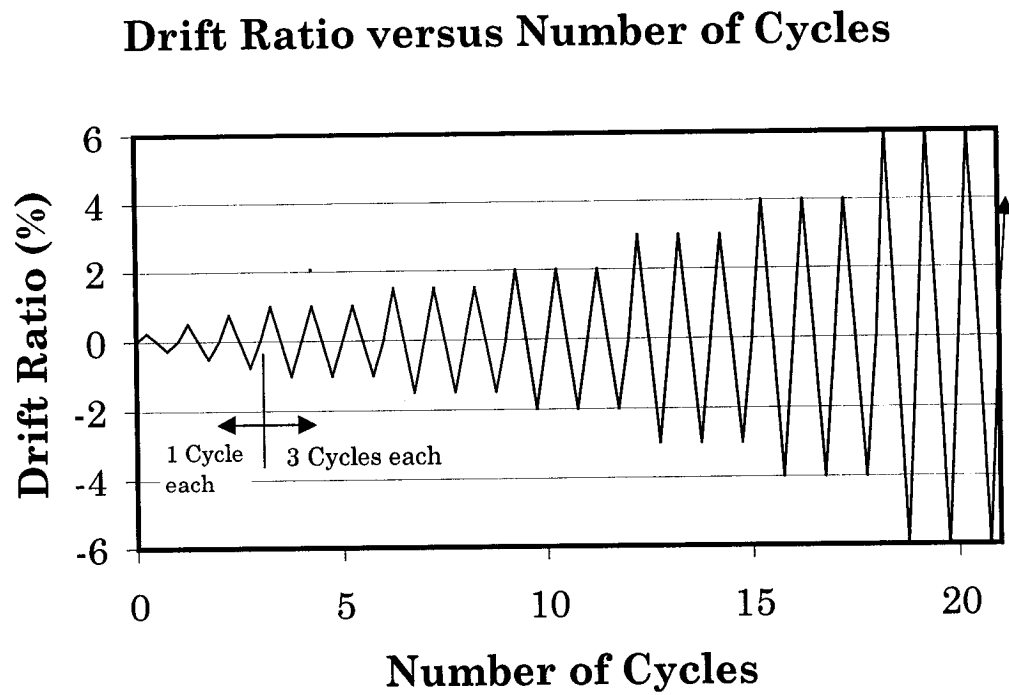
Fig. 3.20-Loading program.

187

CHAPTER 4

EXPERIMENTAL RESULTS AND DISCUSSIONS

4.1 GENERAL OBSERVATIONS

The six model columns developed stable responses, up to drift ratios ranging from Δ/H =3% to Δ/H =8% depending on the transverse reinforcement details and the axial load levels. Fig.4.1 to Fig.4.6 illustrate the crack patterns for the six model columns at various loading stages. Flexural cracks perpendicular to column axis developed first in lower half of the column during initial loading stages corresponding to drift ratios less than 0.5%. The flexural cracks became inclined and extended into the web zone of the columns due to the influence of shear when the peak drift ratio approached Δ/H=1.0%. Concrete cover crushed at the toes of the column, and the highest lateral load carrying capacity was typically recorded during the loading to approach the first peaks in the push and pull directions at peak drift ratio of approximately Δ/H=1.75% to 2.0% for columns with an axial load ratio of 20% or at peak drift ratio of approximately Δ/H=1.0% to 1.5% for columns with the axial load ratio above 30%. Concrete cover spalling gradually spread over the end of the column with the increase of loading cycles and the

188

augmentation of drift displacement. Despite of the concrete cover spalling, the confined core near the column end appeared to rotate in a stable manner, providing a satisfactory column performance until failure typically due to the longitudinal bar buckling occured. Column FHC1-0.2 and FHC3-0.22 developed an ultimate peak drift ratio of Δ/H=6.0% without serious degradation of load carrying capacity. The longitudinal bars of FHC1-0.2 buckled slightly when the column was pushed to the peak at drift ratio Δ/H=8.0%, however, the column was able to carry the lateral force without significant degradation and the full axial load. The sudden buckling of the longitudinal bars caused failure of the column in the pull direction, as evidenced by the sudden drop of lateral and axial loads. Column FHC3-0.2 failed similarly during the third loading cycle at drift ratio Δ/H=6.0%. Other columns with lesser transverse reinforcement or higher axial load compared to these two columns failed more suddenly at smaller drift ratios.

In all cases, no rupture of reinforcement was observed. The buckling of longitudinal bars appeared to be significantly compounded by the opening of the 90 degree anchorage of the cross ties, as shown in Fig.4.7. This was consistent with the observations made during an earlier phase of the program for testing smaller scale HSC columns subjected to eccentric compression loads. (Xiao and Martirossyan, 1996).

189

Δ / H = 1.0%   Δ / H = 2.0%   Δ / H = 3.0%

Δ / H = 4.0%   Δ / H = 6.0%   End of Testing
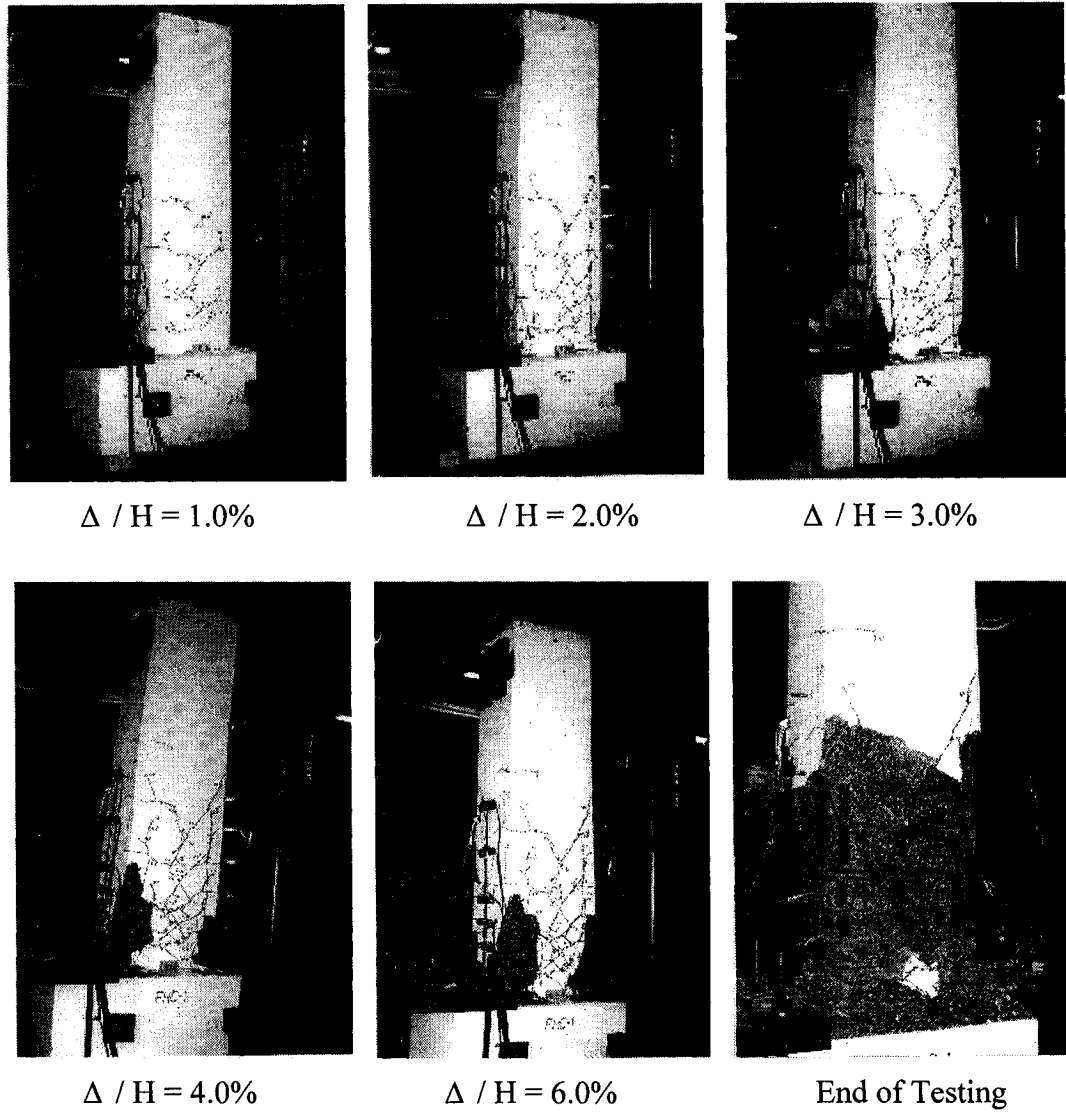
Figure 4.1-Crack Patterns for Column HSC-FF1-0.2 at Various Loading Stages

190
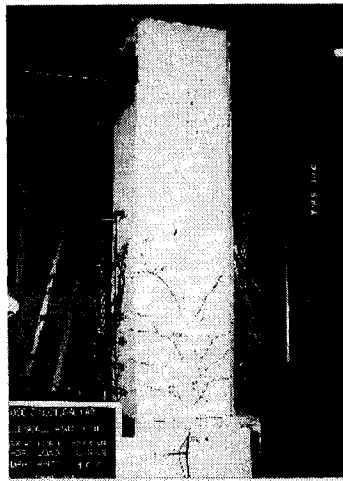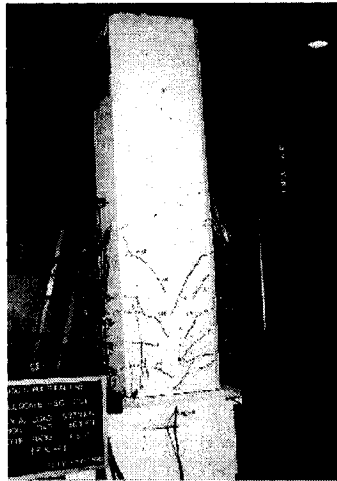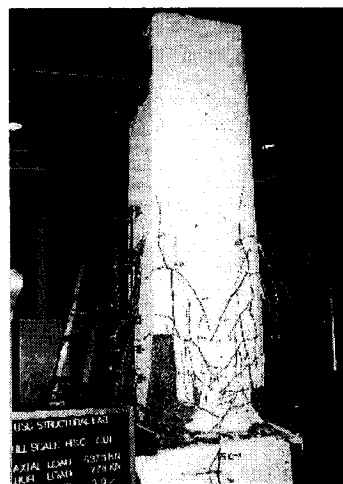
$\Delta / H = 1.0\%$ $\Delta / H = 1.5\%$ $\Delta / H = 2.0\%$

$\Delta / H = 3.0\%$ $\Delta / H = 4.0\%$ End of Testing

Figure 4.2-Crack Patterns for Column HSC-FF2-0.34 at Various Loading Stages

191

Δ/H=1.0% Δ/H=2.0% Δ/H=3.0%
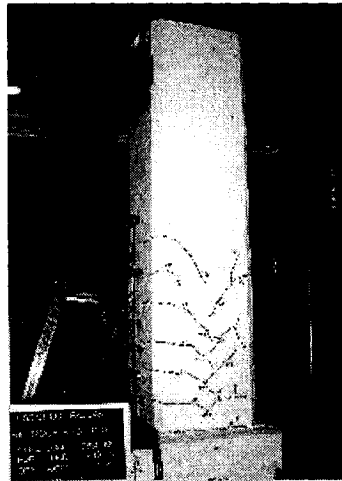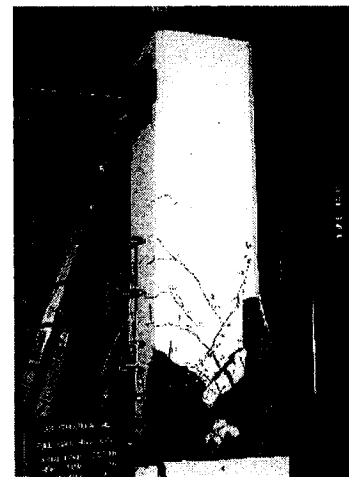
Δ/H=4.0%   Third Peak of Δ/H=4.0% Δ/H=6.0%

Figure 4.3-Crack Patterns for Column HSC-FF3-0.22 at Various Loading Stages

192
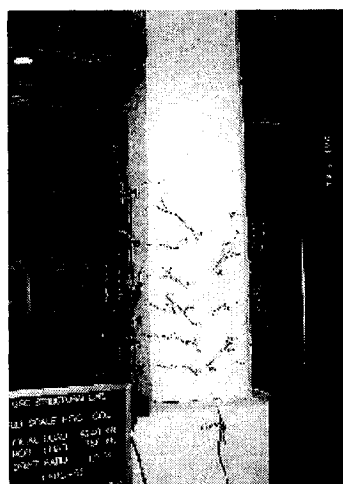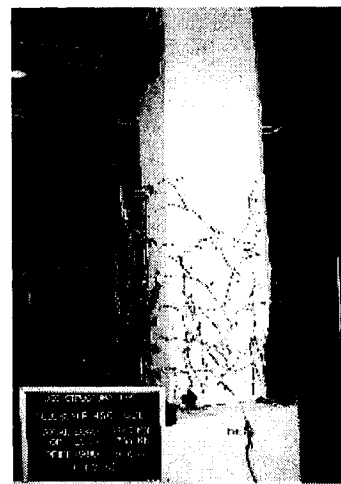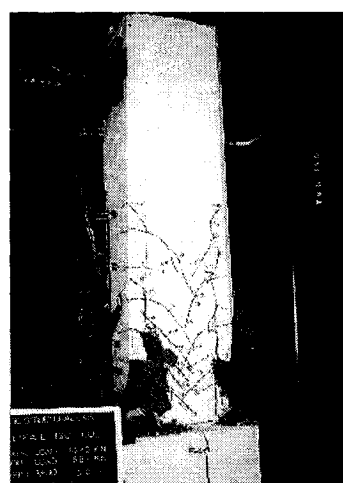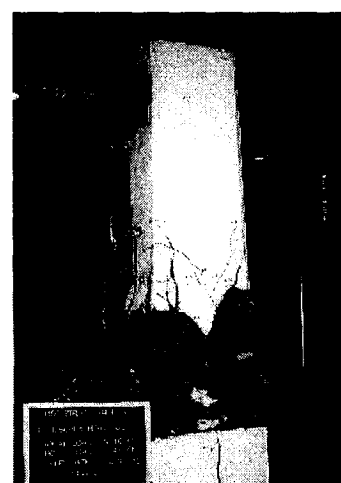
| $\Delta / H = 1.0\%$ | $\Delta / H = 1.5\%$ | $\Delta / H = 2.0\%$ |

| $\Delta / H = 3.0\%$ | $\Delta / H = 4.0\%$ | End of Testing |

Figure 4.4-Crack Patterns for Column HSC-FF4-0.33 at Various Loading Stages

193
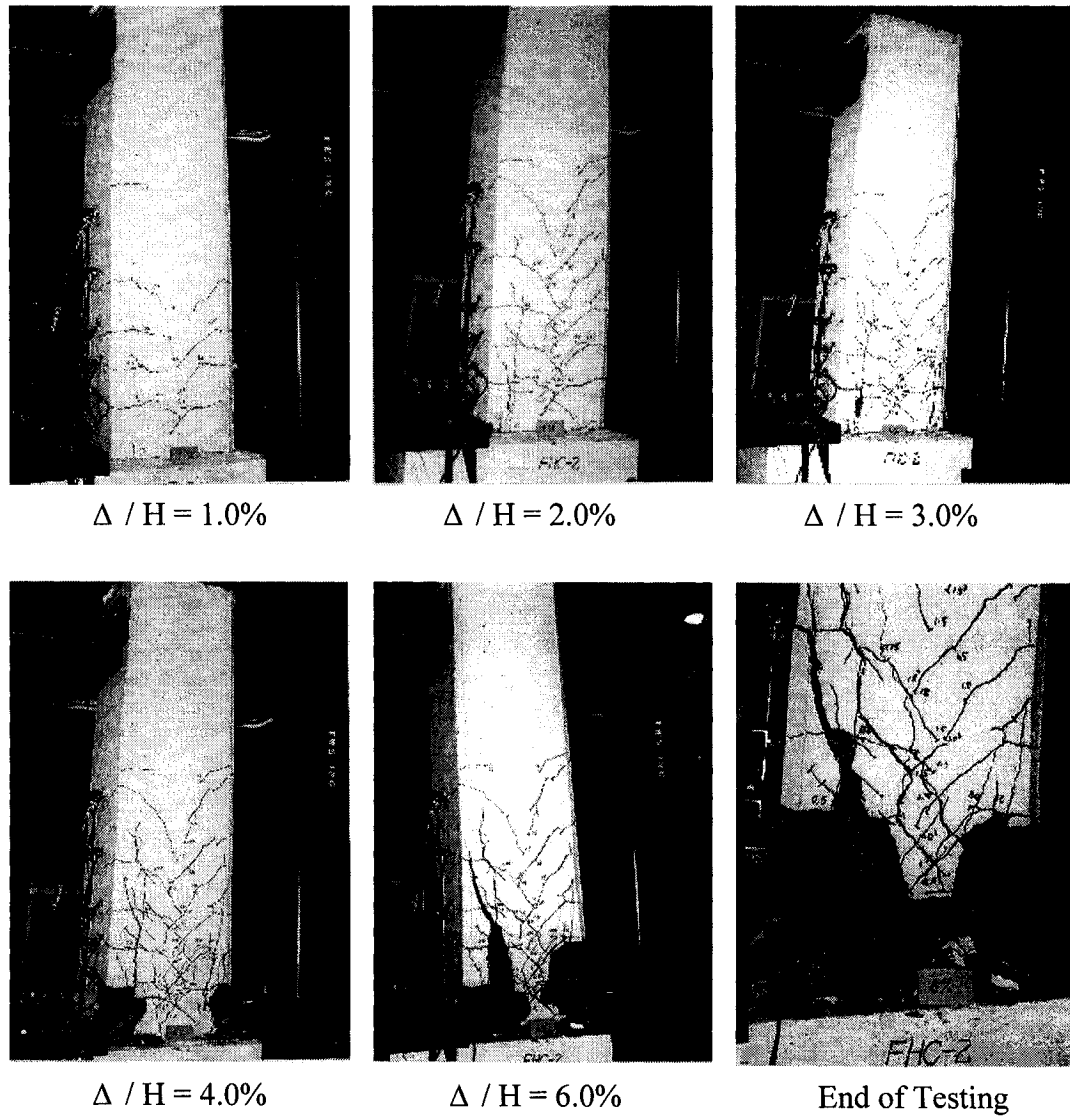
Figure 4.5-Crack Patterns for Column HSC-FF5-0.2 at Various Loading Stages

194

Δ / H = 1.0% Δ / H = 2.0% Δ / H = 3.0%

Δ / H = 4.0% Δ / H = 6.0%   End of Testing
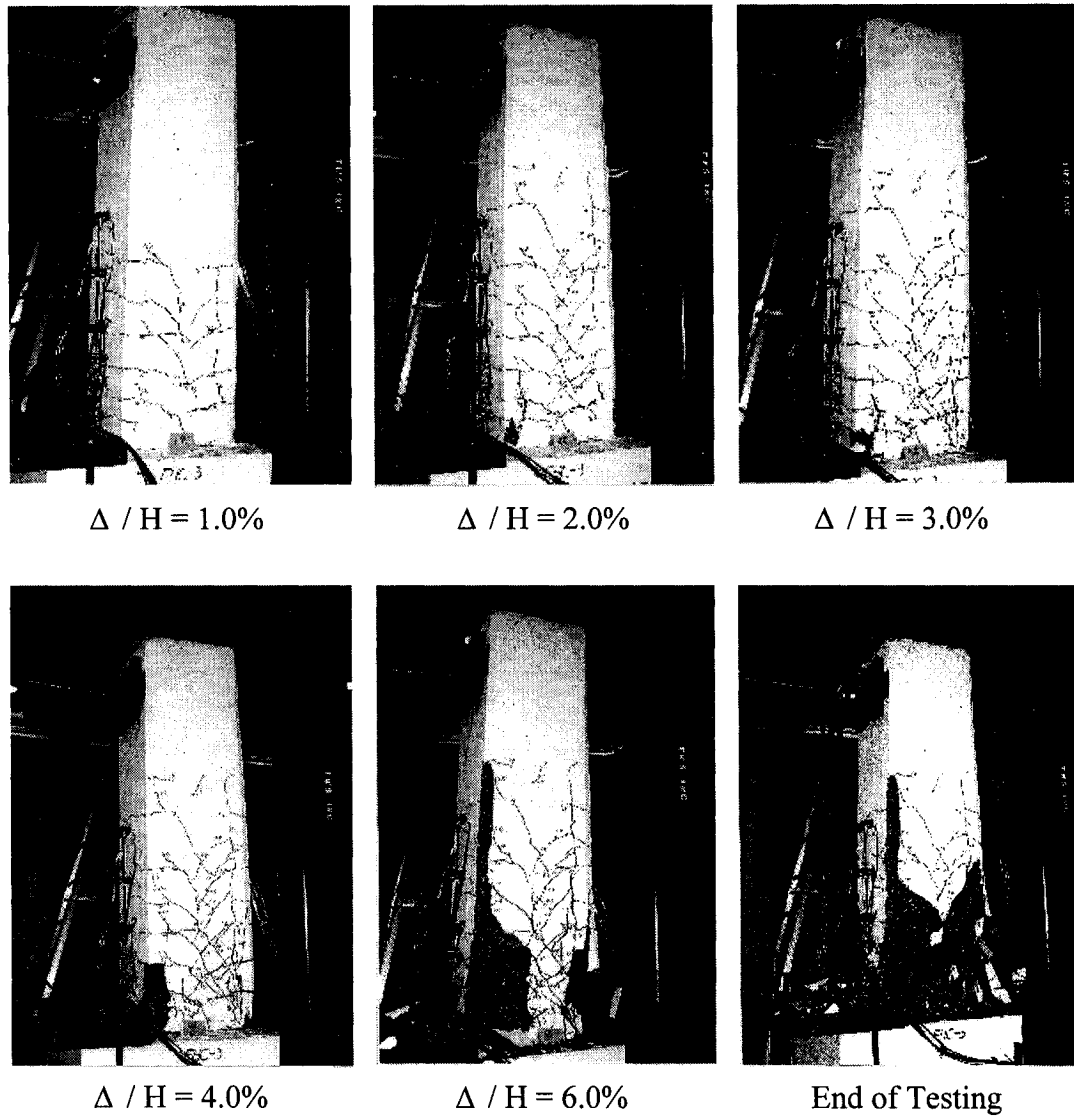
Figure 4.6-Crack Patterns for Column HSC-FF6-0.2 at Various Loading Stages

195
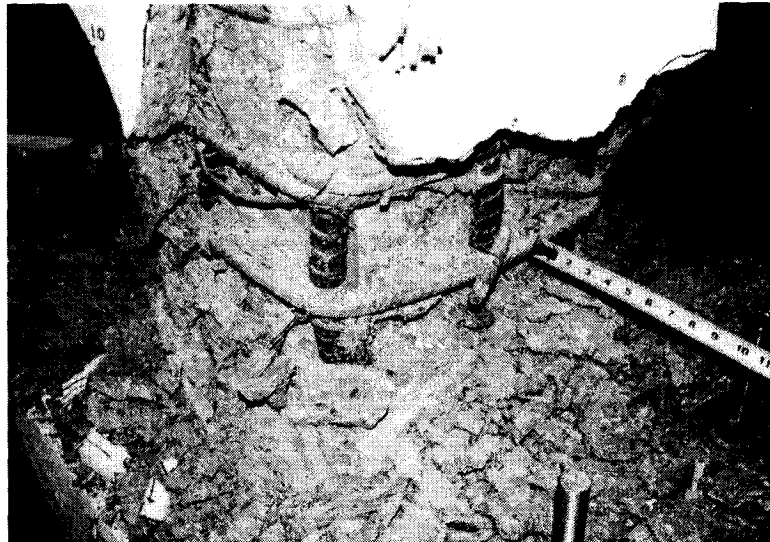
Fig. 4.7-Failure of 90 degree anchorage of cross ties
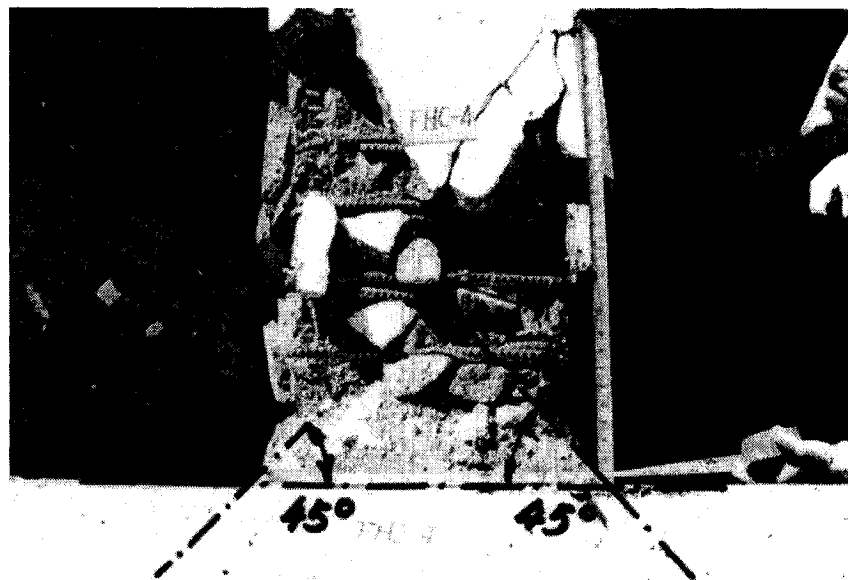
Fig. 4.8-Effect of stub on damage pattern in column

196
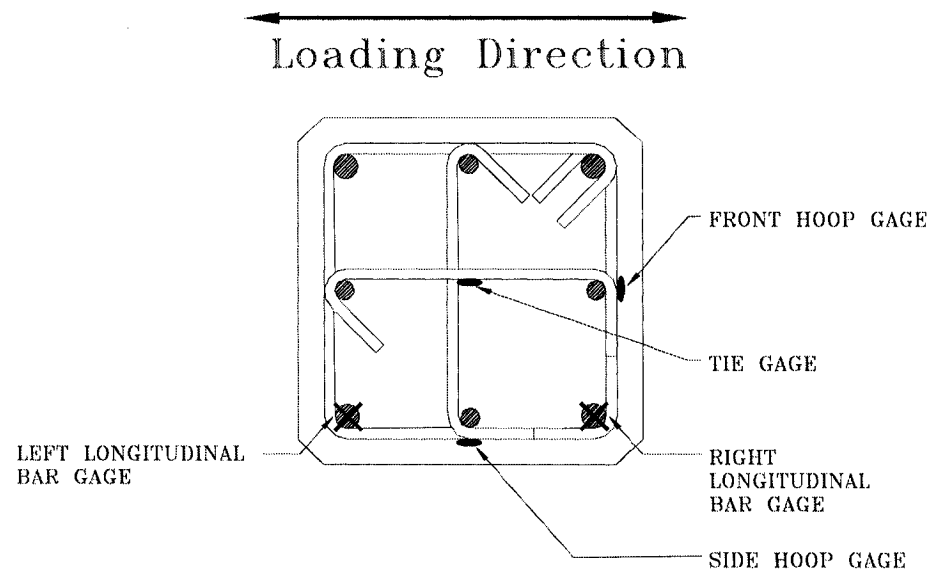
Fig. 4.9-Strain gage locations

197
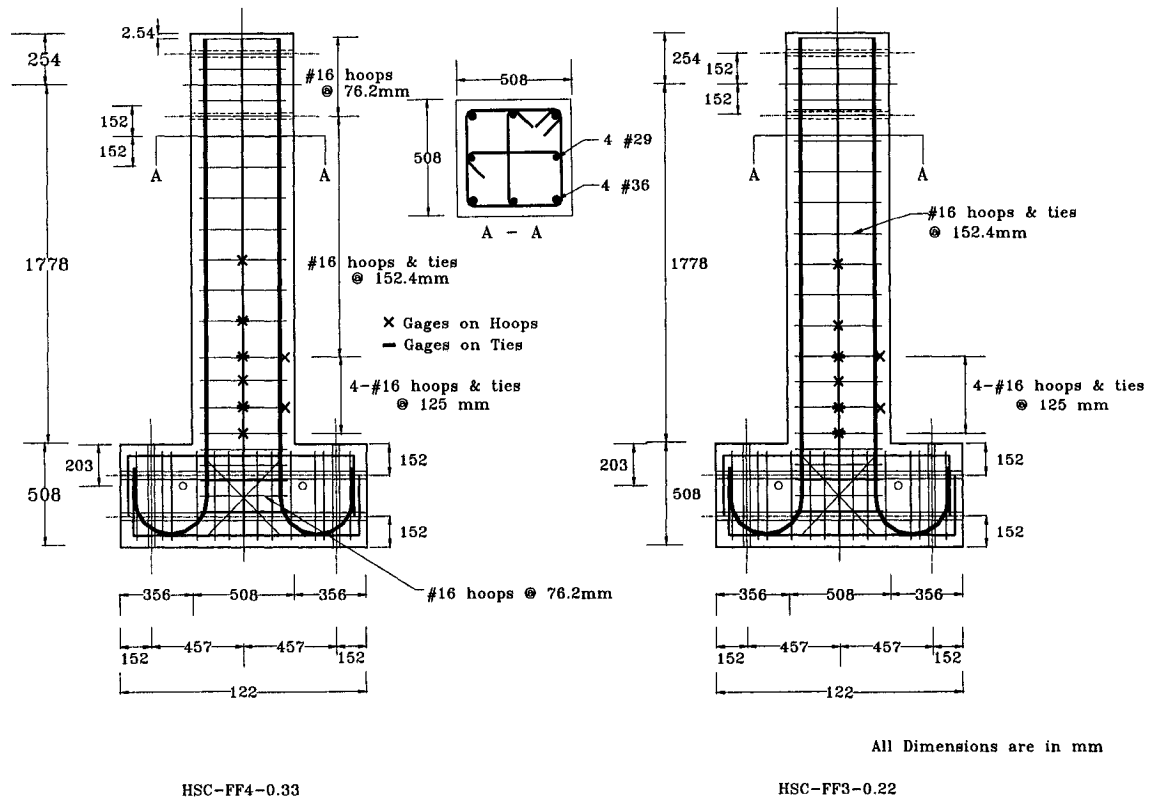
Fig. 4.10(a)-Strain gage locations for FHC4-0.33 and FHC3-0.22.

198
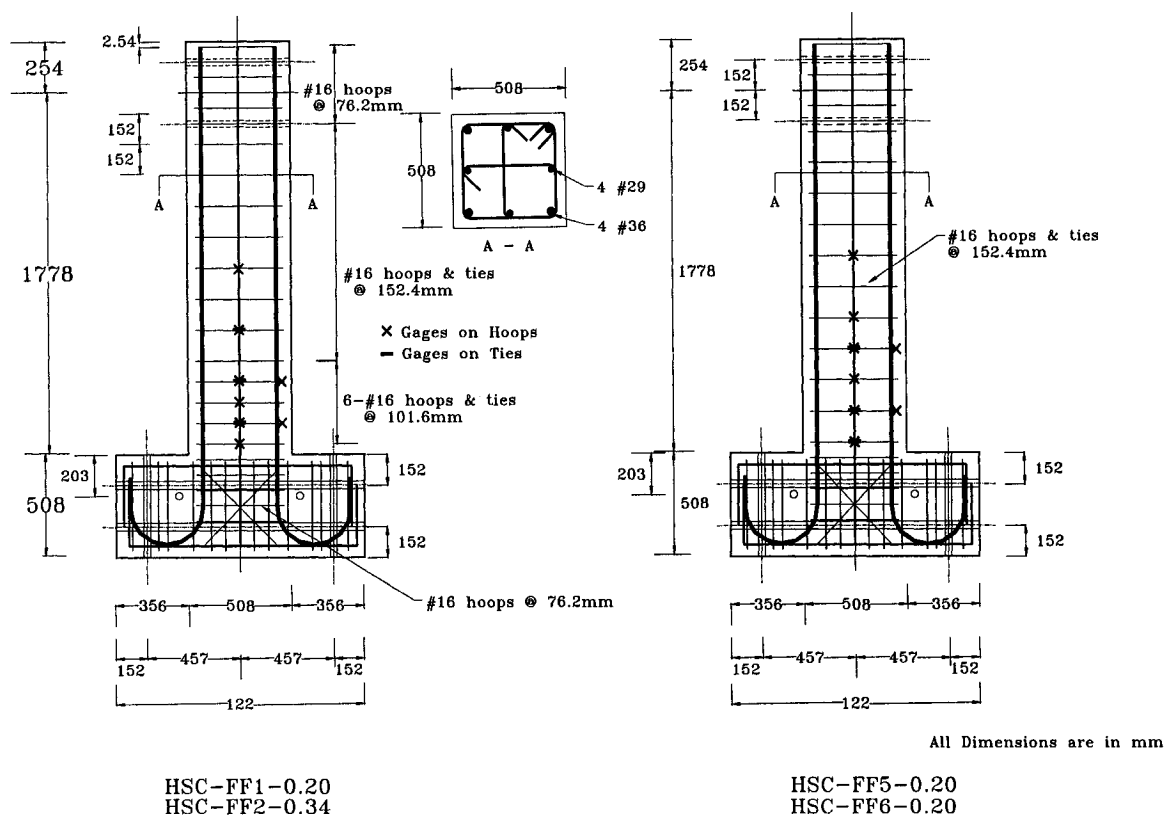
Fig. 4.10(b)-Strain gage locations: for FHC1-0.2 and FHC2-0.34; for FHC5-0.2 and FHC6-0.2.

199

4.2 HYSTERESTIC RESPONSES

Fig.4.11 to Fig.4.16 show the shear force – drift ratio hysteretic relationships for the six full-scale HSC columns. Note that the shear force values shown in Fig.4.11 to Fig.4.16 were obtained by subtracting the horizontal component of the post tensioning force for axial loading from the applied lateral loads, as discussed in previous chapter. Predicted flexural capacity, V_{fACI}, based on the equivalent stress block corresponding to an extreme concrete compressive strain of 0.003 recommended by ACI 318-95 code (1995) and actual material strength is shown by dashed lines. Detailed calculations of the column capacities based on the ACI 318-95 code 1995 can be found in Appendix II. The slopes of the dashed lines and the inclined solid lines passing through the origin of the coordinates represent the P-Δ effect.

200
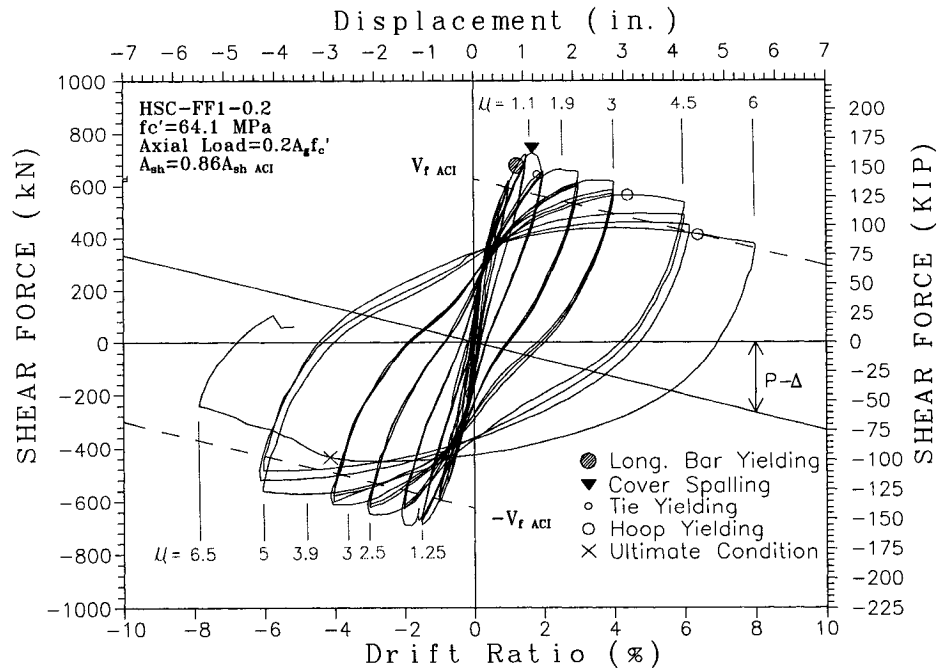
Fig. 4.11-Hysteresis for specimen FHC1-0.2
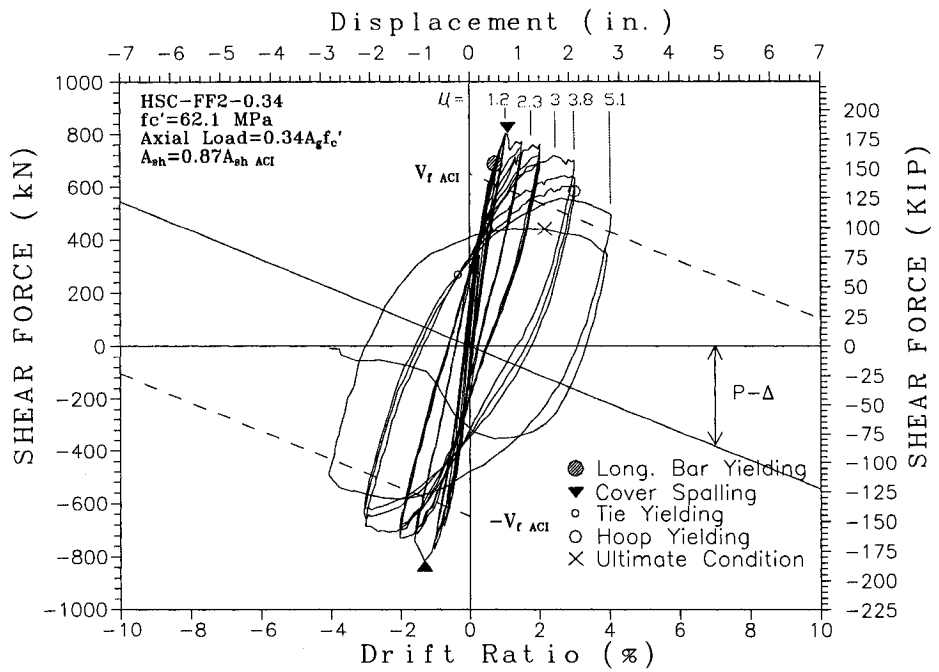
Fig. 4.12-Hysteresis for specimen FHC2-0.34

201
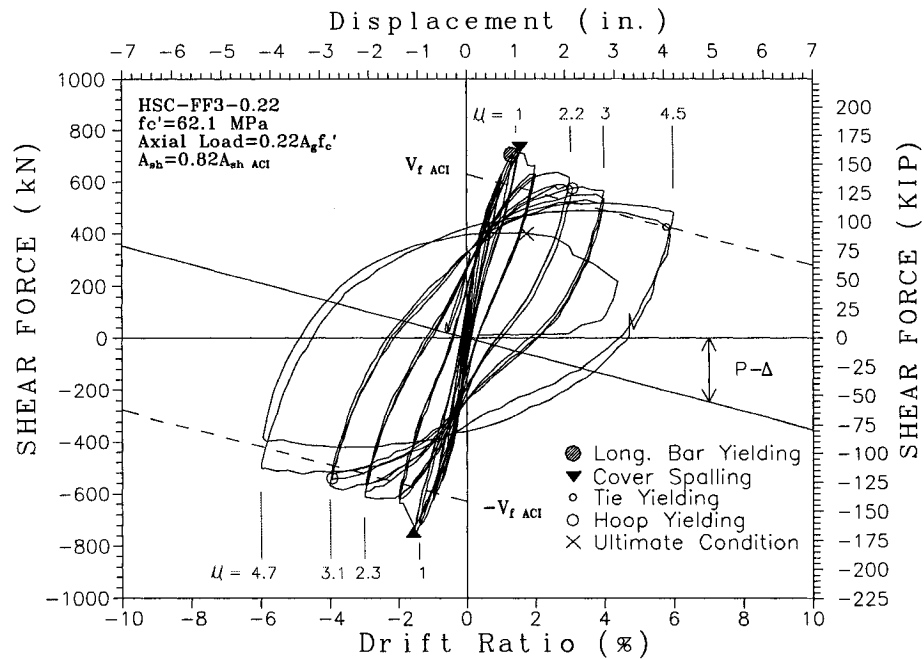
Fig. 4.13-Hysteresis for specimen FHC3-0.22
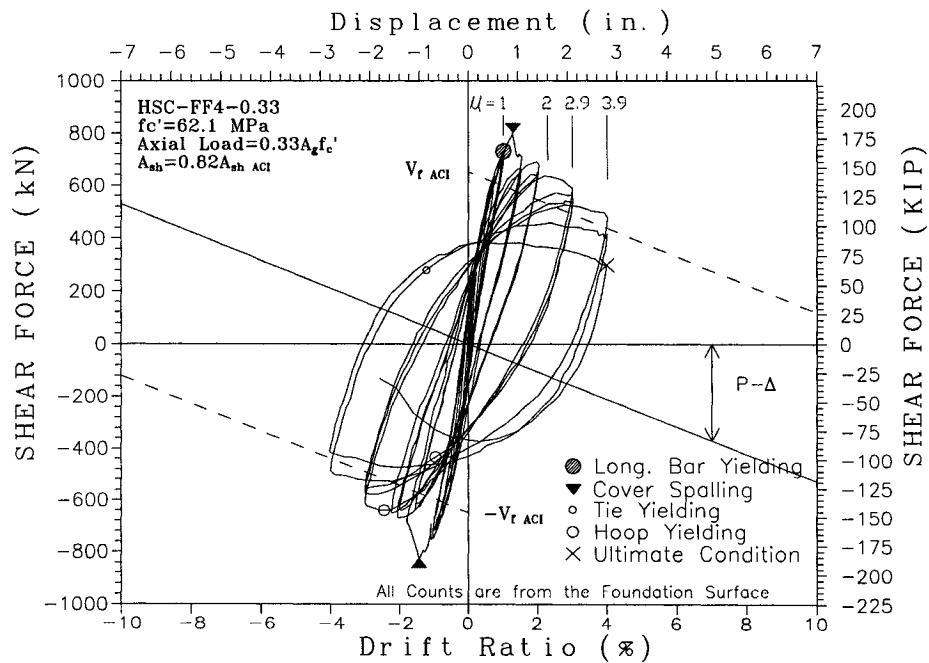
Fig. 4.14-Hysteresis for specimen FHC4-0.33

202
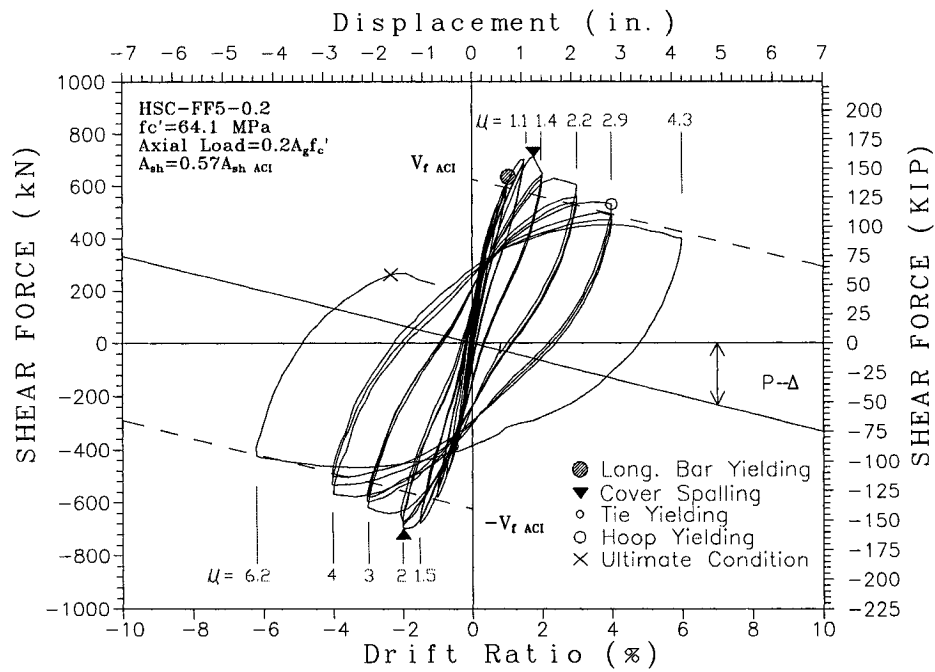
Fig. 4.15-Hysteresis for specimen FHC5-0.2
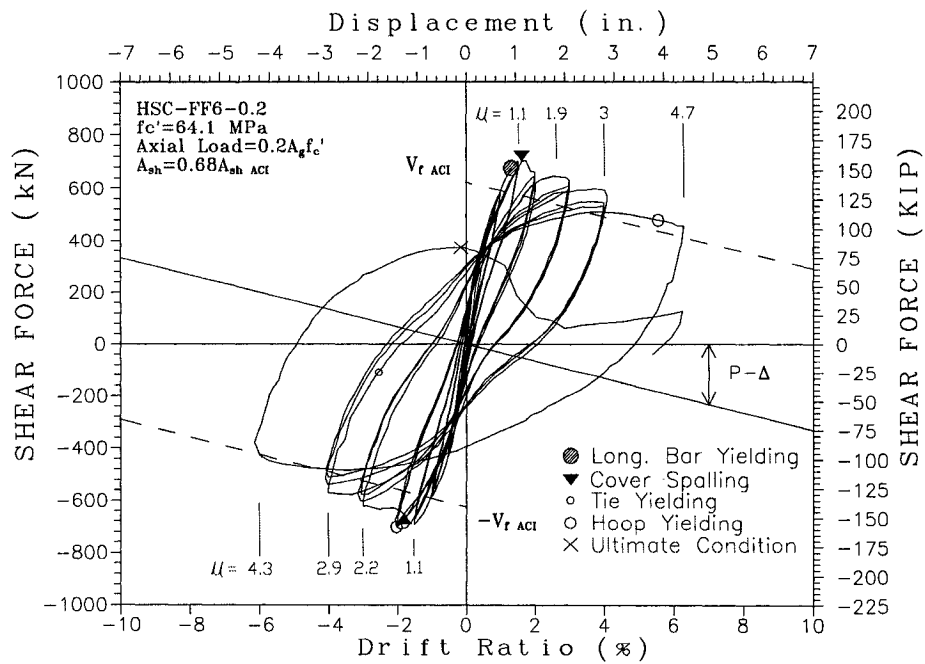
Fig. 4.16-Hysteresis for specimen FHC6-0.2

203

4.3 STAGES OF COLUMN FAILURE

The column deformability (ductility) represent the seismic performance of reinforced concrete columns, and the specimens which were tested for this investigation have shown ideal performances showing stable behaviors after the first peak and spalling of the cover concrete. During the initial stages of load application at a drift ratio of typically less than 0.5 %, the flexural cracks which were initially perpendicular to column axis became gradually became inclined at drift ratio of less than 1.0 %. When the longitudinal reinforcements began to yield, the cracks vertical along the longitudinal reinforcements appeared, showing a bond failure. As the deformation increased further, the concrete crushing at the toe of the columns occurred and shear cracks became apparent. The highest lateral load carrying capacities and the cover spallings were recorded for 1st peaks of cyclic loading at drift ratio of 2 % for 20 % axial load ratio and at drift ratio of 1.5 % for 30 % axial load ratio. The longitudinal bars yielded prior to the transverse hoops, and near the ultimate stage of the loading cycles, the longitudinal reinforcements began to buckle, and this was followed by opening of the transverse hoops along bending of 90 degree tie anchorage. The longitudinal buckling seems to have caused the confinement failure and sudden decrease in the lateral and axial load. The ultimate failure of the specimens were more sudden for smaller drift ratio, for less amount of transverse reinforcement, or for higher

204

axial load ratio. It seems that increased axial load ratio caused significant reduction in column deformability.

According to Sheikh's recent journal publication, the deformability of confined HSC reinforced concrete columns is greatly affected by the axial load ratio, and the performances based on different axial load ratio need to be examined.

The hysteretic behavior of the HSC columns are characterized by three distinct stages: (i.) the initial stage with the full participation of both confined core concrete and the unconfined cover concrete; (ii.) stable behavior with deformation contributed primarily by longitudinal steel yielding and straining of confined core concrete; and (iii.) final failure. The termination of the initial stage and the beginning of the stable stage is typically marked by the crushing and spalling of unconfined cover concrete. The maximum lateral shear force carrying capacity is typically achieved by the HSC columns

immediately before the crushing of cover concrete. The maximum shear force and the corresponding drift ratio depend mainly on the concrete section properties including the axial load levels, and not significantly affected by the configuration of transverse reinforcement. As shown in Fig.4.11 to Fig.4.16, all the full-scale HSC columns developed and exceeded the flexural capacity calculated based on ACI 318-95 code (11). This supports the conclusion from a previous study that

205

the ACI code approach for calculating flexural strength is viable but conservative for HSC columns with concrete compression strength up to about 70MPa (10ksi) to 85MPa (12ksi) (Xiao and Martirossyan, 1997).

Based on the yield strain values of the steel reinforcements that were obtained previously through tensile tests, the first yield points of specific longitudinal and transverse reinforcements within the plastic hinge region were located from the test data and are shown in the hysteresis loops. The location of the strain gauges which are described in the hysteresis loops are shown in Figures 4.9 and 4.10. The Figures 4.9 and 4.10 show specific locations of the strain gauges that were installed on the transverse reinforcements for each of the six columns. The first page of Appendix III shows locations of the strain gauges which were installed on the longitudinal reinforcements for each of the six columns with designation for each strain gage shown. The last group of numbers represents the distance from the column stub in millimeters (at approximately 10, 20, 30, and 40 inches from the stub). The lateral force loading direction is in the plane of the Figures 4.9 and 4.10, and all gauges on the transverse reinforcements measure strains in the lateral force loading direction, except for two gauges on the hoops which were installed perpendicular to the plane of the figures.

206

4.3.1 Specimen 1: FHC1-0.2

Model column FHC1-0.2, which was reinforced with 86% transverse reinforcement required by ACI 318-95 code, was able to develop a ductile response with the peak shear force above V_{fACI} until a drift ratio as large as Δ/H=8.0% was reached, as shown in Fig.4.11. The concrete cover crushing was noticed during the loading to achieve the first peak at Δ/H=1.75%, where the maximum shear force was recorded. The shape of the hysteresis loops for FHC1-0.2 after concrete cover spalling indicates a good energy dissipation capability. The column developed a capacity slightly less than V_{ACI} during the push loading at Δ/H=8.0%, however failed due to longitudinal bar buckling in the pull loading direction.

In the plastic hinge region, the No. 36 (ASTM #11) longitudinal bar in the plastic region reached its first yielding point at $\Delta/H = 1.34\%$ which correspond to a shear force $V_f = 694.2\,\text{kN}$ (156.06 kips). This was followed by first transverse tie yielding at Δ/H=1.87%. The first transverse hoop yielding occurred at much higher drift ratio of Δ/H=6.49%. As shown in Fig. 4.11, the tie reached its yielding point prior to hoop yielding.

207

4.3.2 Specimen 2: FHC2-0.34

With higher axial load level, the initial stiffness of column FHC2-0.34 was higher than its counterpart model FHC1-0.2, as can be seen from comparison of Fig.4.11 and Fig.4.12. However, the increased axial load caused a significant reduction in the column deformability. Concrete cover crushed during the loading to the first peak at Δ/H=1.0%. Column FHC2-0.34 only developed stable response up to drift ratio Δ/H=3.0%, which was half of the ultimate drift ratio achieved by column FHC1-0.20. A drastic degradation occurred during the loading cycle corresponding to a peak drift ratio of 4.0%, however, as shown in Fig.4.12, the column was able to carry a shear force almost equal to the calculated flexural strength based on ACI 318-95 code.

In the plastic hinge region, the transverse hoop reached its yielding point at an earlier stage as compared to the hoop yielding of the previous column FHC1-0.20 with lower axial load. The first No. 36 (#11) longitudinal bar yielding occurred at Δ/h=0.79% at V_f = 697.95 kN (156.9 kips), and the transverse hoop yielded first at Δ/h=0.55% followed by first tie yielding at Δ/h= -0.27%. The yielding of the tie occurred after hoop yielding although the corresponding drift ratio value at tie yielding was less than that of the transverse hoop reinforcement.

208

From above observations, it is noticeable that cover spalling and yielding of all reinforcements occurred earlier in comparison to specimen FHC1-0.2 with lower axial load. Also, it is apparent that higher axial load decreased the deformability of the FHC2-0.34.

4.3.3 Specimen 3: FHC3-0.22

Satisfactory hysteretic response was developed by column FHC3-0.22, which was designed with the transverse reinforcement in the potential plastic hinge region equivalent to 82% of ACI 318-95 code requirement. As shown on Figure 4.13, the hysteresis loops were stable until the second cycle of loading corresponding to peak drift ratio 6.0%, as shown in Fig.4.13. Failure occurred when the longitudinal bars buckled before achieving the third peak at drift $\Delta/H=6.0\%$.

Where the grade 420 (ASTM Grade 60) transverse reinforcements of the columns FHC1-0.20 and FHC2-0.34 were spaced at 100 mm(4 in.) in the plastic hinge region, specimen FHC3-0.22 has Grade 520 (ASTM Grade 75) transverse reinforcement with a 125 mm(5 in.) spacing in the plastic hinge region. The transverse reinforcement provided in the potential plastic hinge region is 82% of ACI requirement, similar to those of the first two columns which are provided with 86% and 87% of ACI requirement, respectively. The longitudinal bar

209

reached its first yield point at Δ/H=1.34% corresponding to $V_f = 711.27$ kN (159.9 kips). The hoop yielded first at Δ/H=3.1% before first tie yielding which occurred at Δ/H=5.85%. It seems that the hoops yielded relatively earlier as the spacing increased from 100 mm (4 in.) to 125 mm (5 in.) when compared to specimen FHC1-0.2. On the other hand, the tie yielding seems to be comparatively delayed for specimen FHC3-0.22 in comparison to FHC1-0.2. Despite above differences in the behavior of reinforcements due to increased hoop and tie spacing to 125 mm (5 in.), specimen FHC3-0.22 performed as well as FHC1-0.2 due to the use of higher grade transverse reinforcement.

4.3.4 Specimen 4: FHC4-0.33

Significant concrete cover spalling was observed for FHC4-0.33 during loading to achieve the first peaks corresponding to drift ratio Δ/H=1.3%, where the maximum shear forces were also recorded for both the push and the pull directions. After this stage the response appeared to be stable with small capacity degradation upon cycling until the third cycle at Δ/H=2.0%. Both physical deterioration and the degradation of load carrying capacity of column HSC-FF4-0.33 accelerated during loading corresponding the peak drift ratio Δ/H=3.0%. As shown in Fig. 4.14, the peak shear forces are all below the calculated flexural strength based on ACI 318-95 code after the first loading cycle at Δ/H=4.0%.

210

Although with much lower peak shear forces achieved, two cycles of loading could be executed corresponding to Δ/H=4.0%. The axial load suddenly dropped during the attempt to start the third loading cycle at Δ/H=4.0%. For this column also with high axial load, hoop yielding occurred prior to tie yielding. Due to higher axial load, the drift ratio values when the transverse tie or tie yielded was smaller as compared to FHC3-0.22. Also, higher grade 520 (ASTM Grade 75) transverse reinforcements provided better performance as compared to the V_{ACI} value as shown in Figure 4.14. With 125 mm (5 in.) spacing of transverse reinforcement, specimen FHC4-0.33 still performed as well as specimen FHC2-0.34 due to the use of higher grade transverse reinforcement.

4.3.5 Specimen 5: FHC5-0.2

The response of FHC5-0.2 was stable up to Δ/H=3.0%, despite a drop of shear force during loading to achieve the first peak at Δ/H=2.0% due to the concrete cover spalling. As shown in Fig.4.15, the degradation of peak shear force of FHC5-0.2 upon recycling becomes apparent for drift ratio $\Delta/H \geq 3.0$%. Particularly in the push loading

direction, the peak shear force reduced below V_{fACI} after first cycle at Δ/H=3.0%. The column failed at the start of the attempted second loading cycle at Δ/H=6.0%.

211

This column with lower axial load has much less transverse reinforcement of 57% of ACI requirement with hoop spacing of 150 mm (6 inches) in the potential plastic region. The hoop yielding occurred first at Δ/H=4.0% corresponding to $V_f = 530.7\,\text{kN}$ (119.3 kips) then tie yielding at Δ/H= -0.56% corresponding to $V_f = -388.0\,\text{kN}$ (-87.2 kips). It seems the first hoop yield occurred earlier for this specimen with greater hoop spacing of 150 mm (6 inches) when compared to the first hoop yield as observed in specimen FHC1-0.2 with hoop spacing of 100 mm (4 inches).

4.3.6 Specimen 6: FHC6-0.2

In comparison with model column FHC5-0.2, improved hysteretic behavior can be seen in Fig.4.16 for column FHC6-0.2, indicating the favorable effects of using higher strength transverse reinforcement. Stable response with peak shear forces reaching or exceeding V_{fACI} was developed by FHC6-0.2 until the third loading cycle corresponding to peak drift ratio Δ/H=4.0%. Column FHC6-0.2 was able to develop the calculated flexural strength based on ACI 318-95 code V_{fACI} at the first peak in the push direction at Δ/H=6.0%, although it failed in the similar manner as FHC5-0.2.

212

This column with 68% of required ACI transverse reinforcement and with grade 520 (ASTM Grade 75) transverse reinforcement at 150 mm (6 in.) spacing provided similar but better performance in comparison to FHC5-0.2. The first yielding of hoop also occurred prior to tie yielding as shown in Fig. 4.16. The increased spacing of 150 mm (6 in.) seems to have resulted in slightly lower performance level when compared to specimen FHC3-0.22 which is provided with transverse reinforcement equivalent to 82% of ACI requirement with spacing of 125 mm (5 inches). Such a small decrease performance for FHC6-0.20 when compared to specimen FHC3-0.22 stems from the fact that FHC6-0.20 uses slightly greater concrete strength of 64.1 MPa (9.3 ksi) and lower axial load ratio of 0.20 where specimen FHC3-0.22 uses similar but slighter lower concrete strength of 62.1 MPa (9.0 ksi.) and slightly higher axial load ratio of 0.22.

213

4.4 DISCUSSION OF DIFFERENT EFFECTS

4.4.1 Influence of Axial Load Ratio

The Figure 4.17(a) shows the peak shear envelopes of two columns that were subjected to different axial loads. The comparison of FHC1-0.2 (Axial Load P=749 kips, ASTM Grade 60 @ 4") and FHC2-0.34 (Axial Load P=1225.4 kips, ASTM Grade 60 @ 4") shows an increase in peak shear value for FHC2-0.34 with higher axial load for the drift ratio range of 0% to 3% but a decrease in the peak shear value for drift ratio greater than 3%. FHC1-0.2 with lower axial load, however, reached greater drift ratio up to 8% before it failed, where FHC2-0.34 failed at a drift ratio of 4%.

Similarly, the comparison of FHC3-0.22 (Axial Load P=792.9 kips, ASTM Grade 75 @ 5") and FHC4-0.33 (Axial Load P=1189.3 kips, ASTM Grade 75 @ 5") in Figure 4.17(b) shows a similar trend. However, the peak shear values of these columns are similar for a drift ratio range of 1.8% to 3%. However, the maximum peak shear value at a drift ratio of approximately 1% shows a substantial increase in the peak shear force due to the increased axial load.

214

It seems that higher axial load level limits the column deformability, and it can also be observed that an increased transverse reinforcement spacing from 100 mm (4 in.) to 125 mm (5 in.) and the use of higher grade transverse reinforcement resulted in similar peak shear values for greater range of drift ratio.
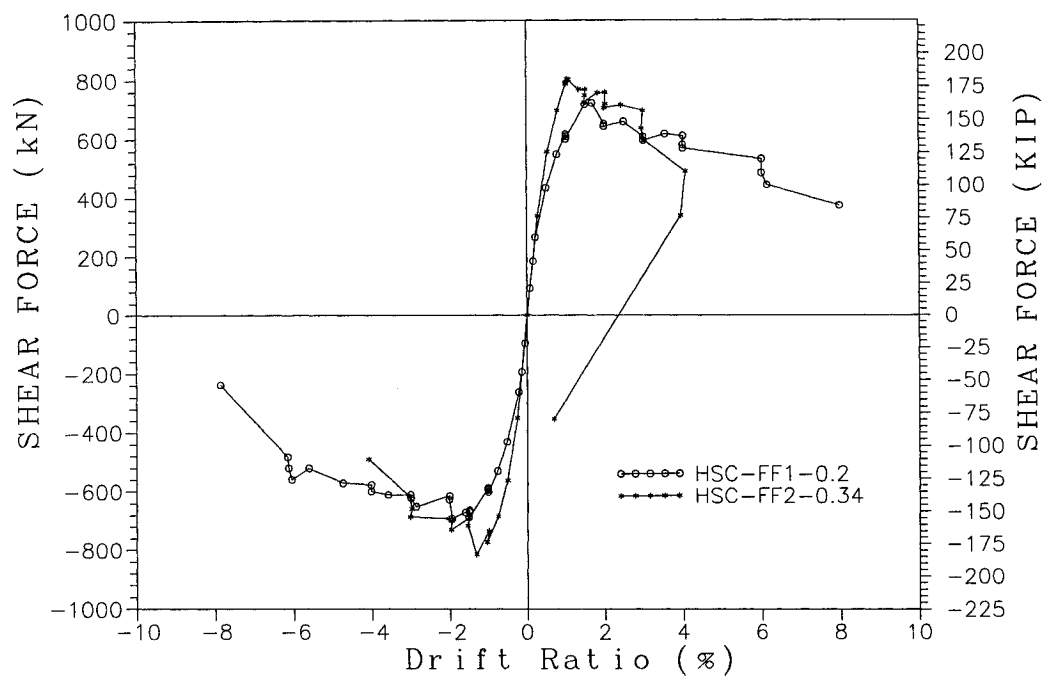
Fig. 4.17 (a)-Influence of axial load ratio

215
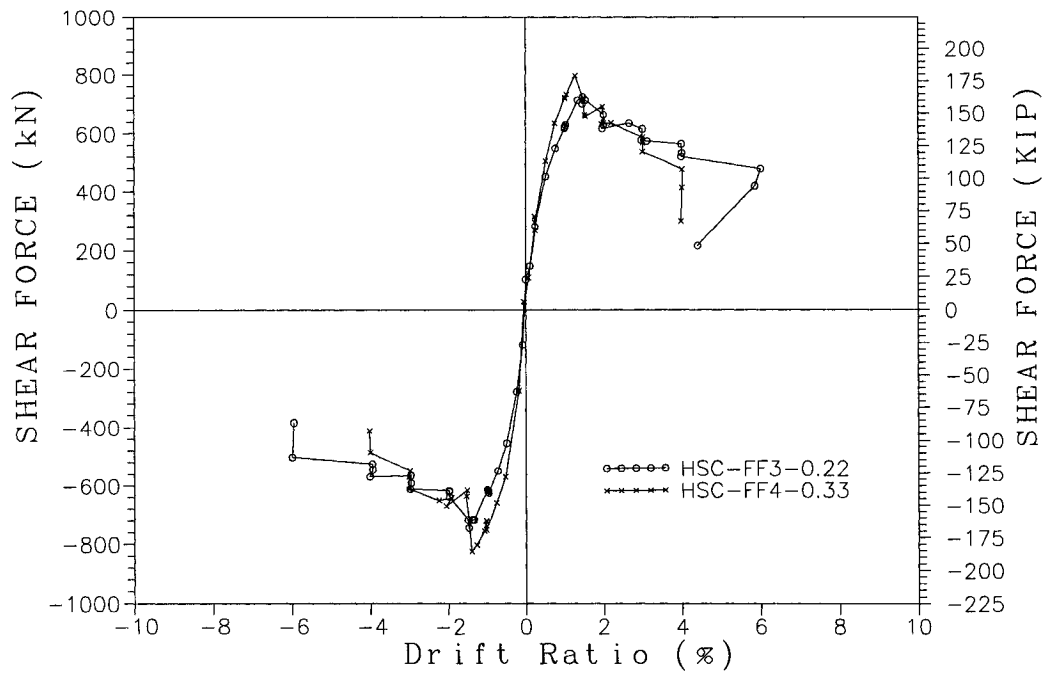
Fig. 4.17(b)-Influence of axial load ratio

4.4.2 Influence of Transverse Reinforcement

The effect of different transverse reinforcement spacing for two columns with similar confinement index from Figure 3.3 is shown in Figures 4.18(a) and (b). For the comparison between FHC2-0.34 (ASTM Grade 60 @ 4") and FHC4-0.33 (ASTM Grade 75 @ 5") which are subjected to high axial loads and for the comparison between FHC1-0.2 (ASTM Grade 60 @ 4") and FHC3-0.22 (ASTM

216

Grade 75 @ 5") which are subjected to lower axial loads, it is apparent that smaller transverse reinforcement spacing of 100 mm (4 in.) as compared to 125 mm (5 in.) gave larger peak shear values. In spite of the fact that the transverse reinforcements of 125 mm (5 in.) spacing are Grade 520 (ASTM Grade 75), the 100 mm (4 in.) spacing still gave higher peak shear values although these columns both have similar confinement index values.

4.4.3 Influence of Transverse Reinforcement Grade Type

The Figure 4.19 shows that specimen FHC6-0.2 with higher Grade 520 (ASTM Grade 75) transverse reinforcement has greater value of peak shear force as compared to that of specimen FHC5-0.2 for drift ratio greater than 2%. With increasing deformation (drift ratio) of the columns, the effect of using higher grade transverse reinforcement seems to increase. The peak shear value for specimen FHC6-0.2 was greater than that of FHC5-0.2 up to the drift ratio of 6% when both columns failed.

217
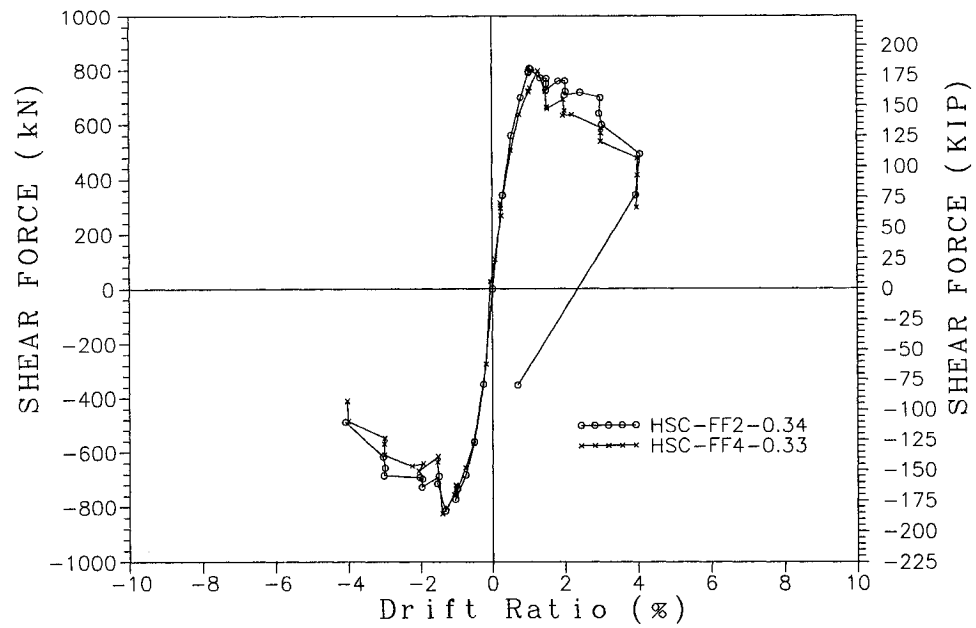
Fig. 4.18(a)-Influence of transverse reinforcement
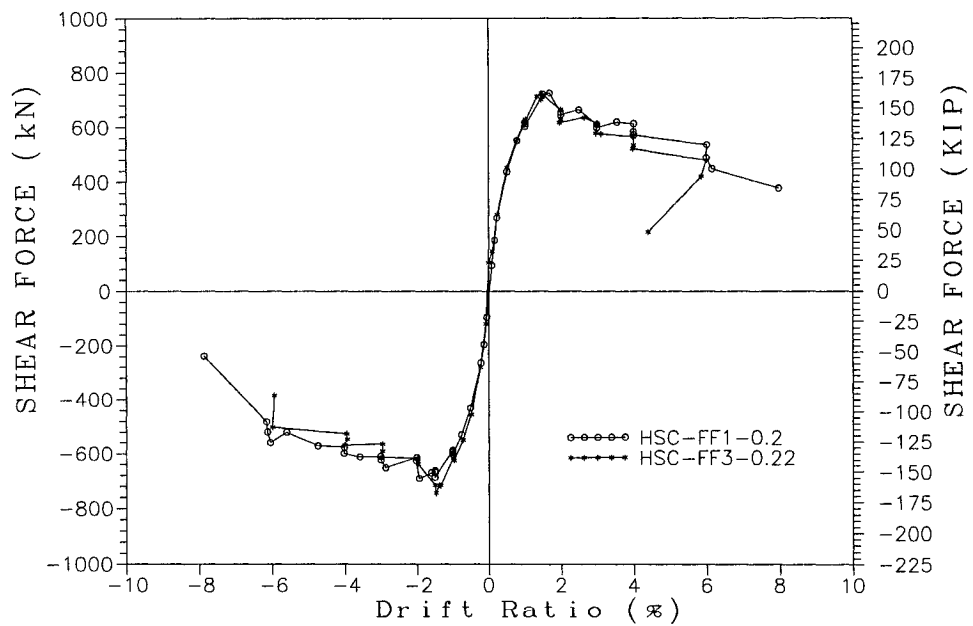
Fig. 4.18(b)-Influence of transverse reinforcement

218
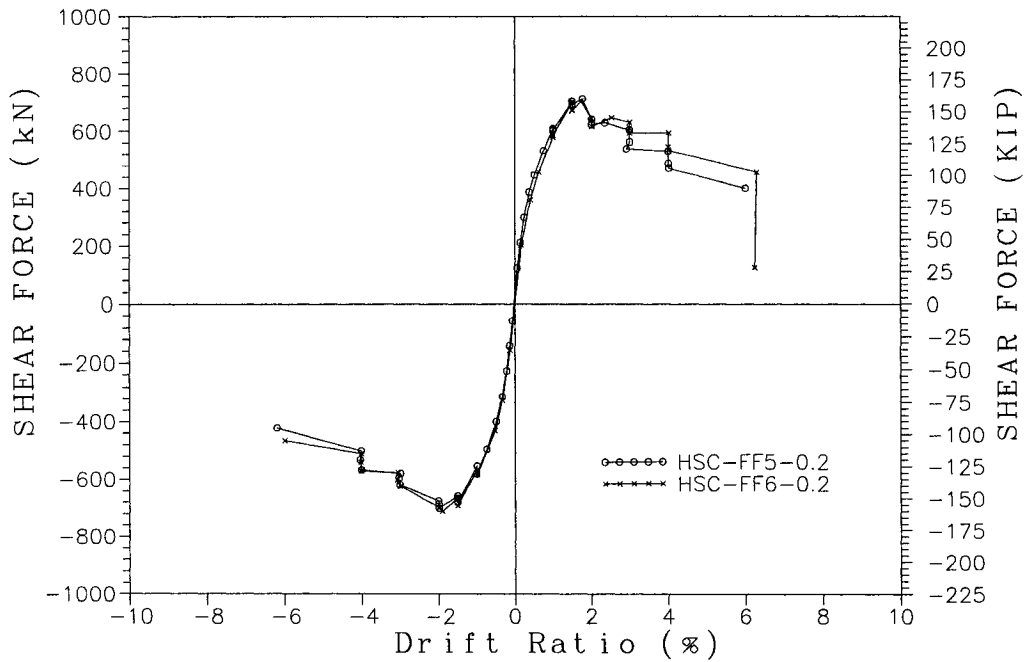
Fig. 4.19-Influence of transverse reinforcement grade type

4.4.4 Discussion of Transverse Reinforcement Spacing

With all parameters equal, the specimens FHC1-0.2 [Axial Load P=3331.7 kN (749 kips), Grade 420 (ASTM Grade 60) @ 100 mm (4"), f_c'=64.1 MPa (9.3 ksi)] and FHC5-0.2 [Axial Load P=3331.7 kN (749 kips), Grade 420 (ASTM Grade 60) @ 150 mm (6"), f_c'=64.1 MPa (9.3 ksi)] are compared with respect to their different transverse reinforcement spacing. As shown in the Figure 4.20(a),

219

specimen FHC5-0.2 with 150 mm (6 in.) spacing has smaller peak shear force values, since shear force transfer is greater through columns with smaller transverse reinforcement spacing. However, the comparison between FHC3-0.22 [Axial Load P=3526.9 kN (792.9 kips), Grade 520 (ASTM Grade 75) @ 125mm (5"), f_c'=62.1 MPa (9.0 ksi)] and FHC6-0.2 [Axial Load P=3331.7 kN (749 kips), Grade 520 (ASTM Grade 75) @ 150mm (6"), f_c'=64.1 MPa (9.3 ksi)] in Figure 4.20(b) only show slight differences in their peak shear values. This seems to be due to the fact that these two columns have slightly different parameters such as different axial loads and concrete compressive strength. The spacing of 125 mm (5 in.) rather than 150 mm (6 in.) seems to have greater effect toward large drift ratio values as shown the figure.

220
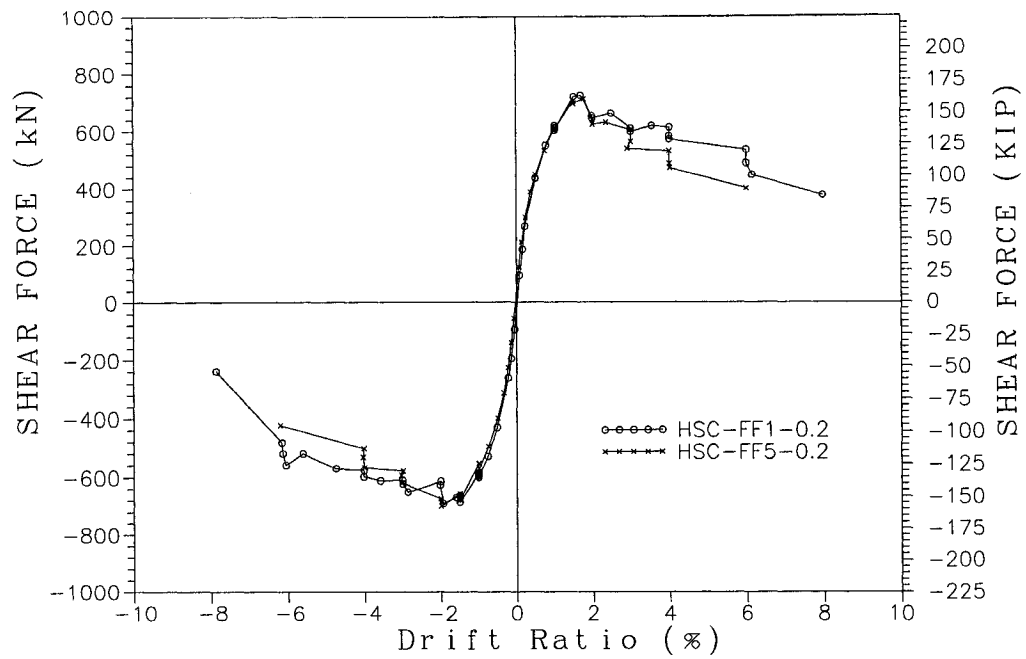
Fig. 4.20(a)-Influence of transverse reinforcement spacing
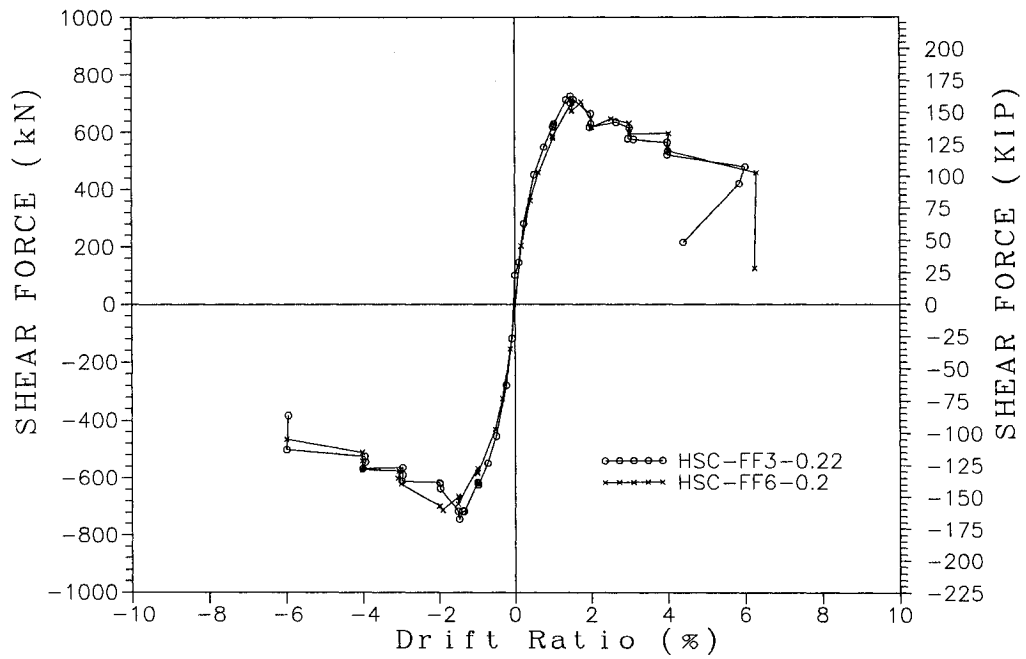
Fig. 4.20(b)-Influence of transverse reinforcement spacing

221

4.5 LONGITUDINAL STRAINS

The peak shear envelope versus longitudinal reinforcement strains measured at 0, 250, 500, 750, and 1000 mm (0, 10, 20, 30, and 40 in.) from the column stubs are shown in Figures 4.21 to 4.26. For each specimen, the positive shear values reflect push-loading and negative shear values reflect pull-loading condition. The longitudinal bar strains are measured both on the right and left sides as shown on Figure 4.9. All positive and negative longitudinal strain values reflect that the longitudinal reinforcements are undergoing tension and compression, respectively.

As shown in Figure 4.21(a) and 4.21(b), during the tension stage of the longitudinal reinforcements, the highest strain values existed within the first 500 mm (20 in.) measured from the column stub for specimen FF1. This is also apparent in Figure 4.1 which shows that the majority of the flexural cracks appears approximately within the first 500mm (20 in.) from the stub. When longitudinal reinforcement underwent compression, largest compressive strains were observed at approximately 750 mm (30 in.) from the column stub. The lowest measured compressive and tensile strains were located at 1000mm (40 in.) from the column stub. The maximum tension strains at distances of 0 mm (0 in.), 250 mm (10 in.), and 500mm (20 in.) from the stub were almost the same with a value of approximately 8000 Micro strain.

222
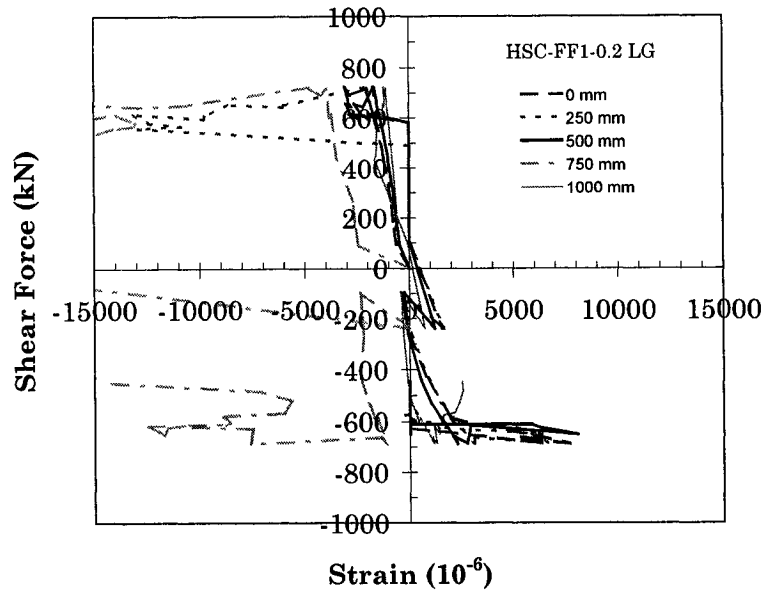
Fig. 4.21(a)-Left peak longitudinal reinforcement strains along column length for specimen FHC1-0.2.
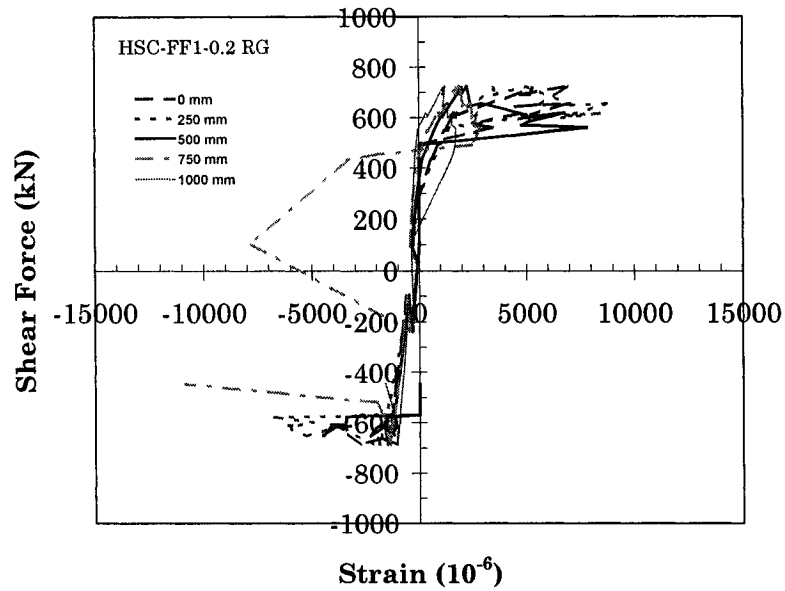
Fig. 4.21(b)-Right peak longitudinal reinforcement strains along column length for specimen FHC1-0.2.

223

Figure 4.22(a) and 4.22(b) show that the maximum tensile strains are located at 0 mm (0 in.), 250mm(10 in.), and 500mm(20 in.) from column stub, where the maximum compressive strains are observed at 250mm (10 in.) from column stub. It is apparent that the locations of highest compressive strains shifted closer to the column stub for specimen FHC2-0.34 when compared those of specimen FHC1-0.2 shown in Figures 4.21(a) and 4.21(b). The tensile strains of specimen FHC2-0.34 have much wider distributions along column length in comparison to those of specimen FHC1-0.2. It seems that such variation of strains is caused by increase level of axial load which increases additional axial forces exerted onto the longitudinal bars. It seems that the plastic hinge length may rotate closer to the column stubs when area is subjected to higher axial load.

For specimen FHC3-0.22, the maximum tensile strains were located 0 mm (0 in.), 250 mm (10 in.), and 500 mm (20 in.) from column stub as shown in Figures 4.23(a) and 4.23(b). The maximum compressive strain was located 250 mm (10 in.) from column stub. Similar to specimen FHC1-0.2, the tensile strains were almost the same up to 500 mm (20 in.) distance from column stub. From a distance of 750 mm (30 in.) from column stub, the tensile strains were drastically reduced.

224

Similar to specimen FHC2-0.34 shown in Figures 4.22(a) and 4.22(b), specimen FHC4-0.33 has wider distribution of maximum tensile strains in comparison to specimen FHC3-0.22. As shown in Figures 4.22(a) and 4.22(b) for specimen FHC2-0.34, the maximum tensile strains for specimen FHC4-0.33 are also located up to a distance of about 500 mm (20 in.) from column stub and the location of the maximum compressive strain is also 250 mm (10 in.) from column stub as shown in Figures 4.24(a) and 4.24(b).

For specimens FHC5-0.2 and FHC6-0.2, similar to specimens FF1 and FF2, also show that the maximum tensile strains are located at 250 mm (10 in.) and 500 mm (20 in.) from column stub as shown in Figures 4.25(a), 4.25(b), 4.26(a), and 4.26(b). This was the case for all specimens except for the right gauge in tension for specimen FF3 and for both right and left gauges of specimen FF4 where the maximum tensile strains were located at the column stub (0mm). The maximum compressive strain for specimen FHC6-0.2 is also located 250 mm (10 in.) from column stub as it was for specimens FHC2-0.34, FHC3-0.22, FHC4-0.33, and FHC5-0.2.

The strain distribution of longitudinal reinforcements indicates a variation of plastic hinge length. Based on the variations in the strain distributions with respect to the axial load level, it can be observed that higher axial loads increase

225

the variations of tensile strains along the column length measured from column stub, particularly in the plastic hinge area up to a distance of about 500 mm (20 in.) from column stub. Also, it is evident that greater the spacing of the transverse reinforcements, there seems to be a greater variation of strains along the column length. Closer spacing of transverse reinforcements increases an even distribution of strains along column length. For all specimens the maximum compressive strains were observed at 250mm (10 in.) from the column stub, except for specimen FHC1-0.2 its maximum value at 750mm (30 in.).
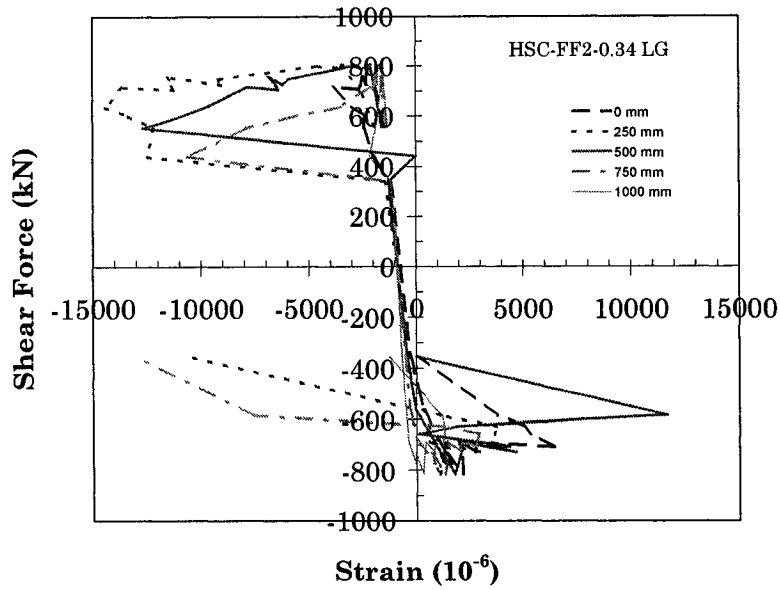
Fig. 4.22(a)-Left peak longitudinal reinforcement strains along column length for specimen FHC2-0.34.
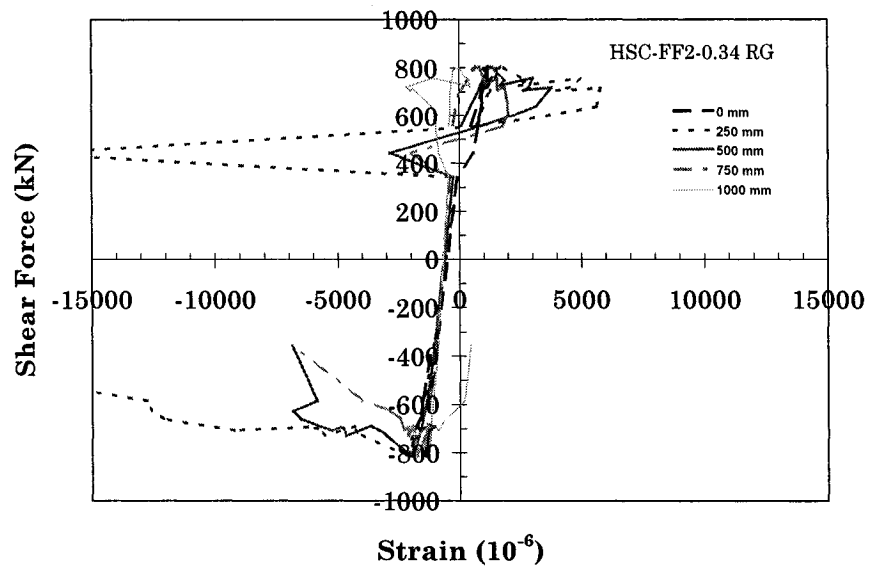
Fig. 4.22(b)-Right peak longitudinal reinforcement strains along column length for specimen FHC2-0.34.

227
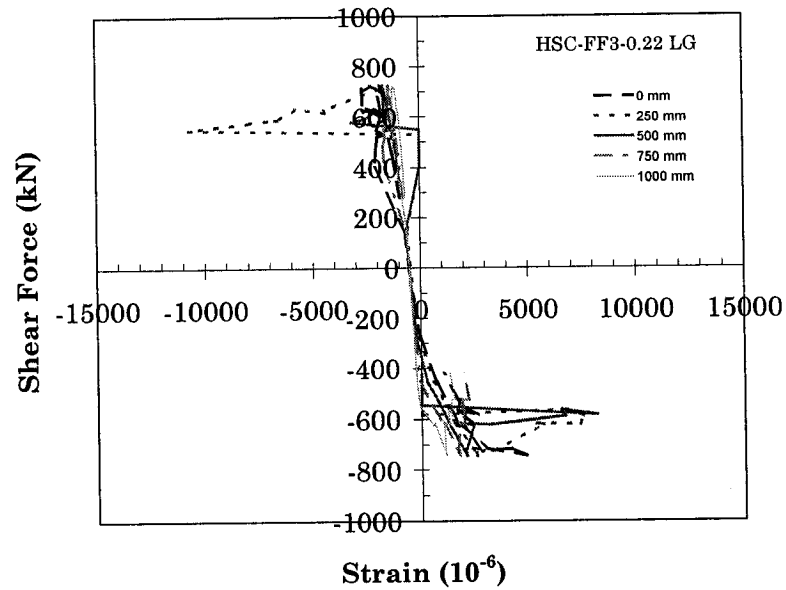
Fig. 4.23(a)-Left peak longitudinal reinforcement strains along column length for specimen FHC3-0.22.
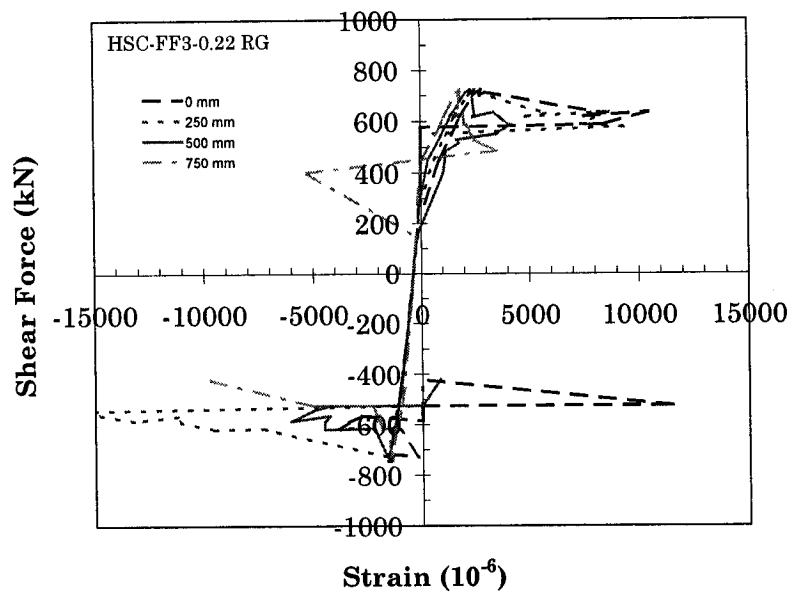
Fig. 4.23(b)-Right peak longitudinal reinforcement strains along column length for specimen FHC3-0.22.

228
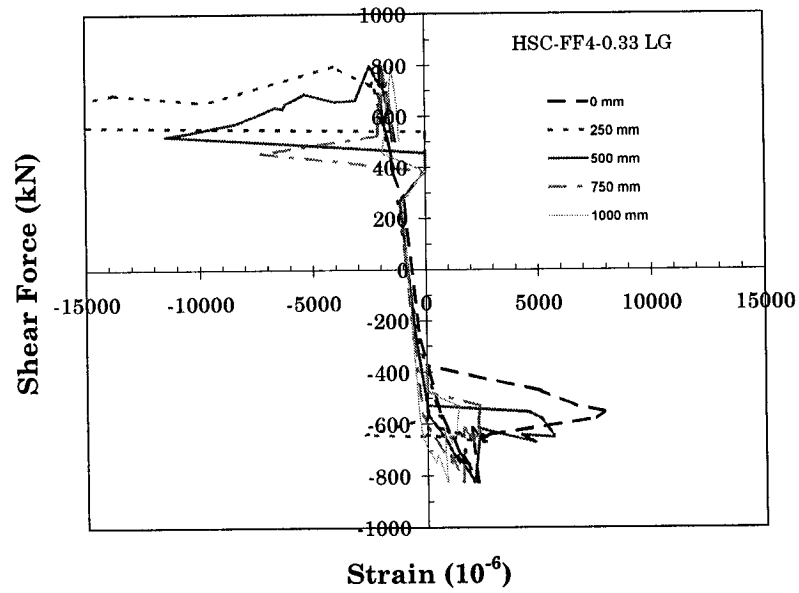
Fig. 4.24(a)-Left peak longitudinal reinforcement strains along column length for specimen FHC4-0.33.
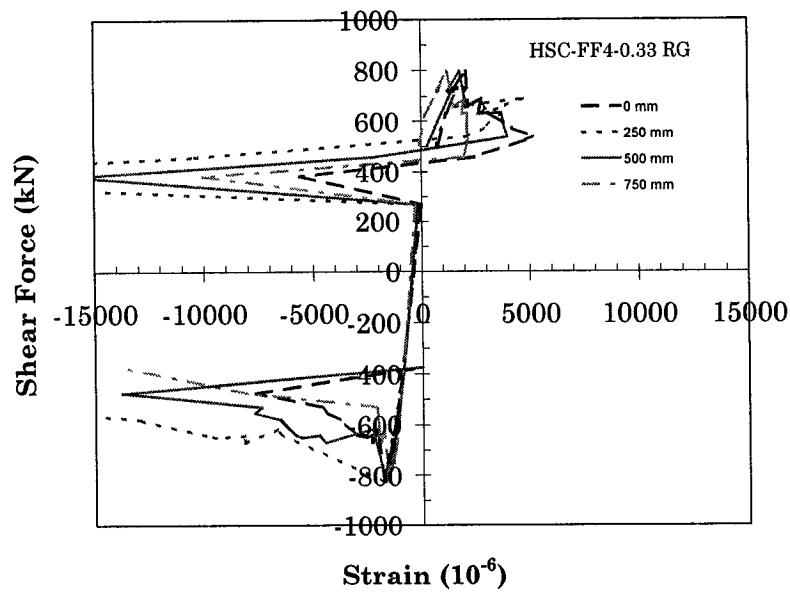
Fig. 4.24(b)-Right peak longitudinal reinforcement strains along column length for specimen FHC4-0.33.

229
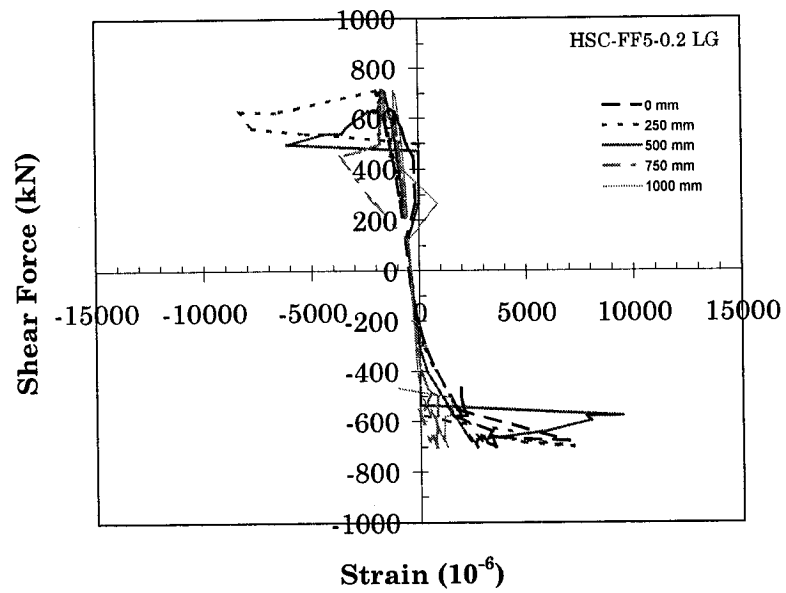
Fig. 4.25(a)-Left peak longitudinal reinforcement strains along column length for specimen FHC5-0.2.
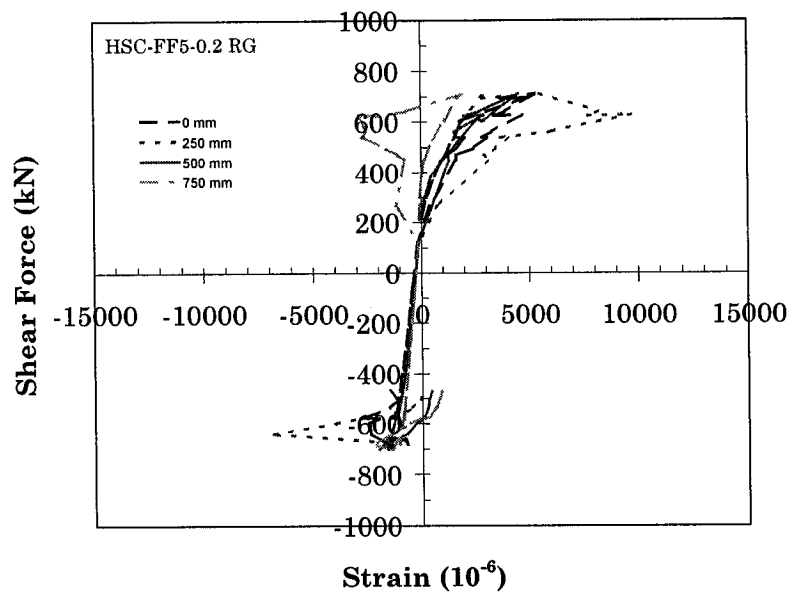
Fig. 4.25(b)-Right peak longitudinal reinforcement strains along column length for specimen FHC5-0.2.

230
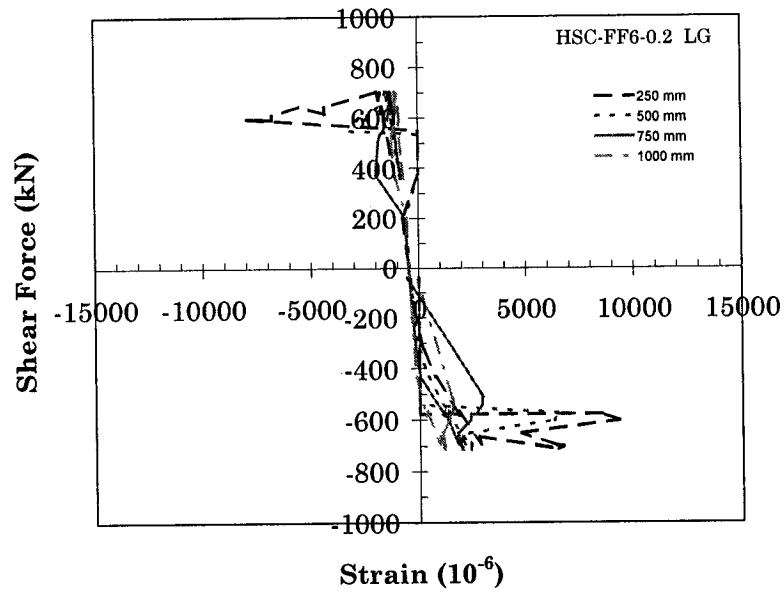
Fig. 4.26(a)-Left peak longitudinal reinforcement strains along column length for specimen FHC6-0.2.
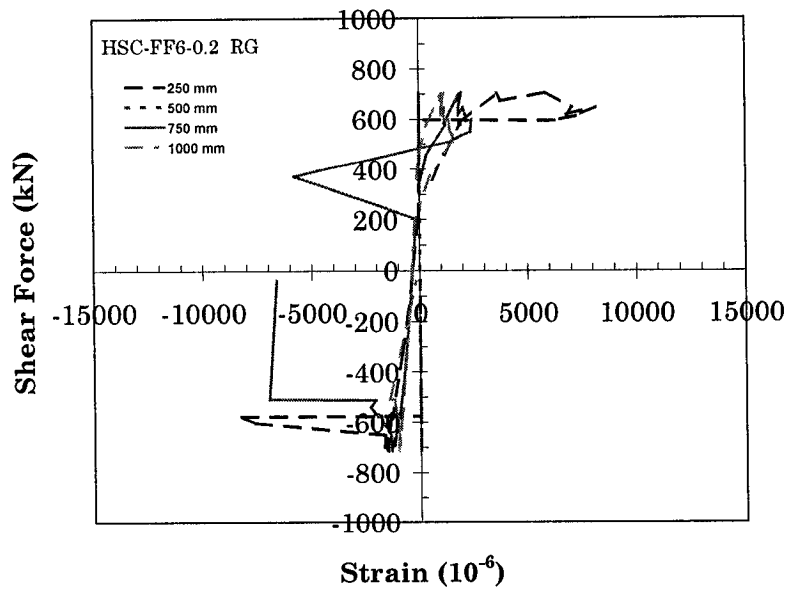
Fig. 4.26(b)-Right peak longitudinal reinforcement strains along column length for specimen FHC6-0.2.

231

The Figures 4.28 to 4.33 show the Shear Force versus Micro-strain relationships obtained from the experiment. For each of the six specimens, the results measured by the lower most longitudinal bar strain gauge in the potential plastic hinge region located at about 250mm (10 in.) from the foundation surface level are shown in (b) figures. Also shown in (a) figures for comparison is the result measured by the upper most longitudinal bar strain gauge which is located outside the potential plastic hinge region at about 1000mm (40 in.) from the foundation surface level.

The Figures 4.27 to 4.32 show values obtained from left longitudinal bar strain gauges on the longitudinal bar away from the horizontal shear force actuator. For each specimen, the upper longitudinal bar strain gauge further away from the foundation surface level reflect smaller tensile strain values as compared to that of the lower longitudinal bar strain gauge. This confirms that the longitudinal bars in the plastic hinge region underwent greater strains throughout the experiments.

In all cases, the positive values of the microstrain means that the longitudinal bar is undergoing tension during "pull" loading, and the negative values of the microstrain means that the longitudinal bar is undergoing compression during "push" loading.

232

It can be seen that the strain hysteresis curves are shifted toward left. This is due to the axial force which is applied onto the longitudinal bars throughout the cyclical lateral force loading on the column. The specimens with high axial load level, FHC2-0.34 and FHC4-0.33, were shifted quite substantially to the left. The overall strain hysteresis curves for the strain gauges 1000 mm (40 in.) above the foundation surface (upper gauges) were much smaller in area as compared to those at 250 mm (10 in.) above the foundation surface (lower gauges). This verifies that much greater energy dissipation occurred in the plastic hinge region as compared to the upper column region.

When the compression force is applied onto the longitudinal bar during "push" loading, the upper gauges underwent much smaller displacements as compared to during "pull" loading. This is due to the role of the concrete which restricted displacement during the compression or "push" phase of loading, where the longitudinal bar was deformed to much greater extent during the tension or "pull" phase of the loading. However, in the plastic hinge region, it is noticeable that such differences in the strain values between tension and compression phases were much less, considering the shift to the left due to the axial load. This is anticipated because there is more rotation in the plastic hinge region as the concrete cracked, allowing more compressive stress to be applied in the compression zone of the column section. For the plastic hinge region, the

233

consecutive strain values were proportionately much greater as compared to previous cycles. This seems to be caused by increase in the column drift as well as the strain hardening effect and the yielding of the bars. By comparison of the results between Figures 4.27 and 4.31, it is apparent that increased transverse reinforcement spacing reduced the energy absorption as evidenced by reduced area of the strain hysteresis curves. Also, the use of high grade steel seems to have increased the overall energy absorption by the longitudinal reinforcement as evidenced by increased area of the strain hysteresis curves for Figure 4.32 in comparison to Figure 4.31.

234
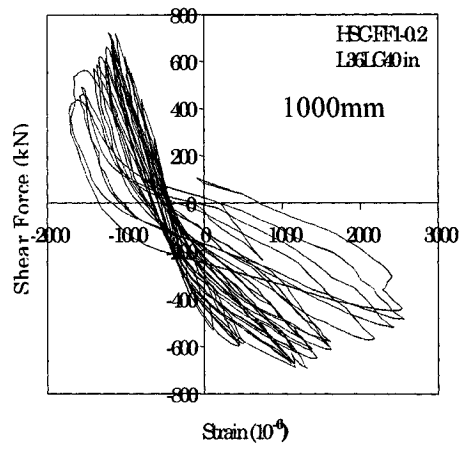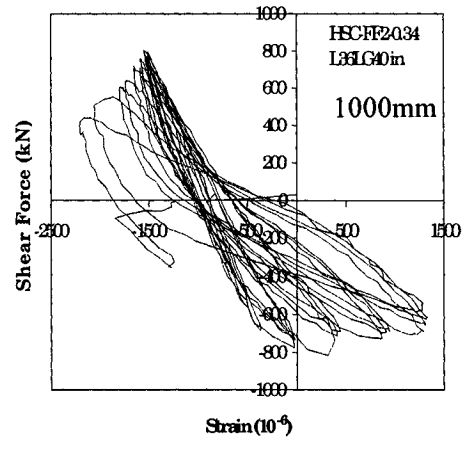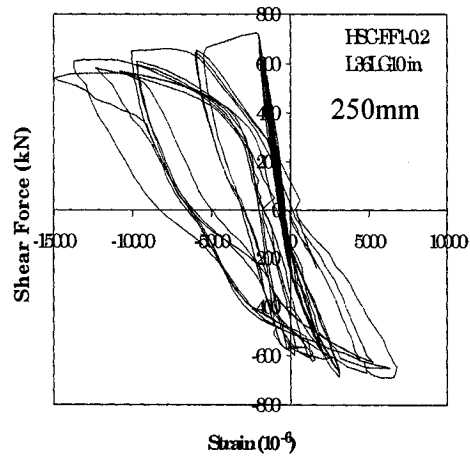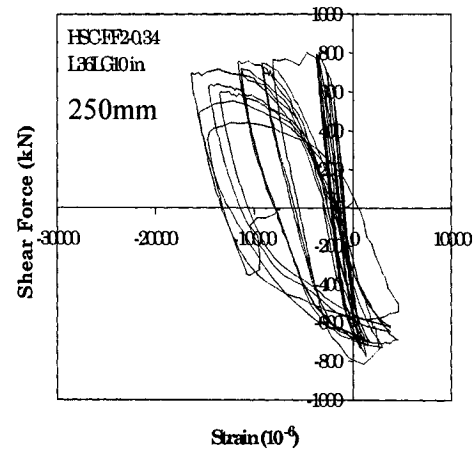
Fig. 4.27-Longitudinal strains.

Fig. 4.28-Longitudinal strains.

235

(a)
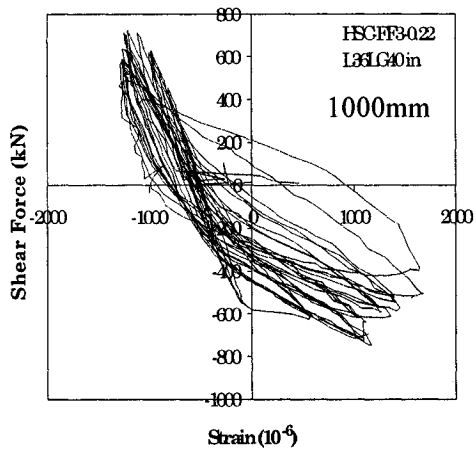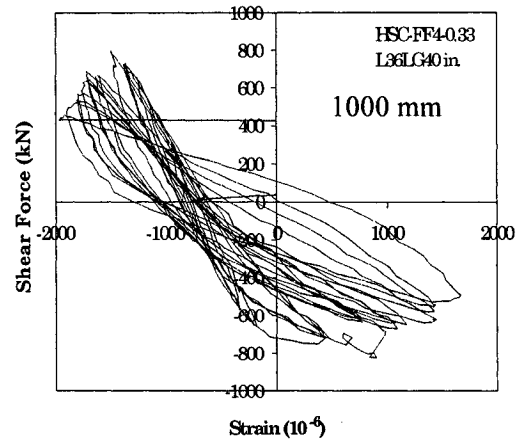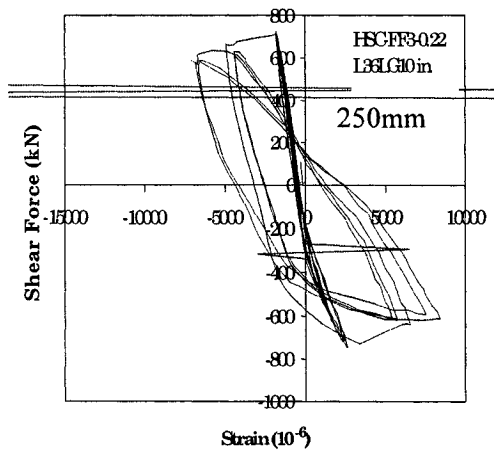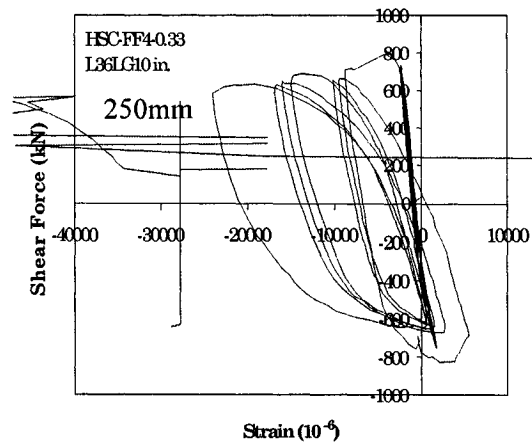
(b)

Fig. 4.29-Longitudinal strains.

(a)

(b)

Fig. 4.30-Longitudinal strains.

236
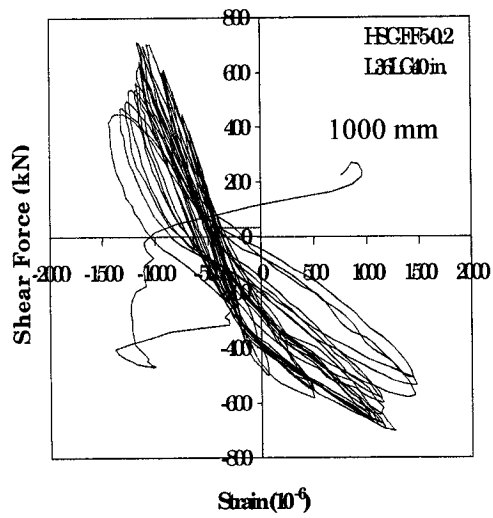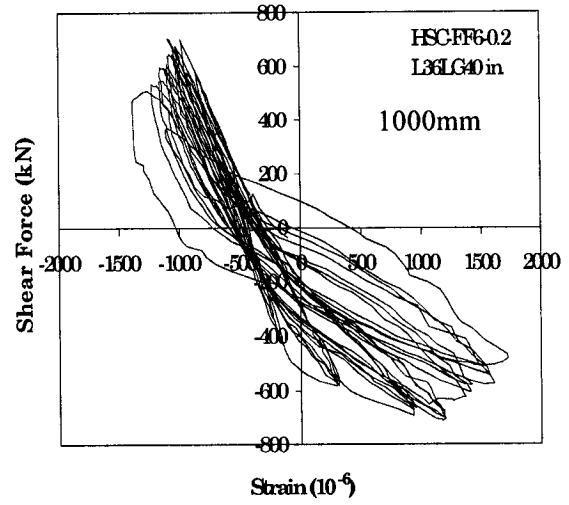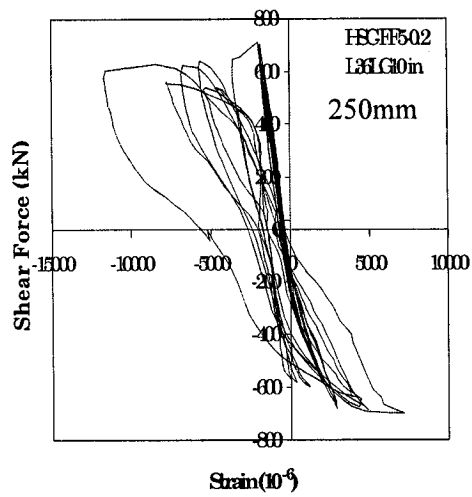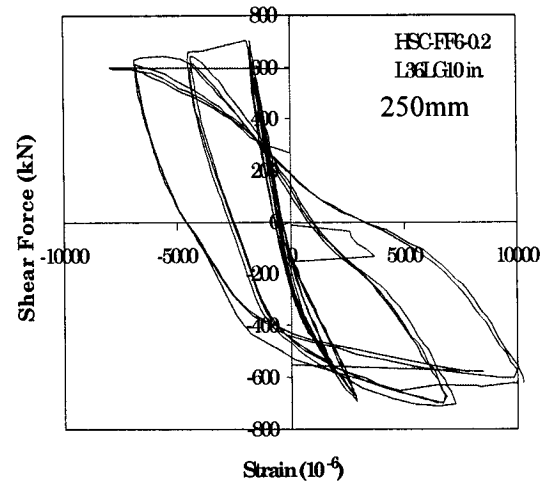
Fig. 4.31-Longitudinal strains

Fig. 4.32-Longitudinal strains

237

The following figures 4.33 to 4.38 show the variation of peak experimental longitudinal reinforcement tensile strains along the column height measured from the stub at each drift. The results correlate to the peak envelope of right longitudinal reinforcement strains as previously shown in figures 4.21 to 4.26. The maximum tensile strain is once again shown to exist within a distance of approximately 0 to 250 mm (10 in.) from the column stub for all specimens. The values logged by a strain gage located at 500 mm (20 in.) from the column stub for specimen FHC6-0.2 is an invalid gage which seems to have failed at early stage of the experiment.

For all specimens the first yielding of the longitudinal bars were reached within the drift ratio range from 0.8% to 1.4% . Figures 4.33 and 4.34 show that maximum strains are reached at 250 mm (10 in.) from the column stub. On the other hand, figures 4.35 and 4.36 show that the locations of maximum strain begin from the column stub. This seems to be due to the increased transverse reinforcement spacing provided for specimens FHC3-0.22 and FHC4-0.33.

As shown in figures 4.37 and 4.38, specimens FHC5-0.2 and FHC6-0.2 with largest transverse reinforcement spacing of 150 mm (6 in.) show maximum longitudinal strains at 250 mm (10 in.) from column stub. The comparison between figures 4.37 and 4.38 show that the use of higher grade transverse steel reinforcement gave slightly less longitudinal strain values at the drift ratios of 2%

238

and 3%, respectively. It seems that axial load levels, transverse reinforcement spacing, and the grade type of transverse reinforcement all affect the strain distribution of the longitudinal reinforcements. The combinations of these factors also may have different effect on such strain distributions.
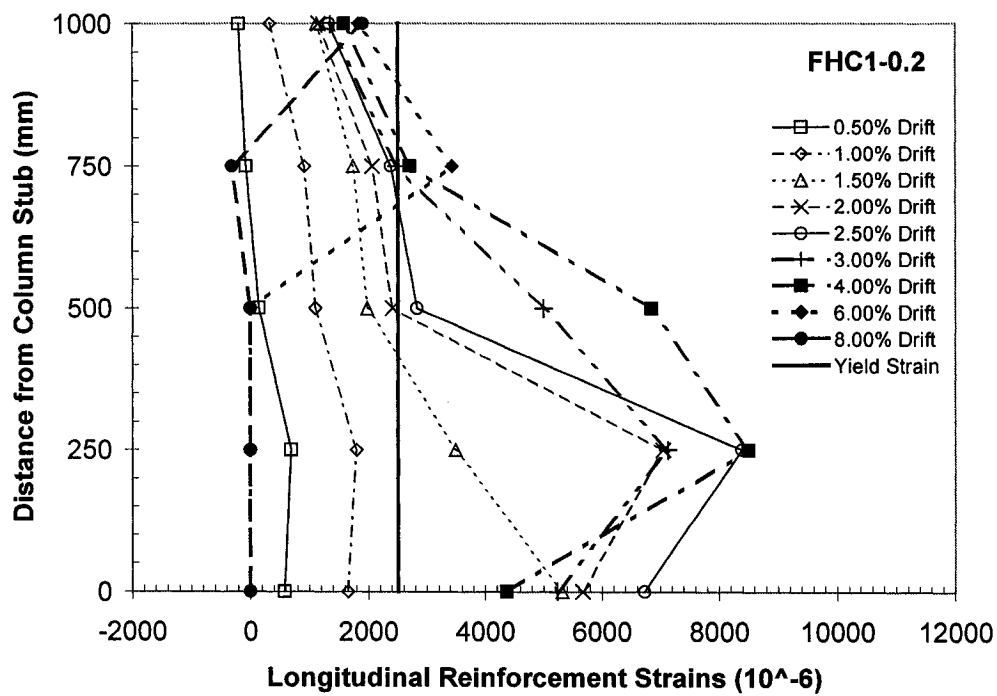
Fig. 4.33-Longitudinal Strains Along Column Height

239
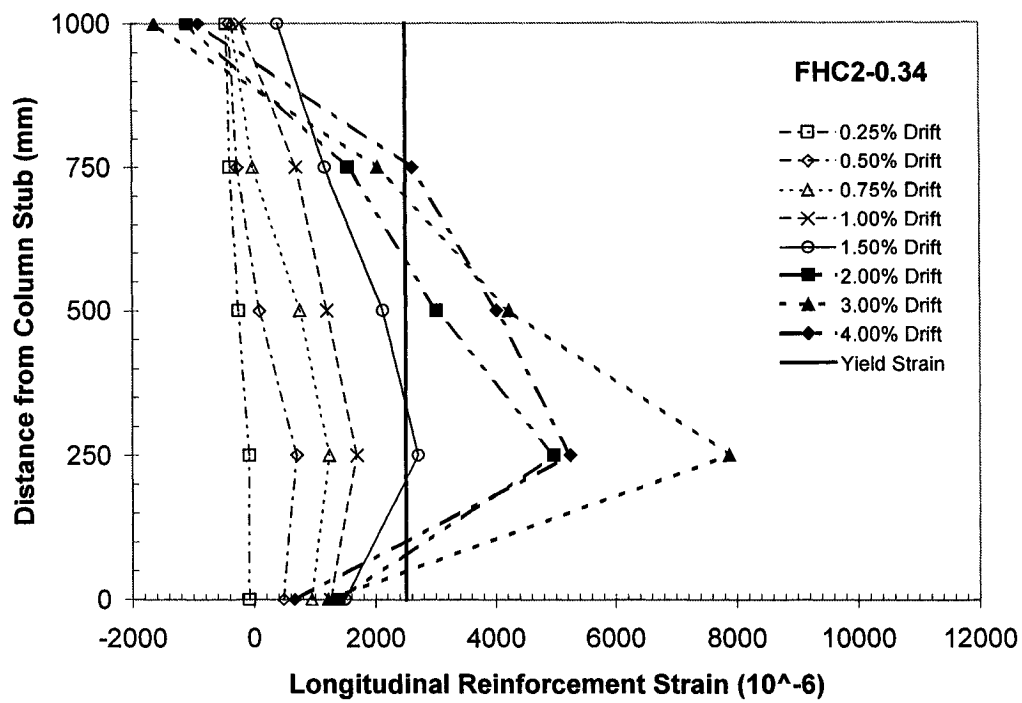
Fig. 4.34-Longitudinal Strains Along Column Height

240
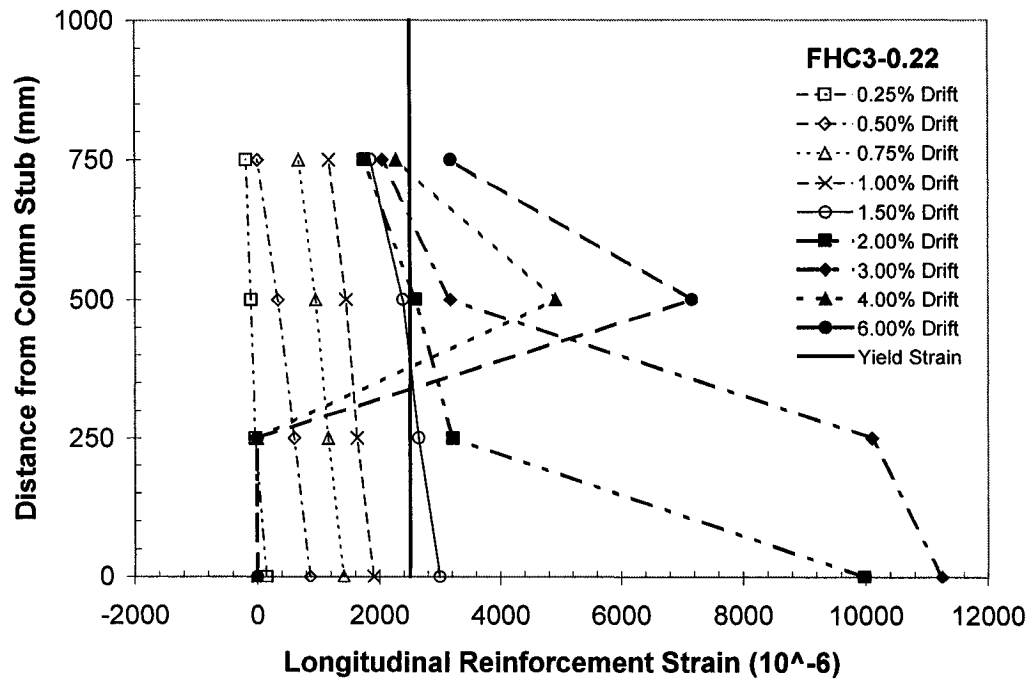
Fig. 4.35-Longitudinal Strains Along Column Height

241
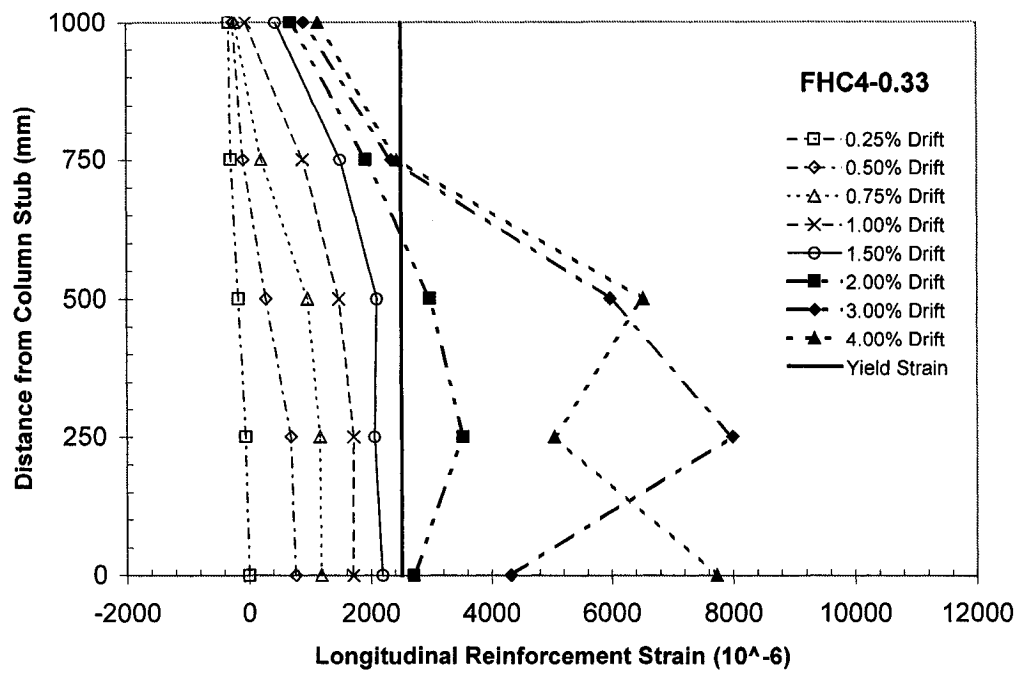
Fig. 4.36-Longitudinal Strains Along Column
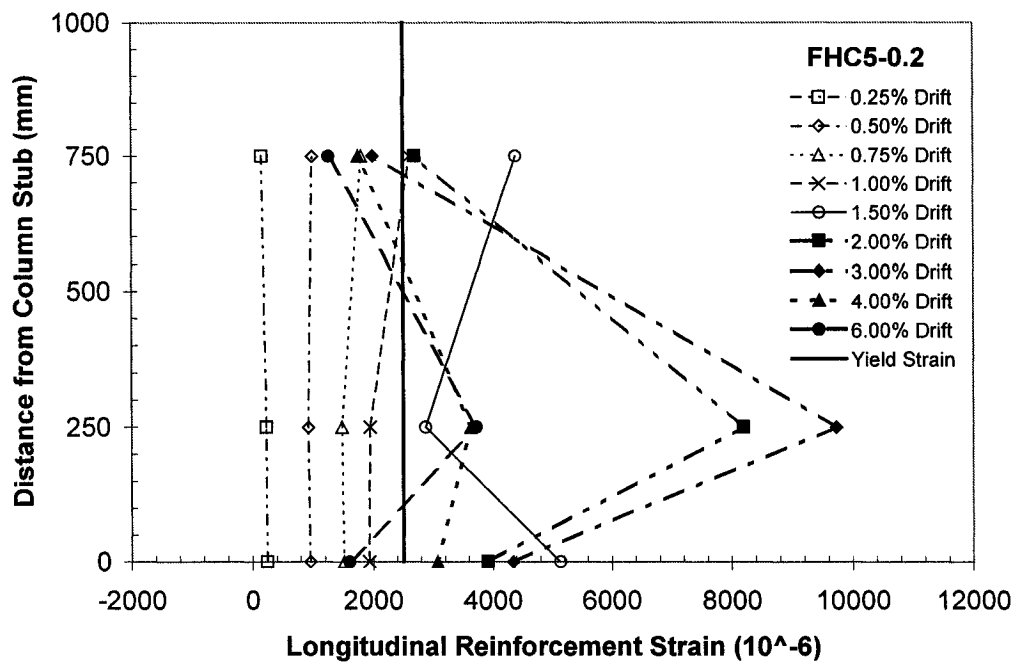
Fig. 4.37-Longitudinal Strains Along Column

243
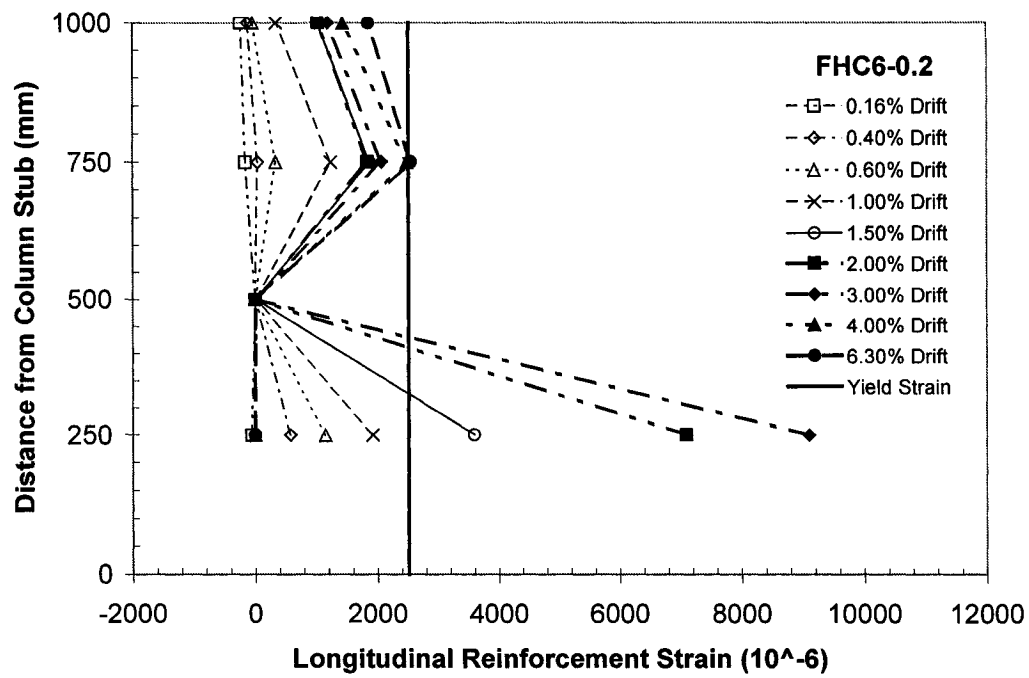
Fig. 4.38-Longitudinal Strains Along Column

244

4.6 TRANSVERSE STRAINS

The hoop and tie strains are shown on Appendix IV. The hoop and tie strains in the plastic hinge region had largest values. Depending on different test parameter values such as the applied axial load, tie or hoop gave larger values of microstrains. In most cases, the second and/or third hoops from the foundation surface level reached the largest maximum strains as compared to other hoops. The Shear Force versus Microstrain relationships for the ties were mostly similar to that of the hoops. The maximum microstrains of ties were either greater or less as compared to those of hoops depending on the location and the test parameters that were considered.

The figures AIV.14 through AIV.19 of Appendix IV show a comparison between the hoop and tie microstrains at two different levels. The last number in the specimen designations show the height of the strain gauges in millimeter unit measured from the foundation surface. The microstrains of the second hoop and tie from the foundation surface which are 14 inches (350mm), 17 inches (425mm), or 20 inches (500mm) from the foundation surface are compared to those of the first hoop and tie from the foundation surface which are only 6 inches (150mm), 7 inches (175mm), or 8 inches (200mm) from the foundation surface. The second column of the figures shows larger values of microstrains for hoops

245

and ties in the upper part of the plastic hinge region in comparison to the strains of the first hoops and ties from the foundation surface as shown in the second column of the figures. It is clear that the largest deformation of transverse reinforcements occurs a distance away from the column stub within the potential plastic hinge region. The Figures 4.10(a) and (b) show the location of the strain gauges on hoops and ties from the foundation surface.

The following Figures 4.39 to 4.44 show Micro-strain versus Drift Ratio relationships for the transverse hoops and ties at three different locations from each column stub. The strain values shown are for side hoop and tie gauges as shown on Figure 4.9. For each specimen, the strains are shown at drift ratios corresponding to the peak shear value of each cycle for positive drift ratios only. For all specimens, except for the transverse tie strains of specimen FHC1-0.2 at 150 mm (5.9 in.) from column stub as shown in Figure 4.39(c), both transverse tie and hoops strain values were highest at farthest location away from the column stubs and lowest near the column stubs. For specimens FHC1-0.2 and FHC2-0.34, hoop strains were higher at a distance of 600 mm (23.6 in.) from column stub where tie strains were higher at distances of 350 mm (13.8 in.) and 150 mm (5.9 in.) from column stub as shown on figures 4.39 and 4.40. The similar strain values were reached at a drift ratio of approximately 5.5% for specimen FHC1-0.2 and 3.0% for specimen FHC2-0.34, except for extremely high value of tie strain

246

for specimen FHC1-0.2 at a distance of 150 mm (5.9 in.) from column stub as shown in figure 4.39(c).

With use of higher grade 520 (ASTM Grade 75) reinforcements, the strains for specimen FHC3-0.22 did not reach yield values for low level of axial load at distances of 425 mm (16.7 in.) from column stub as shown in figure 4.41(a). However, for higher axial load level, specimen FHC4-0.33 also with use of higher grade 520 (ASTM Grade 75) reinforcement and the same spacing, the yield values were exceeded for both tie and hoop strains also at a distance of 425 mm (16.7 in.) from column stub as shown in figure 4.42(b). It appears that tie strains were dominant in comparison to hoop strains for lower axial load levels where both hoop and tie strains were more similar in values for higher axial load levels as shown in figures 4.39 and 4.42. Such dominance in tie strains is more apparent within distance range of 50 mm (2 in.) to 350 mm (13.8 in.) from column stub for specimens FHC1-0.2 and FHC3-0.22 both subjected to low axial load levels as shown in figures 4.39 and 4.41. Both hoop and tie strain values were more similar for specimens FHC2-0.34 and FHC4-0.33 both subjected to high axial loads as shown in figures 4.40 and 4.42. As shown in figures 4.43 and 4.44, specimens FHC5-0.2 and FHC6-0.2 with larger transverse reinforcement spacing in comparison to all other specimens exhibited similar strain values for both ties and hoops. However, strains for specimen FHC6-0.2 with higher grade steel

247

fluctuated in greater magnitude, especially immediately after the cover concrete spalling. On the other hand such behavior was not as drastic for specimen FHC5-0.2.

The specimens FHC1-0.2, FHC2-0.34, FHC3-0.22, and FHC4-0.33 with smaller transverse reinforcement spacing of 125 mm (5 in.) and 100 mm (4 in.) in the plastic hinge area showed relatively large gap in strain values between hoops and ties in comparison to those of specimen FHC5-0.2 and FHC6-0.2 with greater spacing of 150 mm (6 in.); however, for the cases of high axial load level application as for specimens FHC2-0.34 and FHC4-0.33, where such differences in strains of hoops and ties were minimal.

It seems that transverse reinforcement spacing, grade of reinforcement, and axial load levels have affect the strain distributions of hoops and ties in such way that the increased transverse reinforcement spacing seems to provide even strain distributions between hoops and ties while use of higher grade steel seems to delays the yield process, and the increase in axial load level increases the role of the transverse ties.

As axial load increases, the role of hoops seems to increase further as confinement is provided by both hoops and ties in relatively proportional manner. At low axial

248

load levels, the ties seems to be subjected to greater strains during the plastic hinge rotation in comparison to the hoops. The decrease in transverse reinforcement spacing in plastic hinge area seems to have increased the differences in the strain values between hoops and ties especially for low axial load cases as ties are subjected to relatively larger strains even at low drift ratios. For the cases of greater transverse reinforcement spacing, the strains of hoops and ties have similar values until greater drift ratio is reached. In comparison between figures 4.41(c) and 4.43(c), the specimen FHC5-0.2 with greater transverse reinforcement spacing reached 2% drift when the strain differences between hoops and ties begins to increase, where specimen FHC3-0.22 with smaller transverse reinforcement spacing reached less than 1% drift when such strain differences were substantial. Various factors have a role in determination of the behavior in transverse reinforcements during various stages of loading. For all specimens in general, the transverse tie reinforcement is important for all stages of loading especially for high drift ratios.

249
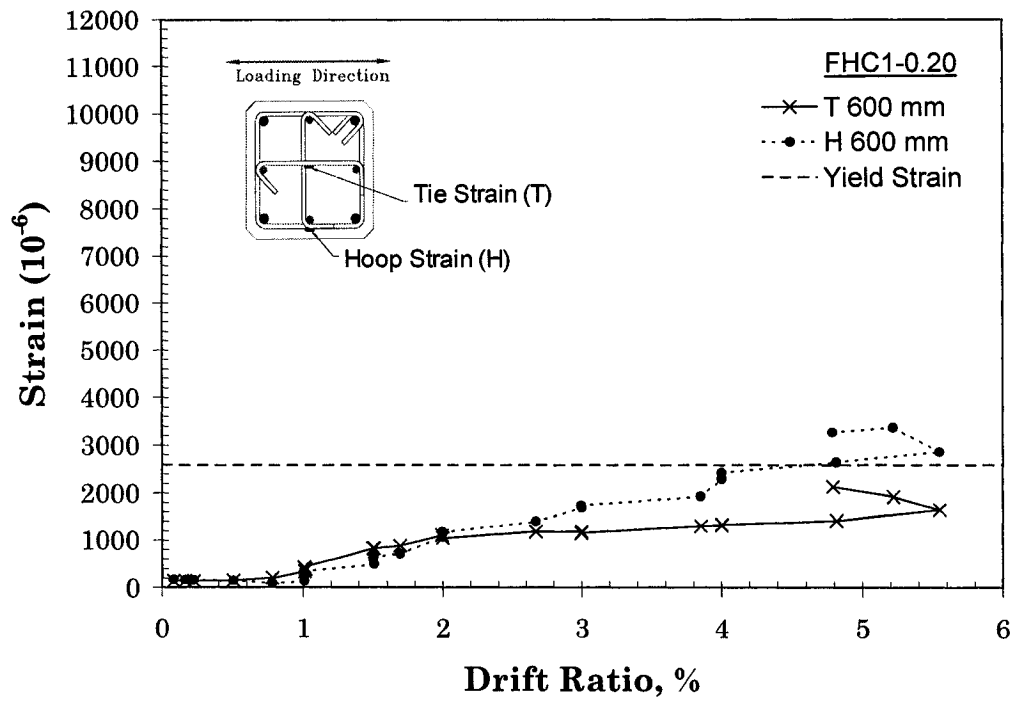
Fig. 4.39(a)-Transverse reinforcement strain versus drift ratio 600mm from column stub.

250
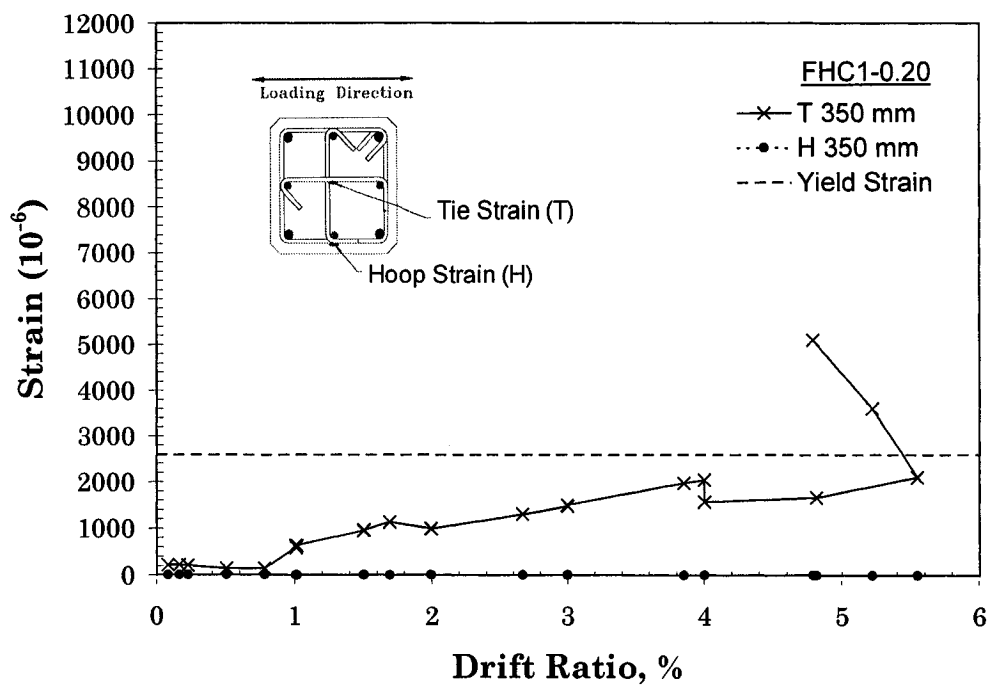
Fig. 4.39(b)-Transverse reinforcement strain versus drift ratio 350mm from column stub.

251
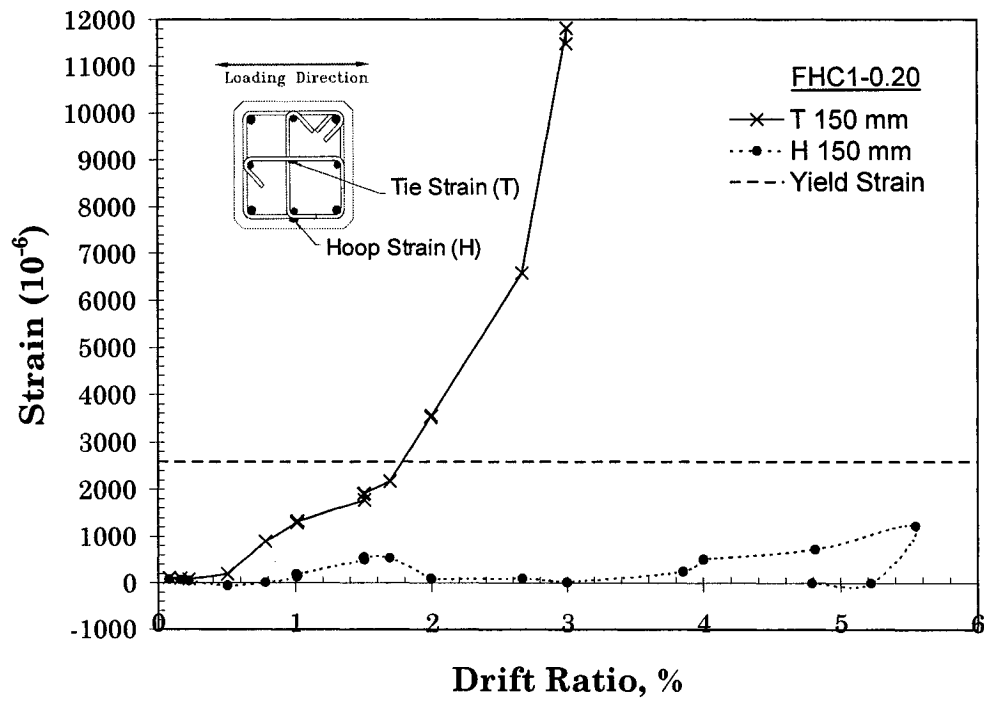
Fig. 4.39(c)-Transverse reinforcement strain versus drift ratio 150mm from column stub.

252
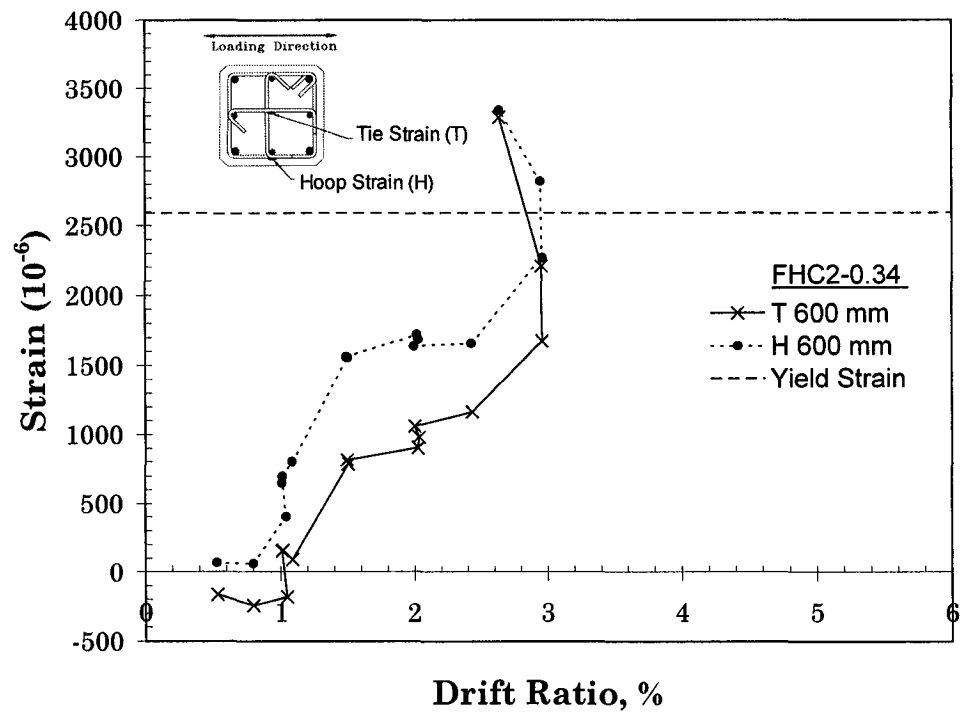
Fig. 4.40(a)-Transverse reinforcement strain versus drift ratio 600mm from column stub.

253
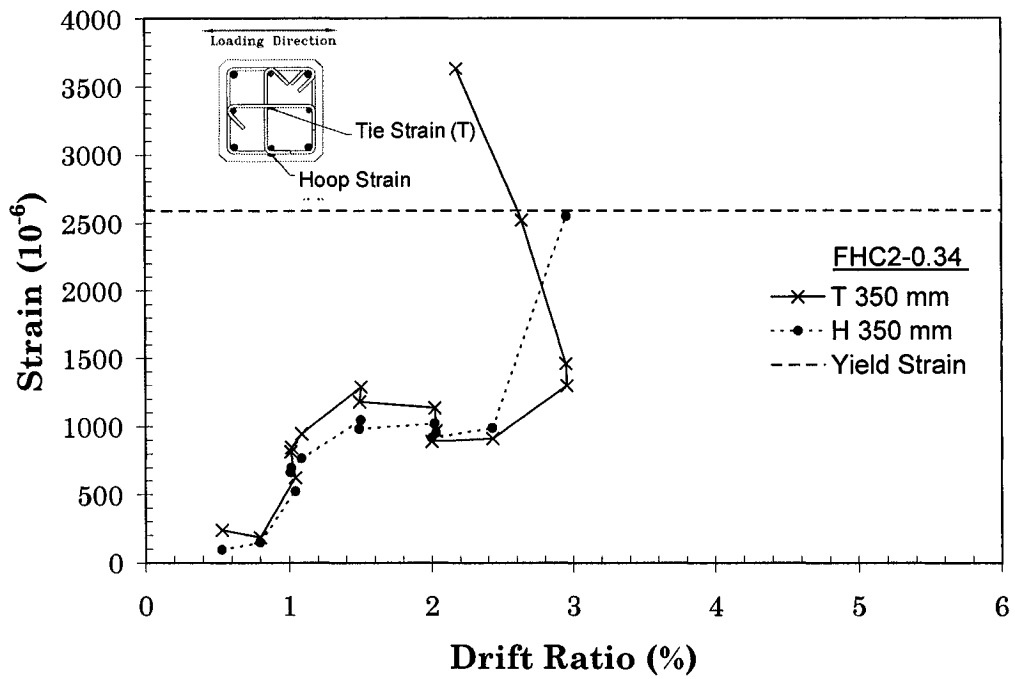
Fig. 4.40(b)-Transverse reinforcement strain versus drift ratio 350mm from column stub.

254
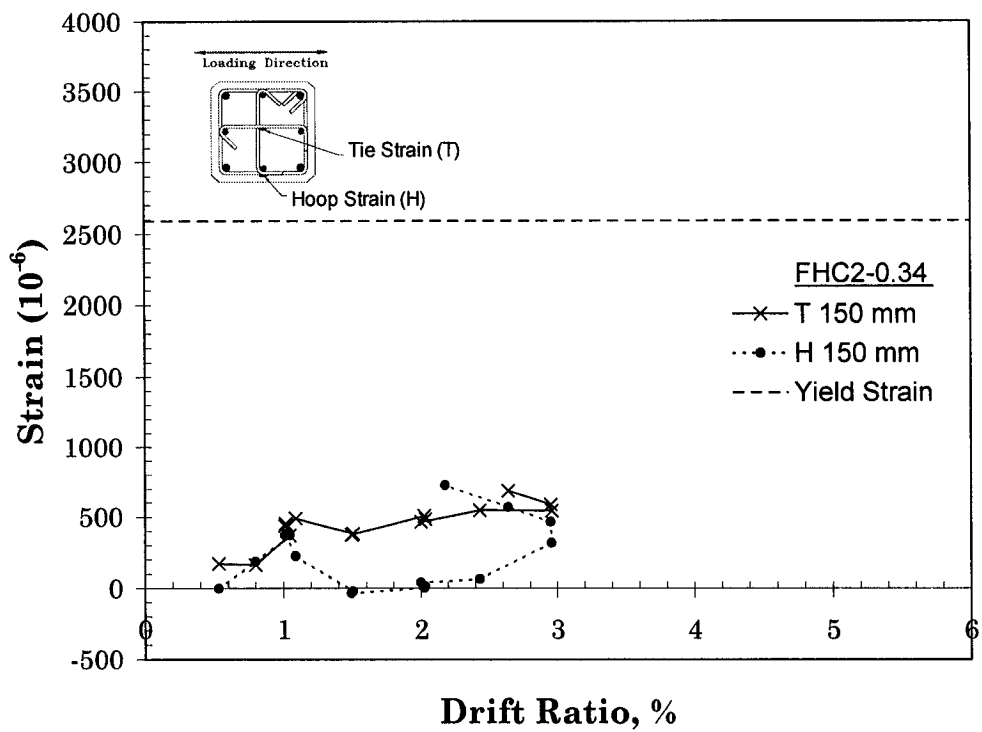
Fig. 4.40(c) -Transverse reinforcement strain versus drift ratio 150 mm from column stub.

255
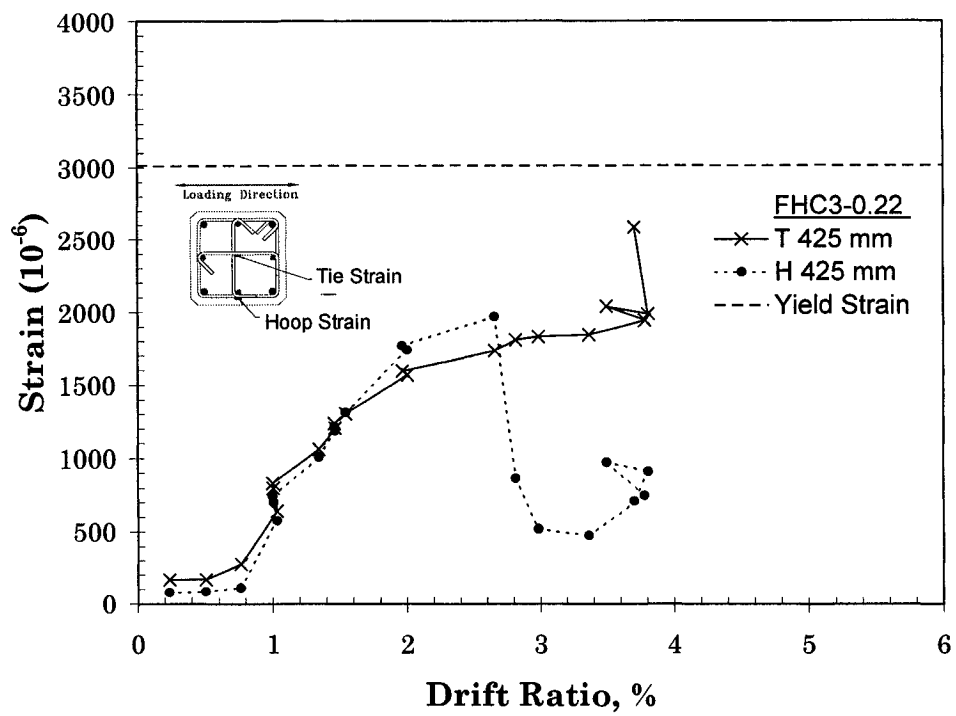
Fig. 4.41(a) -Transverse reinforcement strain versus drift ratio 425 mm from column stub.

256
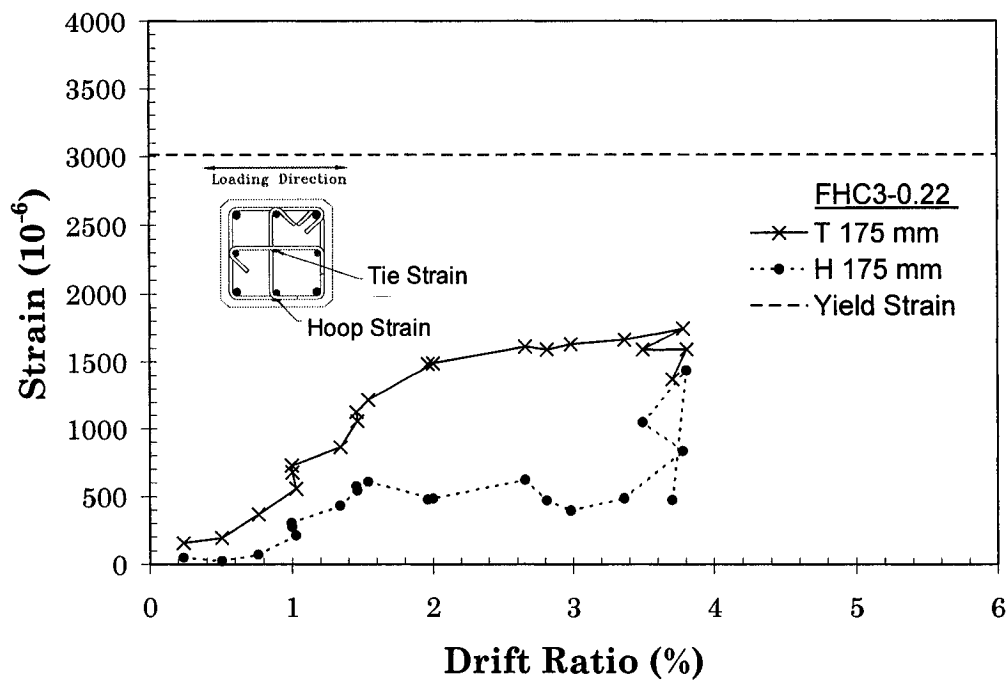
Fig. 4.41(b) -Transverse reinforcement strain versus drift ratio 175 mm
from column stub.

257
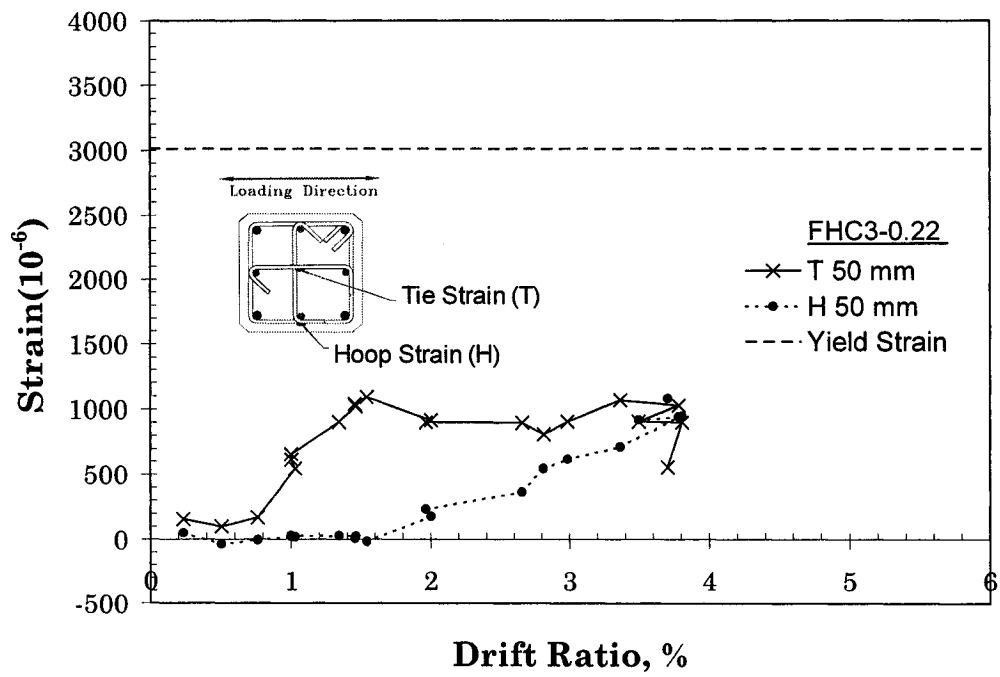
Fig. 4.41(c) -Transverse reinforcement strain versus drift ratio 50 mm from column stub.

258
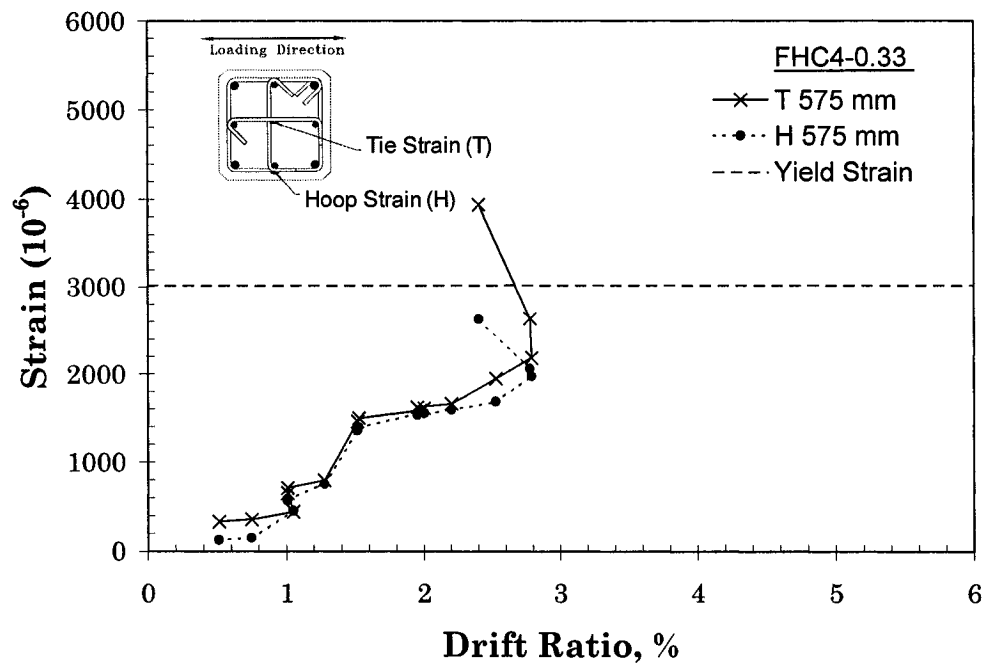
Fig. 4.42(a) -Transverse reinforcement strain versus drift ratio 575 mm from column stub.

259
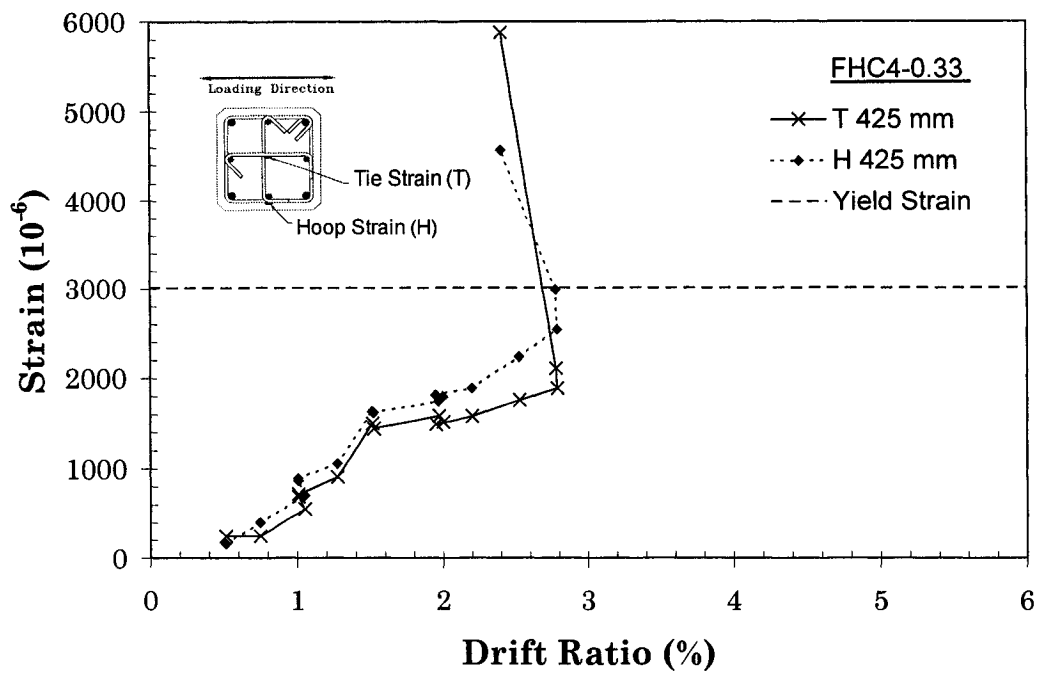
Fig. 4.42(b) -Transverse reinforcement strain versus drift ratio 425 mm from column stub.

260
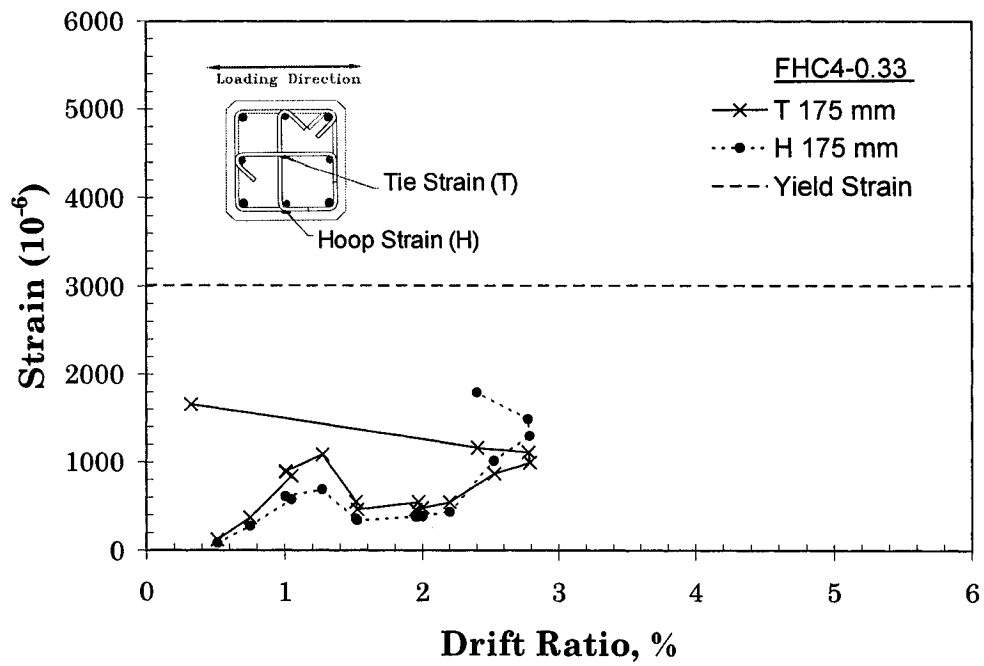
Fig. 4.42(c) -Transverse reinforcement strain versus drift ratio 175 mm from column stub.

261
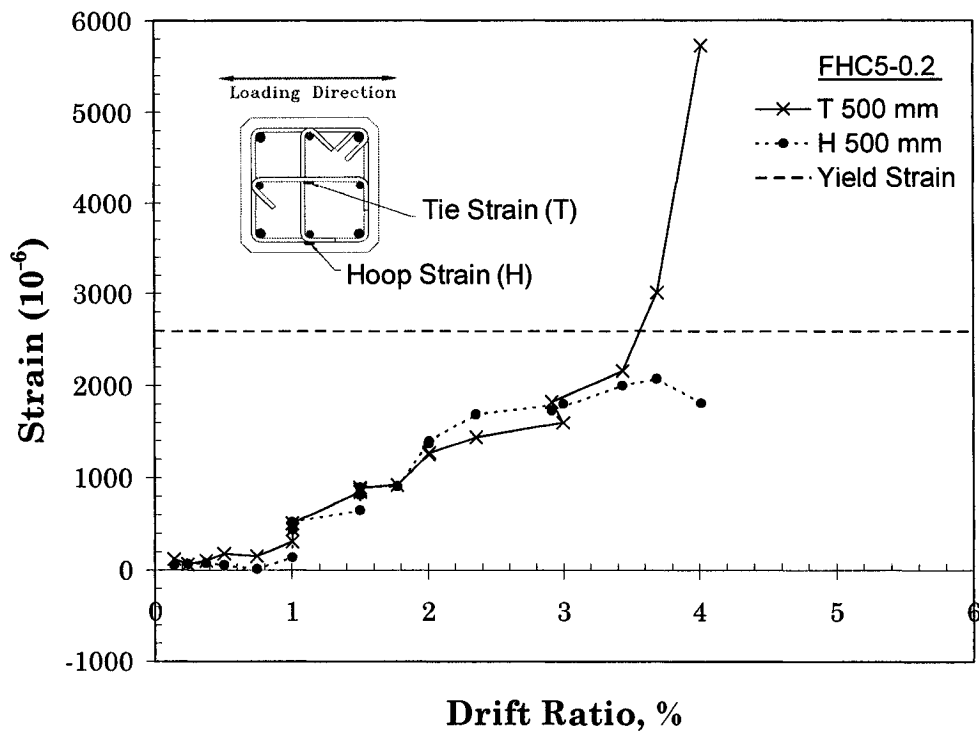
Fig. 4.43(a) -Transverse reinforcement strain versus drift ratio 500 mm from column stub.

262
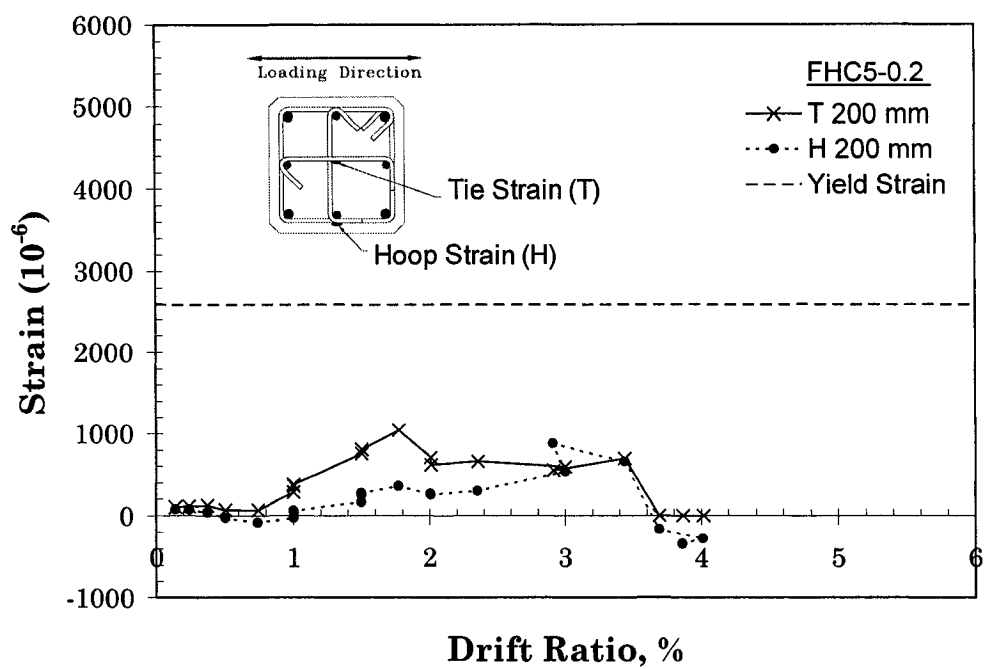
Fig. 4.43(b) -Transverse reinforcement strain versus drift ratio 200 mm from column stub.

263
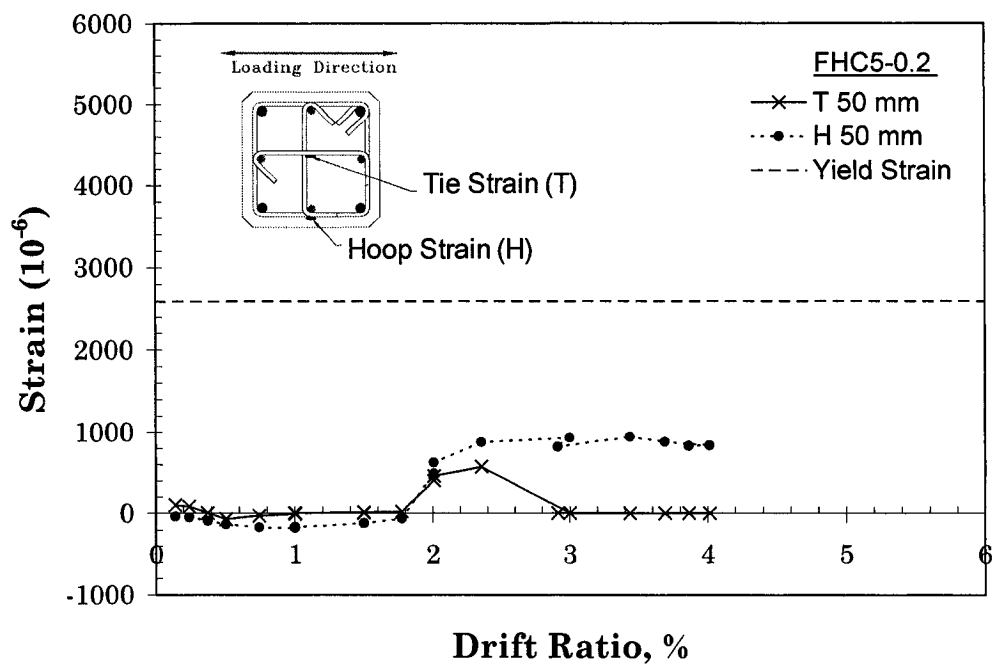
Fig. 4.43(c) -Transverse reinforcement strain versus drift ratio 50 mm from column stub.

264
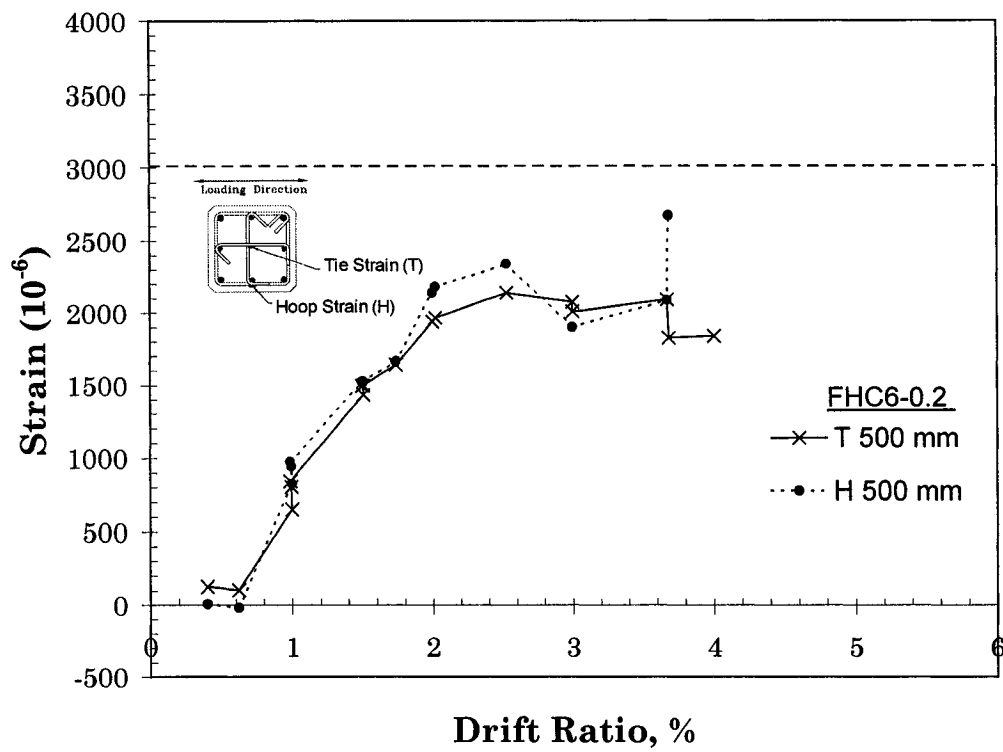
Fig. 4.44(a) -Transverse reinforcement strain versus drift ratio 500 mm from column stub.

265
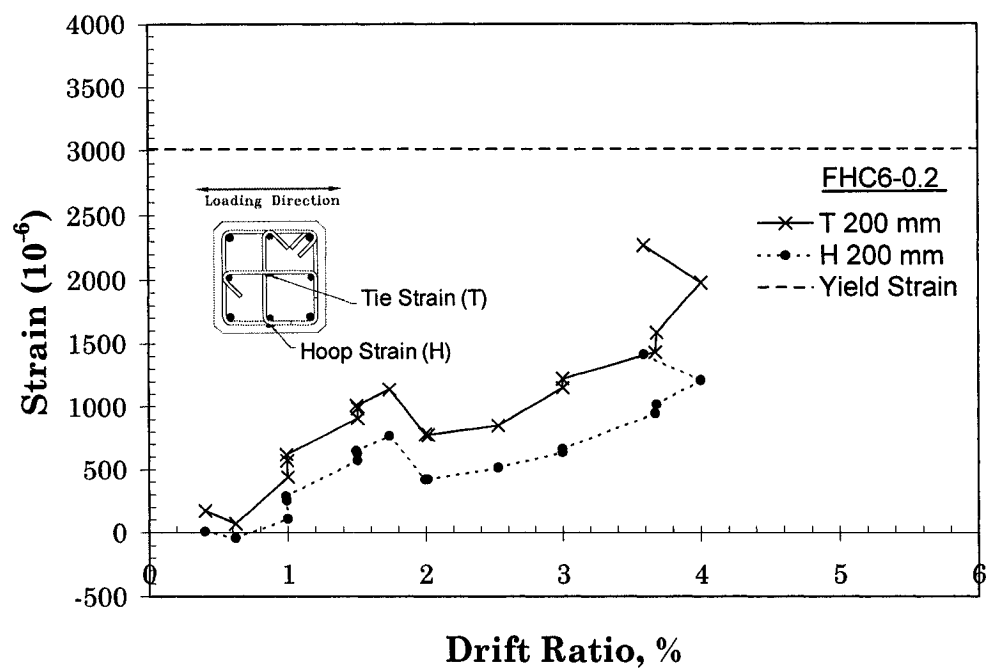
Fig. 4.44(b) -Transverse reinforcement strain versus drift ratio 200 mm
from column stub.

266
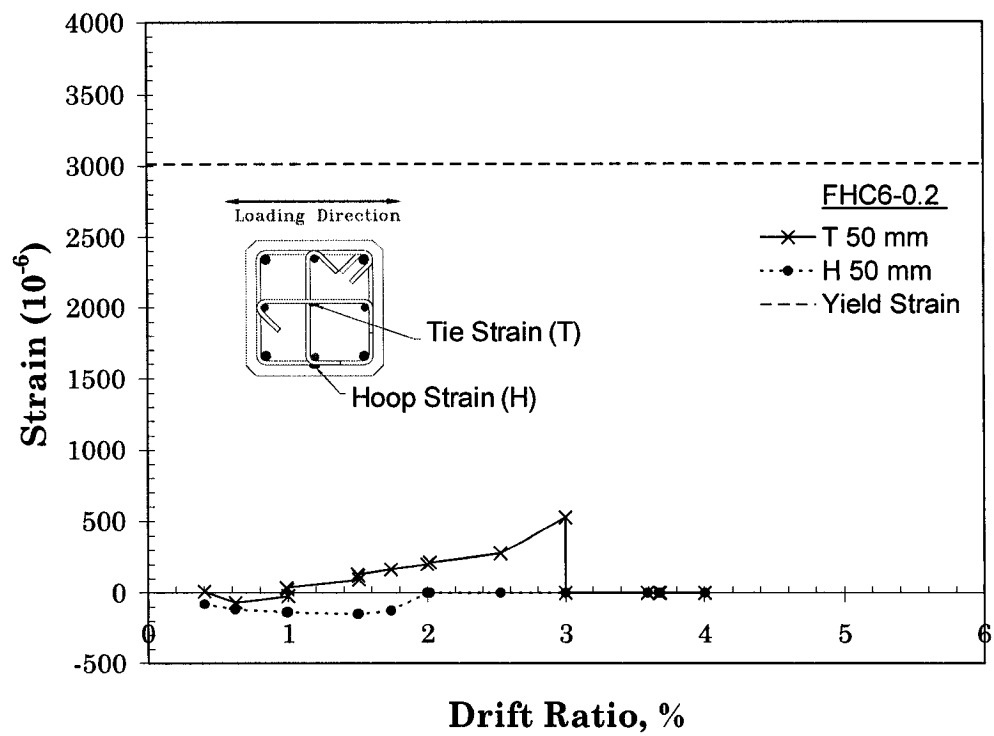
Fig. 4.44(c) -Transverse reinforcement strain versus drift ratio 50 mm from column stub.

267

The following figures 4.45 to 4.56 show the hoop and tie strains along the column height measured from the stub at each peak of loading stages.

The hoop strains of specimen FHC1-0.2 shown figure 4.45 have maximum values at distances of 250 mm (10 in.) and at 600 mm (24 in.) from column stub at a drift ratio of 7.98%. The locations of maximum hoop strains are the same for specimen FHC2-0.34 , however, at a drift ratio of 4.07% as shown in figure 4.46. Due to higher level of axial load applied to specimen FHC2-0.34, the hoop strains have reached its yield strain at much early stage. The tie strain distribution for specimens FHC1-0.2 and FHC2-0.34 shown in figures 4.51 and 4.52 show that maximum tie strains values exist at a distance of 6.0 in. from column stub for specimen FHC1-0.2 which was subjected to lower axial load level. For specimen FHC2-0.34, however, the maximum tie strain exists at a distance of 600 mm (24 in.) from column stub. The tie yield strain was reached much earlier at 2% drift for specimen FHC1-0.2 where it was reached at 4.07% drift for specimen FHC2-0.34. Lower level of axial load level have increased the tie strain values closer to the column stub, where higher axial load level seems to have shifted the location of maximum tie strain further away from column stub.

The maximum hoop strains are located at 300 mm (12 in.) and 425 mm (17 in.) away from column stub for specimens FHC3-0.22 and FHC4-0.34, respectively, as shown in figures 4.47 and 4.48. At drift ratio of 4%, the hoop yield strain was

268

reached for specimen FHC4-0.33 due to higher axial load level, where hoop yield strain was never reached for specimen FHC3-0.22 with lower axial load level. Both tie strains of specimens FHC3-0.22 and FHC4-0.33 did not reach yield values as shown in figures 4.53 and 4.54. The use of higher-grade steel (ASTM Grade 75) resulted in overall lower maximum values of strains for both hoops and ties.

The locations of maximum hoop strains for specimens FHC5-0.2 and FHC6-0.2 are similar to all other specimens as shown in figures 4.49 and 4.50. The maximum values are located at a distance of 350 mm (14 in.) from column stub. Figure 4.50 shows that at 4% drift, specimen FHC6-0.2 with use of higher-grade steel Grade 520 (ASTM Grade 75) gave lower value in comparison to that of specimen FHC5-0.2 of lower grade steel. The tie strains as shown in figures 4.55 and 4.57 indicate that the roles of grade type for the ties are not critical. At greater transverse reinforcement spacing of 125 mm (5 in.) and 150 mm (6 in.), the differences in axial load level did not have much impact on the tie strains as compared to when transverse spacing was less at 100 mm (4 in.) o.c.

For all specimens, the range of maximum hoop strains is 250 mm (10 in.) to 650 mm (26 in.) from column stub. Similarly, the range of maximum strains for the ties is 150 mm (6 in.) to 600 mm (24 in.) from column stub. The variation in tie

269

strains was most drastic for specimens FHC1-0.2 and FHC2-0.34 as compared to those for all other specimens as shown in figures 4.51 and 4.52. Specimens FHC1-0.2 and FHC2-0.34 have smallest transverse reinforcement spacing, and both use low grade steel reinforcements. As transverse reinforcement spacing is increased and as higher grade steel is used, the tie strain distributions were similar as for the remainder of the specimens as shown in figures 4.53 to 4.56.

270
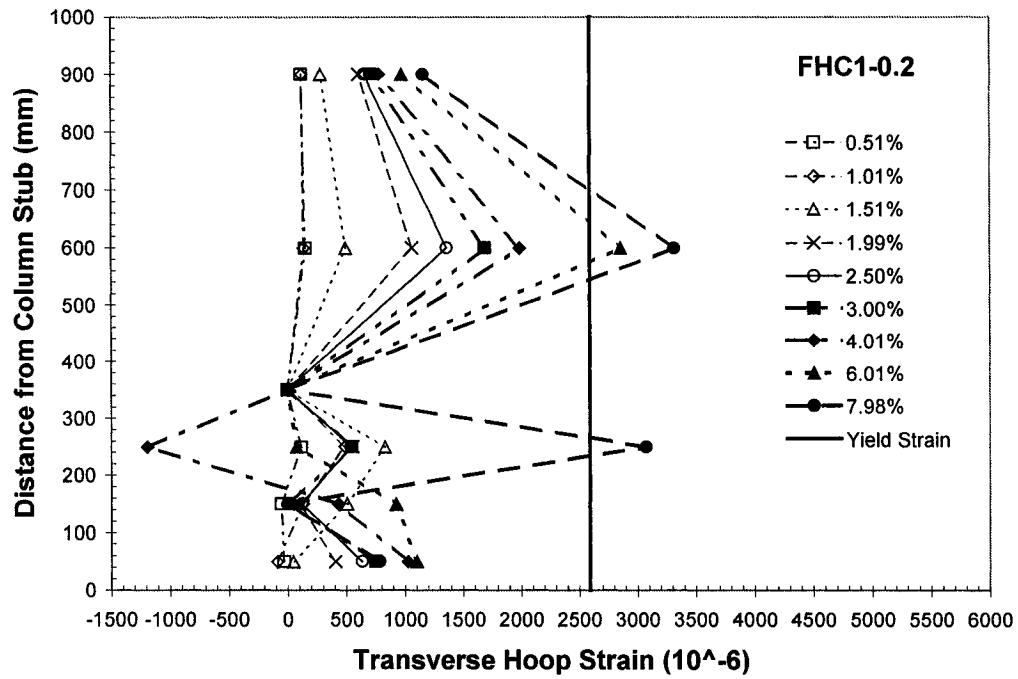
Fig. 4.45-Transverse Hoop Strain Along Column Height.

271
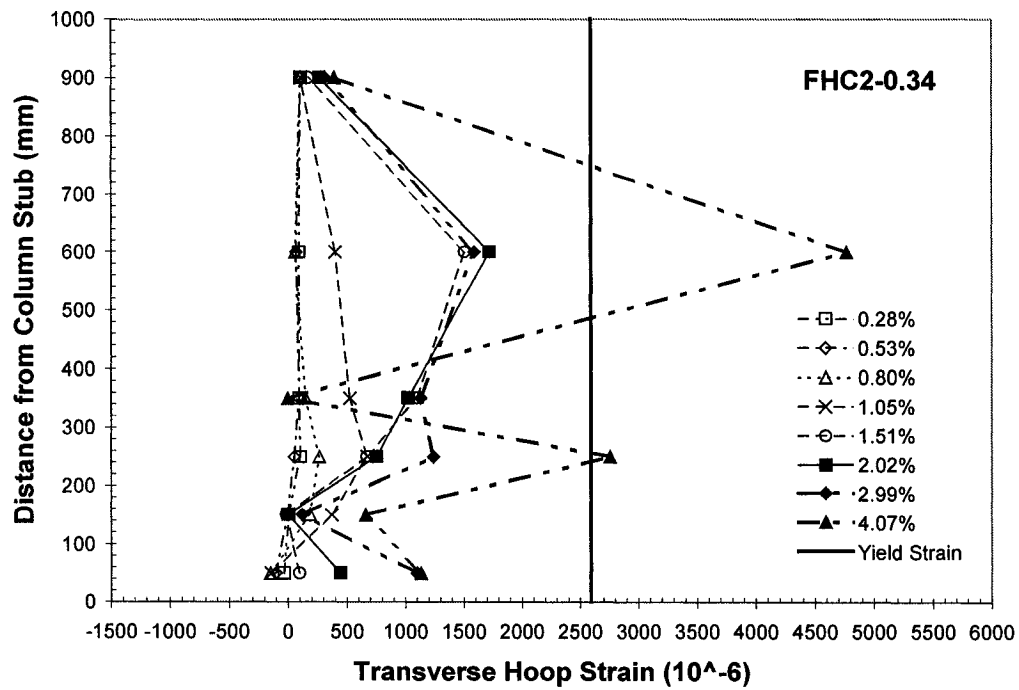
Fig. 4.46-Transverse Hoop Strain Along Column Height.

272
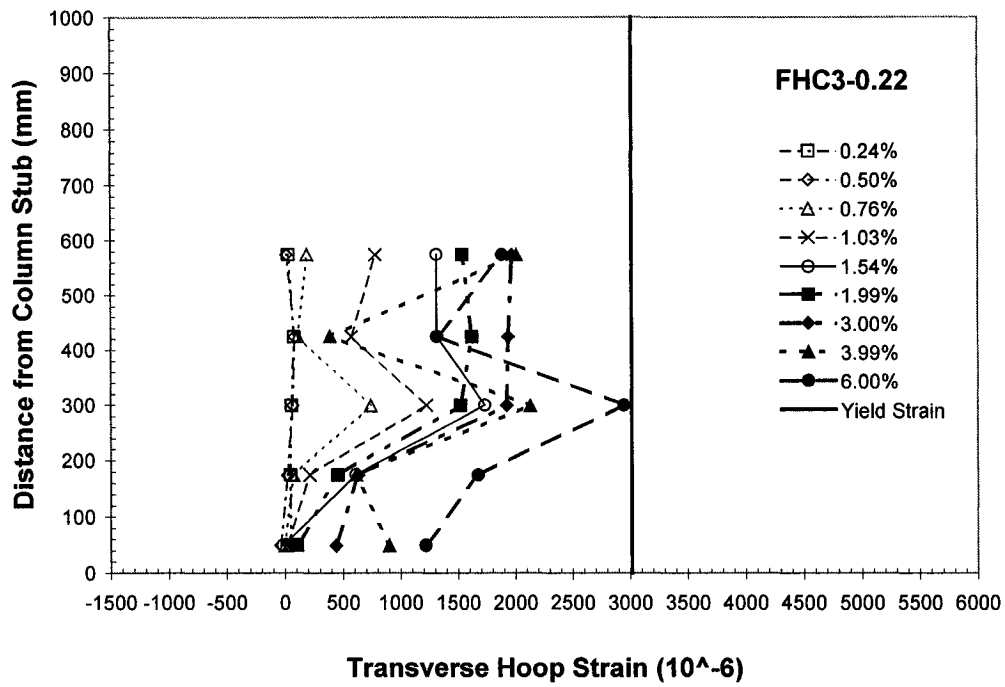
Fig. 4.47-Transverse Hoop Strain Along Column Height.

273
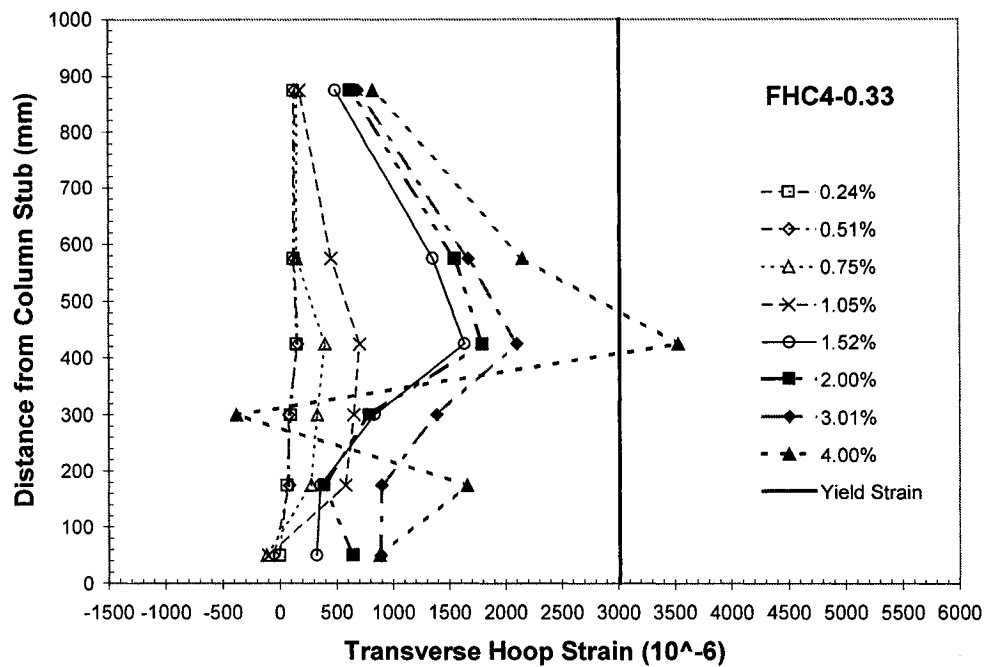
Fig. 4.48-Transverse Hoop Strain Along Column Height.

274
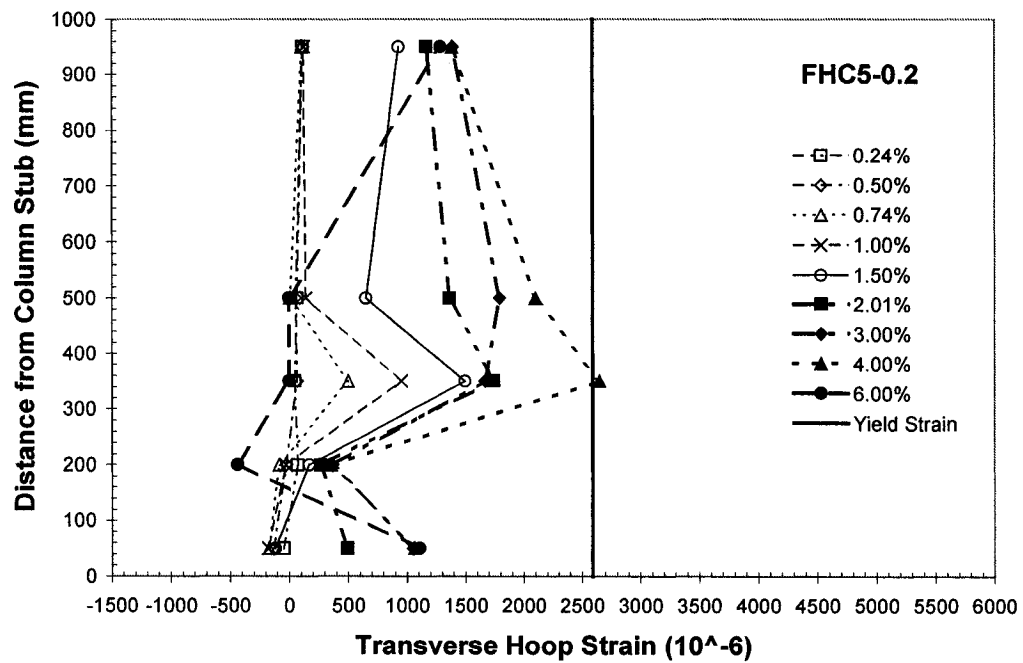
Fig. 4.49-Transverse Hoop Strain Along Column Height.
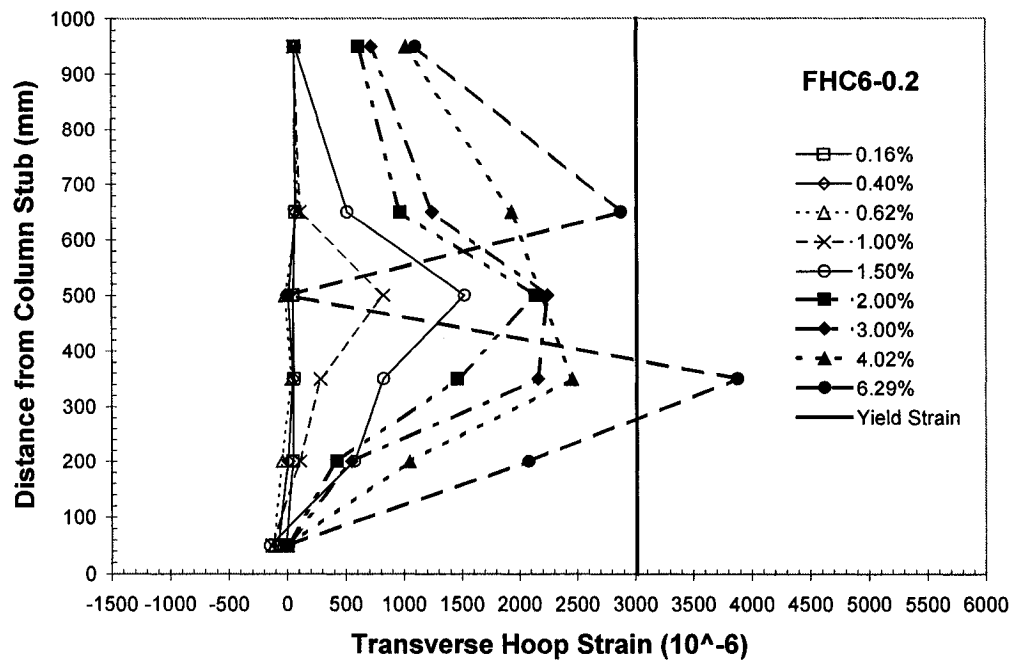
Fig. 4.50-Transverse Hoop Strain Along Column Height

276

Fig. 4.51-Transverse Tie Strain Along Column Height.

277
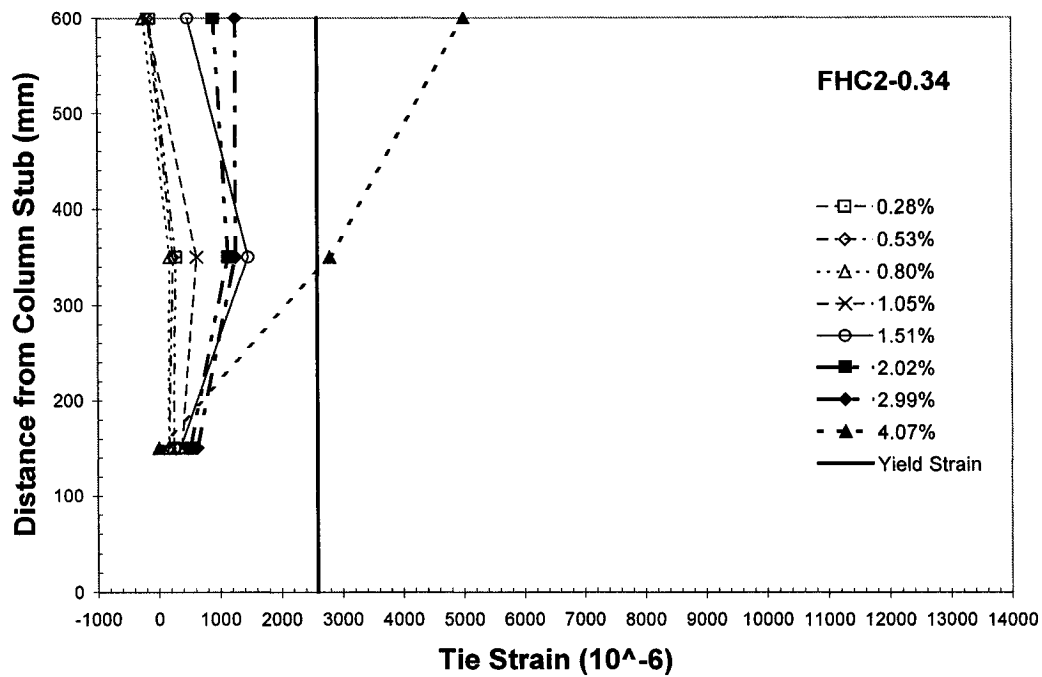
Fig. 4.52-Transverse Tie Strain Along Column Height.

278
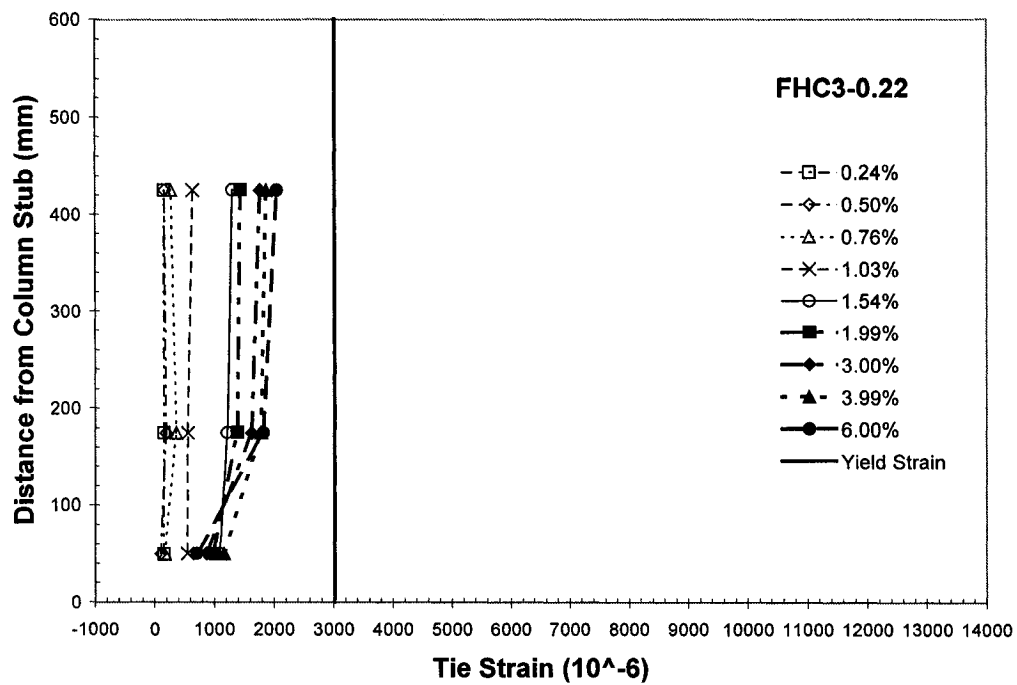
Fig. 4.53-Transverse Tie Strain Along Column Height.

279
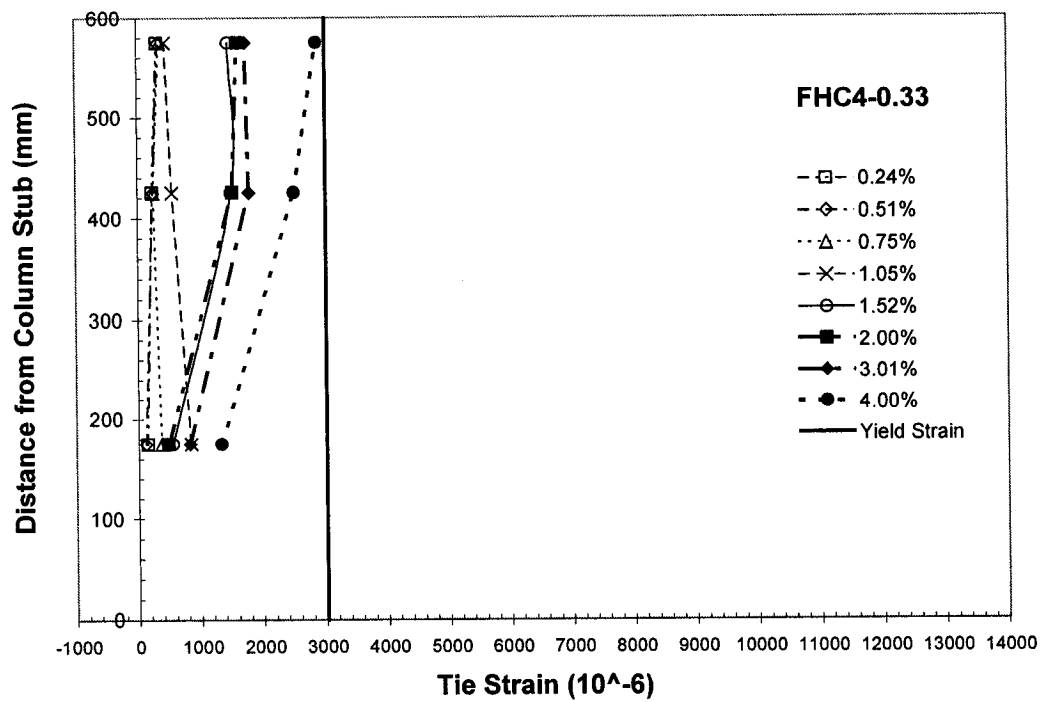
Fig. 4.54-Transverse Tie Strain Along Column Height.

280

Fig. 4.55-Transverse Tie Strain Along Column Height.

281

Fig. 4.56-Transverse Tie Strain Along Column Height.

282

4.7 CURVATURE DISTRIBUTION

The curvature of the plastic hinge region was observed by measuring the curvatures at different heights measured from the foundation surface. The Figures 4.57 to 4.62 show the curvature distribution of columns at each peak shear force value corresponding to each increment of drift ratio. The curvature distributions are presented for the drift ratios in the range from approximately 0.25% to a maximum of 6.00%. However, in most cases, the curvature distributions for only up to 3.00% drift ratios are presented because the linear potentiometers which measured the curvatures either exceeded their maximum displacement capacity or were damaged due to the cover spalling in the plastic hinge region of the columns. Further, there may be an inaccuracy in the curvature measurements for high level of drift ratios typically greater than 2 percent, since the cover concrete began to spall at approximately $\Delta/h = 1.8\%$ for most of the specimen. Despite the difficulties, the curvature distributions show much greater curvature values toward the joint area of the columns.

Based on the observations of the following figures, The first figure for FHC1-0.2 [Axial Load P=3331.7 kN (749 kips), Grade 420 (ASTM Grade 60) @ 100mm (4")] shows a gradual decrease in curvature with increasing column height. For FHC2-0.34 [Axial Load P=5450.85 kN (1225.4 kips), Grade 420 (ASTM Grade

283

60) @ 100mm (4")], the curvature decreased substantially toward the 318 mm (12.5 in.) height. This seems to be due to high axial load level, and therefore greater concentration of force in the plastic hinge region which restricted the deformability of the column. Observing the curvature values for FHC2-0.34 in comparison to FHC1-0.2, it can be noticed that higher axial load seems to distribute forces more evenly through the specimen length. In the plastic hinge region, the curvature values are actually larger than those of FHC1-0.2 at low drift ratios and become smaller at higher drift ratios as the columns undergo large deformations. At 318 mm (12.5 in.) level, for example, the curvatures values for FHC2-0.34 is greater than that of FHC1-0.2 up to a drift ratio of 1.5 percent then becomes smaller from 2 percent drift ratio. A drift ratio range of 1.3 to 2.0 percent is the range in which the longitudinal and tie reinforcement yielded first in the plastic hinge region, where the hoop yielding in the plastic hinge region occurred much later at drift ratio of 3 percent for FHC2-0.34 and 6.5 percent for FHC1-0.2. After yielding of longitudinal and tie reinforcements, the curvature seems to have decreased, since the concrete flexural cracking through the plastic hinge region reduces the curvature of the column surface.

The comparison between the curvature distributions of column FHC3-0.22 [Axial Load P=3526.9 kN (792.9 kips), Grade 520 (ASTM Grade 75) @ 125mm (5")] and FHC4-0.33 [Axial Load P=5290.27 kN (1189.3 kips), Grade 520 (ASTM

284

Grade 75) @ 125mm (5")] shows that distribution of forces are such that the deformability is smaller for FHC4-0.33 with higher axial load as compared to that of FHC3-0.22. The similar trend as FHC1-0.20 and FHC2-0.34 can be seen in the plastic hinge region, where the longitudinal and tie reinforcements for FHC4-0.33 yielded first at approximately 1.0 percent, and only longitudinal reinforcement for FHC3-0.22 yielded first at 1.34 percent. The transverse hoops yielded at 3.1 percent for FHC3-0.22 and at 0.94 percent for FHC4-0.33. This shows that higher axial load decreases the column deformability.

285

Height versus Curvature
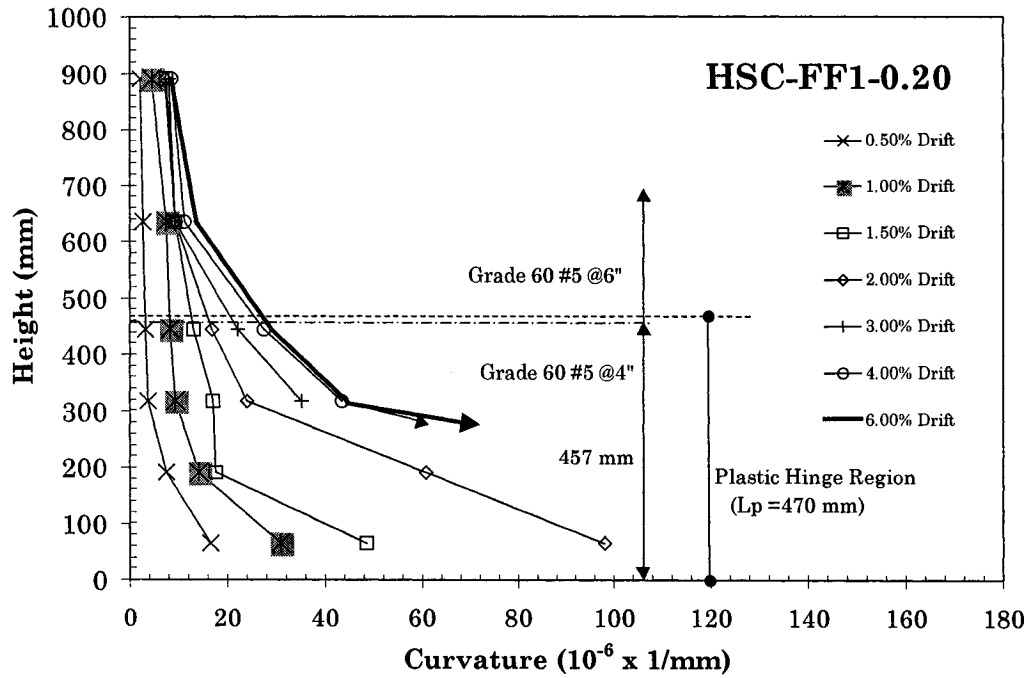
Fig. 4.57-Experimental curvatures in the plastic hinge region

286
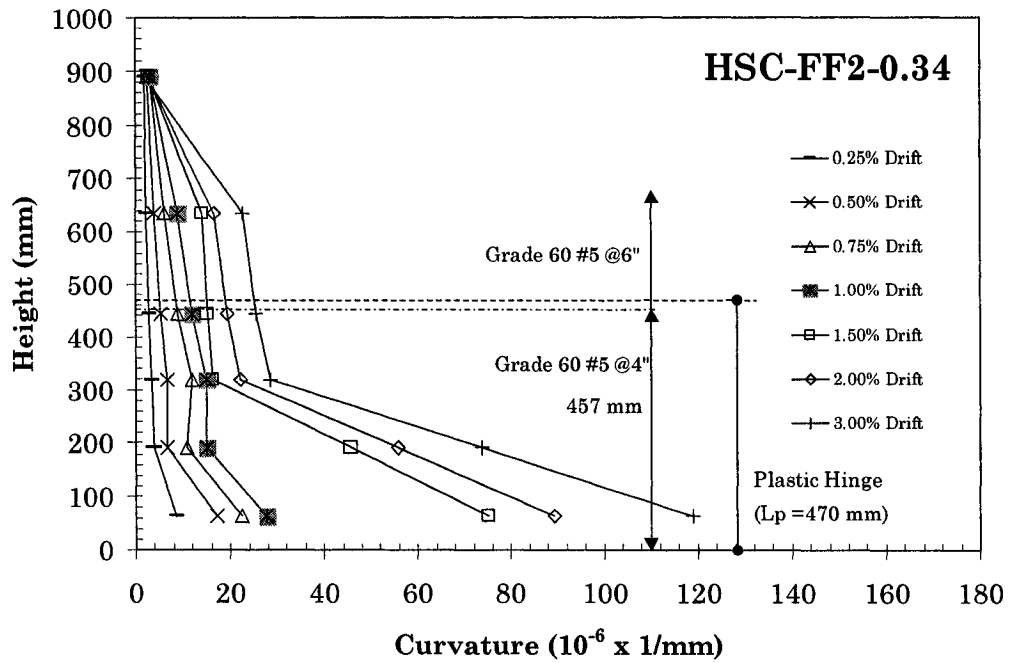
Fig. 4.58- Experimental curvatures in the plastic hinge region

287

Height versus Curvature
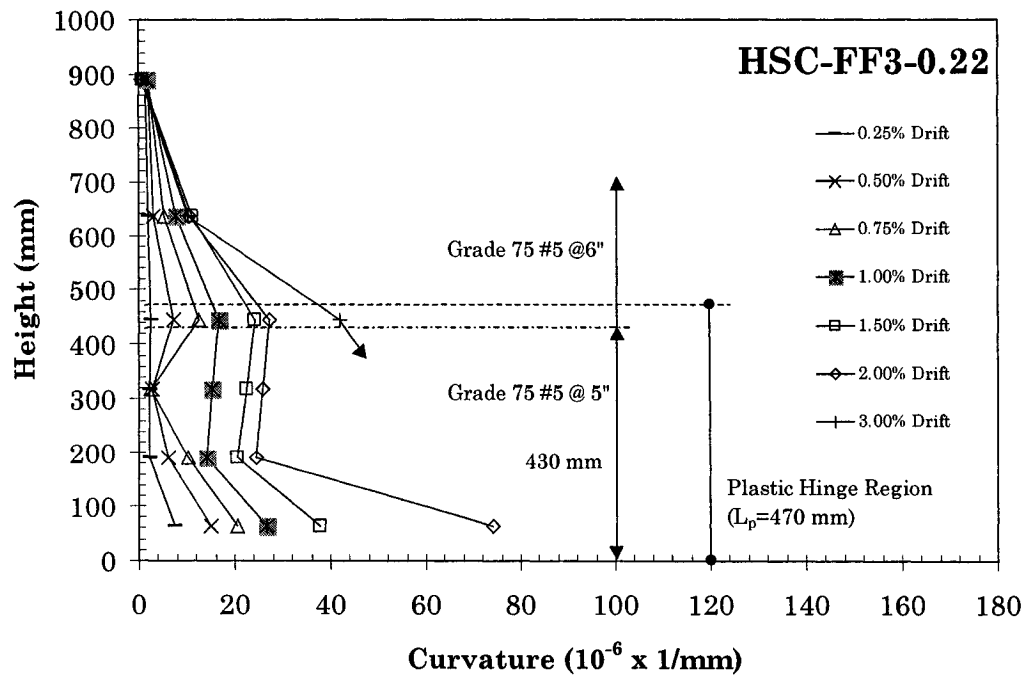
Fig. 4.59- Experimental curvatures in the plastic hinge region

Height versus Curvature
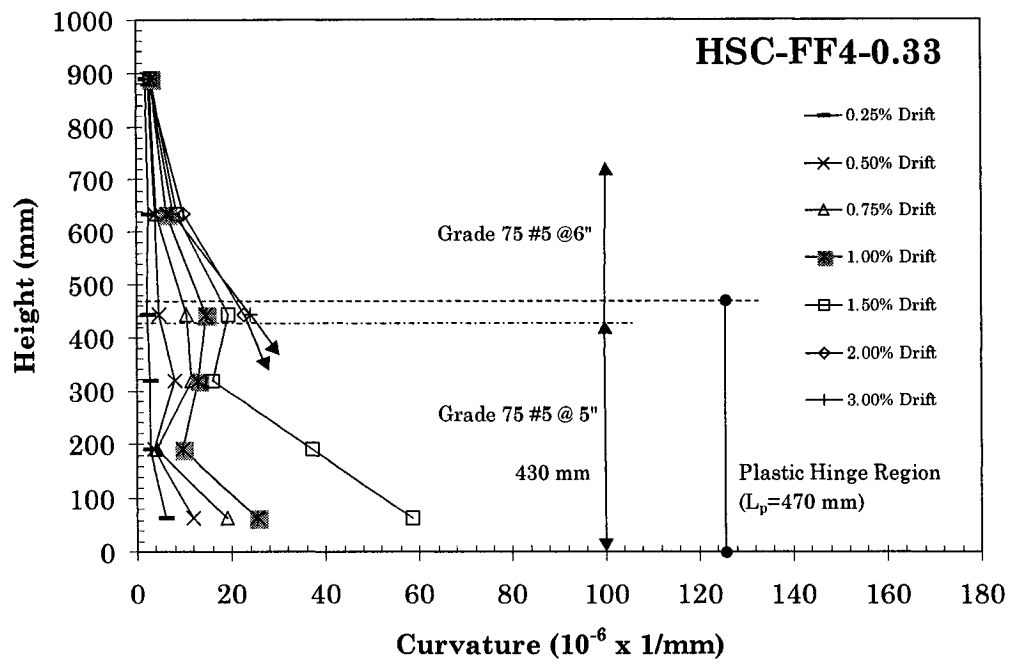
Fig. 4.60- Experimental curvatures in the plastic hinge region

Height versus Curvature
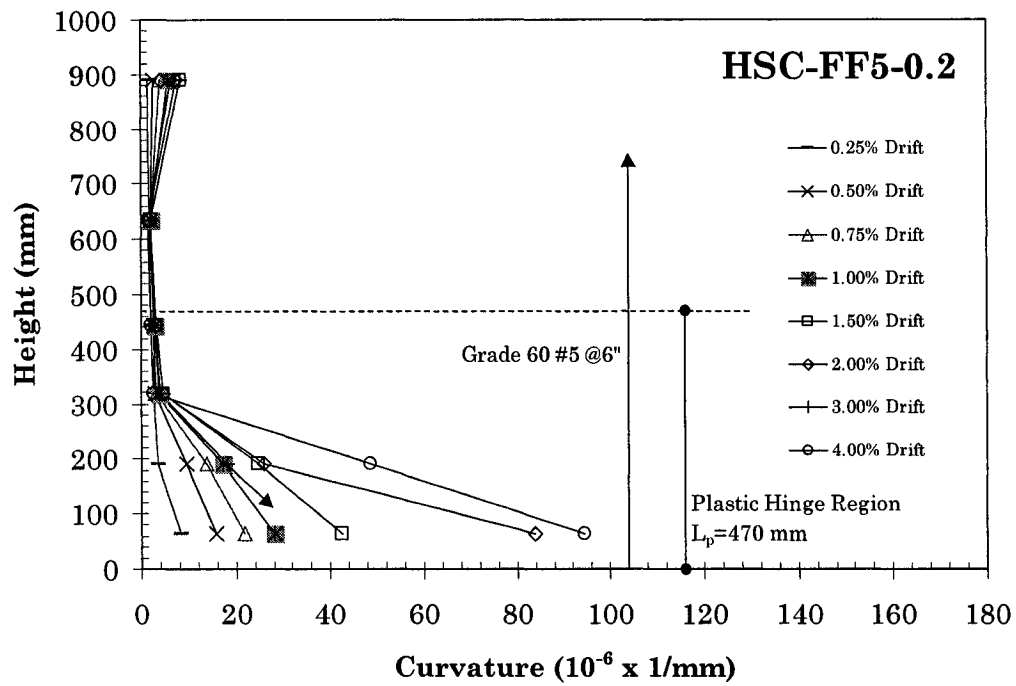
Fig. 4.61 - Experimental curvatures in the plastic hinge region

Height versus Curvature
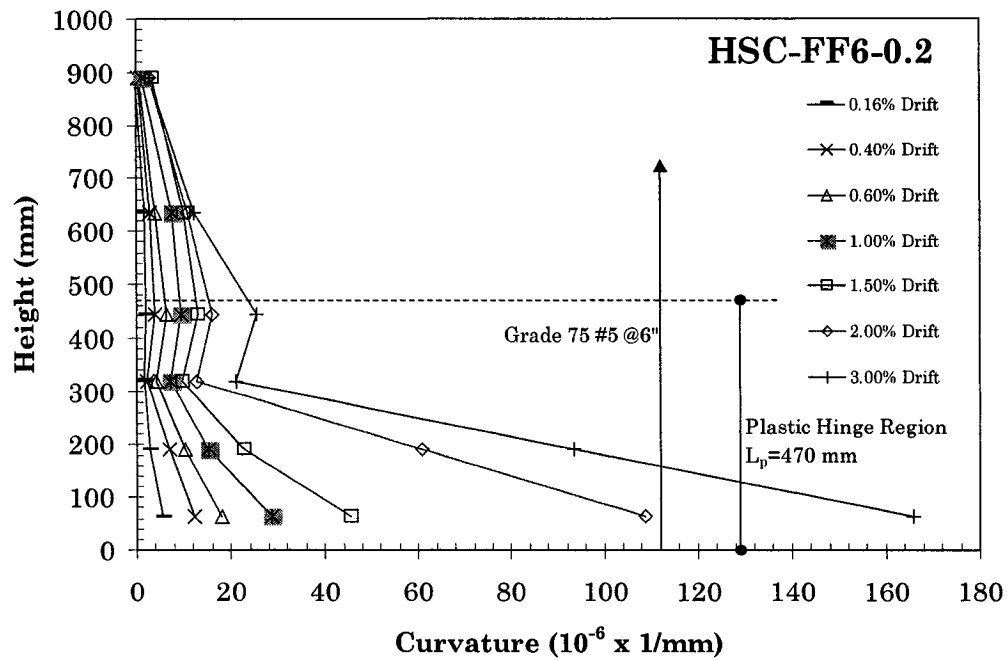
Fig. 4.62- Experimental curvatures in the plastic hinge region

The columns FHC5-0.2 [Axial Load P=3331.7 kN (749 kips), Grade 420 (ASTM Grade 60) @ 150mm (6")] and FHC6-0.2 (Axial Load P=3331.7 kN (749 kips), Grade 520 (ASTM Grade 75) @ 150mm (6")] have similar pattern of curvature distributions. However, for FHC5-0.2, the curvature values were very small in the height range from 318 mm to 635 mm (12.5 in. to 25 in.) due to the fact that the transfer of the lateral shear force was not significant in this region. Similar behavior can be observed for FHC6-0.2. The use of higher-grade transverse reinforcement in FHC6-0.2 seems to have delayed yielding and provided more confinement. It gave comparatively smaller curvature values in the lower plastic hinge region as compared to FHC5-0.2 up to about 1.0 percent drift ratio. However, from 1.5 percent drift ratio, after the longitudinal bar yielded, the curvature became larger as compared to that of FHC5-0.2.

From the observations of the column behavior, it can be deduced that the axial load levels, transverse reinforcement spacing, and the transfer of the shear and the axial load forces to the plastic hinge regions significantly affect the behavior of the columns. It can be observed that with increased transverse reinforcement spacing, the shear force transfer decreased. Also, high axial load level decreased the deformability in the lower region of the plastic hinge. The differences in the curvature distribution for using higher grade transverse reinforcements were not very significant. In this case, the higher grade 520 (ASTM Grade 75) actually

292

seemed to have enhanced more even force distributions through the specimen height, especially for FHC6-0.20.

Based on the experimental data obtained, the locations of greatest curvatures were located as following:

For Specimens FHC1-0.2, FHC2-0.34, and FHC4-0.33, maximum curvatures measured nearest to the center of the experimentally observed plastic hinge were located at 317.5 mm (12.5 in.) from column stubs, and for Specimens FHC3-0.22, FHC5-0.2, and FHC6-0.2, 444.5 mm (17.5 in.) from column stubs. A typical failure pattern is shown on Figure 4.8.

4.8 EFFECT ON PLASTIC HINGE

NZS 3101:1995, New Zealand Concrete Structures Standard, Part 1- The Design of Concrete Structures provides additional requirements for earthquake effects on plastic hinge regions as follows:

Section 8.5.4.1: Potential plastic hinge regions in columns and piers shall be considered to be the end regions adjacent to moment resisting connections over a length from the face of the connections as follows

(a) Where, $N^* \leq 0.25\phi f_c' A_g$, the greater of the longer member cross section dimension in the case of a rectangular cross section or the diameter in the case of a circular cross section, or where the moment exceeds 0.8 of the maximum moment, taking into account dynamic magnification and overstrength actions, at the end of the member;

(b) Where, $0.25\phi f_c' A_g \prec N^* \leq 0.5\phi f_c' A_g$, the greater of 2.0 times the longer member cross section dimension in the case of a rectangular cross section or 2.0 times the diameter in the case of a circular cross section, or where the moment exceeds 0.7 of the maximum moment, taking into account dynamic magnification and overstrength actions, at that end of the member;

(c) Where, $0.5\phi f_c' A_g \prec N^* \leq 0.7\phi N_o$, the greater of 3.0 times the larger member cross section dimension in the case of rectangular cross section or 3.0 times the diameter in the case of a circular cross section, or where the moment exceeds 0.6 of the maximum moment, taking into account dynamic magnification and overstrength actions, at that end of the member.

The variance in axial load levels affects the plastic hinge length and causes shifts in the location of the maximum curvature a distance away from the stub. Greater

294

the axial load level, the location of the maximum curvature shifted its location closer to the column stub as compared to when lower levels of axial loads were applied. Such a shift in the location of the plastic hinge length and its effect on the moment capacity has been taken into consideration in the moment-curvature program that will be introduced in Chapter 5. The existing theoretical plastic hinge length as discussed in Section 2.7 has been implemented in the moment-curvature program for the purpose of moment-curvature analysis.

4.9 SHEAR STRENGTH

In order to assess the range of experimental lateral shear force loads, push over analysis was performed based on the theories of Priestley, Seible, and Calvi et al. as described in "Seismic Design and Retrofit of Bridges", John Wiley & Sons, Inc., 1996. The values predicted are termed 'Shear Demand' as shown in table 4.1.

ASCE-ACI Committee 426 Proposals

The shear strength of reinforced concrete members is considered as a sum of strength of the concrete shear resisting mechanism V_c and the strength of the truss

295

mechanism V_s. The transverse reinforcement is considered to contribute to 45 degree truss, and diagonal concrete strut is considered to contribute to the transfer of the shear force. The expressions are as follows:

$$V_n = V_c + V_s \qquad (4.1)$$

The truss-mechanism strength of transverse reinforcement is given by

$$V_s = \frac{A_v f_y d}{s} \qquad (4.2)$$

where A_v = the total transverse reinforcement area per layer; s = spacing along the axis; f_y = the steel yield strength; and d = the effective depth, normally taken as $0.8h$ or $0.8D$ for rectangular or circular columns, respectively. A simple method for evaluation of V_c is given by

$$V_c = v_b\left(1 + \frac{3P}{f_c' A_g}\right) b_w d \qquad (4.3)$$

where the basic shear stress is given by:

$$v_b = \left(0.067 + 10\rho_w\right)\sqrt{f_c'} \le 0.2\sqrt{f_c'} \quad \text{(MPa)} \qquad (4.4a)$$

$$v_b = \left(0.8 + 120\rho_w\right)\sqrt{f_c'} \le 2.4\sqrt{f_c'} \quad \text{(psi)} \qquad (4.4b)$$

where,

296

ρ_w = the ratio of longitudinal tension reinforcement, taken as $0.5\rho_t$ for columns

$(\rho_t = \dfrac{A_{st}}{A_g}$ = the gross longitudinal reinforcement ratio).

P = the axial load

b_w = the web width taken as D and b for circular and rectangular columns, respectively.

A simplified form of expression applicable to both circular and rectangular columns is given by:

$$V_c = v_b A_e + 0.1P\left(\frac{v_b}{0.2\sqrt{f_c'}}\right)(MPa) = v_b A_e + 0.1P\left(\frac{v_b}{2.4\sqrt{f_c'}}\right)(psi) \qquad (4.5)$$

A_e = $0.8bh = 0.8A_g$ for rectangular columns and $A_e = 0.8D^2 = 1.02A_g$ for circular columns, where A_g is gross column area.

Above ACI 426 equations is based on a prediction of initial flexure-shear cracking and web shear cracking and is based on the fact that shear strength is proportional to the axial load. In considering the initial flexural-shear cracking, it is assumed that there is a linear relationship between shear strength and the inverse of the shear-span-to-depth ratios ($\frac{a}{h}$ or $\frac{a}{D}$), where $a = \frac{M}{V}$, ratio of moment to shear at critical section and h and D are rectangular column depth and circular column diameter, respectively.

297

The expression is applicable to typical range of concrete strengths of 20 MPa $\leq$ $f_c' \leq 35$ MPa $(3{,}000\,psi \leq f_c' \leq 5{,}000\,psi)$ and is generally considered to provide conservative predictions.

Predictive Shear Equations by Priestley et. al.

The shear strength of the columns may also be determined using the predictive shear-strength equations for columns subjected to cyclic lateral shear forces proposed by Priestley, Verma, and Xiao et al. as described in "Seismic Shear Strength of Reinforced Concrete Columns", ASCE *Journal of Structural Engineering,* Vol. 120, No. 8, August 1994 (Priestley et. al., 1994) as follows:

$$V_n = V_c + V_P + V_s \qquad (4.6)$$

where,

V_c = Concrete component dependent on ductility level

V_p = Axial level component dependent on column aspect ratio

V_s = Truss component dependent on content of transverse reinforcement

$$V_c = k\sqrt{f_c'}A_e \qquad (4.7)$$

298

where k depends on the member displacement ductility level and depends on whether loading is uniaxial or biaxial with an upper limit of $0.29\sqrt{f_c'}\,MPa\left(3.5\sqrt{f_c'}\,psi\right)$

$A_e = 0.8A_{gross}$ for both circular and rectangular columns

$$V_p = P\tan\alpha = \frac{D-c}{2a}P \qquad\qquad (4.8)$$

where D = the overall depth or diamter; c = the depth of the compression zone;

$a = L$ for a cantilever column and $\dfrac{L}{2}$ for a column in reversed bending; and

$\alpha = \dfrac{2}{M/_{VD}} \geq 1.0$ = inclination of diagonal compression strut (due to axial load P)

with member axis.

This equation implies that as axial load level is increased its contribution to shear strength will decrease due to increased depth of compression zone, where as aspect ratio for the column increases, the contribution of axial load to shear strength will decrease. However, V_p is not considered to degrade with increasing ductility.

The truss-mechanism component V_s is given as:

$$V_s = \frac{\pi}{2}\frac{A_{sh}f_{yh}D'}{S}\cot 30° \quad \text{for circular columns} \qquad (4.9a)$$

299

$$V_s = \frac{A_v f_{yh} D'}{S} \cot 30° \text{ for rectangular columns} \qquad (4.9b)$$

where D' = the distance between centers of the peripheral hoop or spiral. The above method of the prediction of shear strength is considered to provide conservative design since they are based on experimentally determined material properties. It has not been determined whether the longitudinal reinforcement has effect on the shear strength mechanism.

Shear Strength Requirements of ACI 318-99 Building Code

The shear design provisions of ACI 318-99 Building Code requires that the basic shear strength is greater than or equal to factored shear force V_U such that:

$$\phi V_n \geq V_U \qquad (4.10)$$

$V_n = V_c + V_s$ where V_c is the nominal strength provided by concrete and V_s is the nominal shear strength provided by shear reinforcement.

For members subject to axial compression, a simplified form of expression is given by

$$V_c = 2\left(1 + \frac{N_U}{2000A_g}\right)\sqrt{f_c'} b_w d, \text{ where } \frac{N_U}{A_g} \quad \text{(psi)} \qquad (4.11)$$

300

More detailed expression is given by

$$V_c = \left(1.9\sqrt{f_c'} + 2500\rho_w \frac{V_U d}{M_U - N_U \frac{(4h-d)}{8}} \right) b_w d \qquad (4.12)$$

where maximum value allowed for V_c is:

$$3.5\sqrt{f_c'} b_w d \sqrt{1 + \frac{N_U}{500 A_g}} \qquad (4.13)$$

where,

N_U = Factored axial load normal to cross section taken as positive for compression occurring simultaneously with V_U at section considered.

For shear strength due to the reinforcements provided, the following expression is used:

$$V_s = \frac{A_v f_y d}{s} \le 8\sqrt{f_c'} b_w d \qquad (4.14)$$

The values of nominal shear capacities obtained using various approaches mentioned above for the prediction of shear strengths are shown in table 4.1 for the purpose of comparison to experimental flexural strength.

301

Table 4.1-Shear Capacity

SHEAR CAPACITY KN (KIPS)		ACI 318-95			ASCE-ACI COMMITTEE 426			PRIESTLEY, VERMA, AND XIAO				SHEAR DEMAND KN (KIPS)
SPECIMEN	S mm (in.)	V_c	V_s	V_{tot}	V_c	V_s	V_{tot}	V_c	V_p	V_s	V_n	$V_{Required}$
Column Length												
FF1	150 (6)	274 (61.7)	712 (160.1)	987 (221.8)	514 (115.6)	712 (160.1)	1226 (275.7)	480 (108.0)	310 (69.6)	1262 (283.7)	2052 (461.3)	756 (170.0)
FF2	150 (6)	270 (60.7)	712 (160.1)	982 (220.8)	637 (143.3)	712 (160.1)	1350 (303.4)	473 (106.3)	403 (90.5)	1262 (283.7)	2137 (480.5)	835 (187.8)
FF3	150 (6)	270 (60.7)	838 (188.5)	1108 (249.2)	524 (117.8)	838 (188.5)	1362 (306.3)	473 (106.3)	320 (71.9)	1486 (334.1)	2279 (512.3)	755 (169.7)
FF4	150 (6)	270 (60.7)	840 (188.8)	1110 (249.5)	628 (141.2)	840 (188.8)	1468 (330.0)	473 (106.3)	397 (89.2)	1489 (334.7)	2358 (530.2)	834 (187.6)
FF5	150 (6)	274 (61.7)	712 (160.1)	987 (221.8)	514 (115.6)	712 (160.1)	1226 (275.7)	480 (108.0)	309 (69.4)	1262 (283.7)	2051 (461.1)	746 (167.6)
FF6	150 (6)	274 (61.7)	838 (188.5)	1113 (250.2)	514 (115.6)	838 (188.5)	1353 (304.1)	480 (108.0)	309 (69.5)	1486 (334.1)	2276 (511.6)	738 (165.8)
Plastic Hinge Region												
FF1	100 (4)	274 (61.7)	1068 (240.1)	1342 (301.8)	514 (115.6)	1068 (240.1)	1582 (355.7)	480 (108.0)	310 (69.6)	1893 (425.6)	2683 (603.1)	756 (170.0)
FF2	100 (4)	270 (60.7)	1068 (240.1)	1338 (300.8)	637 (143.3)	1068 (240.1)	1705 (383.4)	473 (106.3)	403 (90.5)	1893 (425.6)	2768 (622.3)	835 (187.8)
FF3	125 (5)	270 (60.7)	1006 (226.2)	1276 (286.9)	524 (117.8)	1006 (226.2)	1530 (343.9)	473 (106.3)	320 (71.9)	1783 (400.9)	2576 (579.1)	755 (169.7)
FF4	125 (5)	270 (60.7)	1008 (226.6)	1278 (287.3)	628 (141.2)	1008 (226.6)	1636 (367.8)	473 (106.3)	397 (89.2)	1787 (401.7)	2656 (597.1)	834 (187.6)
FF5	150 (6)	274 (61.7)	1157 (260.1)	987 (221.8)	514 (115.6)	712 (160.1)	1226 (275.7)	480 (108.0)	309 (69.4)	1262 (283.7)	2051 (461.1)	746 (167.6)
FF6	150 (6)	274 (61.7)	1283 (288.5)	1113 (250.2)	514 (115.6)	838 (188.5)	1353 (304.1)	480 (108.0)	309 (69.5)	1486 (334.1)	2276 (511.6)	738 (165.8)

302

FULL-SCALE EXPERIMENTAL AND ANALYTICAL STUDIES
ON HIGH-STRENGTH CONCRETE COLUMNS

by

Henry Wook Yun

VOLUME II

A Dissertation Presented to the
FACULTY OF THE GRADUATE SCHOOL
UNIVERSITY OF SOUTHERN CALIFORNIA
In Partial Fulfillment of the
Requirements for the Degree
DOCTOR OF PHILOSOPHY
(CIVIL ENGINEERING)

July 2003

Copyright 2003   Henry Wook Yun

CHAPTER 5

ANALYSIS BASED ON MACRO-APPROACH

5.1 INTRODUCTION

The analytical and theoretical studies will be based on two main approaches which are Macro-Model Based and Micro-Model Based Analysis. For the Macro-Model Based analysis the following will be investigated.

5.2 MOMENT CAPACITIES

The experimental column capacities were determined by first adding the increased lateral shear force due to $P - \Delta$ effect to the maximum true shear force, $_{TRUE}V_{MAX}$, exerted onto the specimens, where the true shear force already includes the horizontal component of the applied axial force. From this procedure, the maximum experimental shear capacity, $_{EXP}V_{MAX}$, and the corresponding moment capacity, $_{EXP}M_{MAX}$, are obtained. The $_{EXP}M_{MAX}$ values are then compared to the

303

moment capacities recommended by ACI 318-95 code (1995). The procedures

mentioned above are summarized in the following Table 5.1.

Table 5.1-Column capacity comparison to ACI 318-95 code.

	V_{MAX} (+)	Δ/H (+)	$(V+P\Delta/H)_{MAX}$ (+)	M_{MAX} (+)	V_{MAX} (-)	Δ/H (-)	$(V+P\Delta/H)_{MAX}$ (-)	M_{MAX} (-)	$_{EXP}M_{MAX\,(AVG.)}$	$_{EXP}M_{MAX}/M_{ACI}$	M_{ACI}
	(kips)	(%)	(kips)	(kN*m)	(kips)	(%)	(kips)	(kN*m)	(kN*m)	(%)	(kN*m)
FHC1-0.20	162.80	1.69	175.47	1387.79	125.64	6.06	171.00	1352.40	1370.10	122.37	1119.60
FHC2-0.34(H)*	170.61	2.02	194.97	1541.97	183.13	1.32	199.00	1573.90	1557.94	132.13	1179.10
FHC3-0.22	162.85	1.46	174.90	1383.25	167.29	1.48	179.52	1419.81	1401.53	124.15	1128.90
FHC4-0.33(H)*	179.14	1.27	194.17	1535.71	185.23	1.40	201.92	1597.00	1566.35	132.76	1179.80
FHC5-0.20	160.05	1.77	173.37	1371.15	157.48	2.00	172.39	1363.39	1367.27	122.12	1119.60
FHC6-0.20	158.37	1.74	171.46	1356.06	160.09	1.91	174.45	1379.70	1367.88	122.18	1119.60

*(H) Represent high axial load

The moment capacity of the columns based on the ACI 318-95 Code, M_{ACI},

seems conservative for high axial load levels with $_{EXP}M_{MAX}$ greater by about 32

percent, where for lower axial load, $_{EXP}M_{MAX}$, was greater by only about 22 to 24

percent.

5.3 SUMMARY OF HSC CONFINED STRESS-STRAIN MODELS USED

The Table 5.2 shows a summary of equations for existing confined stress-strain

models and crucial variables that were discussed in Section 2.4. All models are

based on high-strength concrete testing except for Mander model, which was

304

based on normal-strength concrete testing. The table summarizes the equations for each model on each column.

The actual variables presented by each model have been unitized and revised for clarity using the common variables that represent the same parameter. All models present the maximum confined concrete strength in relation to the unconfined concrete strength, where all confinement stresses are calculated in relation to confinement effectiveness coefficients. The longitudinal confined compressive stress of concrete are calculated in relation to peak confined concrete strain and increasing increments of longitudinal compressive concrete strain with all concrete parameters considered including tangent modulus of concrete, spacing, and volumetric ratios. The ascending and descending confined stress-strain curves are typically determined for the ranges of longitudinal compressive confined concrete strains. The ultimate confined concrete strains are defined only for three of the six models presented.

Table 5.2-Confined HSC stress-strain models by different researchers.

	Mander	Yong et al.
Confined Concrete Strength, f_{cc}'	$f_{cc}' = f_c'\left(-1.254 + 2.254\sqrt{1 + \dfrac{7.94 f_l'}{f_c'}} - 2\dfrac{f_l'}{f_c'}\right)$ $f_l' = f_l k_e$ f_l' =effective lateral confining pressure f_l = nominal lateral pressure k_e = confinement effectiveness coefficient for rectangular hoops	$f_{cc}' = k_e\, f_c'$ (Peak Stress Only) f_c' = compressive strength of concrete k_e = confinement effectiveness coefficient
Longitudinal Compressive Concrete Stress, f_c	$f_c = \dfrac{f_{cc}'\, xr}{r - 1 + x^r},\ x = \dfrac{\varepsilon_c}{\varepsilon_{cc}},$ $r = \dfrac{E_c}{E_c - E_{sec}}$ ε_c = longitudinal compressive concrete strain $E_c = 5{,}000\sqrt{f_{co}'}$ Mpa = tangent modulus of elasticity of the concrete (1 MPa = 145 psi) $E_{sec} = \dfrac{f_{cc}'}{\varepsilon_{cc}}$	$f_c = \dfrac{AX + BX^2}{1 + (A - 2)X + (B + 1)X^2}$ for $\varepsilon_c \le \varepsilon_{co}$ $f_c = \dfrac{f_c}{f_o}\ ;\ X = \dfrac{\varepsilon_c}{\varepsilon_{co}}\ ;$ $A = \dfrac{E_c \varepsilon_{co}}{f_o}\ ;$ $B = \left[\dfrac{(A-1)^2}{0.55}\right] - 1\ ;$ $E_c = 27.55 w^{1.5}\sqrt{f_c'}\ ;$ f_c and ε_c = concrete stress and strain, respectively $f_c = \dfrac{CX + DX^2}{1 + (C - 2)X + (D + 1)X^2}$ for $\varepsilon_c \ge \varepsilon_{co}$ $C = \left[\dfrac{(\varepsilon_{2i} - \varepsilon_i)}{\varepsilon_{co}}\right]\left\{\left[\dfrac{\varepsilon_{2i} E_i}{(f_{cc}' - f_i)}\right] - \left[\dfrac{4 \varepsilon_i E_{2i}}{(f_{cc}' - f_{2i})}\right]\right\}$ $D = (\varepsilon_i - \varepsilon_{2i})\left\{\left[\dfrac{E_i}{(f_{cc}' - f_i)}\right] - \left[\dfrac{4 E_{2i}}{(f_{cc}' - f_{2i})}\right]\right\}$

306

Table 5.2 (Continued)

		$E_i = f_i / \varepsilon_i$ and $E_{2i} = f_{2i} / \varepsilon_{2i}$
		$f_i = f_{cc}'\left[0.25\left(\dfrac{f_c'}{f_{cc}'}\right)+0.4\right]$
		$\varepsilon_i = k_e\left[1.4\left(\dfrac{\varepsilon_{co}}{k_e}\right)+0.0003\right]$
		$f_{2i} = f_{cc}'\left[0.025\left(\dfrac{f_{cc}'}{1000}\right)-0.065\right]\ge 0.3 f_{cc}'$
		f_{2i} and ε_{2i} = stress and strain at arbitrarily selected point on the descending branch
		$\varepsilon_{2i} = 2\,\varepsilon_i - \varepsilon_{co}$
Strain at Strength, ε_{cc}	$\varepsilon_{cc} = \varepsilon_{co}\left[1+5\left(\dfrac{f'_{cc}}{f'_{co}}-1\right)\right]$ f'_c = unconfined concrete strength ε_{co} = corresponding strain ≈ 0.002	$\varepsilon_{cc} = 0.00265 + \dfrac{0.0035\left(1-\dfrac{0.734s}{h''}\right)\left(\rho'' f_y\right)^{\frac{2}{3}}}{\sqrt{f_c'}}$ (Peak Strain Only)
Confinement Effectiveness Coefficient, k_e	$k_e = \dfrac{\left(1-\sum\limits_{i=1}^{n}\dfrac{(w'_i)^2}{6b_c d_c}\right)\left(1-\dfrac{s'}{2b_c}\right)\left(1-\dfrac{s'}{2d_c}\right)}{(1-\rho_{cc})}$ w'_i = clear spacing between longitudinal bars s' = clear vertical spacing between spiral or hoop bars b_c and d_c = core dimensions to centerlines of perimeter hoop in x and y directions ρ_{cc} = ratio of area of longitudinal reinforcement to area of core of section	$k_e = 1+0.0091\left(1-\dfrac{0.245s}{h''}\right)\left(\rho'' +\dfrac{nd''}{8sd}\rho\right)\dfrac{f_y}{\sqrt{f_c'}}$ s = the center-to-center spacing of the lateral ties in inches h'' = length of one side of the rectangular ties in inches n = number of longitudinal steel bars d'' = nominal diameter of lateral ties in inches

307

Table 5.2 (Continued)

		d = nominal diameter of longitudinal steel bars in inches
		ρ = volumetric ratio of longitudinal reinforcement
		$\rho^{"}$ = volumetric ratio of lateral reinforcement
		$f_y^{"}$ = yielding stress of the lateral steel in psi
Ultimate Strain, ε_{cu}	Not Available	Not Available

308

Table 5.2 (Continued)

	Azizinamini et al.	Li and Park (Bing et. al. 1994)
Confined Concrete Strength, f_{cc}'	$f_{cc}' = k_e \, f_c'$ (Peak Stress Only) f_c' = compressive strength of concrete k_e = confinement effectiveness coefficient	$f_{cc}' = f_c' \left(1.413 \sqrt{1 + \dfrac{11.4 f_l'}{f_c'} - \dfrac{2 f_l'}{f_c'}} - 0.413 \right)$ f_{cc}' = the peak longitudinal compressive stress for confined concrete f_c' = peak stress of the unconfined concrete ε_{co} = corresponding strain at peak stress of the unconfined concrete f_l' = the effective lateral confining stress $f_l' = \dfrac{1}{2} k_e \rho_s f_{yh}$ f_{yh} = transverse reinforcement yield stress ρ_s = volumetric ratio of the transverse reinforcement k_e = confinement effectiveness coefficient

309

Table 5.2 (Continued)

Longitudinal compressive concrete stress, f_c	$f_c = \left(f_o/\varepsilon_o\right)\varepsilon$ for $0 \leq \varepsilon_c \leq \varepsilon_{cc}$ $f_c = f_{cc}'\left[1 - \alpha(\varepsilon - \varepsilon_o)\right] \geq 0.3 f_{cc}'$ for $\varepsilon_c \geq \varepsilon_{cc}$ $\alpha = \dfrac{0.25\dfrac{f_c' - 0.6}{f_{cc}'}}{3.13 k_e\left[1.4\left(\dfrac{\varepsilon_{cc}}{k_e}\right) + 0.0003\right]}$	$f_c = E_c\varepsilon_c + \dfrac{f_c' - E_c\varepsilon_{co}}{\varepsilon_{co}^2}\varepsilon_c^2$ for $0 \leq \varepsilon_c \leq \varepsilon_{co}$ $E_c = 3200\sqrt{f_c'} + 6900$ Mpa $E_c = 4700\sqrt{f_c'}$ MPa $f_c = f_{cc}' - \dfrac{f_{cc}' - f_c'}{\left(\varepsilon_{cc} - \varepsilon_{co}\right)^2}\left(\varepsilon_c - \varepsilon_{co}\right)^2$ for $\varepsilon_{co} \leq \varepsilon_c \leq \varepsilon_{cc}$ $f_c = f_{cc}' - \beta\dfrac{f_{cc}'}{\varepsilon_{cc}}\left(\varepsilon_c - \varepsilon_{cc}\right) \geq 0.4 f_{cc}'$ for $\varepsilon_{cc} \leq \varepsilon_c$ $\beta = \left(0.048 f_c' - 2.14\right) - \left(0.098 f_c' - 4.57\right)\sqrt{\dfrac{f_l'}{f_c'}}$
Strain at Strength, ε_{cc}	$\varepsilon_{cc} = 0.00265 + \dfrac{0.0035\left(1 - \dfrac{0.734s}{h''}\right)\left(\rho''f_y''\right)^{2/3}}{\sqrt{f_c'}}$ (Peak Strain Only)	$\varepsilon_{cc} = \varepsilon_{co}\left[1.0 + 11.3\left(\dfrac{f_l'}{f_c'}\right)^{0.7}\right]$ for $60\ \text{MPa} \leq f_c' \leq 80\ \text{MPa}$ $\varepsilon_{cc} = \varepsilon_{co}\left[-8.1 + 9.1\exp\left(\dfrac{f_l'}{f_c'}\right)\right]$ for $\quad f_c' \geq 80\ \text{MPa}$ $\varepsilon_{co} = \dfrac{0.7\left(f_c'\right)^{0.3}}{1000}$

310

Table 5.2 (Continued)

Confinement Effectiveness Coefficient, k_e	$k_e = 1 + 0.0091\left(1 - \dfrac{0.245s}{h^{"}}\right)\left(\rho^{"} + \dfrac{nd^{"}}{8sd}\rho\right)\dfrac{f_y^{"}}{\sqrt{f_c^{'}}}$ s = the center-to-center spacing of the lateral ties in inches $h^{"}$ = length of one side of the rectangular ties in inches n = number of longitudinal steel bars $d^{"}$ = nominal diameter of lateral ties in inches d = nominal diameter of longitudinal steel bars in inches ρ = volumetric ratio of longitudinal reinforcement $\rho^{"}$ = volumetric ratio of lateral reinforcement $f_y^{"}$ = yielding stress of the lateral steel in psi	$k_e = \dfrac{(1 - 0.5\alpha)^2 (\beta - 0.5\alpha)}{\beta(1 - 1.6g^{'}\rho_{cc})}\left[1 - \dfrac{8(0.58 + 0.11g^{'})}{\beta}\left(\dfrac{w_i^{'}}{h_c}\right)^2 + \dfrac{0.93}{\beta}\left(\dfrac{w_i^{'}}{h_c}\right)^3\right]$ for square column sections. $\alpha = s^{'}/h$ for square or rectangular sections $s^{'}$ = clear spacing of transverse reinforcement h = depth of the cross section b = width of the cross section $g^{'}$ = the distance between the centers of the longitudinal bars in the extreme faces divided by the core dimension $\beta = b_c/h_c$ b_c = the width of the confined concrete core h_c = the depth of the confined concrete core $w_i^{'}$ = the dimension between longitudinal bars taken from inside to inside ρ_{cc} = longitudinal reinforcement ratio

311

Table 5.2 (Continued)

Ultimate Strain, ε_{cu}	Not Available	$\varepsilon_{cu} = \varepsilon_{co}\left[2 + \left(122.5 - 0.92 f_c'\right)\sqrt{\dfrac{f_l'}{f_c'}}\right]$ for $\quad f_c' \leq 80$ MPa $\varepsilon_{cu} = \varepsilon_{co}\left[2 + \left(82.75 - 0.37 f_c'\right)\sqrt{\dfrac{f_l'}{f_c'}}\right]$ for $\quad f_c' \geq 80$ MPa

312

Table 5.2 (Continued)

	Cusson and Paultre	Martirossyan
Confined Concrete Strength, f'_{cc}	$$f'_{cc}/f'_c = 1.0 + 2.1\left(f'_{le}/f'_c\right)^{0.7}$$ f'_c = maximum strength of unconfined concrete in a member $f'_l = k_e f_l$ f'_l = effective confinement pressure applied to the nominal concrete core k_e = confinement effective coefficient f_l = nominal lateral pressure $$f_l = \frac{f_{hcc}}{s}\left(\frac{A_{shx} + A_{shy}}{c_x + c_y}\right)$$ $$f_l = \frac{f_{hcc}A_{sh}}{sc} \quad \text{for square section}$$ f_{hcc} = stress in the transverse reinforcement at the maximum strengths of confined concrete s = center-to-center tie spacing A_{shx} and A_{shy} = total cross sections of the lateral steel bars perpendicular to the x and the y axis, respectively c_x and c_y = widths of the concrete core parallel to the x and the y axis, repectively	$$f'_{cc} = f'_c + 3.96 \bar{f_r}$$

313

Table 5.2 (Continued)

| Longitudinal compressive concrete stress, f_c | $f_c = f_{cc}\left[\dfrac{k\left(\varepsilon_c/\varepsilon_{cc}\right)}{k-1+\left(\varepsilon_c/\varepsilon_{cc}\right)^k}\right]$ for

$\varepsilon_c \leq \varepsilon_{cc}$

$k = \dfrac{E_c}{E_c - \left(f_{cc}/\varepsilon_{cc}\right)}$

E_c = tangent modulus of concrete

$f_c = f_{cc}\exp\!\left[k_1\left(\varepsilon_c - \varepsilon_{cc}\right)^{k_2}\right]$ for

$\varepsilon_c \geq \varepsilon_{cc}$

$k_1 = \dfrac{\ln 0.5}{\left(\varepsilon_{C50C} - \varepsilon_{cc}\right)^{k_2}}$

$k_2 = 0.58 + 16\left(f_l'/f_c'\right)^{1.4} \approx 1.5$ may be used for the behavior prediction of unconfined concrete | $f_c = \dfrac{f'_{cc}\,xr}{r-1+x^{k_3 r}}$ (Confined)

$f_c = \dfrac{f'_c\,xr}{r-1+x^{k_3 r}}$ (Unconfined)

$x = \dfrac{\varepsilon_c}{\varepsilon_{cc}}$ (Confined)

$x = \dfrac{\varepsilon_c}{\varepsilon_{co}}$ (Unconfined)

$r = \dfrac{E_{50}}{E_{50} - E_{sec}}$ (Confined)

$r = \dfrac{E_{50u}}{E_{50u} - E_{secu}}$ (Unconfined)

$E_{sec} = \dfrac{f'_{cc}}{\varepsilon_{cc}}$ (Confined)

$E_{secu} = \dfrac{f'_c}{\varepsilon_{co}}$ (Unconfined)

$k_3 = \left\{\dfrac{1}{Ln\left[1 - r + \dfrac{1.25\varepsilon_{cu}r}{\varepsilon_{cc}}\right]}{rLn\left[\dfrac{\varepsilon_{cu}}{\varepsilon_{cc}}\right]}\right\}$ |

314

Table 5.2 (Continued)

			(Confined) upper expression value "1" for $0 \le \varepsilon_c \le \varepsilon_{cc}$ lower expression for $\varepsilon_{cc} < \varepsilon_c < \varepsilon_{cu}$ $$k_3 = \left\{ \frac{\begin{cases} 1 \\ Ln\left[1 - r + \dfrac{0.00625r}{\varepsilon_{co}}\right] \end{cases}}{rLn\left[\dfrac{0.005}{\varepsilon_{co}}\right]} \right\}$$ (Unconfined) upper expression value "1" for $0 \le \varepsilon_c \le \varepsilon_{co}$ lower expression for $\varepsilon_{co} < \varepsilon_c < 0.005$ $E_{50} = 46{,}000 \times k_2 \times \sqrt{f'_c}$ (psi) (Confined) $$k_2 = \left(\frac{f_{yeff}}{f_y}\right)^{0.2}$$ $E_{50u} = 46{,}000 \times \sqrt{f'_c}$ (psi) (Unconfined)

315

Table 5.2 (Continued)

Strain at Strength, ε_{cc}	$\varepsilon_{cc} = \varepsilon_{co} + 0.21\left(\dfrac{f_l'}{f_c'}\right)^{1.7}$ ε_{co} = peak strain of unconfined concrete $\varepsilon_{C50C} = \varepsilon_{C50U} + 0.15\left(\dfrac{f_l'}{f_c'}\right)^{1.1}$ with $f_{hcc} = f_{yh}$ ε_{C50C} = strain at which stress drops to 50% of peak strength of confined concrete ε_{C50U} = strain at which stress drops to 50% peak strength of unconfined concrete ≈ 0.004	$\varepsilon_{cc} = \varepsilon_{co}\left[1 + k_1\left(\dfrac{f_{cc}'}{f_c'} - 1\right)\right]$ $k_1 = 5 + 1.3 \times \rho_t \dfrac{f_y}{f_c'}$ ρ_t = transverse reinforcement ratio = $\dfrac{nA_t}{b's}$ f_y = yield strength of transverse reinforcement f_c' = plain concrete strength ε_{co} = peak strain of unconfined concrete b' = width measured from the center lines of the out-most perimeter hoops s = spacing of one pair of transverse steel n = number of the legs of the transverse reinforcement in the vertical cross section within the spacing, s A_t = cross sectional area of one leg of transverse reinforcement .

316

Table 5.2 (Continued)

			f'_l = average transverse confining pressure, a passive confining pressure $$f'_l = \rho_t f_{yeff}$$ f_{yeff} = effective stress in confining steel for the condition when the specimen has reached to its maximum strength. $$f_{yeff} = \min\left(f_y, f_{ye}\right)$$ f_{ye} = effective stress of transverse reinforcement at the point of maximum strength of HSC confined column $$f_{ye} = 11.6 \times \left(\frac{1}{\rho_t} \times \frac{f_y}{f'_c}\right)^{0.26} \quad \text{(ksi)}$$ f_y and f'_c = strengths of transverse steel and the concrete, respectively

317

Table 5.2 (Continued)

Confinement Effectiveness Coefficient, k_e	$$k_e = \frac{\left(1 - \frac{\sum w_i^2}{6c_x c_y}\right)\left(1 - \frac{s'}{2c_x}\right)\left(1 - \frac{s'}{2c_y}\right)}{(1 - \rho_c)}$$ $\sum w_i^2$ = sum of the squares of all the clear spacings between adjacent longitudinal steel bars in a rectangular section s' = clear spacing of ties ρ_c = longitudinal reinforcement ratio in the core section	
Ultimate Strain, ε_{cu}	Not Available	$\varepsilon_{cu} = 0.005 + 0.19 \times \left(\rho_t \frac{f_y}{f_c}\right)^{1.5}$ $\varepsilon_{cu} = 0.005$ assumed for unconfined concrete

318

Table 5.2 (Continued)

	Razvi and Saatcioglu	Bing et. al. (2001)
Confined Concrete Strength, f'_{cc}	$f'_{cc} = f'_c + k_1 f'_l$ $k_1 = 6.7(f'_l)^{-0.17}$ $f'_l = k_2 f_l$ (MPa) $f_l = \dfrac{\sum_{i=1}^{q}(A_s f_s \sin\alpha)_i}{s b_c}$ where q = number of tie legs that cross the side of core concrete for which the average nominal lateral pressure f_l is being computed. f_s = tensile stress in tranverse reinforcement at peak concrete stress, although f_s is often assumed to equal to yield strength f_y of the transverse steel. The value of $f_s = E_s\left(0.0025 + 0.04*\sqrt[3]{\dfrac{k_2\rho_c}{f'_c}}\right) \le f_y$ where f'_{co} is in MPa. The upper limit of yield strength f_{yt} may be taken as 1,400 MPa. Reduction of lateral pressure expressed as: $k_2 = 0.15\sqrt{\left(\dfrac{b_c}{s}\right)\left(\dfrac{b_c}{s_l}\right)} \le 1.0$. s = spacing of transverse reinforcement s_l = spacing of longitudinal reinforcement For rectangular and square columns with different pressures in orthogonal directions due to different tie arrangements in two directions, f'_l is expressed as: $f'_l = \dfrac{f_{lex}b_{cx} + f_{ley}b_{cy}}{b_{cx} + b_{cy}}$ f'_{lx} and f'_{ly} = equivalent lateral pressures acting perpendicular to core dimensions b_{cx} and b_{cy}	$f'_{cc} = f'_c\left[-1.254 + 2.254\sqrt{1 + 7.94\alpha_s\dfrac{f'_l}{f'_c}} - 2\alpha_s\dfrac{f'_l}{f'_c}\right]$ When $f'_c \le 52 MPa$, $\alpha_s = (21.2 - 0.35 f'_c)\dfrac{f'_l}{f'_c}$ When $f'_c > 52 MPa$, $\alpha_s = 3.1\dfrac{f'_l}{f'_c}$, where f'_l is the effective lateral confining pressue expressed as: $f'_l = 0.5 k_e(\rho_x + \rho_y)f_y$ ρ_x = lateral confining steel parallel to x-axis ρ_y = lateral confining steel parallel to y-axis

319

Table 5.2 (Continued)

Longitudinal compressive concrete stress, f_c	$$f_c = \frac{f'_{cc}\left(\dfrac{\varepsilon_c}{\varepsilon_{cc}}\right)r}{r-1+\left(\dfrac{\varepsilon_c}{\varepsilon_{cc}}\right)^r} \quad \text{for } \varepsilon_c \leq \varepsilon_{cc}$$ $$r = \frac{E_c}{E_c - E_{sec}}$$ E_{sec} = secant modulus of elasticity of confined concrete $$E_{sec} = \frac{f'_{cc}}{\varepsilon_{cc}},$$ E_c = modulus of elasticity of unconfined concrete. $$E_c = 3,320\sqrt{f'_c}\,6,900 \quad \text{where } f'_c \text{ is}$$ in MPa. $E_c > E_{sec}$. For $\varepsilon_c \geq \varepsilon_{cc}$, equation is an expression of a linear segment starting from the peak with descending slope defined by the strain corresponding to 85% of peak stress ε_{85}.	When $0 \leq \varepsilon_c \leq \varepsilon_{co}$ $$f_c = E_c\varepsilon_c + \frac{\left(f'_{co} - E_c\varepsilon_{co}\right)}{\varepsilon_{co}^2}\varepsilon_c^2$$ when $\varepsilon_{co} \leq \varepsilon_c \leq \varepsilon_{cc}$ $$f_c = f'_{cc} - \frac{\left(f'_{cc} - f'_c\right)}{\left(\varepsilon_{cc} - \varepsilon_{co}\right)^2} \times \left(\varepsilon_c - \varepsilon_{cc}\right)^2$$ when $\varepsilon_c > \varepsilon_{cc}$ $$f_c = f'_{cc} - \beta\frac{f'_{cc}}{\varepsilon_{cc}} \times \left(\varepsilon_c - \varepsilon_{cc}\right) \geq 0.4f'_{cc}$$ where, f'_{cc} = maximum strength of confined concrete ε_{cc} = axial strain at maximum strength β = coefficient for the slope control of descending branch $$\beta = \left(0.048f'_c - 2.14\right) - \left(0.098f'_c - 4.57\right)\left(\frac{f_l}{f'_c}\right)^{\frac{1}{5}}$$ when $f_y \leq 550MPa$ and $f'_c > 75MPa$ $\beta = 0.07$ when $f_y > 1200MPa$ and $f'_c \leq 80MPa$ $\beta = 0.1$ when $f_y > 1200MPa$ and $f'_c > 80MPa$

320

Table 5.2 (Continued)

Strain at Strength, ε_{cc}	$\varepsilon_{cc} = \varepsilon_{co}\left(1 + 5k_3 k_e\right)$ = strain at peak concrete stress $\varepsilon_{85} = 260 k_3 \rho_c \varepsilon_{cc}\left[1 + 0.5 k_2 \left(k_4 - 1\right)\right] + \varepsilon_{085}$ = The strain corresponding to 85% of peak stress $\rho_c = \dfrac{\displaystyle\sum_{i=1}^{n}\left(A_{sx}\right)_i + \sum_{j=1}^{m}\left(A_{sy}\right)_j}{\left[s\left(b_{cx} + b_{cy}\right)\right]}$ =volumetric ratio $k_3 = \dfrac{40}{f_c'} \leq 1.0$ and $k_4 = \dfrac{f_y}{500} \geq 1.0$ f_y = yield strength of transverse reinforcement $\varepsilon_{co} = 0.0028 - 0.0008 k_3$ = peak strain of unconfined concrete $\varepsilon_{085} = \varepsilon_{co} + 0.0018 k_3^2$ = strain at which stress drops to 85% peak strength of unconfined concrete	Ordinary-strength steel, $\dfrac{\varepsilon_{cc}}{\varepsilon_{co}} = 1.0 + 11.3\left[\dfrac{f_l'}{f_c'}\right]^{0.7}$ Ultra-high-strength steel, $\dfrac{\varepsilon_{cc}}{\varepsilon_{co}} = 2.0 + \left(87 - 1.06 f_{co}'\right)\sqrt{\dfrac{f_l'}{f_c'}}$ when $f_{co}' \leq 50 MPa$ $\dfrac{\varepsilon_{cc}}{\varepsilon_{co}} = 2.0 + \left(53.4 - 0.42 f_{co}'\right)\sqrt{\dfrac{f_l'}{f_c'}}$ when $f_{co}' > 50 MPa$
Confinement Effectiveness Coefficient, k_e	$k_e = \dfrac{k_1 f_l'}{f_c'}$ =strength enhancement coefficient clear spacings between adjacent longitudinal steel bars in a rectangular section	$k_e = \dfrac{\left[1 - \displaystyle\sum_{i=1}^{n}\dfrac{C_i^2}{6 b_c d_c}\right] \times \left[1 - 0.5\dfrac{s'}{b_c}\right] \times \left[1 - 0.5\dfrac{s'}{d_c}\right]}{1 - \rho_{cc}}$ = Confinement effective coefficient ρ_{cc} = volumetric ratio of confining reinforcement to core concrete. s' = clear spacing between hoops

321

Table 5.2 (Continued)

Ultimate Strain, ε_{cu}	Not Available	Normal-strength steel, $\dfrac{\varepsilon_{cu}}{\varepsilon_{co}} = 2.0 + \left(122.5 - 0.92 f_c'\right)\sqrt{\dfrac{f_l'}{f_c'}}$ when $f_c' < 80 MPa$ $\dfrac{\varepsilon_{cu}}{\varepsilon_{co}} = 2.0 + \left(82.75 - 0.37 f_c'\right)\sqrt{\dfrac{f_l'}{f_c'}}$ when $f_c' \geq 80 MPa$ Ultra-high-strength steel, $\dfrac{\varepsilon_{cu}}{\varepsilon_{co}} = 2.0 + \left(70.0 - 0.6 f_c'\right)\sqrt{\dfrac{f_l'}{f_c'}}$ when $f_c' \leq 50 MPa$ $\dfrac{\varepsilon_{cu}}{\varepsilon_{co}} = 2.0 + \left(49.0 - 0.2 f_c'\right)\sqrt{\dfrac{f_l'}{f_c'}}$ when $f_c' > 50 MPa$

322

Table 5.3-Summary of confined HSC peak stress models by different researchers.

Researcher	Confined Concrete Strength	Strain at Strength	Ultimate Strain
Mander	$f_{cc} = f_c\left(-1.254 + 2.254\sqrt{1 + \frac{7.94 f_l}{f_c}} - 2\frac{f_l}{f_c}\right)$	$\varepsilon_{cc} = \varepsilon_{co}\left[1 + 5\left(\frac{f'_{cc}}{f'_c} - 1\right)\right]$	Not available
Yong et al.	$f'_{cc} = k_e\, f'_c$	$\varepsilon_{cc} = 0.00265 + \dfrac{0.0035\left(1 - \frac{0.734s}{h''}\right)\left(\rho'' f_y''\right)^{\frac{2}{3}}}{\sqrt{f'_c}}$	Not available
Azizinamini et. al.	$f'_{cc} = k_e\, f'_c$	$\varepsilon_{cc} = 0.00265 + \dfrac{0.0035\left(1 - \frac{0.734s}{h''}\right)\left(\rho'' f_y''\right)^{\frac{2}{3}}}{\sqrt{f'_c}}$	Not available
Li and Park (Bing et. al. 1994)	$f'_{cc} = f'_c\left(1.413\sqrt{1 + \frac{11.4 f'_l}{f'_c}} - \frac{2 f'_l}{f'_c} - 0.413\right)$	$\varepsilon_{cc} = \varepsilon_{co}\left[-8.1 + 9.1\exp\left(\frac{f'_l}{f'_c}\right)\right]$	$\varepsilon_{cu} = \varepsilon_{co}\left[2 + (82.75 - 0.37 f'_c)\sqrt{\frac{f'_l}{f'_c}}\right]$
Cusson and Paultre	$f'_{cc}/f'_c = 1.0 + 2.1\left(f'_l/f'_c\right)^{0.7}$	$\varepsilon_{cc} = \varepsilon_{co} + 0.21\left(f'_l/f'_c\right)^{1.7}$	$\varepsilon_{C50C} = \varepsilon_{C50U} + 0.15\left(f'_l/f'_c\right)^{1.1}$
Martirossyan	$f'_{cc} = f'_c + 3.96 f'_l$	$\varepsilon_{cc} = \varepsilon_{co}\left[1 + k_1\left(\frac{f'_{cc}}{f'_c} - 1\right)\right]$	$\varepsilon_{cu} = 0.005 + 0.19 \times \left(\rho_l \frac{f_y}{f_c}\right)^{1.5}$
Razvi and Saatcioglu	$f'_{cc} = f'_c + k_1 f'_l$	$\varepsilon_{cc} = \varepsilon_{co}\left(1 + 5 k_3 k_e\right)$	Not available
Bing et. al. (2001)	$f'_{cc} = f'_c\left[-1.254 + 2.254\sqrt{1 + 7.94\alpha_s\frac{f_l}{f_c}} - 2\alpha_s\frac{f_l}{f_c}\right]$	$\dfrac{\varepsilon_{cc}}{\varepsilon_{co}} = 1.0 + 11.3\left[\frac{f'_l}{f'_c}\right]^{0.7}$ $\dfrac{\varepsilon_{cc}}{\varepsilon_{co}} = 2.0 + (87 - 1.06 f'_{co})\sqrt{\frac{f'_l}{f'_c}}$ $\dfrac{\varepsilon_{cc}}{\varepsilon_{co}} = 2.0 + (53.4 - 0.42 f'_{co})\sqrt{\frac{f'_l}{f'_c}}$	$\dfrac{\varepsilon_{cu}}{\varepsilon_{co}} = 2.0 + (122.5 - 0.92 f'_c)\sqrt{\frac{f'_l}{f'_c}}$ $\dfrac{\varepsilon_{cu}}{\varepsilon_{co}} = 2.0 + (82.75 - 0.37 f'_c)\sqrt{\frac{f'_l}{f'_c}}$ $\dfrac{\varepsilon_{cu}}{\varepsilon_{co}} = 2.0 + (70.0 - 0.6 f'_c)\sqrt{\frac{f'_l}{f'_c}}$ $\dfrac{\varepsilon_{cu}}{\varepsilon_{co}} = 2.0 + (49.0 - 0.2 f'_c)\sqrt{\frac{f'_l}{f'_c}}$

323

The concept behind each model as shown on Table 5.3 has been presented in Section 2.4. Typical variables that affect the overall confined concrete stress-stress relationships are: geometry, material properties, effective confinement effective coefficients, volumetric ratio, effective lateral confining stress, and modulus elasticity of concrete. All models were based on the regression analysis based on the data obtained from small-scale tests. For all tests conducted by previous researchers, the specimens were subjected to short-term monotonic concentric or eccentric loading, as it was for the testing by Martirossyan et. al., until failure, except for the test conducted by Azizinamini et. al. where the test columns were subjected to constant axial load and cyclic lateral loads. A conservative estimate was made by Mander et. al. for the ultimate compression strain expressed as:

$$\varepsilon_{cu} = 0.004 + \frac{1.4\rho_s f_{yh}\varepsilon_{su}}{f'_{cc}}$$ where ε_{su} is the steel strain at maximum tensile stress

and $\rho_s = \frac{4A_{sp}}{D's}$ is the volumetric ratio of confining steel. For analytical purposes,

the value of $\varepsilon_{su} = 0.07$ for the longitudinal steel reinforcement was experimentally determined for the specimens. Mander et. al. mentioned that the expression for ultimate compression strain is conservative by at least 50% to estimate ultimate compression strain of sections subjected to bending, or combined bending and axial compressions. Therefore, for the purpose of

324

providing marginal safety to allow for uncertainties in ductility demand, a value of $1.5\varepsilon_{su}$ was used in the moment-curvature program discussed in Section 5.6. The expressions for ε_{su} proposed by Li and Park, Cusson and Paultre, and Martirossyan et. al. are also shown in Table 5.3, where such expressions are not available for the remaining models. Since the expressions for ε_{su} are based on axial confined sections only and not based on combined bending and axial compression, it may be assumed that they are conservative.

Shown in Table 5.4 are the confined concrete stress-strain relationships summarized for the ranges of confined concrete strain. The ranges of strains are shown for ascending portions and descending portions of the confined stress-strain curves, where the expressions are based on regression analysis of experimental data.

325

Table 5.4-Summary of confined HSC stress-strain models by different researchers.

Researcher	Confined Concrete Stress	Strain
Mander	$$f_c = \dfrac{f'_{cc}\, xr}{r - 1 + x^r}$$	All ε_c
Yong et al.	$$f_c = \dfrac{AX + BX^2}{1 + (A - 2)X + (B + 1)X^2}$$ $$f_c = \dfrac{CX + DX^2}{1 + (C - 2)X + (D + 1)X^2}$$	for $\varepsilon_c \leq \varepsilon_{co}$ for $\varepsilon_c \geq \varepsilon_{co}$
Azizinamini et al.	$$f_c = \left(\dfrac{f_o}{\varepsilon_o}\right)\varepsilon$$ $$f_c = f'_{cc}\left[1 - \alpha(\varepsilon - \varepsilon_o)\right] \geq 0.3 f'_{cc}$$	for $0 \leq \varepsilon_c \leq \varepsilon_{cc}$ for $\varepsilon_c \geq \varepsilon_{cc}$
Li and Park (Bing et. al. 1994)	$$f_c = E_c \varepsilon_c + \dfrac{f'_c - E_c \varepsilon_{co}}{\varepsilon_{co}^2}\varepsilon_c^2$$ $$f_c = f'_{cc} - \dfrac{f'_{cc} - f'_c}{(\varepsilon_{cc} - \varepsilon_{co})^2}(\varepsilon_c - \varepsilon_{co})^2$$ $$f_c = f'_{cc} - \beta\dfrac{f'_{cc}}{\varepsilon_{cc}}(\varepsilon_c - \varepsilon_{cc}) \geq 0.4 f'_{cc}$$	for $0 \leq \varepsilon_c \leq \varepsilon_{co}$ for $\varepsilon_{co} \leq \varepsilon_c \leq \varepsilon_{cc}$ for $\varepsilon_{cc} \leq \varepsilon_c$
Cusson and Paultre	$$f_c = f_{cc}\left[\dfrac{k\left(\dfrac{\varepsilon_c}{\varepsilon_{cc}}\right)}{k - 1 + \left(\dfrac{\varepsilon_c}{\varepsilon_{cc}}\right)^k}\right]$$ $$f_c = f_{cc}\exp\left[k_1(\varepsilon_c - \varepsilon_{cc})^{k_2}\right]$$	for $\varepsilon_c \leq \varepsilon_{cc}$ for $\varepsilon_c \geq \varepsilon_{cc}$

326

Table 5.4 (Continued)

Martirossyan	$$f_c = \frac{f'_{cc}\, xr}{r - 1 + x^{k_3 r}} \quad \text{(Confined)}$$ $$f_c = \frac{f'_c\, xr}{r - 1 + x^{k_3 r}} \quad \text{(Unconfined)}$$	$k_3 = 1$ for $$0 \le \varepsilon_c \le \varepsilon_{cc}$$ Expression for k_3 for $$\varepsilon_{cc} < \varepsilon_c < \varepsilon_{cu}$$
Razvi and Saatcioglu	$$f_c = \frac{f'_{cc}\left(\dfrac{\varepsilon_c}{\varepsilon_{cc}}\right) r}{r - 1 + \left(\dfrac{\varepsilon_c}{\varepsilon_{cc}}\right)^{r}}$$ Linear segment starting from the peak with descending slope defined by the strain corresponding to 85% of peak stress ε_{85}	for $\varepsilon_c \le \varepsilon_{cc}$ for $\varepsilon_c \ge \varepsilon_{cc}$,
Bing et. al. (2001)	$$f_c = E_c \varepsilon_c + \frac{\left(f'_{co} - E_c \varepsilon_{co}\right)}{\varepsilon_{co}^2}\varepsilon_c^2$$ $$f_c = f'_{cc} - \frac{\left(f'_{cc} - f'_c\right)}{\left(\varepsilon_{cc} - \varepsilon_{co}\right)^2} \times \left(\varepsilon_c - \varepsilon_{cc}\right)^2$$ $$f_c = f_{cc} - \beta \frac{f'_{cc}}{\varepsilon_{cc}} \times \left(\varepsilon_c - \varepsilon_{cc}\right) \ge 0.4 f'_{cc}$$	for $0 \le \varepsilon_c \le \varepsilon_{co}$ for $\varepsilon_{co} \le \varepsilon_c \le \varepsilon_{cc}$ for $\varepsilon_c > \varepsilon_{cc}$

327

5.4 IDEAL FLEXURAL CAPACITY

The ideal flexural capacity, M_i, is strength based on code specified nominal material strengths and limit state such as $\varepsilon_{cu} = 0.005$ and based on a linear strain distribution across the section. This strength is typically used in Load Factor Design. M_i, in the following cases, is a moment when the measured compressive strain of the concrete reached a value of $\varepsilon_{cu} = 0.005$.

Ideal Moment: Experimental research results and the best prediction of strength of a particular test unit using measured material properties. It corresponds to nominal strength but using measured rather than nominal material strengths which is termed characteristic strength and gives rather conservative estimates of material properties. The ideal moment strength is used primarily to assess the validity of equations used for predicting strength.

Column Failures:

The column failures occurs due to various reasons when inadequately designed for inelastic behavior as follows:

1.　　Flexural strength and ductility failures

2.　　Premature termination of column reinforcement

3. Shear failures

4. Cap beam failures

5. Joint failures

6. Footing failures

7. Longitudinal bar pull out failures

8. Soil failures such as liquefaction

9. Weak beam failure in column-beam connections

10. Lap splice failures due to slippage

11. Transverse reinforcement failure

12. Longitudinal reinforcement buckling

13. Substantial degradation of moment capacity due to cyclical loading

14. Anchorage failures

15. P-Delta Effects

16. Dynamic inelastic time-history response

17. Axial load levels

18. Other material properties

Other factors that affect column failure are the characteristics of the building structure such as period, acceleration response spectra for maximum ground accelerations, and seismic demand for specific geographic location.

329

Mander et. al. introduced a useful estimate of ultimate compressive strain of confined concrete ε_{cu}. The strain is assumed to occur at the initiation of the fracture of transverse confinement steel and is estimated by assuming that strain-energy capacity of the transverse reinforcement as it reaches the peak stress f_{uh} is equal to the total energy absorbed by the confined concrete. This estimate of ultimate compressive strain of confined concrete is conservative by at least 50% when used to estimate the ultimate compressive strain of sections subjected to bending, or combined bending and axial compression. However, it provides sufficient margin of safety to allow for uncertainties in ductility demand.

$$\varepsilon_{cu} = 0.004 + \frac{1.4 \rho_s f_{yh} \varepsilon_{su}}{f'_{cc}}$$, where ε_{su} is the steel strain at maximum tensile stress

and $\rho_s = \dfrac{4 A_{sp}}{D' s}$ is the volumetric ratio of the confining steel. For rectangular

sections, $\rho_s = \rho_x + \rho_y$. The remainder of the terms are as defined previously in the introduction of confined stress-strain models.

For the specimens in consideration, the column shear strength was made sure to exceed the maximum ultimate shear demand of the columns to ensure flexural failure mode. Especially since the ductile design of reinforced concrete columns

330

is mainly relied on the flexural performance, section analysis was performed to obtain moment to curvature relationship and calculated ideal flexural capacity.

5.5 ULTIMATE FLEXURAL CAPACITY

The ultimate flexural capacity, M_U, is reached when the column's longitudinal bar buckles, the hoops or longitudinal bars rupture, or concrete is crushed, or when the moment capacity of the columns drop below 80% of the maximum capacity. These typically cause a substantial loss of the column capacity. From moment-curvature analysis of the critical sections considering concrete confinement, the ultimate conditions are taken to be the lateral shear force V_U and displacement Δ_U corresponding to development of ultimate flexural capacity. According to a the moment-curvature analysis of Priestly, Seible, Xiao, and Verma et al. (*ACI Structural Journal*, September-October, 1994.), the ultimate curvature corresponded to the more critical of ultimate concrete compression strain based on an energy-balance approach, and maximum longitudinal reinforcement tensile strain, taken as $0.7\varepsilon_{SU}$, where ε_{su} is the steel strain corresponding to maximum steel stress (Priestley et. al., 1994).

The objective of this research is to investigate seismic performance and design of

331

high strength concrete full-scale columns. Based on the test data, the Force-Displacement characteristics, load-carrying capacity, and deformability (ductility) of the columns are determined. There are two approaches to determine the aforementioned characteristics. The first is by performing moment-curvature analysis and push-over analysis based on the result in order to obtain the Force-Displacement relationship. The second approach is by considering the confinement design and related parameters to see how they affect the performance, in order to establish an appropriate design guidelines for high strength concrete applications on full-scale reinforced concrete columns and for proper ductility in HSC columns.

In order to establish the Force-Displacement relationship, moment-curvature relationship is calculated in this research for each increment of column curvature in the plastic hinge region. By using currently available confined high strength concrete stress-strain relationship models and steel stress-strain models which are described previously, the columns section is analyzed by using force-equilibrium criteria with the use of Fortran 77 programming. A moment-curvature relationship and corresponding force-displacement relationship obtained by using a particular confined HSC stress-strain model and typical steel stress-strain relationship are compared to those obtained by using other confined HSC stress-strain models.

332

5.6 MOMENT-CURVATURE RELATIONSHIP

Assumptions

The moment-curvature program of Appendix V assumes that plane sections remain plain as the column section deforms with increase in the curvature. The stress-strain relationship of the concrete is based on six different stress-strain theories of confined concrete and takes into consideration the transverse hoop spacing, material properties, and transverse steel area. The empirical formulas which are integrated into the program are based on experimental results by observing the behavior of the confined concrete. The effective concrete area is considered smaller than the total confined concrete area due to the placement of the longitudinal bars within the confined region. The concrete cover of the concrete section is assumed to spall due to cracking as the load increases and as the curvature is increased. This is accomplished by assuming that the cover region of the concrete is not confined with transverse hoop area of zero. The stress in this region is based on the unconfined compressive material property of concrete.

The stress-strain relationship of steel is based currently available Mander Steel Stress-Strain theory and based on its true material properties obtained from

333

tensile testing completed in the laboratory such as yield strength, Young's modulus, and ultimate failure stress. The program calculates the stress for each row of the longitudinal bars based on geometric relationships.

The program also assumes that the concrete cannot take any tension. This was accomplished by letting concrete stress to be zero whenever the concrete strain for any particular concrete strip of the column section is less than or equal to zero. The concrete stress for each concrete strip of the column section is calculated only for positive concrete strains.

Moment-Curvature Program Algorithm Procedure and Description

This program determines the moment-curvature relationship of a rectangular reinforced concrete column sections subjected to constant axial load. The moment-curvature relation is based on the currently available confined concrete stress-strain theories and by using the finite element approach that divides the column section into many strips and adds the contribution of each strip to the stress calculation. The following procedure explains the algorithm of the program that calculates moment values for each increment of curvature in the plastic hinge region.

334

1) Given a curvature PHI(J), the depth of the neutral axis X(I) measured from the left edge of the column is assumed, where the depth of the column section is H.

2) The compression zone is divided into N layers of column strips of equal height DY, where DY=H/N.

3) Based on the assumed curvature PHI(J) and the depth of the neutral axis X(I), the location of each strip of the column section measured from the right edge of the column for the Kth strip, e(K), is determined, based on geometry by e(K)= H − (X(I)/M)*(K-1), where M is the number of strips for the compression zone calculated as M=X(I)/DY.

4) For each strip of the column section within the compression zone, the concrete strain ec(K) is calculated by ec(K)=PHI(J) * (e(K) - (H-X(I))), where H-X(I) represents the length of the tension zone for the given X(I).

5) The stress in each concrete strip is calculated by Mander stress-strain relationship by calling Subroutine FCK which calculates the stress FC(K) for a given strain ec(K) for confined reinforced concrete column. If ec(K) is less than

335

zero in the tension zone, the stress FC(K) calculated by Subroutine FCK is made to be 0, since concrete can not withstand tension.

6) The normal force NC(K) due to the stress FC(K) which is calculated for each strip is added as a single sum.

7) The moment due to concrete stress MC(K) is calculated using the calculated normal force NC(K) around the center of gravity of the column section.

8) Similarly, the strain in each layer of reinforcing steel es(KK) is calculated using the location coordinate YS(KK) measured from the right edge of the column for the given X(I).

es(KK)=PHI(J) * (YS(KK) – (H-X(I)), where H-X(I) represents the length of the tension zone for the given X(I). When the steel strain es(KK) exceeds the yield strength fy of the reinforcing steel, it was made to equal to fy when bi-linear steel stress-strain models is used. For the cases of mild strain hardening, the Mander steel stress-strain model is used.

9) The stress in each layer of the reinforcing steel is calculated by calling Subroutine FSK or Subroutine KING which calculates the steel stress FS(KK)

336

for the given steel strain es(KK), where Subroutine KING is used to consider strain hardening.

10)   The normal force NS(KK) due to the stress FS(KK) which is calculated for each layer of reinforcing steel is added as a single sum.

11)   The moment due to steel stress MS(KK) is calculated using the calculated normal force NS(KK) around the center of gravity of the column section.

12)   The applied axial force PO of the column is compared to the sum of the calculated normal forces NTOT(K) = NC(K) + NS(KK). If the margin of error is within the specified value, the corresponding sum of the moments MTOT(K) = MC(K) + MS(KK) is calculated and printed along with the PHI(J), X(I) which produced this result. Then, the procedure above is repeated for the next incremented value of curvature PHI(J).

13)   If PO – NTOT(K) is not within the specified margin of error, the above procedure is repeated for the next incremented value of the compression zone depth X(I), until this condition is satisfied, before the entire procedure above can be repeated for the next incremented value of curvature PHI(J) .

337

14)   The maximum curvature PHI(J) at the termination of the program is reached at ultimate failure of the column. The ultimate failure of the column is assumed to occur when the moment decreases to 80% of maximum moment with concrete stress of greater than 1.5 times the ideal ultimate confined concrete strain or when longitudinal reinforcement exceeds experimentally determined ultimate tensile strain, whichever occurs first.

Control Parameters

The width of the concrete strip was chosen to be small enough to allow sufficient accuracy of the finite element approach as mentioned above. For each increment of curvature, the calculations are performed to obtain the sum of compressive stresses of each column strip across the depth of the compression zone until convergence is reached. The convergence is achieved when the sum of all the compressive normal forces of all strips of concrete and all rows of steel equal to applied axial load within the specified margin of error before the calculations can be repeated for the next incremented value of curvature.

338

The increment of the curvature was chosen to allow sufficient moment calculations. When the increment of the curvature was too small, it takes much longer time for the program to finish calculations since it must perform iterations for each increment of curvature. This is because for each curvature, the program must scan each compression zone, add the stresses of each strip of the column section and locate the neutral axis location. The following Figure 5.1 illustrates the organization of the program.

339

```
                        ┌─────────────┐
                        │ DATA INPUT  │
                        └─────────────┘
                               │
                               ▼
                   ┌────────────────────────┐
                   │  CURVATURE INCREMENT   │
                   └────────────────────────┘
                               │
                               ▼
                   ┌────────────────────────┐
                   │ COMPRESSION ZONE INCREMENT │
                   └────────────────────────┘
```

CALCULATE CONCRETE AND STEEL STRAINS IN COMPRESSION AND TENSION ZONES

CALCULATE CONCRETE AND STEEL STRESS IN COMPRESSION AND TENSION ZONES

CALCULATE TOTAL CONCRETE AND STEEL AXIAL FORCES = NTOT (I)

APPLIED AXIAL LOAD – NTOT(I) < ERROR

NO

YES

PRINT CURVATURE AND CORRESPONDING total MOMENT, MTOT(I)

PRINT CORRESPONDING STRAINS AND STRESSES OF CONCRETE AND STEEL

CALCULATE CURVATURE, SHEAR FORCE, MOMENT AND CONCRETE STRESS & STRAIN AT FIRST YIELDING OF LONGITUDINAL BAR AND PRINT IDEAL MOMENT AT CONCRETE STRAIN OF 0.005

CALCULATE and print corresponding SHEAR, V, VERSUS LATERAL DISPLACEMENT, Δ

UPDATE MAXIMUM CONFINED CONCRETE STRESS, MOMENT AND SHEAR FORCE AND CORRESPONDING ULTIMATE VALUES (80% OF MAX. ASSUMED)

[MTOT(I) < ULTIMATE MOMENT, MU AND CONCRETE STRAIN, CS > 1.5ECU] OR TENSILE STEEL STRAIN, -SS > ULTSS

NO

YES

PRINT MAXIMUM AND ULTIMATE CURVATURE, DISPLACEMENT, MOMENT, SHEAR, AND CONCRETE STRESS AND STRAINS

STOP

Note: ECU=Empirical ultimate confined concrete strain.
ULTSS=Strain at the ultimate longitudinal bar tensile strength.

Fig. 5.1-Flow Chart for Moment-Curvature Program (Simplified).

340

5.7 MOMENT-CURVATURE ANALYSIS

Numerical Results

The implementations of confined high-strength concrete stress-strain relationship in moment-curvature analysis show that the moment first increases until the first yielding of the longitudinal bars with gradual increase in non-linearity of the moment versus curvatures relationship. Upon first yielding of longitudinal steel, there is a substantial increase in nonlinear behavior due to post-yield behavior of the longitudinal reinforcements and compounded by confinement effect of the transverse reinforcements, as the moment increases further toward the first peak moment capacity of the column. Once the peak moment capacity is reached the first concrete cover spalling occurs, and simultaneously, there is a sudden decrease in the moment value down to below the moment value corresponding to the first longitudinal steel yielding for the columns subjected to lower axial loads. On the other hand, such a sudden decrease is not as drastic for the columns subjected to high axial loads in which case the moment drops to above the its moment value corresponding to the first yielding of longitudinal steel. Thereafter, there is a gradual increase in the moment until a second moment peak is reached as the curvature increases due to the strain-hardening behavior of the longitudinal reinforcements. Typically,

341

the yielding of the transverse reinforcement occurs at greater drift ratios. As the longitudinal steel strain increases further with strain-hardening,the transverse confinement provides the increased ductile column performance. The moment gradually begins to decrease with further increase in the curvature until ultimate column failure is reached. The analytical moment-curvature relationships shown in figures 5.8 to 5.15 show that not all confined high-strength concrete models provide aforementioned moment-curvature behavior. Especially for Mander model, which is based on normal strength concrete testing, does not necessarily reflect each stage of the column failure. Among the high strength concrete models, the Bing et. al. model shown in figure 5.14 does not capture the first peak moment capacity of the specimens. This is because the a β factor used in the model, which controls the descending branch, does not apply to all ranges of ordinary steel strength. Young et. al. model assumes an arbitrarily selected point on the descending branch of the curve which caused it to under predict the post peak behavior of the specimens. It is again noticeable that for large axial load and greater unconfined concrete strength, there is more substantial increase in moment immediately after steel yielding.

With lower axial load or lower unconfined concrete strength, such a drop in the moment at concrete cover spalling was more drastic. This behavior seems to be a result of highers stress exerted on the cover concrete in the compressive

342

region due to lower applied axial load and lower unconfined concrete strength. The slippage of the longitudinal steel or the failure of the transverse hoop would be more gradual in this case. For higher axial load and unconfined concrete strength, there would be more sudden slippage (bonding failure) between the bar and concrete and also due to greater compressive force in the compression zones.

The differences in the basic assumption of longitudinal steel arrangement gave different results as compared to the results obtained from the Moment-Curvature Analysis Program written by David King at the University of Canterbury, February, 1986. The existing Moment-Curvature Analysis Program assumes evenly distributed longitudinal bar placements around the perimeter of the column section, where the program mentioned above assumes that longitudinal steel of different sizes are placed individually in their actual locations as shown in the column section detail of figure 3.1 and AIV.1. Thus, the size and location of reinforcements are realistically considered in this program in comparison to existing Moment-Curvature Analysis Program. The Fortran 77 Code of the new Moment-Curvature Analysis Program is shown in Appendix V.

343

First, the moment-curvature relationship was obtained for all six specimens and is shown below in Tables 5.6 and 5.7 using currently existing confined HSC stress-strain models.

Table 5.6 shows the analytical yield moments, $_{MAN}M_{1Y}$ and $_{MAR}M_{1Y}$, and maximum moments, $_{MAN}M_{MAX}$ and $_{MAR}M_{MAX}$, which are obtained using Mander and Martirossyan Confined Concrete Stress-Strain models, respectively. Table 5.7 shows analytical results using all seven confined HSC stress-strain models and Mander confined concrete stress-strain model which is based on normal strength concrete experiments.

The experimental moment capacities $_{EXP}M_{MAX(Avg.)}$ are summarized in Table 5.5. The experimental yield moment, $M_{1y(Avg.)}$ were obtained from the experimental results when the first yield of the longitudinal reinforcement was reached. It is important to note that the experimental maximum moment values shown in table 5.5 is obtained by multiplication of experimental shear values and the total column length measured from the column stub to the point of load application. Therefore, the moment values table 5.5 are greater than the experimental moment values shown in figures 5.2 to 5.7 since the moment values of figures 5.2 to 5.7 are measured at the point of maximum experimental curvature for each specimen.

344

Table 5.5-Moment capacities from experimental data.

	$M_{1Y}(+)$	$M_{1Y}(-)$	$M_{1y(Avg.)}$	$_{EXP}M_{MAX(Avg.)}$	$^*M_U$	M_{ACI}
	(kN*m)	(kN*m)	(kN*m)	(kN*m)	(kN*m)	(kN*m)
FHC1-0.20	1313.74	1215.01	1264.38	*1370.10*	1001.39	1119.60
FHC2-0.34(H)*	1317.37	1492.99	1405.18	*1557.94*	990.31	1179.10
FHC3-0.22	1352.14	1340.45	1346.30	*1401.53*	787.70	1128.90
FHC4-0.33(H)*	1386.67	1396.28	1391.48	*1566.35*	801.55	1179.80
FHC5-0.20	1329.23	1248.95	1289.09	*1367.27*	333.28	1119.60
FHC6-0.20	1288.97	1272.05	1280.51	*1367.88*	660.02	1119.60

$^*M_U$ represents the ultimate failure of the columns

The figures 5.2 shows the experimental moment versus curvature relationships obtained at peak shear values for each of the six specimens tested. The curvature values were obtained until the linear ports used to measure the curvatures failed. The moment values are obtained by multiplying the experimental shear values by a column length measured from the location of the maximum experimental curvature to the point of lateral load application. The experimental curvature at maximum moment values are located at a distance of approximately 312 mm (12.5 in.) from column stub for specimens FHC3-0.22, FHC5-0.2, and FHC6-0.2 and at approximately 438 mm (17.5 in.) from column stub for specimens FHC1-0.2, FHC2-0.34, and FHC4-0.33.

345

There are shifts in the location of maximum curvature at various stages of loading, and the length of plastic hinge varies depending on the loading conditions.

In general, the location of maximum curvature shifted away from the column stub as drift increased. For the specimens subjected to higher axial loads, there was a greater shift in the location of maximum curvature. For the specimens subjected to lower axial loads, such a shift in the location of maximum curvature was minimal.

346

Moment versus Curvature
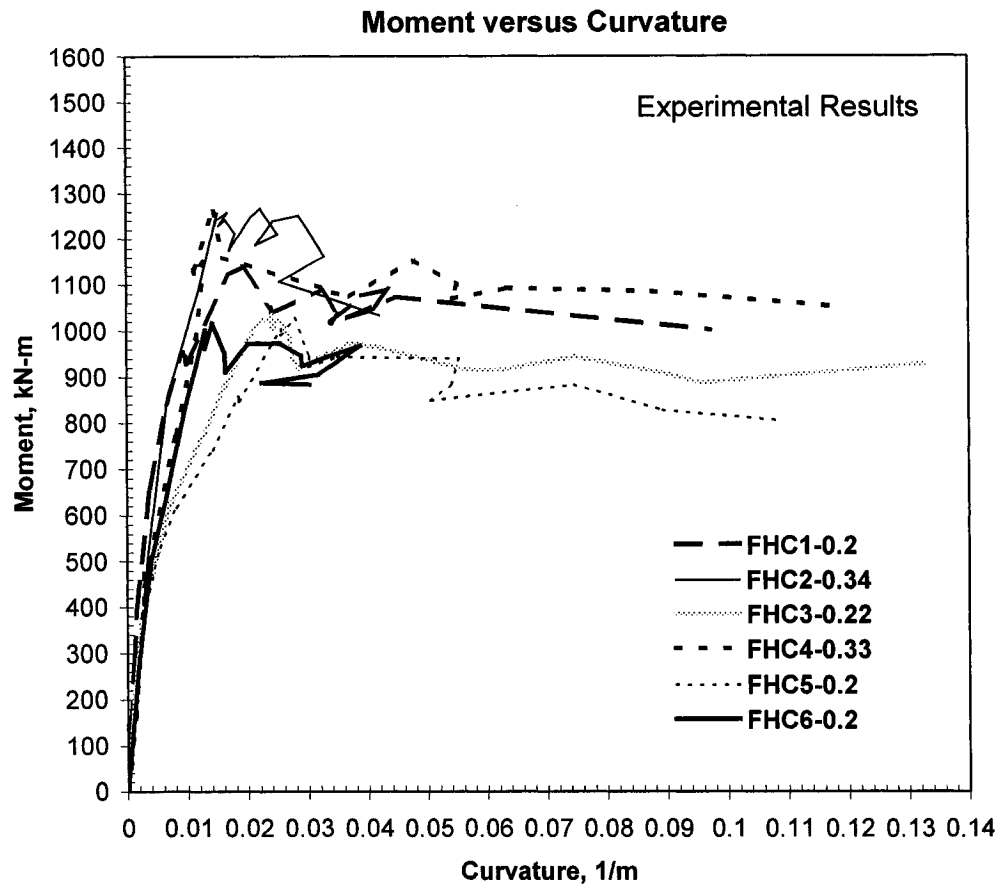
Fig. 5.2-Experimental Moment versus Curvature Relationship

347

Table 5.6-Moment capacities from the moment-curvature program

	Mander Model				*Martirossyan Model*				
	$_{MAN}M_{1Y}$	$_{MAN}M_{MAX}$	$\dfrac{_{EXP}M_{MAX}}{_{MAN}M_{MAX}}$	$^{**}M_i$	$_{MAR}M_{1Y}$	$_{MAR}M_{MAX}$	$\dfrac{_{EXP}M_{MAX}}{_{MAR}M_{MAX}}$	$^{**}M_i$	M_{ACI}
	(kN*m)	(kN*m)		(kN*m)	(kN*m)	(kN*m)		(kN*m)	(kN*m)
FHC1-0.20	1029.79	1060.63	1.29	1006.92	1040.41	1136.06	1.21	1112.71	1119.60
FHC2-0.34(H)*	1109.10	1172.80	1.33	1113.14	1241.73	1247.97	1.25	1243.29	1179.10
FHC3-0.22	1037.43	1066.38	1.31	1013.93	1059.99	1139.04	1.23	1109.19	1128.90
FHC4-0.33(H)*	1102.44	1153.44	1.36	1104.66	1235.44	1242.92	1.26	1242.92	1179.80
FHC5-0.20	1030.78	1033.92	1.32	998.73	1042.60	1135.72	1.20	1119.79	1119.60
FHC6-0.20	1031.86	1040.80	1.31	999.89	1042.60	1135.72	1.20	1119.79	1119.60

* (H) Represent High Axial Load

** Here, M_i corresponds to when concrete strain reaches $\varepsilon_{cu} = 0.005$

Table 5.7-Moment capacities from the moment-curvature program using experimentally determined material properties

MODELS	FHC1-0.20	FHC2-0.34(H)	FHC3-0.22	FHC4-0.33(H)	FHC5-0.20	FHC6-0.20
	(kN-m)	(kN-m)	(kN-m)	(kN-m)	(kN-m)	(kN-m)
Mander	1060.63	1172.80	1066.38	1153.44	1033.92	1040.80
Martirossyan	1136.06	1247.97	1139.04	1242.92	1135.72	1135.72
Li and Park (1994)	1094.09	1246.96	1109.56	1243.40	1094.09	1094.09
Cusson and Paultre	1228.36	1387.47	1239.89	1369.47	1192.24	1209.46
Young et. al.	1100.00	1160.39	1103.76	1166.08	1099.73	1099.47
Azizinamini et. al.	1132.71	1231.65	1132.68	1226.11	1132.92	1132.43
Bing et. al. (2001)	1282.34	1550.20	1306.42	1533.42	1282.34	1282.34
Razvi and Saatcioglu	1023.77	1066.45	1036.14	1068.94	1017.96	1019.82

It can be observed from all tables of moment capacities, Tables 5.5, 5.6, and 5.7, that the first yield of longitudinal reinforcement is substantially delayed for the specimens of high axial load in comparison to the specimens of lower axial loads. It seems that higher axial load induces greater effective confinement of the concrete and less lateral displacement which results in higher moment values at first yield of the longitudinal reinforcement.

As shown in Table 5.6, the experimental results compared to Mander model results are greater by as much as 36% for the columns that are subjected to high axial loads. Compared to Martirossyan model, the experimental results are greater by approximately 26% for the columns that are subjected to high axial loads. On the other hand, the moment capacity values based on ACI 318-95 code, M_{ACI}, again show very conservative values for the columns that are subjected to high axial loads. From above results, it can be deduced that the existing concrete stress-strain models reasonably predict the moment capacity of high strength concrete columns. However, they are still quite conservative, especially for Mander model which over predicted the moment capacities by 29% or greater for every specimen. Figure 5.3 is an analytical result using the moment-curvature program discussed earlier. In this case, Mander model was used to predict the moment-curvature relationships. It is apparent that FHC2-0.34 and FHC4-0.33 with higher applied axial loads both exceed the moment capacities of four other specimens FHC1-0.2, FHC3-0.22, FHC5-0.2, and

349

FHC6-0.2. The first peak of specimens FHC2-0.34 and FHC4-0.33 occur at a moment value of about 1113.14 kN-m and 1104.66 kN-m, respectively, where for other specimens FHC1-0.2, FHC3-0.22, FHC5-0.2, and FHC6-0.2, the first peak occurred at moment values approximately 1030.94 kN-m. The main differences are that for the specimens of higher axial loads, the first yielding of the longitudinal reinforcements were relatively delayed as compared to the other four specimens. The concrete covering spalling occurred much earlier for other four specimens in comparison to those two specimens of higher axial loads. In fact, this was also the case for all other confined concrete models, except for Mander and Bing et. al. models.

Figure 5.4 shows the analytical result using Martirossyan model. Where the higher axial loads resulted in greater moment capacity, this model show distinguished points of the first yield point of the longitudinal reinforcement as well as the point of cover spalling. It can be observed that this model also shows the delay in the first yield and earlier occurrence of cover spalling for the specimens of higher axial loads. Unlike the Mander model, Martirossyan model shows a sudden drop in capacity upon cover concrete spalling for all specimens. The sudden drop is followed by a gradual increase in the moment capacity until the ultimate curvature is reached typically when the compressive concrete strain in the cover region reaches 1.5 times the energy-based theoretical ultimate

350

compressive confined concrete strain, ε_{cu}, and when the moment drops below 80% of the maximum moment value, M_{max}.

It seems that Martirossyan model gave more consistent moment-curvature relationships for all specimens, whether they were subjected to high or low axial loads. Since all values of the moment-curvature program are obtained for each curvature increment, a detailed stages of failures during the initial yielding of the longitudinal reinforcement as well as cover spalling, sudden drop in the capacity at cover spalling, and gradual increase in the capacity in the column due to confinement of concrete are captured.

351
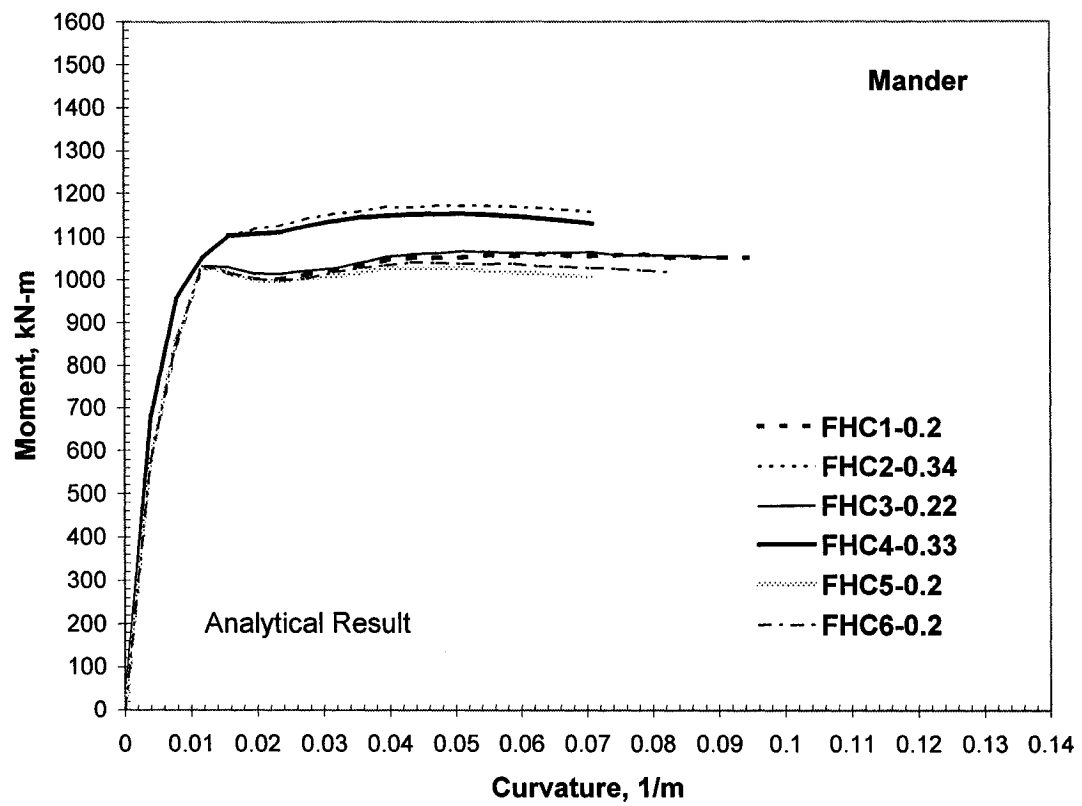
Fig. 5.3-Analytical moment-curvature relationship based on Mander confined concrete stress-strain model.

352
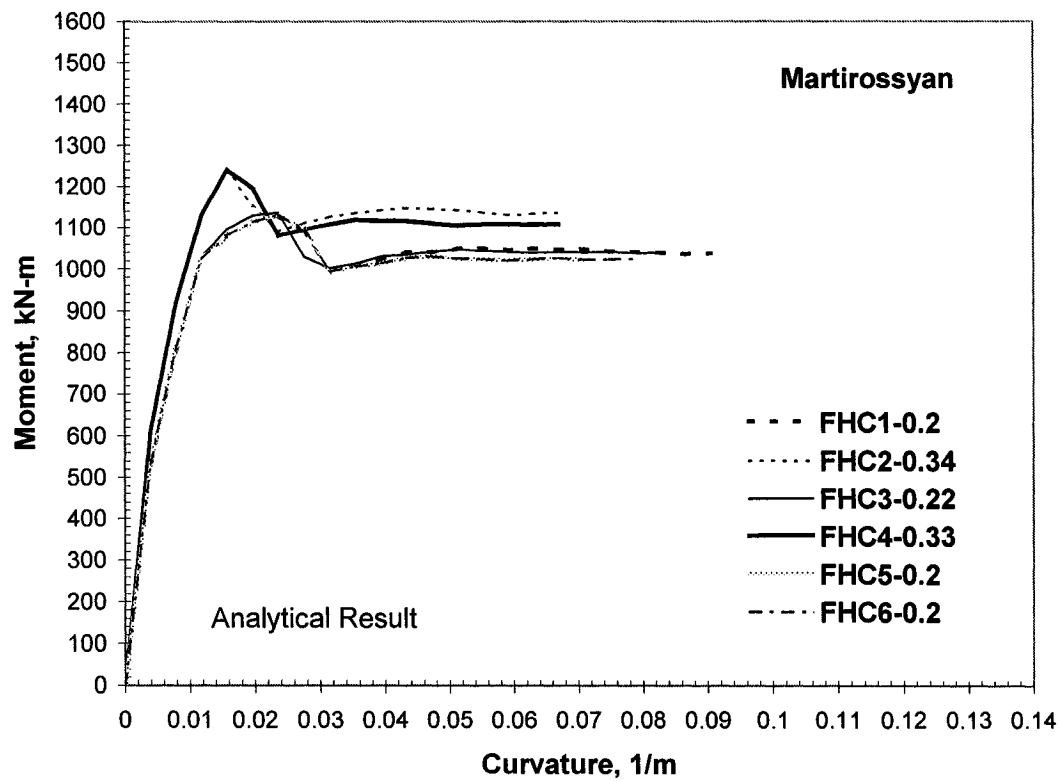
Fig. 5.4-Analytical moment-curvature relationship based on Martirossyan confined concrete stress-strain model.

353
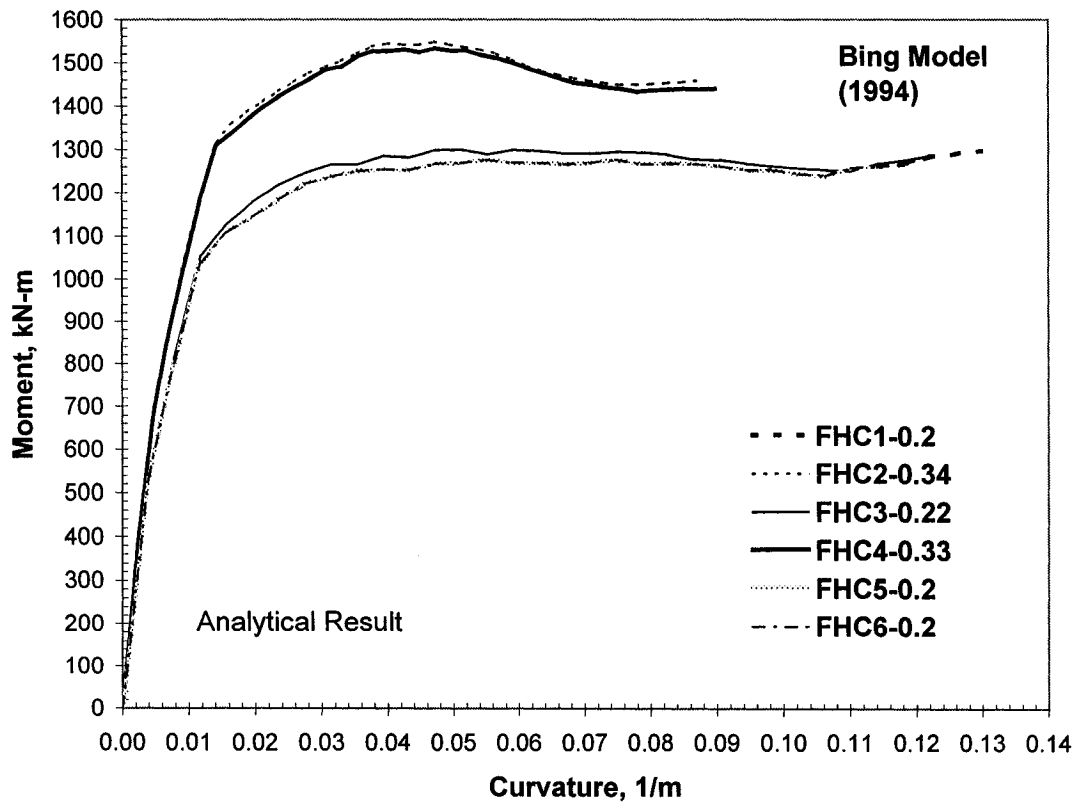
Fig. 5.5-Analytical moment-curvature relationship based on Bing confined concrete stress-strain model.

354
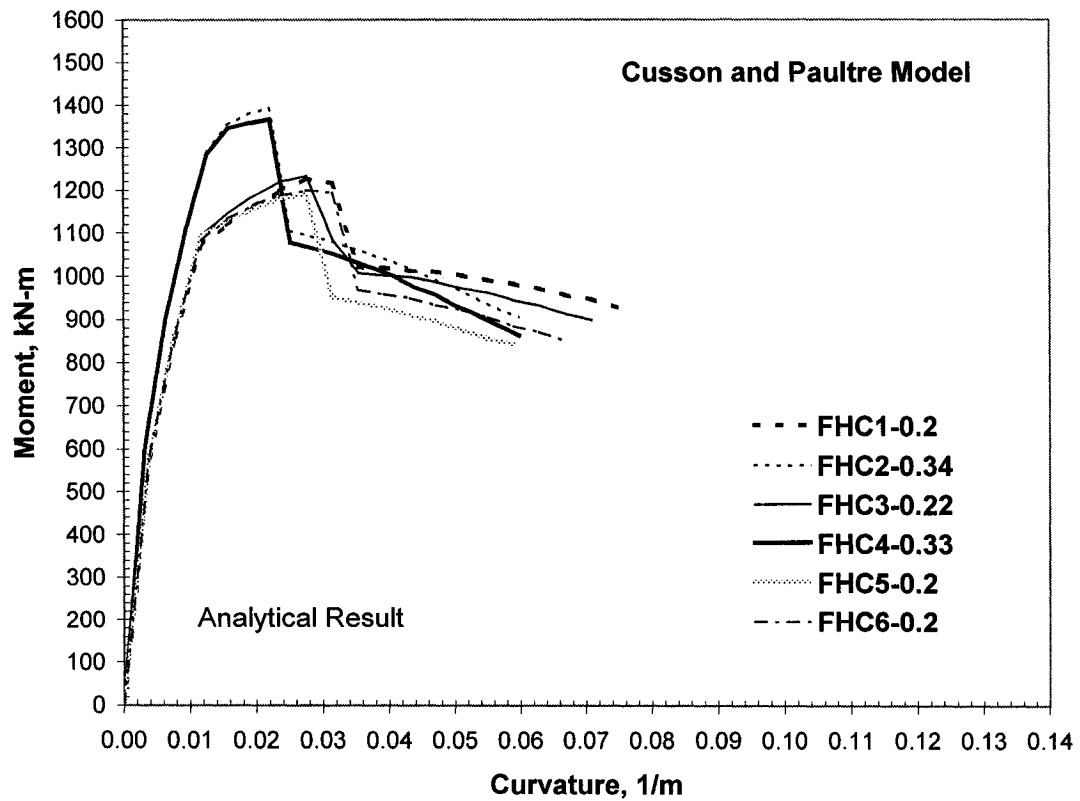
Fig. 5.6-Analytical moment-curvature relationship based on Cusson and Paultre confined concrete stress-strain model.

355
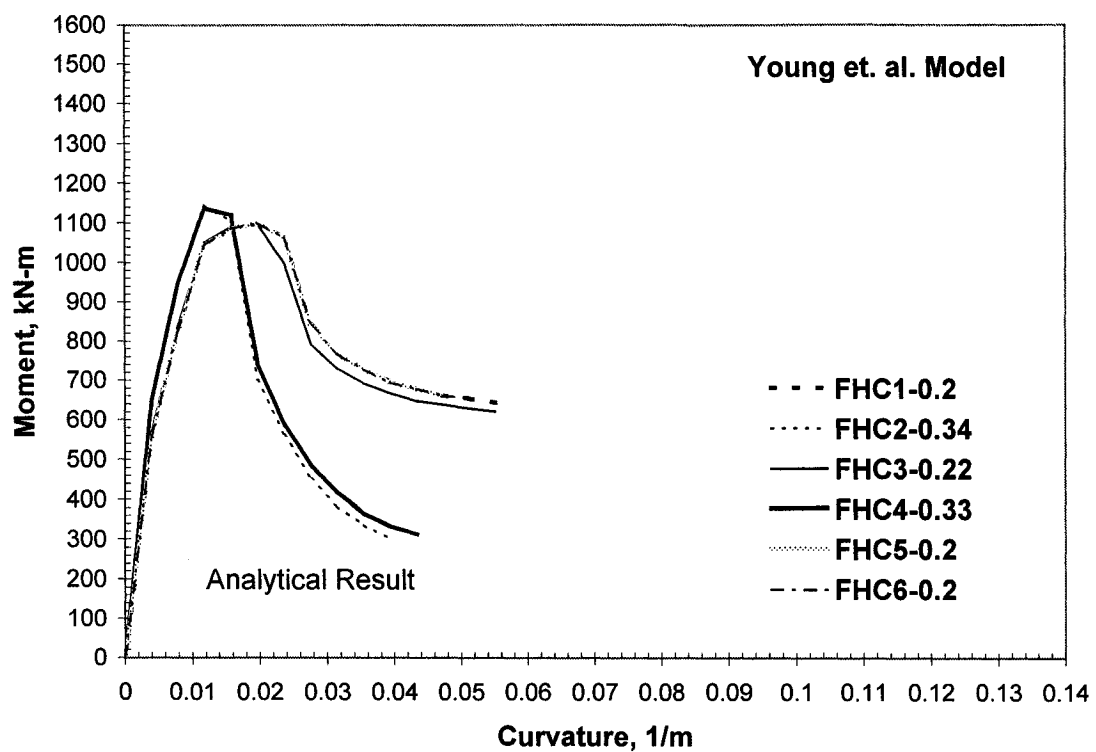
Fig. 5.7-Analytical moment-curvature relationship based on Young et. al. confined concrete stress-strain model.

356
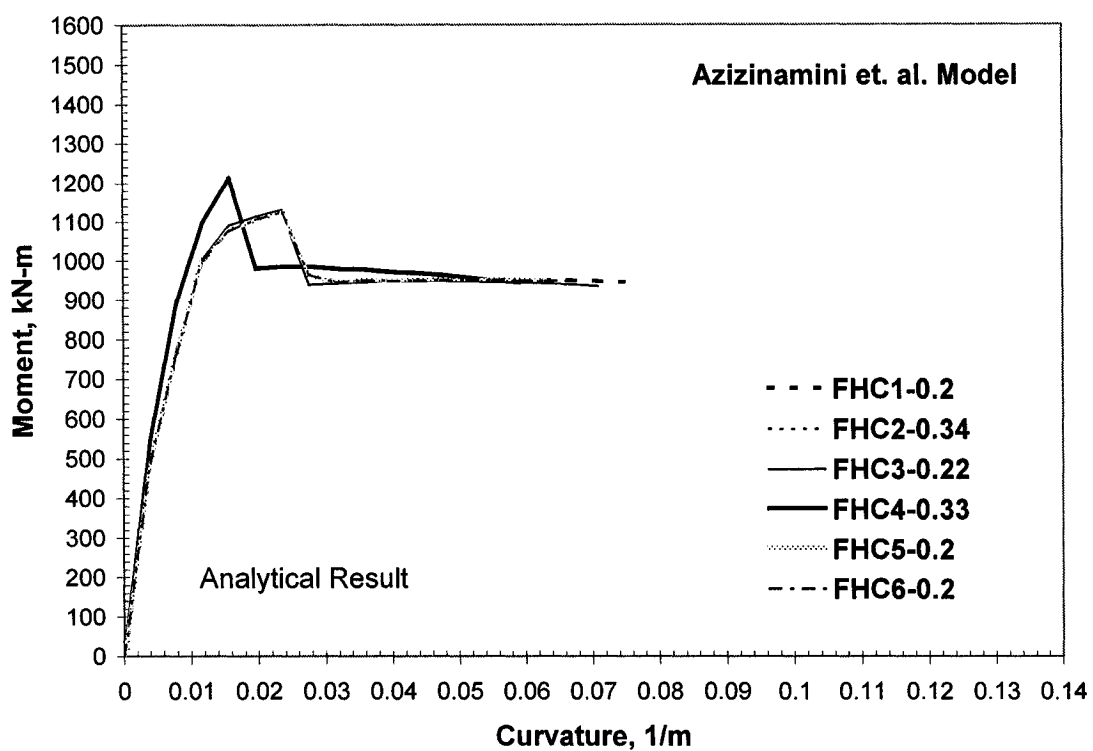
Fig. 5.8-Analytical moment-curvature relationship based on Azizinamini confined concrete stress-strain model.

357
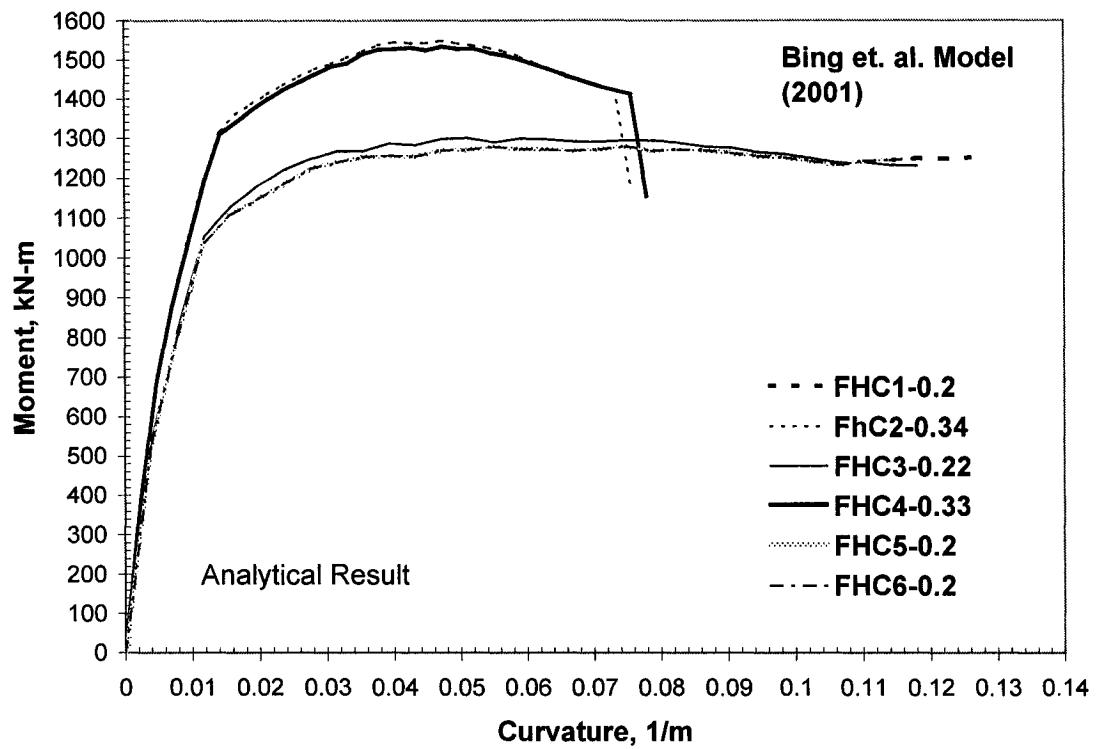
Fig. 5.9-Analytical moment-curvature relationship based on Bing et. al. confined concrete stress-strain model.

358
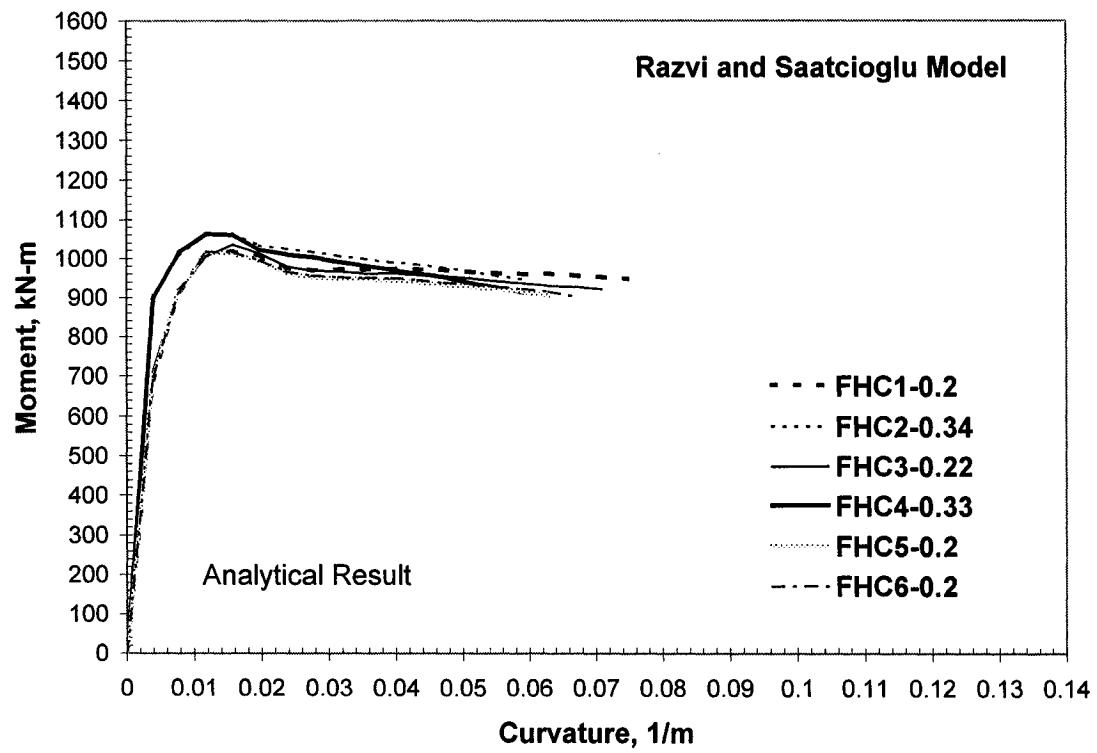
Fig. 5.10-Analytical moment-curvature relationship based on Razvi and Saatcioglu confined concrete stress-strain model.

359

The Figure 5.11 to 5.16 show that the experimental values correlated with the moment values obtained from analytical results quite well, especially for Martirossyan HSC confined concrete stress-strain model. The predictions of the location of first longitudinal rebar yielding and first cover concrete spalling using Martirossyan model gave very good correlation for the majority of the specimens. Despite the slight differences in the composition of the high-strength concrete used, it seems that Martirossyan model which is based on high strength concrete testing gave better prediction in comparison to Mander model which is based on normal strength concrete testing. The estimated ultimate curvature at ultimate column failure which is assumed to occur at ultimate confined concrete compressive strain of $1.5\,\varepsilon_{su}$, as conservatively predicted by Mander el al., provided conservative predictions for all specimens. However, it is important to note that the experimental moment-curvature relationship shown in figures 5.11 to 5.16 do not show a full range of curvature values to ultimate curvature at column failure, since the linear ports which were used to measure the curvatures in the plastic hinge area failed at different stages of loading for each specimen. The specimens FHC3-0.22 and FHC5-0.2, as shown in figures 5.13 and 5.15, respectively, show a drastic variation in the initial slope of experimental the moment-curvature relationship. It seems that their low axial load levels as well as increased transverse reinforcement spacing increased the deformability in the early stages of loading. Specimen FHC6-0.2 with same

360

parameters as specimen FHC5-0.2, except for the use of higher grade transverse reinforcement correlated well with the analytical results during the early stages of loading. Both the decreased transverse reinforcement spacing and increase in axial load level actually increased the performance up to the maximum moment capacity of the columns.
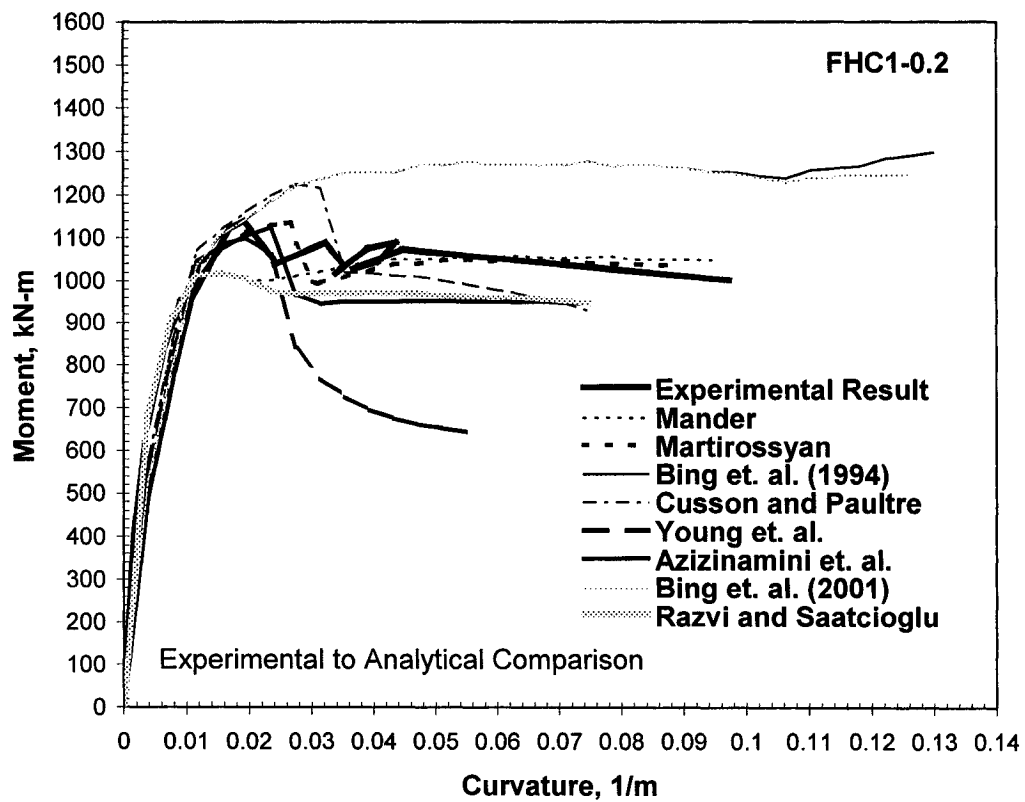
Fig. 5.11-Comparison of experimental to analytical moment-curvature relationships for specimen FHC1-0.2.

361
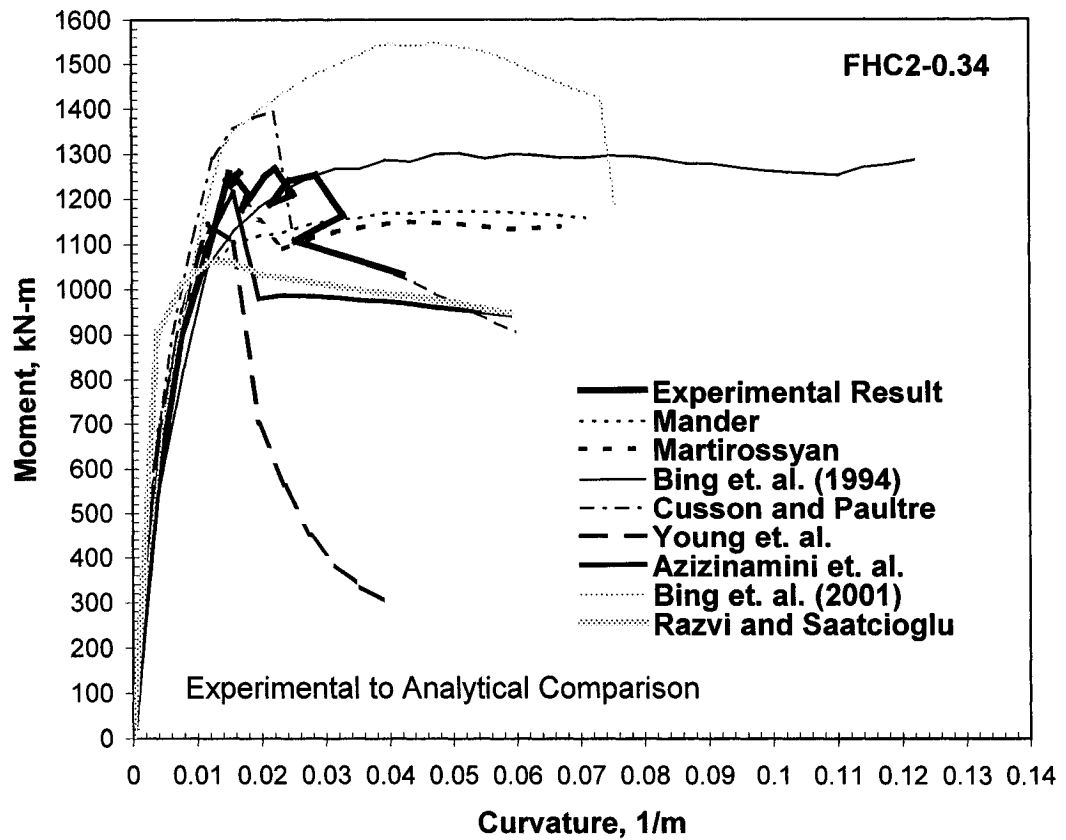
Fig. 5.12-Comparison of experimental to analytical moment-curvature relationships for specimen FHC2-0.34.
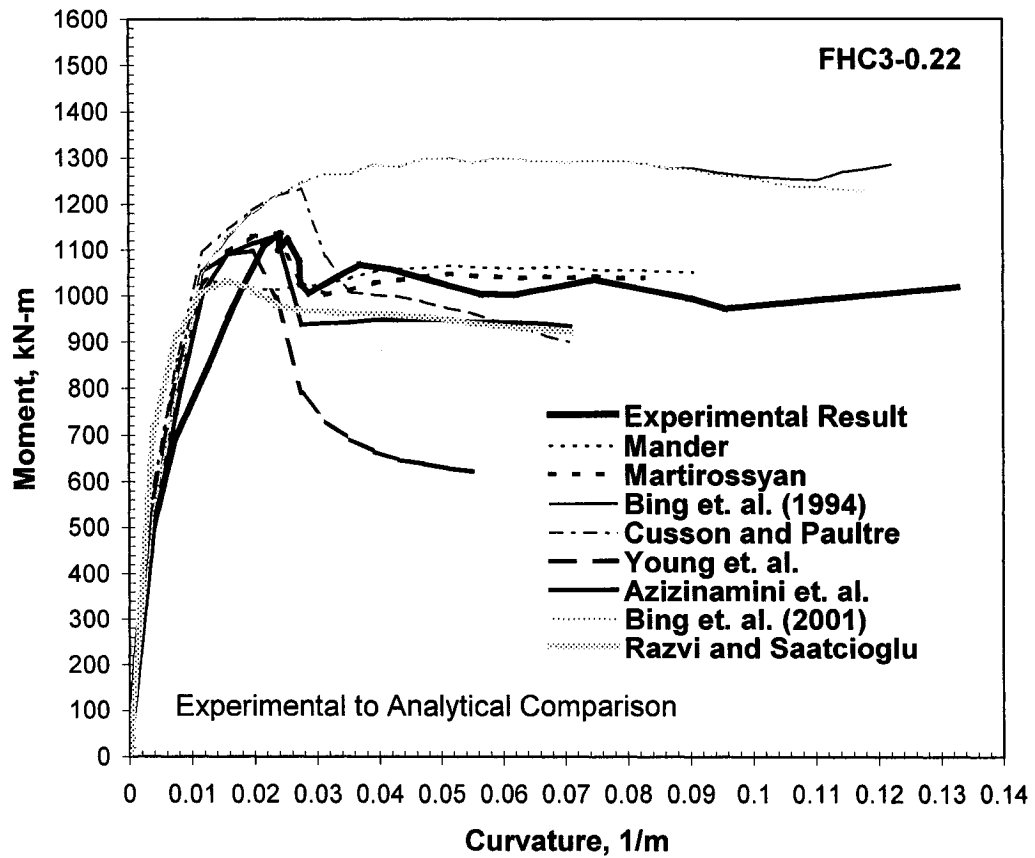
Fig. 5.13-Comparison of experimental to analytical moment-curvature relationships for specimen FHC3-0.22.

363
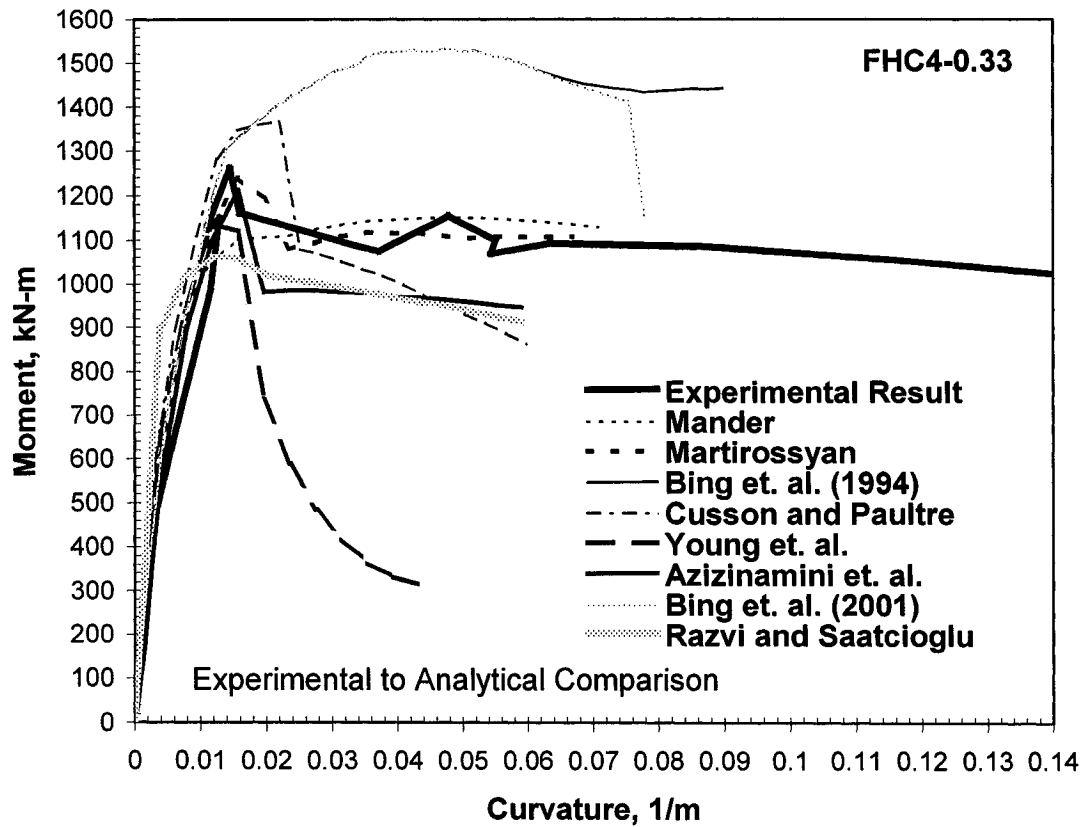
Fig. 5.14-Comparison of experimental to analytical moment-curvature relationships for specimen FHC4-0.33.
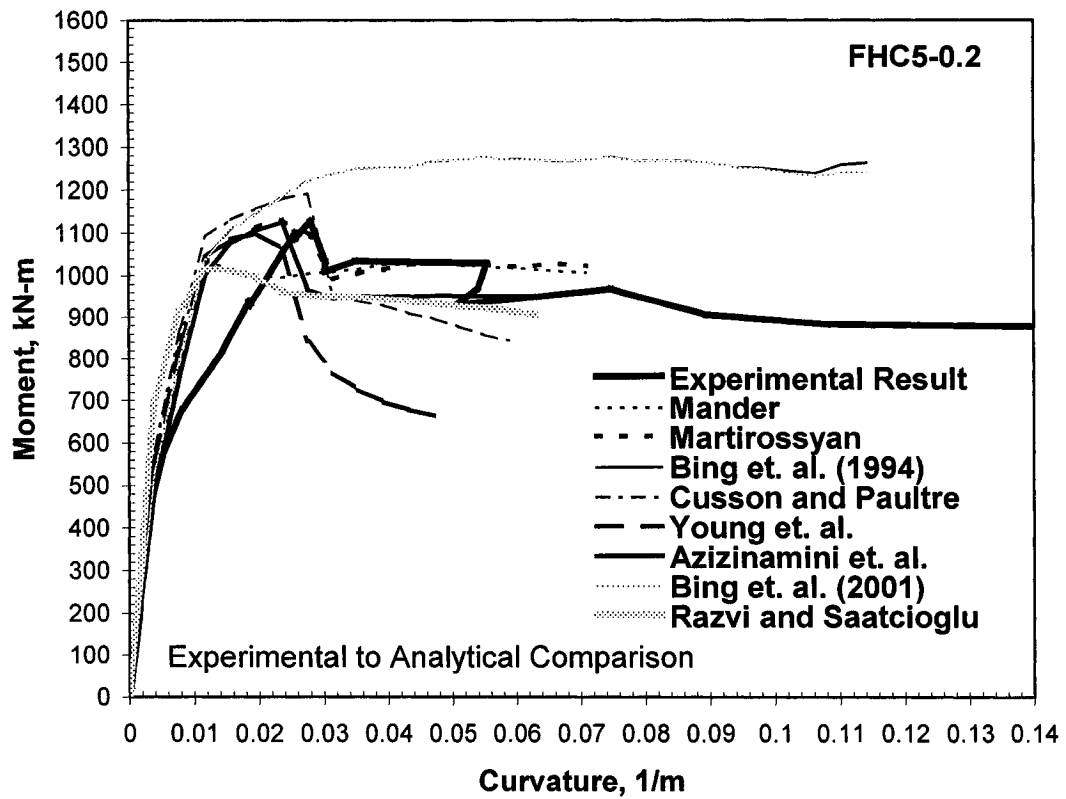
Fig. 5.15-Comparison of experimental to analytical moment-curvature relationships for specimen FHC5-0.2.

365
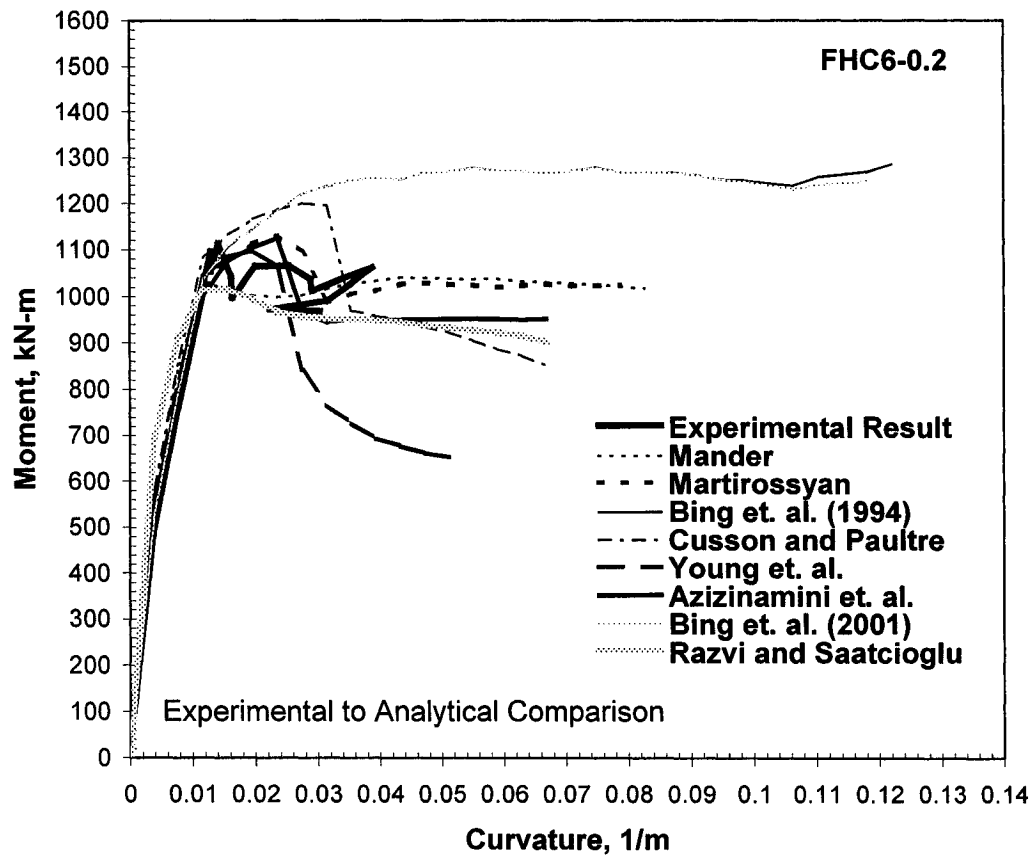
Fig. 5.16-Comparison of experimental to analytical moment-curvature relationships for specimen FHC6-0.2.

366

5.8 SHEAR FORCE VERSUS DISPLACEMENT RELATIONSHIP

5.8.1 Push-Over Analysis

Shear Force versus Displacement Relationship

Derived from the moment-curvature relationships are the lateral force-displacement relationships. These relationships for all six specimens are shown below using the aforementioned method of calculations as discussed in Section 2.7 for the total displacement taking plastic rotation, flexural deformation, and the shear deformation into consideration. Therefore, the lateral force-displacement relationships provide a realistic prediction of column behaviors in comparison to moment-curvature relationships.

The experimental peak shear envelopes are compared to the theoretical shear force versus drift ratio which were derived from the moment-curvature relationships of Section 5.7. They are shown below for each of the six specimens in Figures 5.18 to 5.23. Mild strain-hardening was assumed with the use of Mander steel stress-strain model.

The crucial parameters considered in prediction of column behavior throughout different stages of failure are illustrated in Figure 5.17. The experimentally

367

obtained values of initial longitudinal reinforcement yielding, failure of cover concrete, cover concrete spalling, maximum moment(shear) capacity, and the ultimate column failure points are as previously shown in figures 4.11 to 4.16.
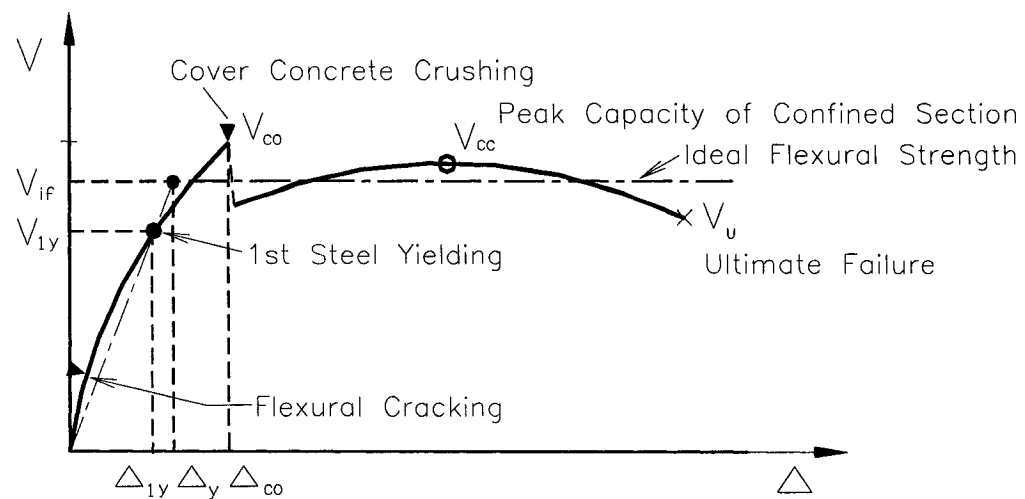
Fig. 5.17-Prediction of column behavior through various stages of failure

5.8.2 Analytical Results

The differences in the confined HSC stress-strain models are such that some models are derived using linear regression-analysis using the experimentally obtained data, and others are based on trial and error approach and iterations.

368

However, the majority of the confined HSC stress-strain models are based on the concept of effectively confined core concrete models, and theoretical peak confined concrete stress which is dependent on various parameters such as volumetric ratios, confinement pressure, and effective confinement values. For all calculations using the Fortran 77 Code of Appendix V, the cover concrete was assumed to spall at a compressive strain of 0.005, and the cover concrete was assumed to have no transverse reinforcement confinement.

The stopping criterion was when one of the following conditions was met whichever occurred first: (1) 1.5 times the conservative estimate for ultimate concrete compressive strain is reached, (2) the moment values after the peak moment capacity was reached decreases to 80% of the ideal moment capacity, and (3) the steel strain of the longitudinal reinforcement exceeded its strain at ultimate tensile strength. An additional stopping criterion is when the compressive stress of the longitudinal reinforcement exceeds it buckling stress. However, the transverse reinforcements typically failed due to anchorage failure of ties, and the longitudinal reinforcements buckled followed by the ultimate failure of column characterized by a sudden loss in the axial load capacity. Therefore, additional criteria were not included at this time in the Fortran 77 Code.

369

Figures 5.18 to 5.23 compare the analytically results, Shear Force versus Displacement relationships, to experimental peak shear envelopes. It can be observed that for the cases of high axial load, the majority of the analytical results underestimated the shear forces at the first yield of the longitudinal reinforcements and the concrete cover spalling was slightly delayed. For the cases of lower axial loads, the first yield of the longitudinal reinforcements correlated quite well with the experimental results. However, the cover spalling at peak shear force were substantially delayed in comparison to the experimental results. In all cases, the concrete cover spalling at peak shear force occurred earlier during the experiments in comparison to the analytical results. The analytical results underestimated the first peak shear capcity for all specimens. Greater the axial load level the distances between the point of the first longitudinal reinforcement yield and the point of concrete cover spalling decreased. With lower axial load levels, the cover concrete spalling was substantially delayed. The majority of the confined HSC stress-models overestimated the post-peak capacity of the specimens at large drift ratios for the cases of high axial loads. For the cases of low axial load levels, the capacities of the specimens correlated well with the analytical results, especially for Cusson and Paultre, Azizinamini et. al., and Razvi and Saatcioglu models. For low axial load levels, the concept of confinement effectiveness of all confined high-strength concrete stress-strain models allows a reasonable

370

prediction of both peak column capacities and post-peak behavior. However, for high axial load levels, the post-peak performance at large drift ratios seems over-estimated.
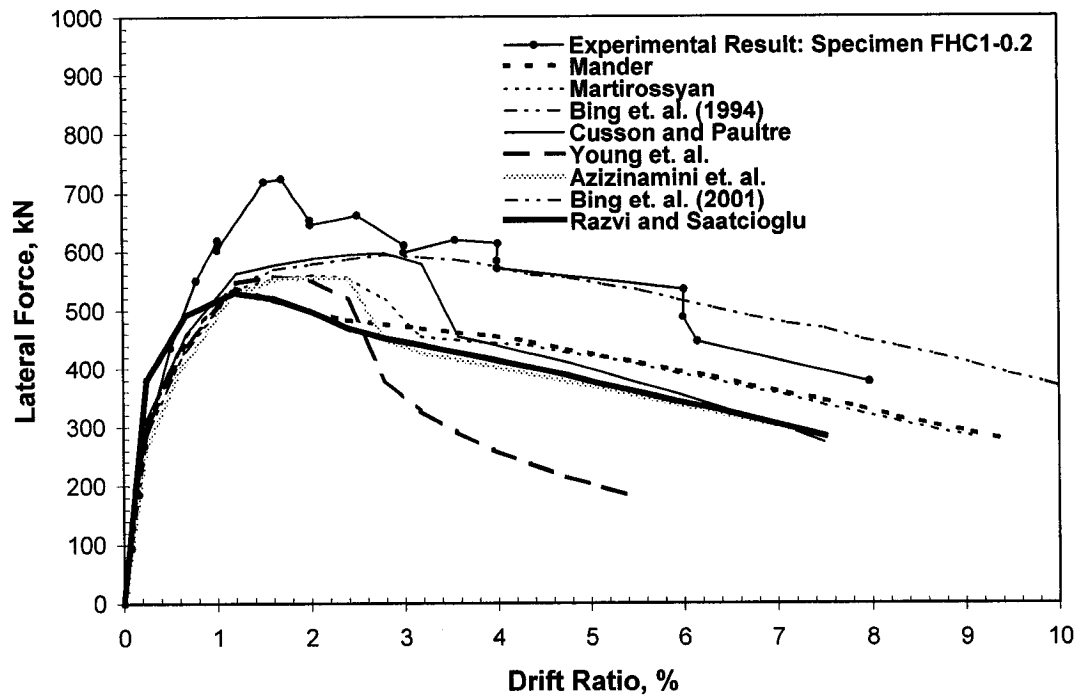
Fig. 5.18-Experimental and Analytical Lateral Force versus Displacement Relationships for Specimen FHC1-0.2

372
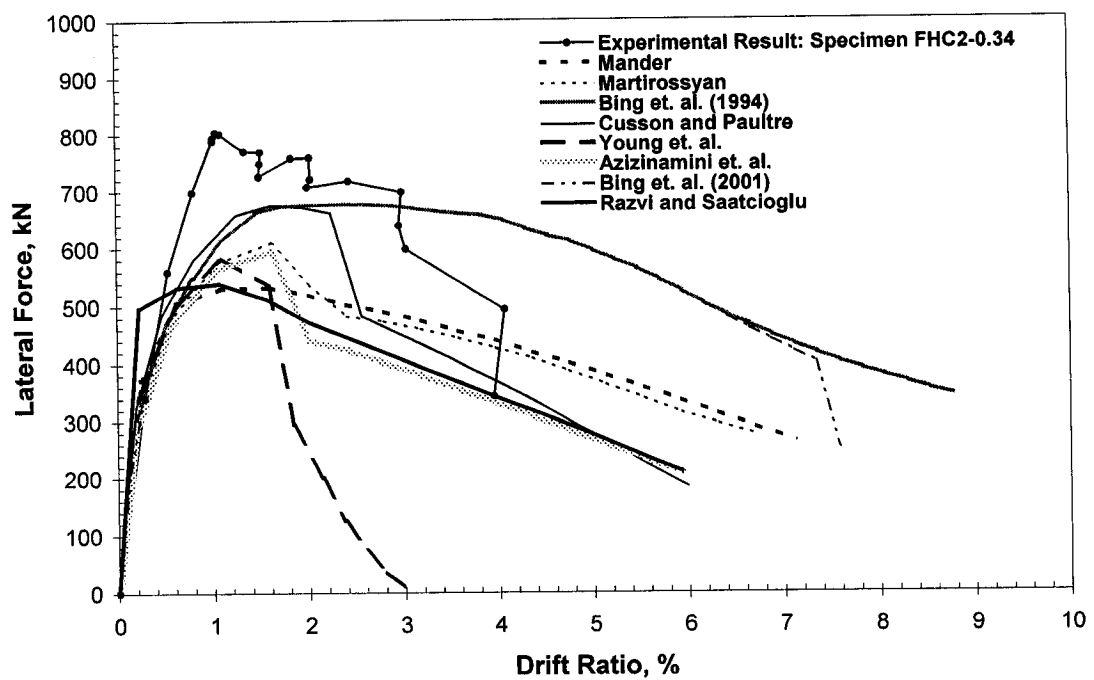
Fig. 5.19- Experimental and Analytical Lateral Force versus Displacement Relationships for Specimen FHC2-0.3

373
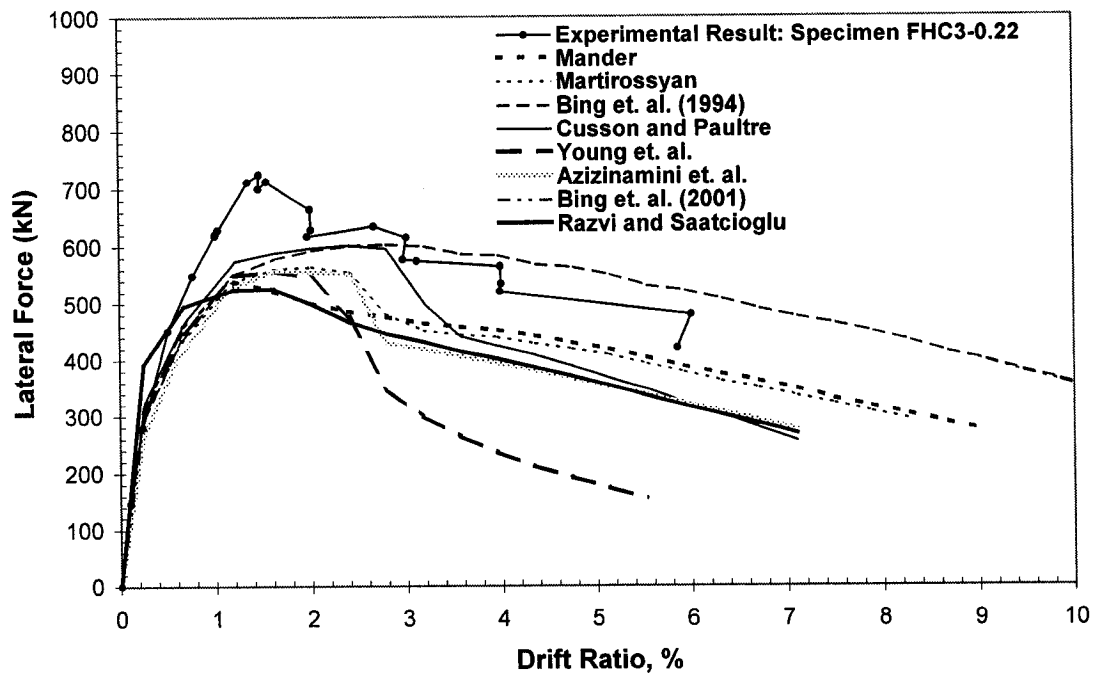
Fig. 5.20-Experimental and Analytical Lateral Force versus Displacement Relationships for Specimen FHC3-0.22

374
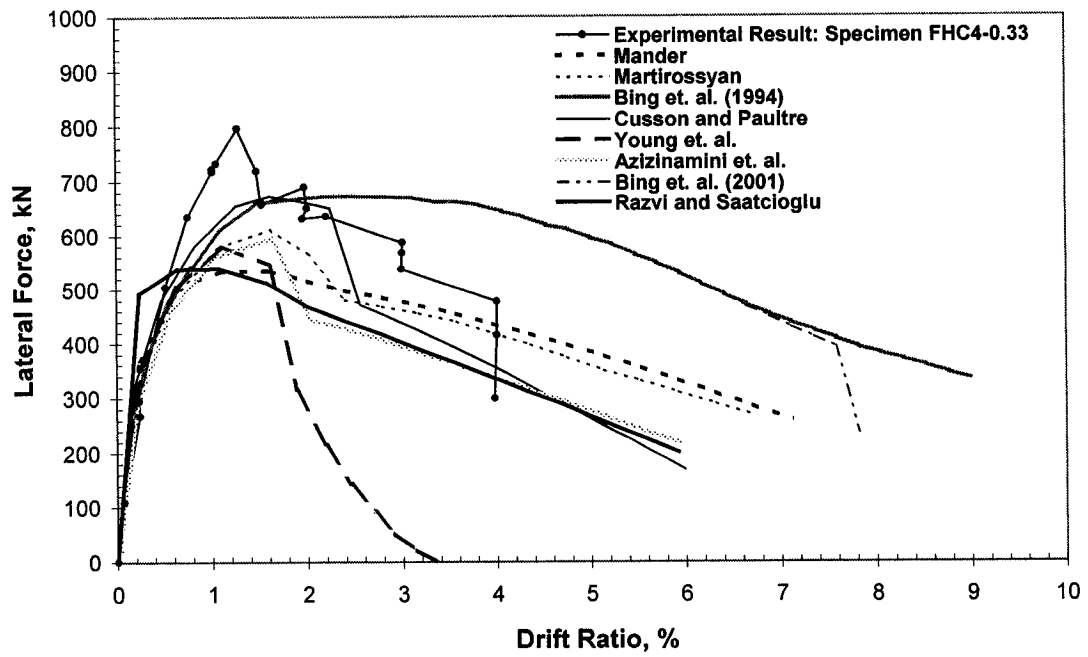
FIG. 5.21- Experimental and Analytical Lateral Force versus Displacement Relationships for Specimen FHC4-0.33

375
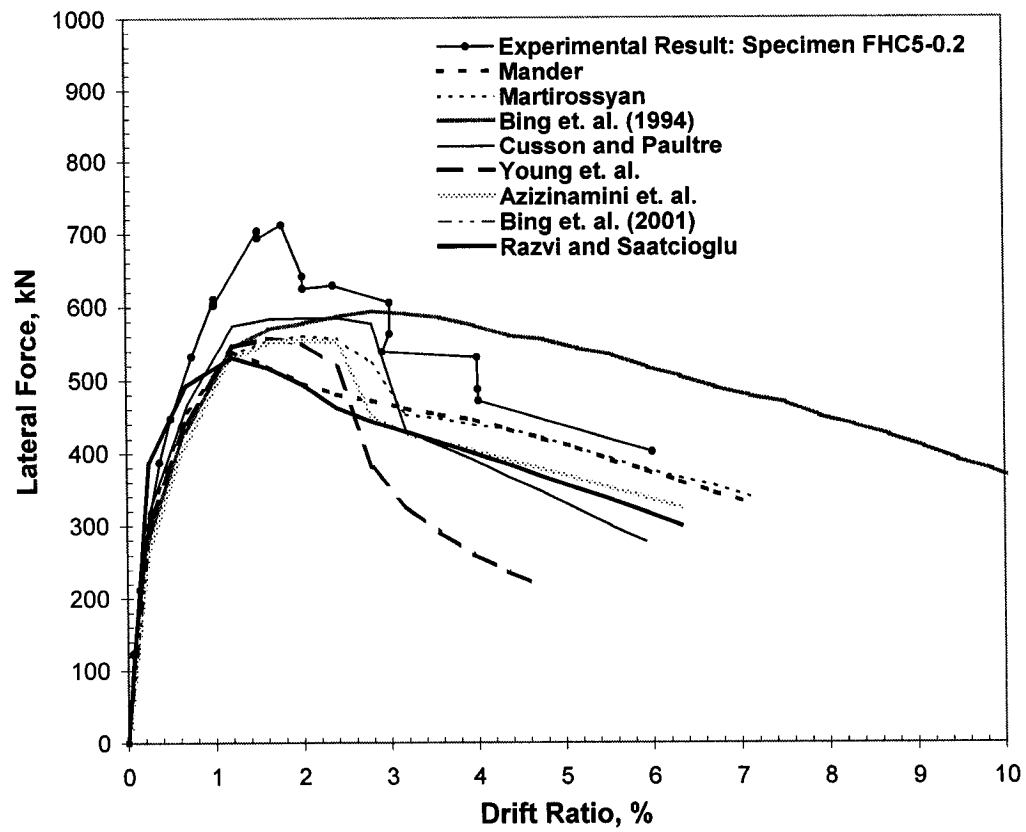
Fig. 5.22-Experimental and Analytical Lateral Force versus Displacement Relationships for Specimen FHC5-0.2

376
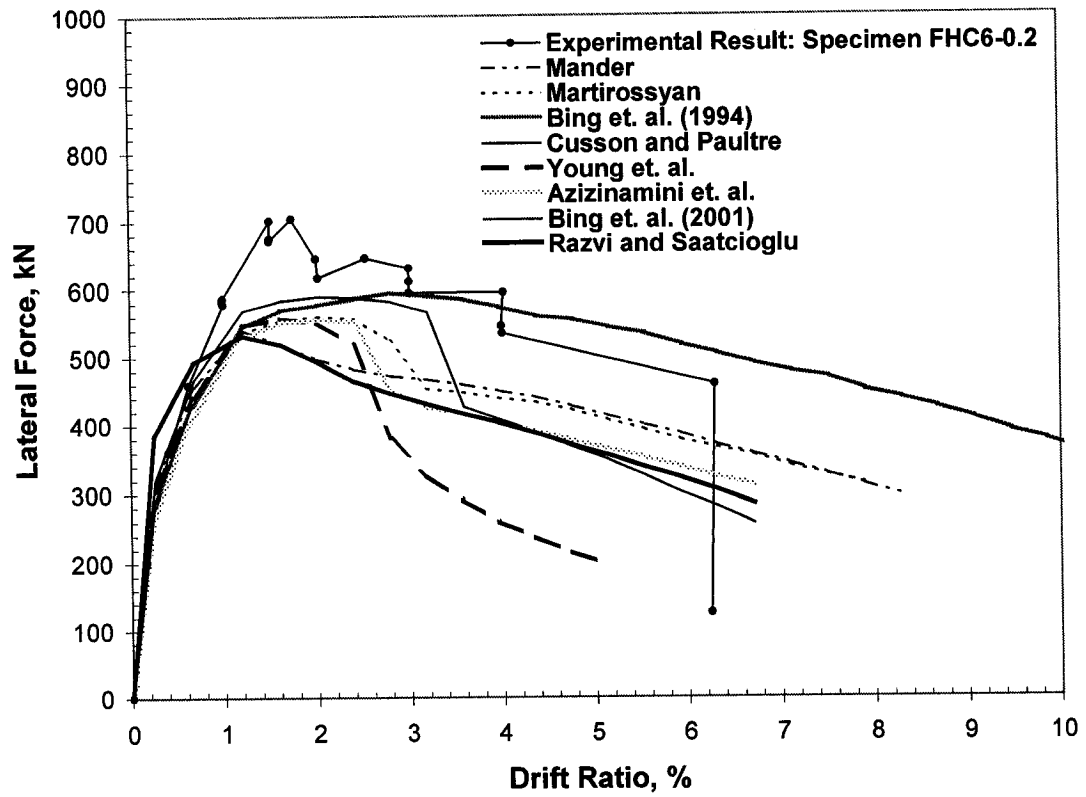
Fig. **5.23-** Experimental and Analytical Lateral Force versus Displacement Relationships for Specimen for specimen FHC6-0.2

377

CHAPTER 6

ANALYSIS BASED ON MICRO-APPROACH

6.1 INTRODUCTION

Since 1940's the method of finite element has been utilized in analysis and design of various structures. The finite element method, which discretize structures into a large number of finite elements, performs a computation to solve a large number of simultaneous equations in order to obtain the desired results such as the stress distribution throughout the model. The method takes the input parameters and combines the compatibility relationships in order to obtain the desired solutions. The large number of equations associated in solving the forces, stresses, and displacements of a typical model is solved with various algorithms which utilizes various iterative techniques which solves a large number of equations simultaneously. The behavior of each finite elements is often expressed in forms of shape functions which are often interpolation with interpolation functions. The theory and approaches are expressed in the form of matrixes to solve the combinations of equations.

378

From the early 1950's to the present, many advances have been made in the finite element method. Initially stiffness matrices for 2-dimensional truss, beam, triangular, and rectangular elements were formulated, and later flat, rectangular-plate bending-element stiffness matrix was developed by Melosh, et. al. in 1961 followed by a development of curved-shell bending-element stiffness matrix. The extension was made to 3-dimensional problems with the development of a tetrahedral stiffness matrix by Martin et. al. Up to 1960's, elastic small strain and displacement material behaviors were considered. Later, large strain and displacement deflection analysis and material non-linearities as well as buckling problems were considered. The initial application of finite element analysis was adopted to non-structural applications such as fluids and heat conduction through variational formulation. In 1976, large-displacement nonlinear dynamic behavior and improved numerical techniques were considered by Belytschko, et. al. The finite element approach to structural analysis still faces difficulties in the simulation of nonlinear materials, geometric non-linearities, and other complexities still being discovered.

The finite element method is used as a method of stress-analysis in relation to prescribed displacement at specific locations of the models presented. The models meet the basic requirements that the deformations of a continuous medium such as concrete is compatible.

379

In this research, the primary goal is to utilize available methods to predict the behavior of high-strength concrete square columns subjected to seismic loads. In an attempt to verify the experimental results in comparison to the results obtained by using the existing HSC confinement theories, a finite element modeling was performed using ADINA computer software. In numerical modeling, workable and reliable material model was used to realistically predict the behavior of HSC subjected to axisymmetric confinement subjected to lateral loading. Various commercially available Finite Element Analysis software allow large strain analysis of reinforced concrete elements. Some of the software currently available are introduced.

6.2 FINITE ELEMENT MODELS AND AVAILABLE SOFTWARE

Various software are now available such as ABAQUS, ANACAP, SAP2000, ANSYS, IFEM, PENTAGON-3D, and COSMOS/M. Among them is ADINA (Accelerated Dynamic Non-linear Analysis) was accessible for the modeling of the specimens. A method of Finite Element Analysis has been chosen as a tool to verify the experimental and analytical results in order to observe detailed micro-mechanical behavior of the column model during the stages of displacement-based loading. Among various types of Finite Element software available,

380

Accelerated Dynamic Non-linear Analysis was utilized to model and simulate the reinforced column behavior. Displacement-based analysis was used in order to efficiently obtain the stress distribution throughout the finite element models.

ABAQUS provides static and dynamic stress and displacement analysis and buckling load predictions for one of its capabilities include control of localized unstable behavior of nonlinear materials for postcollapse or postbuckling cases. The programs copes with the problems of non-converging nonlinear problems by allowing user to define the time step. The program uses fully implicit integration to ensure stability for solution stability for largest strain increments involvingcomplex material behavior

Among available structural analysis programs developed, ANACAP is developed for static or dynamic response and for failure analysis of concrete structures. Its implicit technology is formulated for non-linear responses of concrete cracking, creep, aging, and crushing. Reinforcement yield and bond failure are also considered. Smeared-crack model for general 3-dimensional stress states and rebar slip models for member ductility demand evaluation are one of its many features.

SAP2000 provides modeling of a wide range of structures from bridges to buildings. It allows static and dynamic analysis of 3-dimensional models with the use of truss and shell to non-linear link elements. It allows static pushover analysis with non-linear hinge defined in frame elements. One of its features include 3-dimensional performance-based design of concrete structures by Nonlinear pushover analysis.

ADINA, which is used for the analysis of the specimens, provides a comprehensive finite element linear or non-linear analysis of solids and fluids. Although, the program is not specifically formulated for concrete analysis, it is generally applicable for solids, trusses, beams, pipes, plates, shells, and gaps. Material models for various materials are available. However, the concrete model implemented in currently available program assume only small strains and displacement. Therefore, the analysis performed so far does not provide complete results for large displacements of the specimens. Therefore, the results were obtained up to small displacement strain or until convergence is can be reached.

ANSYS also performs structural simulation of linear or non-linear materials subjected to static or dynamic loads. The program offers complete frictional support and buckling analysis. Its comprehensive features allow for the analysis of complicated assemblies.

6.3 MODELING APPROACH

The appropriate models have been sought to predict the behavior of the reinforced concrete column. The main objective was to use finite element methods to obtain a solution rather than to pursue research on finite element methods.

One of the alternatives of modeling was to perform a very simplified model that consist of prescribed spring stiffness at the plastic hinge area, simple beam elements, and truss rebar elements along the length of the column. However, this type of approach may not allow a three-dimensional observation of stress distribution during the loading process as it occurs during the increments of loading.

Three-dimensional FEM analysis was performed to understand the column behavior. A displacement-based method was used by idealizing the specimen as an assemblage of truss, beam, pipe, and concrete elements interconnected at joints. Linear analysis was performed followed by nonlinear analysis, treating nonlinear analysis as an extension of linear analysis. Once linear analysis was successfully completed, it was verified that the finite element mesh is compatible. The same model was assumed to be displacement-compatible for nonlinear

383

analysis. Various nonlinear formulations were then used to obtain results as trial runs.

The continuum of concrete and all steel reinforcements were first divided into finite elements. The mesh was generated using the preprocessor. The experimentally determined material properties were used. The elements were geometrically assembled to construct a complete model. The loads, in this case prescribed displacements and pressure were applied at the specific lines and surfaces of the elements corresponding to the locations of the experimental load application. The boundary conditions were set by fixing degrees of freedom at specific surfaces and nodal points. Material models were chosen by defining the element types and by prescribing appropriate types of finite elements. The program was then executed to solve simultaneous linear algebraic equations to perform stress analysis. The element strains, displacements, and stress were calculated and displayed in a graphical from using the postprocessor. The combination of different types of elements, shapes, and material properties required defining the appropriate tolerances, number of iterations, kinematics of large versus small displacements and strains, time functions, time steps, type of equation solver, and mesh densities. Due to the complicated geometry of the full-column model, with its reinforcements displaced in all directions and also in

384

interaction with the concrete medium, the full nonlinear analysis of large displacement loading was a challenging task.

Two types of models analyzed are a column section model and a full-column model. The geometry of the section models is equivalent to a quarter of column section due to symmetry. Its thickness is equal to the spacing of transverse reinforcements in the plastic hinge area with the transverse reinforcements placed at middle of the model thickness. The full-column model has its stub fixed in all directions and is geometrically equivalent to specimens FHC1-0.2 and FHC2-0.34 with experimental constant axial loading and monotonic lateral displacement loading. The analysis consists of three groups of models each of which uses various types of elements and parameters to improve the solution obtained and to observe the effect of using different values of material constants of concrete and steel and modeling approaches.

For all models of group one, the transverse reinforcements were modeled using 2-node truss elements. The longitudinal reinforcements were modeled with pipe elements for the quarter column section models and modeled with Hermitian beam-elements with a circular cross sections equal to the area of experimental values for full-column models. All concrete was modeled using 3-D isotropic concrete element. A elasto-plastic bilinear model was assumed for all steel reinforcements. The Kupfer concrete model already implemented in the program

385

was used to simulate the concrete behavior. All geometric dimensions including the locations of the reinforcements were modeled to match those of the specimens as closely as possible. A series of column sections models were analyzed first to observe the behavior during the initial axial loading. Second, the full-column model was analyzed. The intent was to observe the variation of the stress distribution during various stages of loading and to provide understanding of the mechanism which affect the performance of the columns such as the locations of maximum demand in steel stress. All reinforcements were assumed to be perfectly bonded to the concrete elements for simplicity. All models consist of two different versions, those with an assumption that all materials are perfectly elastic, those assuming that all steel reinforcmenets are elasto-plastic combined with all concrete volumes. All elasto-plastic materials were assumed to behave bilinearly with strain-hardening modulus of reinforcements equal to zero.

For all models of group one, the experimental material compressive strength and modulus of elasticity of concrete, $E_c = 57,000\sqrt{f_c'}\,(^{lb}/_{in^2})$ or $4,730\sqrt{f_c'}\,(MPa)$, are used for the concrete with a constant poisson ratio of 0.15. True properties based on material testing are used for all reinforcements with a Poisson ratio of 0.3. All experimentally determined steel yield stress was used with an assumed ultimate plastic strain of 0.03. The experimentally determined maximum concrete

386

stress was assumed to occur at a strain of 0.003 and ultimate concrete stress after failure was assumed as 0.005. For 3-D concrete elements, 8-Node elements were utilized. Various meshing techniques were attempted, but length-based meshing for 8-Node elements for concrete and 2-Node truss and pipe elements were implemented in the models.

The concrete model which was used as 3-D solid elements assumes tensile failure at small principal tensile stress, allows crushing failure at high compression, and assumes a total failure at an ultimate strain. Its nonlinear stress-strain relation allow for the weakening of the material under increasing compressive stresses and models a post-cracking and crushing behavior.

The friction between the concrete elements and all reinforcements were considered for model groups two and three as it will be discussed in Section 6.6 and 6.7.

Concrete Model Uniaxial Stress-Strain Relationship

The general multiaxial stress-strain relations are derived from a uniaxial stress-strain relation as follows:

387

$${}^t\widetilde{\sigma} = \widetilde{E}_0 \, {}^t\widetilde{e}$$

For ${}^t\widetilde{e} \geq 0$, the material is in tension, and the stress-strain relationship is linear

until tensile failure is reached at the stress $\widetilde{\sigma}_t$.

For ${}^t\widetilde{e} \leq 0$,

$$\frac{{}^t\widetilde{\sigma}}{\widetilde{\sigma}_c} = \frac{\left(\dfrac{\widetilde{E}_0}{\widetilde{E}_s}\right)\left(\dfrac{{}^t\widetilde{e}}{\widetilde{e}_c}\right)}{1 + A\left(\dfrac{{}^t\widetilde{e}}{\widetilde{e}_c}\right) + B\left(\dfrac{{}^t\widetilde{e}}{\widetilde{e}_c}\right)^2 + C\left(\dfrac{{}^t\widetilde{e}}{\widetilde{e}_c}\right)^3} \quad \text{and therefore,}$$

$$ {}^t\widetilde{E} = \frac{\widetilde{E}_0\left[1 - B\left(\dfrac{{}^t\widetilde{e}}{\widetilde{e}_c}\right)^2 - 2C\left(\dfrac{{}^t\widetilde{e}}{\widetilde{e}_c}\right)^3\right]}{\left[1 + A\left(\dfrac{{}^t\widetilde{e}}{\widetilde{e}_c}\right) + B\left(\dfrac{{}^t\widetilde{e}}{\widetilde{e}_c}\right)^2 + C\left(\dfrac{{}^t\widetilde{e}}{\widetilde{e}_c}\right)^3\right]^2}$$

$$A = \frac{\left[\dfrac{\widetilde{E}_0}{E_u} + \left(p^3 - 2p^2\right)\dfrac{\widetilde{E}_0}{E_s} - \left(2p^3 - 3p^2 + 1\right)\right]}{\left[\left(p^2 - 2p + 1\right)p\right]}$$

$$B = \left[\left(2\frac{\widetilde{E}_0}{\widetilde{E}_s} - 3\right) - 2A\right]$$

$$C = \left[\left(2 - \frac{\widetilde{E}_0}{\widetilde{E}_s}\right) + A\right]$$

where,

388

$'\tilde{\sigma}$ = uniaxial stress

$\tilde{E}_0$ = uniaxial initial tangent modulus (all uniaxial variables are designated with ~ symbol over them)

$'\tilde{e}$ = uniaxial strain

$\tilde{\sigma}_c$ = maximum uniaxial compressive stress ($\tilde{\sigma}_c \prec 0$)

$\tilde{e}_c$ = uniaxial strain corresponding to $\tilde{\sigma}_c$ ($\tilde{e}_c \prec 0$)

$\tilde{E}_s$ = uniaxial secant modulus corresponding to uniaxial maximum stress,

$$\tilde{E}_s = \frac{\tilde{\sigma}_c}{\tilde{e}_c} .$$

$\tilde{e}_u$ = ultimate uniaxial compressive strain ($\tilde{e}_u \prec 0$)

$\tilde{\sigma}_u$ = ultimate uniaxial compressive stress ($'\tilde{\sigma} \prec 0$)

$$p = \frac{\tilde{e}_u}{\tilde{e}_c}$$

$$\tilde{E}_u = \frac{\tilde{\sigma}_u}{\tilde{e}_u}$$

The relationship assumes monotonic loading conditions, where for unloading conditions, the initial Young's modulus $\tilde{E}_0$ is used. Beyond $\tilde{e}_u$ in compression, it is assumed that stresses are linearly released to zero, using the modulus

$$\tilde{E}_u = \frac{\tilde{\sigma}_u - \tilde{\sigma}_c}{\tilde{e}_u - \tilde{e}_c} .$$

389

For multiaxial stress conditions, the stress-strain relations for material loading conditions are calculated by evaluation of stiffness matrix at time t. For stress increment from time t to $t + \Delta t$, the following relationship is used:

$$\sigma = \hat{C}e$$

where the stress-strain matrix $\hat{C}$ is defined as:

$$C = \frac{1}{(1+v)(1-2v)}\begin{bmatrix} (1-v)^t\widetilde{E}_{p1} & v^t E_{12} & v^t E_{13} & 0 & 0 & 0 \\ & (1-v)^t E_{p2} & v^t E_{23} & 0 & 0 & 0 \\ & & (1-v)^t\widetilde{E}_{p3} & 0 & 0 & 0 \\ & & & 0.5(1-2v)^t E_{12} & 0 & 0 \\ & sym & & & 0.5(1-2v)^t E_{13} & 0 \\ & & & & & 0.5(1-2v)^t E_{23} \end{bmatrix}$$

v is the constant Poisson's ratio and the $^t E_{ij}$ with $i \neq j$ are expressed as:

$$^t E_{ij} = \frac{\left|^t\sigma_{pi}\right|^t\widetilde{E}_{pi} + \left|^t\sigma_{pj}\right|^t\widetilde{E}_{pj}}{\left|^t\sigma_{pi}\right| + \left|^t\sigma_{pj}\right|}$$

In loading conditions, the principal stresses $^t\sigma_{pi}$ with $^t\sigma_{p1} \geq\, ^t\sigma_{p2} \geq\, ^t\sigma_{p3}$ are evaluated. For each principal stress, a tangent Young's modulus $^t\widetilde{E}_{pi}$ corresponding to $^t e_{pi}$ is evaluated using expressions for $^t\widetilde{\sigma}$ introduced earlier, where variables for multiaxial stress conditions, $\widetilde{\sigma}'_c$, $\widetilde{\sigma}'_u$, $\widetilde{e}'_c$, and $\widetilde{e}'_u$ are

390

used. These parameters are expressions for uniaxial stress law under multiaxial stress conditions expressed as:

$$\tilde{\sigma}_u^{'} = \gamma_1 \tilde{\sigma}_u$$

$$\tilde{e}_c^{'} = \left(C_1 \gamma^2_1 + C_2 \gamma_1\right) \tilde{e}_c$$

$$\tilde{e}_u^{'} = \left(C_1 \gamma^2_1 + C_2 \gamma_1\right) \tilde{e}_u$$

where C_1 and C_2 are constants normally 1.4 and –0.4, respectively.

The tensile failures are assumed to occur when the tensile stress in principal stress direction exceeds the tensile failure stress. At failure, the normal and shear stiffnesses and stresses across the plane of failure is reduced and the plane stress conditions are assumed. Thus, the stiffness and shear reduction factors are implemented for the tensile stress calculation.

The behavior after tensile failure is modeled by establishing material stress-strain relationships corresponding to the directions along and perpendicular to the plane of failure rather than using the principal stresses and its directions as it was done for the unfailed material. The subsequent failure planes are assumed to form perpendicular to the direction of the first failure plane whenever a normal stress along the original failure plane has reached its tensile failure stress.

The behavior after compression failure is modeled by an assumption that the material softens in all directions and in multiaxial stress conditions, the material is

391

assumed to be under isotropic conditions. The Young's modulus is assumed to be very small and positive in stiffness calculations. This Young's modulus for strain increment e_{p3} is calculated using the uniaxial stress-strain relationship introduced earlier and expressed as:

$$^tE = \frac{\left[\tilde{\sigma}_{^te_{p3}+e_{p3}} - \tilde{\sigma}_{^te_{p3}} \right]}{e_{p3}}$$

where $^te_{p3}$ and e_{p3} are the strain component at time t measured in direction of the principal stress $^t\sigma_{p3}$. The stress calculation $\sigma = \hat{C}e$ is performed where the matrix $\hat{C}$ corresponds to isotropic conditions with Young's modulus ^tE. When $^te_{p3}$ becomes equal to or less than $\tilde{e}'_u$, the stress are linearly released to zero.

The material model used for the steel reinforcement assumes an idealized isotropic elasto-plastic bilinear behavior with experimental yield stress and ultimate plastic strain specified. The 3-dimensional concrete element model provided by ADINA program is formulated only for small strains although it may be used for both small and large displacements. The model simulates tensile failure at low principal tensile stress, compression crushing failure at high compression, and strain softening at ultimate strain when the concrete completely fails. Since concrete is a very complex material, the model does not necessarily match the actual characteristic of high-strength concrete. In fact, the same model

392

can also be used to simulate the behavior of rock materials. The concrete model offers nonlinear stress-strain relation in consideration for weakening of the material as compressive stresses are increased. The three-dimensional tensile failure envelopes, biaxial concrete compressive failure envelope, triaxial compressive failure envelope, and uniaxial havior under multiaxial stress conditions are defined to model the stress-strain relationship based on the principle of principal stresses.

Column Section Models

In an attempt to simulate the behavior during the initial application of axial loading, a quarter section of specimen FHC1-0.2 100mm (4 inch) in thickness was first modeled. The transverse hoop and ties were placed in the center of its thickness assuming a perfect bond between them and concrete elements.

All material properties of the model matched those of the experiment including the diameters of the transverse hoops. One half of the experimental values were used for the cross-sectional area of the transverse ties that are placed along the two outside edges of the column section models. The boundary conditions of the column section models were set such that the vertical face of the model with transverse ties embedded are fixed in either Y or Z directions to fix displacements

393

in the directions perpendicular to it, where the axial displacement was exerted onto the model in X direction. The axial load was applied until the concrete deformation reached a displacement of 0.254mm (0.01 inch) equivalent to a strain of 0.0025.

Once first crushing or collapse occurred, the program stopped computation. However, the program surpassed the displacement to reach the axial load level applied during the experiment. For the full-column models, the program also stopped computation upon the first crushing of the concrete. The use of very small time steps did not aid computation to achieve the lateral displacement that was induced to the column model. The program seems to have a limited capability to model a concrete crushing in interaction with the reinforcements during large strain applications.

Two versions of the 100 mm (4 inch) thick column section models are coarse meshed and fine meshed. For the coarse mesh model which consist of 99 nodes, the following number of elements are used:

Element group 1: 50 3D solid elements.

Element group 2: 15 general 3D truss elements.

Element group 3: 6 beam-type pipe elements.

394

71 elements total.

The fine mesh model which consist of 575 nodes, the following number of elements are used:

Element group 1: 400 3D solid elements.

Element group 2: 30 general 3D truss elements.

Element group 3: 12 beam-type pipe elements.

442 elements total.
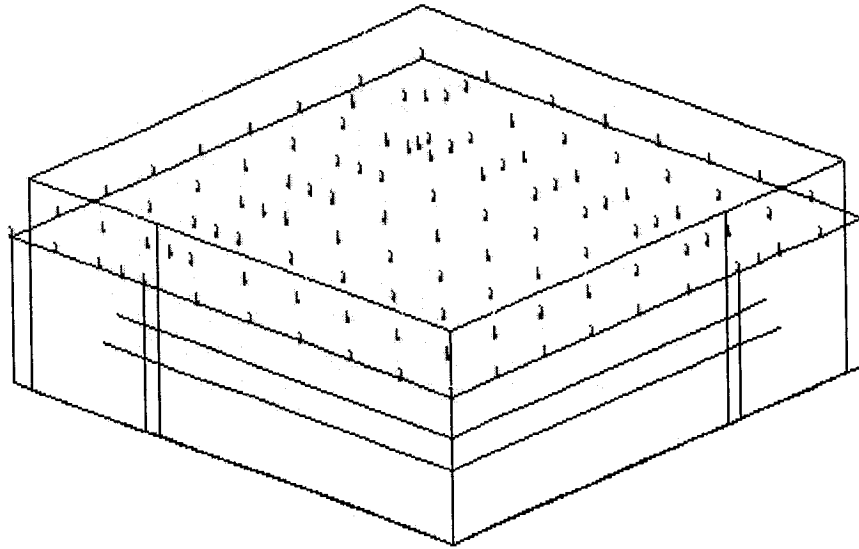
Fig. 6.1-Deformed Shaped in Comparison to Original Shape of Section Models

396
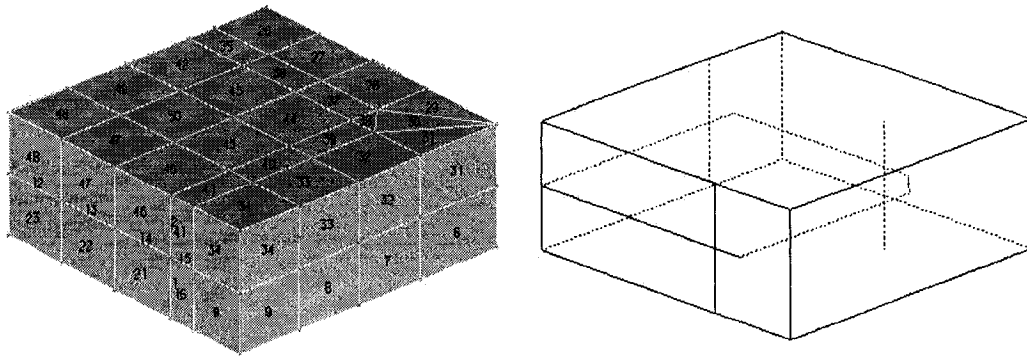
Fig. 6.2-Finite Elements and Reinforcement Location of Section Models
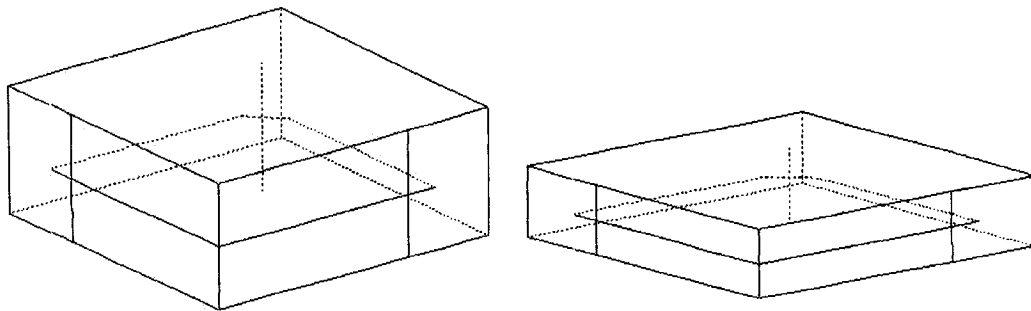
Fig. 6.3-Process of Deformation of Section Models

397

The full-column models consist of 665 nodes with a total of 716 elements divided into 4 element groups as following:

Element group 1: 416 3D solid elements.

Element group 2: 156 general 3D truss elements.

Element group 3: 72 Hermitian beam elements.

Element group 4: 72 Hermitian beam elements.

The top of column stub was fixed in all directions to induce forces in the plastic hinge area.

398
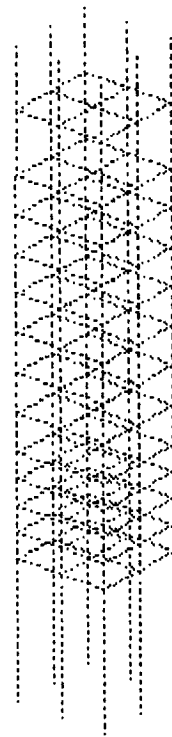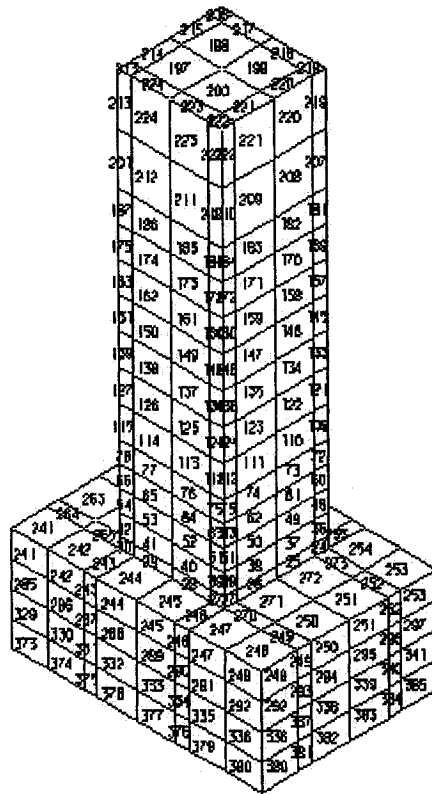
Fig. 6.4-Volume and Steel Elements of Full-Column Model

399
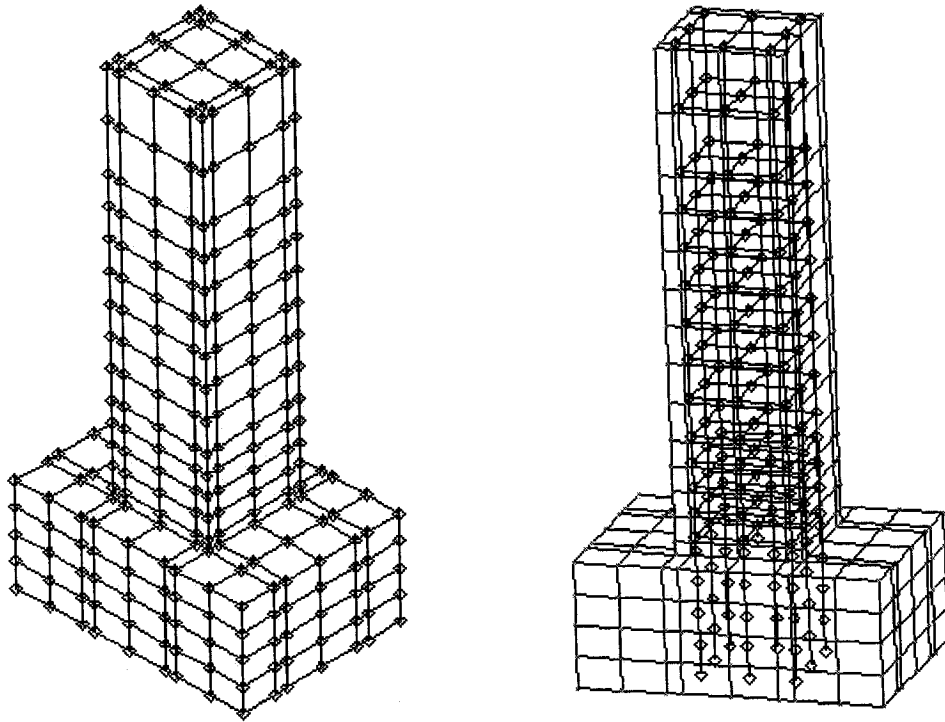
Fig. 6.5-Node Depiction of Full-Column Model

400

Summary of Parameters Used for Finite Element Modeling of Column Section Models:

1.   Quarter Section Model (10" x 10")

2.   Concrete strengths of 62.1 MPa (9.0 ksi), 64.1 MPa (9.3 ksi).

3.   Concrete and Steel Poisson Ratios

4.   FE mesh used - 8 nodes per element

3 x 3 quadrature was used for 8-node elements.

5.   Longitudinal reinforcement was modeled using two-node pipe elements

6.   Tie reinforcement was modeled using 2-node truss elements.

7.   Elasto-plastic stress-strain relationship was used for the steel elements with perfect bond being assumed between the steel and concrete.

8.   Experimental yield stress and initial modulus of elasticity of the reinforcing bars were used.

Summary of Parameters Used for Finite Element Modeling of Full-Column Models:

1.   Full Column Model 508 x 508 mm (20" x 20")

2.   Concrete strengths of 62.1 MPa (9.0 ksi), 64.1 MPa (9.3 ksi).

3.   Experimental Axial Load Levels

401

4. Concrete and Steel Poisson Ratio

5. FE mesh used - 8 nodes per element

3 x 3 quadrature was used for 8-node elements.

6. Longitudinal reinforcement was modeled using two-node Hermitian beam elements

7. Tie reinforcement was modeled using 2-node truss elements.

8. Elasto-plastic stress-strain relationship was used for the steel elements with perfect bond being assumed between the steel and concrete.

9. Experimental yield stress, initial and strain-hardening modulus of elasticity of the reinforcing bars were used.

402
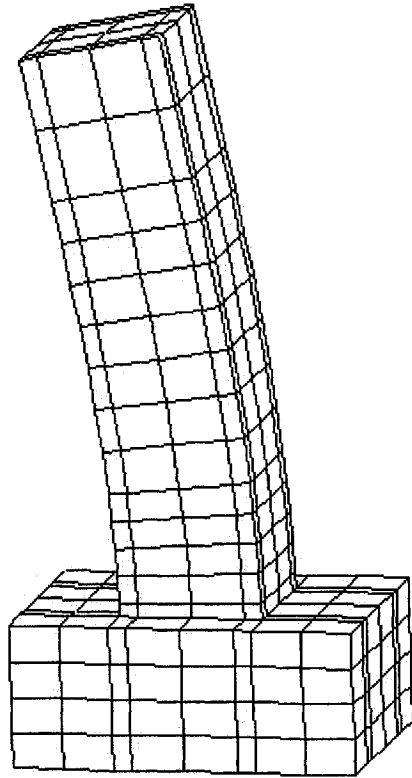
Fig. 6.6-Deformed Shape of Full-Column Model

6.4 ANALYSIS APPROACH

Although an effort has been made to model the behavior of concrete and steel, it is expected that the model cannot predict the actual behavior high strength concrete due to its complex nature and variations. Further, the solutions of

403

concrete problems are known to be difficult due to sudden nonlinear behaviors during cracking and crushing of the material. When combined with steel elements, small increment of loading can cause substantial stress redistributions in the concrete material. Due to this consideration, small incremental time steps were used to avoid difficulty in equilibrium iteration convergence.

Large displacement / Small strain analysis was performed using Full Newton method with 15 iterations for each time step and with translation tolerance of 0.01 for the column section models. For the full-column models, 900 iterations for each time step and translation tolerance of 0.1 were used. For all models, the number of time steps is limited to 50 at increments of 0.2.

Monotonic static loading was assumed for all displacement loading. Fifty load steps at increments of 0.2 was set with maximum displacement or until the solutions can be obtained successfully.

In model group one, FEM models does not consider slippage as it occurs in the experiments. Buckling or rupturing of the transverse reinforcements is not simulated, although other methods using other commericially available FEM software may consider such failure criterias. In the models used, the longitudinal reinforcements were modeled using 2-node 3-D solid pipe, and transverse reinforcements were modeled using 2-node 3-D solid truss elements. In all cases,

404

8-node elements were used for 3-D solid modeling of concrete with specified tangent modulus, compressive strength, tensile strengths, mass density, and ultimate compressive strength into consideration.

The main purpose of the FEM analysis was to simulate the loading conditions to evaluate the general stress distribution in various parts of the specimens. The detailed failure patterns such as steel ruptures and longitudinal steel buckling were not considered as a part of this analysis. However, from the observations of the stress distribution around the reinforcements as the loads are applied and as the specimens were laterally displaced on the full-column FEM model, the column stiffness showed overall consistency with the ACI calculation of column stiffness, EI. Stress-distributions at column sections and throughout the entire column were observed until convergence was achieved to reach the prescribed axial and lateral displacements for each model. Large stress and small strain were assumed with a maximum of 15 iterations executed per time step.

405
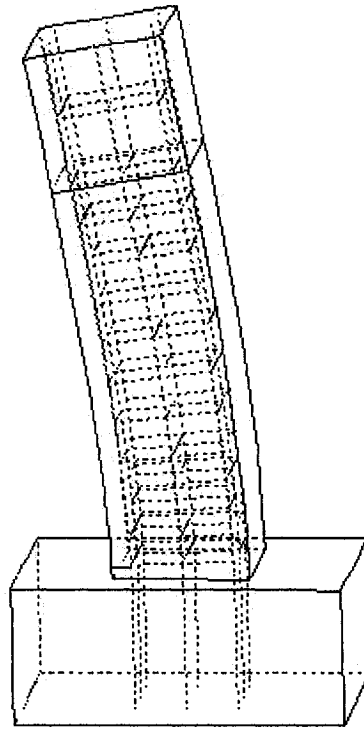
Fig. 6.7-Deformed Shape of Reinforcements

406

Theoretical Considerations in Analysis Approach

Although ADINA program offers its own constitutive relation of concrete, it was not modified for performing large strain analysis. In the past, such constitutive models of concrete were modified by researchers to obtain the desired numerical results on reinforced concrete elements subjected to large displacement and strain.

Xie, et.al. performed a parametric study of high-strength concrete tied columns in 1997.

The study is based on numerical analysis of high-strength concrete tied columns subjected to eccentric compressive loading for rectangular tied columns with concrete strengths of 37.5 to 75 Mpa (5.47 to 10.9 ksi). This numerical investigation considered the configuration, size, and yield strength of ties, concrete strength, depth of cover, and amount of longitudinal reinforcement. The strength and ductility of the tied columns were investigated in relation to the design code sections. The numerical analysis of column models applied eccentric compressive loading using an elasto-plastic three-dimensional finite element model. Three-dimensional finite element nonlinear analysis was performed using a modified form of concrete constitutive model of mathematical formulation proposed by Pramono and Willam, 1989 which is a fracture energy-based plasticity formulation of plain concrete. The failure criterion originally

407

proposed by Leon in 1936 for the shear strength of concrete under combined tension-compression was used to describe the maximum strength surface in the formulation.

Xie et. al., in 1994, proposed a constitutive model of concrete assuming based on the fact that the isotropic failure criterion is a function of the major and minor principal stresses σ_1 and σ_3 and the compressive and tensile concrete strengths. This model implies that the material behaves elastically as long as the stress state lies within an initial yield surface. It has been found that when loading progresses beyond the initial yield surface, plastic flow occurs and the yield surface hardens isotropically up to a failure surface. Until yield surface hardens, it is assumed that the plastic strain rate is governed by a plastic potential different from the yield function. The hardening phase is not associated with the yielding portion and therefore, the resulting constitutive matrix is not symmetric. As plastic flow continues beyond that necessary to reach the failure surface, the material behavior becomes isotropic softening. The strength surface degrades to a residual surface. The plastic flow is then governed by the fracture energy of concrete in tension. Xie et al. extended the range of the model from two to three dimensions, and calibrated the material parameters for high-strength concrete based on the material tests conducted by the authors.

408

Xie et. al., in 1995, customized the existing constituvie model for high-strength concretes containing silica fume using modified Pramono and Willam model. The finite element analysis using the modified formulation successfully captured the load-deformation response, along with important information such as the strain-softening and spalling of the concrete cover, the formation of a triaxial stress state in the concrete in the column core, and the yielding of ties. A number of material parameters defining the concrete behavior were obtained based on the material testing of high-strength concrete including uniaxial compression, triaxial compression, split cylinder, and notched beam tests.

The author used concrete model consisting of 20-node three-dimensional quadratic solid elements with 27 integration points per element. One layer of elements is used for the cover to distinguish from core elements. The reinforcement bars were embedded in concrete elements with numerical integration of the contribution of reinforcement to the element stiffness matrix carried out along the bars only. Complete strain compatibility was assumed between the embedded bars and the concrete medium. Both the longitudinal and transverse reinforcement were assumed to be elastic-perfectly plastic.

With constant axial load applied, the lateral loading was applied monotonically until the applied moment M dropped to zero. The solution strategy was a

displacement control strategy employing a modified Newton-Raphson iteration method.

Argyris et. al., 1973 introduced a nonlinear two-dimensional incremental constitutive law according to Prandtl-Reuss theory of plasticity. This smeared cracking model assumes that concrete is cracked in one direction. The normal stress perpendicular to the crack direction is assumed to drop to zero after cracking, but a small value is retained for the shear modulus G nonlinearly dependent on the deformation perpendicular to the crack direction. When concrete element is cracked in two directions, the same smeared cracking model is also used as previously, assuming the second crack is perpendicular to the first one. For the crushed concrete elements, it is assumed that the crushed element completely loses its strength in all directions and that its stiffness matrix drops to zero. Ideal elasto-plastic constitutive law was used for the steel. The linkage elements which represent bond and nonlinear relation between bond stress and relative slip of steel to concrete (elongation of spring element) is introduced. When the relative slip exceeds a certain value, the stiffness of the linkage element drops to zero.

Kupfer et. al., 1969 introduced two-dimensional cracking and crushing criterion of principal stress for concrete based on simplified failure envelope for concrete

410

under biaxial stresses. If a pair of principal stresses σ_1 and σ_2 lie outside the failure envelope in a section, the concrete element is assumed to crush or crack correspondingly perpendicular to the principal tensile stress. The finite element analysis using this criteria used incremental loading technique. During load increment, the additional stresses and strains of all the elements are determined using the stiffness matrixes of the previous load increment. These stresses and strains are added to those of previous load increments. If no element changes its state, the next load increment is applied. Otherwise the solution for the present load increment is repeated by properly updating the stiffness matrixes of the elements that have changed their state. The failure is assumed to occur until computation stops whenever the mathematical procedure becomes unstable.

The use of ADINA for the specimens is intended only to verify the experimental results and to observe the stress distributions obtained from the analysis using idealized models.

Three versions of the models are used as following:

1. All materials, reinforcements and concrete, are perfectly elastic.

2. All reinforcements are elasto-plastic (bilinear) and concrete model implemented in ADINA is used.

3. All materials are assumed elasto-plastic (bilinear) including concrete.

411

The following plots show concrete and reinforcement stress-strain relationship assumed in the analysis of the models. For each model, the experimental parameters were used for concrete volumes and for the reinforcements.

Uniaxial stress-strain curves
from material property data
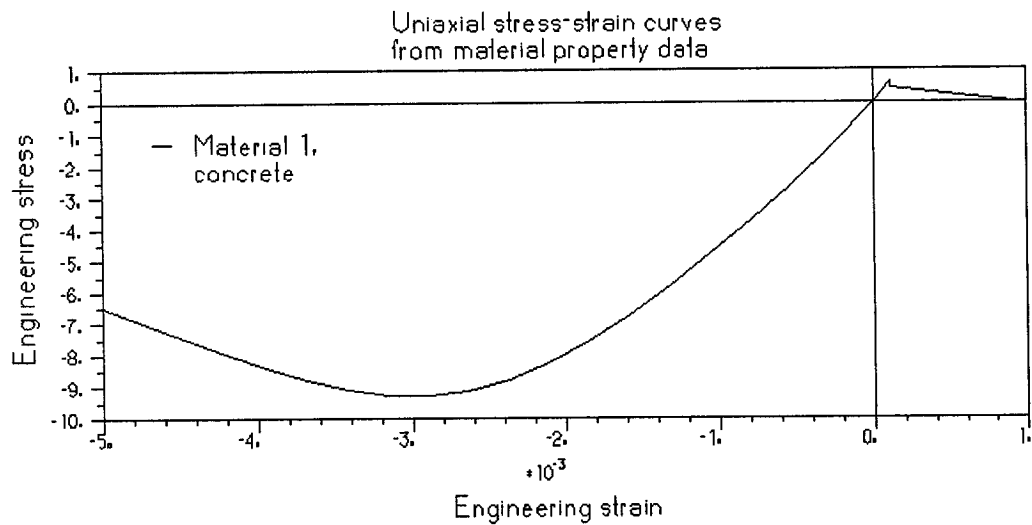
Fig. 6.8-Concrete Stress-Strain Relationship (Values shown in ksi)

412
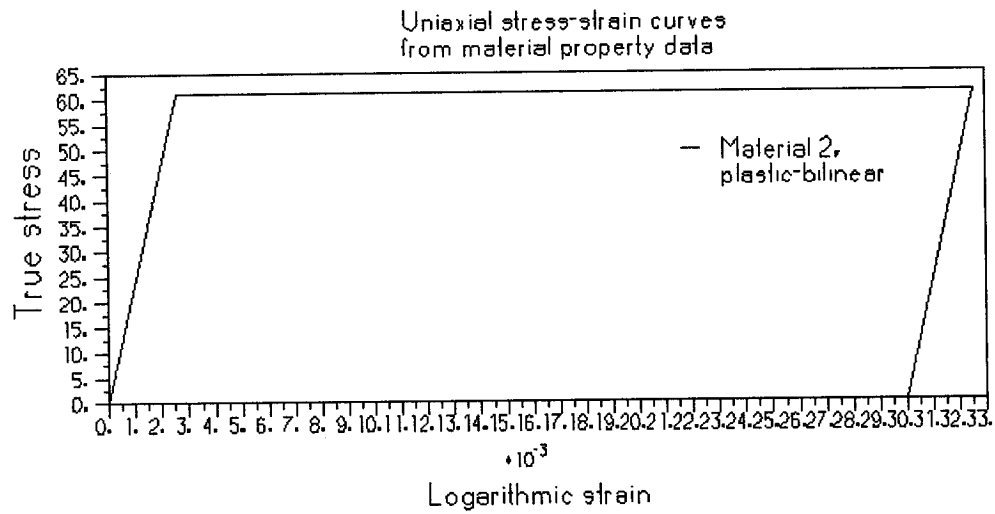
Fig. 6.9-Reinforcement Stress-Strain Relationship (Values shown in ksi)

6.5 RESULTS AND DISCUSSIONS OF MODEL GROUP ONE

Purposes

The purpose of finite element numerical approach is to simulate the behavior of reinforced concrete column and to confirm the validity of the experimental results. An axial displacement was applied to the finite element models of column sections, and resulting axial stress-strain relationships were observed. It

413

was attempted to show that micro-approach to column analysis allows observation of detailed stress distributions of both concrete and reinforcements throughout all stages of loading. The stress contours of the finite element analysis results helps to locate the areas of highly concentrated stress levels and critical regions in the plastic hinge areas. A finite element analysis of full-column models closely depicts the actual behavior of the specimens. A numerical analysis does not necessarily depict the conditions of actual loading conditions. However, it has been attempted to model the specimens as realistically as possible to produce good results.

For column section models that were subjected to axial displacements produced good results. Due to the convergence problems of non-linear analysis, it was a difficult task to analyze finite element models of 3-dimensional concrete elements with its reinforcements perfectly bonded to concrete elements. Upon the first crushing of the concrete, the numerical analysis stops without convergence. Therefore, for non-linear analysis, results have been obtained for a axial displacement of only 0.254 mm (0.01 in). However, the elastic analysis of the column sections with both concrete and reinforcements modeled as perfectly elastic materials provided successful results without limitations in maximum axial displacement.

414

Similarly, the results of full-column models simulating the experimental loading indicate good correlations with the experimental results. As it was for the column section models, due to the convergence problems of non-linear analysis, it was a difficult task to analyze finite element models of 3-dimensional concrete elements with its reinforcements perfectly bonded to concrete elements. Upon the first crushing of the concrete, the numerical analysis stops without convergence. Therefore, for non-linear analysis of the specimens, the results have been obtained for a lateral displacement of only 7.62 mm (0.30 in). However, the elastic analysis of the specimens with both concrete and reinforcements modeled as perfectly elastic materials provided successful results up to a maximum lateral displacement of as much as 203 mm (8.0) inches without convergence problems.

Column Section Model

A quarter of 508 x 508 mm (20 x 20 in.) column section 101.6mm (4 inch) in thickness was modeled for specimen FHC1-0.2, with hoops, ties, and longitudinal reinforcements placed in the center of the 101.6mm (4 inch) thickness was subjected to axial displacement. The 101.6mm (4 inch) is the transverse reinforcement spacing of the plastic hinge region. As a result, the stress distributions and axial load vs. axial displacement relationships were

415

obtained. The same model for specimen FHC2-0.34 with all parameters equal except with lower concrete strength, 62.1 MPa (9.0 ksi) rather than 64.1 MPa (9.3 ksi) was also analyzed to observe the effect of concrete strength on the stress distributions. The analysis of the remaining four FEM models simulating the quarter sections of specimens FHC 3, 4, 5, and 6 which is not included in this study show that greater the transverse hoop spacing, the column stiffness decreases. The use of high grade steel for the transverse reinforcements, on the other hand, resulted in greater column stiffness. The analytical and experimental results correlated well for the initial loading for both elastic and elasto-plastic material models.

The main purpose of the FEM modeling and analysis was to verify the experimental results and obtained insights on the stress distributions. All versions of the FEM models discussed gave results that closely matched those of the analytical and experimental results. The results of fully elastic model and the initial elastic range of the concrete/elasto-plastic material models gave linear slopes that closely matched those of analytical results. For elasto-plastic stage of the monotonic loadings, the change in the initial slope occurred as the displacements increased further.

416

The results of column section models for specimen FHC1-0.2 are shown from in figures 6.10 to 6.13. The first depictions of the stress distribution (a) shown are the entire quarter slice of a column section, where the second depictions (b) show cut section through the section model and the stress distribution at the level of transverse reinforcements.

An axial displacement of 0.254mm (0.01 inch) was applied to fully elastic column section model as shown in the first depiction of figure 6.10. This stress contour of a quarter section figure a of the column shows that during the initial axial loading, the highest stress exist within the concrete cover region followed by the location of No. 29 (ASTM #9) and No. 36 (ASTM #11) longitudinal bars. The same elastic model using finer mesh shown in figure 6.11 (figure a) has a similar pattern of stress distribution with reduced and more refined stress gradients. At a displacement of 0.254mm (0.01 inch), the role of the steel reinforcement is already noticeable due to its high modulus of elasticity. Finer meshes increases the accuracy of actual stress distribution. However, overall load versus displacement relationship remained the same.

The figure 6.10 (b), which show a stress distribution at the level of transverse reinforcements shows that the locations of longitudinal reinforcements has lowest

417

stress values near the area of confined core concrete, assumed to behave elastically in this case.

The stress is slightly decreased toward the center of the confined region away from the confining hoops. At the level of transverse reinforcements, it is apparent that the concrete volumes assumed as elastic material undergoes the highest stress in comparison to the reinforcements.

Figure 6.13 shows a section model using concrete elements and elasto-plastic bilinear reinforcements with the same axial displacement of 0.254mm (0.01 inch) for specimen FHC1-0.2. The model consist of concrete elements of compressive strength 64.1 MPa (9.3 ksi) and elasto-plastic transverse reinforcements. The stress patterns are similar to the fully elastic model of figure 6.11 with greater differences in the stress between the confined and unconfined regions. Figure 6.13(a) shows that during the initial axial loading, the maximum effective stress exists in unconfined concrete cover region adjacent to the confinement hoops followed by the unconfined region of No. 36 (ASTM #11) longitudinal bar located in the corner of the column section. The confined region has the next highest stress distribution followed by the location of No. 29 (ASTM #9) longitudinal bars located midway between No. 36 (ASTM #11) longitudinal bars. The confined region shows that concrete takes majority of the stress as the stress

418

gradually decreases from the location of No. 29 (ASTM #9) longitudinal bars to the center of the column.

Figure 6.13 (b) shows that the highest stress distribution at the level of transverse reinforcements exist in unconfined region adjacent to the confinement hoops followed by confined core of the concrete. The lowest stress values exist at the No. 36 (ASTM #11) longitudinal bar. Within the confined concrete core, the concrete takes majority of the stress as the stress gradually decreases toward the locations of No. 29 (ASTM #9) and No. 36 (ASTM #11) longitudinal reinforcements.

The high stress values located in the confined core concrete are due to the confinement provided by the transverse reinforcements.

Finer meshes increase the accuracy of actual stress distribution. However, overall load versus displacement relationship remained the same.

As shown in figures 6.14 and 6.15, the initial slopes correlated closely with the experimental values for the column section models that consist of bilinear elasto-plastic and Kupfer concrete elements. The experimental result shows slightly greater stress degradation as axial strain increased to 0.0004. The stress versus strain relationships remained the same for both coarse and fine mesh models.

419

Fig. 6.10-FHC1-0.2 Section Model Using Coarse Mesh with All Elastic Materials (Values shown in ksi).

420

Fig. 6.11-FHC1-0.2 Section Model Using Fine Mesh with All Elastic Materials (Values shown in ksi).

421

Fig. 6.12-FHC1-0.2 Section Model Using Coarse Mesh with Concrete and Elasto-Plastic Reinforcements (Values shown in ksi).

422

Fig. 6.13-FHC1-0.2 Section Model Using Fine Mesh with Concrete and Elasto-Plastic Reinforcements (Values shown in ksi).

423

Fig. 6.14-Axial Stress-Stress Relationship of Section Model for FHC1-0.2

424

Fig. 6.15-Comparison of Axial Stress-Stress Relationships Between FEM Model and Experimental Results for Specimen FHC1-0.2.

425

The same axial displacement of 0.254mm (0.01 inch) was applied for the following set of four models for specimen FHC2-0.34 with lower concrete strength of 62.1MPa (9.0 ksi) as shown in figures 6.16 to 6.19. All other material properties remain constant. The results show similar stress distributions in comparison to those for specimen FHC1-0.2. For the column sections models shown in figures 6.16 and 6.17 assume fully elastic behavior for the concrete volumes and all reinforcements. When compared to column section model of specimen FHC1-0.2, the stress values were slightly lower due to the use of lower concrete modulus of elasticity corresponding to 62.1 MPa (9.0 ksi).

The bilinear elasto-plastic / Kupfer concrete models are shown in figures 6.18 and 6.19 The use of concrete elements with lower concrete strength of 62.1MPa (9.0 ksi) shows similar stress distributions. Due to lower concrete strength, the concrete stress generated from the location of No. 36 (ASTM #11) longitudinal bar is more widely spread into the confined region.

During the initial axial loading, all elastic models behave linearly, where the bilinear elasto-plastic / Kupfer concrete models are subject nonlinear behaviors. The figures 6.20 and 6.21 show that the results correlates closely to experimental result.

426

For concrete/elasto-plastic models, the use of higher concrete strength of 64.1 MPa (9.3 ksi) resulted in relatively even stress distribution between the hoops and ties, where the use of lower concrete strength of 62.1 MPa (9.0 ksi) resulted in concentration of stress near the ties.

For the column section analysis, it can be deduced that there is a strength degradation of concrete during the initial axial loading due to change in the micro-mechanical behavior of high strength concrete and due to interaction between concrete and its reinforcements. The stress distribution points out the strong and weak areas of the column section during the initial axial loading and provides a validation of the experimental results. The results show that the confined region in general undergoes lower stress values in comparison to unconfined regions which failed first during the experiment. It seems that greater concrete strength provides even stress distribution between the ties and in confined regions. Even distribution of stress provides greater confinement efficiency and utilization of the reinforcement provided.

The higher concrete strength allows even distribution of stress along the axial direction therefore improving the efficiency of the confinement provided. Close correlations to the experimental results also validate the accuracy of the finite element models considered.

427

When axial displacement greater than 0.254mm (0.01 inch) is applied to the column section models that consist of concrete/elasto-plastic elements, an error messages alerts, 'Divergence, energy greater than 1.E30, model crushed, time step probably too large'. The model stops computation upon first crushing of the concrete.

428

Fig. 6.16-FHC2-0.34 Section Model Using Coarse Mesh with All Elastic Materials (Values shown in ksi).

429

Fig. 6.17-FHC2-0.34 Section Model Using Fine Mesh with All Elastic Materials (Values shown in ksi).

430
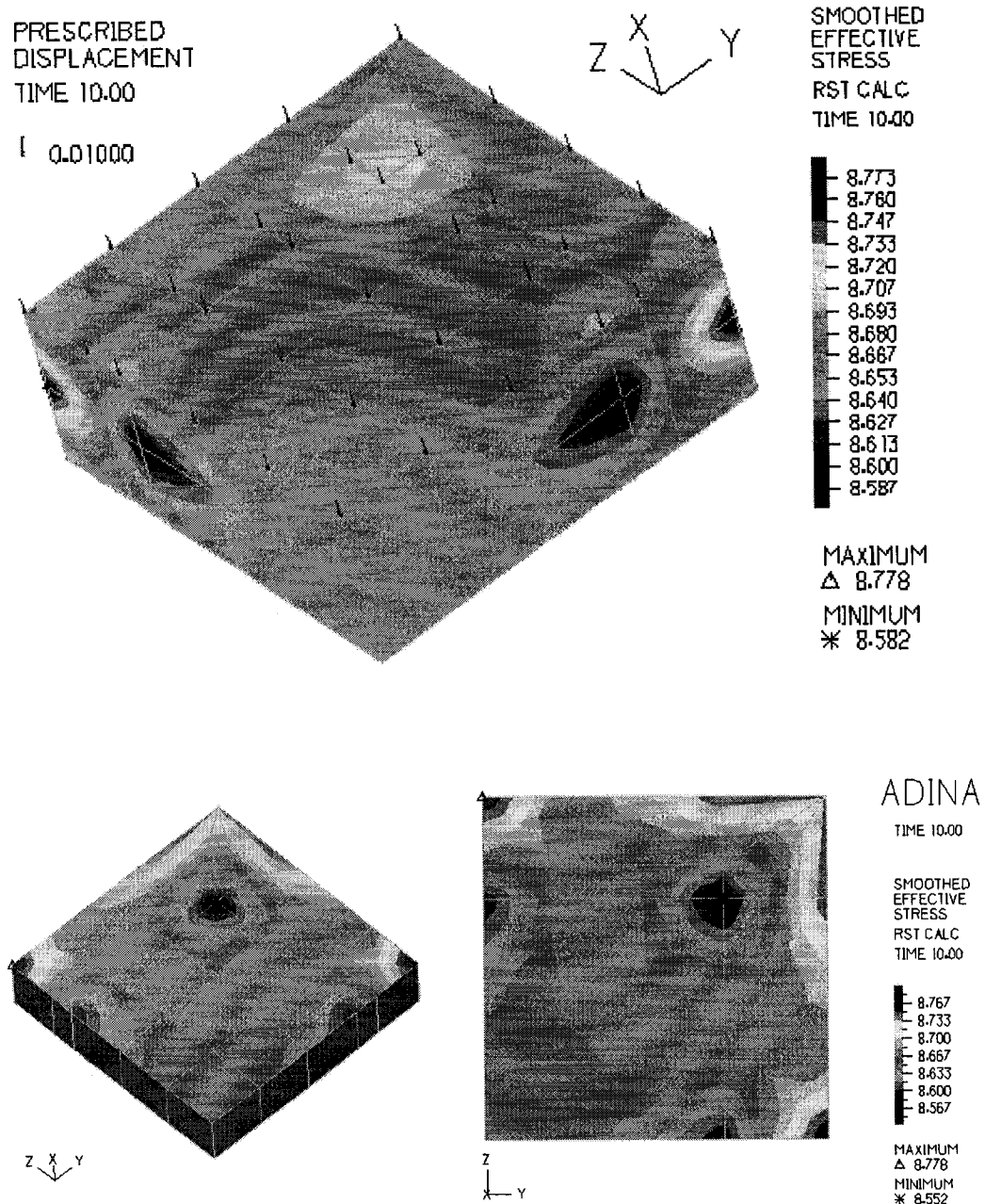
Fig. 6.18-FHC2-0.34 Section Model Using Coarse Mesh with Concrete and Elasto-Plastic Reinforcements (Values shown in ksi).

431
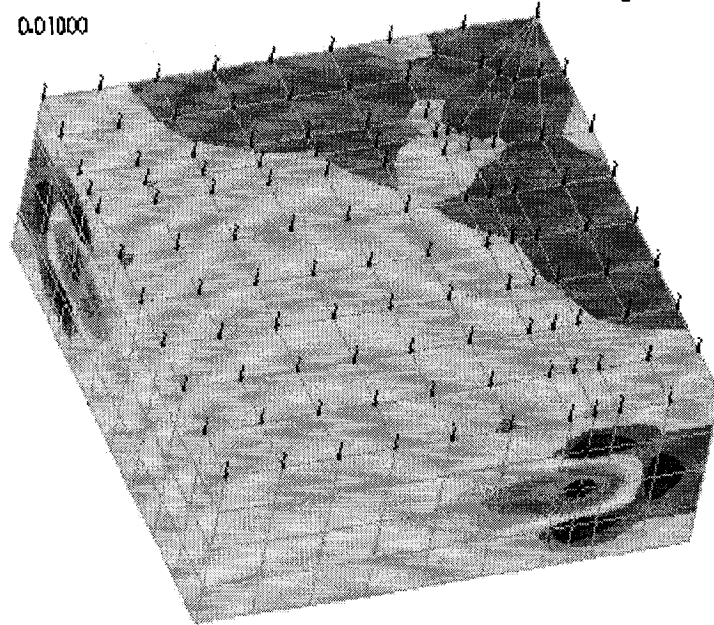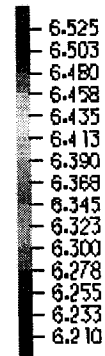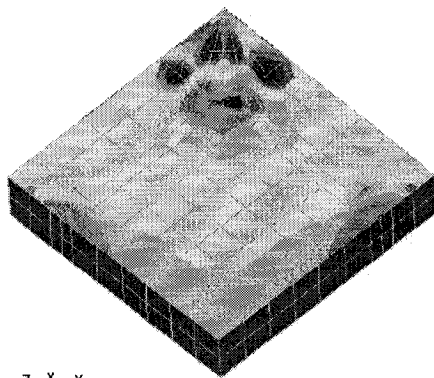
Fig. 6.19-FHC2-0.34 Section Model Using Fine Mesh with Concrete and Elasto-Plastic Reinforcements (Values shown in ksi).

432

Fig. 6.20- Axial Stress-Stress Relationship of Section Model for FHC2-0.34

Fig. 6.21- Comparison of Axial Stress-Stress Relationships Between FEM Model and Experimental Results for Specimen FHC2-0.34.

434

The figure 6.22 shows maximum axial strain along the length of the hoops for all column section models described above at axial displacement of 0.254mm (0.01 inch). For all models, the maximum hoop strain increases away from the location of No. 36 (ASTM #11) longitudinal bars toward the center of the column. This shows that the use of transverse ties help increase the confinement strength of the column since they are provided at the point of maximum hoop strain, the location of maximum hoop strain. The comparison of fully elastic and concrete/elasto-plastic column section models also shows that concrete substantially limits hoop deformation.

435
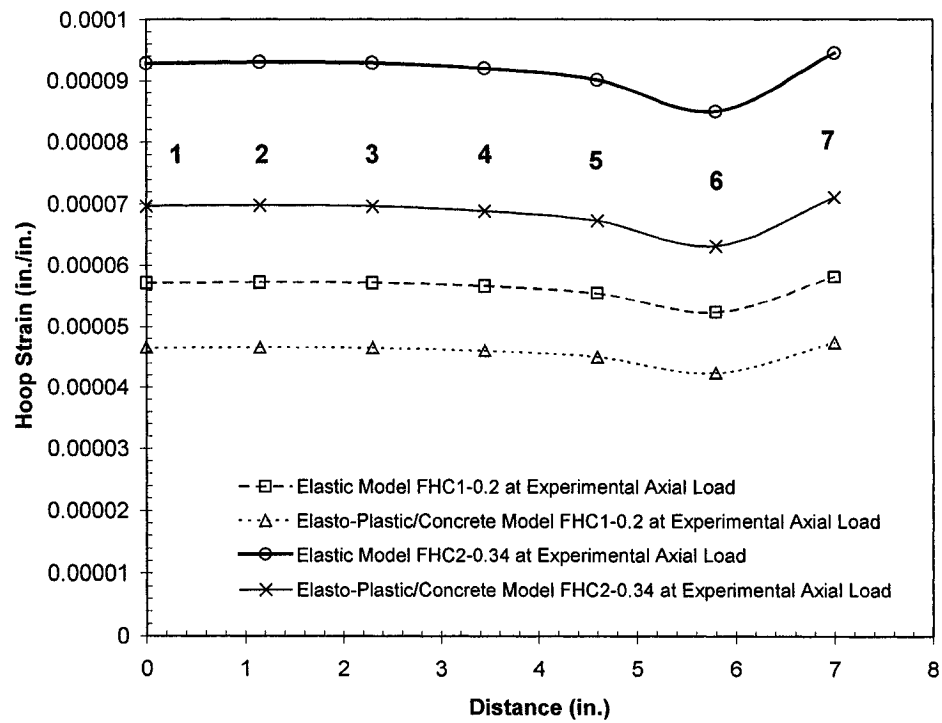
Fig. 6.22-Hoop Strain from Center of Column to Location of Longitudinal Reinforcement at Experimental Axial Loads for Specimens FHC1-0.2 and FHC2-0.34.

436
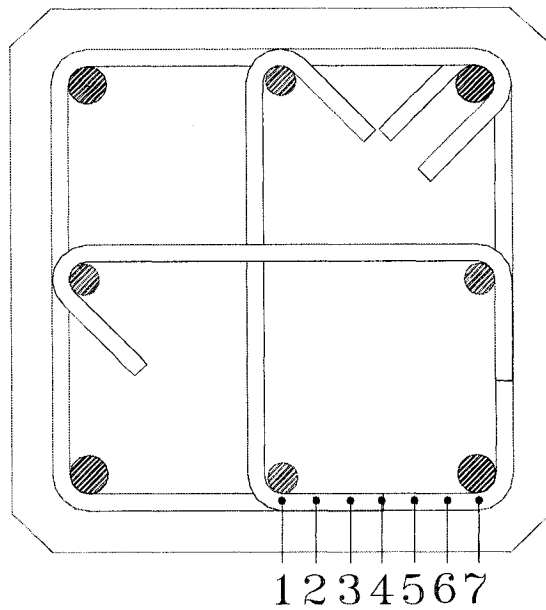
Fig. 6.23-Hoop Strain Locations for Column Section Models.

The analysis of axial deformation and comparisons of resulting stress variations determine the role of the transverse reinforcements. The higher concrete strength allows even distribution of stress along the axial direction therefore improving the efficiency of the confinement provided. Close correlations to the experimental results also validate the accuracy of models considered.

Within an assumption that reinforcements, which are modeled as pipe and truss elements, have complete bond to the concrete elements, the finite element model

437

slightly over predicted the stress versus strain relationships. However, the results provide understanding of improved stress behavior with use of higher strength concrete and help validate the experimental results.

Column Quarter Section Analysis of Specimen H8T76-3 by Martirossyan et. al.

To confirm the validity of the column section analysis previous performed for specimens FHC1-0.2 and FHC2-0.34, a column section analysis was performed for a specimen H8T76-3 tested by Martirossyan et. al. A quarter of 190 x 190 mm (7.5 x 7.5 in.) column section, 95 x 95mm (3.75 x 3.75 in.) section 75mm (3 in.) in thickness, was modeled in the same manner as it was previously accomplished for column sections of specimens FHC1-0.2 and FHC2-0.34.

The following material properties are used in the model.

Concrete:

$f_c' = 73.7$ MPa (10.7 ksi)

438

Reinforcement:

Table 6.1- Material Properties of Specimen H8T76-3

Reinforcement Parameters	8- Longitudinal Reinforcements	Transverse Hoops	Transverse Ties
		Spacing, s = 75mm (3 in.)	
Type	ASTM #4	ASTM #2	ASTM #2
E_s	230,367 MPa (33,412 ksi)	219,880 MPa (31,891 ksi)	219,880 MPa (31,891 ksi)
f_y	530 MPa (76.9 ksi)	506 MPa (73.4 ksi)	506 MPa (73.4 ksi)
f_u	832 MPa (120.7 ksi)	652 MPa (94.6 ksi)	652 MPa (94.6 ksi)

The configuration of specimen H8T76-3 is the same as for specimens FHC1 to

FHC2 previously discussed. The specimen comprises of longitudinal ratio of

2.8% with a total of eight longitudinal reinforcements four at each corner and four

at midpoints between the corner bars with transverse hoops and ties spaced at

75mm (3 in.). The ties have 90 degree bend on one end and 180 degree bend on

the other end.

An axial displacement was applied to the FEM model until the programs stopped

execution upon first cracking of concrete material at axial displacement of

0.213mm (0.0084 in.). Two versions of the models are analyzed, one using

coarse mesh and the other using fine mesh. The analytical results are then

compared to the experimental results.

439
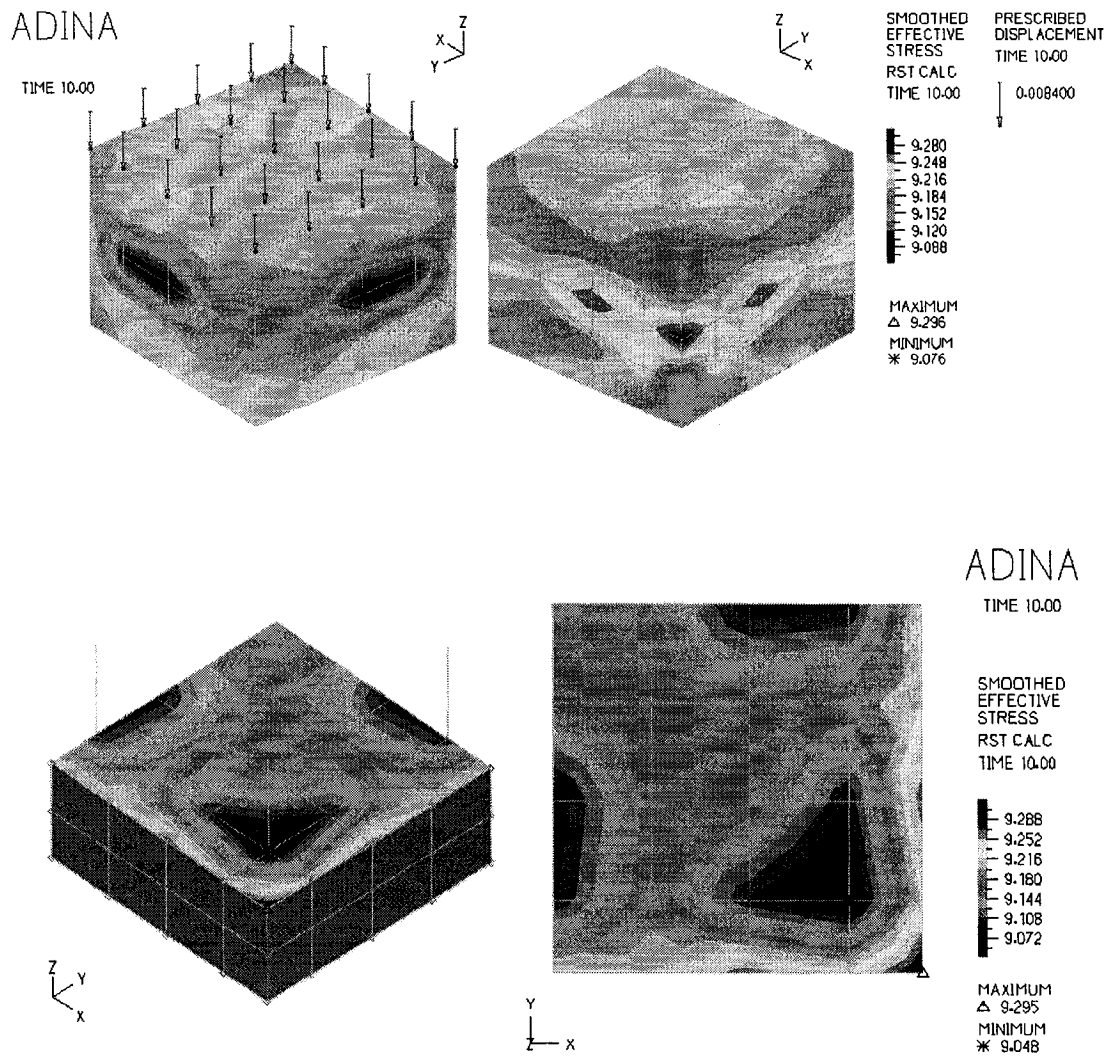
Fig. 6.24-Column Quarter Section Analysis of Specimen H8T76-3 using Coarse Mesh (Values shown in ksi)

440
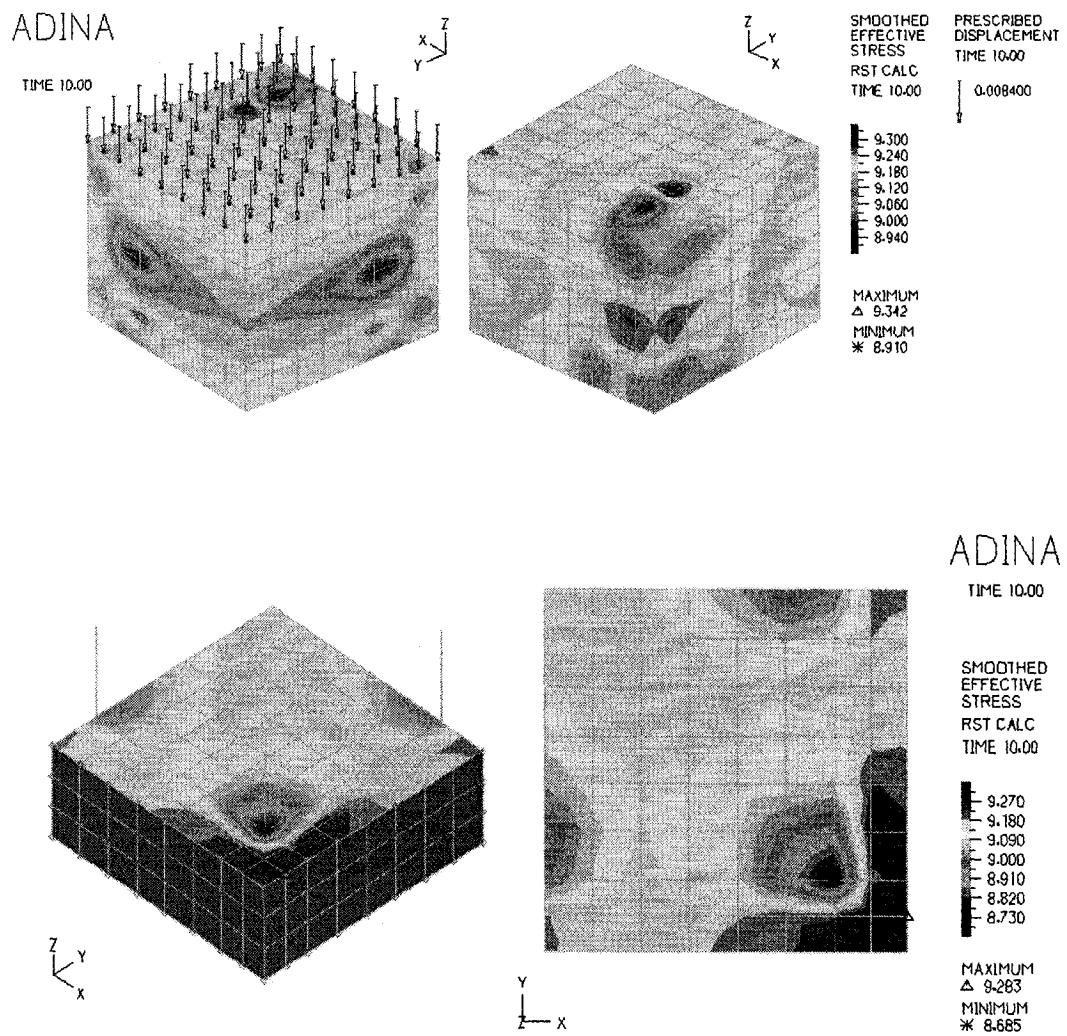
Fig. 6.25-Column Quarter Section Analysis of Specimen H8T76-3 using Fine Mesh (Values shown in ksi)

441
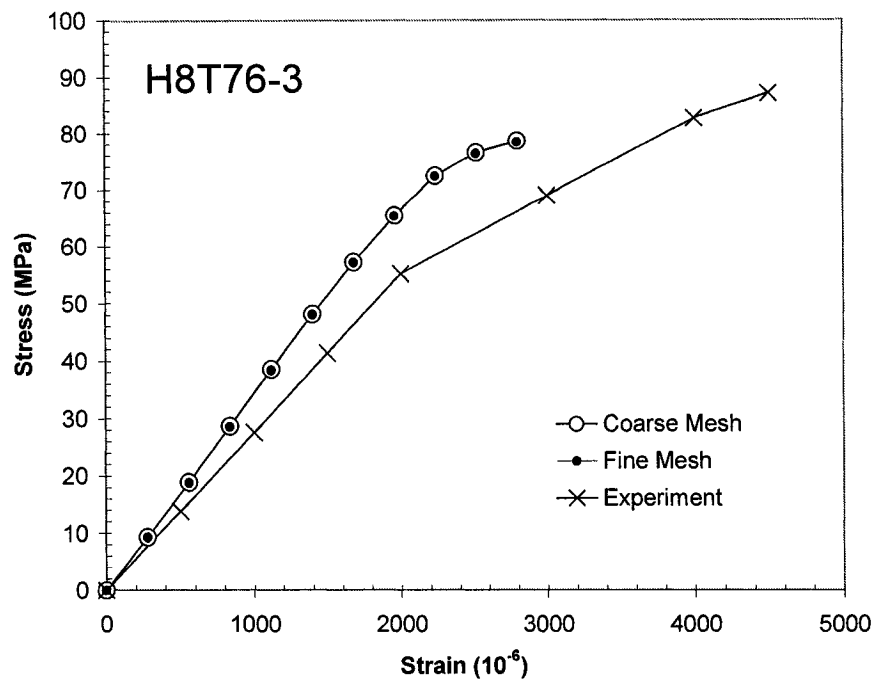
Fig. 6.26-Comparison of Analytical Axial Stress-Strain Relationship of Specimen H8T76-3 to Experimental Result

442

Full-Column Model

Finite element models does not consider repetitive slippage as it occurs in the experiments. Also, buckling or rupturing of the transverse reinforcements is not simulated by finite element analysis (FEA), although other methods using other commericially available FEA software may consider such failure criterias. 8-node elements used for 3-D solid modeling of concrete were specified with tangent modulus, compressive strength, tensile strengths, mass density, and ultimate compressive strength using experimental parameters. The main purpose of the finite element analysis was to simulate the loading conditions to evaluate the general stress distribution in various parts of the specimens. The stress distribution for full-column FE models subjected to constant axial load and lateral displacement are shown below. The resulting lateral load versus displacement relationships show that the column stiffness correlated closely to those of the experimental results.

The analytical result of elastic model for specimen FHC1-0.2 subjected to a maximum of 203 mm (8 inch) lateral displacement is shown below. It is apparent that highest stress values exist at the joint area immediately above the column stub. The stress gradually decreases further away from the column stub. The stress distribution remain the same in both compressive and tensile zones of the

443

column section. The midsection between the compressive and tensile zones shows no change in stress value. The elastic model assumes constant value of Young's modulus for all materials, with lowest value corresponding to experimental parameters prescribed for the concrete modeled as elastic element. The elastic strain distribution of No. 36 (ASTM #11) longitudinal bar along the column length shows highest strains between 150 to 250 mm (6 to 10 inches) away from the column stub for all stages of loading.

444
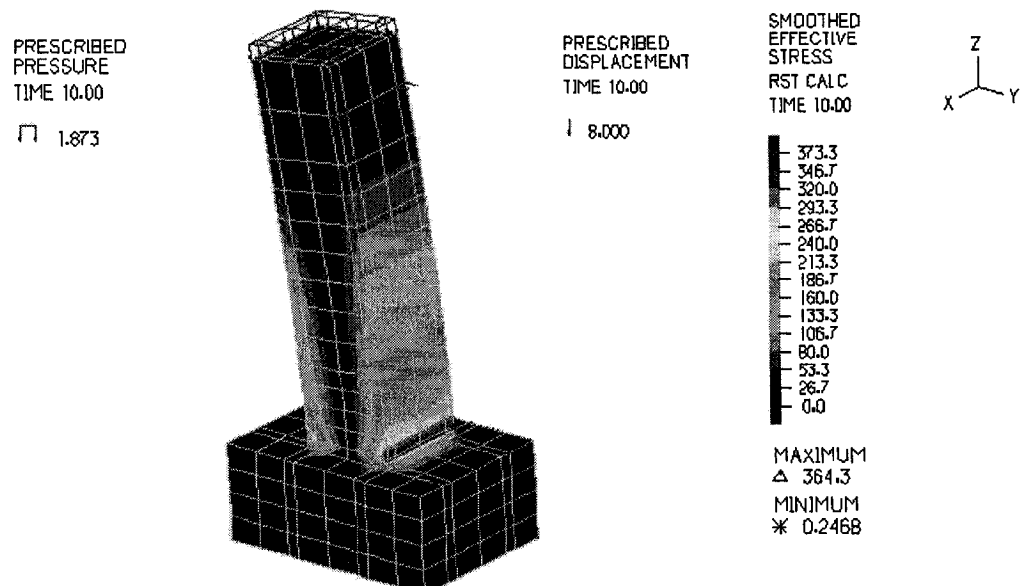
Fig. 6.27-Stress Contour of Elastic FHC1-0.2 Model at Lateral Displacement of 200 mm (8 in) (Values shown in ksi).

445
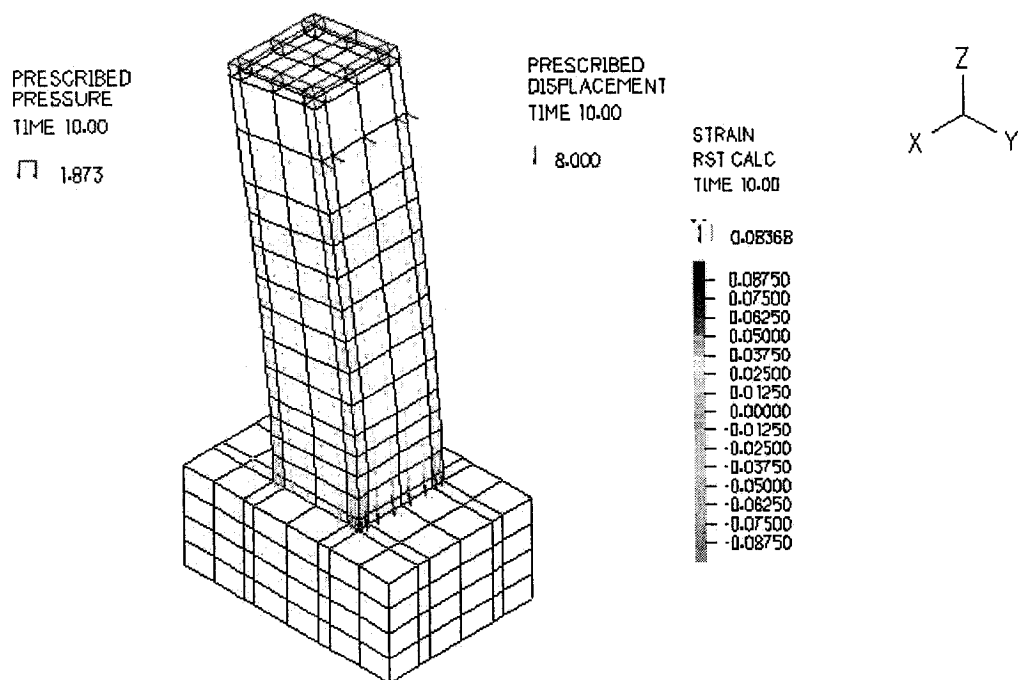
Fig. 6.28-Strain Distribution of Elastic FHC1-0.2 Model at Lateral Displacement of 200 mm (8 in).

446
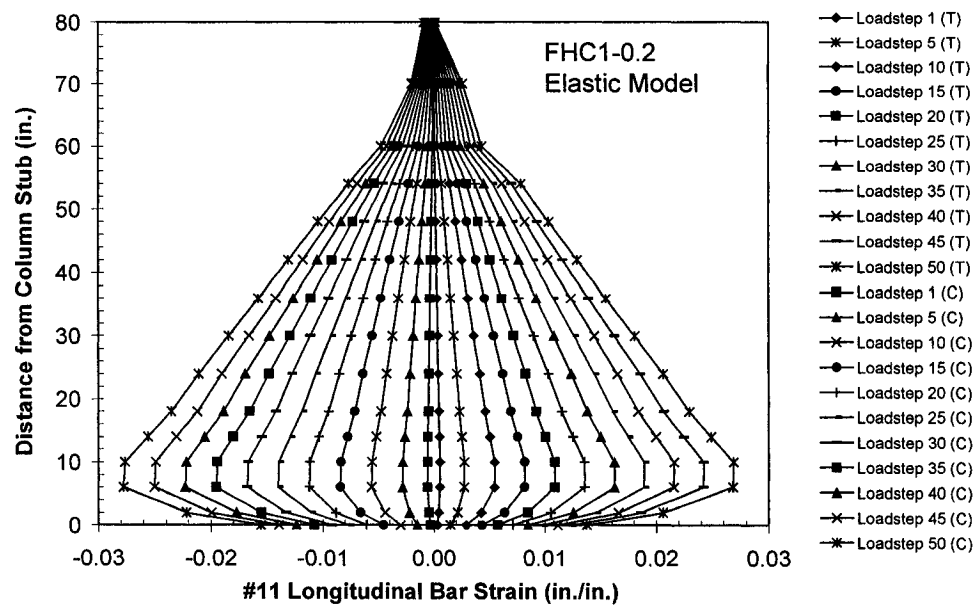
Fig. 6.29-Longitudinal Reinforcement Strains of Elastic FHC1-0.2 Model in Compression and Tension Zones

Both transverse hoops and ties show highest strain values at approximately 229 mm (9 inches) from the column stub. The positive strain values show transverse reinforcements in tension toward the direction of lateral loading at a coordinate of -191 mm (-7.5 in), where the negative strain values show transverse reinforcements in compression at a coordinate of 191 mm (7.5 in). It is apparent

447

that the strain values of the ties are slightly greater in values in comparison to those of hoops.
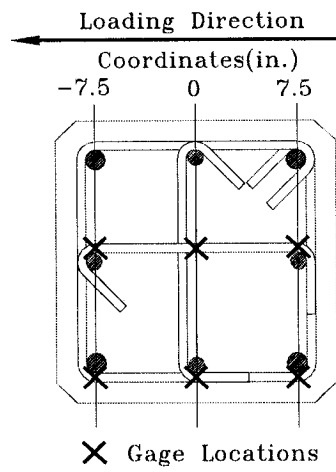
Fig. 6.30-Coordinates (in.) of Hoop and Tie Strain Locations for Full-Column Models
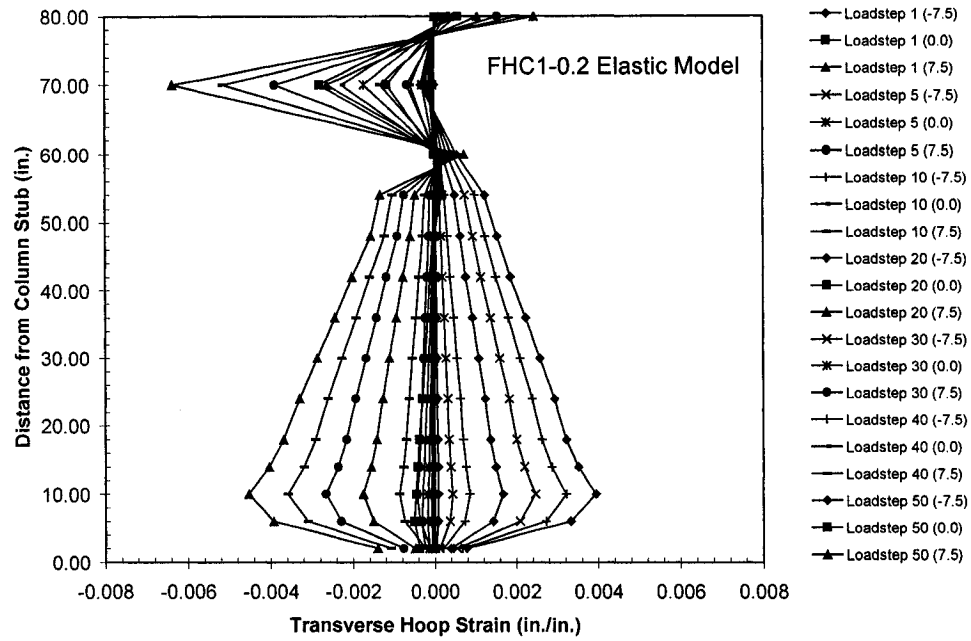
448

Fig. 6.31-Transeverse Hoop Strains for Elastic FHC1-0.2 Model at Loadsteps

449
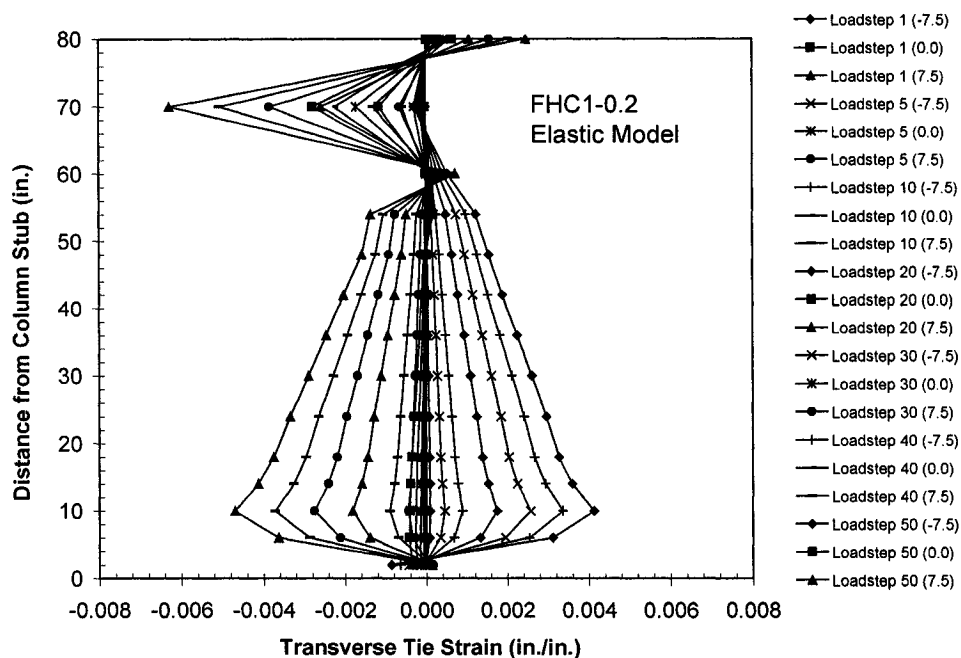
Fig. 6.32-Transeverse Tie Strains for Elastic FHC1-0.2 Model at Loadsteps

The following models show stress distributions at a maximum lateral displacement of 7.62mm (0.30 inches) for specimen FHC1-0.2. The use of concrete elements in the model show highest stress values in the plastic hinge region up to approximately 610mm (24 inches) away from the column stub. A initial concrete crushing in the cover regions shown resulted in the early termination of the push over process.

450
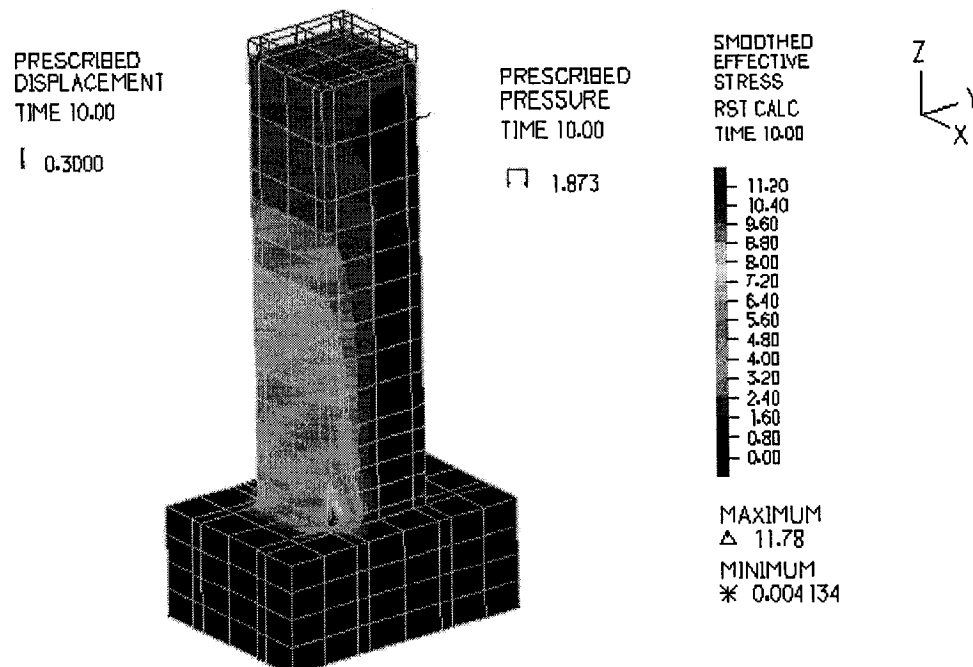
Fig. 6.33- Stress Contour of Elasto-Plastic/Concrete FHC1-0.2 Model at Lateral Displacement of 7.62mm (0.3 in) (Values shown in ksi).

451

The distribution of concrete cracks is shown in the following depiction of model. The flexural cracks occurs in concrete cover along the plastic hinge length as compressive crushing occurs in the concrete cover in the compression zone during the early stages of loading. The deformation shown is magnified for clarity.

452

Development of Cracks (Values shown in ksi)
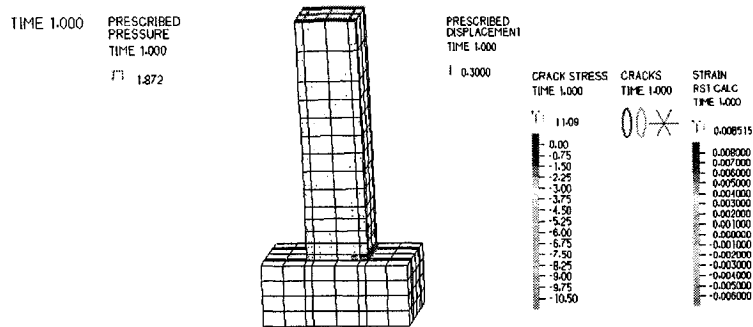
Fig. 6.34-Crack Distribution of Specimen FHC1-0.2 at 0.76mm (0.03 in.) Lateral Displacement
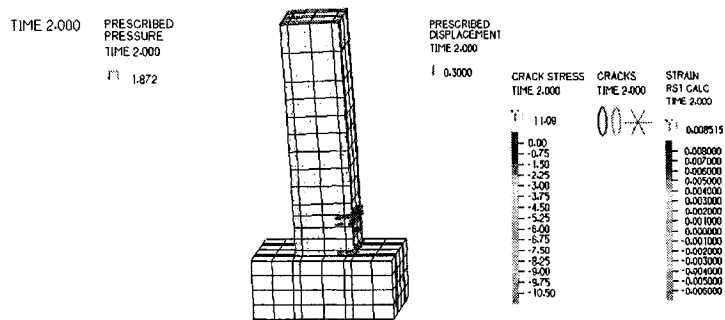
Fig. 6.35-Crack Distribution of Specimen FHC1-0.2 at 1.52mm (0.06 in.) Lateral Displacement
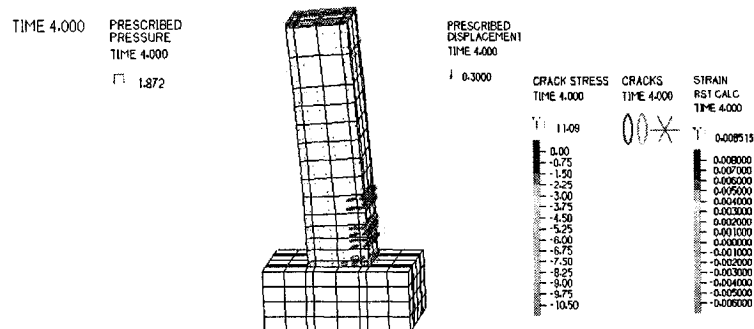
Fig. 6.36-Crack Distribution of Specimen FHC1-0.2 at 3.05mm (0.12 in.) Lateral Displacement

453
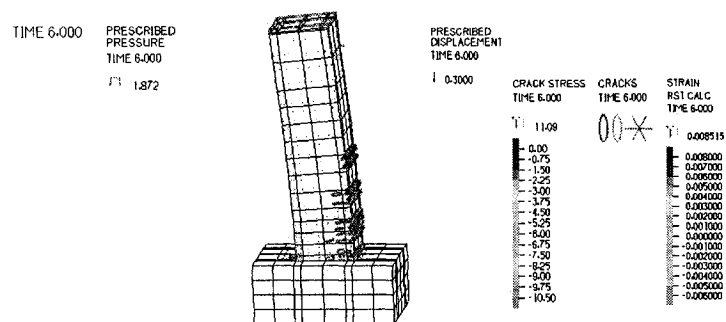
Fig. 6.37-Crack Distribution of Specimen FHC1-0.2 at 4.57mm (0.18 in.) Lateral Displacement
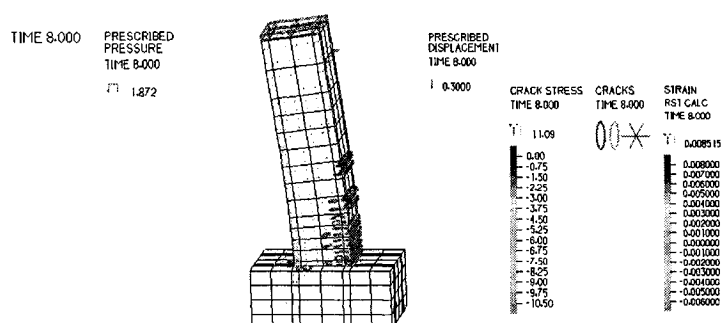
Fig. 6.38-Crack Distribution of Specimen FHC1-0.2 at 6.1mm (0.24 in.) Lateral Displacement
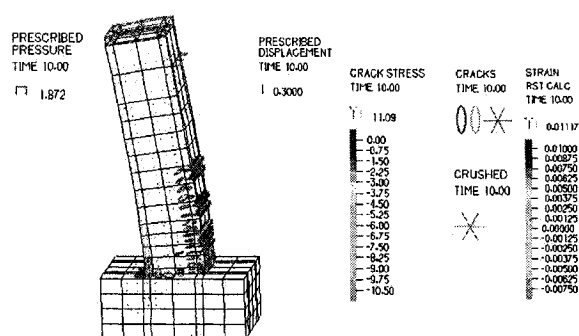
Fig. 6.39-Crack Distribution of Specimen FHC1-0.2 at 7.62mm (0.3 in.) Lateral Displacement

454
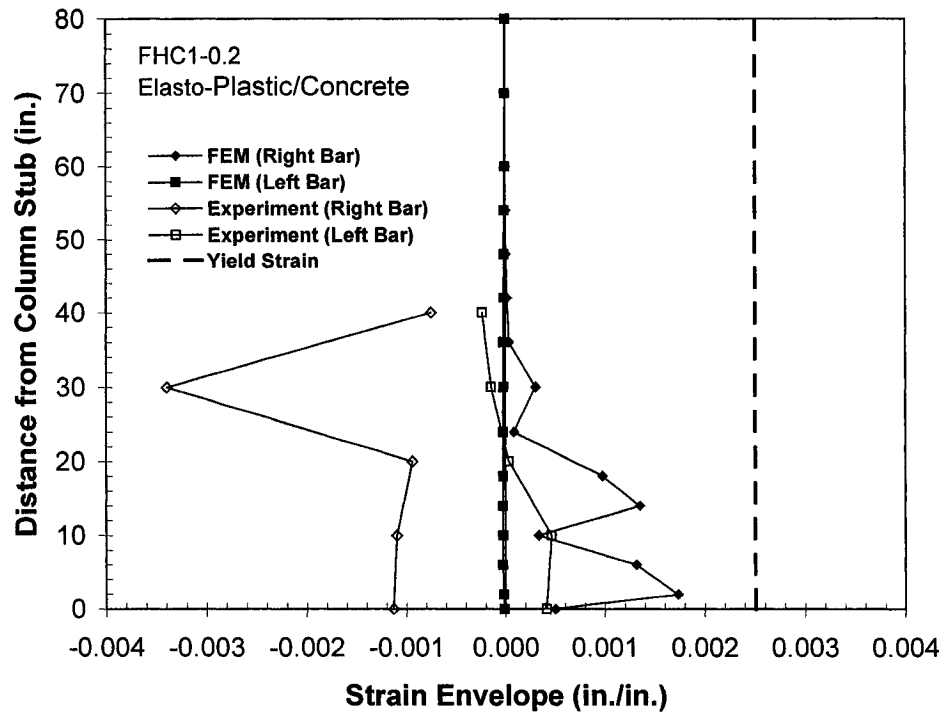
Fig. 6.40-Longitudinal Bar Strain Envelope Along Column Length at Lateral Displacement of 7.62mm (0.3 in).

See Appendix III for the locations of experimental gage locations for the longitudinal bars.

In contrast to the results of the elastic model discussion previously, the models using concrete elements showed higher strain values at the locations of first and fourth transverse reinforcements from the column stub as shown in the chart above.

455

The following chart shows strain envelope of transverse reinforcements for loading up to the same lateral displacement of 7.62mm (0.30 inches) at 0.43% Drift.
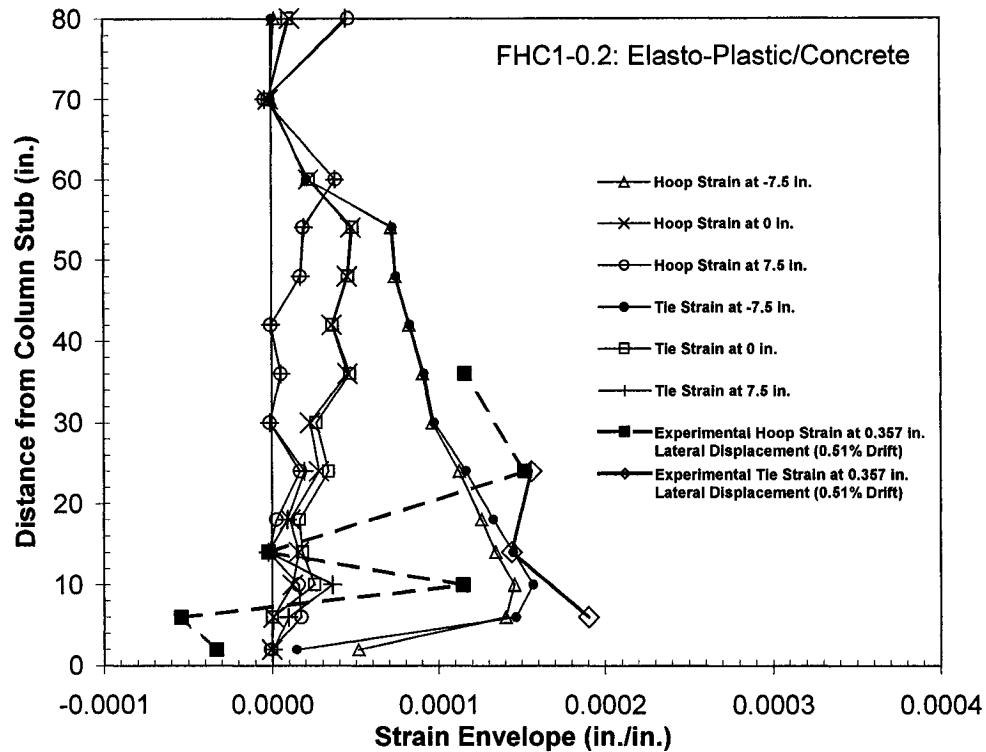
Fig. 6.41-Hoop and Tie Strains for FHC1-0.2 Model at 7.62mm (0.3 in.) Lateral Displacement (0.43% Drift).

The maximum strain values in the transverse reinforcements were similar for both hoops and ties. In contrast to the results obtained for elastic model discussed, all axial strain of the transverse reinforcements remain in tension. The highest strain

456

values for hoops and ties exist at approximately 250mm (10 inches) from the column stub, where the axial strain value for No. 36 (ASTM #11) longitudinal bar remains lowest at this location. It seems that the longitudinal bar strains are reduced at the locations of transverse reinforcements at low level of axial load. When the effective confinement is relatively low, the flexural effect seems to dominate between the transverse reinforcements.
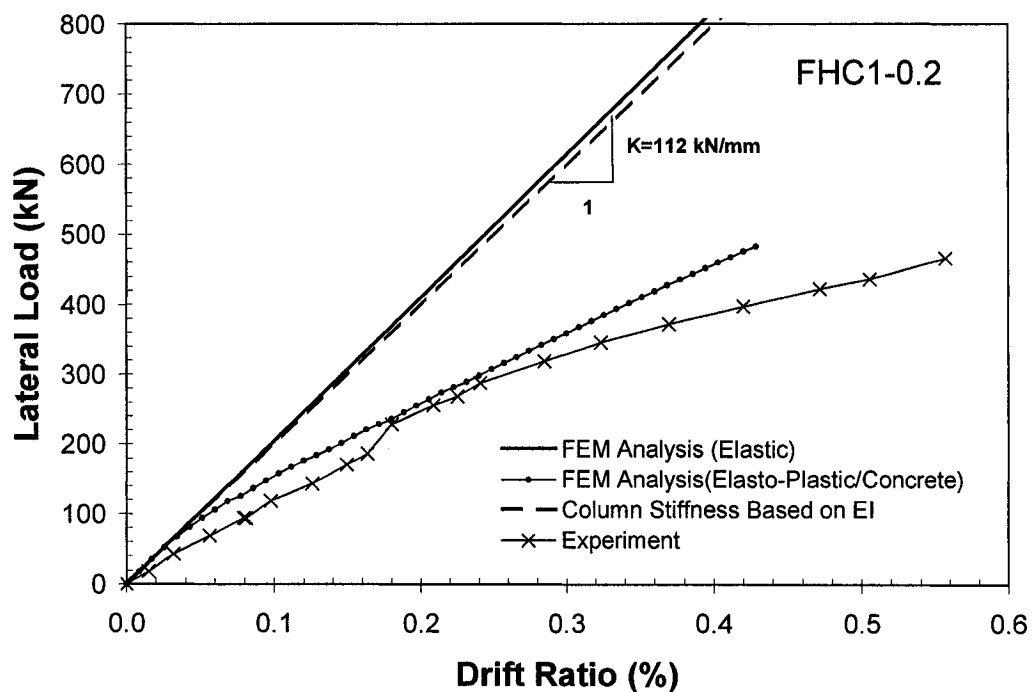
Fig. 6.42-Lateral Force vs. Drift Ratio Relationships for Specimen FHC1-0.2.

The load versus displacement relationship above shows a close correlation to the experimental result. With an assumption that the reinforcements are perfectly

457

embedded in concrete, the finite element analysis result slightly over predicts the experiment values.

The analytical results for the model of specimen FHC2-0.34 subjected to a maximum lateral displacement of 150mm (6 inches) show similar trends as those of specimen FHC1-0.2. However, for the elastic model, the stress values are higher due to higher axial load application although the variations in the stress remain the same with highest values existing immediately above the column stub.
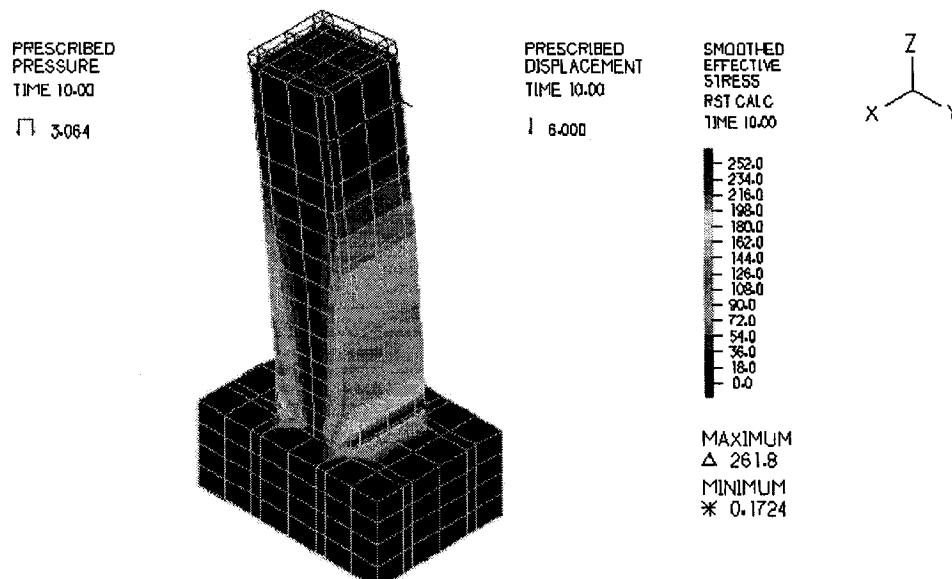
Fig. 6.43-Stress Contour of Elastic FHC2-0.34 Model at Lateral Displacement of 150mm (6 in) (Values shown in ksi).

458
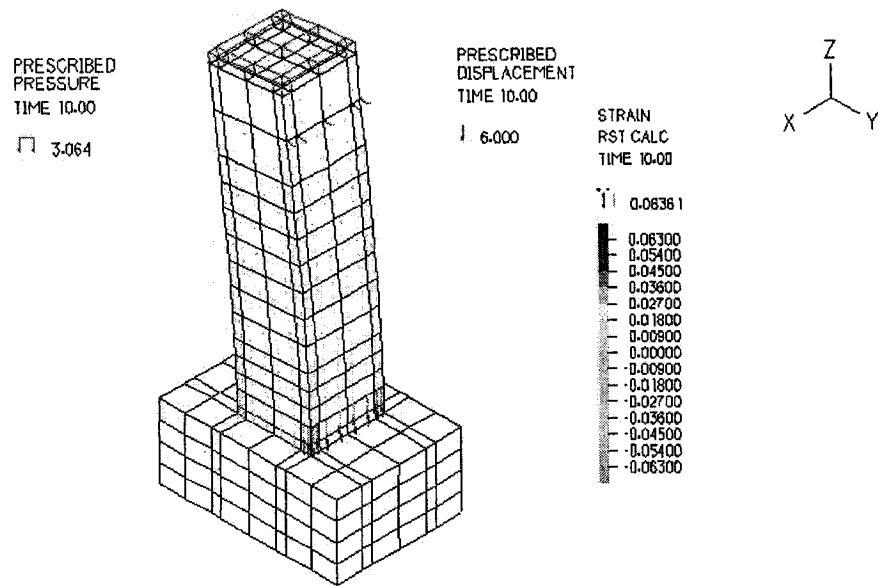
Fig. 6.44-Strain Distribution of Elastic FHC2-0.34 Model at Lateral Displacement of 150mm (6 in) (Values shown in ksi).

459
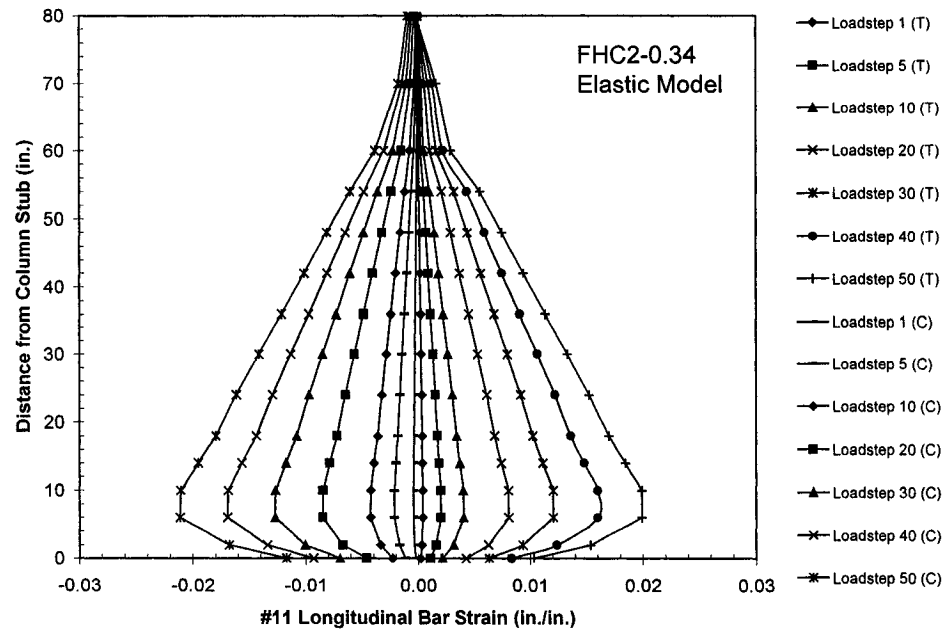
Fig. 6.45-Longitudinal Reinforcement Strains of Elastic FHC2-0.34 Model in Compression and Tension Zones

For specimen FHC2-0.34, the highest strain values of No. 36 (ASTM #11)

longitudinal bar also exists between a distances of 150 to 250mm (6 to 10 inches)

away from the column stub, similar to specimen FHC1-0.2.

The strain envelopes for the transverse reinforcements also remain similar to that

of specimen FHC1-0.2. Also, the location of maximum axial strain for both

hoops and ties remain 250mm (10 inches) away from column stub.
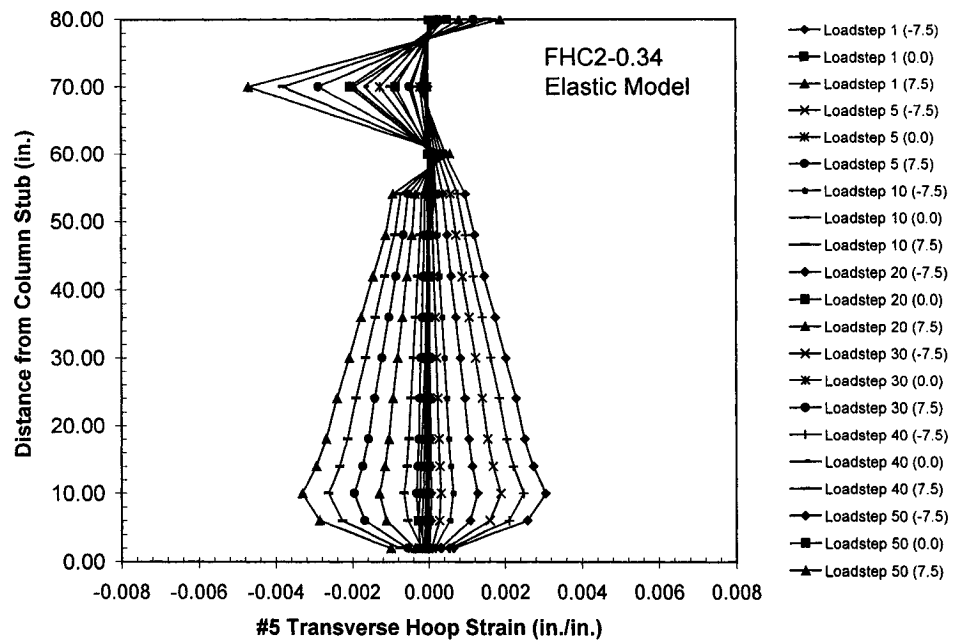
460

Fig. 6.46-Transeverse Hoop Strains for Elastic FHC2-0.34 Model at Loadsteps

461
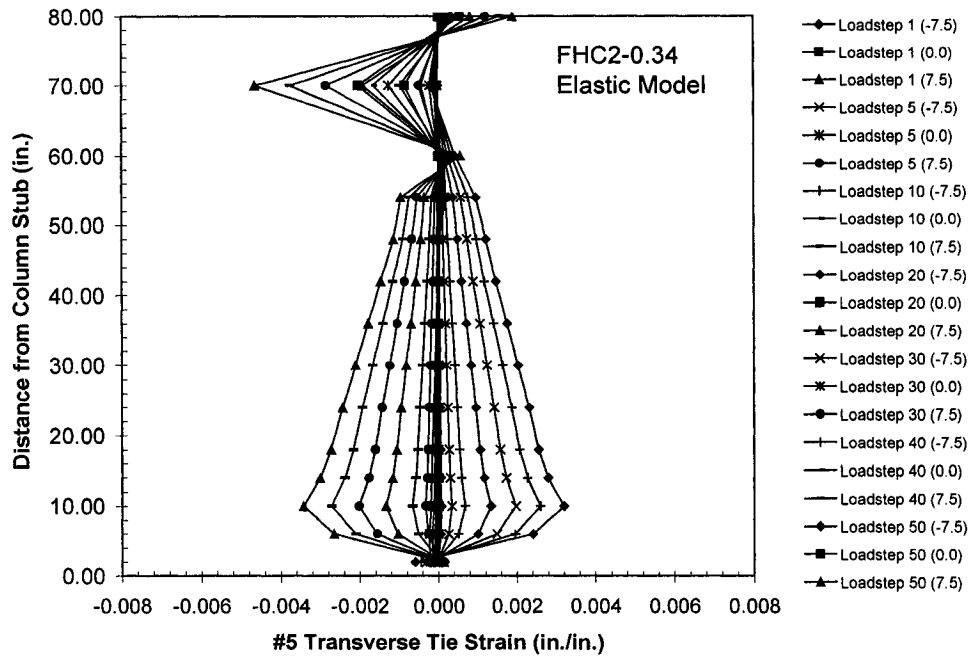
Fig. 6.47-Transeverse Tie Strains for Elastic FHC2-0.34 Model at Loadsteps

The following results of concrete model for specimen FHC2-0.34 using elasto-plastic elements for the reinforcing bars shows similar patterns in comparison to specimen FHC1-0.2. However, length of plastic hinge at a maximum of 5 mm (0.2 inch) lateral displacement is approximately 450mm (18 inches) measured from the column stub rather than 610mm (24 inches) as it was the case for FHC1-0.2. In comparison to specimen FHC1-0.2 which was subjected to a maximum lateral displacement of 7.62mm (0.3 inches), specimen FHC2-0.34 shows concentration of cracks closer to column stub. There are greater extent of compressive cracking and crushing due to higher axial loading. The strain

462

envelope of No. 36 (ASTM #11) longitudinal bar shows that the both compressive and tensile bars in compression as shown in chart above at lateral displacement of 5 mm (0.2 inches). The No. 36 (ASTM #11) longitudinal bar in tension zone is in tension only up to approximately 508 mm (20 inches) from column stub. It was observed that for specimen FHC1-0.2, No. 36 (ASTM #11) longitudinal bar in tension zone was in tension for almost the entire length of the column at lateral displacement of 7.62mm (0.3 inches).

It can be noticed that the depth of compression zone has also increased due to higher axial load level.

PRESCRIBED
PRESSURE
TIME 10.00

⊓ 3.064

PRESCRIBED
DISPLACEMENT
TIME 10.00

I 0.2000

SMOOTHED
EFFECTIVE
STRESS
RST CALC
TIME 10.00

- 9.333
- 8.667
- 8.000
- 7.333
- 6.667
- 6.000
- 5.333
- 4.667
- 4.000
- 3.333
- 2.667
- 2.000
- 1.333
- 0.667
- 0.000

MAXIMUM
△ 9.883
MINIMUM
✳ 0.009560
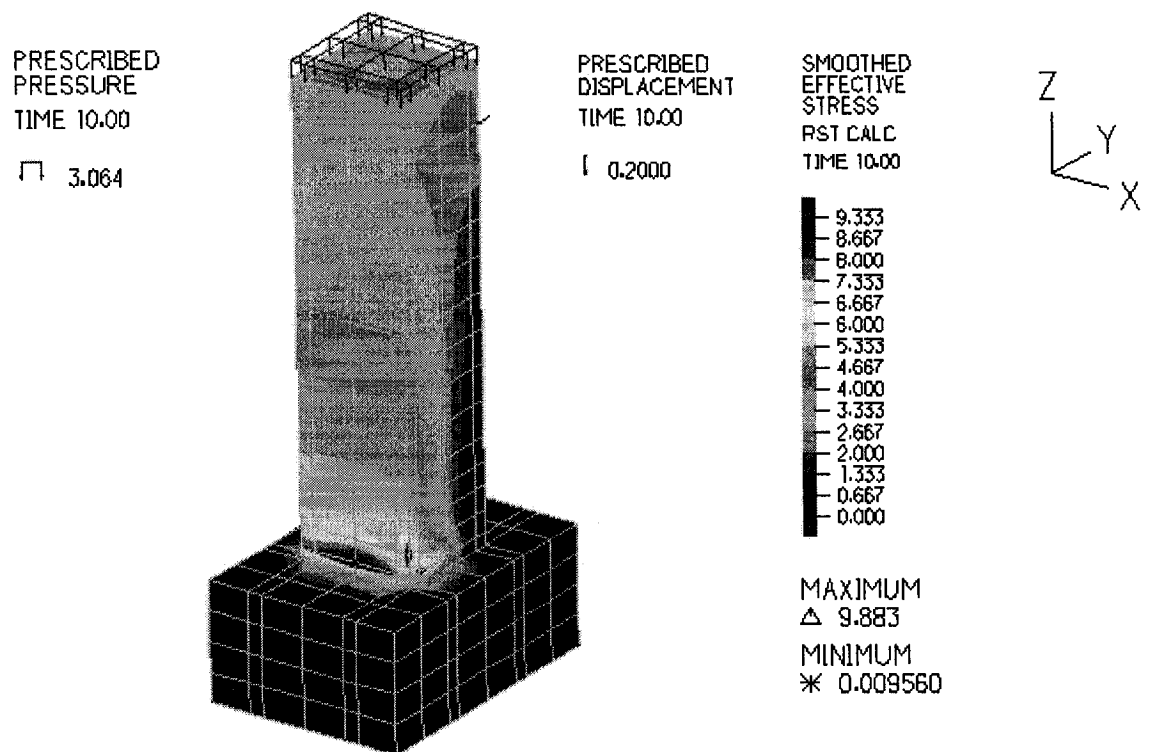
Fig. 6.48- Stress Contour of Elasto-Plastic/Concrete FHC2-0.34 Model at Lateral Displacement of 5 mm (0.2 in) (Value shown in ksi).

464

Development of Cracks (Values shown in ksi)
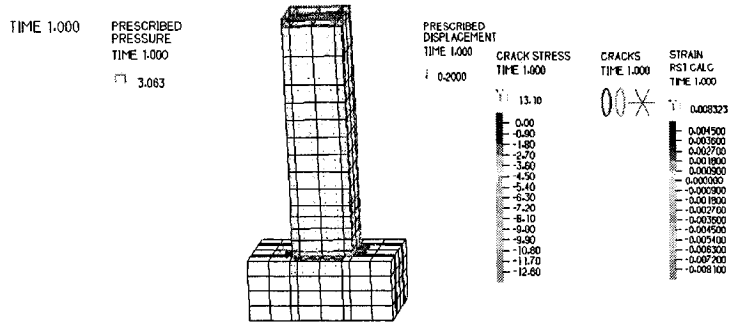
Fig. 6.49-Crack Distribution of Specimen FHC2-0.34 at 0.5mm (0.02 in.) Lateral Displacement
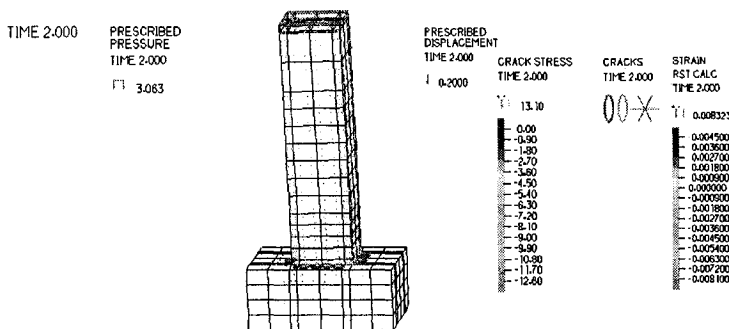
Fig. 6.50-Crack Distribution of Specimen FHC2-0.34 at 1mm (0.04 in.) Lateral Displacement
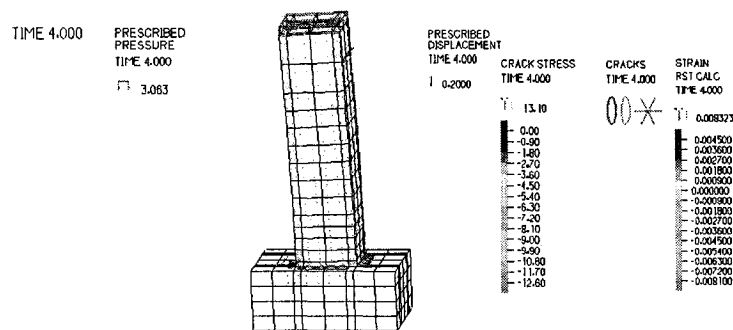
Fig. 6.51-Crack Distribution of Specimen FHC2-0.34 at 2mm (0.08 in.) Lateral Displacement

465
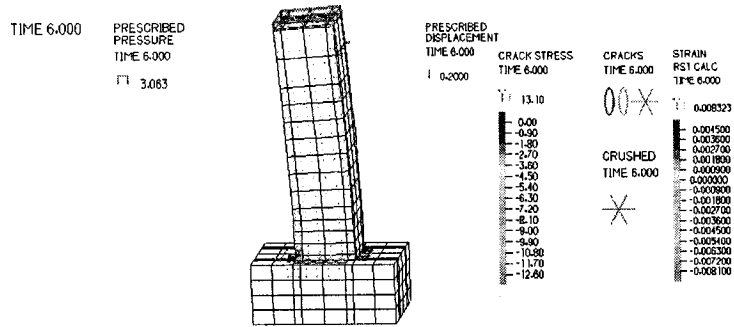
Fig. 6.52-Crack Distribution of Specimen FHC2-0.34 at 3mm (0.12 in.) Lateral Displacement
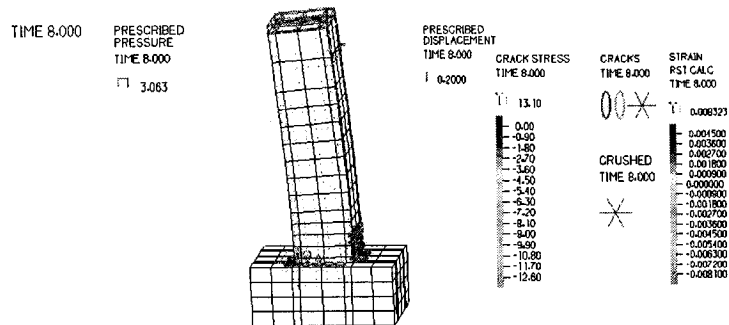
Fig. 6.53-Crack Distribution of Specimen FHC2-0.34 at 4mm (0.16 in.) Lateral Displacement
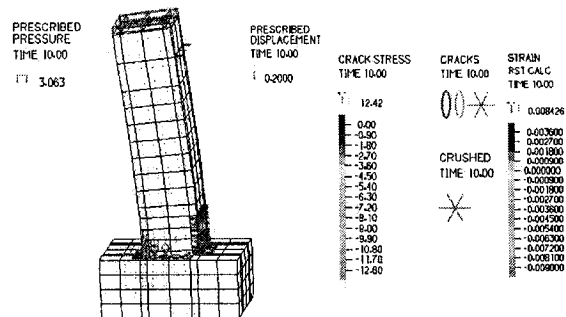
Fig. 6.54-Crack Distribution of Specimen FHC2-0.34 at 5mm (0.2 in.) Lateral Displacement

466
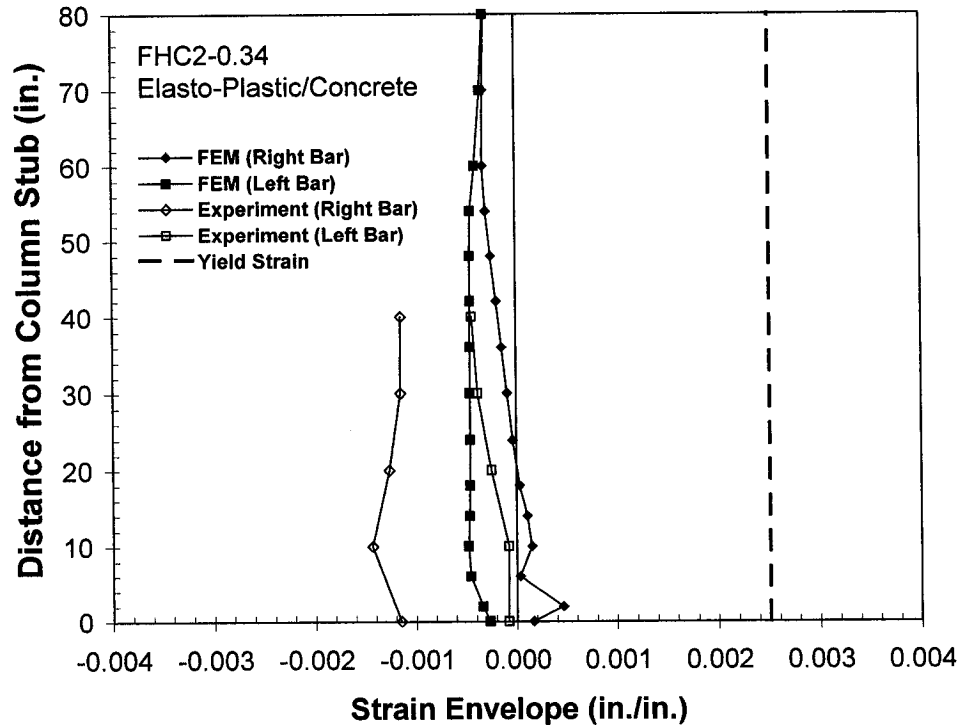
Fig. 6.55-Longitudinal Bar Strain Envelope along Column Length at Lateral Displacement of 5mm (0.2 in.)

For the transverse reinforcements, the axial strain envelopes remain in tension as shown in following charts. The highest confinement is provided by the first hoop at 50mm (2 inches) from the column stub and provided by ties at approximately 250mm (10 inches) from the column stub. The results of specimen FHC1-0.2 show that the longitudinal bar strain is smaller in value at the location of confinement. However, the axial strain of No. 36 (ASTM #11) longitudinal bar for specimen FHC2-0.34 is actually greater in value at the location of transverse reinforcement. As higher axial load is applied, it seems that longitudinal bars

467

exert higher stress in the confining hoop and ties causing greater elongation at the location of transverse reinforcements.

The following charts show transverse hoop and tie strains at a lateral displacement of 5mm (0.2 inches) at 0.286% drift for specimen FHC2-0.34.
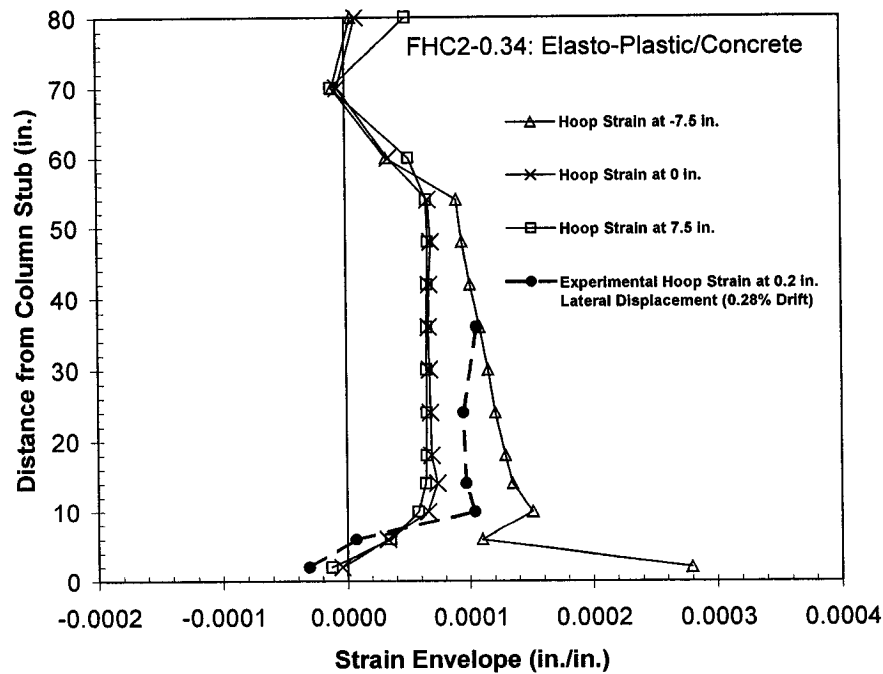
Fig. 6.56-Hoop Strains for FHC2-0.34 Model at 5mm (0.2 in.) Lateral Displacement (0.28% Drift).

468
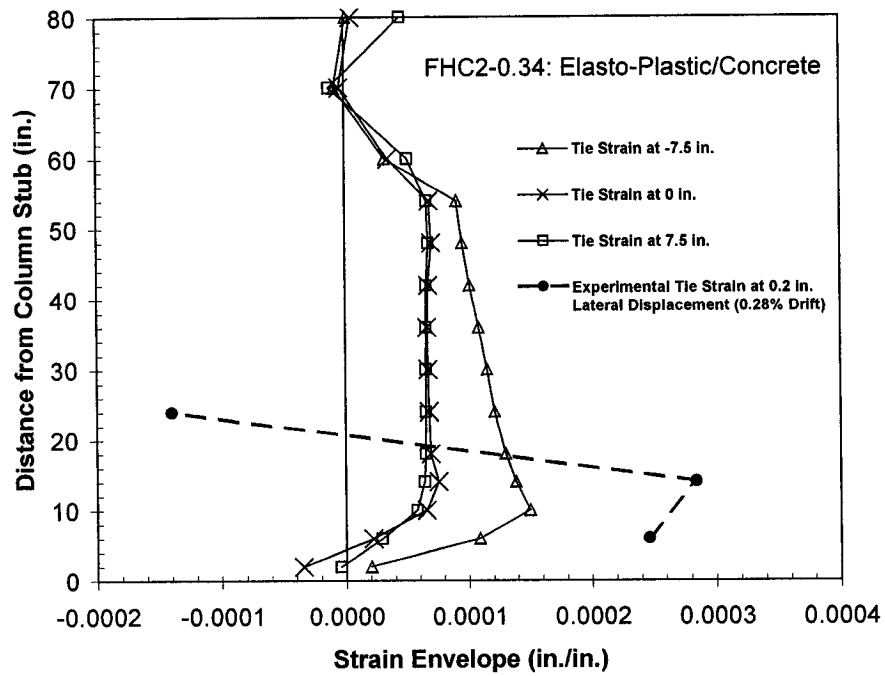
Fig. 6.57-Tie Strains for FHC2-0.34 Model at 5mm (0.2 in.) Lateral Displacement at 0.28% Drift.

469
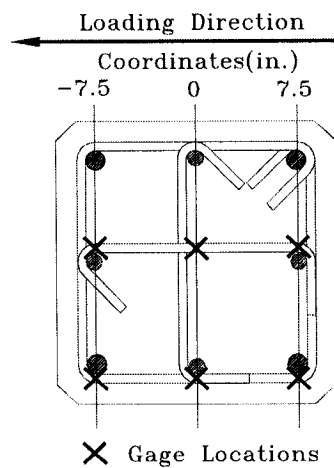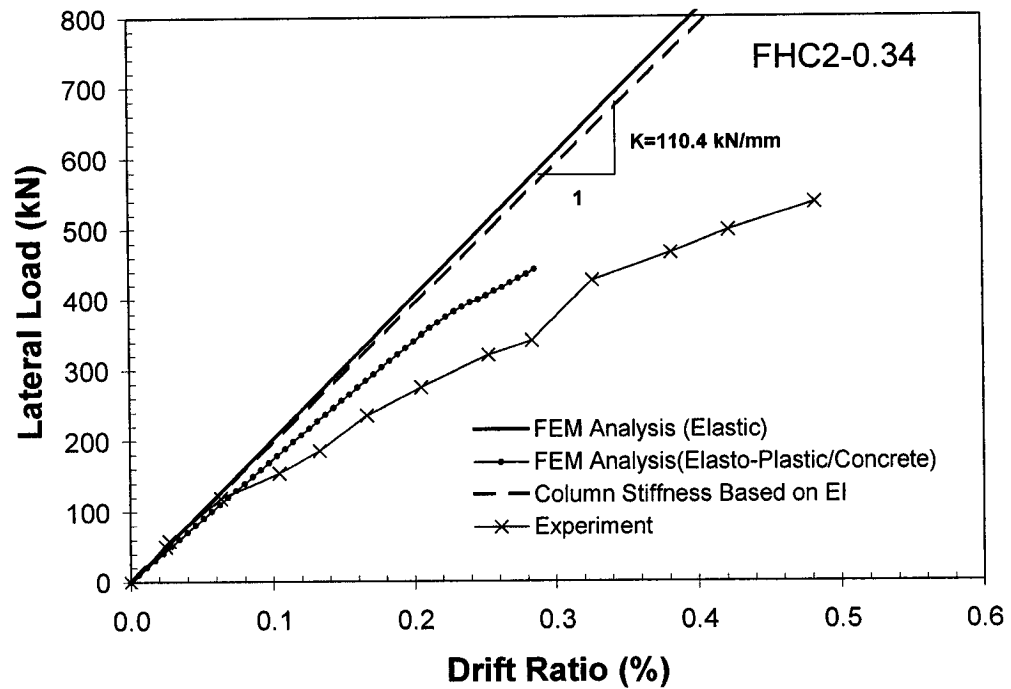
Fig. 6.58-Lateral Force vs. Drift Ratio Relationships for Specimen FHC2-0.34.

The load versus displacement above shows that the non-linear curve shows higher stiffness in comparison to that of specimen FHC1-0.2. It seems that higher axial load level actually increases the stiffness of the column even though the column deformability is decreased. The assumption of perfect bond between the concrete volumes and the reinforcements and an idealization of the placement of the reinforcements gave higher values. However, the slope of nonlinear curve during

470

the process of strength degradation show good correlation to the experimental result.

The ADINA program performed full Newton-Raphson interation methods with 50 time steps at 0.20 seconds each until convergence was achieved to reach the prescribed axial and lateral displacements for each model. Large stress and small strain were assumed with a maximum of 900 iterations executed per time step.

FEM model of the entire specimen FHC1-0.2 was analyzed with lateral loading applied at the height of 1780 mm (70 inches) measured from the top of the column stub. The column stub was completely fixed in all directions and axial load was applied to the column in vertical Z-direction only with a constant pressure equivalent to the experimental loads. Despite the convergence problems, a verification of experimental and analytical results were achieved through the FEM analysis.

For the first version of attempted full-column models using concrete elements which were discussed previously, the model did not converge or obtained non-positive stiffness matrix even beyond a very small lateral displacement due to instability in the plastic hinge area when both truss and Hermitian beam elements were used. Therefore, it was attempted to use beam and lateral pipe elements to

471

model the reinforcements and finer meshes in the plastic hinge area was used in order to achieve convergence, therefore, achieving successful executions of the program.

However, the major problem was that the program stopped before the prescribed displacements are reached. The message that the model stopped abnormally appears until the prescribed displacements had to be reduced to reach convergence. Also, upon the first crushing of the concrete near the cover region, the program stopped, and the input time step, in other words, the energy input exceeded the energy criteria used by the program causing the program to stop before reaching convergence.

The equilibrium iterations performed for each time step were used to re-establish equilibrium stiffness reformed to continue iteration for each consecutive step, based on energy criteria set by the program. Therefore, automatic time stepping (ATS) feature of the program along with smaller time steps and greater number of iterations were used to improve the convergence problems.

Despite many efforts to push-over beyond the concrete crushing and the point of peak shear capacity of the column, it was concluded that the large differences in the non-linearity of the two materials, concrete and steel, caused divergence of the solution beyond the elastic stage of the their deformations.

472

A trial run of the full-column model analysis for specimen FHC1-0.2 consisted of elasto-plastic bilinear elements for all materials including the concrete volumes. The model did not consider the micro-mechanics of the concrete material and assumed perfectly bilinear elasto-plastic behavior of all materials. Thus, the load versus displacement model response gave almost double the analytical result obtained from the Macro-approach in Chapter 5 due to the fact that plastic tensile stress remains throughout the analysis, where the tensile stress was assumed to be close to zero value for the concrete material model at a relatively small strain value. However, the result gave an anticipated pattern of degradation in the column capacity due to the elasto-plastic behavior of the elements.

When concrete material is idealized as elasto-plastic material with the same compressive and tensile strengths, it was possible to perform analysis to a greater lateral displacement. As the elasto-plastic material retained its tensile strength even at large values tensile strain, the values of lateral force versus displacement relationship were approximately 219% of the experimental result.

From the observation of the stress distribution obtained, the center of plastic hinge is located at approximately 356mm (14 inches) from the column stub. The maximum plastic strain in tension zone reached as high as 0.1295 at maximum lateral displacement of 150mm (6.0 inches) at 8.57% Drift Ratio. All volumes

473

within 610mm (24 inches) from the column stub reached their yield values. The concrete materials were assumed to behave bilinearly with an yield stress of 64.1 MPa (9.3 ksi) for the purpose of idealization. This analysis does not necessarily reflect in any way close to the experimental results since the use of elasto-plastic material with full tension value is unable to simulate the behavior of concrete material. However, it provides an insight on the stress contours for before and after the peak loads. The result hows that the damage is localized over a well defined hinge region. Further, the numerical model does not necessarily reflect the effect of cover spalling or strength degradations due to various failure modes of HSC columns such as cover-core interface failure due to tension across it.

6.6 RESULTS AND DISCUSSIONS OF MODEL GROUP TWO

New Set of Full-Column Analysis for Specimens FHC1-0.2 and FHC2-0.34

The Coulomb friction coefficient of 0.6 was used to model the contact between the reinforcements and their adjoining surfaces in all directions. As a result, greater lateral displacements were achieved. Further, FEM models with no concrete cover were analyzed to observe the stress distribution during the initial stage of the loading. With no concrete cover in the model, greater lateral

474

displacements were achieved without convergence problems since the crushing of the cover concrete in contact with the reinforcements was delayed. For the model with all concrete cover in place, the analysis stopped at smaller lateral displacement upon the first crushing in the cover concrete. In all models, the use of contact friction increased the achievable lateral displacements. However, the convergence problems due to large differences in non-linearity of concrete and steel persisted. Despite the difficulties, the analysis provided a further verification of the experimental results and insights on the behavior of concrete in the confined regions.

Energy-based BFGS Matrix Update method with line searches and 300 iterations per time step were used. The energy tolerance was set to 0.5 to improve convergence. The pipe elements were used for all reinforcements. The cross section of the pipe elements are given a radius equal to one half of its diameter.

Two versions of full-column models are: one with all of its cover concrete removed and the other with all of its concrete cover in place. Both models include two double sided three-dimensional contact surface groups.
The full-column model with all cover concrete removed consist of following number of elements and nodes:
441 nodes.

475

5 element groups:

Element group 1: 240 3D solid elements.

Element group 3: 56 beam-type pipe elements.

Element group 4: 56 beam-type pipe elements.

Element group 5: 8 3D solid elements.

Element group 6: 168 beam-type pipe elements.

528 elements total.

The full-column model with all cover concrete in place consist of following

number of elements and nodes:

665 nodes.

5 element groups:

Element group 1: 392 3D solid elements.

Element group 3: 56 beam-type pipe elements.

Element group 4: 56 beam-type pipe elements.

Element group 5: 24 3D solid elements.

Element group 6: 168 beam-type pipe elements.

696 elements total.

A constant poisson ratio of 0.15 and ACI recommended modulus of elasticity was

used for all concrete elements. For the full-column model, numerical problems

also occurred due to the complexity of the concrete material as well as due to

476

large differences in non-linearity of both concrete and its reinforcements. Kupfer concrete elements implemented in the program and pipe elements were used to capture the realistic mechanics of the materials. The non-linear analysis using iterative methods did not converge to provide solutions for large lateral displacements. Especially, upon the first crushing of the concrete, the solution diverged and the problem stopped execution. To resolve the problem, smaller time steps, automatic time stepping (ATS) methods, greater number of iterations, and BFGT method using line search were used. Also, the energy tolerance was increased to 0.5, and the strain-hardening modulus of all reinforcements were set to equal to 3% of their respective Young's modulus. Despite many attempts to surpass the displacement at the column peak capacity, the divergence problem upon first crushing of the concrete was inevitable. Therefore, it was further attempted to prescribe a Coulomb friction coefficient of 0.6 between the reinforcements and all of its adjoining surfaces for the entire model. This approach improved the results, and computation up to greater lateral displacement was feasible. However, the convergence problems persisted. It seems that the there is a limit to perform large displacement analysis of reinforced concrete FEM models due to large differences in the non-linearity between concrete and its reinforcements. Of all material models available, it seems that concrete model is one of the most complex ones since in reality, concrete is a very complex material.

477

A static push over analysis with constant axial load for full-column model with all cover concrete removed as shown in figure 6.59 reached a lateral displacement of 35.6mm (1.4 inches) with use of high tangent modulus of 68,950 MPa (10,000 ksi) for all reinforcements to reach convergence. When actual bilinear elasto-plastic model is used for the reinforcements with tangent modulus equal to 3% of elastic Young's modulus, the results were obtained up to lateral displacement of 25.4mm (1.0 inch) for specimen FHC1-0.2 with no cover concrete. Upon first yielding of longitudinal reinforcement, the no-cover model of both specimens FHC1-0.2 and FHC2-0.34 show the stresses initially concentrated in the plastic hinge area is distributed along the column span is dispersed manner as concrete and the reinforcements deform in different manner. The phenomenon occurred along the entire length of the column for specimen FHC1-0.2 but occurred only in the vicinity of the plastic hinge area for specimen FHC2-34. The damage is more concentrated in the plastic hinge area for higher axial load applications.

For the full-column model with all concrete cover in place as shown in figure 6.60, it was possible to obtain solution and to verify the experimental results up to a displacement of approximately 13.2mm (0.52 inches). At early stages of loading, the cover concrete in the plastic hinge area are subjected to highest stress values and the stress value is substantially less within the confined region. The

478

specimen FHC1-0.2 is provided with an axial load ratio of 0.2 and concrete compressive stress of f_c'=64.2 MPa (9.3 ksi). The depth of compression zone on the column section of plastic hinge increased at the initial stage of loading and decreased as lateral displacement is increased up to 13.2mm (0.52 inches). The confinement effect of core concrete gradually decreases away from column stub reaching almost zero value at the location of lateral load application. The greatest concrete tensile stress in the plastic hinge area is located approximately 254mm (10 inches) from the column stub at a lateral displacement of 13.2mm (0.52 inches).

The specimen FHC2-0.34 is subjected to higher axial load ratio of 0.34 and concrete strength of f_c'=62.1 MPa (9.0 ksi). The depth of compression on the column section in the plastic hinge area is much greater in comparison to that of specimen FHC1-0.2. The confinement effect of the core concrete seems to decrease at a greater rate toward the point of lateral load application. The greatest concrete tensile stress in the plastic hinge area is located approximately 457mm (18 inches) from the column stub at a lateral displacement of 12.7mm (0.5 inches).

The increased compression depth of column section in the plastic hinge due to higher axial load level results in increased energy dissipation and higher

479

concentration of stresses in the plastic hinge area as well as in the column span, causing greater amount of crack damages both in confined and unconfined regions.

The lateral force versus drift ratio results are shown in figure 6.61 for the model without and with cover concrete. The cover concrete provides greater initial capacity, however, a limited displacement can be reached, where the model without any cover concrete converged at greater lateral displacement as previously mentioned. This shows that if crushing of the cover concrete in contact with the reinforcements is avoided, analytical results may be obtained up to a greater lateral displacement. The figures 6.62 to 6.64 show that a peak capacity is reached for the model without any concrete cover, where the model with all cover in place converged up to a limited drift ratio.

480
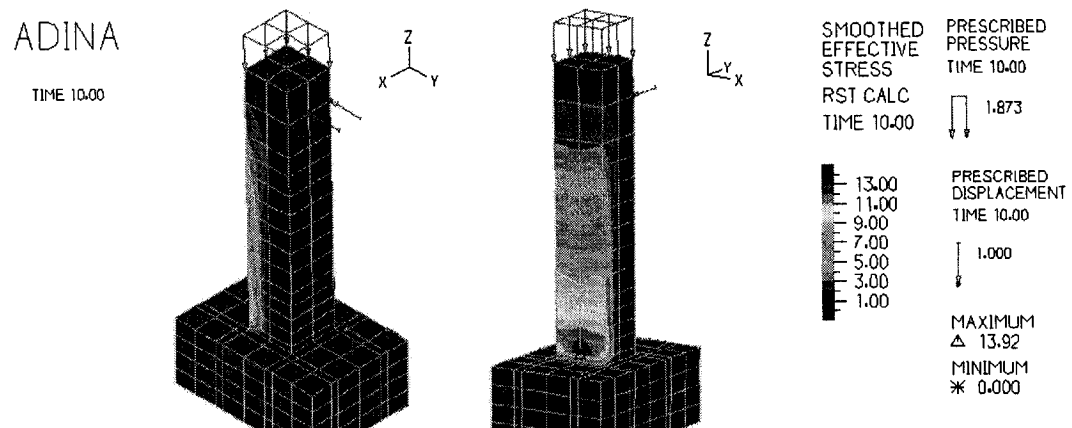
Fig. 6.59-Specimen FHC1-0.2 with all cover concrete removed (Values shown in ksi)
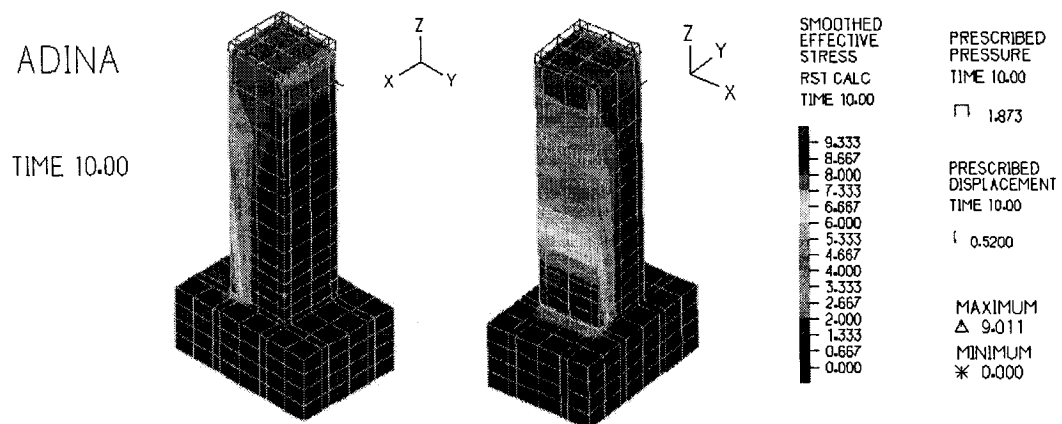
Fig. 6.60-Specimen FHC1-0.2 with all concrete cover in place (Values shown in ksi)

481
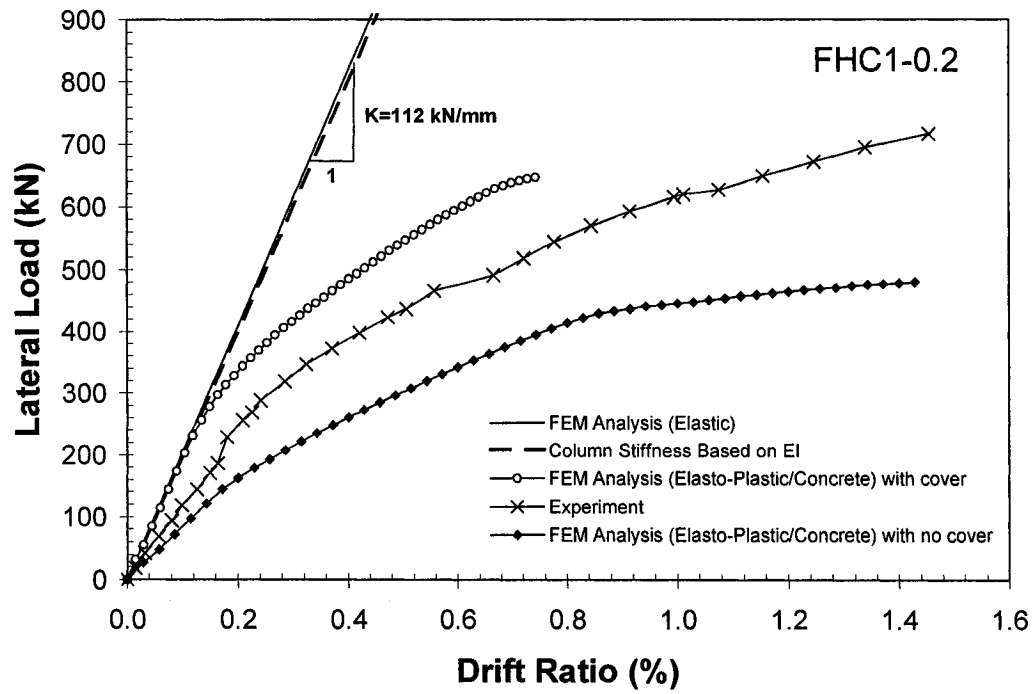
Fig. 6.61- Comparison of Lateral Force vs. Drift Ratio Relationships for Specimen FHC1-0.2 with to Experimental Results.

482
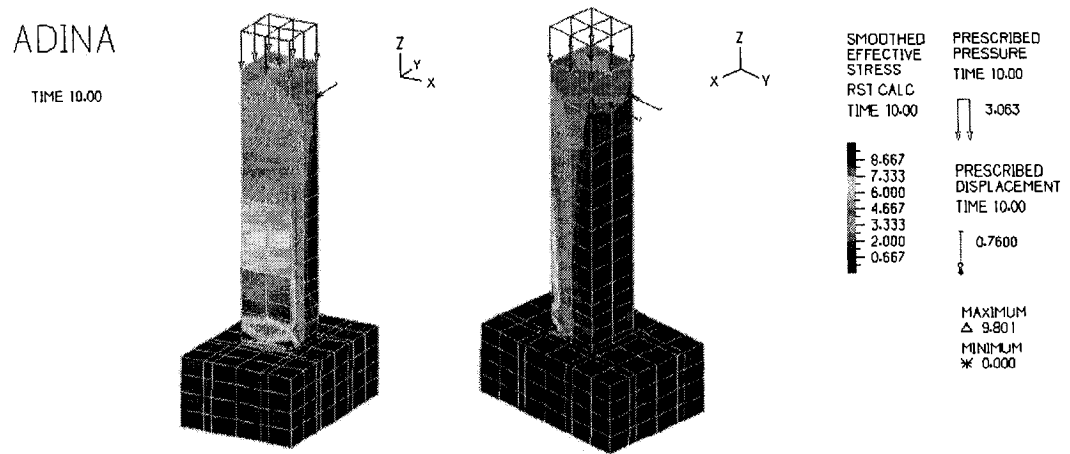
Fig. 6.62-Specimen FHC2-0.34 with all cover concrete removed (Values shown in ksi)
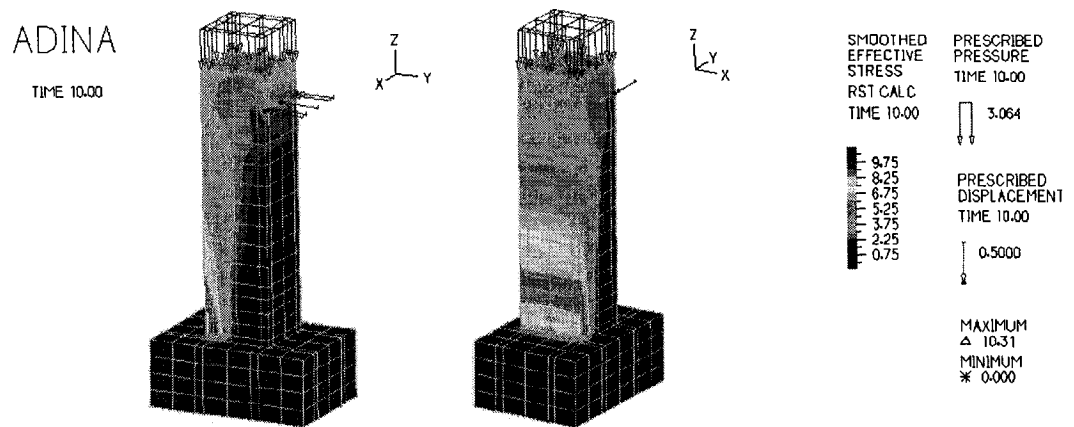
Fig. 6.63-Specimen FHC2-0.34 with all concrete cover in place (Values shown in ksi)

483
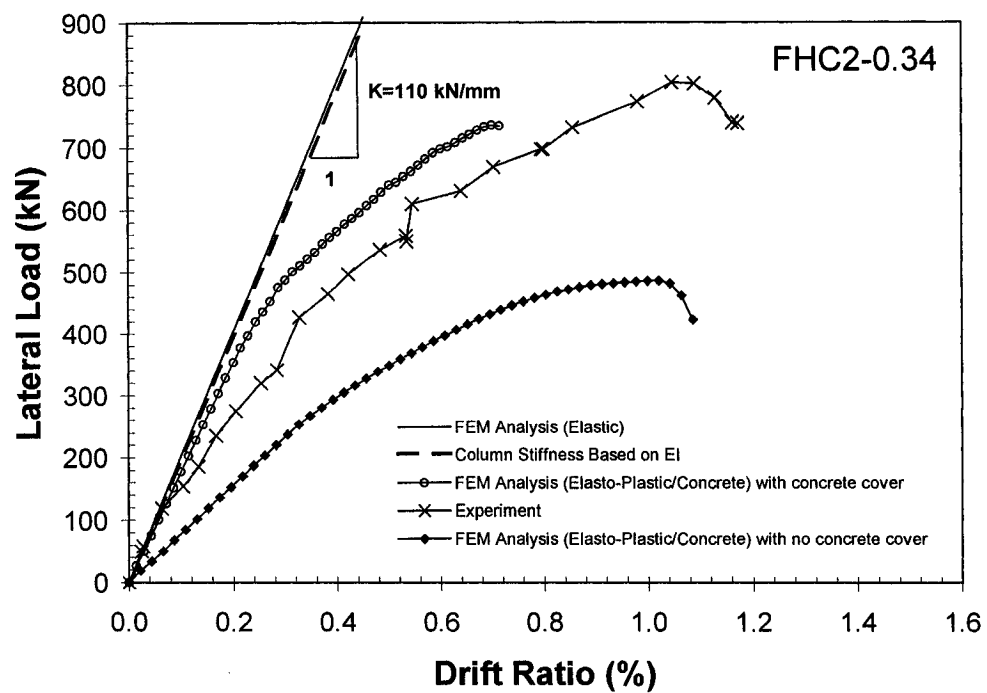
Fig. 6.64- Comparison of Lateral Force vs. Drift Ratio Relationships for Specimen FHC2-0.34 to Experimental Results.

484

Trial Analysis for Specimens FHC1-0.2 and FHC2-0.34

A trial analysis for the identical model of specimens FHC1-0.2 and FHC2-0.34 with all cover in place was performed with use of an empirical equation of modulus of elasticity of high-strength concrete. The equation is as following:

$$E_c = 18,000\sqrt{f_c'} + 2.1 \times 10^6 \text{ (psi)}$$

An increased constant value of poisson ratio of concrete, 0.18, and unusually high values of strain-hardening modulus of all reinforcements, which are almost identical to the initial modulus of elasticity of reinforcements, were used to observe the their effect on achievable lateral displacement and corresponding peak shear values of the model. This approach resulted in increased achievable lateral displacements of up 33.5mm (1.32 in.) for specimen FHC1-0.2 and 25.2mm (0.992 in.) for specimen FHC2-0.34 without convergence problems. Due to unrealistically high values of the strain-hardening modulus of the reinforcements, the results greatly overestimated the experimental values as shown in figures 6.65 and 6.66. However, the cracking and stress distributions were obtained at lateral displacements approximately corresponding to the experimental peak shear values of specimens FHC1-0.2 and FHC2-0.34 as following as shown in the following figures 6.67 to 6.98.

485

The figures 6.67 to 6.72 show stress distribution of the full-column for specimen

FHC1-0.2 at various drift ratios up to a maximum drift of 1.89%. The point of

highest stress is located at approximately 50.8mm (2 inches) from the column

stub. The stress distribution of column cross sections at various distances away

from column stub in the plastic hinge area are shown in figure 6.73 at drift ratio of

1.89%. The results indicate that the maximum stress of the cross section is

located at the intersection of the cover concrete and the confinement hoop in the

compressive zone. A stress distribution of a mid-cut section of the column also

indicate the same location of maximum stress.

The crack distributions as shown in figures 6.74 to 6.79 indicate that an

approximate length of substantially damaged zone at drift ratio of 1.89% is

508mm (20 inches), where the empirical plastic hinge length as described in

section 2.7 was 470mm (18.5 inches).

As shown in figure 6.83, the first crushing of cover concrete occurred at a drift

ratio of 1.21%. The figures 6.80 to 6.85 show that initial horizontal flexural

cracks formed at 0.26%, and the crack formation propagated from the concrete

cover to the center of the confined concrete where shear cracks began to form as

the drift ratio increased.

For full-column model of specimen FHC2-0.34, the stress distributions shown in

figures 6.86 to 6.89 indicate a similar as those of specimen FHC1-0.2 with

486

greater depth of compression zone. A cut section of the model as shown in figure 6.90 also indicate that the maximum stress is located at the boundary between the cover concrete and the confinement hoop in the compression zone of the column cross section at drift ratio of 1.42%. The figures 6.91 to 6.94 show that the length of the most damaged zone indicated by cracks is approximately 14 inches (356mm) at a drift ratio of 1.42%, less than that of specimen FHC1-0.2. The crack distributions shown in figures 6.95 to 6.98 indicate that first crushing of cover concrete occurred at approximately 1% drift ratio. The formation of flexural cracks in the concrete cover did not propagate as closely to the center of the confined concrete in comparison to specimen FHC1-0.2. The comparison of figures 6.83 and 6.97 at the same drift ratio of 1.20% demonstrates that the specimen FHC1-0.2 with lower axial load level has greater amount of flexural cracks with less crushing of cover concrete in comparison to specimen FHC2-0.34 subjected to high axial load.

487
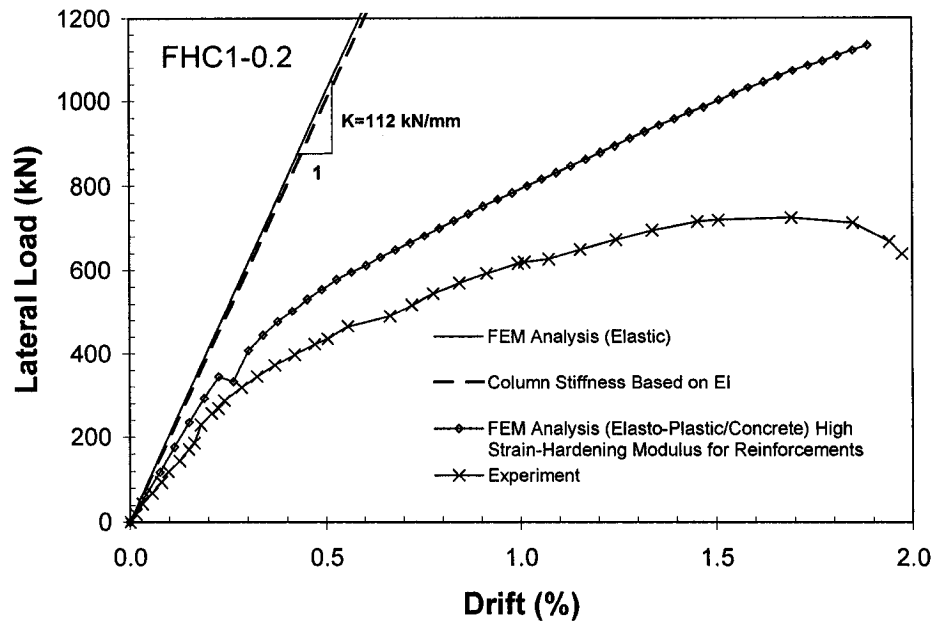
Fig. 6.65- Comparison of Lateral Force vs. Drift Ratio Relationships for Model Specimen FHC1-0.2 with Reinforcements of High Strain-Hardening Modulus.

488
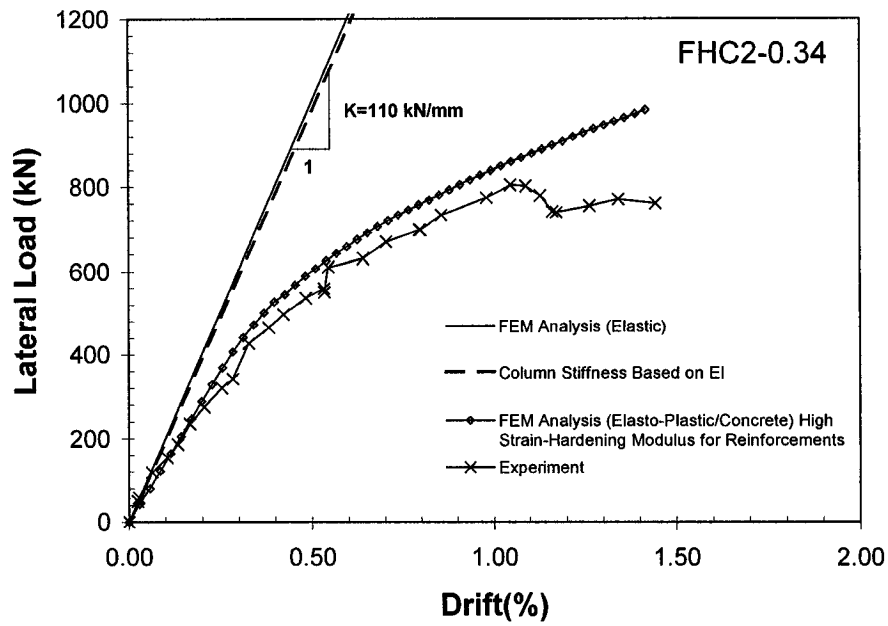
Fig. 6.66- Comparison of Lateral Force vs. Drift Ratio Relationships for Model Specimen FHC2-0.34 with Reinforcements of High Strain-Hardening Modulus.

489
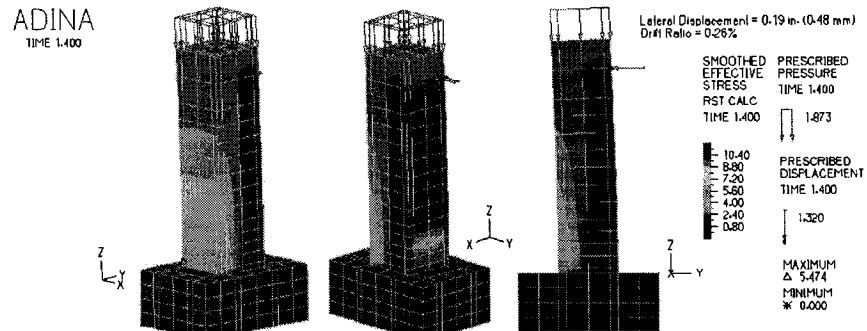
Fig. 6.67-Effective Stress Distribution of Specimen FHC1-0.2 at Drift Ratio of 0.26%.
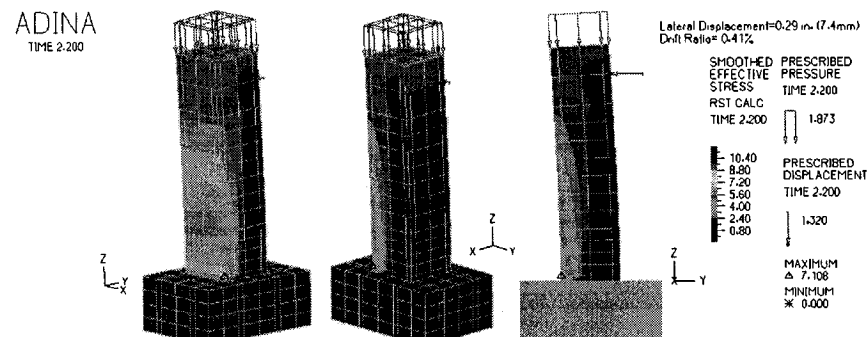
Fig. 6.68-Effective Stress Distribution of Specimen FHC1-0.2 at Drift Ratio of 0.41%.
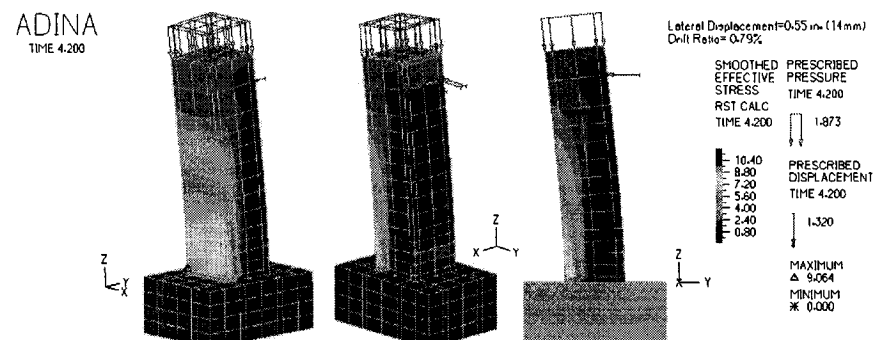
Fig. 6.69-Effective Stress Distribution of Specimen FHC1-0.2 at Drift Ratio of 0.79%.

490

ADINA
TIME 6.400

Lateral Displacement=0.85in. (21.5mm)
Drift Ratio= 1.21%

SMOOTHED PRESCRIBED
EFFECTIVE PRESSURE
STRESS TIME 6.400
RST CALC
TIME 6.400   1.873

    10.40   PRESCRIBED
    8.80   DISPLACEMENT
    7.20   TIME 6.400
    5.60
    4.00   1.320
    2.40
    0.80
                   MAXIMUM
                   △ 9.728
                   MINIMUM
                   ✳ 0.000
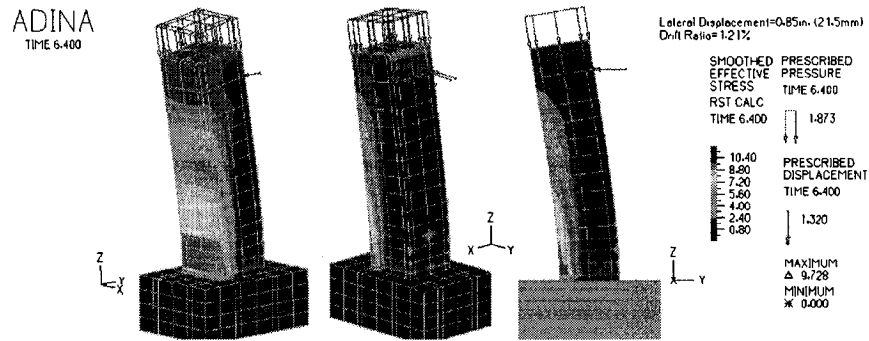
Fig. 6.70-Effective Stress Distribution of Specimen FHC1-0.2 at Drift Ratio of 1.21%.

ADINA
TIME 8.600

Lateral Displacement= 1.14in. (28.8mm)
Drift Ratio= 1.62%

SMOOTHED PRESCRIBED
EFFECTIVE PRESSURE
STRESS TIME 8.600
RST CALC
TIME 8.600   1.873

    10.40   PRESCRIBED
    8.80   DISPLACEMENT
    7.20   TIME 8.600
    5.60
    4.00   1.320
    2.40
    0.80
                   MAXIMUM
                   △ 10.48
                   MINIMUM
                   ✳ 0.000
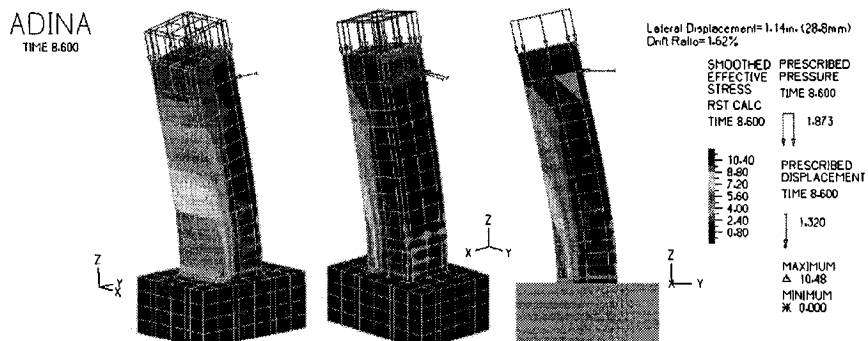
Fig. 6.71-Effective Stress Distribution of Specimen FHC1-0.2 at Drift Ratio of 1.62%.

ADINA
TIME 10.00

Lateral Displacement= 1.32in.(33.5mm)
Drift Ratio= 1.89%

SMOOTHED PRESCRIBED
EFFECTIVE PRESSURE
STRESS TIME 10.00
RST CALC
TIME 10.00   1.873

    10.40   PRESCRIBED
    8.80   DISPLACEMENT
    7.20   TIME 10.00
    5.60
    4.00   1.320
    2.40
    0.80
                   MAXIMUM
                   △ 10.91
                   MINIMUM
                   ✳ 0.000
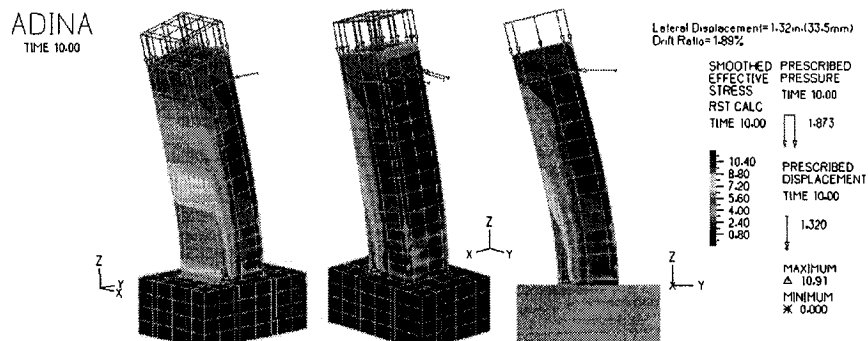
Fig. 6.72-Effective Stress Distribution of Specimen FHC1-0.2 at Drift Ratio of 1.89%.

491
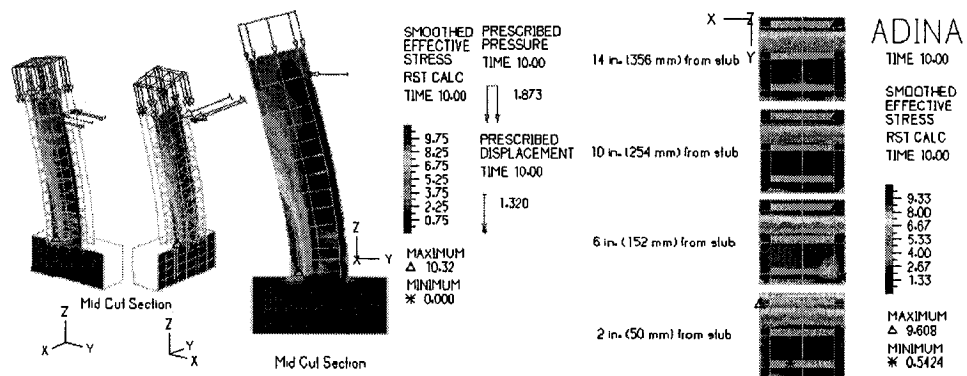
Fig. 6.73- Stress Distribution of Column Cross Section in Plastic Hinge Area for Specimen FHC1-0.2 at Drift Ratio of 1.89%.

492
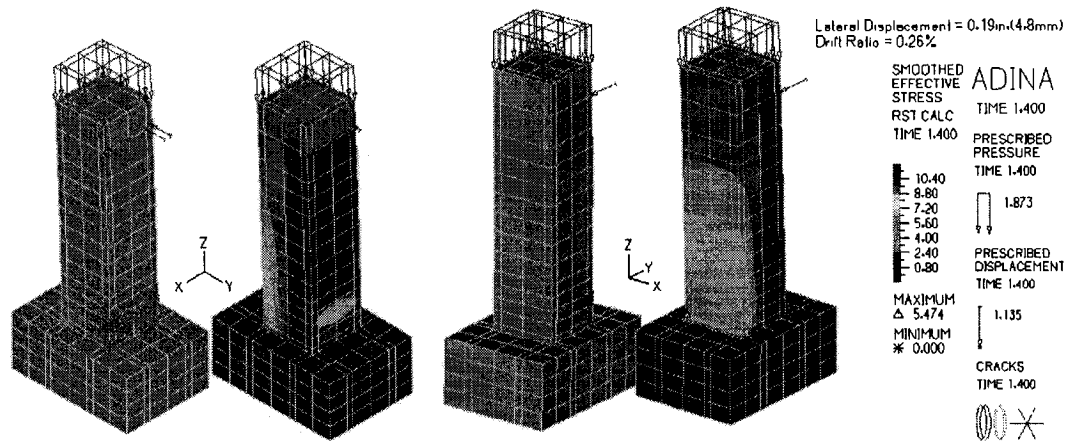
Fig. 6.74-Crack Distribution of Specimen FHC1-0.2 at Drift Ratio of 0.26%.
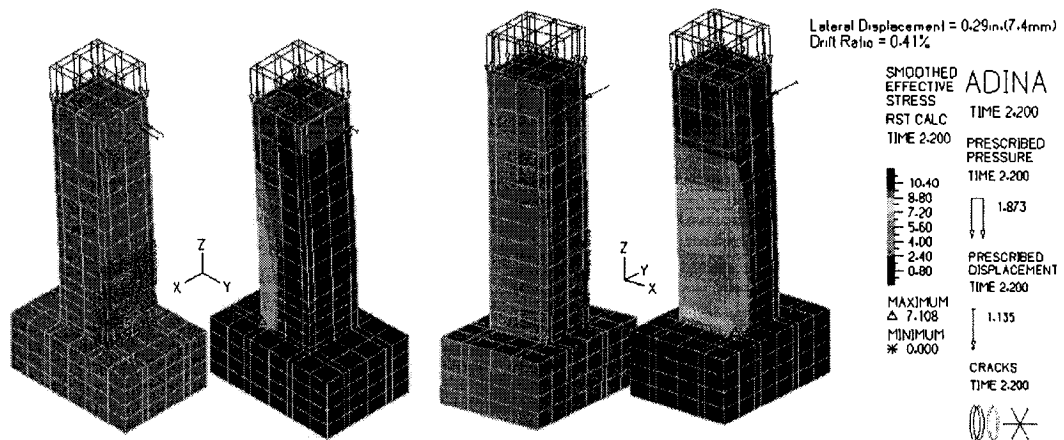
Fig. 6.75-Crack Distribution of Specimen FHC1-0.2 at Drift Ratio of 0.41%.

493
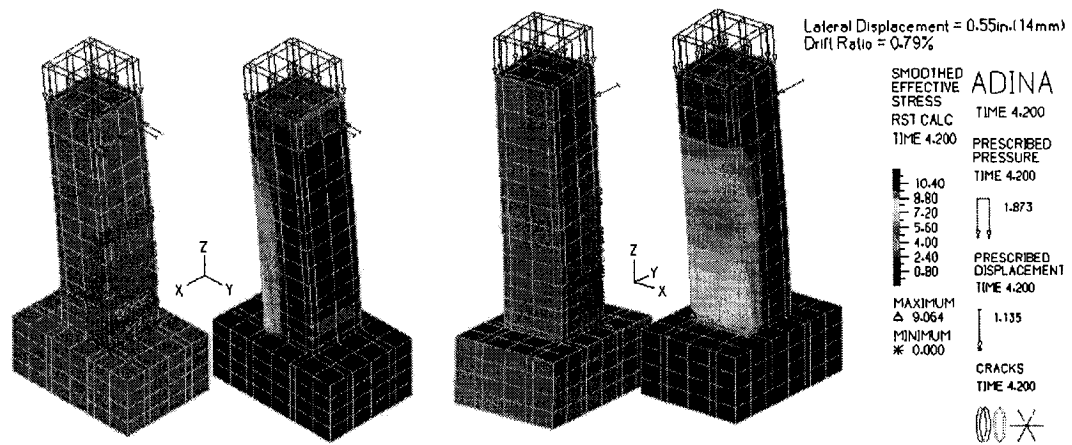
Fig. 6.76-Crack Distribution of Specimen FHC1-0.2 at Drift Ratio of 0.79%.
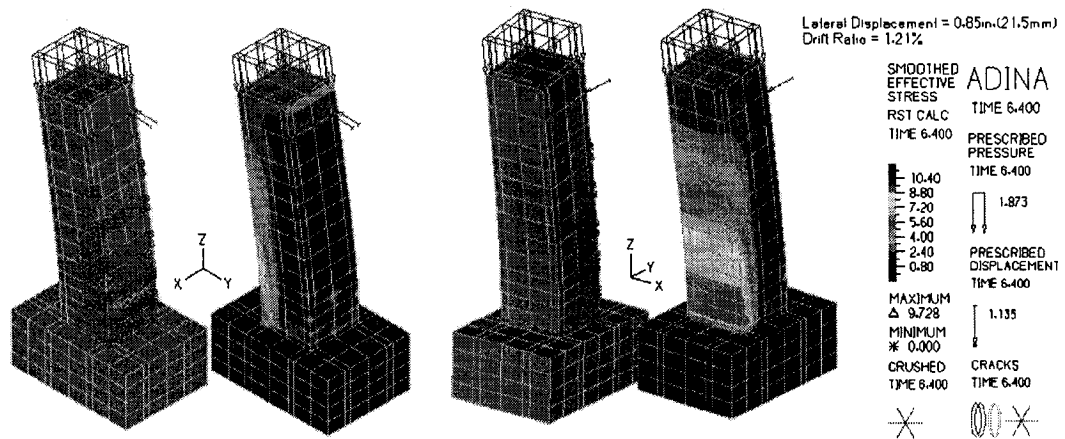
Fig. 6.77-Crack Distribution of Specimen FHC1-0.2 at Drift Ratio of 1.21%.

494
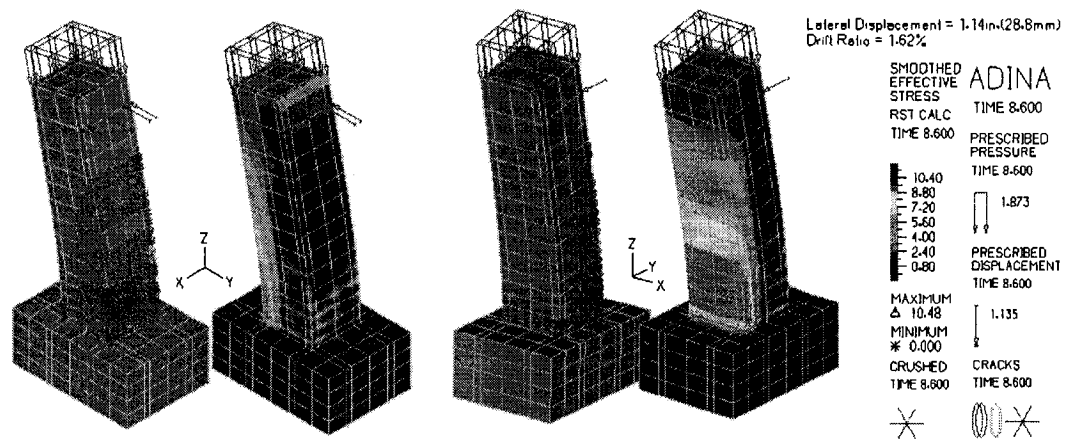
Fig. 6.78-Crack Distribution of Specimen FHC1-0.2 at Drift Ratio of 1.62%.
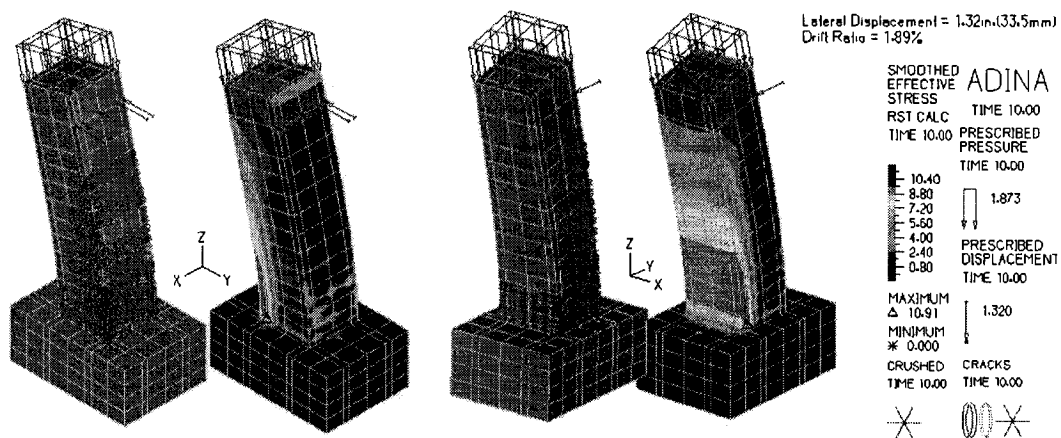
Fig. 6.79-Crack Distribution of Specimen FHC1-0.2 at Drift Ratio of 1.89%.

495
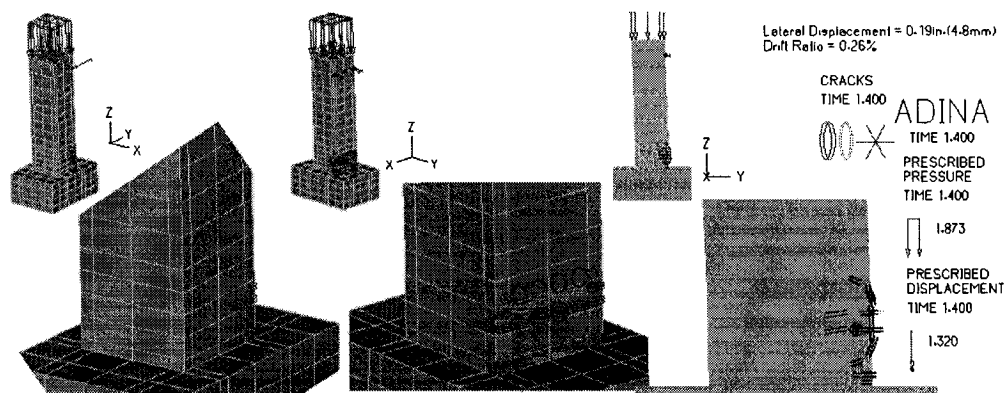
Fig. 6.80-Crack Distribution of Plastic Hinge Area for Specimen FHC1-0.2 at Drift Ratio of 0.26%.
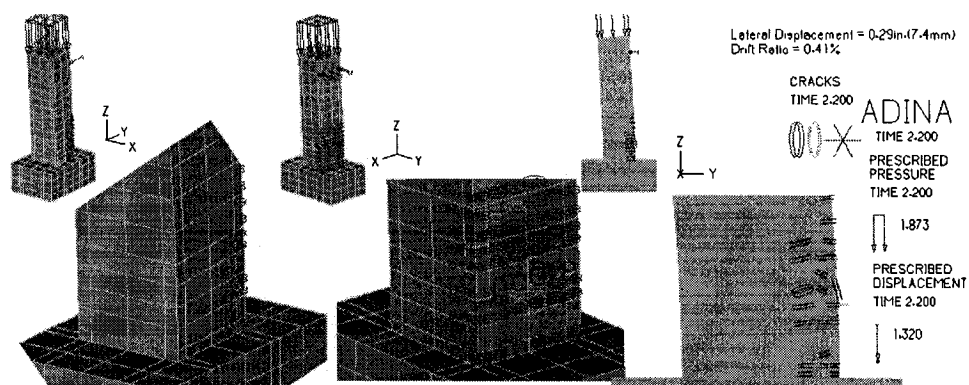
Fig. 6.81-Crack Distribution of Plastic Hinge Area for Specimen FHC1-0.2 at Drift Ratio of 0.41%.

496
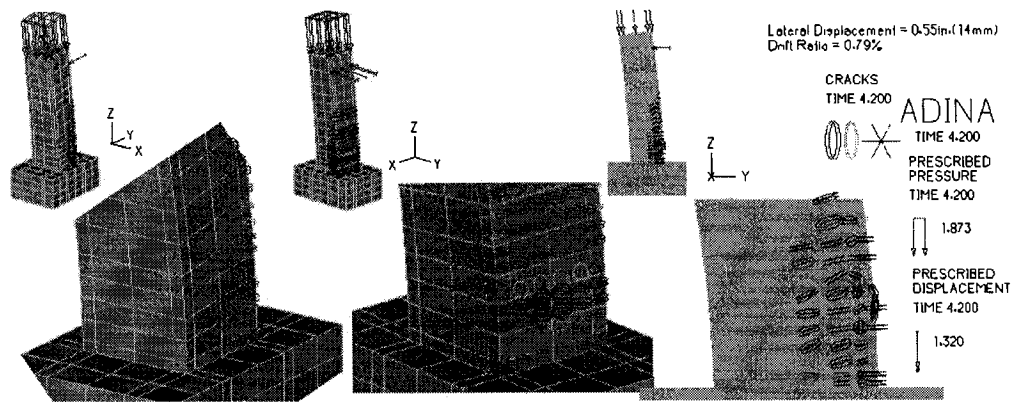
Fig. 6.82-Crack Distribution of Plastic Hinge Area for Specimen FHC1-0.2 at Drift Ratio of 0.79%.
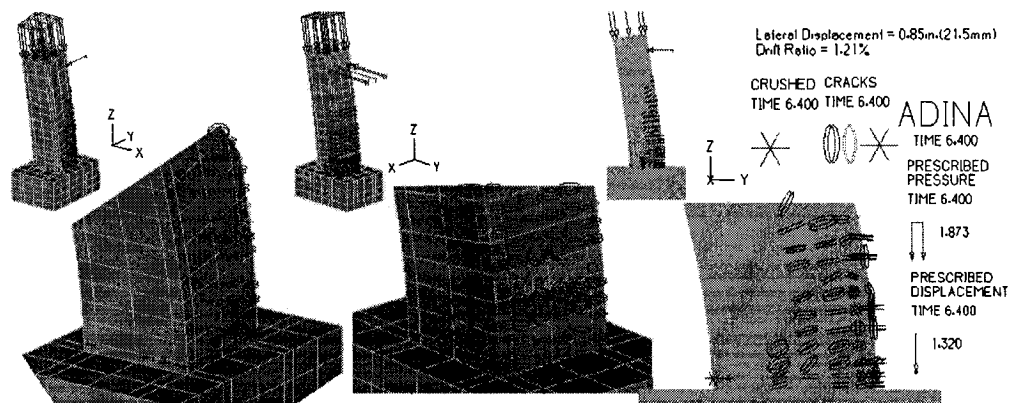
Fig. 6.83-Crack Distribution of Plastic Hinge Area for Specimen FHC1-0.2 at Drift Ratio of 1.21%.

497
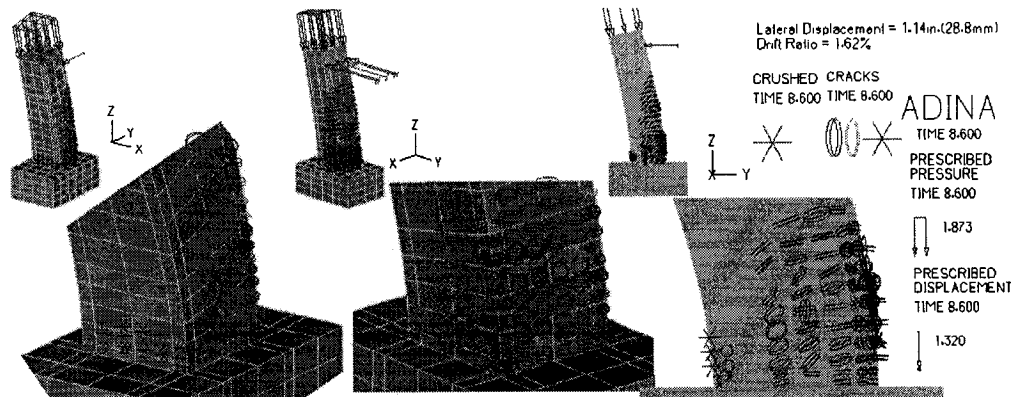
Fig. 6.84-Crack Distribution of Plastic Hinge Area for Specimen FHC1-0.2 at Drift Ratio of 1.62%.
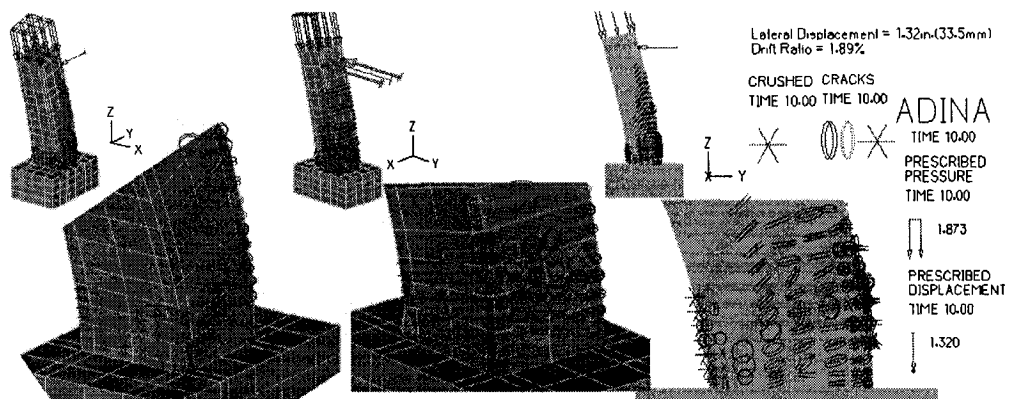
Fig. 6.85-Crack Distribution of Plastic Hinge Area for Specimen FHC1-0.2 at Drift Ratio of 1.89%.

498
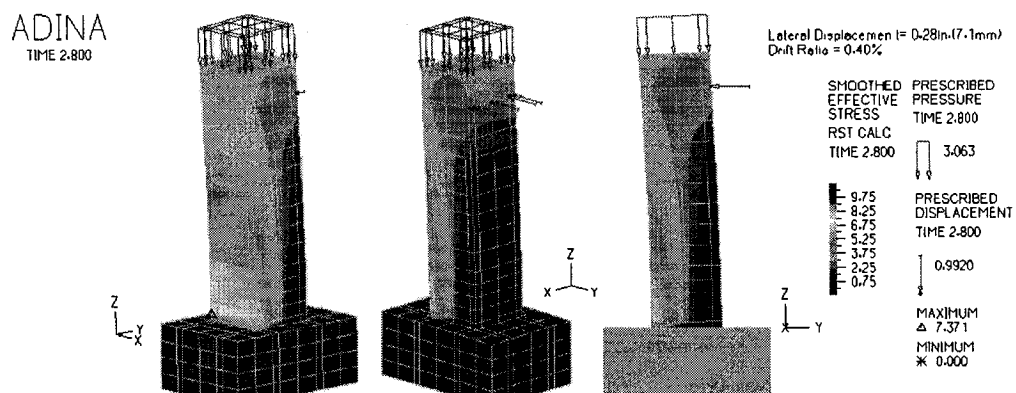
Fig. 6.86-Effective Stress Distribution of Specimen FHC2-0.34 at Drift Ratio of 0.4%.
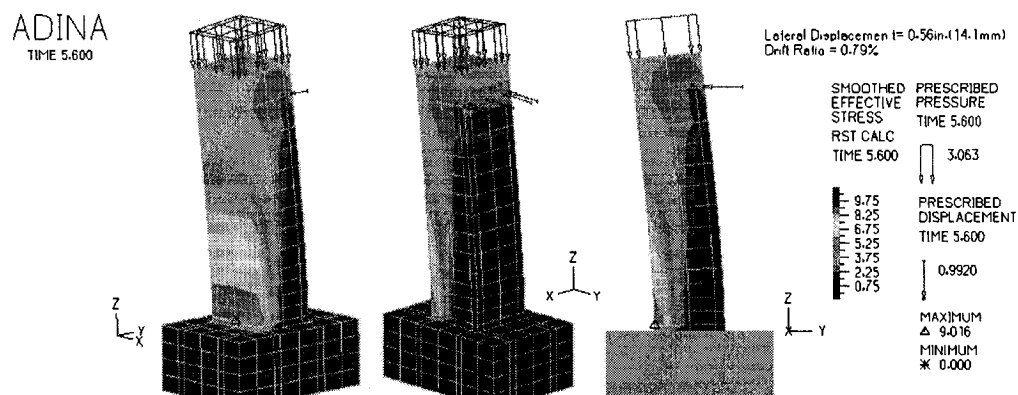
Fig. 6.87-Effective Stress Distribution of Specimen FHC2-0.34 at Drift Ratio of 0.79%.

499
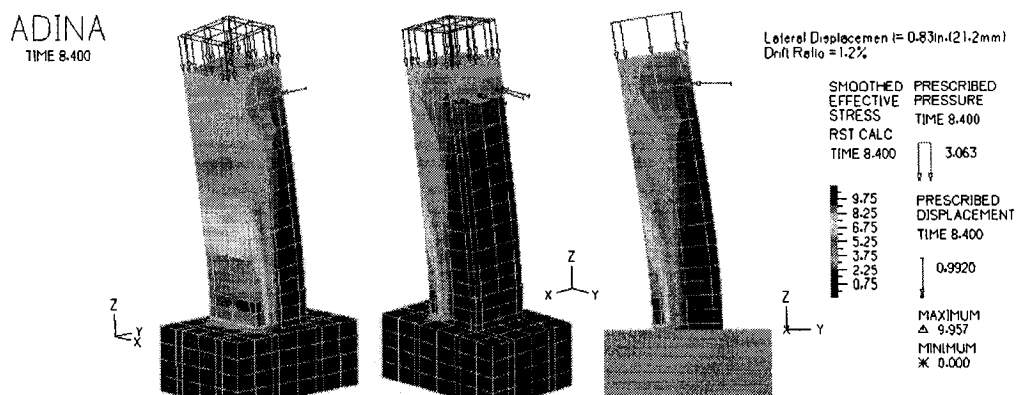
Fig. 6.88-Effective Stress Distribution of Specimen FHC2-0.34 at Drift Ratio of 1.2%.
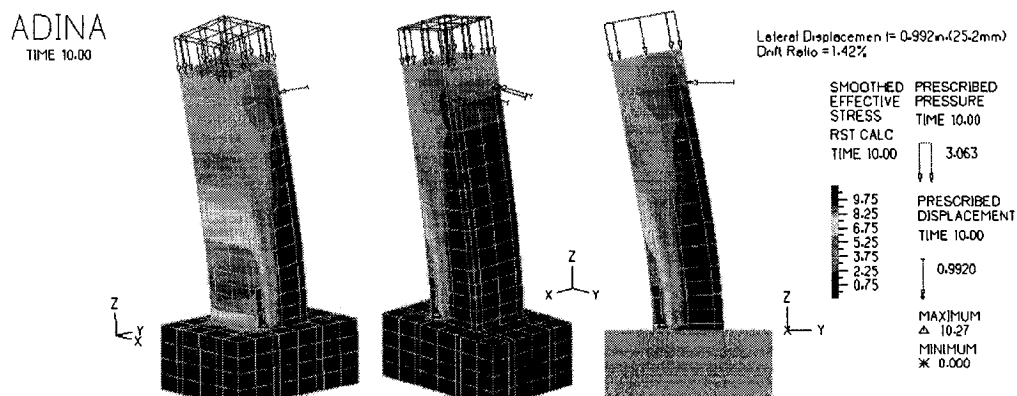
Fig. 6.89-Effective Stress Distribution of Specimen FHC2-0.34 at Drift Ratio of 1.42%.

500
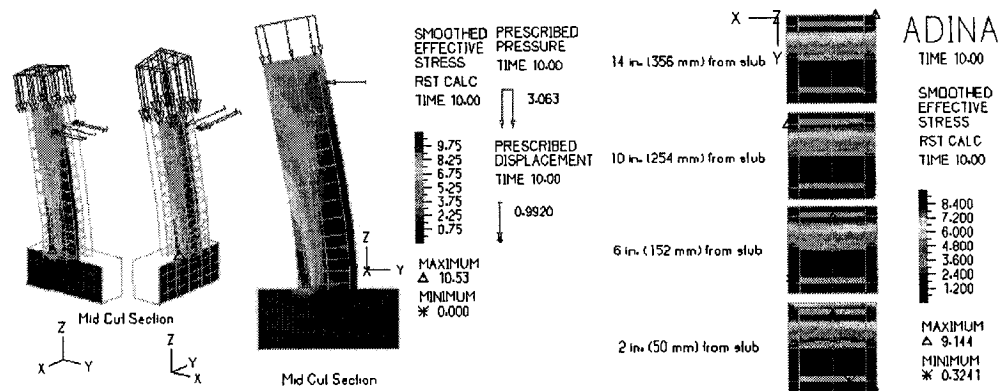
Fig. 6.90- Stress Distribution of Column Cross Section in Plastic Hinge Area for Specimen FHC2-0.34 at Drift Ratio of 1.42%.

501
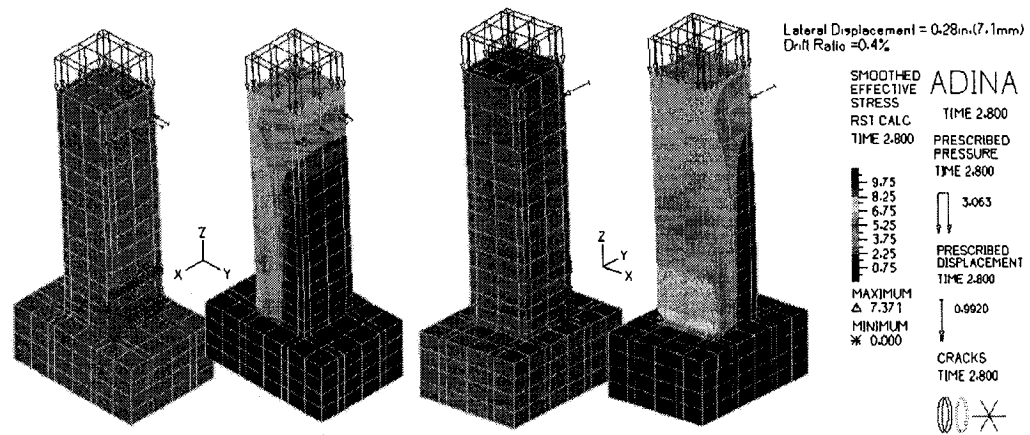
Fig. 6.91-Crack Distribution of Specimen FHC2-0.34 at Drift Ratio of 0.4%.
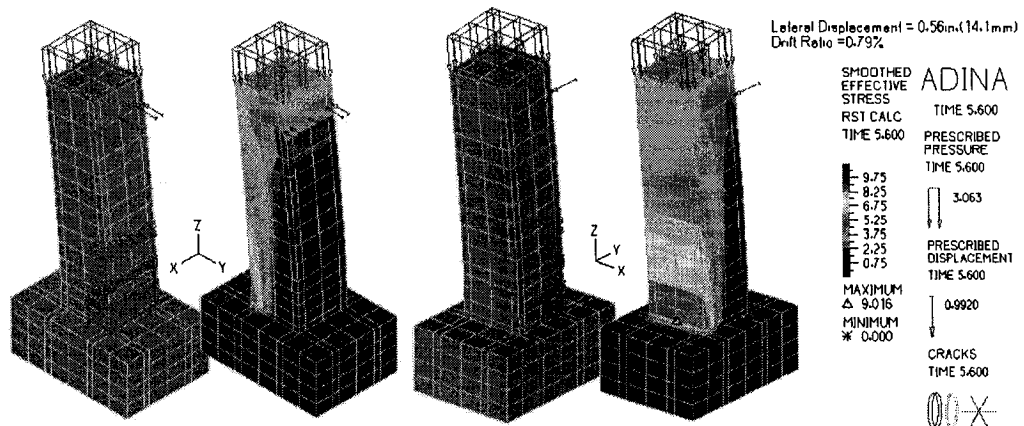
Fig. 6.92-Crack Distribution of Specimen FHC2-0.34 at Drift Ratio of 0.79%.

502
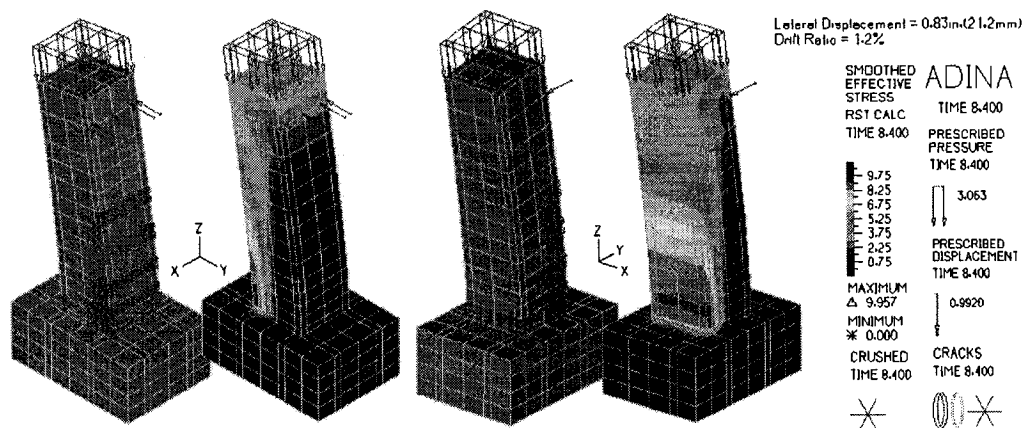
Fig. 6.93-Crack Distribution of Specimen FHC2-0.34 at Drift Ratio of 1.2%.
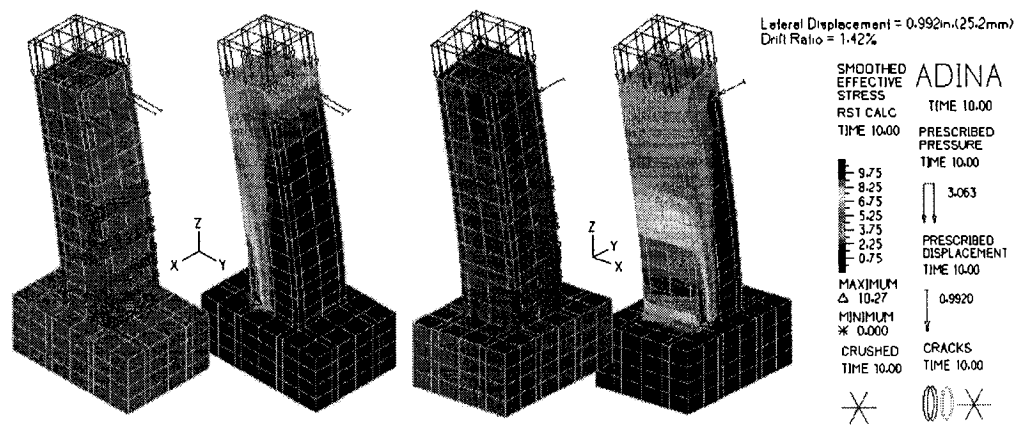
Fig. 6.94-Crack Distribution of Specimen FHC2-0.34 at Drift Ratio of 1.42%.

503
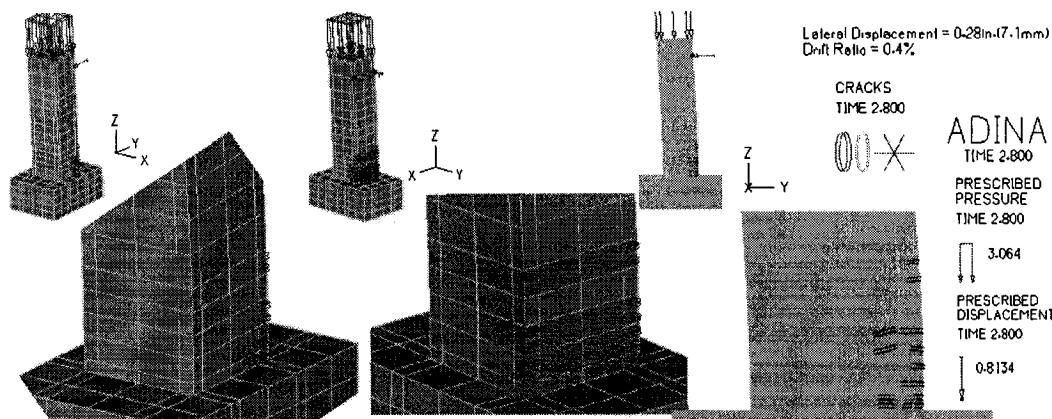
Fig. 6.95-Crack Distribution of Plastic Hinge Area for Specimen FHC2-0.34 at Drift Ratio of 0.4%.
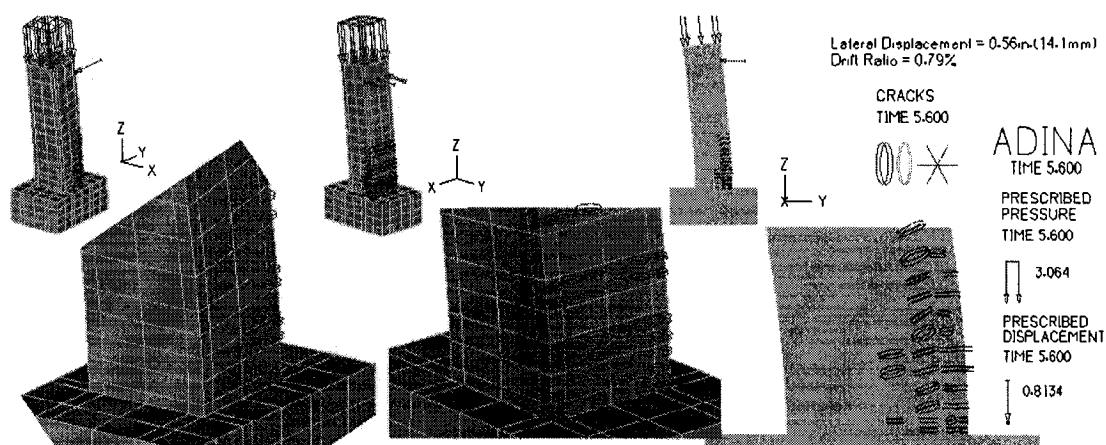
Fig. 6.96-Crack Distribution of Plastic Hinge Area for Specimen FHC2-0.34 at Drift Ratio of 0.79%.

504
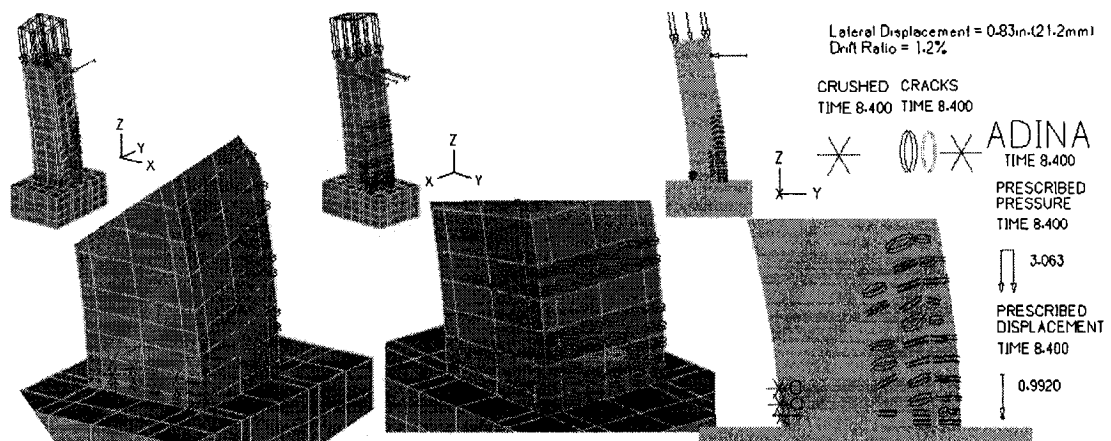
Fig. 6.97-Crack Distribution of Plastic Hinge Area for Specimen FHC2-0.34 at Drift Ratio of 1.2%.
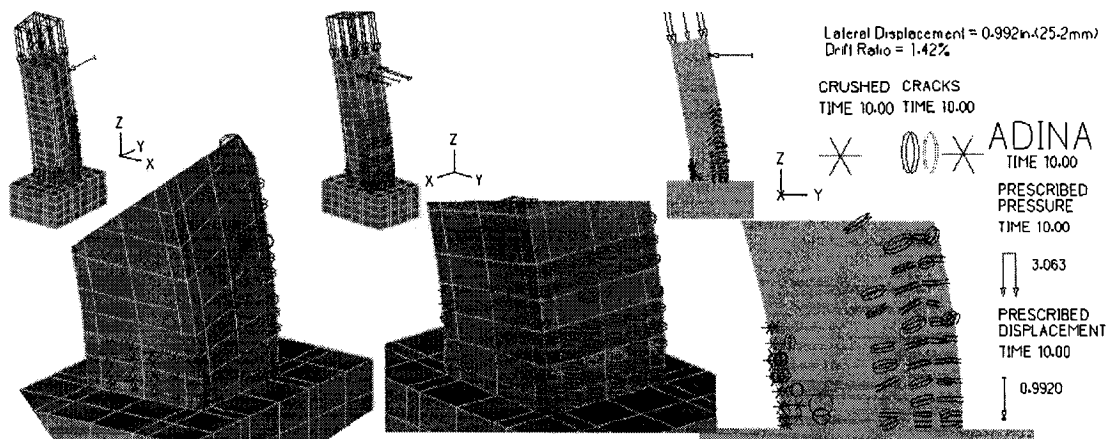
Fig. 6.98-Crack Distribution of Plastic Hinge Area for Specimen FHC2-0.34 at Drift Ratio of 1.42%.

505

6.7 RESULTS AND DISCUSSIONS OF MODEL GROUP THREE

With all parameters equal as previous full-column models of group two (Section

6.6), an increased constant poisson ratio of 0.2 was set for the following models

of specimens FHC1-0.2 and FHC2-0.34. Further, the strain-hardening modulus of

all reinforcements were interpolated from the average of experimental tensile test

results. The empirical modulus of elasticity of concrete for high strength concrete

as previously mentioned in Section 6.6 was used. The figures 6.99 and 6.100

show that analysis using finite element method correlated well with the

experimental results up to the column peak capacities for specimens FHC1-0.2

and FHC2-0.34.

Considering the assumptions made in finite element modeling such as idealized

geometry, assumed friction coefficient between the concrete and its

reinforcements, and the use of material properties which mostly resemble the high

strength concrete, the results were remarkably accurate when compared to the

experimental values. The stress distributions, crack formation, and overall

mechanical behavior was shown to correlate to the experimental results. To

enhance the future finite element modeling of reinforced concrete members, it is

advisable to prescribe contact friction between the concrete and steel elements

and to make sure that all material properties are properly input. Further, a true

506

value of strain-hardening modulus should be used to reduce convergence problems. Automatic time step using small time steps are recommended, where times steps which are too small will require tremendous amount of processing time and a large disk space. The modeling should always begin with a simple preliminary model to confirm proper execution. Linear analysis should be performed first prior to engaging in a non-linear analysis to avoid complications. Proper unit should be chosen from the beginning of the modeling to avoid the need to manually convert all units after the modeling is completed. It is advisable to always work copies of the original model in consideration of future revision of the model. The element and line numbers used for meshing and defining the elements should be save in a separate data file for future references. The time spent in planning the model and consideration of various alternatives of the model prior to making a final choice is extremely important.

When poisson ratio for concrete element is too low, the only small lateral displacement is reached without convergence problems. When poisson ratio is higher, a limited but greater lateral displacement can be reached without any convergence problems. Further, it is important to set the tolerances appropriately in order to achieve convergence. The convergence tolerances are set as following:

507

Energy convergence: 0.5

Contact Force convergence: 0.2

Minimum reference contact force: 0.02

Line search convergence tolerance for BFGS method of iteration: 0.5

Setting the true strain-hardening modulus of all reinforcements greatly enhanced

the convergence between the concrete and the plastic reinforcement of the

iterations near the peak shear capacity of the column models as this helped reduce

a sudden change in the non-linear behavior at first yielding of the reinforcements,

resulting in numerical divergence. .

A proper choice elements is important by reviewing the their features and

allowable use.

Among the finite elements available for modeling the reinforcements modeled as

plastic-bilinear. The use of 2-node 3-D truss elements gave unstable results upon

cracking of the concrete. The 2-node 3-D rectangular Hermititan beam elements

did not converge well with the 8-node 3-D elements used for concrete since the

interpolations of the model involves all six degrees of freedom at each of its

nodes. All plastic-bilinear materials are based on the von Mises yield condition,

associated flow rule using the von Mises yield function with an assumption of

isotropic or kinematic, bilinear or multilinear hardening rule. The rectangular

508

beam element is formulated based on the Bernoulli-Euler beam theory, where stress-strain relation of circular or rectangular beam elements are based on the classical flow theory with the von Mises yield condition derived from the three-dimensional stress-strain law in which case the stresses τ_{ss} and τ_{tt} and the strain γ_{st} are zero. The elastic-plastic stress-strain matrix for the normal stress τ_{rr} and the two shear stresses τ_{rs} and τ_{rt} are obtained using static condensation. The beam-type element matrices are formulated using the Hermitian displacement functions which give the displacement interpolation matrix.

The pipe-beam elements, which worked best to model the reinforcements, has six displacement degrees of freedom per node (3 translations and 3 rotations). The pipe-beam elements may be used for linear or nonlinear behavior with large displacements and small strain as it is for the concrete element that also assumes large displacement and small strains. Only Newton-Cotes numerical integration is used for computation of beam element stiffness matrix and internal force vector along the length of the element. No integration is required over the cross section.

Despite the many challenges faced during the process of three-dimensional finite element modeling of reinforced concrete, the purpose of the verifying the experimental results by FEM analysis was accomplished. The results were adequate and provided insights on the stress and crack distributions which varied during the initial loading of the columns up to the peak capacity values.

509
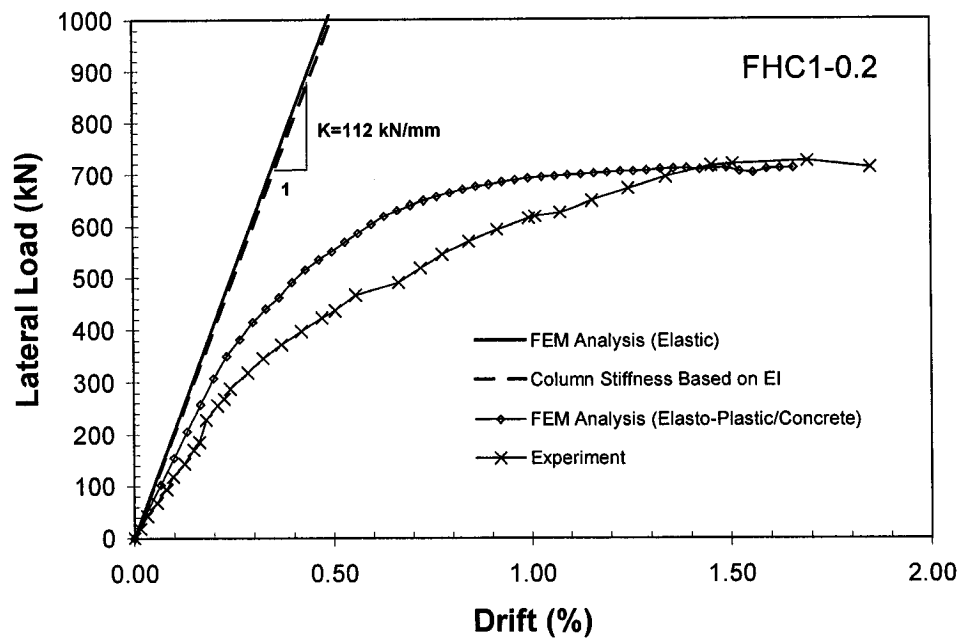
Fig. 6.99- Comparison of Lateral Force vs. Drift Ratio Relationships for Specimen FHC1-0.2 to Experimental Results.

510
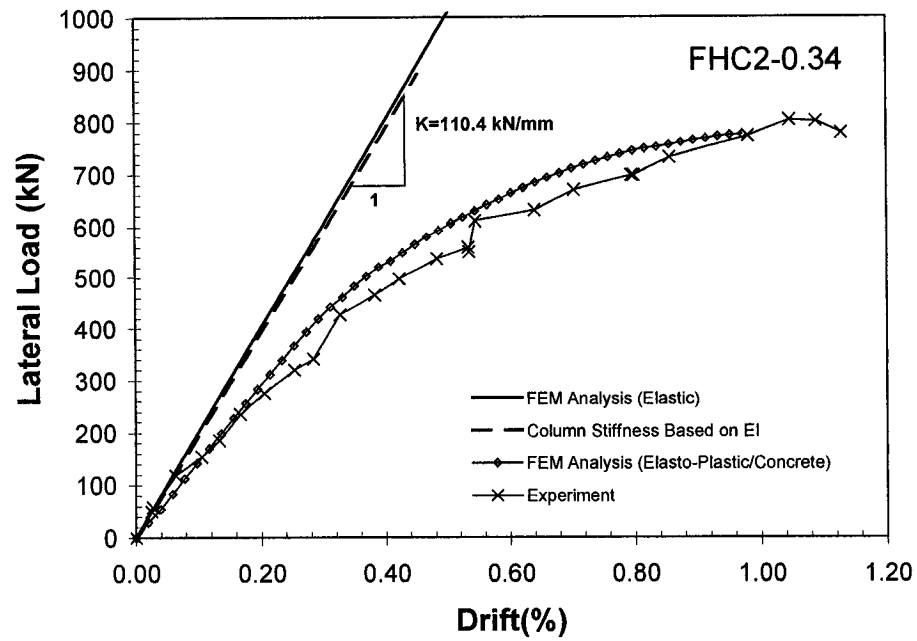
Fig. 6.100- Comparison of Lateral Force vs. Drift Ratio Relationships for Specimen FHC2-0.34 to Experimental Results.

511

CHAPTER 7

SUMMARY AND CONCLUSIONS

7.1 SUMMARY

This study constituted a study of an experimental behavior and analysis of six full-scale high strength reinforced concrete column, under combined axial and lateral cyclic quasi-statical loading. The combined state was introduced by application of either low or high levels of axial loads and a cyclically applied lateral force, simulating the lateral seismic loading. The variation of material size, properties and their placements induced different behavior and performance levels. Currently applicable codes for reinforced high-strength concrete members subjected to both axial and flexural loads during seismic loading have been investigated; the current requirements in high-strength concrete applications in reinforced columns were investigated in consideration for performance-based design. A curvature-based moment-curvature analysis and derived lateral force-displacement relationships along with a experimental verification by finite element analysis were performed to understand column behavior in detail. The investigation and application of existing confined high-strength concrete stress-

512

stress relationships were implemented in the moment-curvature analysis to predict the column behavior. This provided insights of the high-strength concrete application in the performance-based design.

The following are a summary of findings based on different phases of experimental and analytical studies that have been performed.

7.2 CONCLUSIONS

1.   A loading system has been developed for testing large to full-scale model columns. The main feature of the system is a lever arm amplifier for axial loading up to 6,000 kN (about 1,400 kip). Axial loading capacity of the system can be further increased by further strengthening the lever arm amplifier or combining the lever arm system with additional post-tensioning bars.

2.   A significant discrepancy was noticed between the values obtained from the compressive strength testing of concrete cylinders cured in the air-dry condition and those cured in the standard wet curing tank.

513

3.   The hysteretic behavior of the HSC columns are characterized by three distinct stages: (i.) the initial stage with the full participation of both confined core concrete and the unconfined cover concrete; (ii.) stable behavior with deformation contributed primarily by longitudinal steel yielding and straining of confined core concrete; and (iii.) final failure.

4.   The termination of the initial stage and the beginning of the stable stage is typically marked by the crushing and spalling of unconfined cover concrete. The maximum lateral shear force carrying capacity is typically achieved by the HSC columns immediately before the crushing of cover concrete. The maximum shear force and the corresponding drift ratio depend mainly on the concrete section properties including the axial load levels, and not significantly affected by the configuration of transverse reinforcement.

5.   The stable behavior after concrete cover spalling, which is the most important for seismic design, is significantly affected by both the level of axial load and the details of transverse reinforcement. Model columns reinforced with transverse reinforcement of more than 82% of the ACI-318-95 requirement developed ductile response with an ultimate drift ratio of 6.0% when the axial load was $0.2A_g f'_c$. The ultimate drift ratios reduced for model columns with less transverse reinforcement or higher axial load levels.

514

6.   Analysis based on the equivalent compressive stress block corresponding to an ultimate concrete compressive strain of 0.003 recommended by ACI 318-95 code can provide a predictable but conservative estimation to the flexural strength of the HSC full-scale column models tested in this study.

7.   High axial load level reduced column deformability.

8.   Use of higher grade confinement increased performance. The use of high-strength transverse reinforcement was found effective in providing additional confinement and ductility.

9.   ACI 318-99 Transverse Reinforcement Requirement under-predicts column performance for high axial levels. Although all the six specimens were substandard design based on ACI, the ACI 318-95 code equation governing the transverse reinforcement design for earthquake resistant columns does not result in consistent performance. The current code design for transverse reinforcement appeared to be over-conservative for lower axial load levels but less conservative for higher axial load levels.

515

10. Performance-based criteria requires consideration of all column parameters as well as the target performance levels for the determination of required transverse reinforcement.

11. Hysteretic behavior reveals that columns undergo a various stages of failures until ultimate failure is reached.

12. The highest strains are typically observed at approximately 250 mm from column stub for both longitudinal and transverse reinforcements in the center region of the plastic hinge area.

13. The location of plastic hinge shifted lower higher the axial load level.

14. The transverse hoops typically undergo greater strains further away from column stub in comparison to transverse ties. On the other hand, the transverse ties undergo comparatively greater strains closer to column stub.

15. The failure of all the model columns was dominated by the buckling of longitudinal reinforcement, followed by the total crushing of core concrete. The failure might have been initiated or at least compounded by the opening of the 90

516

degree anchorage of the cross ties. Neither longitudinal nor transverse bars fractured.

16.   The ultimate failure was caused by buckling of longitudinal bars as 90 degree bend of transverse ties bend outward in the plastic hinge region.

17.   A development of curvature-based moment-curvature analysis program is able to provide a prediction of column behavior including the various stages of column failures.

18.   The theoretical models of confined HSC stress-strain relationships based on the concept of confinement effectiveness are able to provide a prediction of lateral force versus drift ratio relationships.

19.   The existing HSC confinement theories in general provide conservative prediction of the lateral force versus drift ratio relationships. For high axial load application, however, the prediction over estimates the column capacity at large drift ratios since the proposed descending curves of the theories are determined in arbitrary manner based on the experimental values.

20.   The range of concrete strength and the strength of reinforcements tested by previous researchers are wide, and the results are not anticipated to correlate accurately to the experimental results. The moment-curvature analysis closely captured the point of initial longitudinal yield. However, the point of cover spalling at peak column capacities are predicted to occur at a greater drift ratios in comparison to the experimental results since the lateral force versus drift ratio relationship, derived from the moment-curvature relationships, assumes a fixed empirical plastic hinge length.

21.   The finite element analysis of column section model subjected to axial displacement provided good results in comparison to experimental axial load - displacement relationships and is shown to be able to predict the axial stress-strain relationships of confined concrete.

22.   The finite element analysis of column section models show that the location of highest stress is located at the concrete cover and particularly at the location of bond between the transverse hoops and the cover concrete for all cases. Within the confined core of the concrete, the area of highest stress is located at the location of the longitudinal reinforcements at midlevel between transverse reinforcement spacing. On the other hand, highest stress is located in the

518

confined concrete core with the lowest stress located at the longitudinal bars at the level of transverse reinforcements.

23. Higher concrete strength concrete provided better stress distributions through the column sections.

24. The finite element analysis result for experimental simulation of full-column model correlated well to the experimental results for both specimens FHC1-0.2 and FHC2-0.34.

25. For full-column finite element models, there are more concrete crushing near the column stub for the cases of high axial load applications in comparison to the cases of low axial load applications at the same drift ratio. On the other hand, at the same drift ratio, the columns with higher axial load has less flexural and shear cracks on the tension side in comparison to those of the columns of low axial loads.

26. The finite element analysis of full-column models indicate that initial cracks developed are concentrated closer to column stubs for high axial load levels, where they are spread out in column axial direction for low axial load

519

levels. The level of flexural and shear crack penetration into the confined core concrete is greater for the columns of low axial load at the same drift ratio.

27.   The finite element analysis approach requires good planning and proper usage of the elements. It is recommended to use contact friction between the concrete and its reinforcements to obtain good results. A true strain-hardening modulus of elasticity of concrete should be used for all reinforcements.

28.   The finite elements analysis method, which can provide a full three-dimension analysis of reinforced concrete members, can be used as an analytical tool. It can provide good predictions of the extent of damaged areas with stress and crack distributions.

29.   To achieve further design efficiency of HSC columns, improved transverse reinforcement design including the use of higher strength steel and more effective details should be developed and evaluated.

More model columns with wider ranges of parameters should be tested using the newly developed testing system to refine and develop the performance based design procedure for seismic resistant HSC columns.

520

It is author's hope that the findings of this study lead to economic and reliable high performance high strength concrete design procedures that may be applied in practice.

REFERENCES

ACI Committee 318, (1995), "Building Code Requirements for Reinforced Concrete and Commentary (ACI 318-95/ACI 418R-95)," American Concrete Institute, Farmington Hills, Mich., 369.

ACI 211.4R-93, "Guide for Selecting Proportions for High-Strength Concrete With Portland Cement and Fly Ash", Reported by ACI Committee 211, American Concrete Institute, Box 19150, Redford Station, Detroit, Michigan 48219.

Ahmad. S. M., and Shah, S.P. (1982). "Stress-strain curves of concrete confined by spiral Reinforcement." *Am. Concr. Inst. J.,* 79(6), 484-490.

Azizinamini, A.; Kuska, B.S.S.; Brungardt, P.; and Harfield, E., (1994), "Seismic Behavior of Square High-Strength Concrete Columns," *ACI Structural Journal,* American Concrete Institute, V.91, No.10, May-June, pp.336-345.

Bayrak, O. (1995). "High Strength Concrete Columns Subjected to Earthquake Type Loading,

Bayrak, O., and Sheikh, S. A. (1996). "Confinement Steel Requirements of High Strength Concrete Columns." *Proc., 11th World Conf. On Earthquake Engrg.,* 8.

Bayrak, O. (1995). "High Strength Concrete Columns Subjected to Earthquake Type Loading, " MACc thesis, Dept. of Civl. Engrg., Univ. of Toronto, Toronto, Ont., Canada, 239.

Bayrak, O. and Sheikh, S. A. September (1998)., "Confinement Reinforcement Design Considerations for Ductile HSC Columns." *Journal of Structural Engineering.* 999-1010.

Bing et. al. "Stress-Strain Behavior of High-Strength Concrete Confined by Ultra-High- and Normal-Strength Transverse Reinforcements." *ACI Structural Journal,* American Concrete Institute, Vol. 98, No. 3, May-June 2001, pp. 395-406.

Bresler, B., and Bertero, V. V. (1975). "Influence of high strain rate and cyclic loading on behavior of unconfined and confined concrete in compression." *Proc. 2nd Can. Conf. on Earthquake Engrg.,* McMaster Univ., 1-32..

522

Code of Practice for the Design of Concrete Structures, (NZS 3101:1982), Standards Association of New Zealand, Wellington, 1982, Part 1, 127 p., and Part 2, 156 P.

"Code of Practice for the Design of Concrete Structures." (1995a). Part1: The Design of Concrete Structures, NZS 3101: 1995, New Zealand Standards, Wellington, New Zealand, 256.

"Code of Practice for the Design of Concrete Structures." (1995b). Part II: Commentary on the Design of Concrete Structures, NZS 3101: 1995, New Zealand Standards, Wellington, New Zealand, 264.

Cusson, D. and Paultre, P., (Vol. 120, March, 1994), "High-Strength Concrete Columns Confined by Rectangular Ties." *Journal of Structural Engineering,* ASCE. 783-805.

Cusson, D. and Paultre, P., (Vol. 121, March, 1995), "Stress-Strain Model for Confined High-Strength Concrete." *Journal of Structural Engineering,* ASCE. 468-477.

Giraldi, Almerigo. "High-Strength Concrete in Washington, D.C." Concrete International. March, 1989, pg. 52-55.

Hester, T. W., editor, (1990), "High-Strength Concrete," American Concrete Institute, Special Publication, SP-121, 786p.

Jensen, Jens Jacob. "High Strength Concrete Research.", Cement and Concrete Research Institute, Norwegian Concrete Engineering, 1990, pg. 23. (Above)

Joint ACI-ASCE Committee 441, (1997), "High-Strength Concrete Columns: State of the Art," *ACI Structural Journal,* American Concrete Institute, V.94, No.3, May-June, pp.323-335.

Kent, D.C.:, and Park, R., "Flexural Members with Confined Concrete," *Journal of Structural Division,* ASCE, 97(7), 1971, pp. 1969-1990.

Khoury, S.S., and Sheikh, S.A. (1991). "Behavior of normal and high strength confined concrete columns with and without stubs." *Res. Rep. No. UHCEE 91-4,* Dept. of Civ. And Envir. Engrg., Univ. of Houston, Tex., 345.

523

King, D.J.; Priestley, M.J.N.; and Park, R., "Computer Program for Concrete Column Design," Research Report No. 86/12, Department of Civil Engineering, University of Canterbury, Christchurch, New Zealand, May, 1986.

Li, B. and Park, R., (1994), "Strength and Ductility of Reinforced Concrete and Frames Constructed Using High-Strength Concrete," Department of Civil Engineering, University of Canterbury, New Zealand.

Malhotra, V.M., editor, (1994), "High-Performance Concrete," American Concrete Institute, Special Publication, SP-149, 844p.

Mander, J.B., Priestley, M.J.N., and Park, R. (1988a). "Observed stress-strain behavior of confined concrete." *J. Struct. Engrg.,* ASCE, 114(8), 1827-1849.

Mander, J.B., Priestley, M.J.N., and Park, R. (1988b). "Theoretical stress-strain model for confined concrete." *J. Struct. Engrg.,* ASCE, 114(8), 1804-1826.

Mander, J.B., Priestley, M.J.N., and Park, R. (1984). "Seismic design of bridge piers." *Research report No. 84-2,* Univ. of Canterbury, New Zealand.

Mau, S.T., and El-Mabsout, M. (1989). "Inelastic buckling of reinforcing bars." *J. engrg. Mech.,* ASCE, 11591), 1-17.

Mitchell, D., and Paultre, P. (1994). "Ductility and overstrength in seismic design of reinforced concrete structures." *Can. J. Civ. Engrg.,* Ottawa, Canada, 21(6), 1049-1060.

Moreno, Jaime. "The State of the Art of High-Strength Concrete in Chicago." Concrete International, January, 1990, pg. 35-39

Park, R., and Paulay, T. (1975). *Reinforced concrete structures.* John Wiley and Sons, New York, N.Y.

Park, R., Priestley, M.J.N., and Gill, W.D. (1982). "Ductility of square-confined concrete columns." *J. Struct. Div.,* ASCE, 108(4), 929-950.

Park, Robert, November (1998). "Design and Behavior of RC Columns Incorporating High-Strength Materials." *Concrete International.,* 55-62.

Paulay, T., and Priestley, M.J.N. (1992). *Seismic design of reinforced concrete and masonry buildings.* Wiley Interscience, New York, N.Y.

524

Popovics, S. (1973). "A numerical approach to the complete stress-strain curves for concrete." *Cement and Concr. Res.,* 3(5), 583-599.

Priestley, M.J.N., Verma, R., and Xiao, Y. (1994). "Seismic Shear Strength of Reinforced Concrete Columns." *Journal of Structural Engineering,* ASCE, 120(7), 2310-2329.

Priestley, M.J.N.; Seible, F.; Xiao, Y.; and Verma, R., "Steel Jacket Retrofit of Squat RC Bridge Columns for Enhanced Shear Strength – Part 1 – Theoretical Considerations and Test Design," *ACI Structural Journal,* American Concrete Institute, Vol. 91, No. 4, July-August 1994, pp.394-405.

Priestley, M.J.N., and Park, R., "Strength and Ductility of Concrete Bridge columns Under Seismic Loading," *ACI Structural Journal,* V. 84, No. 1, Jan.-Feb. 1987, pp. 69-76.

Priestley, Seible, and Calvi (1996), Seismic Design and Retrofit of Bridges. John Wiley & Sons, Inc.

Rangan, Vijaya. November (1998). "High-Performance High-Strength Concrete: Design Recommendations." *Concrete International.,* 63-68.

Razvi and Saatcioglu (1999). "Confinement Model for High-Strength Concrete." *Journal of Structural Engineering, ASCE, Vol. 125, No. 3, March, 1999, pp. 281-289.*

Roy, H.E.H., and Sozen, M.A. (1964). "Ductility of concrete." *Proc. Int. Symp. on the Flexural Mech. of Reinforced Concrete,* ASCE-American Concrete Institute, 213-224.

Scribner, C. F. (1986). "Reinforcement buckling in reinforced concrete flexural members." *ACI J.,* 83(6), 966-973.

Shah, S. P., and Ahmad, S. H. (eds). (1993). *High Performance Concrete: Properties and Applications.* McGraw-Hill, Inc. New York, N.Y.

Sheikh, S.A., and Khoury, S. S. (1993). "Confined concrete columns with stubs." *ACI Struct. J.,* 90(4), 414-431.

Sheikh, S.A., and Khoury, S.S. (1997). "A performance-based approach for the design of confining steel in tied columns." *ACI Struct. J.,* 94(4), 421-431.

Sheikh, S.A., and Toklucu, M.A. (1993). "Reinforced concrete columns confined by circular spirals and hoops." *ACI Struct. J.,* 90(5), 542-553.

Sheikh, S. A., and Uzumeri, S. M., "Strength and Ductility of Tied Concrete Columns," *Journal of the Structural Division,* ASCE, Vol.106, No. ST5, May 1980, pp. 1079-1102.

Sheikh, S.A.; Shah, D.V.; and Khoury, S.S., (1994), "Confinement of High-Strength Concrete Columns," *ACI Structural Journal,* American Concrete Institute, V.91, No.1, January-February, pp.100-111.

Smith, Gregory J. and Rad, Franz N., "Economic Advantages of High-Strength Concretes in Columns.", Concrete International, April, 1989.

Watson, S., Zahn, F.A., Park, R. (1994). "Confining Reinforcement for Concrete Columns.", *Journal of Structural Engineering,* ASCE, 1798-1823.

Watson, S., and Park, R. (1994). "Simulated seismic load tests on reinforced concrete columns." *J. Struct. Engrg.,* ASCE, 120(6), 1825-1849.

Watstein, D. (1953). "Effect of straining rate on the compressive strength and elastic properties of concrete." *Am. Concr. Inst. J.,* 24(8), 729-744.

Watson, S., Zahn, F.A., and Park, R. (1994). "Confining reinforcement for concrete columns." *J. Struct. Engrg.,* ASCE, 120(6), 1798-1824.

Xiao, Y. and Martirossyan, A., (1997), "Seismic Performance of High-Strength Concrete Columns," *ASCE Journal of Structural Engineering,* Vol.124(3), March, pp.241-251.

Xiao, Y.; Anderson, J.C.; and Martirossyan, A., "Reinforcement Design for High Strength Concrete Columns Using Local Materials In Southern California," USC *Structural Engineering Research Program,* Report No. USC-SERP-95/1, Department of Civil Engineering, University of Southern California, March 1995, 150p.

Xiao, Y. and Martirossyan, A., "Performance of High Strength Concrete Columns Subjected to Eccentric Loading," USC *Structural Engineering Research Program,*

Report No. USC-SERP-96/2, Department of Civil Engineering, University of Southern California, February 1996, 40p.

Yong Y. K., Nour, M. G., and Nawy, E. G., (Vol. 114, February, 1988), "Behavior of Laterally Confined High-Strength Concrete under Axial Loads.", *Journal of Structural Engineering,* ASCE., 332-351.

Zahn, F.A., Park, R., and Priestley, M.J.N. (1986). "Design of reinforced concrete bridge columns for strength and ductility." *Research Report 86-7,* Univ. of Canterbury, Christchurch, New Zealand.

527

APPENDIX I.

TEST SETUP DESIGN DETAILS

528

C4—Full Scale Column Lever–Arm

Front View

Side view

I-I View

W14 x 145

Existing Stiffners

All holes are 1.5" in Diameter

PL-8

PL-11

PL-12

PL-10

W14 x 145
L=32.0

PL-10

W14 x 145-L=32.0

PL-9

PL-11

* The 96" long W14 x 145
  will be supplied by USC

* G50 Steel required

* All welds 70ksi

ALL DIMENSIONS ARE IN INCHES

Design	Y. Xiao, H.W. Yun
Drawing	H.W. Yun
Date	July 1, 1997

529

Existing Stiffners

W14 x 145

96.0

56.0

14.0

1.0

14.78

Side view

* The 96" long W14 x 145 will be supplied by USC
* G50 Steel required
* All welds 70ksi

14.78

W14 x 145

8.0 6.0
6.0
32.0
32.0
6.0
8.0 6.0

W14 x 145

Front View

ALL DIMENSIONS ARE IN INCHES

Drawn by: Henry W. Yun
University of Southern California

C4—Full Scale Column Lever—Arm

530

C4-Full Scale Column "1400k" Connector

Side View of Vertical Connectors

Design	Y. Xiao, H.W. Yun	
Drawing	H.W. Yun	
Date	August 20, 1997	

C4-Full Scale Column Test Setup

2

Note:

* Two assemblies needed
* Grade 50 steel or equivalent
* 70 ksi welds
* Paint eye brackets with black
* Paint tubes with dark red color

ALL DIMENSIONS ARE IN INCHES

21.0

6.5 — 11.5 — 3.0

1/8
60°

2.0
4.0
2.0
2.0
4.0
16.0
2.0

Front View

Note

* Need 4 sets of the eye brackets

* Full penetration welds

* Grade 50 Steel

* 70 ksi welds

* Black paint

ALL DIMENSIONS ARE IN INCHES

PL-5

φ1.5" holes

PL-4

5" hole

5.0
10.0
5.0

2.0
5.0
6.0
16.0
5.0
6.0
2.0

6.5 — 11.5 — 3.0

14.5

21.0

Side View

φ1.5" holes

2.0

6.0
5.0
16.0
6.0
5.0

2.0

2.0
2.0

2.0 — 4.0 — 4.0 — 2.0

16.0

Top View

Design	Y. Xiao, H.W. Yun
Drawing	H.W. Yun
Date	August 25, 1997

C4—Full Scale Column End Details

Eye Bracket

3

Note:

* All welds for the ends of the tube are fillet all around

* 70 ksi welds

* The details shown in this sheet are for the two ends of two identical tubes

* Paint tubes with dark red color

ALL DIMENSIONS ARE IN INCHES

Design	Y. Xiao, H.W. Yun
Drawing	H.W. Yun
Date	September 4, 1997

4 C4—Full Scale Column Tube End Detail

534

APPENDIX II.

ANALYSIS OF COLUMN CAPACITIES BASED ON ACI 318-95 CODE

SAMPLE CALCULATIONS

ULTIMATE FLEXURAL STRENGTH

PROJECT NAME:	Full-Scale HSC Col.	DATE	February 18, 2002
ENGINEER:	Yan Xiao		**HSC-FF1,5,6-0.2**
MODIFIED:	Dr. Xiao		February 18, 2002

DIMENSIONS OF THE SECTION

Section top flange Width, b (in)	20.00
Section total hight h (in)	20.00
Clear cover	1.50
Area of the Section, Ag (in^2)	400.00
Moment of Ineritia, I (in^4)	82065.0

CONCRETE PROPERTIES

Specified Compressive Strength of Concrete, f 'c (psi)	9.3
Young's Modulus of Concrete, Ec (ksi)	5496.880934
β 1	0.65
If consider 0.85 for concrete strength reduciton	**yes**
Concrete strength reduciton	0.85

PROPERTIES OF LONGITUDINAL STEEL

Type of the Rebars	astm 605-g60
Specified Tensile Strength of Prestressing Tendons, f y (ksi)	68.6
Young's Modulus of Steel, Es (ksi)	29000
Yield Strain, ε y	0.00237
Number of layers	3
Area of steel layer -1 As1 (sq.in.)	4.12
Area of steel layer -2 As2 (sq.in.)	2.00
Area of steel layer -3 As3 (sq.in.)	4.12
Postion of steel layer-1 to centroid (in.)	-7.24
Postion of steel layer-2 to centroid (in.)	0.00
Postion of steel layer-3 to centroid (in.)	7.24

LOADS

Ultimate Moment, Mu (ft-k)	not used
Ultimate Axial Load, Pu (kip)	750.00

Trial Values of Compression Zone

Compression zone depth, x (in.)	**8.13**
stress block depth, a (in.)	5.29

Calculation of Steel Strain and Stress

Layer-1 strain, ε d	-0.003359
Layer -1 stress, fs2 (ksi)	-68.6
Layer-2 strain, ε d	-0.000689
Layer -2 stress, fs2 (ksi)	-20.0
Layer-3 strain, ε d	0.001982
Layer -3 stress, fs2 (ksi)	57.5
Layer-1 force (kip)	-282.6
Layer-2 force (kip)	-39.9
Layer-3 force (kip)	236.8
Layer-1 moment (kip-in)	2046.3
Layer-2 moment (kip-in)	0.0
Layer-3 moment (kip-in)	1714.4

Internal Foces

Steel Axial force Fs	-85.8
Concrete Axial force Fc	835.8
Total Internal axial force F (kip)	**750.0**
Steel moment Ms	3760.7
Concrete moment Mc	6148.7
Total Internal Moment Mn(kip-in)	**9909.4**
Total Internal Moment Mn(kip-ft)	**825.8**
Total Internal Moment Mn(kNm)	1119.6

Check Axial Equilibrium

F-P	**0.01**
%	**0.00**

536

UNIVERSITY OF SOUTHERN CALIFORNIA

ULTIMATE FLEXURAL STRENGTH

PROJECT NAME:	Full-Scale HSC Col.	DATE:	February 18, 2002
ENGINEER:	Yan Xiao		**HSC-FF2-0.34**
MODIFIED:	Dr. Xiao		February 18, 2002

DIMENSIONS OF THE SECTION

Section top flange Width, b (in)	20.00
Section total hight h (in)	20.00
Clear cover	1.50
Area of the Section, Ag (in^2)	400.00
Moment of Ineritia, I (in^4)	82065.0

CONCRETE PROPERTIES

Specified Compressive Strength of Concrete, f'c (psi)	9
Young's Modulus of Concrete, Ec (ksi)	5407.494799
β 1	0.65
If consider 0.85 for concrete strength reduciton	**yes**
Concrete strength reduciton	0.85

PROPERTIES OF LONGITUDINAL STEEL

Type of the Rebars	astm 605-g60
Specified Tensile Strength of Prestressing Tendons, f y (ksi)	68.6
Young's Modulus of Steel, Es (ksi)	29000
Yield Strain, ε y	0.00237
Number of layers	3
Area of steel layer -1 As1 (sq.in.)	4.12
Area of steel layer -2 As2 (sq.in.)	2.00
Area of steel layer -3 As3 (sq.in.)	4.12
Postion of steel layer-1 to centroid (in.)	-7.24
Postion of steel layer-2 to centroid (in.)	0.00
Postion of steel layer-3 to centroid (in.)	7.24

LOADS

Ultimate Moment, Mu (ft-k)	not used
Ultimate Axial Load, Pu (kip)	1225.40

Trial Values of Compression Zone

Compression zone depth, x (in.)	**11.30**
stress block depth, a (in.)	7.34

Calculation of Steel Strain and Stress

Layer-1 strain, ε d	-0.001579
Layer -1 stress, fs2 (ksi)	-45.8
Layer-2 strain, ε d	0.000344
Layer -2 stress, fs2 (ksi)	10.0
Layer-3 strain, ε d	0.002267
Layer -3 stress, fs2 (ksi)	65.7
Layer-1 force (kip)	-188.7
Layer-2 force (kip)	19.9
Layer-3 force (kip)	270.9
Layer-1 moment (kip-in)	1365.9
Layer-2 moment (kip-in)	0.0
Layer-3 moment (kip-in)	1961.0

Internal Foces

Steel Axial force Fs	102.1
Concrete Axial force Fc	1123.3
Total Internal axial force F (kip)	**1225.4**
Steel moment Ms	3326.9
Concrete moment Mc	7109.4
Total Internal Moment Mn(kip-in)	**10436.3**
Total Internal Moment Mn(kip-ft)	**869.7**
Total Internal Moment Mn(kNm)	**1179.1**

Check of Axial Equilibrium

F-P	*0.03*
%	**0.00**

537

UNIVERSITY OF SOUTHERN CALIFORNIA

PROJECT NAME:	Full-Scale HSC Col.	DATE	February 18, 2002
ENGINEER:	Yan Xiao		**HSC-FF3-0.22**
MODIFIED:	Dr. Xiao		February 18, 2002

DIMENSIONS OF THE SECTION

Section top flange Width, b (in)	20.00
Section total hight h (in)	20.00
Clear cover	1.50
Area of the Section, Ag (in^2)	400.00
Moment of Ineritia, I (in^4)	82065.0

CONCRETE PROPERTIES

Specified Compressive Strength of Concrete, f 'c (psi)	9
Young's Modulus of Concrete, Ec (ksi)	5407.494799
β 1	0.65
If consider 0.85 for concrete strength reduciton	yes
Concrete strength reduciton	0.85

PROPERTIES OF LONGITUDINAL STEEL

Type of the Rebars	astm 605-g60
Specified Tensile Strength of Prestressing Tendons, f y (ksi)	68.6
Young's Modulus of Steel, Es (ksi)	29000
Yield Strain, ε y	0.00237
Number of layers	3
Area of steel layer -1 As1 (sq.in.)	4.12
Area of steel layer -2 As2 (sq.in.)	2.00
Area of steel layer -3 As3 (sq.in.)	4.12
Postion of steel layer-1 to centroid (in.)	-7.24
Postion of steel layer-2 to centroid (in.)	0.00
Postion of steel layer-3 to centroid (in.)	7.24

LOADS

Ultimate Moment, Mu (ft-k)	not used
Ultimate Axial Load, Pu (kip)	793.00

Trial Values of Compression Zone

Compression zone depth, x (in.)	**8.64**
stress block depth, a (in.)	5.62

Calculation of Steel Strain and Stress

Layer-1 strain, ε d	-0.002987
Layer -1 stress, fs2 (ksi)	-68.6
Layer-2 strain, ε d	-0.000473
Layer -2 stress, fs2 (ksi)	-13.7
Layer-3 strain, ε d	0.002042
Layer -3 stress, fs2 (ksi)	59.2
Layer-1 force (kip)	-282.6
Layer-2 force (kip)	-27.4
Layer-3 force (kip)	243.9
Layer-1 moment (kip-in)	2046.3
Layer-2 moment (kip-in)	0.0
Layer-3 moment (kip-in)	1766.0

Internal Forces

Steel Axial force Fs	-66.1
Concrete Axial force Fc	859.1
Total Internal axial force F (kip)	**793.0**
Steel moment Ms	3812.3
Concrete moment Mc	6179.3
Total Internal Moment Mn(kip-in)	**9991.5**
Total Internal Moment Mn(kip-ft)	**832.6**
Total Internal Moment Mn(kNm)	**1128.9**

Check Axial Equilibrium

F-P	*0.03*
%	**0.00**

538

UNIVERSITY OF SOUTHERN CALIFORNIA

ULTIMATE FLEXURAL STRENGTH

PROJECT NAME:	Full-Scale HSC Col.	DATE	February 18, 2002
ENGINEER:	Yan Xiao		**HSC-FF4-0.33**
MODIFIED:	Dr. Xiao		February 18, 2002

DIMENSIONS OF THE SECTION

Section top flange Width, b (in)	20.00
Section total hight h (in)	20.00
Clear cover	1.50
Area of the Section, Ag (in^2)	400.00
Moment of Ineritia, I (in^4)	82065.0

CONCRETE PROPERTIES

Specified Compressive Strength of Concrete, f 'c (psi)	9
Young's Modulus of Concrete, Ec (ksi)	5407.494799
β 1	0.65
If consider 0.85 for concrete strength reduciton	**yes**
Concrete strength reduciton	0.85

PROPERTIES OF LONGITUDINAL STEEL

Type of the Rebars	astm 605-g60
Specified Tensile Strength of Prestressing Tendons, f y (ksi)	68.6
Young's Modulus of Steel, Es (ksi)	29000
Yield Strain, ε y	0.00237
Number of layers	3
Area of steel layer -1 As1 (sq.in.)	4.12
Area of steel layer -2 As2 (sq.in.)	2.00
Area of steel layer -3 As3 (sq.in.)	4.12
Postion of steel layer-1 to centroid (in.)	-7.24
Postion of steel layer-2 to centroid (in.)	0.00
Postion of steel layer-3 to centroid (in.)	7.24

LOADS

Ultimate Moment, Mu (ft-k)	not used
Ultimate Axial Load, Pu (kip)	1189.30

Trial Values of Compression Zone

Compression zone depth, x (in.)	**11.08**
stress block depth, a (in.)	7.20

Calculation of Steel Strain and Stress

Layer-1 strain, ε d	-0.001667
Layer -1 stress, fs2 (ksi)	-48.3
Layer-2 strain, ε d	0.000293
Layer -2 stress, fs2 (ksi)	8.5
Layer-3 strain, ε d	0.002253
Layer -3 stress, fs2 (ksi)	65.3
Layer-1 force (kip)	-199.1
Layer-2 force (kip)	17.0
Layer-3 force (kip)	269.2
Layer-1 moment (kip-in)	1441.7
Layer-2 moment (kip-in)	0.0
Layer-3 moment (kip-in)	1948.8

Internal Foces

Steel Axial force Fs	87.1
Concrete Axial force Fc	1102.2
Total Internal axial force F (kip)	**1189.3**
Steel moment Ms	3390.5
Concrete moment Mc	7051.9
Total Internal Moment Mn(kip-in)	**10442.5**
Total Internal Moment Mn(kip-ft)	**870.2**
Total Internal Moment Mn(kNm)	**1179.8**

Check axial equilibrium

F-P	*-0.04*
%	0.00

539

APPENDIX III.

LONGITUDINAL REINFORCEMENT STRAINS

Strain response of longitudinal bars of the six model columns are shown in Figures AIII.2 to 7. The strain gauge name designations are explained in the following figure.

Loading Direction

L36L   L36R

Loading Direction

L36LG1000			L36RG1000
L36LG750			L36RG750
L36LG500			L36RG500
L36LG250			L36RG250
L36LG0			L36RG0

Foundation Surface
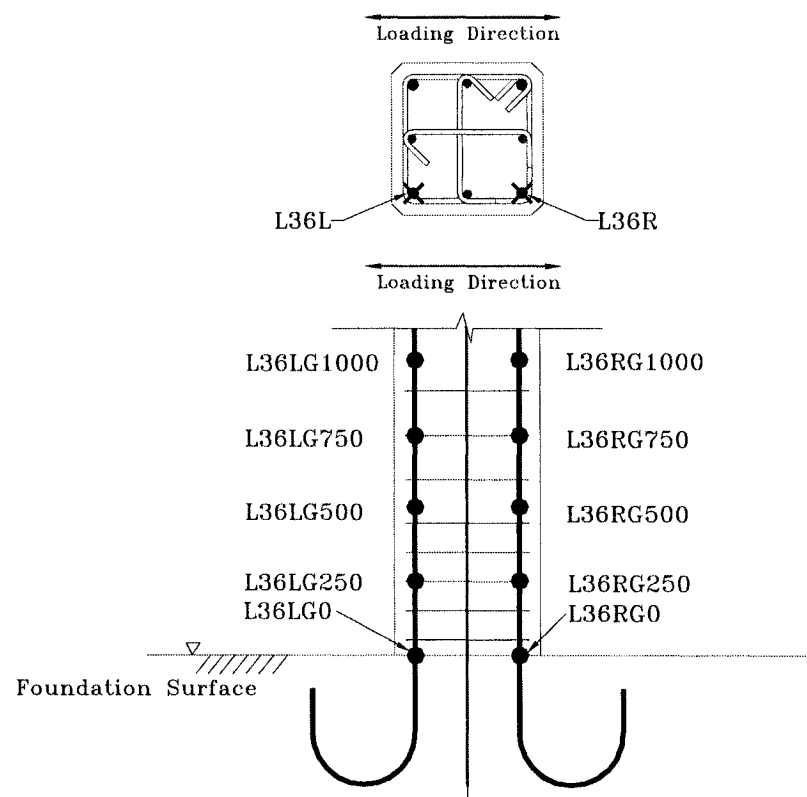
Fig. AIII.1 Strain Gage Locations of Longitudinal Reinforcement.

540
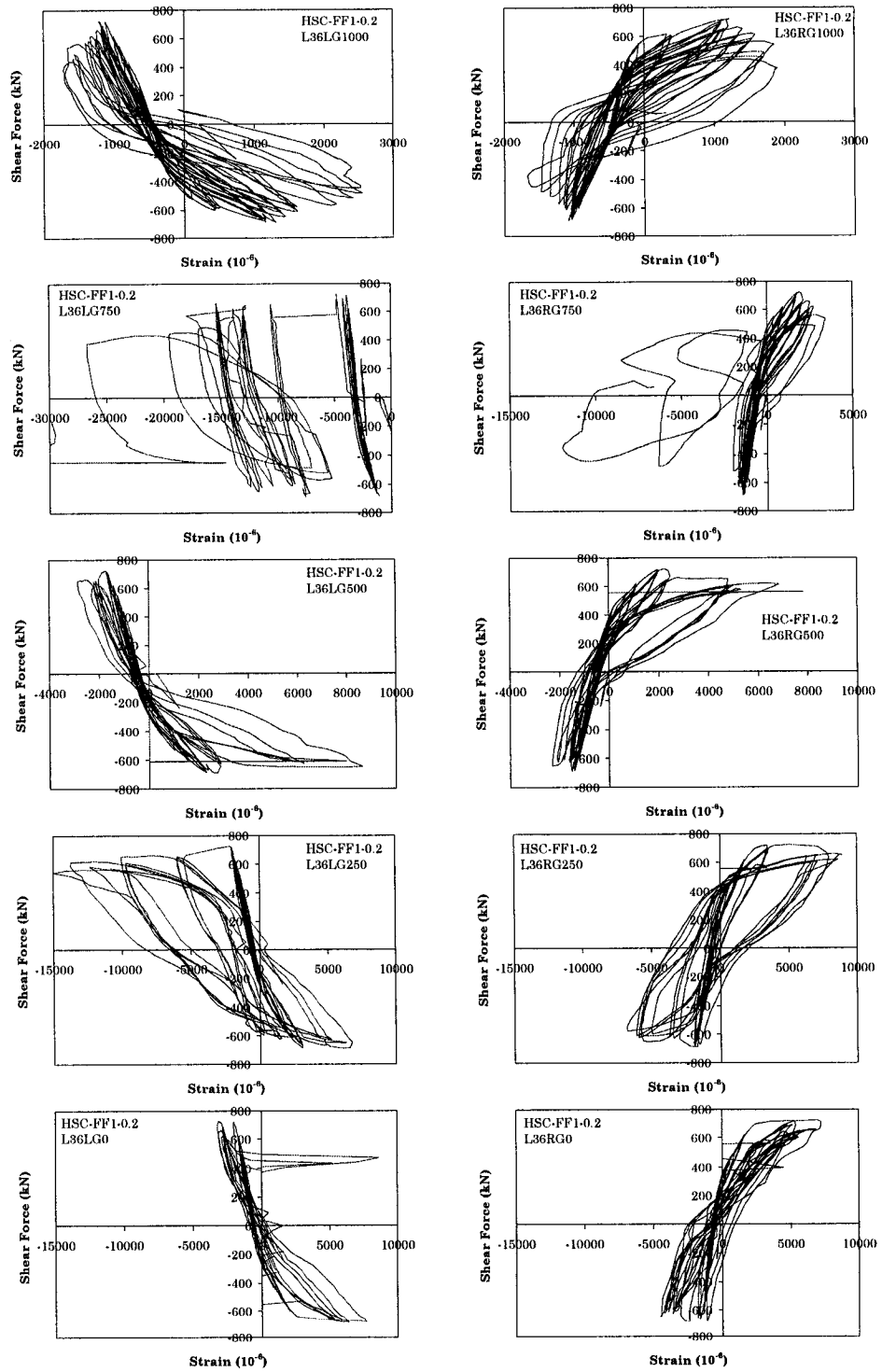
Fig. AIII.2 Strains of Longitudinal Bars for Model Column HSC-FF1-0.2

541
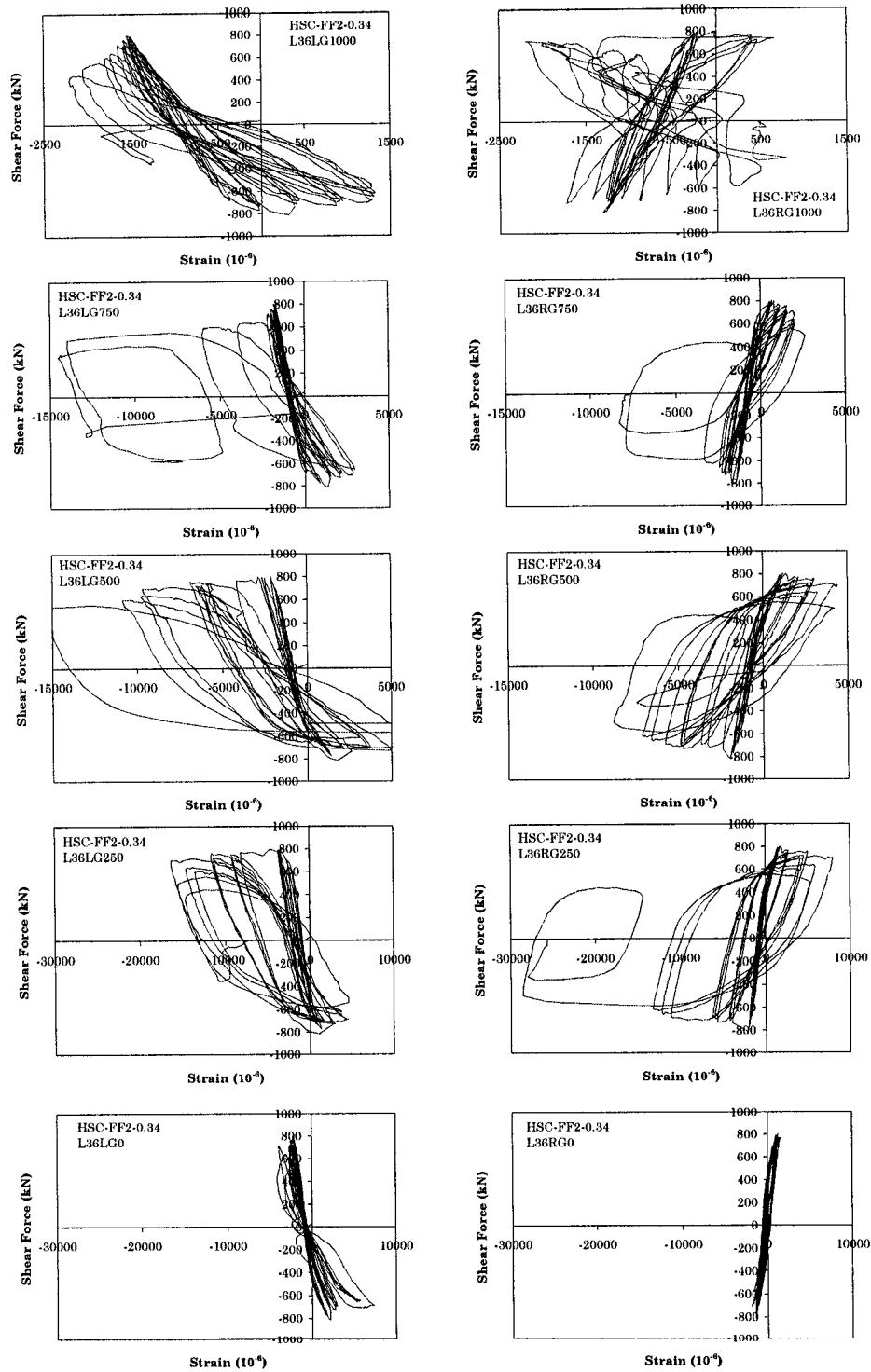
Fig. AIII.3 Strains of Longitudinal Bars for Model Column HSC-FF2-0.34

542
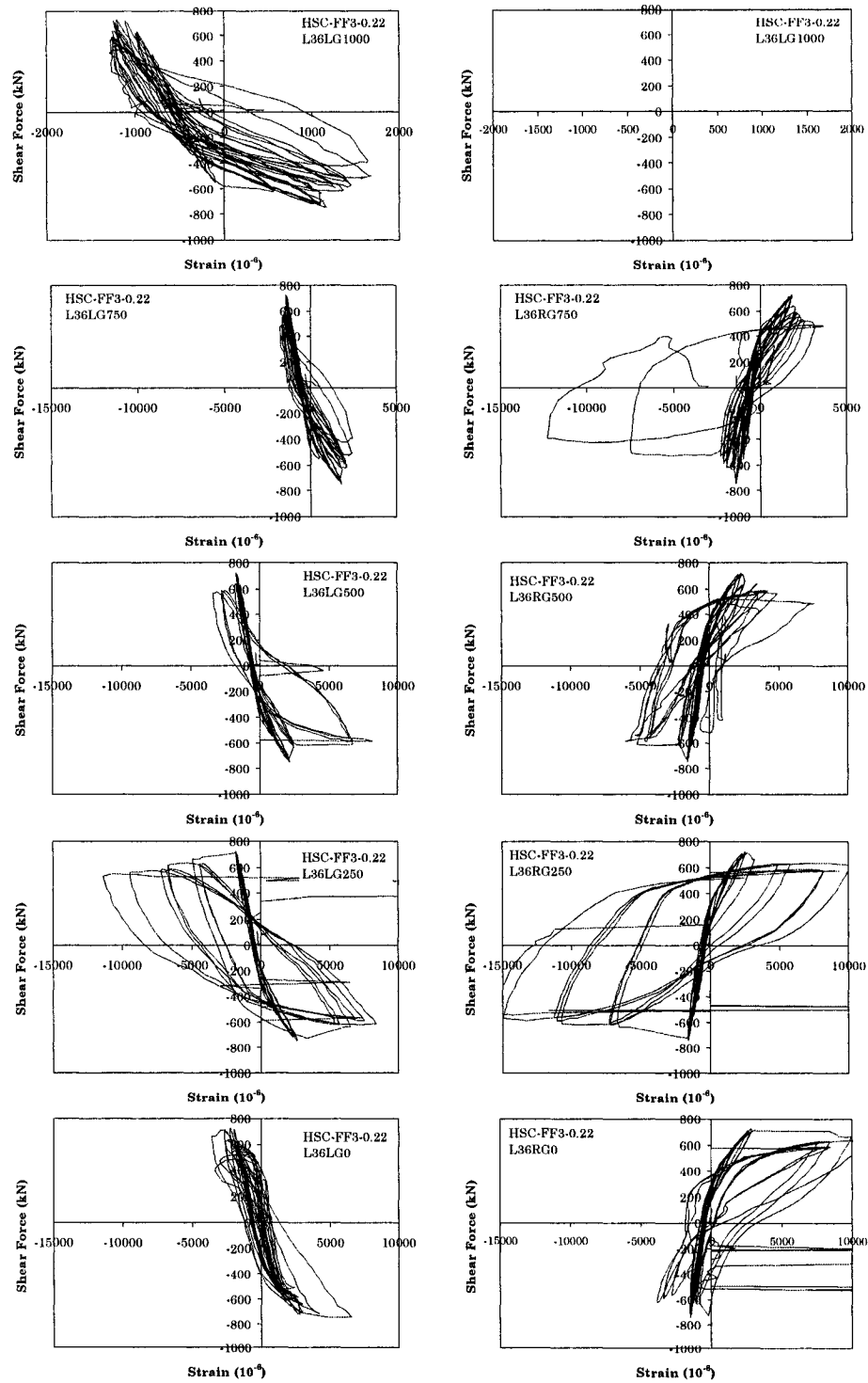
Fig. AIII.4 Strains of Longitudinal Bars for Model Column HSC-FF3-0.22

543
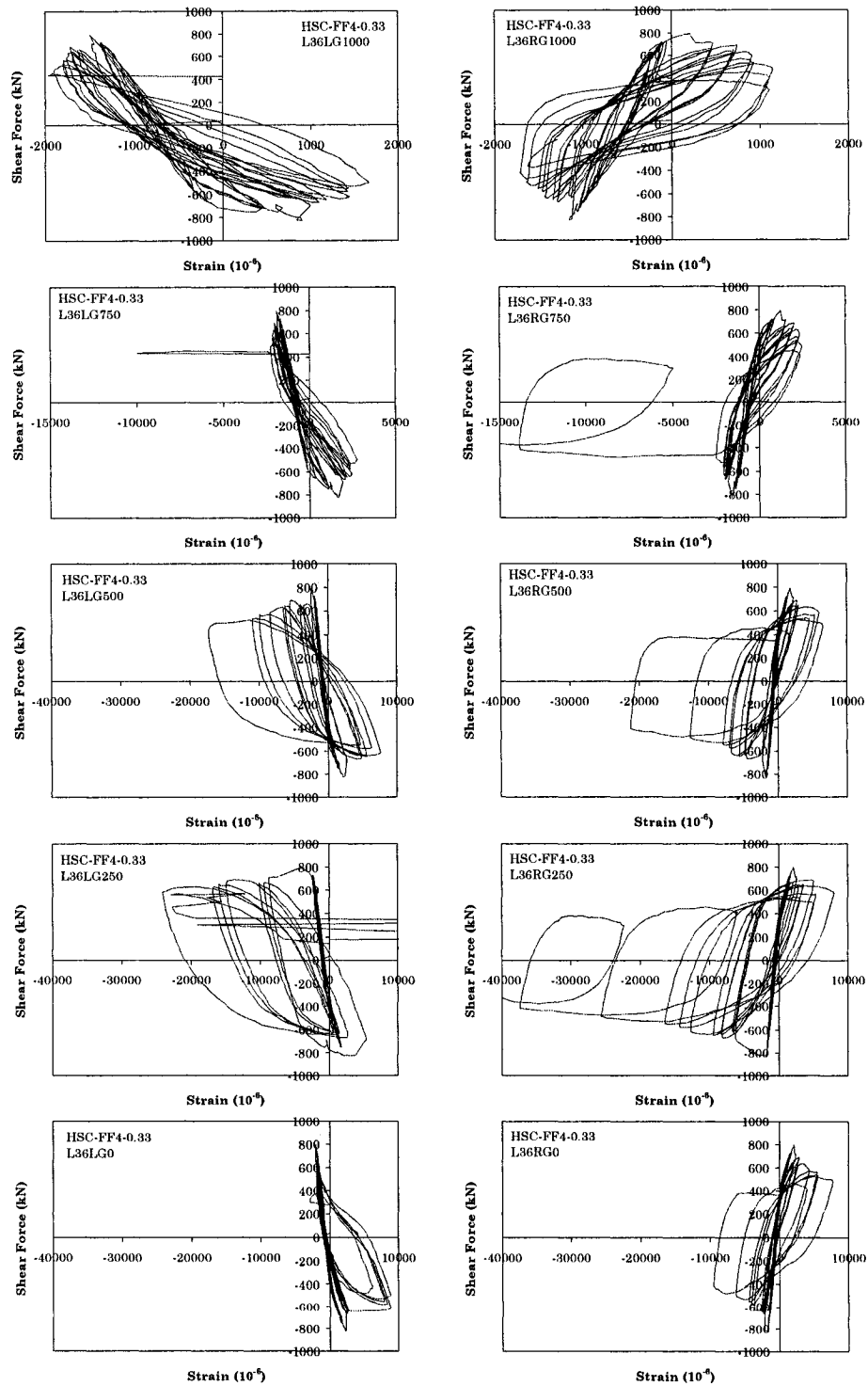
Fig. AIII.5 Strains of Longitudinal Bars for Model Column HSC-FF4-0.33

544
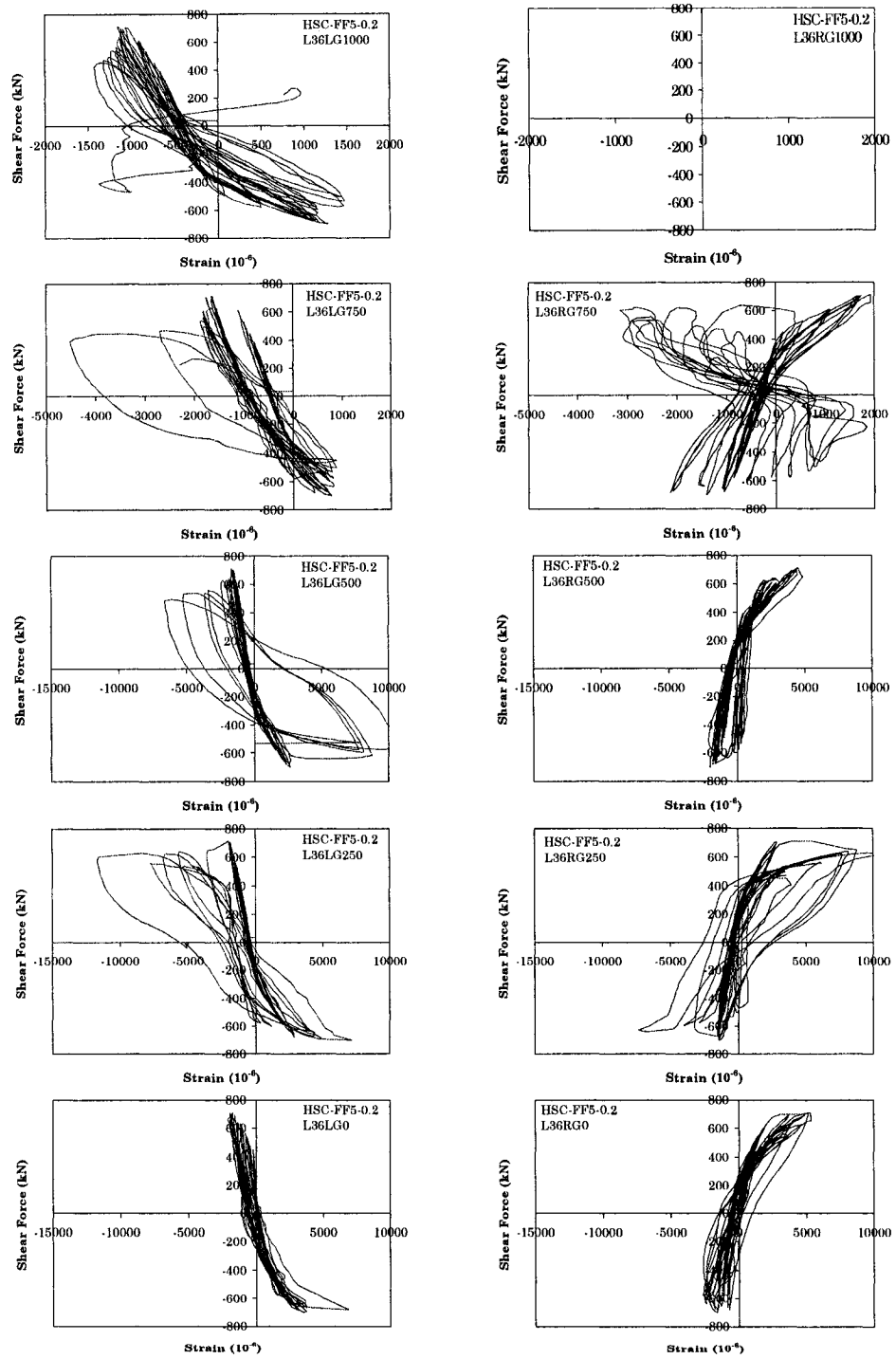
Fig. AIII.6 Strains of Longitudinal Bars for Model Column HSC-FF5-0.2
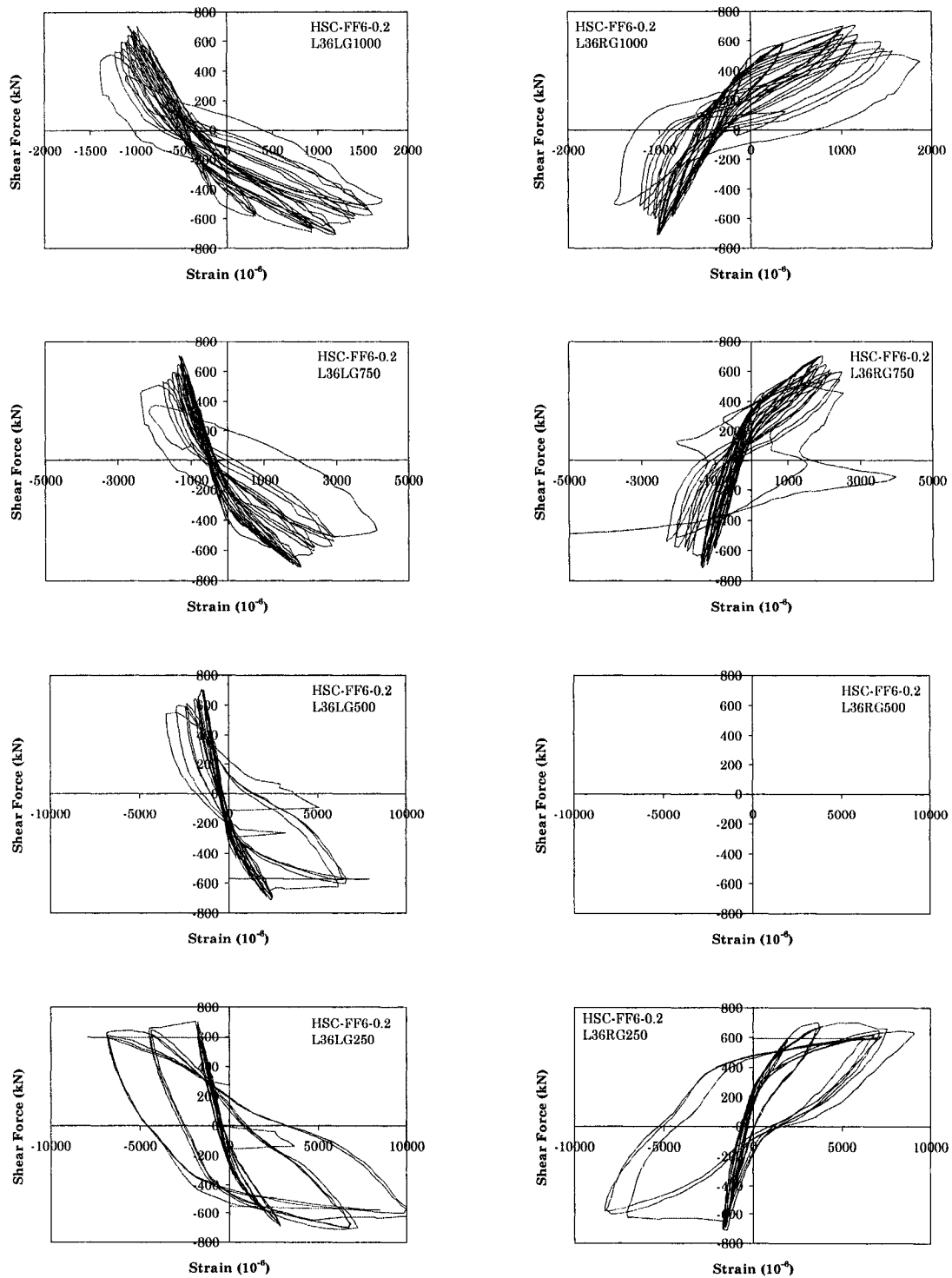
Fig. AIII.7 Strains of Longitudinal Bars for Model Column HSC-FF6-0.2

546

TRANSVERSE REINFORCEMENT STRAINS

Strain responses of transverse reinforcements are provided in this appendix. The gauge name designations are shown in the following figures. The last number following the character "G" in the gage name describes the height in mm of the hoop or tie above the bottom loading stub.
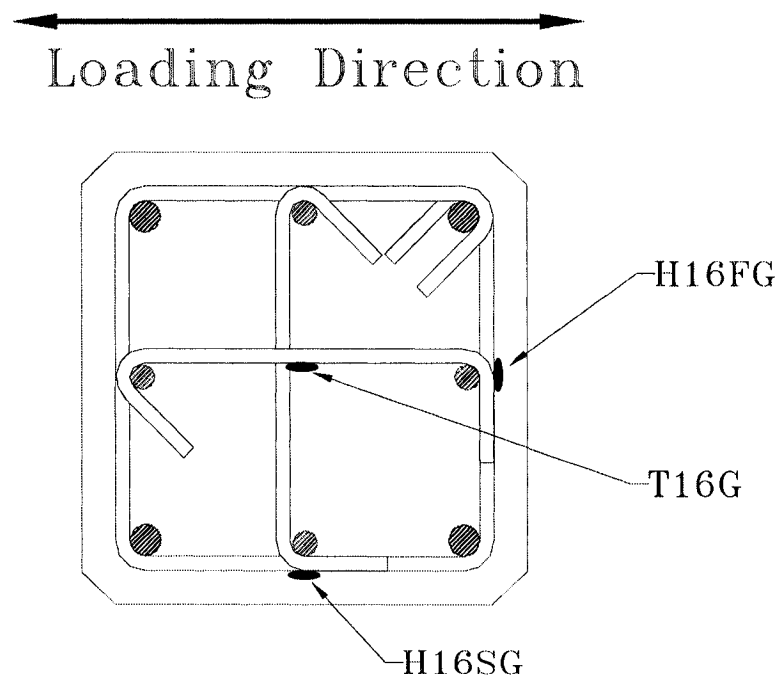
Fig. AIV.1-Strain Gage Locations of Hoops and Ties

547
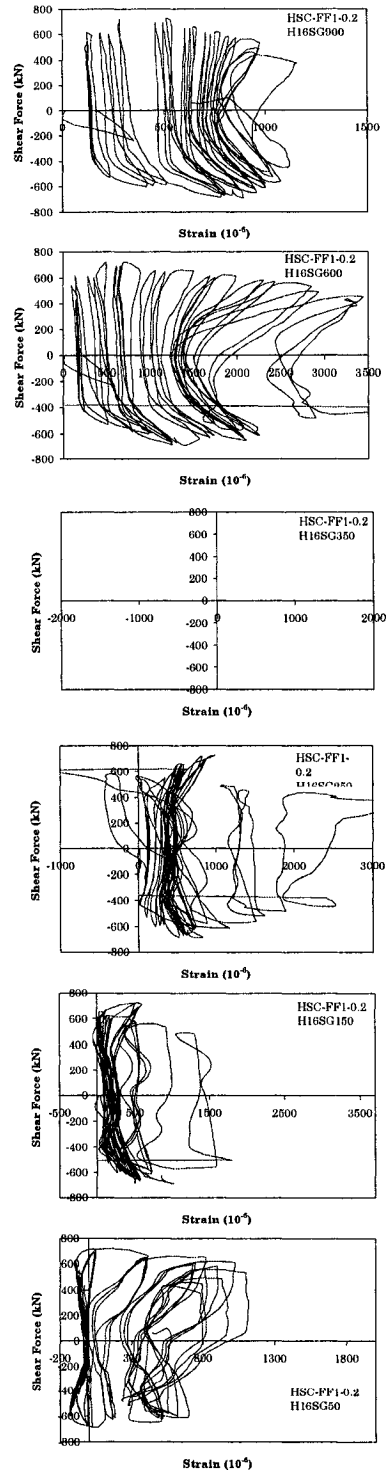
Fig. AIV.2 Hoop Strains for Model Column HSC-FF1-0.2
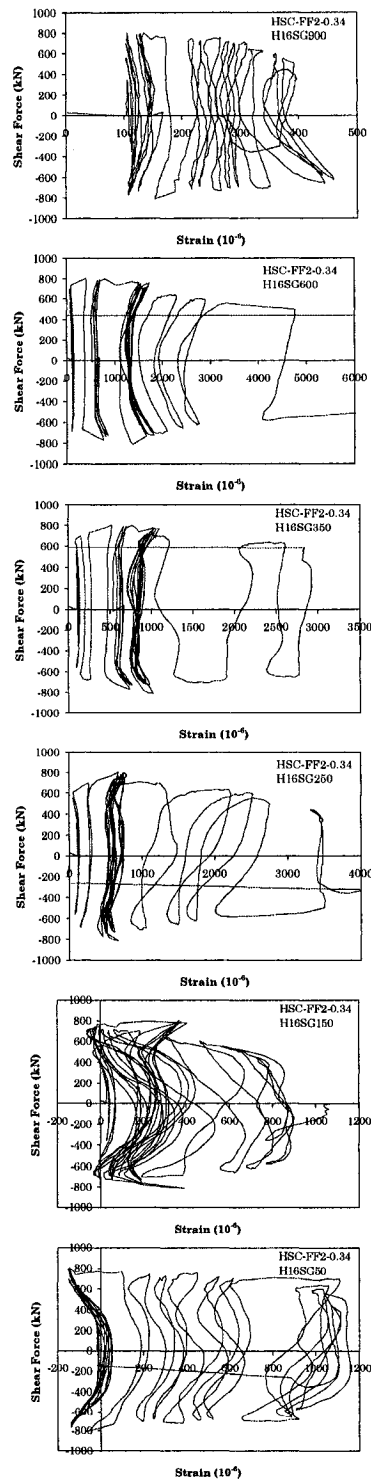
Fig. AIV.3 Hoop Strains for Model Column HSC-FF2-0.34

549
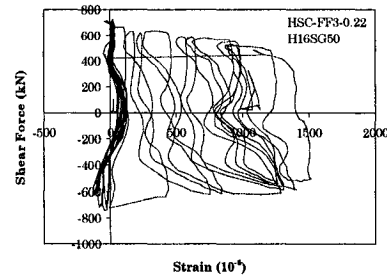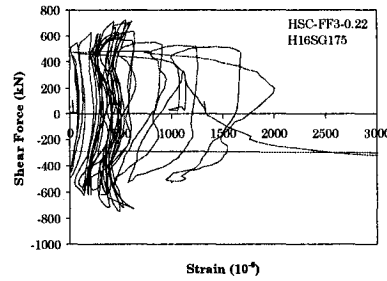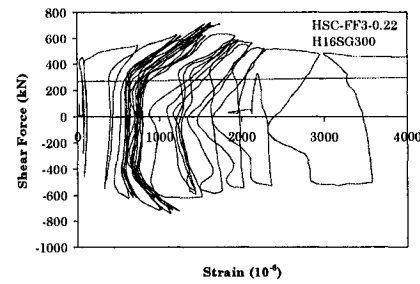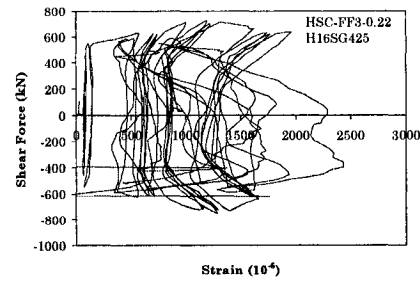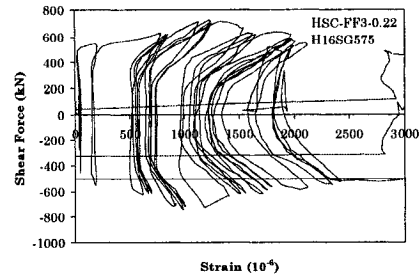
Fig. AIV.4 Hoop Strains for Model Column HSC-FF3-0.22

550
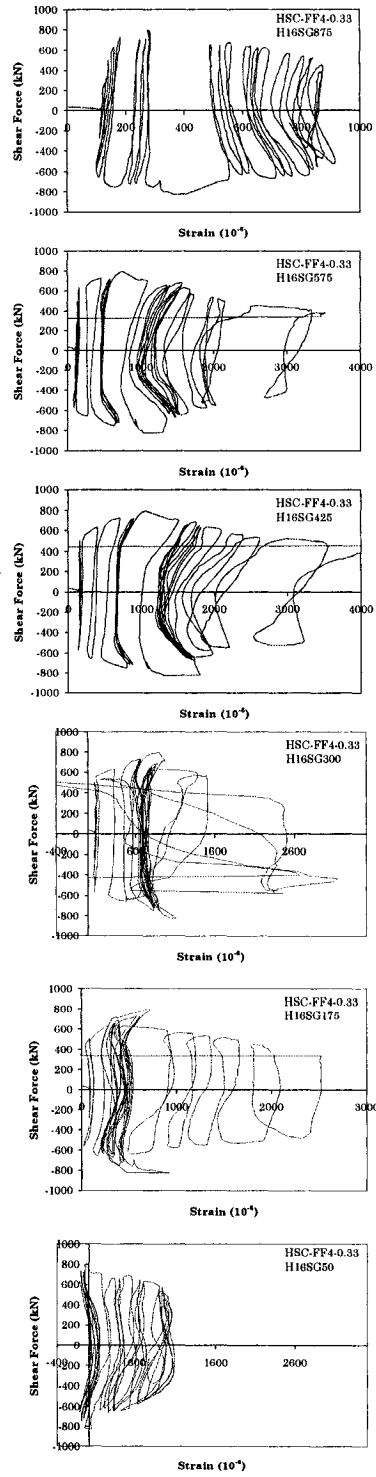
Fig. AIV.5 Hoop Strains for Model Column HSC-FF4-0.33

551
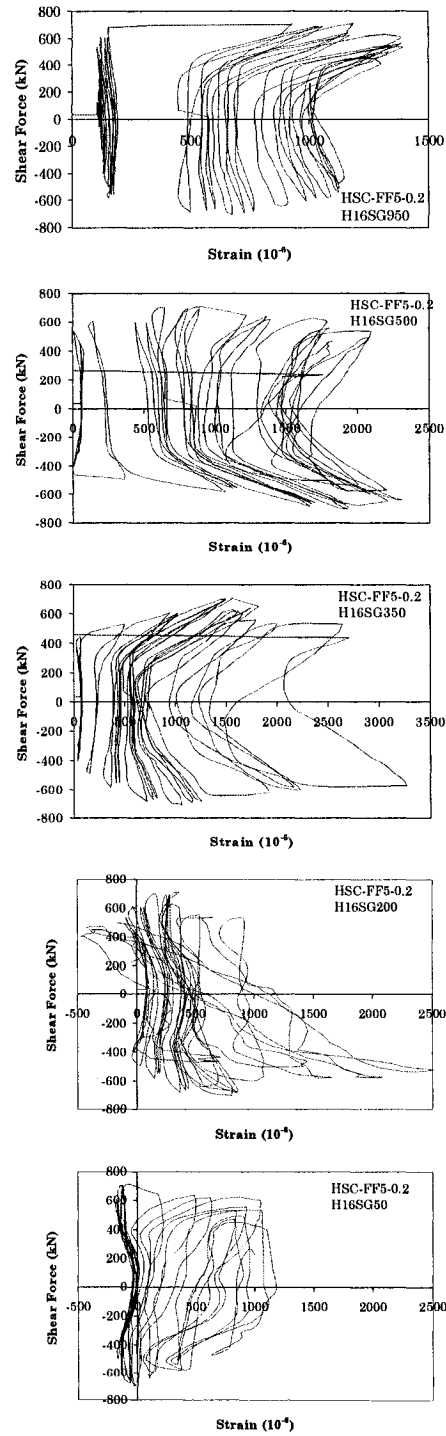
Fig. AIV.6 Hoop Strains for Model Column HSC-FF5-0.2

552
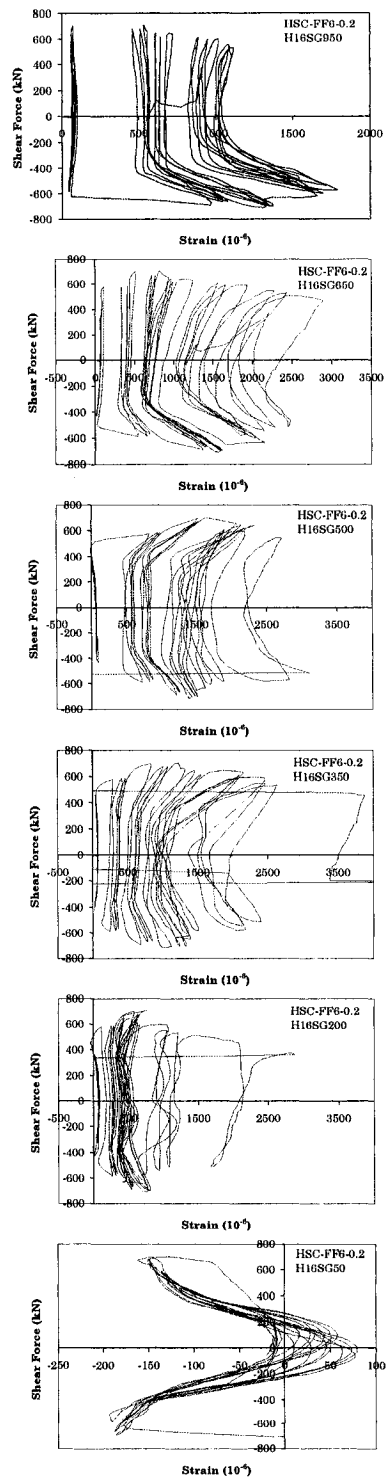
Fig. AIV.7 Hoop Strains for Model Column HSC-FF6-0.2

553
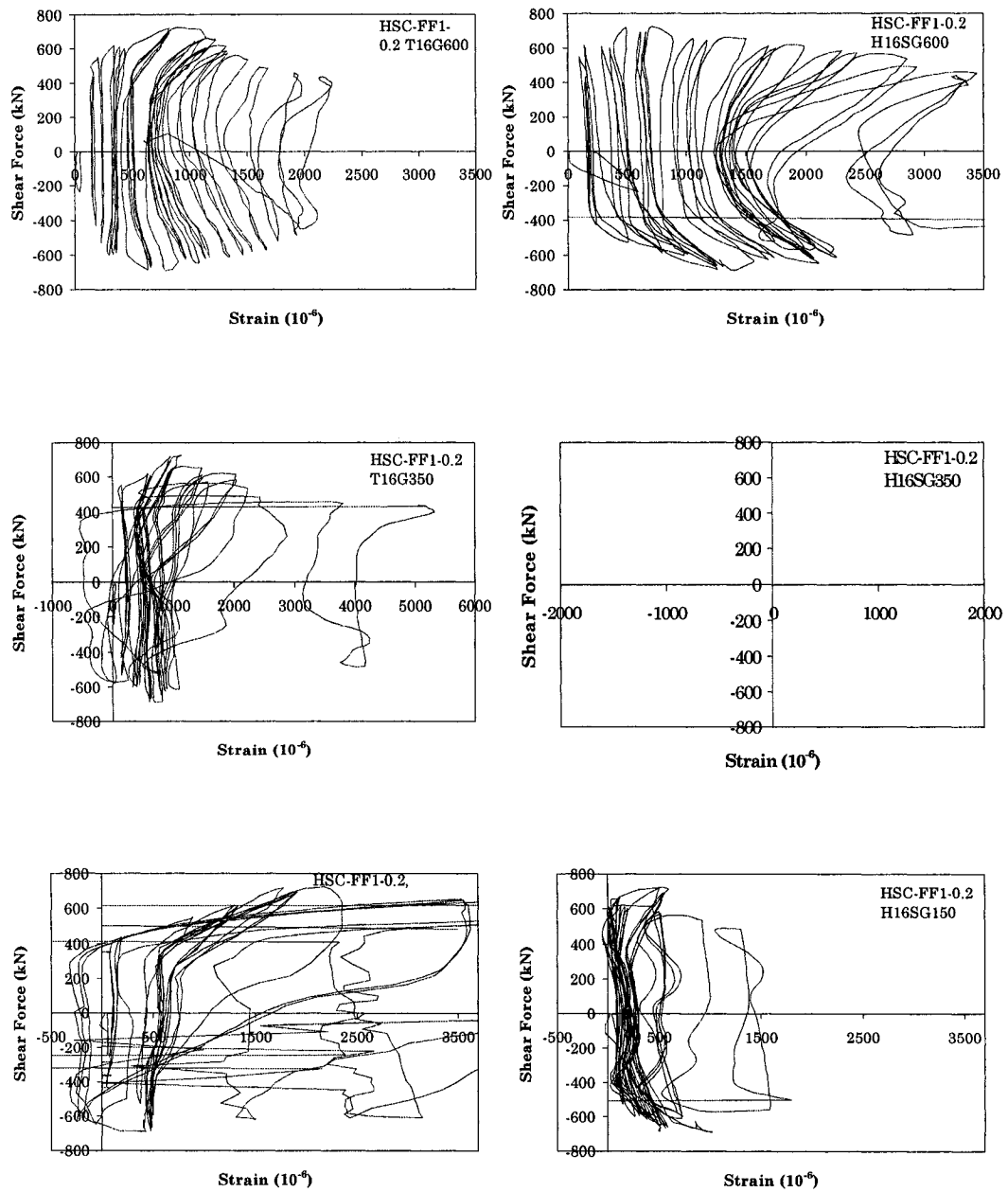
Fig. AIV.8 Comparisons of Tie and Hoop Strains for Model Column HSC-FF1-0.2
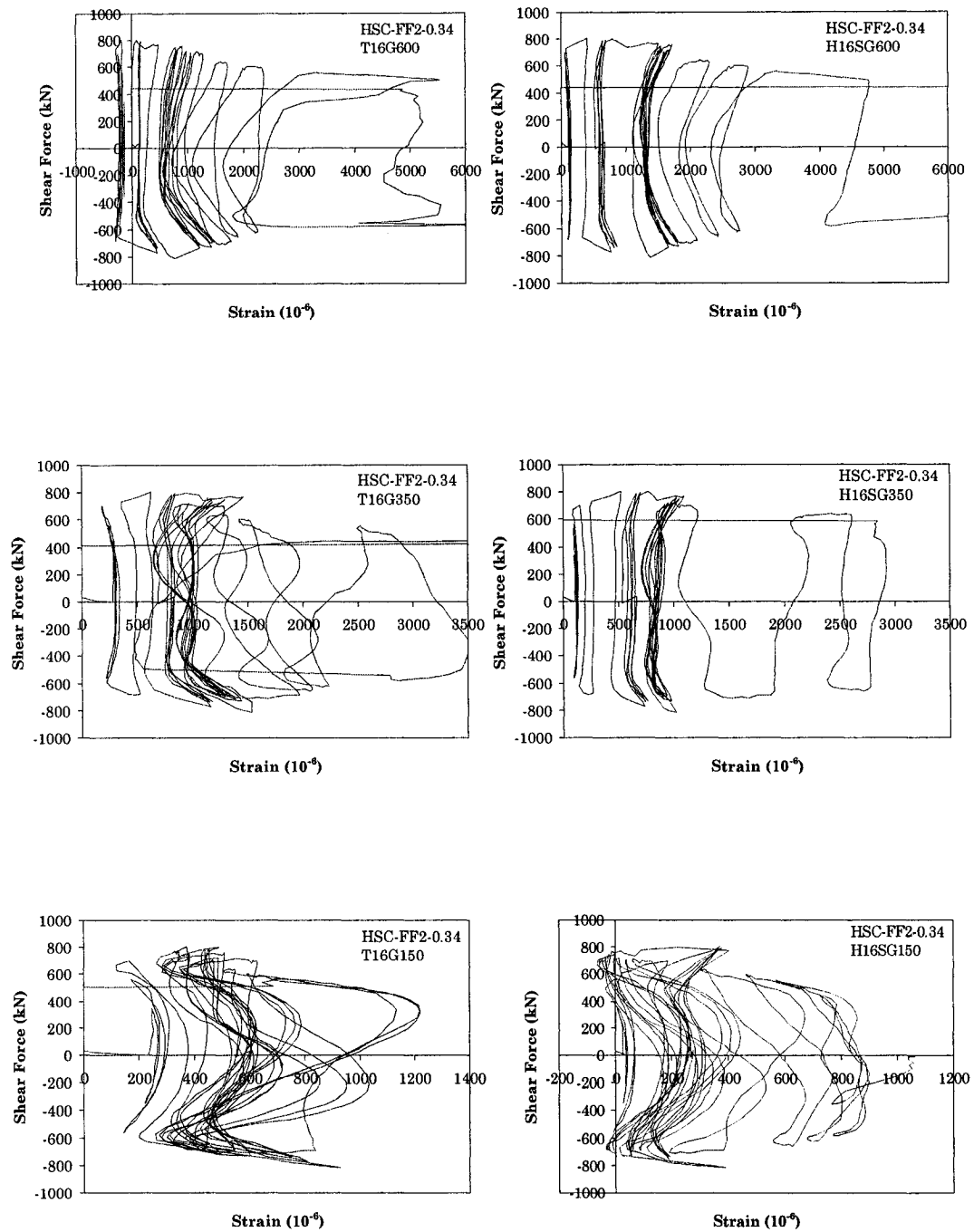
Fig. AIV.9 Comparisons of Tie and Hoop Strains for Model Column HSC-FF2-0.34
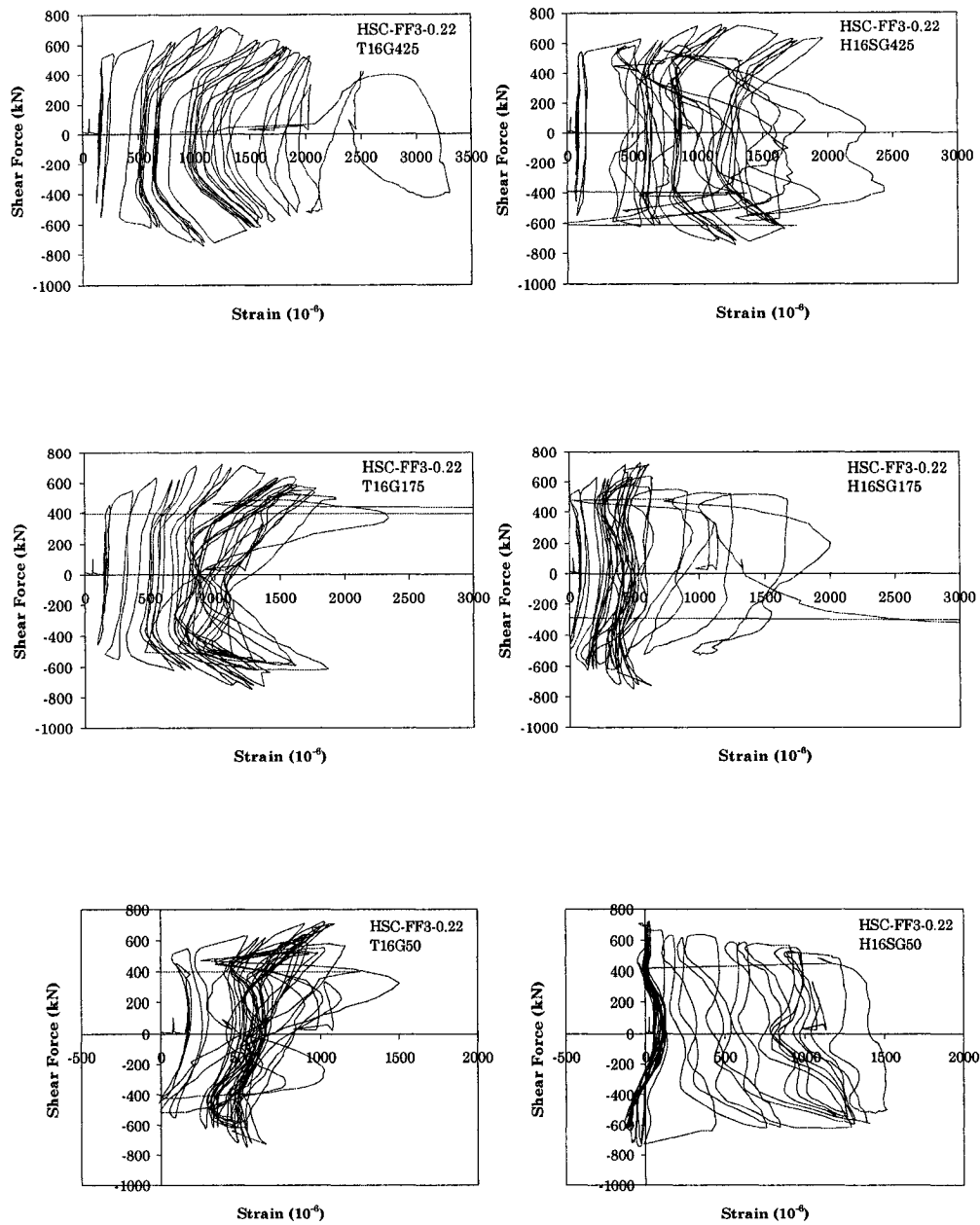
Fig. AIV.10 Comparisons of Tie and Hoop Strains for Model Column HSC-FF3-0.22
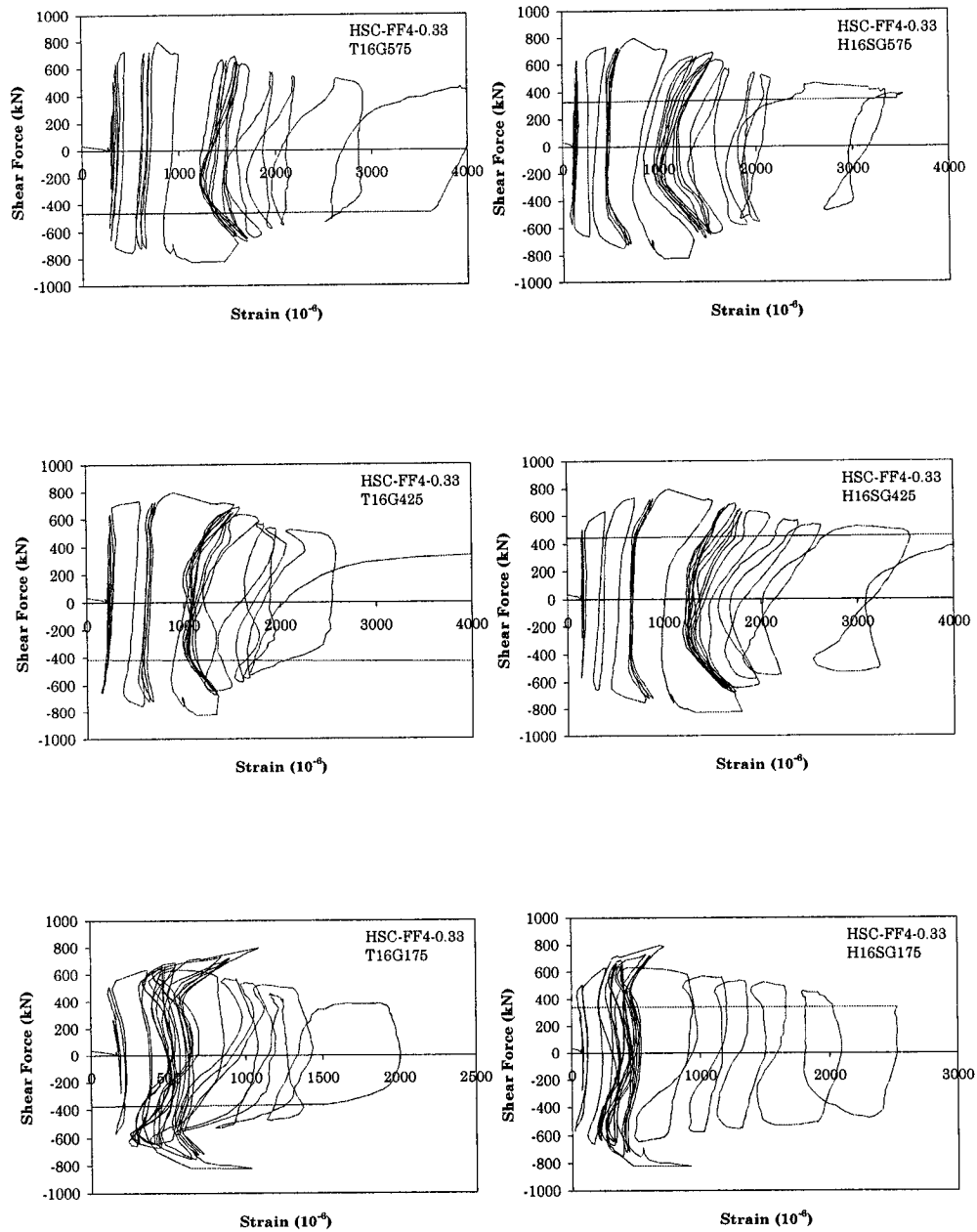
Fig. AIV.11 Comparisons of Tie and Hoop Strains for Model Column HSC-FF4-0.33

557
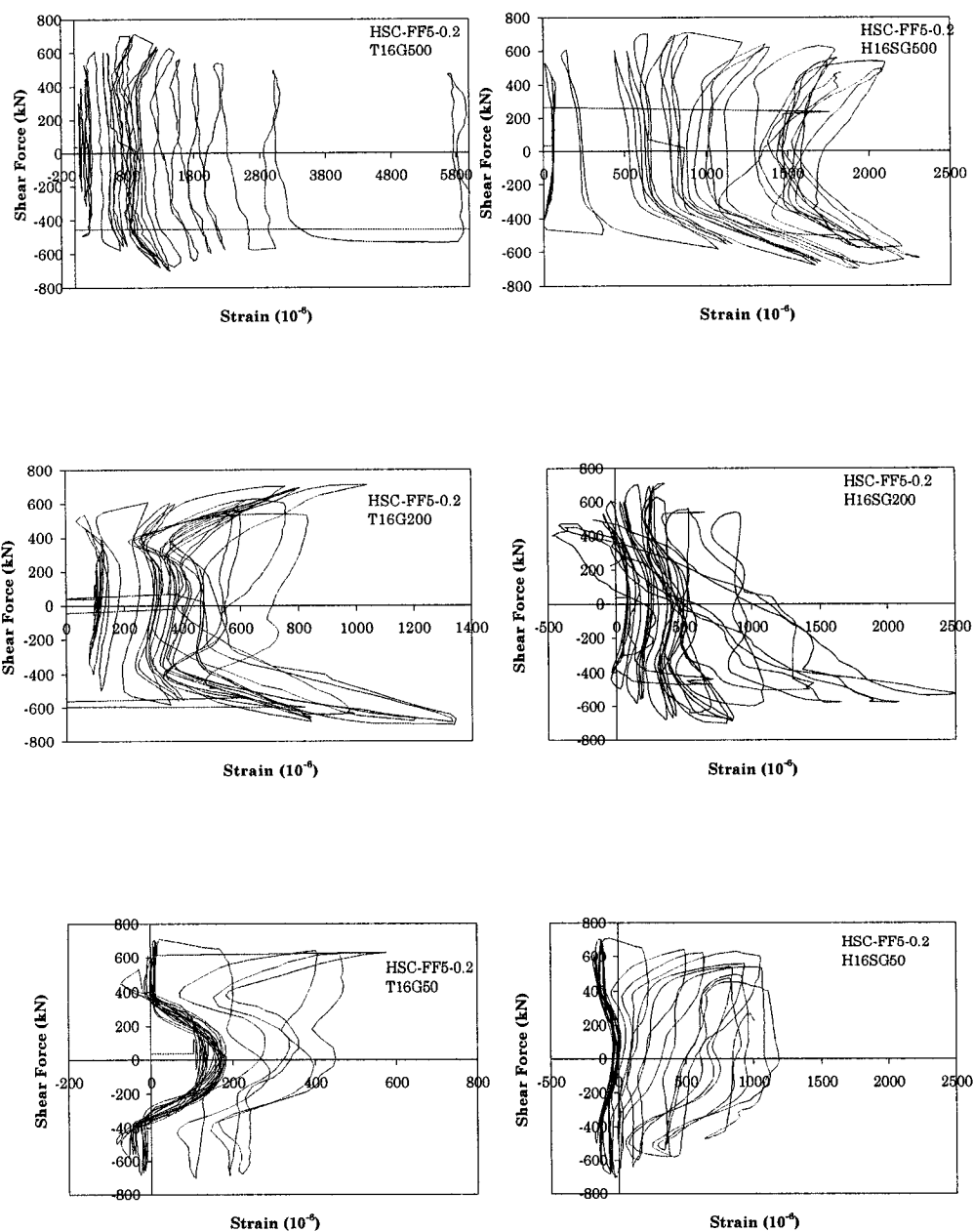
Fig. AIV.12 Comparisons of Tie and Hoop Strains for Model Column HSC-FF5-0.2

558
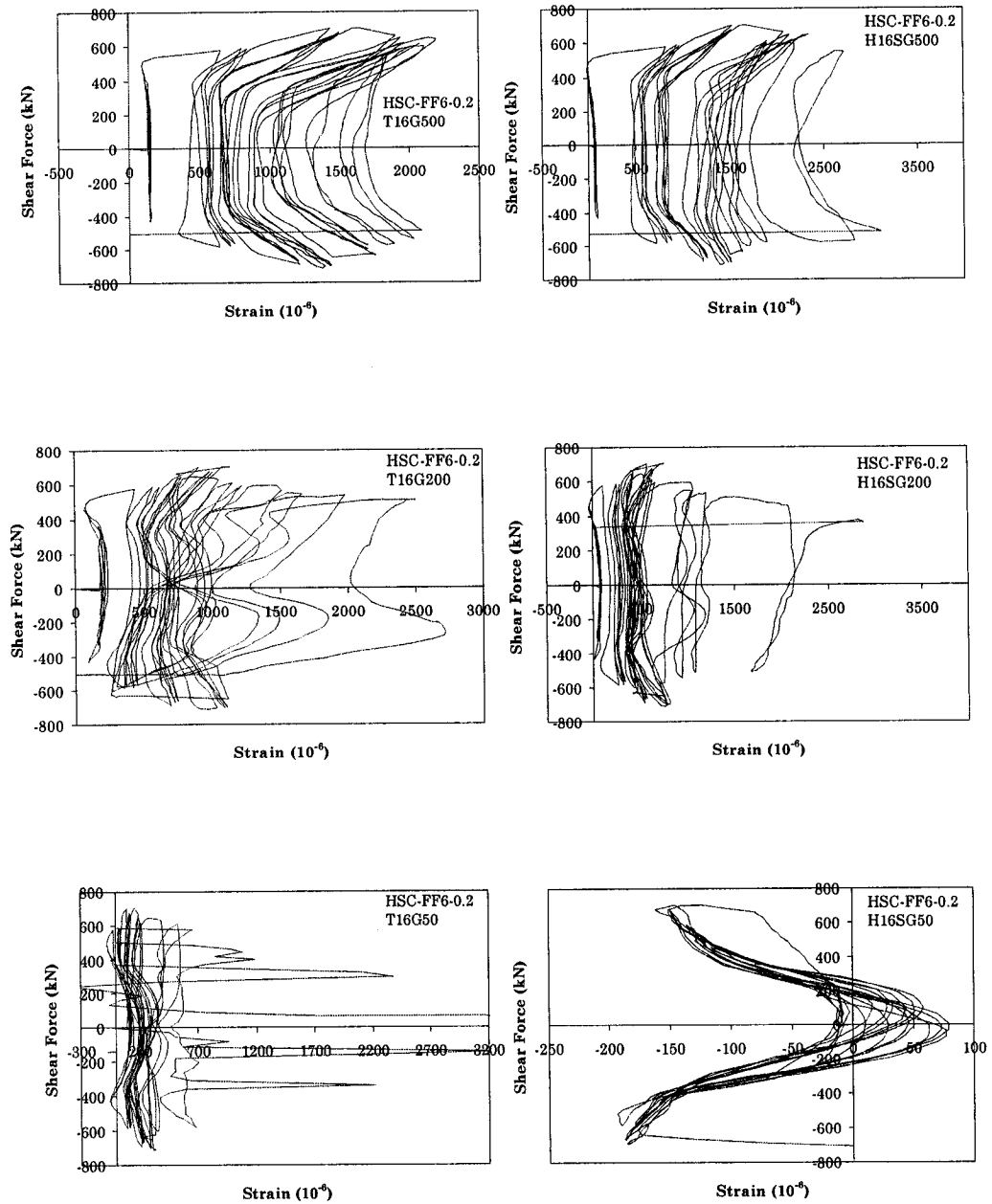
Fig. AIV.13 Comparisons of Tie and Hoop Strains for Model Column HSC-FF6-0.2

559
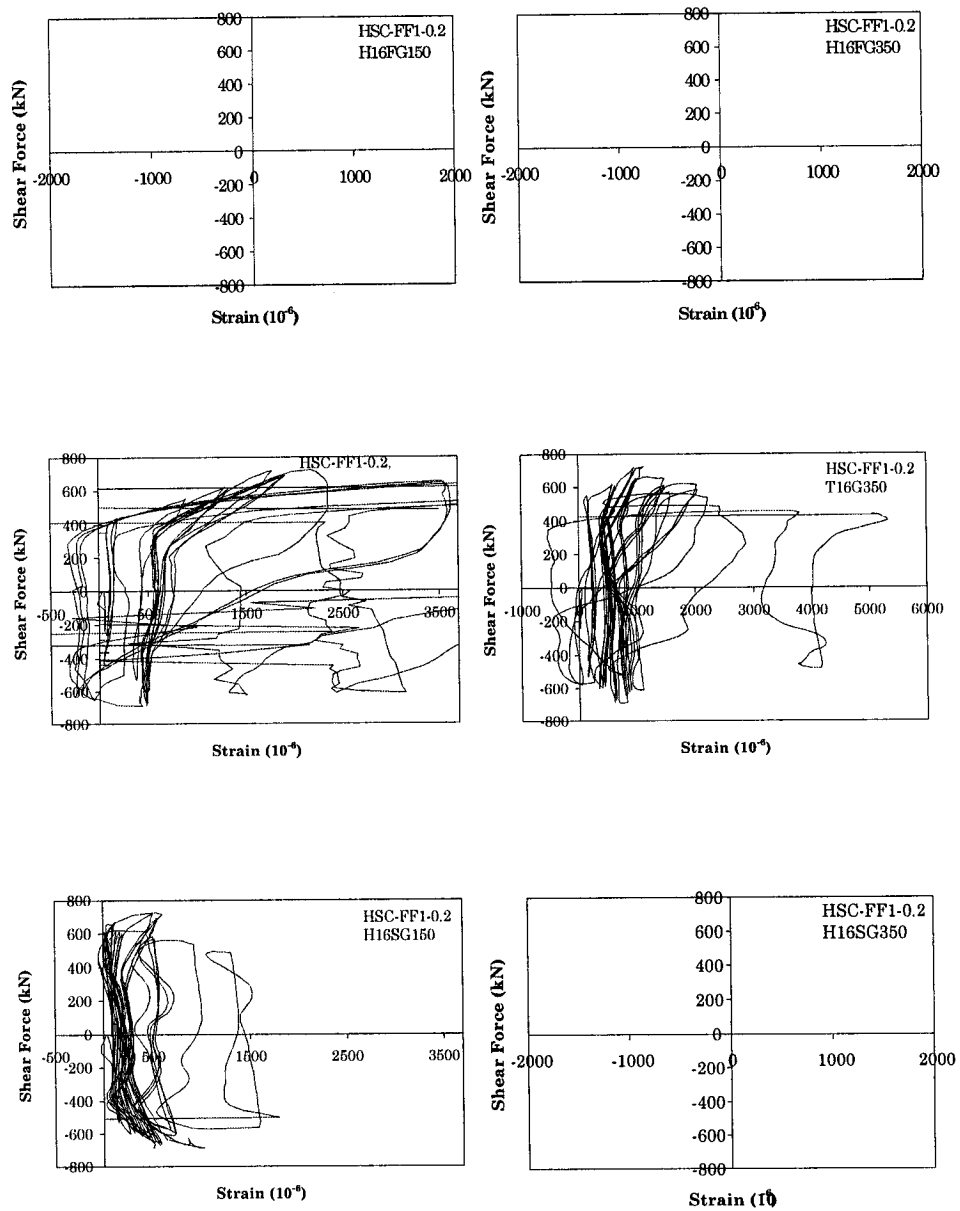
Fig. AIV.14 Transverse Reinforcement Strains in Cross Sections of
Column HSC-FF1-0.2
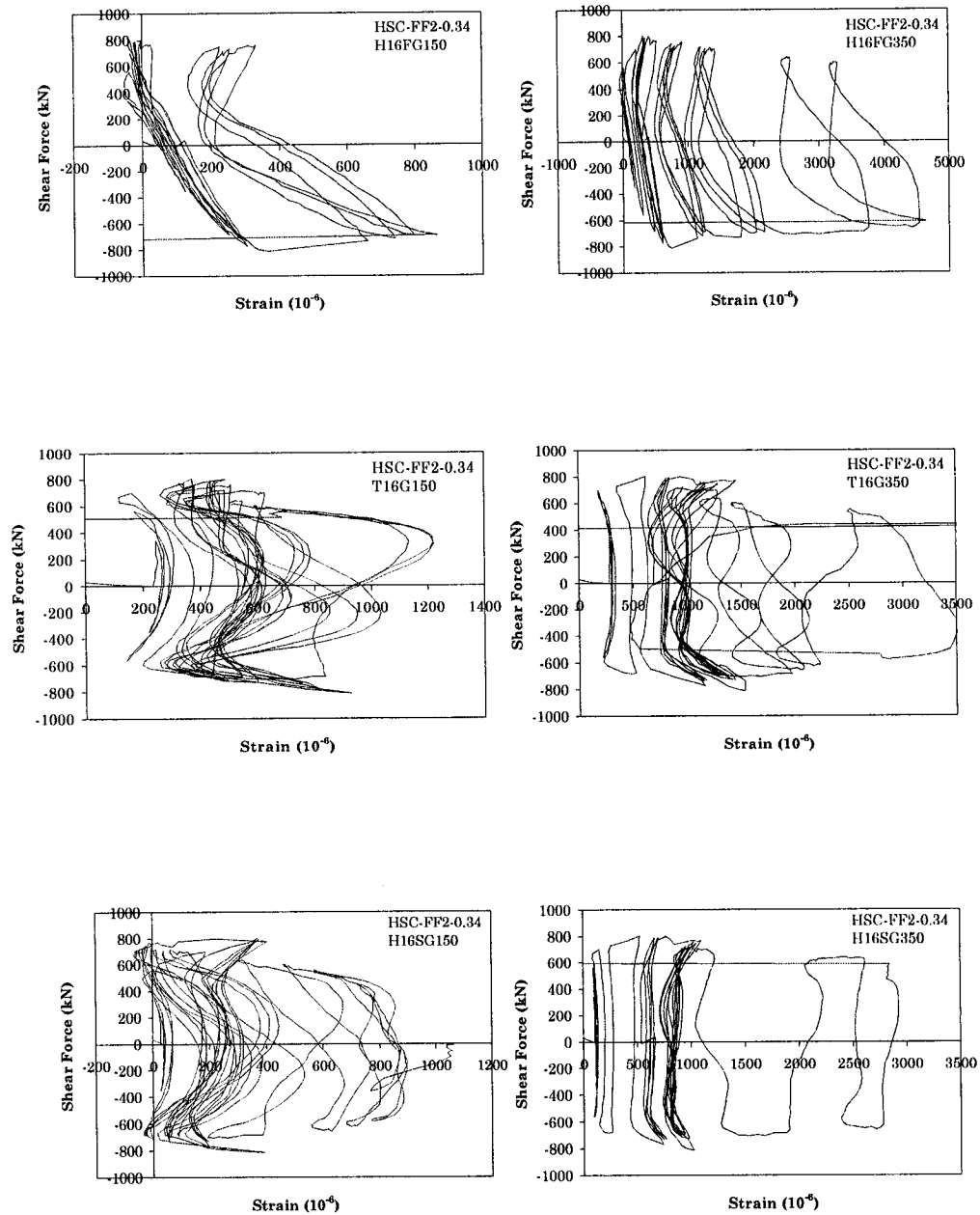
Fig. AIV.15 Transverse Reinforcement Strains in Cross Sections of Column HSC-FF2-0.34

561
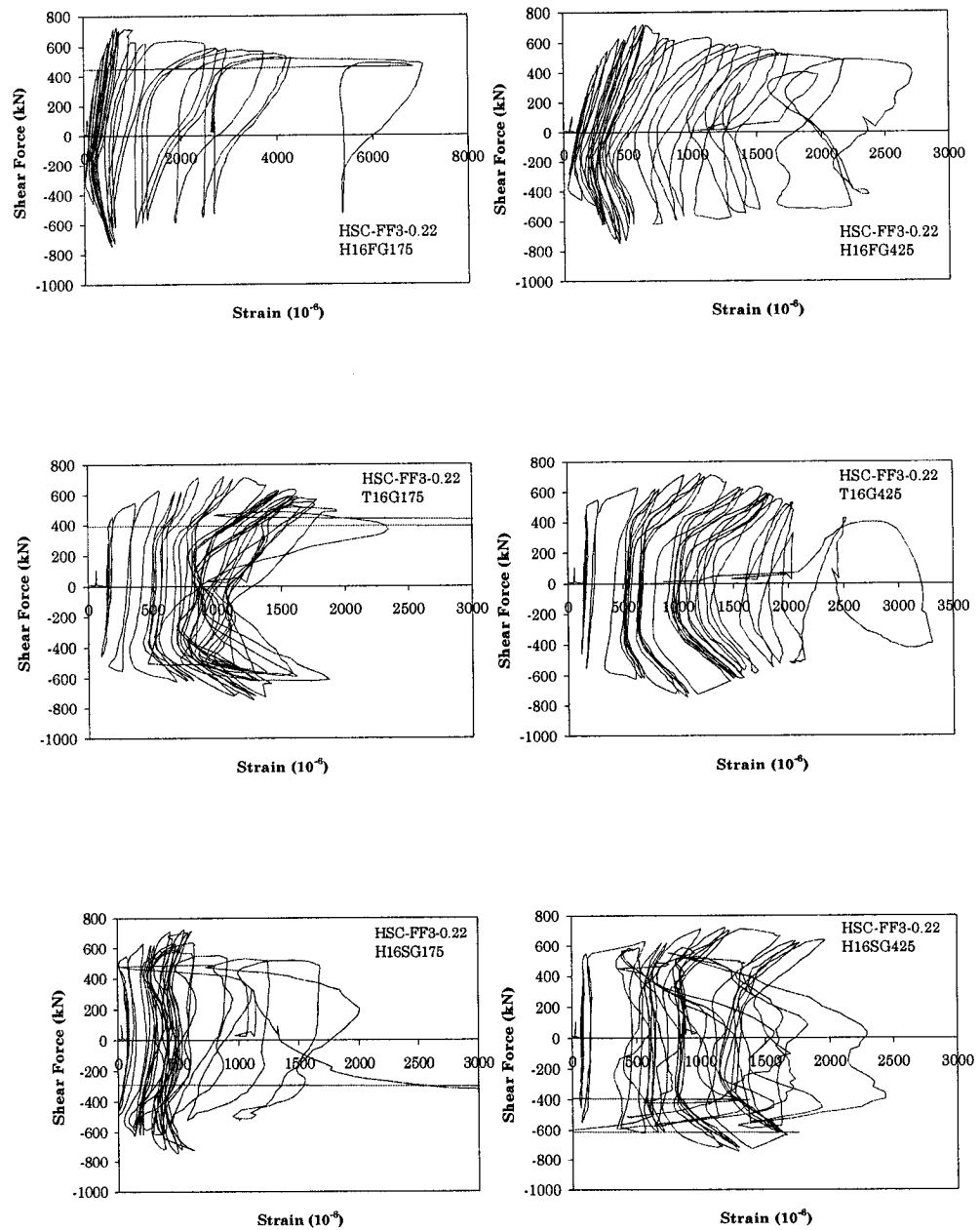
Fig. AIV.16 Transverse Reinforcement Strains in Cross Sections of Column HSC-FF3-0.22

562
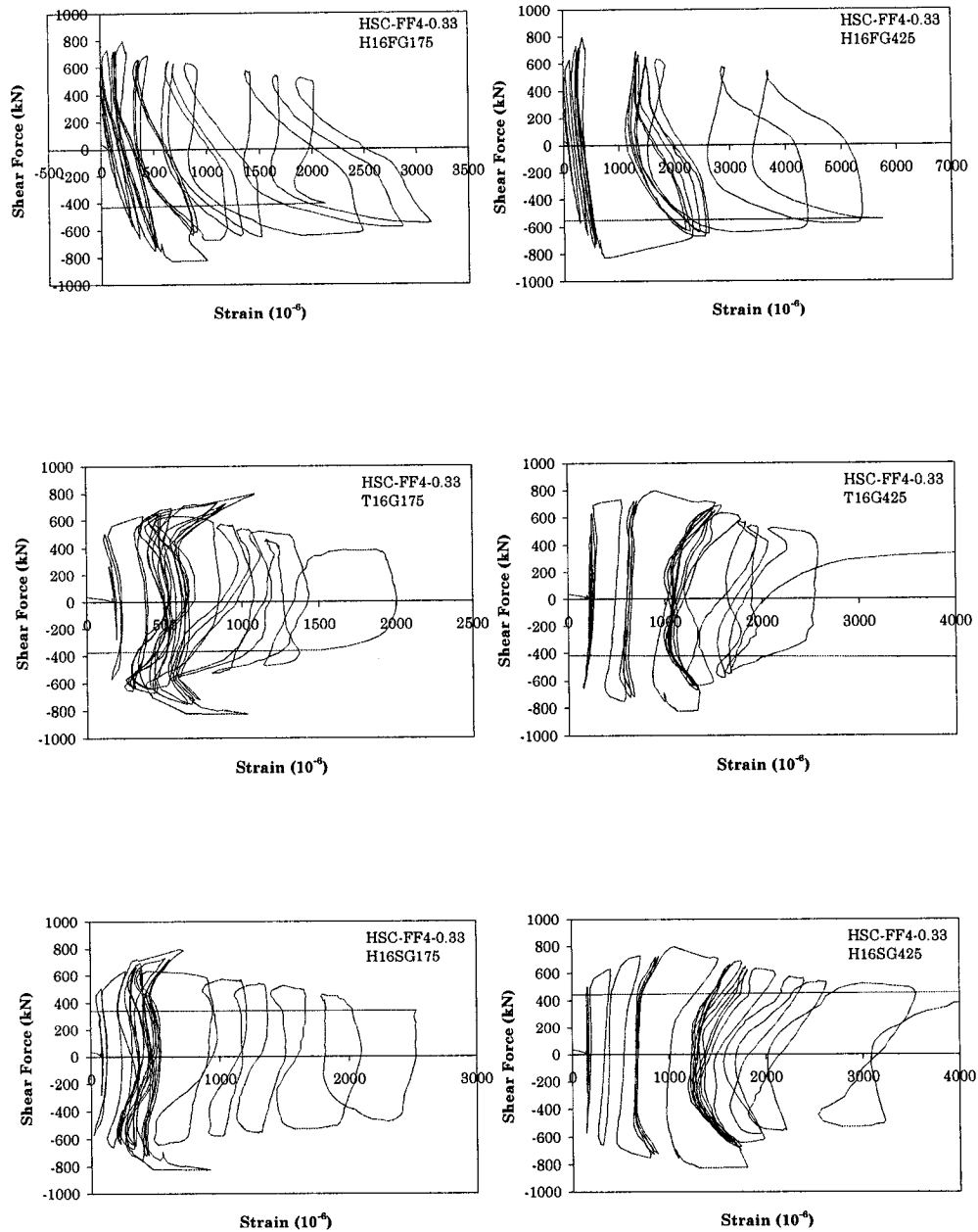
Fig. AIV.17 Transverse Reinforcement Strains in Cross Sections of Column HSC-FF4-0.33
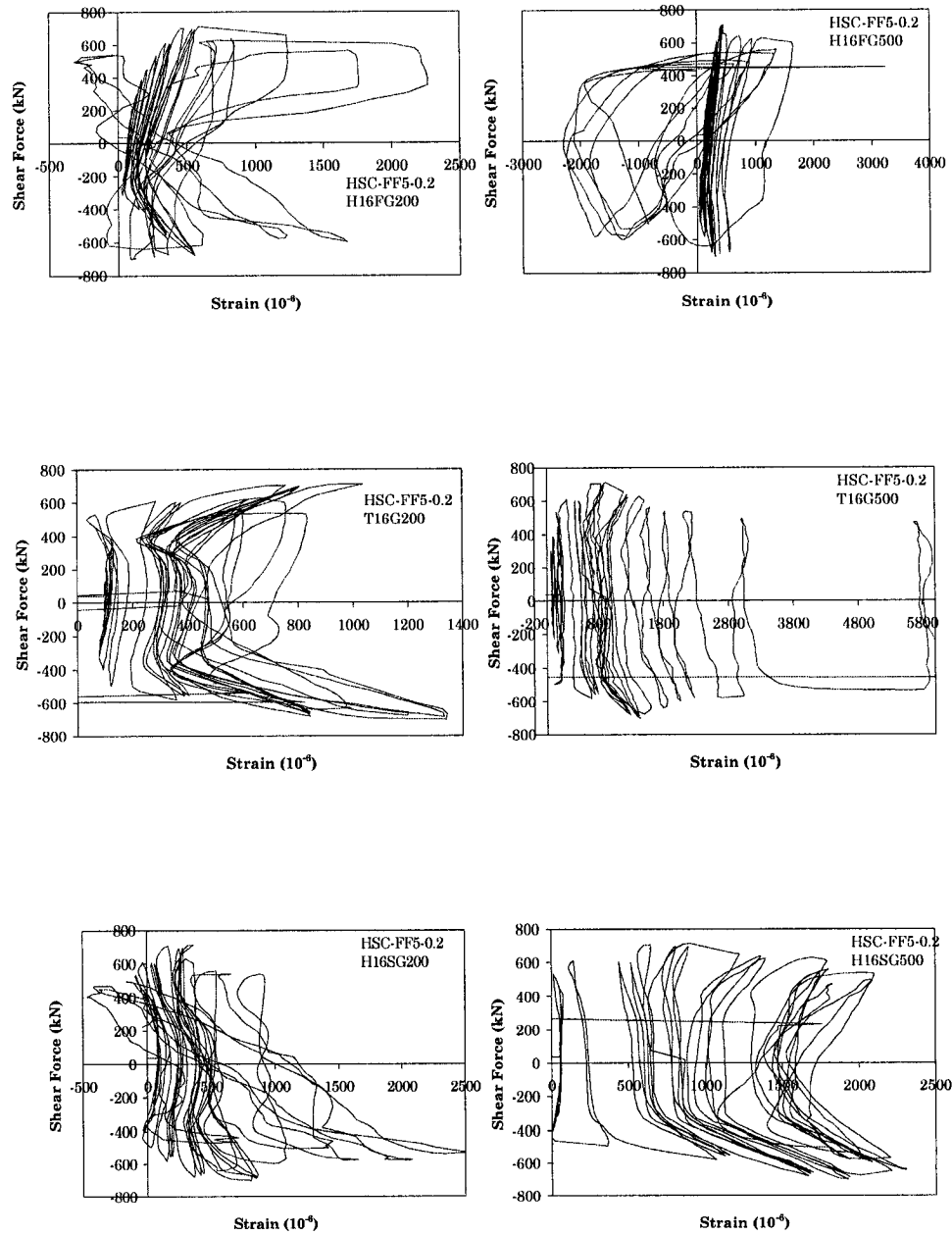
Fig. AIV.18 Transverse Reinforcement Strains in Cross Sections of Column HSC-FF5-0.2

564
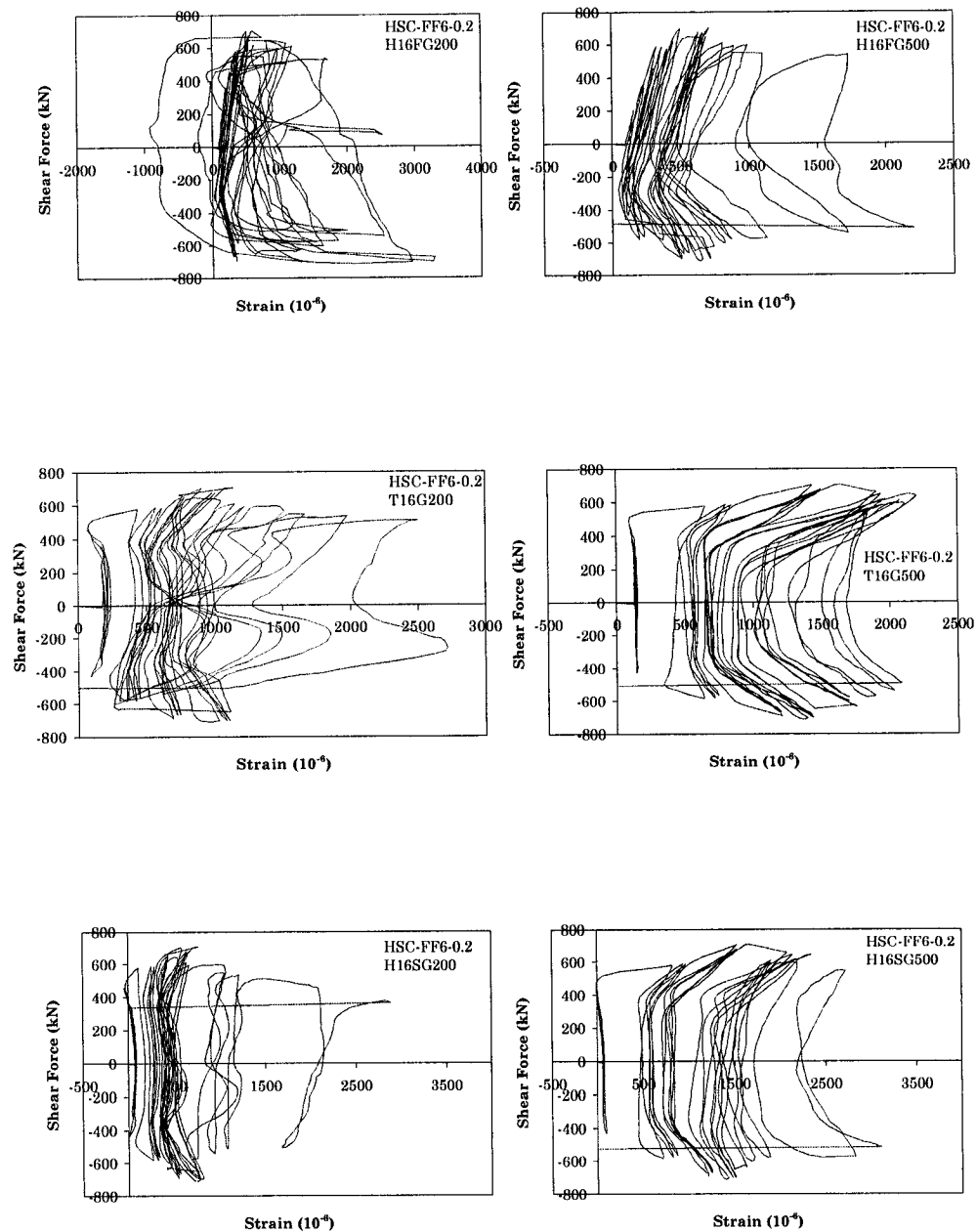
Fig. AIV.19 Transverse Reinforcement Strains in Cross Sections of Column HSC-FF6-0.2

APPENDIX V.

MOMENT-CURVATURE PROGRAM

Following is the new Moment-Curvature and Lateral Force-Displacement Fortran 77 Code which contains six NSC and seven HSC Confined Concrete Stress-Strain Models that currently exist. The code also offers options to consider mild or high steel strain-hardening using Mander and King stress-strain models.

566

```
          PROGRAM MOMENTCURVATURE
          IMPLICIT DOUBLEPRECISION(A-H,O-Z)
!         THIS CASE IS FOR SQUARE SECTION COLUMN
!         ALL COVER CONCRETE CONSIDERED ON ALL SIDES OF THE COLUMN
          REAL AS(50), YS(50), PHI(10000000)
          REAL ES(100000), X(100000),E1(100000),EC(100000)
          REAL NC(100000),MC(100000),MS(100000),NS(100000)
          REAL FS(100000),FC(100000),COUNT,FC1(100000)
          REAL PO,W,H,DY,N,HS,AH,AH1,AL,FYH,FYS,WCR,I
          REAL COVER,DH,DL,AIN,AST
          REAL FCOMP,ESTEEL,ECONCRETE,IN,IN1,OUT,OUT1,OUTT,J,ST
          REAL NN, AT, BB, CS, SS,L
          REAL E,FK
          REAL ERROR,MTOT(100000),NTOT(100000)
          REAL PH,MT,HEIGHT,FFSS,LS,MY,VY,PHIY
          REAL MAXMTOT,VU,FU,ULTSS
          REAL MU
          REAL ROX,ROY,RO,FCC,ECC
!         REAL ECU
          REAL FCONC,CONCSTRAIN,CONCSTRESS,CONCFORCE
          REAL SSCOMP,FFSSCOMP,DELI
          INTEGER NUM
!         REAL CENERGY(100000),SENERGY(100000),BALANCE
!         REAL CTOT,STOT
!         REAL ULTSTRAIN
!         REAL CORECS,FCOREC

          INTEGER NL,K,KK,M,STEELTYPE,MODELTYPE,FLAG

          OPEN (UNIT=2,FILE='N1(1)MC.XLS')
          OPEN (UNIT=3,FILE='N1(1)VD.XLS')
          OPEN (UNIT=4,FILE='VALUE1N(1).XLS')
          OPEN (UNIT=5,FILE='TENKG1N(1).XLS')
          OPEN (UNIT=6,FILE='COVCONC1N(1).XLS')
          OPEN (UNIT=7,FILE='CONC1N(1).XLS')
          OPEN (UNIT=8,FILE='COMKG1N(1).XLS')
          OPEN (UNIT=9,FILE='1(1)MC(METRIC).XLS')
          OPEN (UNIT=10,FILE='1(1)VD(METRIC).XLS')
!         OPEN (UNIT=9,FILE='CORECONC1(I)H.XLS')

          MODELTYPE=1
          STEELTYPE=1

!         STEELTYPE=0    FOR NO STRAIN HARDENING CONSIDERED
!         STEELTYPE=1    FOR MILD STEEL
!         STEELTYPE=2     FOR HIGH STRENGTH STEEL

!         MODELTYPE=1    FOR MANDER STRESS-STRAIN MODEL         **
!         MODELTYPE=2    FOR ARMEN STRESS-STRAIN MODEL *
!         MODELTYPE=3    FOR LI STRESS-STRAIN MODEL (1994) *
!         MODELTYPE=4    FOR CUSSON AND PAULTRE'S MODEL *
!         MODELTYPE=5    FOR YOUNG,NOUR, AND NAWY'S MODEL *
!         MODELTYPE=6    FOR AZIZINAMINI,KUSKA,BRUNGARDT,AND HATFIELD MODEL *
!         MODELTYPE=7    FOR SAATCIOGLU AND RAZVI'S MODEL (1992) **

!         MODELTYPE=8    FOR SAKINO'S MODEL
!         MODELTYPE=9 RICHART'S MODEL
!         MODELTYPE=10 FAFITIS AND SHAH'S MODEL
!         MODELTYPE=11 FOR SHEIKH AND UZUMERI'S MODEL
```

567

```
!        MODELTYPE=12 FOR KENT AND PARK'S MODEL (NOT INCLUDED IN THIS PROGRAM)

!        MODELTYPE=13 NEW BING LI STRESS-STRAIN MODEL (2001) *
!        MODELTYPE=14 NEW RAZVI AND SAATCIOGLU MODEL (1999) *

!        * HSC MODEL NUMBERS: 2,3,4,5,6,13,14
!        ** NSC MODEL NUMBERS: 1, 7
!        WORK WITH MODEL NUMBER 1,2,3,4,5,6,13, AND 14

!        FC1(100000)=UNCONFINED CONCRETE STRESS FOR SIDE COVER
!        NN=# OF THE LEGS OF THE TRANSVERSE REINFORCEMENT IN THE
!                   VERTICAL CROSS SECTION WITHIN THE SPACING HS
         NN=3
!        NL=# OF ROWS OF LONGITUDINAL BARS
         NL=3
!        AS() = SUM OF AREAS FOR EACH ROW OF LONGITUDINAL STEEL
         AS(1)=4.12
         AS(2)=2.00
         AS(3)=4.12
!        YS() = COORDINATE FROM THE EDGE OF THE COLUMN
         YS(1)=17.24
         YS(2)=10.00
         YS(3)=2.76
         L=8.
!        L=# OF LONGITUDINAL BARS
         PO=749
         W=20.
         H=20.
         LS=70
!        LS=SHEAR SPAN LENGTH IN INCHES
         HEIGHT=70
!        HEIGHT= COLUMN HEIGHT IN INCHES
         ESTEEL=27363
         FCOMP=9.3
         ECONCRETE=57.*((FCOMP*1000)**0.5)
!        N=100.
         N=400.
!        N=300
!        N=# OF STRIPS OF THE COLUMN SECTION
         HS=4.0
!        HS=HOOP SPACING
!        AH=TRANSVERSE BAR AREA (HOOPS OR TIES)
         AH=0.31
         AH1=0.0
!        AT=CROSS SECTIONAL AREA OF ONE LEG OF TRANSVERSE
!                   REINFORCEMENT
!        FOR #5 BAR
         AT=AH
         AL=1.27
!        AL=AVERAGE LONGITUDINAL BAR AREA
         DH=(4.*AH/3.142)**0.5
         DL=(4.*AL/3.142)**0.5
         FYH=60.9
!        FYH = YIELD STRENGTH OF HOOPS/TIES
         FYS=68.2
!        FYS = YIELD STRENGTH OF LONGITUDINAL BARS
         COVER=1.5
         FU=114.5
!        FU=ULTIMATE LONGITUDINAL BAR TENSILE STRENGTH (KSI)
         WCR=(W-(2*COVER)-(2*DH)-(3*DL))/2
!        WCR=CLEAR SPACE BETWEEN LONGITUDINAL BARS
!        BB=WIDTH MEASURED FROM THE CENTER LINES OF THE OUT MOST
```

568

```
!                     PERIMETER HOOPS
              BB=W-(2*COVER)-DH
              DO 10 I=1,NL
              AST=AST+AS(I)
!             AST=TOTAL LONGITUDINAL STEEL AREA
10            CONTINUE
              AIN=L*((WCR**2.0)/6)
!             AIN=AREA OF INEFFECTUALLY CONFINED CORE CONCRETE
              DY=H/N
              NUM=(COVER+DH)/DY
              COUNT=0
              DELI=0
              FLAG=1
              PHI(J)=0
              X(I)=0
              CS=0
              MC(I)=0
              SS=0
              MS(I)=0
              MTOT(I)=0
              WRITE(2,25) COUNT,PHI(J),X(I),CS,MC(I),SS,MS(I),MTOT(I)
              WRITE(*,25) COUNT,PHI(J),X(I),CS,MC(I),SS,MS(I),MTOT(I)
              WRITE(9,27) COUNT,PHI(J)*39.37,X(I)*2.54,CS,MC(I)*0.11298,SS,MS(I)*0.11298,MTOT(I)*0.11298
25
              FORMAT(2X,'COUNT=',F5.0,2X,'PHI(J)=',F10.8,2X,'X(I)=',F5.2,2X,'ec(I)=',F10.8,2X,'MC(I)=',F8.2,2X,'
              es(I)=',F10.8,2X,'MS(I)=',2X,F8.2,2X,'MTOT(I)=',F9.2,2X)
27            FORMAT(2X,'COUNT=',F5.0,2X,'PHI(J)[1/M]=',F10.8,2X,'X(I)[CM]=',F5.2,2X,'ec(I)=',F10.8,2X,'MC(I)[
              kN*M]=',F8.2,2X,'es(I)=',F10.8,2X,'MS(I)[kN*M]=',2X,F8.2,2X,'MTOT(I)[kN*M]=',F9.2,2X)
              DELI=0
              V=0
              WRITE(3,26) DELI, V
              WRITE(*,26) DELI, V
              WRITE(10,29) DELI*2.54, V*4.44822, DELI*100/LS, V*4.44822
26            FORMAT(2X,'DELI=',F8.2,2X,'V=',F8.2,2X)
29            FORMAT(2X,'DELI[CM]=',F8.2,2X,'V[KN]=',F8.2,2X,'DRIFT RATIO[%]=',F8.2,2X,'V[KN]=',F8.2,2X)

              GOTO 123
122           FLAG=2
123           DO 1 J=0,0.018,0.0001
                      PHI(J)=J
                      DO 2 I=1,8*N
                              X(I)=DY*I
                              NC(0)=0
                              MC(0)=0
                              NS(0)=0
                              MS(0)=0
                      M=X(I)/DY
!             X(I)= DEPTH OF THE COMPRESSION ZONE
!             M=# OF STRIPS FOR COMPRESSION ZONE
!                             CS=0
!                             SS=0
                              ES(0)=0
                              EC(0)=0
                              DO 3 K=1, M
                                      E1(K)=(H)-(DY*(K-1))
                                      EC(K)=PHI(J)*(E1(K)-(H-X(I)))
                                      IN=EC(K)
                                      IF ((EC(K).GT.0.0).AND.(E1(K).LE.H-COVER-
                                      (DH/2)).AND.(E1(K).GE.COVER+(DH/2))) THEN
                                              IF (MODELTYPE.EQ.1) THEN
                                      CALL FCK(IN,FCOMP,HS,AH,W,H,FYH,COVER,DH,AST,AIN,OUT)
                                              ELSEIF (MODELTYPE.EQ.2) THEN
```

569

```
                    CALL AFCK(IN,NN,AT,BB,HS,FYS,FCOMP,OUT)
                        ELSEIF (MODELTYPE.EQ.3) THEN
                    CALL LI (AH,BB,AST,FYH,FCOMP,HS,DH,DL,W,H,WCR,IN,OUT)
                        ELSEIF (MODELTYPE.EQ.4) THEN
            CALL CUSPAU(IN,FYH,HS,DH,AST,W,H,BB,WCR,L,AH,FCOMP,ESTEEL,OUT)
                        ELSEIF (MODELTYPE.EQ.5) THEN
                    CALL YON(HS,BB,DH,AST,W,H,DL,FYH,FCOMP,AH,L,IN,OUT)
                        ELSEIF (MODELTYPE.EQ.6) THEN
                    CALL AZI(HS,BB,DH,AST,W,H,DL,FYH,FCOMP,AH,L,IN,OUT)
                        ELSEIF (MODELTYPE.EQ.7) THEN
                    CALL SAARAZ(BB,FYH,HS,FCOMP,IN,OUT,AH)
                        ELSEIF (MODELTYPE.EQ.8) THEN
                    CALL SAK(FCOMP,BB,COVER,DH,DL,HS,FYH,AH,IN,OUT,W)
                        ELSEIF (MODELTYPE.EQ.9) THEN
                    CALL RICH(FYH,FCOMP,AH,BB,HS,IN,OUT)
                        ELSEIF (MODELTYPE.EQ.10) THEN
                    CALL FAFSHA(IN,FCOMP,HS,BB,AH,FYH,OUT)
                        ELSEIF (MODELTYPE.EQ.11) THEN
                CALL SHUZ(OUT,IN,AH,L,COVER,W,DH,DL,BB,AST,FCOMP,HS,FYH)
                        ELSEIF (MODELTYPE.EQ.13) THEN
        CALL BINGLI(COVER,AIN,AH,AST,FYH,FCOMP,HS,DH,W,H,IN,OUT,STEELTYPE)
                        ELSEIF (MODELTYPE.EQ.14) THEN
        CALL RAZSAAT(DH,DL,COVER,W,NN,ESTEEL,BB,FYH,HS,FCOMP,IN,OUT,AH)
                        ENDIF
                            FC(K)=OUT
                    ELSEIF ((EC(K).LE.0.0).OR.(E1(K).LT.0.0)) THEN
                        FC(K)=0.0
                        FC1(K)=0.0
            ELSEIF ((EC(K).GT.0.0).AND.(E1(K).LE.H).AND.(E1(K).GT.H-COVER-(DH/2))) THEN
                        IF (MODELTYPE.EQ.1) THEN
                    CALL FCKK(IN,FCOMP,HS,AH1,W,H,FYH,COVER,DH,AST,AIN,OUTT)
                        ELSEIF (MODELTYPE.EQ.2) THEN
                    CALL AFCKK(IN,FCOMP,OUTT)
                        ELSEIF (MODELTYPE.EQ.3) THEN
                    CALL LII (BB,AST,FYH,FCOMP,HS,DH,DL,W,H,WCR,IN,OUTT)
                        ELSEIF (MODELTYPE.EQ.4) THEN
            CALL CUSPAUU(IN,FYH,HS,DH,AST,W,H,BB,WCR,L,AH,FCOMP,ESTEEL,OUTT)
                        ELSEIF (MODELTYPE.EQ.5) THEN
                    CALL YONW(HS,BB,AST,W,H,DL,FYH,FCOMP,L,IN,OUTT)
                        ELSEIF (MODELTYPE.EQ.6) THEN
                    CALL AZIZ(HS,BB,AST,W,H,FYH,FCOMP,IN,OUTT)
                        ELSEIF (MODELTYPE.EQ.7) THEN
                    CALL SAARAZZ(FYH,FCOMP,IN,OUTT)
                        ELSEIF (MODELTYPE.EQ.8) THEN
                    CALL SAKK(FCOMP,BB,COVER,DH,DL,HS,FYH,IN,OUTT,W)
                        ELSEIF (MODELTYPE.EQ.9) THEN
                    CALL RICHH(FYH,FCOMP,AH,BB,HS,IN,OUTT)
                        ELSEIF (MODELTYPE.EQ.10) THEN
                    CALL FAFSHAA(IN,FCOMP,OUTT)
                        ELSEIF (MODELTYPE.EQ.11) THEN
                CALL SHUZZ(OUTT,IN,L,COVER,W,DH,DL,BB,AST,FCOMP,HS,FYH)
                        ELSEIF (MODELTYPE.EQ.13) THEN
                    CALL BINGLII(FYH,FCOMP,IN,OUTT,STEELTYPE)
                        ELSEIF (MODELTYPE.EQ.14) THEN
        CALL RAZSAATT(DH,DL,COVER,W,NN,ESTEEL,BB,FYH,HS,FCOMP,IN,OUTT)
                        ENDIF
                            FC(K)=OUTT
            ELSEIF ((EC(K).GT.0.0).AND.(E1(K).LT.COVER+(DH/2)).AND.(E1(K).GE.0.0)) THEN
                        IF (MODELTYPE.EQ.1) THEN
                    CALL FCKK(IN,FCOMP,HS,AH1,W,H,FYH,COVER,DH,AST,AIN,OUTT)
                        ELSEIF (MODELTYPE.EQ.2) THEN
                    CALL AFCKK(IN,FCOMP,OUTT)
```

```
                    ELSEIF (MODELTYPE.EQ.3) THEN
          CALL LII (BB,AST,FYH,FCOMP,HS,DH,DL,W,H,WCR,IN,OUTT)
                    ELSEIF (MODELTYPE.EQ.4) THEN
   CALL CUSPAUU(IN,FYH,HS,DH,AST,W,H,BB,WCR,L,AH,FCOMP,ESTEEL,OUTT)
                    ELSEIF (MODELTYPE.EQ.5) THEN
          CALL YONW(HS,BB,AST,W,H,DL,FYH,FCOMP,L,IN,OUTT)
                    ELSEIF (MODELTYPE.EQ.6) THEN
          CALL AZIZ(HS,BB,AST,W,H,FYH,FCOMP,IN,OUTT)
                    ELSEIF (MODELTYPE.EQ.7) THEN
          CALL SAARAZZ(FYH,FCOMP,IN,OUTT)
                    ELSEIF (MODELTYPE.EQ.8) THEN
          CALL SAKK(FCOMP,BB,COVER,DH,DL,HS,FYH,IN,OUTT,W)
                    ELSEIF (MODELTYPE.EQ.9) THEN
          CALL RICHH(FYH,FCOMP,AH,BB,HS,IN,OUTT)
                    ELSEIF (MODELTYPE.EQ.10) THEN
          CALL FAFSHAA(IN,FCOMP,OUTT)
                    ELSEIF (MODELTYPE.EQ.11) THEN
        CALL SHUZZ(OUTT,IN,L,COVER,W,DH,DL,BB,AST,FCOMP,HS,FYH)
                    ELSEIF (MODELTYPE.EQ.13) THEN
          CALL BINGLII(FYH,FCOMP,IN,OUTT,STEELTYPE)
                    ELSEIF (MODELTYPE.EQ.14) THEN
   CALL RAZSAATT(DH,DL,COVER,W,NN,ESTEEL,BB,FYH,HS,FCOMP,IN,OUTT)
                    ENDIF
                         FC(K)=OUTT
          ELSEIF ((EC(K).GT.0.0).AND.(E1(K).LE.H).AND.(E1(K).GE.0.0)) THEN
                    IF (MODELTYPE.EQ.1) THEN
          CALL FCKK(IN,FCOMP,HS,AH1,W,H,FYH,COVER,DH,AST,AIN,OUTT)
                    ELSEIF (MODELTYPE.EQ.2) THEN
          CALL AFCKK(IN,FCOMP,OUTT)
                    ELSEIF (MODELTYPE.EQ.3) THEN
          CALL LII (BB,AST,FYH,FCOMP,HS,DH,DL,W,H,WCR,IN,OUTT)
                    ELSEIF (MODELTYPE.EQ.4) THEN
   CALL CUSPAUU(IN,FYH,HS,DH,AST,W,H,BB,WCR,L,AH,FCOMP,ESTEEL,OUTT)
                    ELSEIF (MODELTYPE.EQ.5) THEN
          CALL YONW(HS,BB,AST,W,H,DL,FYH,FCOMP,L,IN,OUTT)
                    ELSEIF (MODELTYPE.EQ.6) THEN
          CALL AZIZ(HS,BB,AST,W,H,FYH,FCOMP,IN,OUTT)
                    ELSEIF (MODELTYPE.EQ.7) THEN
          CALL SAARAZZ(FYH,FCOMP,IN,OUTT)
                    ELSEIF (MODELTYPE.EQ.8) THEN
          CALL SAKK(FCOMP,BB,COVER,DH,DL,HS,FYH,IN,OUTT,W)
                    ELSEIF (MODELTYPE.EQ.9) THEN
          CALL RICHH(FYH,FCOMP,AH,BB,HS,IN,OUTT)
                    ELSEIF (MODELTYPE.EQ.10) THEN
          CALL FAFSHAA(IN,FCOMP,OUTT)
                    ELSEIF (MODELTYPE.EQ.11) THEN
        CALL SHUZZ(OUTT,IN,L,COVER,W,DH,DL,BB,AST,FCOMP,HS,FYH)
                    ELSEIF (MODELTYPE.EQ.13) THEN
          CALL BINGLII(FYH,FCOMP,IN,OUTT,STEELTYPE)
                    ELSEIF (MODELTYPE.EQ.14) THEN
   CALL RAZSAATT(DH,DL,COVER,W,NN,ESTEEL,BB,FYH,HS,FCOMP,IN,OUTT)
                    ENDIF
                         FC1(K)=OUTT
                    ENDIF
       NC(K)=NC(K-1)+(W-(2*COVER+DH))*(X(I)/M)*FC(K)+(2*COVER+DH)*(X(I)/M)*FC1(K)
   MC(K)=MC(K-1)+(W-(2*COVER+DH))*(X(I)/M)*FC(K)*(E1(K)-(H/2))+(2*COVER+DH)*(X(I)/M)*FC1(K)*(E1(K)-
   (H/2))
                    NC(I)=NC(K)
                    MC(I)=MC(K)
                    IF (E1(K).EQ.H) THEN
                         CS=EC(K)
                         FCONC=OUTT
```

571

```
!                            FCONC= CONCRETE STRESS AT CONCRETE STRAIN 'CS'
                             ENDIF
!                           ELSEIF (E1(K).EQ.DY*NUM) THEN
!                                   CORECS=EC(K)
!                                   FCOREC=FC(K)
       CORECS=CONFINED CONCRETE STRAIN AT EDGE OF CONFINED CORE
!                           FCOREC=CONFINED CONCRETE STRESS AT EDGE OF CONFINED CORE
!                           ENDIF
3                           CONTINUE
                            DO 99 P=1,M,DY
                            CONCFORCE=NC(P)+NC(P-1)
99                          CONTINUE
                            ROX=3*AH/(HS*BB)
                            ROY=3*AH/(HS*BB)
                            RO=0.5*(ROX+ROY)
                            ULTSS=0.07
!                           ULTSS=STEEL STRAIN AT MAXIMUM TENSILE STRESS
!                                   (EXPERIMENTALLY DETERMINED)
                            CALL FCCP(FCOMP,HS,AH,W,H,FYH,COVER,DH,AST,AIN,ECC,FCC)
                            ECU=0.004+(1.4*RO*FYH*ULTSS/FCC)
!                           ECU=0.07
!                           ECU=ULTIMATE CONFINED CONCRETE STRAIN
!                           FCC=MAXIMUM CONFINED CONCRETE STRESS (MANDER BASED)
!                           ULTSS=STEEL STRAIN AT MAXIMUM TENSILE STRESS
!                           RO=VOLUMETRIC RATIO OF CONFINING STEEL
!              ULTSS=STRAIN AT THE ULTIMATE LONGITUDINAL BAR TENSILE
!                               STRENGTH (IN/IN)
                            ST=FYS/ESTEEL
                            DO 4 KK=1,NL
                                    ES(KK)=PHI(J)*(YS(KK)-(H-X(I)))
                            IF (STEELTYPE.EQ.0) THEN
                                    IF ((ES(KK).LE.ST).AND.(ES(KK).GE.0))THEN
                                            IN1=ES(KK)
                                            CALL FSK(ESTEEL,IN1,OUT1)
                                            FS(KK)=OUT1
                                    ELSEIF ((ES(KK).GE.-ST).AND.(ES(KK).LT.0))THEN
                                            IN1=ES(KK)
                                            CALL FSK(ESTEEL,IN1,OUT1)
                                            FS(KK)=OUT1
                                    ELSEIF (ES(KK).GT.ST) THEN
                                            FS(KK)=FYS
                                    ELSEIF (ES(KK).LT.-ST) THEN
                                            FS(KK)=-FYS
                                    ENDIF
                            ELSEIF ((STEELTYPE.EQ.1).OR.(STEELTYPE.EQ.2)) THEN
                                    E=ES(KK)
                                    CALL KING(E,ST,ESTEEL,FYS,STEELTYPE,FK)
                                    FS(KK)=FK
                            ENDIF
                                    NS(KK)=NS(KK-1)+FS(KK)*AS(KK)
                                    MS(KK)=MS(KK-1)+FS(KK)*AS(KK)*(YS(KK)-(H/2))
                                    NS(I)=NS(KK)
                                    MS(I)=MS(KK)
                                    SSCOMP=ES(1)
                                    FFSSCOMP=FS(1)
                                    SS=ES(3)
                                    FFSS=FS(3)
4                           CONTINUE
               NTOT(I)=NC(I)+NS(I)

               ERROR=ABS(PO-NTOT(I))/PO
               IF (ERROR.LE.0.02) THEN
```

572

```
!                        IF (ERROR.LE.0.03) THEN
                                COUNT=COUNT+1.0
                                MTOT(I)=MC(I)+MS(I)
                                IF ((MTOT(I).GE.0.0).AND.(FLAG.EQ.1)) THEN
                                        WRITE(2,13) COUNT,PHI(J),X(I),CS,MC(I),SS,MS(I),MTOT(I)
                                        WRITE(*,13) COUNT,PHI(J),X(I),CS,MC(I),SS,MS(I),MTOT(I)
                                        WRITE(9,28)
COUNT,PHI(J)*39.37,X(I)*2.54,CS,MC(I)*0.11298,SS,MS(I)*0.11298,MTOT(I)*0.11298
13
                FORMAT(2X,'COUNT=',F5.0,2X,'PHI(J)=',F10.8,2X,'X(I)=',F5.2,2X,'EC(I)=',F10.8,2X,'MC(I)=',F8.2,2X,'ES(
I)=',F10.8,2X,'MS(I)=',2X,F8.2,2X,'MTOT(I)=',F9.2,2X)
28
                FORMAT(2X,'COUNT=',F5.0,2X,'PHI(J)[1/M]=',F10.8,2X,'X(I)[CM]=',F5.2,2X,'EC(I)=',F10.8,2X,'MC(I)[KN
*M]=',F8.2,2X,'ES(I)=',F10.8,2X,'MS(I)[KN*M]=',2X,F8.2,2X,'MTOT(I)[KN*M]=',F9.2,2X)


                        ENDIF
                        PH=PHI(J)
                        MT=MTOT(I)


                        CONCSTRAIN=CONCFORCE/(W*X(I))/ECONCRETE
                        CONCSTRESS=CONCFORCE/(W*X(I))

                        IF (FLAG.EQ.1) THEN
                                CALL YIELD(CS,SS,ST,MT,PH,HEIGHT,MY,VY,PHIY,VU,PO,DELI)
                                MU=VU*HEIGHT
!                               MU=ULTIMATE MOMENT
                                WRITE (*,20) -SS,-FFSS
                                WRITE (5,20) -SS,-FFSS
20                              FORMAT(2X,'ES(3)=',2X,F10.8,3X,'FS(3)=',F15.8)
!               -SS=TENSION STRAIN OF THE LONGITUDINAL REINFORCEMENT BAR
!               -FFSS=TENSION STRESS OF THE LONGITUDINAL REINFORCEMENT BAR
                                WRITE (*,21) CS,FCONC
                                WRITE (6,21) CS,FCONC
21                              FORMAT(2X,'EC(K)=',2X,F10.8,3X,'FC(K)=',F15.8)
!               CS=STRAIN OF THE EDGE CONCRETE
!               FCONC=STRESS OF THE EDGE CONCRETE
!                               WRITE (*,25) CORECS,FCOREC
!                               WRITE (9,25) CORECS,FCOREC
!25                             FORMAT(2X,'COREEC(K)=',2X,F10.8,3X,'COREFC(K)=',F15.8)
!               CORECS=CONCRETE CORE EDGE STRAIN
!               FCOREC=CONCRETE CORE EDGE STRESS
                                WRITE (*,22) CONCSTRAIN,CONCSTRESS
                                WRITE (7,22) CONCSTRAIN,CONCSTRESS
22                              FORMAT(2X,'CONCSTRAIN=',2X,F10.8,3X,'CONCSTRESS=',F15.8)
!               CONCSTRAIN=STRAIN OF ALL COMPRESSIVE ZONE CONCRETE
!               CONCSTRESS=STRESS OF ALL COMPRESSIVE ZONE CONCRETE
                                WRITE (*,23) SSCOMP,FFSSCOMP
                                WRITE (8,23) SSCOMP,FFSSCOMP
23                              FORMAT(2X,'SSCOMP=',2X,F10.8,3X,'FFSSCOMP=',F15.8)
!       SSCOMP=COMPRESSION STRAIN IN THE LONGITUDINAL REINFORCEMENT BAR
!       FFSSCOMP=COMPRESSION STRESS OF THE LONGITUDINAL REINFORCEMENT BAR
                                GOTO 111
                        ELSEIF (FLAG.EQ.2) THEN
                                FFSS=-FFSS
                                CALL
VD(PH,MT,MY,VY,PHIY,HEIGHT,DL,FFSS,FYS,LS,FCOMP,W,H,PO)
                                GOTO 222
                        ENDIF
                ELSE
                        GOTO 2
                ENDIF
2               CONTINUE
```

```
111                     IF (((MTOT(I).LE.MU).AND.(-SS.GE.ULTSS)).OR.(CS.GE.1.5*ECU)) THEN
                            MAXMTOT=MAXVAL(MTOT)
                            VMAX=MAXMTOT/HEIGHT
                            WRITE(4,18) MAXMTOT,VMAX
                            WRITE(*,18) MAXMTOT,VMAX
18                          FORMAT(2X,'MAXMTOT=',F8.2,2X,'VMAX=',F8.2,2X)
                            GOTO 122
                        ENDIF


222                     IF (((MTOT(I).LE.MU).AND.(-SS.GE.ULTSS)).OR.(CS.GE.1.5*ECU)) THEN
                            WRITE(4,16) 1.5*ECU
                            WRITE(*,16) 1.5*ECU
16          FORMAT(2X,'IDEAL ENERGY BASED ULTIMATE CONFINED CONCRETE STRAIN=',F10.8,2X)
                            WRITE(4,24) CS
                            WRITE(*,24) CS
24          FORMAT(2X,'ACTUAL FINAL CONFINED CONCRETE STRAIN=',F10.8,2X)
                            WRITE(4,19) FCC
                            WRITE(*,19) FCC
19          FORMAT(2X,'MAXIMUM CONFINED CONCRETE STRESS=',F5.2,2X)
                            STOP
                        ENDIF


1       CONTINUE
        STOP
        END


        SUBROUTINE KING(E,ST,ESTEEL,FYS,STEELTYPE,FK)
        REAL FSU,FYS,ESH,ESU,ST,R,MM,FK,A,B,ESTEEL,EE,AA,BB
        INTEGER STEELTYPE
        FSU=1.5*FYS
        IF (STEELTYPE.EQ.1) THEN
                ESH=14*ST
                ESU=0.14+ESH
        ELSEIF (STEELTYPE.EQ.2) THEN
                ESH=3.24*ST
                ESU=0.12
        ENDIF
                R=ESU-ESH
                MM=((FSU/FYS)*(((30*R)+1)**2)-(60*R)-1)/(15*(R**2))
                A=(MM*(E-ESH)+2)/(60*(E-ESH)+2)
                B=(E-(ESH*(60-MM)))/(2*((30*R+1)**2))
        IF ((E.GT.ST).AND.(E.LE.ESH))THEN
                FK=FYS
        ELSEIF ((E.GT.ESH).AND.(E.LE.ESU))THEN
                FK=FYS*(A+B)
        ELSEIF ((E.LT.-ST).AND.(E.GE.-ESH))THEN
                FK=-FYS
        ELSEIF ((E.LT.-ESH).AND.(E.GE.-ESU))THEN
                EE=-E
                AA=(MM*(EE-ESH)+2)/(60*(EE-ESH)+2)
                BB=(EE-(ESH*(60-MM)))/(2*((30*R+1)**2))
                FK=-FYS*(AA+BB)
        ELSEIF ((E.LE.ST).AND.(E.GE.0))THEN
                FK=ESTEEL*E
        ELSEIF ((E.GE.-ST).AND.(E.LT.0))THEN
                FK=ESTEEL*E
        ENDIF
        RETURN
```

574

```fortran
                  END


                  SUBROUTINE YIELD(CS,SS,ST,MT,PH,HEIGHT,MY,VY,PHIY,VU,PO,DELI)
                  REAL SS,ST,MT,PH,HEIGHT,MY,VY,PHIY
                  REAL VI,MI,PHII
                  IF (ABS(ABS(SS)-ST).LE.0.0003) THEN
                          MY=MT
                          VY=(MT-PO*DELI)/HEIGHT
                          PHIY=PH
                          WRITE(4,15) MY,VY,PHIY
                          WRITE(*,15) MY,VY,PHIY
15                        FORMAT(2X,'MY=',F8.2,2X,'VY=',F8.2,2X,'PHIY=',F10.8,2X)
                  ENDIF
                  IF (ABS(CS-0.005).LE.0.0003) THEN
                          MI=MT
                          VI=(MT-PO*DELI)/HEIGHT
                          PHII=PH
                          VU=0.8*VI
                          WRITE(4,17) MI,VI,PHII,VU
                          WRITE(*,17) MI,VI,PHII,VU
17                        FORMAT(2X,'MI=',F8.2,2X,'VI=',F8.2,2X,'PHII=',F10.8,2X,'VU=',F8.2,2X)
                  ENDIF
                  RETURN
                  END



                  SUBROUTINE VD(PH,MT,MY,VY,PHIY,HEIGHT,DL,FFSS,FYS,LS,FCOMP,W,H,PO)
                  REAL V,MT,HEIGHT,MY,VY,PHIY,PH,FYS,FFSS,DL
                  REAL LH,HE,DELF1,DELF2,DELF,ECONCRETE,FCOMP,AGROSS,IGROSS
                  REAL DELSY,DELS,DELI,LS,PO


                  LH=(0.08*LS*FFSS/FYS)+(0.15*DL*FFSS)
!                 LH=PLASTIC HINGE LENGTH              (INCHES)
                  HE=2*HEIGHT+(2*0.15*DL*FFSS)
!                 HE=EFFECTIVE HEIGHT OF THE COLUMN TAKING INTO CONSIDERATION THE PLASTIC HINGE
!                         FORMATION  (INCHES)
                  DELF1=(HE/2-(LH/2))*LH*PH
!                 DELF1=DEFLECTION DUE TO PLASTIC HINGE ROTATION
                  DELF2=(PH/3)*((2*HEIGHT/2-(0.08*2*HEIGHT*FFSS/(2*FYS)))**2)
!                 DELF2=DEFLECTION DUE TO COLUMN BENDING
                  DELF=DELF1+DELF2
!                 DELF=TOTAL FLEXURAL DEFLECTION
                  ECONCRETE=57.*((FCOMP*1000)**0.5)
                  AGROSS=W*H
                  IGROSS=W*(H**3)/12
                  DELSY=VY*LS*ECONCRETE*IGROSS/(0.9*AGROSS*0.4*ECONCRETE*MY/PHIY)
                  DELS=V*DELSY/VY
!                 DELS=TOTAL DEFLECTION DUE TO SHEAR DEFORMATION
                  DELI=DELS+DELF
!                 DELI=TOTAL DEFLECTION
!                 V=SHEAR FORCE IN KIPS
                  V=(MT-PO*DELI)/HEIGHT
                  IF (DELI.GE.0.0) THEN
                          WRITE(3,14) DELI, V
                          WRITE(*,14) DELI, V
                          WRITE(10,30) DELI*2.54, V*4.44822, DELI*100/LS, V*4.44822
14                FORMAT(2X,'DELI=',F8.2,2X,'V=',F8.2,2X)
30                FORMAT(2X,'DELI[CM]=',F8.2,2X,'V[KN]=',F8.2,2X,'DRIFT RATIO[%]=',F8.2,2X,'V[KN]=',F8.2,2X)
                  ENDIF
                  RETURN
                  END
```

575

```
!       RESULTS SHOULD BE:
!       X(I),PHI(J),NTOT(I),MTOT(I)
!       WHERE X(I)=NEUTRAL AXIS AT CONVERGENCE
!       WHERE PHI(J)=CURVATURE
!       WHERE NTOT(I)=AXIAL LOAD(KIPS) AT CONVERGENCE
!       WHERE MTOT(I)=MOMENT (KIPS-IN.) AT CONVERGENCE
!       CONVERGENCE=WHEN APPLIED AXIAL LOAD PO=NTOT(I)
!                     WITHIN PRESET ERROR MARGIN AS SHOWN ABOVE.


        SUBROUTINE FCCP(FCOMP,HS,AH,W,H,FYH,COVER,DH,AST,AIN,ECC,FCC)
        REAL BC,DC,AIN,COVER,W,H,ROX,ROY,AH,DH,FLX
        REAL FLY,FYH,KE,ECO,FCO,FCC,ECC,AST,AC
        REAL AE,SP,ROCC,ACC,ECONCRETE
        REAL FCOMP
        ECONCRETE=57.*((FCOMP*1000)**0.5)
        SP=HS-DH
        BC=W-(2.*COVER)-DH
        DC=H-(2.*COVER)-DH
        AC=BC*DC
        ROCC=AST/AC
        AE=(AC-AIN)*(1.-(SP/(2.*BC)))*(1.-(SP/(2.*DC)))
        ACC=AC*(1-ROCC)
        KE=AE/ACC
        ROX=3.*AH/(HS*DC)
        ROY=3.*AH/(HS*BC)
        FLX=ROX*FYH*KE
        FLY=ROY*FYH*KE
        FL=0.5*(FLX+FLY)
        ECO=0.002
        FCO=FCOMP
        FCC=FCO*(-1.254+(2.254*((1.+7.94*FL/FCO)**0.5))-2.*FL/FCO)
        ECC=ECO*(1.+(5.*(FCC/FCO-1.)))
        RETURN
        END


        SUBROUTINE FCK(IN,FCOMP,HS,AH,W,H,FYH,COVER,DH,AST,AIN,OUT)
        REAL BC,DC,AIN,COVER,W,H,ROX,ROY,AH,DH,FLX
        REAL FLY,FYH,KE,ECO,FCO,FCC,ECC,X,R,AST,AC
        REAL AE,SP,ROCC,ACC,ESEC,ECONCRETE
        REAL IN,OUT,FCOMP
        ECONCRETE=57.*((FCOMP*1000)**0.5)
        SP=HS-DH
        BC=W-(2.*COVER)-DH
        DC=H-(2.*COVER)-DH
        AC=BC*DC
        ROCC=AST/AC
        AE=(AC-AIN)*(1.-(SP/(2.*BC)))*(1.-(SP/(2.*DC)))
        ACC=AC*(1-ROCC)
        KE=AE/ACC
        ROX=3.*AH/(HS*DC)
        ROY=3.*AH/(HS*BC)
        FLX=ROX*FYH*KE
        FLY=ROY*FYH*KE
        FL=0.5*(FLX+FLY)
        ECO=0.002
        FCO=FCOMP
        FCC=FCO*(-1.254+(2.254*((1.+7.94*FL/FCO)**0.5))-2.*FL/FCO)
        ECC=ECO*(1.+(5.*(FCC/FCO-1.)))
```

576

```
                      ESEC=FCC/ECC
                      R=ECONCRETE/(ECONCRETE-ESEC)
                      X=IN/ECC
                      OUT=FCC*X*R/(R-1+(X**R))
                      RETURN
                      END


                      SUBROUTINE AFCK(IN,NN,AT,BB,HS,FYH,FCOMP,OUT)
                      REAL FCO,FCC,X,R
                      REAL ESEC,ECONCRETE
                      REAL IN,OUT,FCOMP
                      REAL RHOT, NN, AT, BB, FYE, FYH, HS
                      REAL FYEFF,FR,K1,ECO,ECC,K2
                      REAL ECU,K3
 !                    RHOT=TRANSVERSE REINFORCEMENT RATIO
 !                    NN=NUMBER OF THE LEGS OF THE TRANSVERSE REINFORCEMENT IN THE
 !                            VERTICAL CROSS SECTION
 !                    AT=CROSS SECTIONAL AREA OF ONE LEG OF TRANSVERSE REINFORCEMENT
 !                    BB=WIDTH MEASURED FROM THE CENTER LINES OF THE OUT MOST
 !                            HOOPS
 !                    HS=HOOP SPACING
                      RHOT=(NN*AT)/(BB*HS)
 !                    FYE=EFFECTIVE STRESS OF TRANSVERSE REINFORCEMENT
 !                            AT THE POINT OF MAX. STRENGTH OF HSC CONFINED COLUMN
                      FYE=11.6*(((1/RHOT)*(FYH/FCOMP))**0.26)
 !                    FYEFF=EFFECTIVE STRESS OF CONFINING REINFORCEMENT AT THE
 !                            PEAK POINT
                      FYEFF=MIN(FYH,FYE)
                      FR=RHOT*FYEFF
                      FCO=FCOMP
                      FCC=FCO+(3.96*FR)
                      K1=5+(1.3*RHOT*FYH/FCO)
                      ECO=1.4*(FCO**0.27)/1000
                      ECC=ECO*(1+(K1*((FCC/FCO)-1)))
                      K2=(FYEFF/FYH)**0.2
                      ECONCRETE=46.*K2*((FCO*1000)**0.5)
                      ESEC=FCC/ECC
                      R=ECONCRETE/(ECONCRETE-ESEC)
                      ECU=0.005+(0.19*((RHOT*FYH/FCO)**1.5))
                      X=IN/ECC
                      IF ((IN.GE.0).AND.(IN.LE.ECC)) THEN
                              K3=1
                      ELSEIF ((IN.GT.ECC).AND.(IN.LT.ECU)) THEN
                              K3=LOG(1-R+(1.25*ECU*R/ECC))/(R*LOG(ECU/ECC))
                      ENDIF
                      OUT=FCC*X*R/(R-1+(X**(K3*R)))
                      RETURN
                      END


                      SUBROUTINE LI (AH,BB,AST,FYH,FCOMP,HS,DH,DL,W,H,WCR,IN,OUT)
                      REAL IN,BETA,FCOMP,FYH,RHOS,AST,BB,WCR,FL,KE,SPRIME,H
                      REAL GPRIME,W,ROCC,ALPHA,ECO,ECONCRETE,FCC
                      REAL OUT,ECC,ECU,A,B,C,D,AH,BETA1
                      SPRIME=HS-DH
 !                    GPRIME=(0.5*BB)/(BB-DL)
                      GPRIME=(BB)/(BB-DL)
                      ECONCRETE=(3200*SQRT(FCOMP*6.89655)+6900)*145/1000
                      RHOS=3*AH/(HS*BB)
                      BETA=1
                      ALPHA=SPRIME/H
```

577

```
                    ROCC=AST/(W*H)
                    A=((1-(0.5*ALPHA))**2)*(BETA-(0.5*ALPHA))
                    B=BETA*(1-(1.6*GPRIME*ROCC))
                    C=(8*(0.58+(0.11*GPRIME))/BETA)*((WCR/BB)**2)
                    D=(0.93/BETA)*((WCR/BB)**3)
                    KE=(A/B)*(1-C+D)
  !                 FL=0.5*KE*RHOS*FYH
                    FL=KE*RHOS*FYH
                    ECO=0.7*((FCOMP*1000)**(0.3))/1000
                    FCC=FCOMP*(1.413*SQRT(1+(11.4*FL/FCOMP))-(2*FL/FCOMP)-0.413)
                    IF (FCOMP.LT.11.6) THEN
                            ECC=ECO*(1.0+(11.3*((FL/FCOMP)**0.7)))
                    ELSEIF (FCOMP.GE.11.6) THEN
                            ECC=ECO*(-8.1+(9.1*EXP(FL/FCOMP)))
                    ENDIF
                    IF (FCOMP.LT.11.6) THEN
                            ECU=ECO*(2+(122.5-(0.92*FCOMP*6.895))*SQRT(FL/FCOMP))
                    ELSEIF (FCOMP.GE.11.6) THEN
                            ECU=ECO*(2+((82.75-(0.37*FCOMP*6.895))*SQRT(FL/FCOMP)))
                    ENDIF
                    IF ((IN.GE.0).AND.(IN.LT.ECO)) THEN
                            OUT=(ECONCRETE*IN)+((FCOMP-(ECONCRETE*ECO))*(IN**2)/(ECO**2))
                    ELSEIF ((IN.GE.ECO).AND.(IN.LT.ECC)) THEN
                            OUT=FCC-((FCC-FCOMP)*((IN-ECO)**2)/((ECC-ECO)**2))
                    ELSEIF (IN.GE.ECC) THEN
                    BETA1=((0.048*FCOMP*6.895)-2.14)-(((0.098*FCOMP*6.895)-4.57)*((FL/FCOMP)**(1/3)))
                            OUT=FCC-(BETA1*FCC*(IN-ECC)/ECC)
                            IF (OUT.LT.(0.4*FCC)) THEN
                                    OUT=0.4*FCC
                            ENDIF
                    ENDIF
                    IF (OUT.LT.0) THEN
                            OUT=0
                    ENDIF
                    RETURN
                    END


                    SUBROUTINE CUSPAU(IN,FYH,HS,DH,AST,W,H,BB,WCR,L,AH,FCOMP,ESTEEL,OUT)
                    REAL FYH,HS,SPRIME,FHCC,AST,W,H,RHOC,CX,CY,WCR,KE,BB,ECONCRETE
                    REAL ASHX,ASHY,ASH,FLE,C,OUT,FCOMP,ECC,EC50U,EC50C,EHCC,ESTEEL
                    REAL KK,K1,K2,AC,AH,ECO,TOLERANCE,A,B,D,F,L,IN
                    ECONCRETE=57.*((FCOMP*1000)**0.5)
                    AC=W*H
                    CX=BB
                    CY=BB
                    SPRIME=HS-DH
                    RHOC=AST/AC
                    ASHX=3*AH
                    ASHY=3*AH
                    FHCC=FYH
                    A=1-(L*(WCR**2)/(6*CX*CY))
                    B=1-(SPRIME/(2*CX))
                    D=1-(SPRIME/(2*CY))
                    F=1-RHOC
                    KE=A*B*D/F
                    ASH=ASHX+ASHY
                    C=CX+CY
  20                FLE=KE*FHCC*ASH/(HS*C)
                    FCC=FCOMP*(1.0+(2.1*((FLE/FCOMP)**0.7)))
                    ECO=FCOMP/ECONCRETE
                    ECC=ECO+(0.21*((FLE/FCOMP)**1.7))
```

578

```
          EC50U=0.004
          EC50C=EC50U+(0.15*((FLE/FCOMP)**1.1))
          EHCC=0.5*ECC*(1-(FLE/FCC))
          FHCC=ESTEEL*EHCC
          NFLE=KE*FHCC*ASH/(HS*C)
          TOLERANCE=ABS(NFLE-FLE)/100
          IF (TOLERANCE.LE.0.1) THEN
                  IF (IN.LE.ECC) THEN
                          KK=ECONCRETE/(ECONCRETE-(FCC/ECC))
                          OUT=FCC*(KK*(IN/ECC)/(KK-1+((IN/ECC)**KK)))
                          GOTO 10
                  ELSEIF (IN.GT.ECC) THEN
                          K2=0.58+(16*((FLE/FCOMP)**1.4))
                          K1=LOG(0.5)/((EC50C-ECC)**K2)
                          OUT=FCC*EXP(K1*((IN-ECC)**K2))
                          GOTO 10
                  ENDIF
          ELSE
                  GOTO 20
          ENDIF
10        IF (OUT.GE.0) THEN
                  GOTO 30
          ELSEIF (OUT.LT.0) THEN
                  OUT=0
          ENDIF
30        RETURN
          END


          SUBROUTINE YON(HS,BB,DH,AST,W,H,DL,FYH,FCOMP,AH,L,IN,OUT)
          REAL HS,AX,AY,BB,W,H,FY,FYH,DH,EO,FO,FI,EI,F2I,E2I,ECONCRETE
          REAL WEIGHT,IN,OUT,EINIT,E2INIT,X,A,B,C,D,AST,RHO,RHOP
          REAL KK,DL,FCOMP,P,Q,R,S,T,AH,L
!         L=NUMBER OF LONGITUDINAL BARS
          FY=FYH*1000
          WEIGHT=150
          AX=3*AH
          AY=3*AH
          RHOP=(AX+AY)/(HS*(BB+BB))
          RHO=AST/(W*H)
          P=0.245*HS/BB
          Q=RHOP+(L*DH*RHO/(8*HS*DL))
          R=FY/SQRT(FCOMP*1000)
          KK=1.0+(0.0091*(1-(P*Q*R)))
          S=1-(0.734*HS/BB)
          T=(RHOP*FY)**(2/3)
          EO=0.00265+((0.0035*S*T)/SQRT(FCOMP*1000))
          FO=KK*FCOMP
          FI=FO*(0.25*(FCOMP/FO)+0.4)
          EI=KK*(1.4*(EO/KK)+0.0003)
          F2I=FO*((0.025*FO)-0.065)
          IF (F2I.LT.(0.3*FO)) THEN
                  F2I=0.3*FO
          ENDIF
          E2I=(2*EI)-EO
!         E2I IS A STRAIN
          ECONCRETE=27.55*((WEIGHT)**1.5)*SQRT(FCOMP*1000)/1000
          X=IN/EO
          A=ECONCRETE*EO/FO
          B=((A-1)**2/0.55)-1
          IF (IN.LE.EO) THEN
                  OUT=(A*X+B*(X**2))*FO/(1+(A-2)*X+(B+1)*(X**2))
```

579

```
!                          OUT=OU/1000
                    ELSEIF (IN.GT.EO) THEN
                           EINIT=FI/EI
                           E2INIT=F2I/E2I
                           C=((E2I-EI)/EO)*((E2I*EINIT)/(FO-FI)-(4*EI*E2INIT)/(FO-F2I))
                           D=(EI-E2I)*(EINIT/(FO-FI)-4*E2INIT/(FO-F2I))
                           OUT=((C*X)+(D*(X**2)))*FCOMP/(1+((C-2)*X)+((D+1)*(X**2)))
!                          OUT=OU/1000
                           IF (OUT.LT.(0.3*FO)) THEN
                                  OUT=0.3*FO
                           ENDIF
                    ENDIF
                    IF (OUT.LT.0) THEN
                    OUT=0
                    ENDIF
                    RETURN
                    END


                    SUBROUTINE AZI(HS,BB,DH,AST,W,H,DL,FYH,FCOMP,AH,L,IN,OUT)
                    REAL HS,AX,AY,BB,W,H,FY,FYH,DH,EO,FO,FI,EI,F2I,E2I,ECONCRETE
                    REAL WEIGHT,IN,OUT,EINIT,E2INIT,X,A,B,C,D,AST,RHO,RHOP
                    REAL KK,DL,FCOMP,P,Q,R,S,T,AH,L,ALPHA
!                    L=NUMBER OF LONGITUDINAL BARS
                    FY=FYH*1000
                    WEIGHT=150
                    AX=3*AH
                    AY=3*AH
                    RHOP=(AX+AY)/(HS*(BB+BB))
                    RHO=AST/(W*H)
                    P=0.245*HS/BB
                    Q=RHOP+(L*DH*RHO/(8*HS*DL))
                    R=FY/SQRT(FCOMP*1000)
                    KK=1.0+(0.0091*(1-(P*Q*R)))
                    S=1-(0.734*HS/BB)
                    T=(RHOP*FY)**(2/3)
                    EO=0.00265+((0.0035*S*T)/SQRT(FCOMP*1000))
                    FO=KK*FCOMP
                    FI=FO*(0.25*(FCOMP/FO)+0.4)
                    EI=KK*(1.4*(EO/KK)+0.0003)
                    F2I=FO*((0.025*FO)-0.065)
                    IF (F2I.LT.(0.3*FO)) THEN
                           F2I=0.3*FO
                    ENDIF
                    E2I=(2*EI)-EO
                    ECONCRETE=27.55*((WEIGHT)**1.5)*SQRT(FCOMP*1000)/1000
                    X=IN/EO
                    A=ECONCRETE*EO/FO
                    B=((A-1)**2/0.55)-1
                    IF (IN.LE.EO) THEN
!                          OUT=((A*X)+(B*(X**2)))*FO/(1+((A-2)*X)+((B+1)*(X**2)))
!                          OUT=OU/1000
                           OUT=(FO/EO)*IN
                    ELSEIF (IN.GT.EO) THEN
                           EINIT=FI/EI
                           E2INIT=F2I/E2I
                           C=((E2I-EI)/EO)*(((E2I*EINIT)/(FO-FI))-((4*EI*E2INIT)/(FO-F2I)))
                           D=(EI-E2I)*((EINIT/(FO-FI))-(4*E2INIT/(FO-F2I)))
!                          OUT=((C*X)+(D*(X**2)))*FCOMP/(1+((C-2)*X)+((D+1)*(X**2)))
!                          OUT=OU/1000
                           ALPHA=(0.25*(FCOMP-0.6)/FO)/((3.13*KK)*((1.4*EO/KK)+0.0003))
                           OUT=FO*(1-(ALPHA*(IN-EO)))
```

```fortran
                IF (OUT.LT.(0.3*FO)) THEN
                        OUT=0.3*FO
                ENDIF
        ENDIF
        IF (OUT.LT.0.0) THEN
        OUT=0
        ENDIF
        RETURN
        END


        SUBROUTINE SAARAZ(BB,FYH,HS,FCOMP,IN,OUT,AH)
        REAL EO1,E1,E85,RHO,E085,IN,OUT,AH,FCCP,FCO,ALPHA,K2,BB
        REAL FYH,FL,K1,FCOMP,KK,FLE,FY,OU
        FCO=FCOMP*6.895
!       FCO IS IN MPA
        ALPHA=90
        FY=FYH*6.895
        FL=(3*AH)*FY*SIND(ALPHA)/(HS*BB)
!       FL IS IN MPA
        K1=6.7*((FL)**(-0.17))
        K2=1.0
        EO1=0.002
        FLE=K2*FL
        KK=K1*FLE/FCO
        E1=EO1*(1+(5*KK))
        RHO=6*AH/(HS*BB)
        E085=0.0038
        E85=(260*RHO*E1)+E085
        FCCP=FCO+(K1*FL)
        IF (IN.LT.E1) THEN
        OU=FCCP*(((2*(IN/E1))-((IN/E1)**2))**(1/(1+(2*KK))))
        ELSEIF (IN.GE.E1) THEN
!       OU=E1*(0.15*FCCP)/(E85-E1)+FCCP-((0.15*FCCP/(E85-E1))*IN)
        OU=FCCP-((0.15*FCCP/(E85-E1))*IN)
        ENDIF
        IF (OU.GT.FCCP) THEN
        OU=FCCP
        ENDIF
        OUT=OU/6.895
!       OUT IS IN KSI
        IF (OUT.LT.0) THEN
        OUT=0.0
        ENDIF
        RETURN
        END


        SUBROUTINE SAK(FCOMP,BB,COVER,DH,DL,HS,FYH,AH,IN,OUT,W)
        REAL ALPHA,BETA,GAM,SIGB,KS,BB,HS,DH,KAPPA,FYH,SIGH,SIGP
        REAL MU,RHOH,AH,CSIGB,D,ECONCRETE,EO,KK
        REAL X,A,OUT,IN,FCOMP,C,COVER,KAY,ECO,DL,W
        SIGB=FCOMP
        KS=11.5
        C=(W-(2*DH)-DL-(2*COVER))/2
        KAPPA=KS*(DH/C)*(1-(HS/(2*BB)))
        ALPHA=1.5
        BETA=-0.00168
        GAM=0.50
        MU=1.0
        SIGH=FYH
        SIGP=MU*SIGB
```

581

```
RHOH=3*AH/(HS*BB)
CSIGB=SIGP+(KAPPA*RHOH*SIGH)
KK=CSIGB/SIGP
D=ALPHA+(BETA*SIGB)+(GAM*SQRT((KK-1)*SIGB/23))
KAY=1.0
ECONCRETE=4*KAY*(SIGB**(1/3))*(100000)*((GAM/2.4)**2)
EO=0.5243*((SIGB)**0.25)*(0.001)
IF (KK.LE.1.5) THEN
        ECO=EO*(1+(4.7*(KK-1)))
ELSEIF (KK.GT.1.5) THEN
        ECO=EO*(3.35+(20*(KK-1.5)))
ENDIF
X=IN/ECO
A=ECONCRETE*ECO/CSIGB
OUT=CSIGB*((A*X)+((D-1)*X*X))/(1+((A-2)*X)+(D*X*X))
IF (OUT.LT.0) THEN
OUT=0
ENDIF
END


SUBROUTINE RICH(FYH,FCOMP,AH,BB,HS,IN,OUT)
REAL AH,BB,HS,KK,FR,FCOMP,FCCP,ECO,ECONCRETE,ECC,IN,OUT
ECONCRETE=57*SQRT(FCOMP*1000)
FR=3*AH*FYH/(BB*HS)
KK=4.1
FCCP=FCOMP+(KK*FR)
ECO=FCOMP/ECONCRETE
ECC=ECO*(1+(5*((FCCP/FCOMP)-1)))
IF (IN.LT.ECC) THEN
OUT=FCCP*IN/ECC
ELSEIF (IN.GE.ECC) THEN
OUT=FCCP+(ECC*0.15*FCCP/(0.00736-ECC))-(0.15*FCCP*IN/(0.00736-ECC))
ENDIF
IF (OUT.LT.0) THEN
OUT=0
ENDIF
RETURN
END


SUBROUTINE FAFSHA(IN,FCOMP,HS,BB,AH,FYH,OUT)
REAL ECONCRETE,ASH,LAMBDA,KK,IN,FCOMP,K1
REAL HS,BB,FYH,FR,FCCP,ECC,A,WEIGHT,AH,OUT
K1=4.1
!       K1 IS FROM RICHART'S MODEL
ASH=3*AH
WEIGHT=150
ECONCRETE=33*(WEIGHT**1.5)*SQRT(FCOMP*1000)/1000
FR=ASH*FYH/(BB*HS)
FCCP=FCOMP+K1*FR
ECC=FCCP/ECONCRETE
A=ECONCRETE*ECC/FCCP
LAMBDA=1-(25*FR*(1-EXP((-3.24*FCOMP)**9))/FCOMP)
KK=24.65*FCOMP*EXP(-0.01*FR/LAMBDA)
IF ((IN.GE.0).AND.(IN.LE.ECC)) THEN
        OUT=FCCP*(1-((1-(IN/ECC))**A))
ELSEIF (IN.GT.ECC) THEN
        OUT=FCCP*EXP(-KK*((IN-ECC)**1.15))
ENDIF
IF (OUT.LT.0) THEN
        OUT=0
```

582

```
                ENDIF
                RETURN
                END


                SUBROUTINE SHUZ(OUT,IN,AH,L,COVER,W,DH,DL,BB,AST,FCOMP,HS,FYH)
                REAL C,W,COVER,DH,DL,L,BB,KS,BC,AST,POCC,FCOMP,ACO,RHO
                REAL FSP,Z,ES1,FCCP,EOO,ECONCRETE,ES2,F,G,AH,IN,OUT
  !             REAL ES85
                RHO=3*AH/(BB*HS)
                BC=W-(2*COVER)-(2*DH)
                ACO=BC**2
                POCC=FCOMP*(ACO-AST)
                FSP=FYH
                C=(W-(2*COVER)-(2*DH)-DL)/2
        KS=1.0+((2.73*BB*BB/POCC)*(1-(L*C*C/(5.5*BB*BB)))*((1-(HS/(2*BB)))**2)*SQRT(RHO*FSP))
                Z=0.5/(0.75*RHO*SQRT(BB/HS))
                FCCP=KS*FCOMP
                ES1=0.55*KS*FCOMP*(0.000001)*1000
                ECONCRETE=57*SQRT(FCOMP*1000)
                EOO=FCOMP/ECONCRETE
                F=1-(5*((HS/BB)**2))
                G=RHO*FSP*1000/SQRT(FCOMP*1000)
                ES2=EOO*(1+(0.81*F*G/C))
  !             ES85=(0.225*RHO*SQRT(BB/HS))+ES2
                IF (IN.LE.ES1) THEN
                        OUT=(-FCCP*((IN-ES1)**2)/(ES1**2))+FCCP
                ELSEIF ((IN.GT.ES1).AND.(IN.LE.ES2)) THEN
                        OUT=FCCP
                ELSEIF (IN.GT.ES2) THEN
  !             .AND.(IN.LE.ES85)) THEN
                        OUT=FCCP+(ES2*Z)-(Z*IN)
                        IF (OUT.LE.(0.3*FCCP)) THEN
                                OUT=0.3*FCCP
                        ENDIF
  !     ELSEIF (IN.GT.ES85) THEN
  !             OUT=0.3*FCCP
                ENDIF
                IF (OUT.LT.0) THEN
                        OUT=0.0
                ENDIF
                RETURN
                END


        SUBROUTINE BINGLI(COVER,AIN,AH,AST,FYH,FCOMP,HS,DH,W,H,IN,OUT,STEELTYPE)
                REAL IN,FCOMP,FYH,AST,FL,KE,SP,H,AH
                REAL W,ROCC,ALPHAS,ECO,ECONCRETE,FCC,COVER
                REAL OUT,ECC,ECU,BETA1,AIN,ROX,ROY,FLX,FLY,FCO,BC,DC,DH,AC
                INTEGER STEELTYPE
                SP=HS-DH
                BC=W-(2.*COVER)-DH
                DC=H-(2.*COVER)-DH
                AC=BC*DC
                ROCC=AST/AC
                KE=ABS((1-AIN)*(1.-(0.5*SP/BC))*(1.-(0.5*SP/DC))/(1-ROCC))
                ROX=3.*AH/(HS*DC)
                ROY=3.*AH/(HS*BC)
                FLX=ROX*FYH*KE
                FLY=ROY*FYH*KE
                FL=0.5*KE*(ROX+ROY)*FYH
                IF (FCOMP.LE.7.5) THEN
```

583

```
                ALPHAS=(21.2-(0.35*FCOMP*6.895))*FL/FCOMP
        ELSEIF (FCOMP.GT.7.5) THEN
                ALPHAS=3.1*FL/FCOMP
        ENDIF
        FCO=FCOMP
        FCC=FCO*(-1.254+2.254*SQRT(1.+7.94*ALPHAS*FL/FCO)-2.*ALPHAS*FL/FCO)
        ECO=0.7*((FCO*1000)**(0.3))/1000
        IF ((STEELTYPE.EQ.0).OR.(STEELTYPE.EQ.1)) THEN
                        ECC=ECO*(1.+11.3*((FL/FCO)**0.7))
        ELSEIF (STEELTYPE.EQ.2) THEN
                IF (FCO.LE.7.2)THEN
                                ECC=ECO*(2.+(87-1.06*FCO*6.895)*((FL/FCO)**0.5))
                ELSEIF (FCO.GT.7.2)THEN
                                ECC=ECO*(2.+(53.4-0.42*FCO*6.895)*((FL/FCO)**0.5))
                ENDIF
        ENDIF
        ECONCRETE=(3200*SQRT(FCO*6.895)+6900)*145/1000
 !      RHOS=3*AH/(HS*BB)

        IF ((FYH.GE.0).AND.(FYH.LE.79.77).AND.(FCO.GT.10.88)) THEN
                BETA1=((0.048*FCO*6.895)-2.14)-(((0.098*FCO*6.895)-4.57)*((FL/FCO)**(1/3)))
        ELSEIF ((FYH.GE.0).AND.(FYH.LE.79.77).AND.(FCO.LE.10.88)) THEN
                BETA1=0.2
        ELSEIF ((FYH.GT.79.77).AND.(FYH.LE.174))THEN
                BETA1=0.2
        ELSEIF ((FYH.GT.174).AND.(FCO.LE.11.6)) THEN
                BETA1=0.07
        ELSEIF ((FYH.GT.174).AND.(FCO.GT.11.6))          THEN
                BETA1=0.1
        ENDIF


        IF ((STEELTYPE.EQ.0).OR.(STEELTYPE.EQ.1)) THEN
                IF (FCO.LT.11.6) THEN
                        ECU=ECO*(2+(122.5-(0.92*FCO*6.895))*SQRT(FL/FCO))
                ELSEIF (FCO.GE.11.6) THEN
                        ECU=ECO*(2+((82.75-(0.37*FCO*6.895))*SQRT(FL/FCO)))
                ENDIF
        ELSEIF (STEELTYPE.EQ.2) THEN
                IF (FCO.LT.7.2) THEN
                        ECU=ECO*(2+(70-(0.6*FCO*6.895))*SQRT(FL/FCO))
                ELSEIF (FCO.GE.7.2) THEN
                        ECU=ECO*(2+((49-(0.2*FCO*6.895))*SQRT(FL/FCO)))
                ENDIF
        ENDIF
        IF ((IN.GE.0).AND.(IN.LT.ECO)) THEN
                OUT=(ECONCRETE*IN)+((FCO-(ECONCRETE*ECO))*(IN**2)/(ECO**2))
        ELSEIF ((IN.GE.ECO).AND.(IN.LE.ECC)) THEN
                OUT=FCC-((FCC-FCO)*((IN-ECO)**2)/((ECC-ECO)**2))
        ELSEIF (IN.GT.ECC) THEN
                OUT=FCC-(BETA1*FCC*(IN-ECC)/ECC)
                IF (OUT.LT.(0.4*FCC)) THEN
                        OUT=0.4*FCC
                ENDIF
        ENDIF
        IF (OUT.LT.0) THEN
                OUT=0
        ENDIF
        RETURN
        END
```

584

```fortran
      SUBROUTINE RAZSAAT(DH,DL,COVER,W,NN,ESTEEL,BB,FYH,HS,FCOMP,IN,OUT,AH)
      REAL E01,E1,E85,RHO,E085,IN,OUT,AH,FCCP,FCO,ALPHA,K2,BB
      REAL FYH,FL,K1,FCOMP,KK,FLE,OU,ESTEEL,NN
      REAL ESEC,ECONCRETE,R,K3,K4,FS,LS,W,COVER,DH,DL,HS
      BC=W-(2.*COVER)-DH
!     INCOMING 'ESTEEL','FCOMP' IN KSI
      ECONCRETE=(3320*SQRT(FCOMP*6.895)+6900)/6.895
!     ECONCRETE ABOVE IN KSI
      FCO=FCOMP*6.895
!     FCO ABOVE IN MPA
      LS=(W-(2*COVER)-(2*DH)-DL)/2
      K2=0.15*SQRT((BC/HS)*(BC/LS))
      ALPHA=90
      RHO=NN*AH/(HS*BB)
      FS=ESTEEL*6.895*(0.0025+0.04*((K2*RHO)/(6.895*FCOMP))**1/3)
      IF (FS.GT.FYH) THEN
      FS=FYH
      ENDIF
      FL=(NN*AH)*FS*SIND(ALPHA)/(HS*BB)
!     FL IS IN MPA
      FLE=K2*FL
      K1=6.7*((FLE)**(-0.17))
      K3=40/(FCOMP*6.895)
      K4=FYH*6.895/500
      IF (K4.LT.1.0) THEN
      K4=1.0
      ENDIF
      FCCP=FCO+(K1*FL)
      E01=0.0028-0.0008*K3
      KK=K1*FLE/FCO
      E1=E01*(1+(5*K3*KK))
      ESEC=FCCP/E1
      R=ECONCRETE/(ECONCRETE-ESEC)
      E085=E01+0.0018*(K3**2)
      E85=260*K3*RHO*E1*(1+0.5*K2*(K4-1))+E085
      IF (IN.LT.E1) THEN
              OU=FCCP*(IN/E1)*R/(R-1+(IN/E1)**R)
      ELSEIF (IN.GE.E1) THEN
              OU=FCCP-((0.15*FCCP/(E85-E1))*IN)
      ENDIF
      IF (OU.GT.FCCP) THEN
      OU=FCCP
      ENDIF
      OUT=OU/6.895
!     OUT IS IN KSI
      IF (OUT.LT.0) THEN
      OUT=0.0
      ENDIF
      RETURN
      END


      SUBROUTINE FSK(ESTEEL,IN1,OUT1)
      REAL IN1,OUT1
      REAL ESTEEL
      OUT1=IN1*ESTEEL
      RETURN
      END


      SUBROUTINE FCKK(IN,FCOMP,HS,AH1,W,H,FYH,COVER,DH,AST,AIN,OUTT)
      REAL BC,DC,AIN,COVER,W,H,ROX,ROY,AH1,DH,FLX
```

```
REAL FLY,FYH,KE,ECO,FCO,FCC,ECC,X,R,AST,AC
REAL AE,SP,ROCC,ACC,ESEC,ECONCRETE
REAL IN,OUTT,FCOMP
ECONCRETE=57.*((FCOMP*1000)**0.5)
SP=HS-DH
BC=W-(2.*COVER)-DH
DC=H-(2.*COVER)-DH
AC=BC*DC
ROCC=AST/AC
AE=(AC-AIN)*(1.-(SP/(2.*BC)))*(1.-(SP/(2.*DC)))
ACC=AC*(1-ROCC)
KE=AE/ACC
ROX=3.*AH1/(HS*DC)
ROY=3.*AH1/(HS*BC)
FLX=ROX*FYH*KE
FLY=ROY*FYH*KE
FL=0.5*(FLX+FLY)
ECO=0.002
FCO=FCOMP
FCC=FCO*(-1.254+(2.254*((1.+7.94*FL/FCO)**0.5))-2.*FL/FCO)
ECC=ECO*(1.+(5.*(FCC/FCO-1.)))
ESEC=FCC/ECC
R=ECONCRETE/(ECONCRETE-ESEC)
X=IN/ECC
OUTT=FCC*X*R/(R-1+(X**R))
IF (IN.GT.0.005) THEN
OUTT=0.0
ENDIF
RETURN
END


SUBROUTINE AFCKK(IN,FCOMP,OUTT)
REAL FCO,FCC,X,R
REAL ESEC,ECONCRETE
REAL IN,OUTT,FCOMP
REAL ECO,ECC
REAL ECU,K3
FCO=FCOMP
FCC=FCO
ECO=1.4*(FCO**0.27)/1000
ECC=ECO
ECONCRETE=46.*((FCO*1000)**0.5)
ESEC=FCC/ECC
R=ECONCRETE/(ECONCRETE-ESEC)
ECU=0.005
X=IN/ECC
IF ((IN.GE.0).AND.(IN.LE.ECC)) THEN
        K3=1
ELSEIF ((IN.GT.ECC).AND.(IN.LT.ECU)) THEN
        K3=LOG(1-R+(0.00625*R/ECC))/(R*LOG(ECU/ECC))
ENDIF
OUTT=FCC*X*R/(R-1+(X**(K3*R)))
IF (IN.GT.0.005) THEN
OUTT=0.0
ENDIF
RETURN
END


SUBROUTINE LII(FCOMP,IN,OUTT)
REAL IN,FCOMP
```

586

```
!          REAL ECO,X,EO,KK,ECONCRETE,R
!          REAL OUTT
!          ECONCRETE=(3200*SQRT(FCOMP*6.89655)+6900)*145/1000
!          ECONCRETE=53.6*((FCOMP*1000)**0.5)
!          ECO=0.7*((FCOMP)**(0.3))/1000
!          X=IN/ECO
!          EO=FCOMP/ECO
!          IF (X.LE.1.0) THEN
!                KK=0.67+(FCOMP/62)
!          ELSEIF (X.GT.1.0) THEN
!                KK=1
!          ENDIF
!          R=ABS(ECONCRETE/(ECONCRETE-EO))
!          OUTT=FCOMP*X*R/(R-1+(X**(R*KK)))
!          IF ((OUTT.LT.0).OR.(IN.GT.0.005)) THEN
!          OUTT=0
!          ENDIF


           SUBROUTINE LII (BB,AST,FYH,FCOMP,HS,DH,DL,W,H,WCR,IN,OUTT)
           REAL IN,BETA,FCOMP,FYH,RHOS,AST,BB,WCR,FL,KE,SPRIME,H
           REAL GPRIME,W,ROCC,ALPHA,ECO,ECONCRETE,FCC
           REAL OUTT,ECC,ECU,A,B,C,D,AH,BETA1
           AH=0
           SPRIME=HS-DH
!          GPRIME=(0.5*BB)/(BB-DL)
           GPRIME=(BB)/(BB-DL)
           ECONCRETE=(3200*SQRT(FCOMP*6.89655)+6900)*145/1000
           RHOS=3*AH/(HS*BB)
           BETA=1
           ALPHA=SPRIME/H
           ROCC=AST/(W*H)
           A=((1-(0.5*ALPHA))**2)*(BETA-(0.5*ALPHA))
           B=BETA*(1-(1.6*GPRIME*ROCC))
           C=(8*(0.58+(0.11*GPRIME))/BETA)*((WCR/BB)**2)
           D=(0.93/BETA)*((WCR/BB)**3)
           KE=(A/B)*(1-C+D)
!          FL=0.5*KE*RHOS*FYH
           FL=KE*RHOS*FYH
           ECO=0.7*((FCOMP*1000)**(0.3))/1000
           FCC=FCOMP*(1.413*SQRT(1+(11.4*FL/FCOMP))-(2*FL/FCOMP)-0.413)
           IF (FCOMP.LT.11.6) THEN
                   ECC=ECO*(1.0+(11.3*((FL/FCOMP)**0.7)))
           ELSEIF (FCOMP.GE.11.6) THEN
                   ECC=ECO*(-8.1+(9.1*EXP(FL/FCOMP)))
           ENDIF
           IF (FCOMP.LT.11.6) THEN
                   ECU=ECO*(2+(122.5-(0.92*FCOMP*6.895))*SQRT(FL/FCOMP))
           ELSEIF (FCOMP.GE.11.6) THEN
                   ECU=ECO*(2+((82.75-(0.37*FCOMP*6.895))*SQRT(FL/FCOMP)))
           ENDIF
           IF ((IN.GE.0).AND.(IN.LT.ECO)) THEN
                   OUTT=(ECONCRETE*IN)+((FCOMP-(ECONCRETE*ECO))*(IN**2)/(ECO**2))
           ELSEIF ((IN.GE.ECO).AND.(IN.LT.ECC)) THEN
                   OUTT=FCC-((FCC-FCOMP)*((IN-ECO)**2)/((ECC-ECO)**2))
           ELSEIF (IN.GE.ECC) THEN
           BETA1=((0.048*FCOMP*6.895)-2.14)-(((0.098*FCOMP*6.895)-4.57)*((FL/FCOMP)**(1/3)))
                   OUTT=FCC-(BETA1*FCC*(IN-ECC)/ECC)
                   IF (OUTT.LT.(0.4*FCC)) THEN
                           OUTT=0.4*FCC
                   ENDIF
           ENDIF
```

587

```
                    IF (OUTT.LT.0) THEN
                            OUTT=0
                    ENDIF

                    RETURN
                    END


        SUBROUTINE CUSPAUU(IN,FYH,HS,DH,AST,W,H,BB,WCR,L,AH,FCOMP,ESTEEL,OUTT)
                    REAL FYH,HS,SPRIME,FHCC,AST,W,H,RHOC,CX,CY,WCR,KE,BB,ECONCRETE
                    REAL ASHX,ASHY,ASH,FLE,C,OUTT,FCOMP,ECC,EC50U,EC50C,EHCC,ESTEEL
                    REAL KK,K1,K2,AC,AH,ECO,TOLERANCE,A,B,D,F,L,IN
                    ECONCRETE=57.*((FCOMP*1000)**0.5)
                    AC=W*H
                    CX=BB
                    CY=BB
                    SPRIME=HS-DH
                    RHOC=AST/AC
                    ASHX=3*AH
                    ASHY=3*AH
                    FHCC=FYH
                    A=1-(L*(WCR**2)/(6*CX*CY))
                    B=1-(SPRIME/(2*CX))
                    D=1-(SPRIME/(2*CY))
                    F=1-RHOC
                    KE=A*B*D/F
                    ASH=ASHX+ASHY
                    C=CX+CY
20                  FLE=KE*FHCC*ASH/(HS*C)
                    FCC=FCOMP*(1.0+(2.1*((FLE/FCOMP)**0.7)))
                    ECO=FCOMP/ECONCRETE
                    ECC=ECO+(0.21*((FLE/FCOMP)**1.7))
                    EC50U=0.004
                    EC50C=EC50U+(0.15*((FLE/FCOMP)**1.1))
                    EHCC=0.5*ECC*(1-(FLE/FCC))
                    FHCC=ESTEEL*EHCC
                    NFLE=KE*FHCC*ASH/(HS*C)
                    TOLERANCE=ABS(NFLE-FLE)/100
                    IF (TOLERANCE.LE.0.1) THEN
                            IF (IN.LE.ECC) THEN
                                    KK=ECONCRETE/(ECONCRETE-(FCC/ECC))
                                    OUTT=FCC*(KK*(IN/ECC)/(KK-1+((IN/ECC)**KK)))
                                    GOTO 10
                            ELSEIF (IN.GT.ECC) THEN
                                    K2=1.5
                                    K1=LOG(0.5)/((EC50C-ECC)**K2)
                                    OUTT=FCC*EXP(K1*((IN-ECC)**K2))
                                    GOTO 10
                            ENDIF
                    ELSE
                            GOTO 20
                    ENDIF
10                  IF ((OUTT.GE.0).AND.(IN.LE.0.005)) THEN
                            GOTO 30
                    ELSEIF ((OUTT.LT.0).OR.(IN.GT.0.005)) THEN
                            OUTT=0
                    ENDIF
30                  RETURN
                    END


        SUBROUTINE YONW(HS,BB,AST,W,H,DL,FYH,FCOMP,L,IN,OUTT)
```

588

```
                    REAL HS,AX,AY,BB,W,H,FY,FYH,DH1,EO,FO,FI,EI,F2I,E2I,ECONCRETE
                    REAL WEIGHT,IN,OUTT,EINIT,E2INIT,X,A,B,C,D,AST,RHO,RHOP
                    REAL KK,DL,FCOMP,P,Q,R,S,T,AH1,L
   !                L=NUMBER OF LONGITUDINAL BARS
                    AH1=0.0
                    DH1=0.0
                    FY=FYH*1000
                    WEIGHT=150
                    AX=3*AH1
                    AY=3*AH1
                    RHOP=0
                    RHO=AST/(W*H)
                    P=0.245*HS/BB
                    Q=RHOP+(L*DH1*RHO/(8*HS*DL))
                    Q=0
                    R=FY/SQRT(FCOMP*1000)
                    KK=1.0+(0.0091*(1-P)*Q*R)
                    S=1-(0.734*HS/BB)
                    T=(RHOP*FY)**(2/3)
                    EO=0.00265+((0.0035*S*T)/SQRT(FCOMP*1000))
                    FO=KK*FCOMP
                    FI=FO*(0.25*(FCOMP/FO)+0.4)
                    EI=KK*(1.4*(EO/KK)+0.0003)
                    F2I=FO*((0.025*FO)-0.065)
                    IF (F2I.LT.(0.3*FO)) THEN
                            F2I=0.3*FO
                    ENDIF
                    E2I=(2*EI)-EO
                    ECONCRETE=27.55*((WEIGHT)**1.5)*SQRT(FCOMP*1000)/1000
                    X=IN/EO
                    A=ECONCRETE*EO/FO
                    B=((A-1)**2/0.55)-1
                    IF (IN.LE.EO) THEN
                    OUTT=((A*X)+(B*(X**2)))*FO/(1+((A-2)*X)+((B+1)*(X**2)))
   !                OUTT=OUU/1000
                    ELSEIF (IN.GT.EO) THEN
                            EINIT=FI/EI
                            E2INIT=F2I/E2I
                            C=((E2I-EI)/EO)*(((E2I*EINIT)/(FO-FI))-((4*EI*E2INIT)/(FO-F2I)))
                            D=(EI-E2I)*((EINIT/(FO-FI))-(4*E2INIT/(FO-F2I)))
                            OUTT=((C*X)+(D*(X**2)))*FCOMP/(1+((C-2)*X)+((D+1)*(X**2)))
   !                        OUTT=OUU/1000
                    ENDIF
                    IF ((OUTT.LT.0).OR.(IN.GT.0.005)) THEN
                            OUTT=0
                    ENDIF
                    RETURN
                    END


                    SUBROUTINE AZIZ(HS,BB,AST,W,H,FYH,FCOMP,IN,OUTT)
                    REAL HS,AX,AY,BB,W,H,FY,FYH,DH1,EO,FO,FI,EI,F2I,E2I,ECONCRETE
                    REAL WEIGHT,IN,OUTT,EINIT,E2INIT,X,A,B,C,D,AST,RHO,RHOP
                    REAL KK,FCOMP,P,Q,R,S,T,AH1,ALPHA
   !                L=NUMBER OF LONGITUDINAL BARS
                    AH1=0.0
                    DH1=0.0
                    FY=FYH*1000
                    WEIGHT=150
                    AX=3*AH1
                    AY=3*AH1
                    RHOP=0
```

589

```
RHO=AST/(W*H)
P=0.245*HS/BB
Q=0
R=FY/SQRT(FCOMP*1000)
KK=1.0+0.0091
S=1-(0.734*HS/BB)
T=(RHOP*FY)**(2/3)
EO=0.00265
FO=KK*FCOMP
FI=FO*(0.25*(FCOMP/FO)+0.4)
EI=KK*(1.4*(EO/KK)+0.0003)
F2I=FO*((0.025*FO)-0.065)
IF (F2I.LT.(0.3*FO)) THEN
        F2I=0.3*FO
ENDIF
E2I=(2*EI)-EO
ECONCRETE=27.55*((WEIGHT)**1.5)*SQRT(FCOMP*1000)/1000
X=IN/EO
A=ECONCRETE*EO/FO
B=((A-1)**2/0.55)-1
IF (IN.LE.EO) THEN
!       OUTT=((A*X)+(B*(X**2)))*FO/(1+((A-2)*X)+((B+1)*(X**2)))
!       OUTT=OUU/1000
        OUTT=(FO/EO)*IN
ELSEIF (IN.GT.EO) THEN
        EINIT=FI/EI
        E2INIT=F2I/E2I
        C=((E2I-EI)/EO)*(((E2I*EINIT)/(FO-FI))-((4*EI*E2INIT)/(FO-F2I)))
        D=(EI-E2I)*((EINIT/(FO-FI))-(4*E2INIT/(FO-F2I)))
!       OUTT=((C*X)+(D*(X**2)))*FCOMP/(1+((C-2)*X)+((D+1)*(X**2)))
!       OUTT=OUU/1000
        ALPHA=(0.25*(FCOMP-0.6)/FO)/((3.13*KK)*((1.4*EO/KK)+0.0003))
        OUTT=FO*(1-(ALPHA*(IN-EO)))
        IF (OUTT.LT.(0.3*FO)) THEN
                OUTT=0.3*FO
        ENDIF
ENDIF
IF ((OUTT.LT.0.0).OR.(IN.GT.0.005)) THEN
        OUTT=0
ENDIF
RETURN
END


SUBROUTINE SAARAZZ(FYH,FCOMP,IN,OUTT)
REAL EO1,E1,E85,RHO,E085,IN,FCCP,FCO,ALPHA
REAL FYH,FL,K1,FCOMP,KK,FLE,FY,OU,OUTT
FCO=FCOMP*6.895
ALPHA=90
FY=FYH*6.895
FL=0
!       FL IS IN MPA
K1=0
EO1=0.002
FLE=0
KK=0
E1=EO1*(1+(5*KK))
RHO=0
E085=0.0038
E85=(260*RHO*E1)+E085
FCCP=FCO+(K1*FL)
IF (IN.LT.E1) THEN
```

```
                    OU=FCCP*(((2*(IN/E1))-((IN/E1)**2))**(1/(1+(2*KK))))
                    ELSEIF (IN.GE.E1) THEN
!                   OU=E1*(0.15*FCCP)/(E85-E1)+FCCP-((0.15*FCCP/(E85-E1))*IN)
                    OU=FCCP-((0.15*FCCP/(E85-E1))*IN)
                    ENDIF
                    IF (OU.GT.FCCP) THEN
                    OU=FCCP
                    ENDIF
                    OUTT=OU/6.895
!                   OUTT IS IN KSI
                    IF ((OUTT.LT.0.0).OR.(IN.GT.0.005)) THEN
                    OUTT=0.0
                    ENDIF
                    RETURN
                    END


                    SUBROUTINE SAKK(FCOMP,BB,COVER,DH,DL,HS,FYH,IN,OUTT,W)
                    REAL ALPHA,BETA,GAM,SIGB,KS,BB,HS,DH,KAPPA,FYH,SIGH,SIGP
                    REAL MU,RHOH,CSIGB,D,ECONCRETE,EO,KK,DH1,AH1
                    REAL X,A,OUTT,IN,FCOMP,C,COVER,KAY,ECO,DL,W
                    SIGB=FCOMP
                    KS=11.5
                    DH1=0.0
                    C=(W-(2*DH)-DL-(2*COVER))/2
                    KAPPA=KS*(DH1/C)*(1-(HS/(2*BB)))
                    ALPHA=1.5
                    BETA=-0.00168
                    GAM=0.50
                    MU=1.0
                    SIGH=FYH
                    SIGP=MU*SIGB
                    AH1=0
                    RHOH=3*AH1/(HS*BB)
                    CSIGB=SIGP+(KAPPA*RHOH*SIGH)
                    KK=CSIGB/SIGP
                    D=ALPHA+(BETA*SIGB)+(GAM*SQRT((KK-1)*SIGB/23))
                    KAY=1.0
                    ECONCRETE=4*KAY*(SIGB**(1/3))*(100000)*((GAM/2.4)**2)
                    EO=0.5243*((SIGB)**0.25)*(0.001)
                    IF (KK.LE.1.5) THEN
                            ECO=EO*(1+(4.7*(KK-1)))
                    ELSEIF (KK.GT.1.5) THEN
                            ECO=EO*(3.35+(20*(KK-1.5)))
                    ENDIF
                    X=IN/ECO
                    A=ECONCRETE*ECO/CSIGB
                    OUTT=CSIGB*((A*X)+((D-1)*X*X))/(1+((A-2)*X)+(D*X*X))
                    IF ((OUTT.LT.0).OR.(IN.GT.0.005)) THEN
                    OUTT=0
                    ENDIF
                    END


                    SUBROUTINE RICHH(FYH,FCOMP,AH,BB,HS,IN,OUTT)
                    REAL AH,BB,HS,KK,FR,FCOMP,FCCP,ECO,ECONCRETE,ECC,IN,OUTT
                    ECONCRETE=57*SQRT(FCOMP*1000)
                    FR=3*AH*FYH/(BB*HS)
                    KK=0
                    FCCP=FCOMP+(KK*FR)
                    ECO=FCOMP/ECONCRETE
                    ECC=ECO*(1+(5*(FCCP/FCOMP-1)))
```

591

```
                    IF (IN.LT.ECO) THEN
                    OUTT=FCCP*IN/ECO
                    ELSEIF (IN.GE.ECO) THEN
                    OUTT=(2*FCCP)-(FCCP*IN/ECO)
                    ENDIF
                    IF ((OUTT.LT.0).OR.(OUTT.GT.0.005)) THEN
                    OUTT=0
                    ENDIF
                    RETURN
                    END


                    SUBROUTINE FAFSHAA(IN,FCOMP,OUTT)
                    REAL ECONCRETE,ASH,LAMBDA,KK,IN,FCOMP
                    REAL FR,FCCP,ECC,A,WEIGHT,OUTT,K1
                    K1=4.1
   !                K1 IS FROM RICHART'S MODEL
                    ASH=0
                    WEIGHT=150
                    ECONCRETE=33*(WEIGHT**1.5)*SQRT(FCOMP*1000)/1000
                    FR=0
                    FCCP=FCOMP+K1*FR
                    ECC=FCCP/ECONCRETE
                    A=ECONCRETE*ECC/FCCP
                    LAMBDA=1
                    KK=24.65*FCOMP*EXP(-0.01*FR/LAMBDA)
                    IF ((IN.GE.0).AND.(IN.LE.ECC)) THEN
                            OUTT=FCCP*(1-((1-(IN/ECC))**A))
                    ELSEIF (IN.GT.ECC) THEN
                            OUTT=FCCP*EXP(-KK*((IN-ECC)**1.15))
                    ENDIF
                    IF ((OUTT.LT.0).OR.(IN.GT.0.005)) THEN
                            OUTT=0
                    ENDIF
                    RETURN
                    END


                    SUBROUTINE SHUZZ(OUTT,IN,L,COVER,W,DH,DL,BB,AST,FCOMP,HS,FYH)
                    REAL C,W,COVER,DH,DL,L,BB,KS,BC,AST,POCC,FCOMP,ACO,RHO
                    REAL FSP,Z,ES1,FCCP,EOO,ECONCRETE,ES2,F,G,AH1,OUTT,IN
   !                REAL ES85
                    AH1=0.0001
                    RHO=3*AH1/(BB*HS)
                    BC=W-(2*COVER)-(2*DH)
                    ACO=BC**2
                    POCC=FCOMP*(ACO-AST)
                    FSP=FYH
                    C=(W-(2*COVER)-(2*DH)-DL)/2
   KS=1.0+((2.73*BB*BB/POCC)*(1-(L*C*C/(5.5*BB*BB)))*((1-(HS/(2*BB)))**2)*SQRT(RHO*FSP))
                    Z=0.5/(0.75*RHO*SQRT(BB/HS))
                    FCCP=KS*FCOMP
                    ES1=0.55*KS*FCOMP*(0.000001)*1000
                    ECONCRETE=57*SQRT(FCOMP*1000)
                    EOO=FCOMP/ECONCRETE
                    F=1-(5*((HS/BB)**2))
                    G=RHO*FSP*1000/SQRT(FCOMP*1000)
                    ES2=EOO*(1+(0.81*F*G/C))
   !                ES85=(0.225*RHO*SQRT(BB/HS))+ES2
                    IF (IN.LE.ES1) THEN
                            OUTT=(-FCCP*((IN-ES1)**2)/(ES1**2))+FCCP
                    ELSEIF ((IN.GT.ES1).AND.(IN.LE.ES2)) THEN
```

                                                                    592

```
                    OUTT=FCCP
          ELSEIF (IN.GT.ES2) THEN
!         .AND.(IN.LE.ES85)) THEN
                    OUTT=FCCP+(ES2*Z)-(Z*IN)
!         ELSEIF (IN.GT.ES85) THEN
!         OUTT=0.0
          ENDIF
          IF ((OUTT.LT.0).OR.(IN.GT.0.005)) THEN
                    OUTT=0.0
          ENDIF
          RETURN
          END


          SUBROUTINE BINGLII(FYH,FCOMP,IN,OUTT,STEELTYPE)
          REAL IN,FCOMP,FL
          REAL ALPHAS,ECO,ECONCRETE,FCC
          REAL OUTT,ECC,ECU,BETA1,FCO
          INTEGER STEELTYPE
          REAL FYH
          FL=0
          ALPHAS=0
          FCO=FCOMP
          FCC=FCO
          ECO=0.7*((FCOMP*1000)**(0.3))/1000
          IF ((STEELTYPE.EQ.0).OR.(STEELTYPE.EQ.1)) THEN
                             ECC=ECO
          ELSEIF (STEELTYPE.EQ.2) THEN
                             ECC=2*ECO
          ENDIF
          ECONCRETE=(3200*SQRT(FCO*6.89655)+6900)*145/1000
          IF ((FYH.GE.0).AND.(FYH.LE.79.77).AND.(FCO.GT.10.88)) THEN
                    BETA1=(0.048*FCO*6.895-2.14)
          ELSEIF ((FYH.GE.0).AND.(FYH.LE.79.77).AND.(FCO.LE.10.88)) THEN
                    BETA1=0.2
          ELSEIF ((FYH.GT.79.77).AND.(FYH.LE.174))THEN
                    BETA1=0.2
          ELSEIF ((FYH.GT.174).AND.(FCO.LE.11.6)) THEN
                    BETA1=0.07
          ELSEIF ((FYH.GT.174).AND.(FCO.GT.11.6))          THEN
                    BETA1=0.1
          ENDIF

          IF ((STEELTYPE.EQ.0).OR.(STEELTYPE.EQ.1)) THEN
                    IF (FCO.LT.11.6) THEN
                             ECU=2*ECO
                    ELSEIF (FCO.GE.11.6) THEN
                    ECU=2*ECO
                    ENDIF
          ELSEIF (STEELTYPE.EQ.2) THEN
                    IF (FCO.LT.7.2) THEN
                             ECU=2*ECO
                    ELSEIF (FCO.GE.7.2) THEN
                             ECU=2*ECO
                    ENDIF
          ENDIF
          IF ((IN.GE.0).AND.(IN.LT.ECO)) THEN
                    OUTT=(ECONCRETE*IN)+((FCO-ECONCRETE*ECO)*(IN**2)/(ECO**2))
          ELSEIF (IN.GE.ECC) THEN
                    OUTT=FCC-(BETA1*FCC*(IN-ECC)/ECC)
                    IF (OUTT.LT.(0.4*FCC)) THEN
                             OUTT=0.4*FCC
```

```
                ENDIF
        ENDIF
        IF (OUTT.LT.0) THEN
                OUTT=0
        ENDIF
        RETURN
        END


        SUBROUTINE RAZSAATT(DH,DL,COVER,W,NN,ESTEEL,BB,FYH,HS,FCOMP,IN,OUTT)
        REAL E01,E1,E85,RHO,E085,IN,OUTT,AH,FCCP,FCO,ALPHA,K2,BB
        REAL FYH,FL,K1,FCOMP,KK,FLE,OU,ESTEEL,NN
        REAL ESEC,ECONCRETE,R,K3,K4,FS,LS,W,COVER,DH,DL,HS
        AH=0
        BC=W-(2.*COVER)-DH
!       INCOMING 'ESTEEL','FCOMP' IN KSI
        ECONCRETE=(3320*SQRT(FCOMP*6.895)+6900)/6.895
!       ECONCRETE ABOVE IN KSI
        FCO=FCOMP*6.895
!       FCO ABOVE IN MPA
        LS=(W-(2*COVER)-(2*DH)-DL)/2
        K2=0.15*SQRT((BC/HS)*(BC/LS))
        ALPHA=90
        RHO=NN*AH/(HS*BB)
        FS=ESTEEL*6.895*(0.0025+0.04*((K2*RHO)/(6.895*FCOMP))**1/3)
        IF (FS.GT.FYH) THEN
        FS=FYH
        ENDIF
        FL=(NN*AH)*FS*SIND(ALPHA)/(HS*BB)
!       FL IS IN MPA
        FLE=K2*FL
        K1=6.7*(0)
        K3=40/(FCOMP*6.895)
        K4=FYH*6.895/500
        IF (K4.LT.1.0) THEN
        K4=1.0
        ENDIF
        FCCP=FCO+(K1*FL)
        E01=0.0028-0.0008*K3
        KK=K1*FLE/FCO
        E1=E01*(1+(5*K3*KK))
        ESEC=FCCP/E1
        R=ECONCRETE/(ECONCRETE-ESEC)
        E085=E01+0.0018*(K3**2)
        E85=260*K3*RHO*E1*(1+0.5*K2*(K4-1))+E085
        IF (IN.LT.E1) THEN
                OU=FCCP*(IN/E1)*R/(R-1+((IN/E1)**R))
        ELSEIF (IN.GE.E1) THEN
                OU=FCCP-((0.15*FCCP/(E85-E1))*IN)
        ENDIF
        IF (OU.GT.FCCP) THEN
        OU=FCCP
        ENDIF
        OUTT=OU/6.895
!       OUTT IS IN KSI
        IF (OUTT.LT.0) THEN
        OUTT=0.0
        ENDIF
        RETURN
        END
```

594